

CRANFIELD UNIVERSITY

Kevin Stevens

An Investigation into Heat Dissipation from a Stationary Commercial Vehicle
Disc Brake in Parked Conditions

School of Engineering

EngD

Academic Year: 2013

Supervisors: Dr Marko Tirović
Dr Heather Skipworth

2013

CRANFIELD UNIVERSITY

School of Engineering

EngD

Academic Year: 2013

Kevin Stevens

An Investigation into Heat Dissipation from a Stationary Commercial
Vehicle Disc Brake in Parked Conditions

Supervisors: Dr Marko Tirović
Dr Heather Skipworth

2013

© Cranfield University 2013. All rights reserved. No part of this
publication may be reproduced without the written permission of the
copyright owner.

Abstract

Detailed understanding of heat dissipation from a stationary disc brake is of considerable importance for vehicle safety. This is essential for both park braking on inclines and for preventing brake fluid boiling in hydraulic brakes. Despite the experience proving the significance of such conditions, there is very little published data dealing with this phenomenon, and even ECE Regulation 13 does not specify hot parking braking performance. The problem of heat dissipation from stationary brake may appear simplistic but it is actually more complex than from a rotating disc, due to the lack of symmetry through or a dominant mode of heat transfer as natural convection is the only driving force behind the airflow. All three heat transfer modes exist in a transient process, with complex heat transfer paths within and between brake components.

This Thesis investigates the cooling performance of a Commercial Vehicle (CV) brake whilst in stationary conditions. The research is predominantly orientated towards the thermal aspects of Electric Parking Brake (EPB) application in CVs. Contraction of large brake components after hot parking may lead to vehicle rollaway on inclines, with tragic consequences. An extensive theoretical and experimental study was conducted. An analytical model of a disc brake in free air was developed, enabling good prediction of disc temperatures and average surface convective heat transfer coefficients (h_{conv}) over the entire cooling range. A comprehensive CFD modelling of the 3-dimensional flowfield around the disc brake was also conducted, as well as predicting the surface convection coefficient distribution. Shear Stress Turbulence model was found to be most suitable for such studies. FE models were created to predict temperatures in all components of the brake assembly. A special Thermal Rig was developed for experimental validations, which uses an induction heater for heating the disc brake, and numerous surface mounted and embedded thermocouples for measuring component temperatures, as well as 'free standing' for determining air temperatures in specific points. IR cameras provided further temperature field information.

The results clearly show little influence of the conductive heat dissipation mode. The study also showed, for the experimental arrangement used, a constant value of surface emissivity ($\varepsilon = 0.92$). With well-defined conductive and radiative heat dissipation modes, the emphasis was placed on investigating convective heat dissipation from a stationary disc brake. It has been demonstrated that the anti-coning straight vane design of brake disc does not cool effectively in stationary conditions. Expected 'chimney effects' in disc vent channels do not materialise due to large scale recirculation regions preventing airflow from entering the channels, which

drastically reduces the convective cooling. Complex thermal interactions between the large assembly components are explained, with typical cooling time being just over an hour for disc brake cooling from 400°C to 100°C.

Extracted heat transfer coefficients were used for establishing a complex FE assembly model, which enables accurate prediction of temperatures of individual components over the entire cooling period. The developed approach is used for predicting temperature of the existing brake assembly but is equally suited for generating new designs with more favourable characteristics. In addition to being a powerful design tool for assisting in EPB design and validation process, the methodology developed offers wide applications, such as thermal optimisation of the caliper housing for the installation of continuous wear monitoring sensors, smart slack adjusters (for low friction drag brakes), etc.

EPBs in passenger cars have been successfully used for over 10 years now. They use a relatively simple approach for ensuring safe parking from hot by over-clamping (applying approximately twice the required actuating force) and re-clamping (repeated application after the vehicle has been parked). Large CV actuating forces prevent the use of over-clamping as this could damage the disc, whilst re-clamping would need to be repeated several times over a much longer period of time, requiring the vehicle battery to power the electronic systems for a longer period of time without recharging. Neither approach is acceptable, requiring a more in-depth thermal study of the CV brake in stationary conditions, as investigated in this Thesis. In addition to technical, there are marketing and financial aspects which make EPB introduction and acceptance in commercial vehicles very different to passenger car applications.

Such an investigation was conducted, exploring the market the CV EPB will be sold in and whether it would accept the new technology. Two questionnaire analyses were carried out, with the second giving the respondent detailed information about the EPB. It was found that using an informed, knowledge based approach yielded more positive feedback to the proposed product. The outcome may be even considered more contrary than expected, rather than instigating mistrust, the new CV EPB technology created interest. Furthermore, reports of pneumatic malfunction indicated that independence from the pneumatic system should be used as the key selling point for the EPB, for all beneficiary segments.

Keywords:

Benefit analysis, questionnaire analysis, numerical modelling, CFD, FE, disc brake cooling, brake assembly

Acknowledgements

This is an opportunity I would like to take to thank and show my deepest appreciation to my supervisor, Dr Marko Tirović. Throughout my (extended) four year time working as your student, I have thoroughly enjoyed our random conversations. Your trips to the office were always entertaining! More importantly, under your tuition, I have developed not only in knowledge, but as a person. Your enthusiasm and passion for subject of Engineering hasn't been matched by anyone I ever met. When I arrived at Cranfield I was not convinced in my ability as an Engineer, I leave as a confident, mature man with an excellent job and future career prospects. I am of no doubt that your influence has made this possible. For this, I say the sincerest thank you!

Secondly, without the backing of Meritor I would have never had the opportunity to complete this doctorate. I would especially like to thank Paul, Martin and Peter at the Cwmbran facility. The guidance and advice you always gave was helpful. I wish you all the best in the future, please keep in touch.

I would also like to express my gratitude to Dr Heather Skipworth who gave me guidance on the commercial aspects of this thesis.

I am lucky to have the family that I do. You have all been very understanding with me over the past 8 (plus) years of university education, and the years before that. I realise I'm not the easiest person to be around when exam time comes around so thank you for putting up with me! To my sister, Lisa. You're the person who gets me the most and I know I can count on you for anything. You have always been there and I know you always will be. I hope I can return the favour. To my Mum and Dad, I would most like to thank you for the upbringing you gave me. I am privileged to say that I have become a person I am proud of and to what I have achieved already. Your love and advice throughout my life has made this possible and it is this that I am most thankful for. Jason, you have been a huge influence in my life and a person I admire. One final thought goes out to my Grandpa. Unfortunately he is no longer around to see me graduate, I know he would have been proud of me. Wherever you are, know you won't ever be forgotten.

There are three fellow researchers I would like to pay a special tribute to. Without you guys the days at Cranfield would have been much harder than they were. Lucia, you're awesome! Never forget that, and a Kit-Kat won't ever taste the same again. Stam, AKA The Bear, it was a pleasure to share an office with you for three years. The friendly banter was epic. For his

mathematical brilliance, I would like to say thank you to Stewart, your help was invaluable! Plus, your outrageous comments brightened up my days!

Finally, there is Malachy. I'm not sure either one of us really understood what we were letting ourselves in for when we started the MBA. Utter fear brought us together in its early stages, followed by the legendary revision session. Four years on and you have become one of my best friends. But dude please, take advice from Bane's dietary expertise and realise that a bowl of cereal is not dinner!

Table of Contents

<u>Section Number and Title</u>	<u>Page Number</u>
Abstract	i
Acknowledgements	v
Table Of Contents	vii
List of Figures	xiii
List of Tables.....	xxiii
List of Equations	xxv
List of Abbreviations.....	xxvii
Nomenclature	xxix
Publications	xxxiii
1 Introduction and Research Objectives.....	1
1.1 Research Aims and Objectives	7
2 Review of Meritor and the European Commercial Vehicle Braking Market.....	9
2.1 Introduction to the Business Problem	9
2.2 Technological Lock-In.....	11
2.3 Meritor Profile	14
2.4 Market Analysis.....	16
2.5 IAA Hannover Show 2010.....	20
2.6 Benefit Analysis.....	21
3 Obtaining an EPB Route to Market.....	27
3.1 Questionnaire Objectives	27
3.1.1 Further Information	29
3.2 Explanatory Questionnaire.....	30
3.2.1 Explanatory Questionnaire Flowchart	30
3.2.2 Population and Questionnaire Sample Size.....	31
3.2.2.1 End Users	33
3.2.2.2 End Buyers.....	35
3.2.2.3 OEM's	37
3.2.3 Administering the Questionnaire.....	37
3.2.4 Constructing the Questionnaire	40
3.2.4.1 Question Types.....	40
3.2.4.2 Response Types and Scales.....	41
3.2.5 Pilot Questionnaire	42
3.2.6 Explanatory Questionnaire Results	44
3.2.6.1 SECTION 2: Attitudes to New Products.....	45
3.2.6.2 SECTION 3: Customer Needs	52
3.2.6.3 SECTION 4: Braking and EPB Specific.....	53
3.2.6.4 SECTION 5: Brand Awareness.....	57
3.2.7 Explanatory Questionnaire Discussion.....	59
3.3 Knowledge Based Questionnaire	61
3.3.1 Discussion	72

4 Literature Review	75
4.1 Electric Parking Brake	76
4.2 Heat Transfer	80
4.2.1 Conduction	80
4.2.1.1 Thermal Conductance	82
4.2.1.2 Harman Technique	83
4.2.1.3 Parallel Thermal Conductance	83
4.2.1.4 3ω Technique	83
4.2.1.5 Laser Flash	83
4.2.1.6 Fourier Number	85
4.2.2 Convection.....	85
4.2.2.1 Boundary Layer Theory	86
4.2.2.2 Reynolds Number.....	88
4.2.2.3 Prandtl Number	89
4.2.2.4 Grashof Number.....	89
4.2.2.5 Rayleigh Number	90
4.2.2.6 Nusselt Number.....	90
4.2.3 Radiation	92
4.3 Heat Transfer Coefficients.....	93
4.4 Natural Convection	99
4.5 CFD Modelling and Forced Convection Cooling.....	100
4.6 FE Modelling Investigations.....	103
4.7 Thermal Stresses	108
4.8 Hot Spotting and Third Body Layer	110
4.9 Friction Pair Materials and Friction Coefficient Studies	114
4.10 New Technologies	118
4.11 Literature Summary	121
5 Experimental Equipment and Procedures	125
5.1 Laboratory Equipment	125
5.1.1 The Thermal Rig.....	125
5.1.2 Temperature Measurements	126
5.1.3 Measurement and Data Logging Equipment	127
5.1.3.1 CompactRIO	127
5.1.3.2 Thermocouple Modules	128
5.1.3.3 Universal Module – NI 9219.....	128
5.1.3.4 Output Voltage Module – NI 9263	129
5.1.3.5 High Speed Digital I/O Module – NI 9401	129
5.1.3.6 LabVIEW Program	129
5.1.4 Displacement and Input Force Transducers	131
5.1.5 Pressure Transducer.....	131
5.1.6 Induction Heater Coil System	132
5.2 Material Properties of Brake Assembly Components.....	133
5.2.1 Brake Caliper.....	133
5.2.2 Disc Brake	134
5.2.3 Friction Materials	135

5.3	Uncertainty analysis.....	137
5.4	Static Testing Method.....	142
5.5	Equipment Calibration.....	144
5.5.1	Displacement Transducer Calibration Method.....	144
5.5.2	Strain Gauge Calibration Method.....	146
5.5.3	Calibration Validation.....	150
5.6	Cooling Test Methods.....	153
5.7	Experimental Methodology Development.....	157
5.7.1	Influence of the Wheel on Disc Brake Cooling.....	157
5.7.2	Input Force Readings.....	159
5.7.2.1	Thermal Loading of the Caliper.....	163
5.7.2.2	Integration Box Reliability.....	164
5.7.2.3	Strain Gauge Temperature Correction.....	166
5.7.3	Thermal Set in the Brake Pads due to Preheating Input Pressure.....	169
5.7.4	Worst Case Pad Conditioning Testing.....	173
6	FE Thermal Modelling of a Parking Application.....	177
6.1	FE Model Creation.....	177
6.1.1	The Disc Brake.....	177
6.1.2	Brake Pad Friction Material – T3016.....	179
6.1.3	The Backplate.....	182
6.2	FE Model Preparation.....	184
6.2.1	Initial Parking Application Conditions.....	184
6.2.1.1	Radiation.....	187
6.2.1.2	Convection.....	188
6.2.1.3	Conduction.....	189
6.2.2	Preheating Results.....	190
6.3	Cooling Test Simulation Results.....	195
6.4	Chapter Summary.....	200
7	Analytical Investigation into Disc Brake Cooling.....	201
7.1	Analytical Modelling of a Vertically Positioned Disc.....	201
7.1.1	Rectangle Section Properties.....	212
7.1.2	Disc Brake Friction Surface Convection Heat Transfer Coefficient.....	215
7.2	Numerical Modelling.....	217
7.3	Chapter Summary.....	222
8	CFD Modelling of Airflow and Heat Transfer from a Stationary Ventilated Disc Brake.....	225
8.1	Validation Equipment and Procedure.....	225
8.2	CFD Model Construction.....	227
8.2.1	Volume Mesh Generation.....	228
8.2.2	CFD Model Setup.....	231
8.2.2.1	Laminar Model.....	232
8.2.2.2	$k - \epsilon$ Model.....	233
8.2.2.3	$k - \omega$ Model.....	233
8.2.2.4	SST Model.....	233
8.2.2.5	Turbulence Modelling Comparison.....	234
8.3	CFD Results.....	236

8.3.1 Flange Airflow and Heat Plume Existence Testing.....	236
8.3.2 Airflow Results.....	239
8.3.3 Qualitative Airflow Validation.....	247
8.3.3.1 Flow Regime Around the Hat Section	248
8.3.3.2 CFD Qualitative Validation	250
8.3.3.3 Effect of the Caliper on the Airflow.....	255
8.4 Distribution of Heat Transfer Coefficients	258
8.4.1 Convective Heat Transfer Distribution at High Temperatures.....	258
8.4.2 Changes in Convective HTC Values During Cooling Phase.....	262
8.5 Chapter Summary	271
9 Detailed Thermal Analysis of Disc Brake Cooling.....	273
9.1 Component Analysis Experimental Method.....	273
9.2 Disc Only Experimental Cooling Temperatures	276
9.2.1 With Gasket and Blocked vanes.....	277
9.2.2 Further Disc Only Experiments.....	286
9.2.3 Hat Temperatures	291
9.3 Conduction Coefficient Calculations.....	293
9.4 Emissivity	294
9.5 Chapter Summary	297
10 Full Brake Assembly FE Analysis	299
10.1 Disc Brake Temperatures.....	300
10.1.1 Experimental Disc Temperatures	300
10.1.2 Initial Disc Only Modelling.....	302
10.1.3 Effect of Additional Brake Components on the Disc Brake.....	307
10.2 Brake Pad Temperatures	308
10.3 Pad Carrier Temperatures	310
10.3.1 FE Model Alterations	312
10.3.2 Pad Carrier Final Heating FE Temperatures	318
10.3.3 Influence of Other Caliper Components on Pad Carrier	320
10.4 Bridge and Housing Temperatures	321
10.4.1 Bridge Final Heating Temperatures	321
10.4.2 Housing Final Heating Temperatures.....	322
10.4.3 FE Model Development – Bridge and Housing	323
10.4.4 Bridge and Housing Heating FE Results	325
10.5 Piston Temperatures.....	328
10.5.1 FE Development and Results	329
10.6 Full Assembly Cooling Temperatures and FE Predictions.....	332
10.7 Brake Assembly Showcase Model.....	339
10.8 Chapter Summary	341
11 Summary and Conclusions.....	343
11.1 Discussion.....	344
11.2 Research Contributions.....	347
11.3 Recommendations for Future Work.....	348
Appendix A - Minutes Of Meritor Survey Meeting With Thibaut Grosdemouge	353
Appendix B - Pilot Questionnaire	357

Appendix C – Pilot Questionnaire Flowchart	379
Appendix C.1 Personal Information	379
Appendix C.2 New Products.....	380
Appendix C.3 Customer Needs.....	381
Appendix C.4 Direct EPB.....	382
Appendix C.5 Brand Recognition.....	383
Appendix D - Explanatory Questionnaire.....	385
Appendix E - Knowledge-Based Questionnaire	413
Appendix F - Designed Pneumatic Ram Modification	431
Appendix G - National Instruments Module Data Sheets.....	435
Appendix H - LM 120 Offest D-Elsa 225 Brake	451
Appendix I - Standard 434/234 Straight Radial Vane Ventilated Rotor	453
Appendix J - Service Chamber.....	455
Appendix K - Analytical Disc Cooling Modelling, Cases 1 and 2	457
Appendix K.1 - Lumped HTC - Case 1	457
Appendix K.1.1 - Numerical Solution.....	458
Appendix K.1.1.1 - Solver	458
Appendix K.1.1.2 - Results	459
Appendix K.1.1.3 - Cooling Equation.....	462
Appendix K.2 Case 2 - Variable Radiation.....	464
Appendix K.2.1 - Numerical Solution.....	464
Appendix K.2.2 - Improved Cooling Equation	466
Appendix K.2.2.1 - Asymptotic Assumption.....	466
Appendix K.2.2.2 - Comparing β Coefficients.....	468
Appendix K.2.2.2.1 - Order 1	469
Appendix K.2.2.2.2 - Order β	470
Appendix L - Temperature Dependent Air Properties	473
Appendix M - Contact Pressure	479
Appendix N - MatLab Program	483
References.....	491

List of Figures

<u>Figure Number</u>	<u>Page Number</u>
Figure 1.1: Cut through of the current service chamber and the spring parking chamber	2
Figure 1.2: The LM 120 Offset D-Elsa Brake Assembly.....	4
Figure 1.3: Exploded view of the parts making up the Mechanism component, located in the Housing Unit	5
Figure 2.1: ArvinMeritor 2010 sales of brake configurations by global region.....	16
Figure 2.2: European brake supplier market share 2010.....	17
Figure 2.3: OEM market share 2010.....	18
Figure 2.4: Tiers of the brake market.....	22
Figure 2.5: Benefit analysis for the EPB based on author’s experience.	23
Figure 3.1: General questionnaire flowchart.....	31
Figure 3.2: Q2.3 All Results - driver features appear to be the most important.....	46
Figure 3.3: Question 2.6 shows little resistance to an electric actuation method.....	51
Figure 3.4: Question 3.6 shows the benefit segments don’t know the amount of weight loss needed for them to realise a benefit.....	53
Figure 3.5: Improved Benefit analysis to include independence from air.....	55
Figure 3.6: Only 1/3 of respondents knew of the EPB component.....	56
Figure 3.7: People strongly agree with the statement “ <i>The brake system is highly important to the overall CV performance.</i> ”	58
Figure 3.8: People generally agree with the statement “ <i>There is little difference in quality between brake systems from the various brake manufacturers.</i> ”	58
Figure 3.9: Meritor is the least known brake brand of brake manufacturers.....	59
Figure 3.10: Knowledge based questionnaire flowchart	62
Figure 3.11: 58% believes reducing size and weight of the parking chamber is a useful feature.	63
Figure 3.12: 52% of respondents agree that removing pneumatic parts is a useful CV feature..	65
Figure 3.13: Reducing the compressed air reservoir was described as a useful CV feature by 58% of questionnaire respondents.....	65
Figure 3.14: Aided hill start functionality is useful according to 70% of respondents.	66
Figure 3.15: Use of the EPB as an Immobiliser appears.....	67

Figure 3.16: Single button operation is seen as useful, but with more scepticism than other features.....	68
Figure 3.17: The parking chamber will no longer need an air supply to operate is useful according to 50% of respondents	69
Figure 3.18: Final benefit analysis	71
Figure 3.19: 66% of respondents believe say the EPB would be beneficial to a CV.....	72
Figure 3.20: An illustration of the suggested marketing strategy made to Meritor.....	74
Figure 4.1: Common types of disc brake design a) standard outer hat design, b) outer with neck, c) inner hat and d) inner hat with hole.....	76
Figure 4.2: Passenger vehicle EPB	77
Figure 4.3: Electric brake cable type EPB (Slosarczyk <i>et al.</i> 2008).	78
Figure 4.4: Thermal contact resistance example.....	82
Figure 4.5: Typical velocity profile in hydrodynamic boundary layer (turbulent).	86
Figure 4.6: Transition from laminar to turbulent flow. The boundary layer thickness not to scale (Anderson 2007).....	87
Figure 4.7: h_{conv} vs rotational speed for CV disc (Voller 2003).	94
Figure 4.8: Influence of dissipation modes against rotational disc brake speed (Voller <i>et al.</i> 2003).....	95
Figure 4.9: Varying emissivity values (Voller <i>et al.</i> 2003).....	96
Figure 4.10: 1D model to calculate hub temperatures (Abbas <i>et al.</i> 1969).....	104
Figure 4.11: Full car model (Pavlidis and Siskos 2010).	108
Figure 4.12: Hotspot classifications (Panier <i>et al.</i> 2004)	112
Figure 4.13: Negative stick-slip phenomenon (Gao and Kuhlmann-Wilsdorf 1990).	115
Figure 4.14: Annular disc brake design for automotive use (Erlston and Miles 2005).....	119
Figure 5.1: Full Thermal Rig.....	126
Figure 5.2: LabVIEW closed-loop motor controller.....	130
Figure 5.3: Connection between the pressure transducer and the NI-9219.....	132
Figure 5.4: a.) Installed induction heater coil and b.) the induction box.....	133
Figure 5.5: Thermocouple system error when using the NI 9211 module (National Instruments NI 9211 Datasheet).....	140
Figure 5.6: Thermocouple system error when using the NI 9213 module (National Instruments NI 9213 Datasheet).....	140

Figure 5.7: Thermocouple system error when using the NI 9214 module (Instruments NI 9214 Datasheet).....	141
Figure 5.8: Internal caliper output ratio as a function of pushrod travel.....	143
Figure 5.9: Correctly fitted plates (1) between the brake pads (2, steel dummy plates in this instance) and the pistons (3), to create the gap clearance.....	144
Figure 5.10: Displacement transducer (1) calibration equipment, incorporating a self-locating pin (2) to locate the pushrod from the service chamber (3) in the Instron machine head unit (4).	145
Figure 5.11: Calibration results of the displacement transducer.....	146
Figure 5.12: Use of weights to exert a known compression load on the load cell.....	147
Figure 5.13: Calculated gain from the load cell.....	148
Figure 5.14: Fixturing used to calibrate the strain gauge located on the pushrod, housed in the service chamber (1), using the load cell (2) and displacement transducer (3).....	149
Figure 5.15: Calibration graphs used for the second set of static tests.....	150
Figure 5.16: Third static test comparison of FER 4567 friction material.....	152
Figure 5.17: Third static test comparison of T3016 friction material.....	153
Figure 5.18: Disc Brake temperatures taken from an actual drive cycle (Data provided by P. Gibbens, Meritor H.V.B.S).....	154
Figure 5.19: Rubbing thermocouple placement on the disc brake.....	155
Figure 5.20: Positions and labels of thermocouples in the pads.....	156
Figure 5.21: Positions and labels of thermocouples on the caliper.....	156
Figure 5.22: The full cooling test time cycle with two preheating clamps and the wheel present.....	158
Figure 5.23: There is a negligible difference in the cooling phase when the wheel is attached and when not attached.....	159
Figure 5.24: Presence of a pressure drop during the cooling tests.....	160
Figure 5.25: Measured actuator displacement during the coolback phase of the cooling test for FER 4567 pads, total initial clearance gap of 1.70 mm and an input pressure of 7 bar ...	161
Figure 5.26: Measured input force during the coolback phase of the cooling test for FER 4567 pads, total clearance gap of 1.70 mm and an input pressure of 7 bar.....	162
Figure 5.27: Bridge temperatures during the cooling phase.....	163
Figure 5.28: Positions and labels of thermocouples on the caliper.....	164
Figure 5.29: Zero shift from the integration box produces a large effect on the calculated clamp force.....	165
Figure 5.30: Second zero shift test confirming randomness of the shifting.....	165

Figure 5.31: Graph taken from the Vishay technical support document Tech Note TN-504-1 displaying the amount of additional strain generated in the strain gauge from the effects of temperature (Vishay Micro-Measurements 2007).....	167
Figure 5.32: Temperature rise of the pushrod during the coolback phase.	168
Figure 5.33: Cooling test with 2 preheating clamps at 6 bar.....	170
Figure 5.34: Cooling test with 2 preheating clamps at 1 bar.....	171
Figure 5.35: Cooling test with 5 preheating clamps at 1 bar.....	171
Figure 5.36: Cooling rates in the backplate from 150°C.....	173
Figure 5.37: Total measured brake assembly contraction using various pad materials, in various thermal states.	175
Figure 6.1: CAD model of the disc brake provided by Meritor.....	177
Figure 6.2: Fully simplified disc geometry used for FE analysis – ID side.	178
Figure 6.3: Disc segmented by simplified vane shape.	179
Figure 6.4: Sectioning pattern placed on the T3016 pad friction material.....	180
Figure 6.5: Pad section put into disc as well.	181
Figure 6.6: Fully meshed disc.....	182
Figure 6.7: a.) The brake pad and disc sections put into front side of backplate, and b.) piston rings located on the rear of the backplate.....	183
Figure 6.8: Mesh techniques for various backplate divisions.	184
Figure 6.9: Outboard disc friction surface temperatures during the preheating sequence.	185
Figure 6.10: Outboard pad temperatures during the preheating sequence.	186
Figure 6.11: Uniformly distributed heat flux into the disc friction surface.....	186
Figure 6.12: Surface radiation boundary conditions set on the disc brake a.) OD axial surface and b.) disc brake friction surface.....	188
Figure 6.13: Standard convection from highlighted surfaces.....	189
Figure 6.14: Conduction interaction at the disc/friction material interface.....	190
Figure 6.15: Approximate thermocouple node positions in ABAQUS.....	191
Figure 6.16: FE model results for the preheating sequence for the thermocouple position Disc Out High Top (see Figure 5.19 and Figure 6.15).....	192
Figure 6.17: Predicted temperatures reached at the end of the first heating sequence (see Figure 5.19 and Figure 6.15 for thermocouple positions).....	193
Figure 6.18: First heating procedure comparisons for the Disc Out Top positions (see Figure 5.19 and Figure 6.15).....	194

Figure 6.19: First heating procedure comparisons for the Pad Out positions (see Figure 5.20 and Figure 6.15)	195
Figure 6.20: Outboard disc cooling results from FE (see Figure 6.15 for thermocouple positions)	196
Figure 6.21: Outboard pad cooling results from FE (see Figure 6.15 for thermocouple positions)	197
Figure 6.22: Average friction surface experimental data with the corresponding FE predictions	199
Figure 6.23: POS average temperature with erroneous results omitted.	200
Figure 7.1: How the contact face surfaces area was broken down into simplified geometry (not to scale).....	203
Figure 7.2: Arc area integration results.	204
Figure 7.3: Prandtl number across the arc section at different temperatures.	205
Figure 7.4: Grashof number across the arc section at different temperatures.	206
Figure 7.5: Rayleigh number across the arc section at different temperatures.	207
Figure 7.6: Mean Nusselt number for temperature and horizontal position for Churchill and Chu (1975) relationship.....	208
Figure 7.7: Mean Nusselt number for temperature and horizontal position for McAdams (1954) relationship.	209
Figure 7.8: Calculated h_{conv} values for the arc section - Churchill and Chu relationship.	210
Figure 7.9: Mean h_{conv} values across the arc for various temperatures.....	212
Figure 7.10: Calculated dimensionless parameters for a rectangular section.....	214
Figure 7.11: Mean h_{conv} values for the rectangle area against various temperatures.....	215
Figure 7.12: Mean h_{conv} values for the full simplified geometry with various temperatures.	216
Figure 7.13: Comparison of the three different cases shows the fully variable case to be superior.....	219
Figure 7.14: Simplified hat geometry.	220
Figure 7.15: Dimensionless parameters for both cylinders representing hat geometry	221
Figure 7.16: Variable convective HTC over both cylinders.	222
Figure 8.1: Thermocouple names and positions.....	226
Figure 8.2: Smoke machine testing with light planes to aid flow visualisation.	227
Figure 8.3: CFD model domain.....	228
Figure 8.4: Mesh generated for CFD investigation, with a.) the full volume mesh, b.) finer mesh around the disc brake and c.) prism layer close to the surface	229

Figure 8.5: Open surfaces set to 20°C.....	231
Figure 8.6: Typical convergence graphs for a.) mass and momentum, and b.) heat transfer....	235
Figure 8.7: Predicted plume presence from CFD modelling located on the flange face.....	237
Figure 8.8: Additional thermocouple positions for plume existence test.....	238
Figure 8.9: Close up view of velocity streamlines on the flange surface light plane.....	239
Figure 8.10: The plane used at the vanes centre to analyse CFD results.	240
Figure 8.11: Velocity streamlines from the central vanes light plane.....	241
Figure 8.12: Velocity streamlines within the vane channels (surfaces have been removed)	242
Figure 8.13: Central vanes located plane demonstrating high in-vane upper temperatures.....	243
Figure 8.14: Airflow streamline CFD results in the axial plane at the outboard friction surfaces on the lower half of the disc brake (cross section view).....	245
Figure 8.15: Airflow streamline CFD results in the axial plane at the outboard friction surfaces on the upper half of the disc brake.	246
Figure 8.16: Pressure change from atmospheric conditions.....	247
Figure 8.17: Light plane in the Flange location, suggesting flow over the hat is the laminar regime.....	248
Figure 8.18: Light plane in the Flange location showing flow fluctuations.....	250
Figure 8.19: The presence of weak vortices creating holes in the light plane.....	251
Figure 8.20: Airflow forced into upper ID regions does not travel through the vanes channels.	252
Figure 8.21: Evidence of exiting ID airflow causing the upper inlet blockage.....	253
Figure 8.22: Existence of an external region.....	254
Figure 8.23: Caliper presence causes more air to be entrained over the free side of the disc ...	255
Figure 8.24: Passages between caliper not providing air passages to vane inlets.	256
Figure 8.25: Bridge component acting as a barrier to upper OD vane channel inlets.....	257
Figure 8.26: <i>hconv</i> distribution of the in-vane surfaces when the friction surfaces are at 350°C.	259
Figure 8.27: <i>hconv</i> distribution off the outboard friction surface at 350°C.	260
Figure 8.28: Convective heat transfer distribution over hat section outer surface.	262
Figure 8.29: The recirculation region in the axial plane, on the lower half of the disc (Figure 8.14).....	263
Figure 8.30: Upper velocity streamlines in light plane C at 213°C (can compare with Figure 8.15).....	264

Figure 8.31: Velocity streamlines in light plane B at 112°C.....	265
Figure 8.32: Lower velocity streamlines in light plane C at 49°C.....	266
Figure 8.33: Increased area of high convective heat dissipation over the hat section, at 49°C.	267
Figure 8.34: Upper velocity streamlines in light plane C at 49°C.....	268
Figure 8.35: CFD <i>hconv</i> values compared to the analytical values predicted in Chapter 7.....	269
Figure 9.1: Position of the disc brake thermocouple holders.....	274
Figure 9.2: Thermal Rig modifications showing a.) the vertical air thermocouples and b.) the three hat thermocouples.....	276
Figure 9.3: Temperatures varying less than $\pm 2^{\circ}\text{C}$ before cooling starts, thermal equilibrium conditions.....	278
Figure 9.4: Temperatures prior to and including the start of the cooling phase.....	280
Figure 9.5: 350°C cooling profiles for all five experiments from the +000 DOO thermocouple - for case 1.....	282
Figure 9.6: Standard deviation values for the average blocked vanes, with gasket experiments.....	283
Figure 9.7: Averaged outboard disc brake surface temperatures, at the 350°C reference.....	284
Figure 9.8: Averaged inboard disc brake surface temperatures, at the 350°C reference.....	284
Figure 9.9: Averaged circumferential temperatures at the start of the cooling phase.....	286
Figure 9.10: Comparing the averaged cooling data for the three disc only cases.....	288
Figure 9.11: Thermal gradient across the disc brake/wheel carrier interface.....	289
Figure 9.12: The results of disc brake/wheel carrier testing confirms the thermal gradient between the pair to a 70% experimental confidence level.....	291
Figure 9.13: Bulk rotor temperatures drop below hat temperatures during the cooling phase (see Figure 9.2 for thermocouple positions).....	292
Figure 9.14: Thermal image of the initial parking application, showing the Spot temperature SP01 position (located on the outboard 0° friction surface) and the adjacent +000 DOO thermocouple.....	295
Figure 9.15: Emissivity results over the full cooling phase.....	297
Figure 10.1: Outboard brake “disc only” thermal equilibrium temperatures.....	301
Figure 10.2: Inboard brake “disc only” thermal equilibrium temperatures.....	301
Figure 10.3: Highlighted conduction path for the simplified disc brake and wheel carrier model.....	302
Figure 10.4: Cooling from wheel carrier external surfaces.....	304

Figure 10.5: Surfaces selected for a radiation interaction between the disc brake and wheel carrier.....	304
Figure 10.6: Predicted FE disc brake and wheel carrier temperature distribution at thermal equilibrium (initial cooling temperatures).....	306
Figure 10.7: FER 4567 brake pads being held against the disc brake with a G clamp – experiment two	309
Figure 10.8: Average outboard pad carrier surface temperatures.	311
Figure 10.9: Average inboard pad carrier surface temperatures.	312
Figure 10.10: Reduction in disc surface area available for radiation with installation of the pad carrier.....	313
Figure 10.11: Radiation interaction between the disc and the pad carrier surfaces.	314
Figure 10.12: Surface area used for both the radiation and gap conduction interactions between the disc brake circumferential surface and the pad carrier	315
Figure 10.13: Radiation interaction between the hat and pad carrier.....	316
Figure 10.14: Surfaces used in attempt to artificially create a vertical thermal gradient	317
Figure 10.15: Pad carrier flange surface thermal boundary conditions.....	318
Figure 10.16: Schematic diagram of airflow a.) flowing through the housing or b.) being blocked by the mechanism.	321
Figure 10.17: Average recorded bridge temperatures	322
Figure 10.18: Housing final heating (initial cooling) temperatures	323
Figure 10.19: Radiation and gap conduction surfaces between bridge and disc brake outer surface	324
Figure 10.20: Radiation from disc brake friction surface a.) outboard to internal bridge surfaces, and b.) inboard to housing flange surface.....	325
Figure 10.21: Piston temperatures from experiment 6	328
Figure 10.22: Full FE caliper assembly model – experiment 6.....	329
Figure 10.23: Radiation interaction between inboard friction surface and the mechanism	330
Figure 10.24: FE modelling of a stationary application – experiment 06	333
Figure 10.25: FE modelling of a parking– 02 Disc, FER 4567.....	335
Figure 10.26: FE modelling of a stationary application – 04 Disc, Pad Carrier	336
Figure 10.27: Predicted bridge temperatures compared to experimental data – experiment 5 .	337
Figure 10.28: Predicted housing temperatures compared to experimental data – experiment 6	338
Figure 10.29: Piston and disc brake predicted temperatures from the final FE model – experiment 6.	339

Figure 10.30: Temperature contour plots of brake assembly during the first 2 hours of the cooling phase.....	340
Figure 11.1: Designed pneumatic ram system for friction testing	350

List of Tables

<u>Table Number</u>	<u>Page Number</u>
Table 3.1: Breakdown of CV End Users in the UK (taken from the Office of National Statistics 2011).....	35
Table 3.2: Estimated number of people with sufficient CV knowledge in the End Buyer segment.....	37
Table 3.3: Q2.3 – Segmented results for the most important CV features.....	47
Table 3.4: Q2.3 – Segmented results for the least important CV features.....	48
Table 4.1: Parameters for the McAdams relationship for <i>Num</i> (McAdams 1954)	91
Table 4.2: Values for the Morgan equation with ranging <i>Ra</i> (Morgan 1975)	92
Table 4.3: Emissivity values used by Voller <i>et al.</i> (2003)	96
Table 4.4: Order of wear rate and μ level influences for CV brake pad materials (Lu <i>et al.</i> 2002).	117
Table 4.5: Brake pad makeup (Jang <i>et al.</i> 2004).....	117
Table 5.1: Spheroidal Graphite Iron material properties for the pad carrier, bridge and housing components (from Meritor HVBS).	134
Table 5.2: Material properties for the disc brake (from Meritor HVBS).	135
Table 5.3: T3016 friction material properties (from Meritor HVBS).	136
Table 5.4: FER 4567 friction material properties (from Meritor HVBS).	136
Table 5.5: Brake pad backplate material properties (from Meritor HVBS).....	136
Table 5.6: Experimental results of the static tests.....	151
Table 5.7: Meritor’s static test results.	151
Table 6.1: <i>hcond</i> values for the disc brake/friction material interface.....	190
Table 6.2: Average, maximum and minimum temperatures for the Disc Out High Top thermocouple.....	198
Table 7.1: Coefficients relating to equation (7.4)	211
Table 8.1: CFD model tests – convergence times.....	234
Table 8.2: CFD model results compared to experimental results - % difference from measured.	236
Table 8.3: Plume test results (Ambient temperature set at 20°C)	238
Table 9.1: Summary of the rotational thermal properties at 100 rpm.	287

Table 9.2: Times and subsequent temperatures when the hat thermocouples become higher than the bulk rotor temperature	293
Table 9.3: Calculated <i>hcond</i> values for all assembly contacting surface, using equations (4.23) and (4.24).....	294
Table 10.1: <i>hconv</i> values used during heating stage of FE simulation, based on 100 rpm rotational speed from Voller (2003) and iteration results.....	303
Table 10.2: Final heating (initial parking) temperature comparisons – 01 Disc.....	307
Table 10.3: Gap conductance values used – 04 Disc, Pad Carrier.....	315
Table 10.4: Final heating (initial parking) temperature comparisons – 04 Disc, Pad Carrier...	319
Table 10.5: Final heating (initial parking) temperature comparisons – 05 Disc, Pad Carrier, Bridge, Housing.....	327
Table 10.6: Breakdown of the number of elements in the full FE model.	330
Table 10.7: Final heating (initial parking) temperature comparisons – 06 Disc, Pad Carrier, Bridge, Housing, Mechanism, Pistons.....	331
Table 10.8: Final <i>hconv</i> values used in the stationary parking simulations – reduced values by 15%.....	333
Table 11.1: Average disc brake temperature taken from averaged experimental data – blocked vanes, gasket installed. Ambient temperature = 24.1°C.....	459

List of Equations

<u>Equation Number</u>	<u>Page Number</u>
(4.1).....	81
(4.2).....	81
(4.3).....	82
(4.4).....	82
(4.5).....	82
(4.6).....	84
(4.7).....	85
(4.8).....	86
(4.9).....	86
(4.10).....	86
(4.11).....	87
(4.12).....	87
(4.13).....	87
(4.14).....	89
(4.15).....	89
(4.16).....	91
(4.17).....	91
(4.18).....	91
(4.19).....	91
(4.20).....	91
(4.21).....	91
(4.22).....	92
(4.23).....	96
(4.24).....	107
(5.1).....	131
(5.2).....	132
(5.3).....	133
(5.4).....	135
(5.5).....	136
(5.6).....	136
(5.7).....	160
(5.8).....	160
(5.9).....	160
(7.1).....	197
(7.2).....	198
(7.3).....	198
(7.4).....	198
(7.5).....	199

(7.6).....	199
(7.7).....	199
(7.8).....	199
(7.9).....	201
(7.10).....	201
(7.11).....	209
(7.12).....	209
(7.13).....	211
(7.14).....	214
(8.1).....	226
(8.2).....	228
(9.1).....	275
(9.2).....	276
(9.3).....	277
(10.1).....	317

List of Abbreviations

ABS	Anti-lock Brake System
BBW	Brake-By-Wire
BSL	Baseline
CFD	Computational Fluid Dynamics
CU	Cranfield University
CV	Commercial Vehicle
DAR	Drive Away Release
DIC	Digital Imaging Correlation
DSC	Differential Scanning Calorimeter
ECU	Electronic Control Unit
EPB	Electronic Parking Brake
EQ	Explanatory Questionnaire
HGV	Heavy Goods Vehicle
HTC	Heat Transfer Coefficient
IAA	International Automotive Exhibition
ID	Inner Diameter
IR	Infrared
KBQ	Knowledge Based Questionnaire
NAO	Non-Asbestos Organic
LVS	Light Vehicle System
NO _x	Nitrous Oxides
OD	Outer Diameter
ODE	Ordinary Differential Equation
OEM	Original Equipment Manufacturer
PTC	Parallel Thermal Conductance
SST	Shear Stress Transport
TCR	Thermal Contact Resistance

Nomenclature

<u>Symbol</u>	<u>Description</u>	<u>Unit</u>
α	Thermal diffusivity	m^2/s
α_G	Thermal expansion of strain gauge	K^{-1}
α_{opt}	Opshaft Ratio	
α_S	Thermal expansion of substrate	
β_G	Coefficient of temperature resistance	
ε	Emissivity	
ε	Turbulent eddy dissipation rate	J/s
$\varepsilon_{T/0}$	Thermal output function	
θ	Surface temperature	K
λ_a		
μ	Friction coefficient	
ξ	Effusivity	$\left(\frac{J^2}{s m^4 K^2}\right)^{1/2}$
ρ	Density	kg/m^3
σ	Stefan-Boltzman constant, taken at 5.67E-8	
τ	Stress tensor	Pa
ν	Poisson's ratio	
ϕ	Heat flux	W/m^2
φ	Cooling rate parameter	s^{-1}
σ	Standard deviation	
χ	Probability of making a type I error	
ψ	Probability of accepting a null hypothesis (type II error)	
φ	Power of the test	
ω	Specific dissipation rate	
A	Surface area	m^2
A_{arc}	Surface area of arc	m^2
A_{int}	Surface area at contact interface	m^2
A_{rec}	Surface area of rectangular area	m^2
C	Constant	
C_p	Specific heat capacity	$J/kg K$
D	Diameter	m

E	Energy	J
E_{axle}	Energy per axle	J
E_d	Energy per disc brake	J
E_{surf}	Energy entering a single disc brake friction surface	J
F_G	Gauge factor in a strain gauge	
F_I	Gauge factor	
Fo	Fourier Number	
Gr	Grashof number	
H_N	Alternative Hypothesis	
H_0	Null Hypothesis	
h	Bulk heat transfer coefficient	W/m^2K
h_{cond}	Conduction heat transfer coefficient	W/m^2K
h_{conv}	Convection heat transfer coefficient	W/m^2K
h_{outer}	Heat transfer coefficient on out disc brake surfaces	W/m^2K
h_{rad}	Radiation heat transfer coefficient	W/m^2K
h_{vanes}	In-vane heat transfer coefficient	W/m^2K
k	Thermal conductivity	W/m^2K
k	Turbulent kinetic energy	J
K	Constant	J
K_t	Transverse sensitivity of strain gauge	
l	Length	m
L	Characteristic length	m
m_d	Mass of the disc brake	kg
Nu	Nusselt number	
P	Power	W
Pr	Prandtl number	
p -value	Observed significance value	
\dot{Q}	Rate of heat transfer	kW
r	Radius	m
R	Length through which conduction occurs	m
Ra	Rayleigh number	
R_{cond}	Thermal contact resistance	m^2K/W
Re	Reynolds number	
t	Time	s

T	Absolute temperature	K
T_{∞}	Ambient temperature	K
T_d	Bulk disc brake temperature	K
T_{int}	Absolute temperature difference at contact interface	K
T_w	Wall temperature	K
T_{surf}	Surface temperature	K
V	Vehicle speed	m/s
V_{∞}	Free stream velocity	m/s
x_{cr}	Critical point	m
y_{arc}	Height of edge above horizontal centreline	m
y_{rec}	Height of rectangle	m
γ^+		

Subscripts

o	Outer
i	Inner
$cond$	Conduction
$conv$	Convection
rad	Radiation
d	Disc brake

List of Publications from this Research

Stevens, K., Leiter, R., Taylor, M., Gibbens, P., Roberts, P., Jackson, J., Thomas, P. and Tirović, M. (2010) 'Thermal Aspects in Electronic Parking Braking of Commercial Vehicles', in GRRT, ed. *6th European Conference on Braking*, Lille, France, 327-334.

Stevens, K., Tirović, M., Roberts, P., Taylor, M. and Gibbens, P. (2012) 'Heat Transfer from Commercial Vehicle Brake Disc Assemblies in Parked Conditions', in ATZlive, ed. *chassis.tech plus*, Munich, Germany, Springer, 721-739.

1 Introduction and Research Objectives

Electric parking brakes (EPB) have been installed in cars for 10 years now, providing many advantages to car OEMs and customers alike. Convenient parking brake application, packaging and ergonomic advantages are complemented with smart operation (required clamp application only, 'hill hold' and 'hill start'), improving comfort and safety. Replacing the traditional parking lever system with a brake by wire (BBW) removes the ratchet mechanism and the tensioned cable and linkages between the handbrake lever and the brake itself. Both space saving in the passenger compartment and vehicle mass reduction is achieved. The latter helps lower carbon dioxide (CO₂) emissions and improve fuel consumption, reducing the running costs for all the vehicles using this technology.

The main driving force towards developing EPBs for installation on Commercial Vehicles (CV) is the reduction of energy consumption, by the reduction of compressed air usage. Furthermore, reduction of actuator mass and dimensions are particularly attractive for variety of vehicles, in particular vehicles with independent suspension. Smart features which can be easily integrated, increasing driver comfort and vehicle safety are also beneficial.

Currently, parking braking of heavy CVs (lorries, coaches and busses) is achieved by using the energy stored in a pre-loaded steel spring within the parking chamber (see Figure 1.1). Compressed air is used to release the park brake, by compressing the spring and moving the parking pushrod away from the service chamber. In an EPB actuator, this function is to be replaced with a smart electric actuator. Demands on the air compressor are reduced, which allows it to be reduced in terms of required driven power, size and mass. Furthermore, compressed air storage requirements also reduce, lowering the size and/or amount of compressed air reservoirs required. Ultimately, these changes could lead to a potential reduction in manufacturing costs by using the smaller, cheaper components.

A typical mass saving of 29 kg/axle is estimated (Wilde and Leiter 2007) by using these proposed component changes. At frequent start-stop situations (such as buses) much less compressed air will be used (for service braking only and no air for parking) hence the energy/fuel saving of 8-10 % is predicted (Wilde and Leiter 2007). Even higher reduction in fuel consumption can be achieved in some communal vehicles, such as rubbish collecting lorries with extremely frequent parking brake application (practically at every house). In inter-city operations (coaches and lorries), the parking demands are much lower but smaller compressor, reduced volumes of air reservoirs and component mass reduction, will result in an estimated fuel saving of up to 2%. As commercial vehicles form the backbone of the UKs

freight distribution and public road transportation systems, the reduced running costs should reduce the overall cost base of the UK economy.

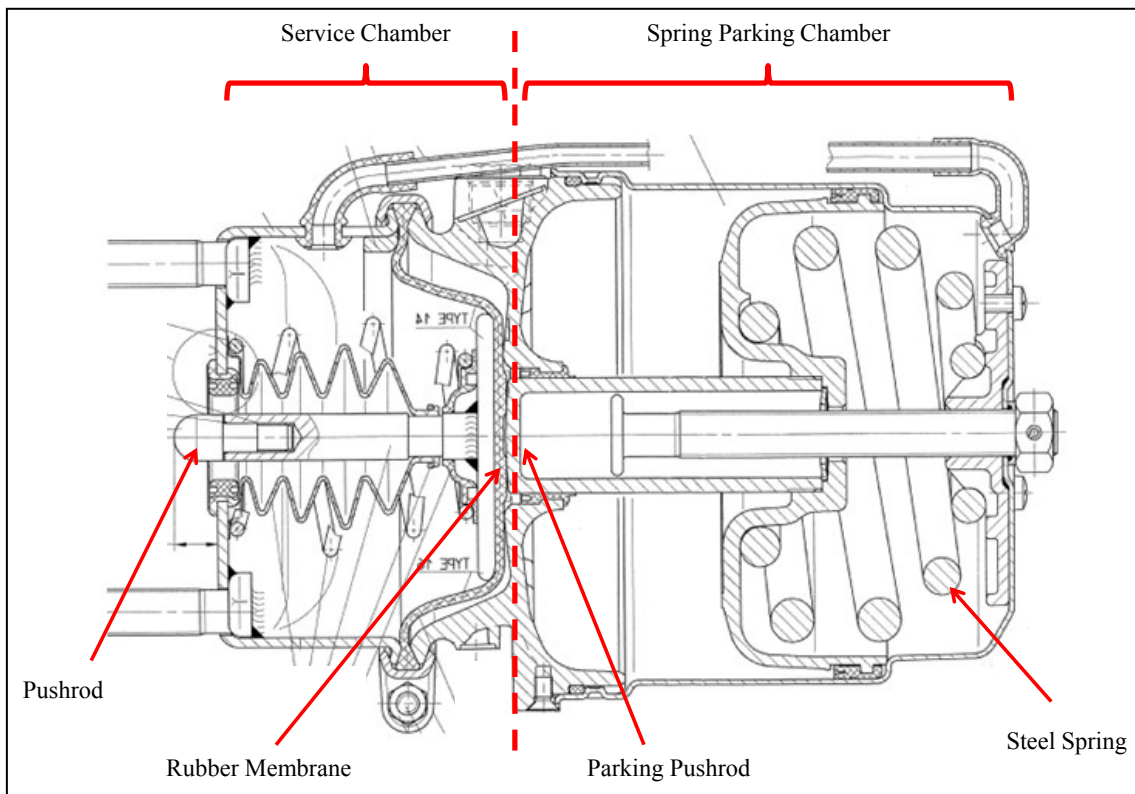


Figure 1.1: Cut through of the current service chamber and the spring parking chamber

Even with the potential to reduce manufacturing costs, simplifying the brake assembly installation, improving the fuel economy and reducing CO₂ emissions, EPBs are yet to be introduced in CVs. Differences in the thermal characteristics between passenger cars and CV brake assemblies, specifically the disc brakes, is one of the key technical factors preventing the introduction. A passenger car will typically have a laden mass of between 1 to 2 tonnes. Sufficient brake parking force is generated by disc brakes having an approximate mass of 3-5 kg, with a thickness of 12 mm (solid disc) and 25mm (ventilated disc). The outer diameter (OD) is of the order of 240 mm.

Comparing this to a CV brake, the disc has a mass an order of magnitude larger, at approximately 35 kg. Required disc brake thickness is 45 mm and OD typically 434 mm. In passenger cars axle loading is around 1,000 kg per axle, in CVs around 10,000 kg. CVs also have a lower power to weight ratio, hence lower engine braking, creating the need to be equipped with retarders. However, the retarder/engine braking of the CV does not proportionally equal the braking force provided by the car engine braking, resulting in a higher

acceleration downhill and increasing the braking demand. Heat dissipation characteristics from a CV are worse than for a passenger car generally due to being shielded more from the airflow, lower speeds and lower wheel angular velocities for the same vehicle speeds (due to larger wheels).

Thermal heating of the brake assembly, predominately the disc and pads is an effect of the friction braking process. Bulk temperatures reached within the CV and passenger car disc brakes are comparable, creating proportionally more expansion to occur in the CV disc brake, due to the larger sizes. Cooling will be much prolonged owing to the additional energy storage capability. A parking brake will always be applied when the disc brake is “hot” as, by definition, it will be applied after the vehicle has been in use, creating thermal expansion in the brake. When parked, and if left for long enough, the brake assembly will cool down to ambient temperature. During this cooling phase, contraction of the brake system naturally occurs as heat is dissipated from the system. To understand how this effect causes an issue, in Figure 1.2 the Elsa 225 brake assembly is presented, which incorporates service and parking chambers (see also Figure 1.1). What is being emphasized here is the amount components present in the caliper system able to store thermal energy and the additional heat paths created as a consequence. With heat being passed to one component to another, it becomes difficult to predict the volume of expansion/contraction at a given point in time in this highly transient system.

A brake caliper, consisting of the Housing Unit, Bridge and Pad Carrier, as well as a brake disc and pads are also shown in Figure 1.2. Meritor HVBS, the sponsors of this research, provided this brake assembly as a prime candidate for EPB introduction. To operate the brake, the driver presses down on the foot pedal, which regulates the flow of pressurised air into the service chamber (Figure 1.1). Situated inside the back of the service chamber is a rubber membrane, which is resting on the pushrod. Compressed air will cause axial movement of the membrane, pushrod and brake activation (a more detailed explanation is given in Appendix E).

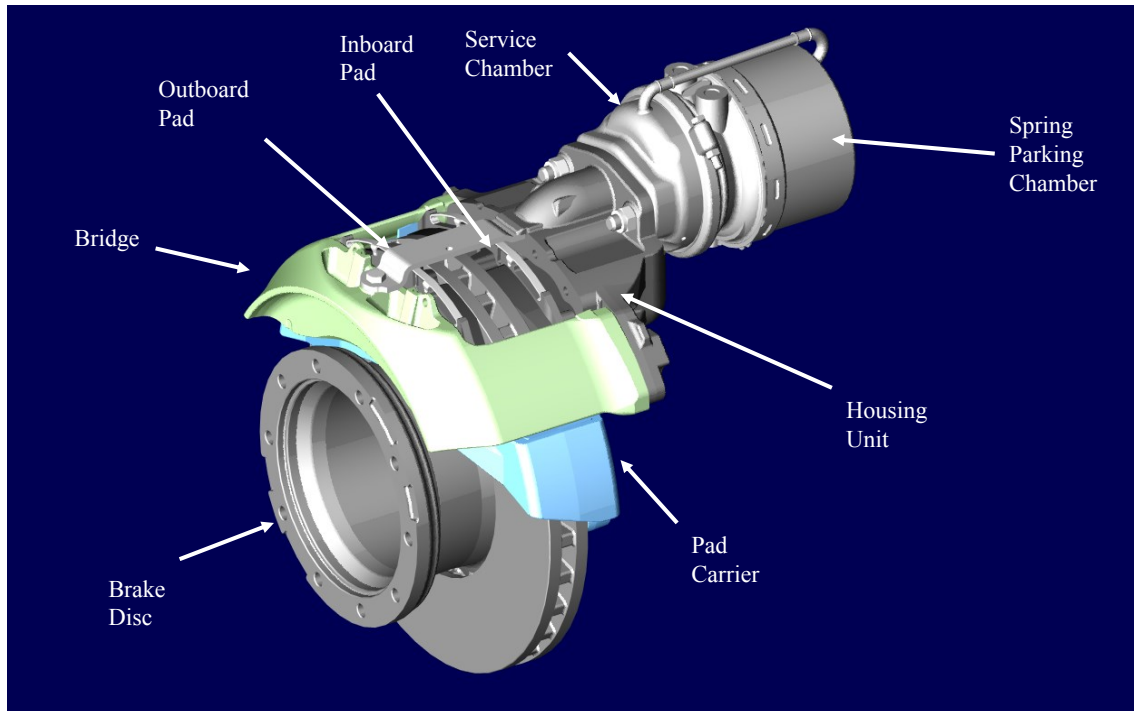


Figure 1.2: The LM 120 Offset D-Elsa Brake Assembly

The pushrod output locates in the housing unit, where it pushes against an off-centred operating shaft (Figure 1.3). Movement of the pushrod rotates the off-centred shaft, reducing the displacement within the system whilst adopting mechanical advantages to increase the force acting on the pistons. The two pistons push the inboard pad against the disc brake. As a reaction to the applied force, the housing unit, being fastened (bolted) to the bridge (Figure 1.2), slides axially in the opposite direction, pulling the outboard pad against the other side of the disc. In such a manner, a clamp force is created. This force is also called actuating force, since it activates the brake. If the disc is to rotate, friction is developing at the disc/pad interfaces, generating friction forces, which are reacted by the pad carrier (Figure 1.2) and transferred to the axle.

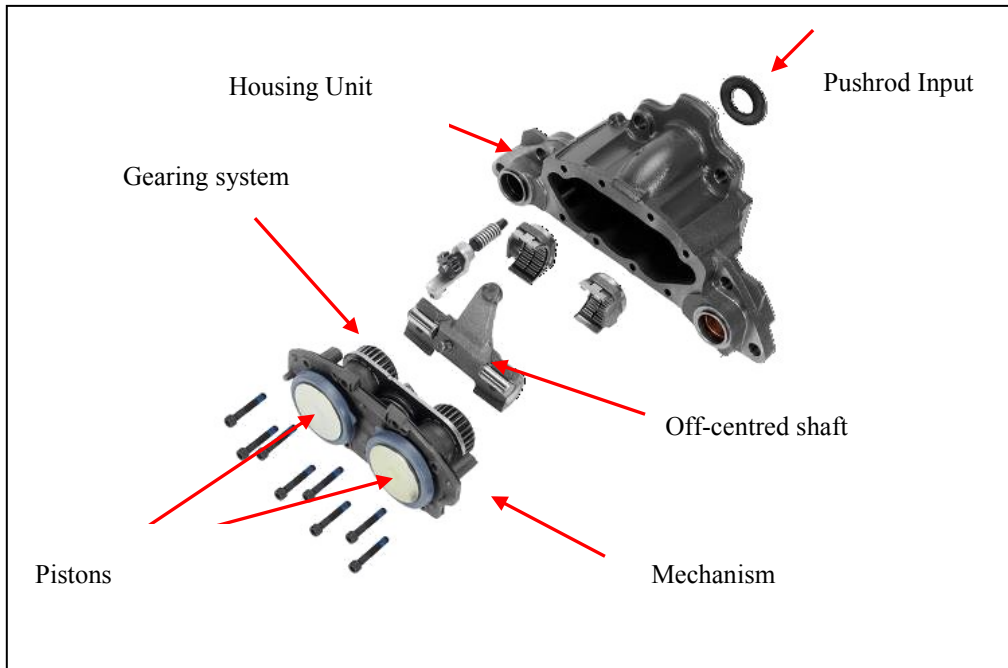


Figure 1.3: Exploded view of the parts making up the Mechanism component, located in the Housing Unit

If the parking brake is to be activated, the process of the force transfer is identical, with the only exception that it starts by releasing the air from the Spring Parking Chamber (Figure 1.1), which results in relaxation of the preloaded steel spring, which pushes parking pushrod onto the membrane and (service) pushrod. From here on, the process is the same, with the off-centred shaft pushing the pistons (Figure 1.3) and inboard pad, and the bridge actuating outboard pad (Figure 1.2). It should be noted here that when parking chamber is actuated, by releasing the compressed air, the parking pushrod will press against the membrane and (service) pushrod, activating the brake, irrelevant of whether the service chamber is actuated (pressurised) or not. The only difference is that if the service chamber is pressurised, the parking pushrod will have some 'free travel' before acting upon the membrane and (service) pushrod.

It should be noticed that the off-centred shaft provides a ratio of about 15, increasing the force but reducing the travel, hence it is a paramount for the brake assembly to be properly adjusted. This is achieved by an automatic slack adjuster, using gearing system shown in Figure 1.3. Such high ratio is necessary in order to achieve required clamping force but as a direct consequence any displacement on the disc/pad interface will cause much higher displacement of the pushrod. Practically, thermal disc and pad shrinkage, permanent pad set and other effects could have negative consequences on the pushrod movement and actuating force reduction.

The basic concept of an EPB actuator is to replace the Spring Parking Chamber (shown in Figure 1.1 and Figure 1.2) with a smaller spring, actuated by an electronic system (which is still under development). The EPB spring will have a similar diameter but will be shorter and lighter than the current spring used. Being more compact and 'stiffer', the EPB actuator has its advantages but also potential disadvantages. Keeping a spring in the system is advantageous to the design as it inherently self-corrects against thermal contraction without external control.

Disc and pad temperatures will depend upon the braking duties and vehicle loading condition. Prolonged parking of the fully laden vehicle on the incline after heavy braking duties, such as repeated or drag braking on the incline, are particularly critical for all vehicles. For heavy commercial vehicles, with disc and pads being of considerable thickness, thermal expansion can be very pronounced at high temperatures. As the disc and pads cool down, they will shrink, the pushrod will retract, reducing the amount of clamp force at the friction interface. The situation is made worse by increase in caliper temperature and its expansion.

In the case of the spring parking actuator (Figure 1.1), this condition will cause expansion (relaxation) of the spring and reduction of the clamp force. Due to relatively long spring stroke and high preload, the consequences are unlikely to be dangerous for a brake in good condition, with correctly functioning slack adjuster. However, use of an EPB actuator, compact and stiff, would require a much better understanding of thermal processes to assure safe parking in all conditions.

It should be noted here that passenger car EPBs use two methods in preventing vehicle rollaway in hot parking conditions. Firstly, the clamp force applied in all conditions is much higher than required (typically 100% higher) and secondly, so called automatic 're-parking' in hot parking conditions. By measuring the frequency of brake application, brake pressure and vehicle speed, a thermal model within parking brake ECU predicts brake temperatures. If the vehicle is parked, and the model estimates higher brake temperatures, the electrical EPB actuator is re-activated. This is typically done 3 minutes after the vehicle is parked. Despite this period being too short, it is considered better to take this action sooner, since the vehicle battery may be disconnected. Also, vehicle ECUs are being switched off. The main measure in preventing passenger car rollaway in hot parking conditions remains the severe 'over-clamping'.

The above approach cannot be simply 'transferred' from passenger to commercial vehicles. The clamp forces in commercial vehicles are already very high, up to 240 kN which approximately equates to 80% of the disc material's yield strength. Therefore, over-clamping is not a possible option to prevent permanently damaging the disc. Re-clamping in a short period of time is

ineffective for CVs due to the much larger amounts of energy, size and volume (mass) of the components involved. It is therefore a paramount need to develop a thorough, methodical and in-depth understanding of heat transfer within the brake assembly, the temperature changes and heat dissipation from individual brake components.

Parking brake performance for HGV's in Europe and many other countries is governed by the United Nations Economic Commission for Europe (UNECE) Regulation 13 (ECE Regulation No. 13 2008). For CVs, ECE Regulation 13 Annex 4, paragraph 2.3.1 states that "*The parking brake system shall, even if it is combined with one of the other braking systems, be capable of holding the laden vehicle stationary on an 18 per cent up or down-gradient.*" Interestingly, there is no requirement to demonstrate parking performance in "hot" conditions, ignoring the thermal contraction phenomenon and the resultant variability in clamp force. Nevertheless, the safety remains paramount and both the braking system and the vehicle manufacturers must assure the vehicle is safely immobilised when parked in any conditions that can be reasonably expected. This is particularly important for commercial vehicles, since the engine braking effects (leaving the parked vehicle in gear) are much smaller and any rollaway is likely to have tragic consequences due to the sheer mass and size of these vehicles.

1.1 Research Aims and Objectives

This investigation had two distinct research aims that are related to the introduction of the CV EPB. These are described below.

The first research aim focussed on the commercial aspects of the project. The aim was:

To understand the benefits of the EPB and how to successfully market them.

To achieve this aim, there were two main objectives that had to be completed, which were:

1. To obtain a complete appreciation of the benefits on offer by the CV EPB.
2. To understand the barriers to market and potential ways they could be overcome.

The benefits of the CV EPB will be delivered to multiple customer segments downstream of Meritor. By developing the understanding of what the EPB offers and how these benefits are experienced by the individual customer segments, a marketing strategy that targets specific customer segments was possible to maximise the chances of a successful product introduction. These objectives were completed by conducting questionnaires and analysing the results, discussed in detail in Chapter 3.

The second research aim was focussed on the technical aspects of the project. The aim was:

To understand the heat flow around a stationary brake assembly.

A number of research objectives needed completing to realise the technical research aim, of which there were four:

1. To identify the worst case for CV hot parking.
2. To develop tools and techniques for predicting thermal behaviour of the brake assembly with reference to its parking function.
3. To identify the level of variability in heat transfer coefficients over the temperature range relevant to a CV parking application.
4. To validate the thermal behaviour tools using unique experimental processes that simulates a parking application.

As already demonstrated, many technical challenges have to be overcome by the introduction of the CV EPB, primarily due to the increase in thermal mass which alters the EPB performance compared to a passenger car. With such a large system, there are numerous active heat paths in operation during a parking brake application that affects the clamping force. Having a solid understanding of how the heat flows through the system and ultimately dissipated from it, enables accurate predictions of the system capabilities during the design phase. Out of scope for this project was any investigation into the changeable friction force experienced at the disc brake and pad interfaces and therefore, this project does not investigate the brake clamp forces during a parking application.

2 Review of Meritor and the European Commercial Vehicle Braking Market

The main topic under investigation during this thesis is how to model the interactions of a CV brake assembly, subjected to purely natural convection conditions. The aim is to generate a tool that aids Meritor in the design phase of the proposed EPB. Before this work is conducted however, a study is to be carried out on the current state of the CV braking market, as well as finding Meritor's position within it. In Chapter 2, it shall be shown that the pneumatic spring parking chamber currently holds a state of technical lock-in that must be breached before a successful introduction of the EPB can occur.

2.1 Introduction to the Business Problem

It has become common practice for all industries now to take responsibility for the CO₂ and other greenhouse pollutant gases they produce and exhaust into the atmosphere. It is no secret that the automotive industry, and the transport industry as a whole, has one of the largest impacts on greenhouse effects, with a study conducted by the International Energy Agency (2008) estimating the transportation industry is responsible for 26% of the global manmade CO₂ emissions. The problem of greenhouse gases is a global issue; the more these gases are exhausted into the atmosphere, the warmer the global climate will become. Over the past 20 years awareness of the problem has come to light, resulting in vast quantities of research being dedicated to improving the situation.

European legislation has been a key driving force in the reduction of vehicle emissions within Europe, and in particular, road vehicles. A series of regulations have been introduced since the initial meeting of the EC Environment Council in Brussels in 1998 (ENDS 1999), called Euro I–VI, which set maximum emissions levels required before a manufacturer is allowed to sell a new model vehicle. Each introduction has tightened the emissions limit further; forcing automotive OEMs to produce cleaner vehicles. In 2011 the introduction of Euro V will legislate for any new vehicles. However, research and design work is not concentrating on this regulation but looking to the future to find ways of meeting the Euro VI requirements that are to be introduced in 2014, reducing the allowed nitrous oxides (NO_x) emissions from Heavy Goods Vehicles (HGV) by a further 55%, down to only 125 mg/km.

The Department for Transport is a public agency aimed at developing and improving the transportation in the UK. Their statistics show that there were 482,000 HGVs on the UK roads in 1990. Since then there has been a steady decrease in numbers, although this trend is predicted

to reverse with an expected rise between 1990 and 2025 of 50 - 100%. Lorries and other CVs operating on the UK roads are vital for any business as equipment, material and finished goods all need to be moved from one place to another. Unfortunately, there is a heavy cost associated with transportation, predominantly from rising fuel prices. In response, OEMs are attempting to design vehicles which not only have cleaner emission engines but have reduced overall vehicle weight as well. Reducing the vehicle weight will result in less fuel required to power the same drive cycle, generating a saving on a firm's variable cost. Alternatively, a lighter vehicle will be able to carry more goods before reaching the maximum 44 tonnes limit imposed on vehicles operating on UK roads. Subsequently, an improvement in the fleet efficiency can be realised as additional products can be placed on each vehicle before reaching weight limit, enabling more products being transported by fewer vehicles resulting in lower emissions.

To design lighter, more fuel efficient CVs it is important that tier 1 and 2 suppliers produce individual products and sub-assemblies that help generate small but incremental weight savings. However, some components are easier to reduce weight in than others. For example, by simply reducing the volume of lubrication in a component to the minimum required level, such as in the differential (providing there is still a sufficient amount to not hamper performance) a small weight savings will be achieved. A double advantage achieved by doing this process is that a material cost saving is made whilst developing a more desirable greener component. Typically though, not all vehicle sub-systems have this luxury. Safety critical brake systems are a good example where simple design alterations won't bring the coupled benefits. During a braking application, a large proportion of a vehicles kinetic energy is transformed into thermal energy that is predominately dissipated into the disc brake. Having a braking system with a large mass allows more of the thermal energy to be stored, increasing the brake efficiency. Understandably then, there is a reluctance amongst CV customers to purchase lightweight brake components in fear of a potentially inferior brake performance they may give in comparison to current designs.

Meritor is attempting to help OEMs meet the Euro VI legislative requirements by the introduction of the EPB mechanism. The proposed new product will replace the current spring parking chamber to actuate the brake system when the CV becomes stationary. The spring is large in both size and mass, generating opportunities to reduce weight in the brake system. Additionally, a size reduction would also become a possibility, making it more appealing to the OEM as it would be easier to fit the parking chamber into a wheel arch. Weight savings though, will not come exclusively from the removal or reduction of the large spring, further advantages will be realised as heavy air lines between the cabin and each individual brake can be eliminated. In their place, light weight electrical cables would be used. A size reduction of the

pressurised air reservoir could also occur as the required volume of pressurised air would subsequently reduce. Due to the infancy of the EPB design, an accurate prediction of total vehicle weight saving cannot be made. Yet, providing costs remain neutral, any weight saving will be seen as positive.

Here lies the crux of the problem for Meritor; OEMs are demanding smaller, more lightweight braking systems to help meet ever stringent legislation whilst CV customers, such as logistics providers, have been told and realise that bigger brakes are safer. Therefore, this project will attempt to find a solution to the problem of how to market a product to buyers that contradicts the advice they have previously been given.

2.2 Technological Lock-In

Unlike car brakes, CV use pneumatic actuation systems opposed to hydraulics. The primary reason for using pneumatics over hydraulics is the simplicity of the connections when coupling multiple vehicle units together whilst maintaining the ability to control to all the brakes from the tractor unit. Secondly, any leakage from the brake lines would result in air being ejected into the atmosphere rather than hazardous brake fluid. With the advancement in science and technology, funding is being heavily invested in electronically actuated braking systems, better known as BBW systems. The advantages here are large weight savings, easier packaging solutions and an increase of space in the driver compartment. Whilst development of the full BBW system is continuing, electronic actuation has partially been introduced to the car braking field via the introduction of the EPB by TRW back in 2003 (Schuette and Waeltermann 2005). Yet, it appears such a move to electronic actuation has been met with heavier resistance in the CV braking field, as the preferred actuation method remains the inferior pneumatic technology even though advantages of an EPB system have been demonstrated in the passenger car environment. Such persistence with the inferior pneumatics spring parking chamber is a classic example of technological lock-in.

David (1985) was one of the first authors to publish work on the lock-in phenomena. He described the path taken by the QWERTY keyboard configuration in gaining dominance over superior alternatives. Launched in the 1870's, QWERTY became and remains the worldwide keyboard standard today, even though the competing Dvorak layout gave time savings between 20% and 30%. At the time, buyers had no preference to which keyboard layout their typewriters had, just as long as outcome was completed to sufficient quality. Typists, on-the-other-hand, wanted typewriters that they had been trained to touch-type on. With every typist that became trained on the QWERTY design, the probability of the design becoming the standard increased.

The reasoning behind this was that it is easier and cheaper to replace equipment with the different layout than retraining a workforce. Economies of scale also influence an employer's thinking as the unit price drops the more they buy. Why the first few typists chose to learn QWERTY and their thinking behind their decisions are unknown but the effects are evident; these random historical events have dictated how everyone who has interacted with a computer ever since. An analytical investigation conducted by Arthur (1989) has shown that it is not always the optimum solution which becomes standardised, as shown in the QWERTY example.

Evidently, to break the current strangle-hold held on the market by pneumatic spring chambers, the CV EPB must escape the technical lock-in. To do this, Cowan and Hulten (1996) claim that “...it is not enough that the competing technology is better.” Subsequently, Cowan and Hulten suggested six impact factors that could help break technical lock-in, these are:

- Crisis in the existing technology
- Technical breakthrough producing a cost saving
- Regulation
- Changes in taste
- Scientific results
- Niche markets

Confidence in an existing technology is not easily destroyed. Huge sums of money are spent developing and testing technologies, so why should it belief in the technology suddenly disappear? It would take a serious failure for these proceedings to transpire. A historical case of this impact factor has been discussed by Cowan and Gunby (1996) where pesticides now have less effect at preventing insects from damaging crops compared to when they were first introduced forcing alternative solutions to be found. Unfortunately for the EPB, the spring parking chamber has been in service for a surplus of 30 years with an absence of serious failures, making it doubtful that they will become dangerous and lose their customer confidence within the foreseeable future. This impact factor is therefore unlikely to help the CV EPB break the technological lock-in currently suffocating the market. The costs associated with the EPB are also unlikely to help the escape from technological lock-in as the unit complexity will increase, leading to a probable price increase. There is an argument that the removal of other vehicle components will make the EPB overall cost neutral, or possibly even a slight cost reduction, but certainly not by a significant enough margin to claim cost will be a leading factor for change. Additionally, the scientific results factor would struggle to impact the on the spring parking chambers hold on the current market as the CV EPB is not designed to outperform the

current solution as both will keep a vehicle from rolling away. However, supplementary functionality offered may prove to be the key selling point for the EPB.

Nevertheless, hope for the EPB is obtained through the Regulation impact factor. The Euro VI emission standards coming into effect in 2014 will force OEMs to produce cleaner vehicles for use on European roads. OEMs are therefore looking for sub-assemblies like the EPB to help meet the incoming emission requirements. Furthermore, as society becomes further aware of the environmental issues at hand, personal preferences are changing towards greener options. Potential escape from technical lock-in may ultimately stem from the changes in taste impact factor.

Finally, niche markets can produce a unique opportunity to develop interesting and innovative products which may otherwise never enter a market. A niche market can be defined as a small proportion within a market, with a particular need or interest that differs slightly from the market norm. Foxon (2002) argues that targeting a niche market provides excellent opportunities for innovation introduction into locked-out markets as a firm is able to gain knowledge of the new technology by the method of 'learning-by-doing.' Gaining of knowledge allows costs reduction in the learning stage, which ultimately increases returns. At which point, the new innovation may become favourable to the rest of the market and break the lock-in effect. Yet, with only five major players in the CV braking market, it is hard to envisage where a niche marketing opportunity can arise.

Furthermore, Foxon proposes a seventh impact factor; Policy. It is claimed that the role of the government can be instrumental in overcoming technological lock-in. With the correct mix of incentives offered, such as tax breaks for ultra-low emission vehicles, the EPB could almost instantly become the parking component of choice for CV OEMs. It is not only the purchasers where policy can be influential, Carrillo-Hermosilla (2006) has shown through analytical techniques that social factors can prevent the breakout of a locked-in technology. In this case, policy can be the catalyst for changing public perception and in some cases could help society cope with an almost spontaneous change in preferred technology.

Within the automotive industry policy is currently influencing the ever increasing trend of alternative methods to power the vehicle instead of the internal combustion engine, such as hybrids and electric engines. Dijk and Yarime (2010) hold techno-economic mechanisms culpable for the lock-in of the internal combustion engines. The internal combustion engine has evolved to a technologically advanced power source with over 100 years of research behind them. A huge amount of funding will be needed to bring another technology to the performance

level already achieved by the combustion engine. Therefore, greater actual performance returns are realised for the same funding on products which have techno-economic mechanisms acting on them. Policy is being deployed to help public acceptance of the alternative technologies with reduced or free road tax for hybrid and electric vehicles. In addition to the green tax scheme, an incentive was introduced in 2011 where the government will subsidise £5,000 for every purchase of any new electric vehicle (Jha 2009). Dijk and Yarime point to California's Air Resources Board and Toyota (with the introduction of the Prius) for their efforts pushing change back in 2000, which started the public acceptance for alternatively fuelled vehicles where others had failed previously.

2.3 Meritor Profile

Marketing issues faced by Meritor for the introduction of the EPB have been described, but before investigating the optimum marketing direction to take with the EPB, a brief look into the Meritor profile will be conducted. Understanding a company's strengths will build up a picture of what they specialise in and what anchors the marketing strategy should be founded on.

Timken Detroit Axle was originally formed back in 1909, producing truck axles. The movement towards trucks over traditional horse-drawn carriages enabled a workforce to produce four times the total work, covering a special area six times greater, for only 15% of the storage area due to stabling needs of the horses. However, it was not until the start of the First World War that significant development of trucks began. During the war periods, production of military components became another source of revenue for the company, adding to the axle business. With further acquisitions and mergers post World War Two, Timken Detroit Axle traded under the name Rockwell Spring and Axle Company (later to becoming Rockwell International) until its automotive division was separated in 1997 to form Meritor Automotive. Meritor Automotive thrived well in a competitive market, leading to a merger with Arvin Industries in 2000 when ArvinMeritor was established.

ArvinMeritor was a global Tier 1 supplier whose business interests were in providing integrated systems, modules and components to a number of original equipment manufacturers (OEMs) as well as delivering an aftermarket service for the CV, transportation and industrial sectors. In doing so, ArvinMeritor serviced the bus and coach, commercial truck, trailer, off-highway, military and other industrial OEMs aftermarkets. The fundamental systems that ArvinMeritor produced were brakes and braking systems, roofs and door systems, axles, undercarriages and drivelines (ArvinMeritor 2010).

Although ArvinMeritor traded as a single business group, internally the business was run as four separate units; Commercial Truck, Industrial, Aftermarket and Trailer, and Light Vehicle Systems (LVS). Of the four, the greatest amount of revenue was generated by the Commercial Truck segment, reported in the ArvinMeritor 2009 Annual Report to generate \$1,566m by supplying drivetrain systems and components (including braking and braking systems, suspension systems, axles and drivelines), predominately to Medium- and Heavy-Duty trucks. Supply of the same systems and components to large industrial vehicles, such as buses, fire and emergence vehicles, military and other off-highway vehicles are categorised in the Industry segment, along with all business concluded in the Asia Pacific region. Finally, the LVS is mostly made of the Body Systems business, supplying roof and door systems to passenger car OEMs.

During the 2008-2009 global recession, the automotive industry suffered globally, with almost every company involved in the sector recording a huge decrease in sales; ArvinMeritor were no exception as the reported revenues for 2009 were down by 35.7% from the previous year (ArvinMeritor 2009). The downturn offered an unusual opportunity for ArvinMeritor to focus more closely on what was important to the company and redirected the business strategy towards a new goal. Described in the ArvinMeritor 2010 Annual Report it was “...to focus on targeted investments with potentially higher margins.” Production of components and assemblies for both Commercial and Industrial Vehicles have become the core business focus, along with the continuing Aftermarket service they provide. Enhancement of their market share was designed on utilising the quality of the company’s products and geographical strengths. However, many global trends were identified that could impact the business strategy, either positively or negatively, which include (ArvinMeritor 2010):

- Increasingly stringent regulations relating to the emissions levels produced by all vehicles.
- OEMs continuing consolidation and globalisation of its suppliers
- Growth of developing countries presenting new market opportunities
- Increasing demand from OEMs for modules and complete systems over individual components
- A drive in enhanced fuel efficiency via engineering and technology based improvements

Although being the second largest source of revenue for ArvinMeritor in 2009, a reaction to the new business strategy caused divestment of many supplementary businesses within this segment, allowing ArvinMeritor to focus more closely on the business strategy. Consequently,

as of 2010, ArvinMeritor operated with only three business segments, selling off the LVS fraction and ultimately, diverging the Arvin brand. The core business being refocused on Medium- to Heavy-Goods vehicle systems, company branding reverted back to Meritor, as it was prior to the merger in 2000.

With today's global demand for products, Meritor operates in most of the global continents, with a separate design and manufacturing headquarters in each. Doing so allows Meritor to meet the local demand of various customers. An example of local trends differing around the world lies with the sale of brakes systems. In general, there are two main brake configurations; drum brakes and disc brakes. As seen in Figure 2.1, the European market is very different to other markets as 80% of CVs use the disc brake configuration over the drum brake, the pattern is reversed in all other geographical regions.

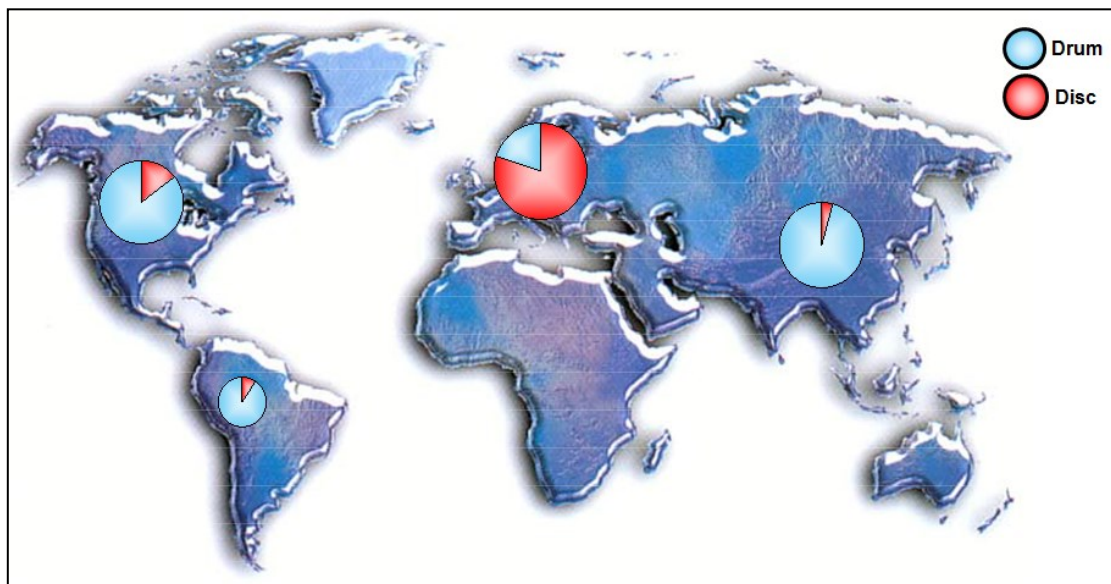


Figure 2.1: ArvinMeritor 2010 sales of brake configurations by global region.

2.4 Market Analysis

As discussed earlier, the EPB unit is being designed to replace the spring parking chamber on a disc brake, to actuate the brake for a parking application. In light of the data presented in Figure 2.1, this research will focus solely on the European braking market (EBM) as this is the only global market where the disc brake configuration is sold in large quantities, and hence the majority market for any incoming CV EPB. Within the EBM, Meritor has four main competitors competing in the brakes and braking systems segment: Knorr-Bremse, Wabco, Brembo and Haldex.

Knorr-Bremse is the largest player in the braking field, holding a majority market share of 58% according to 2010 statistics (see Figure 2.2), doubling the sales revenue generated by the next largest player, which was Meritor (ArvinMeritor at the time). Knorr-Bremse utilise their knowledge in the pneumatic systems to great effect, enabling them to offer a complete brake system, including air treatment units and compressors, compared to just the brake assembly itself (Datamonitor 2010a). Advanced knowledge of the pneumatic braking technology has helped Knorr-Bremse to also take a strong position in the rail braking market in addition to road vehicles. Meritor produced the market statistics seen in Figure 2.2 and Figure 2.3 by surveying and analysing the publicly available sales data.

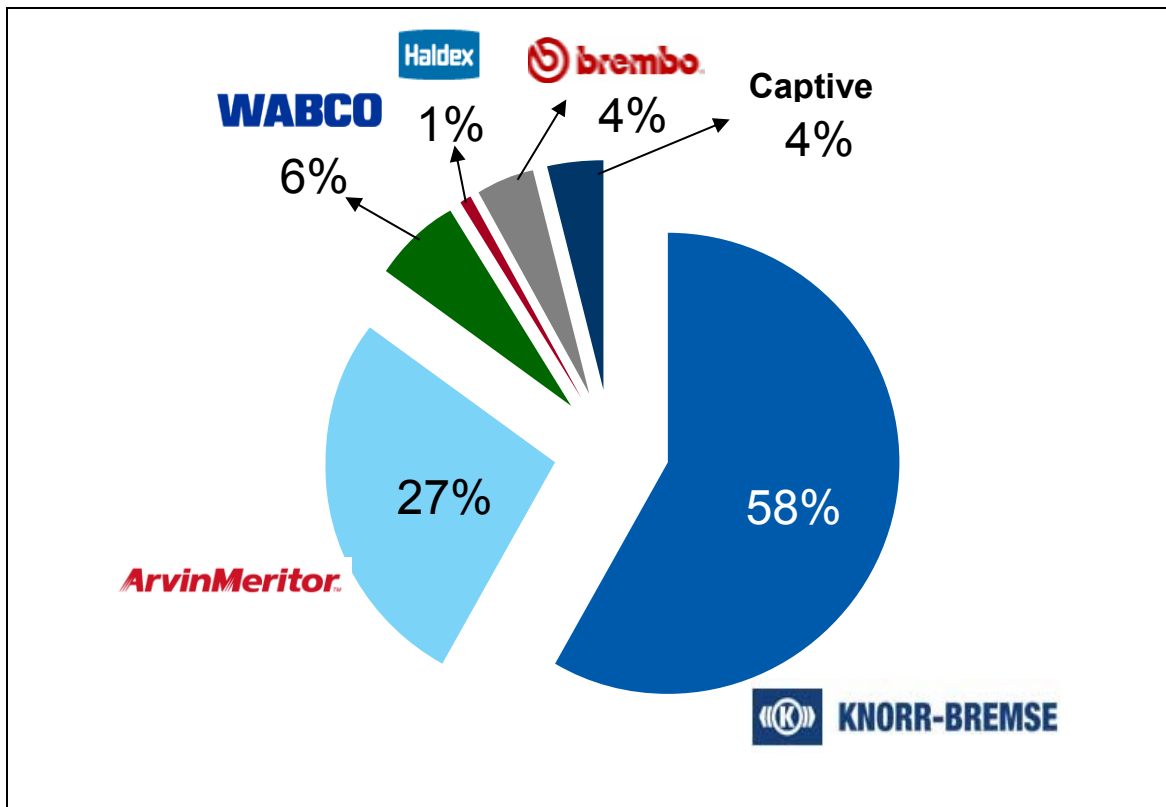


Figure 2.2: European brake supplier market share 2010.

Wabco holds a smaller population of the market, only 6%, yet they are still an important figure. They offer a more varied product range, from car brakes all the way through to heavy-vehicle brakes as part of their speciality in safety and control systems. Currently, Wabco and Meritor are partnering a joint venture into Anti-Locking Brake systems (ABS) as well as other vehicle control products (Datamonitor 2010b). Both Brembo and Haldex are smaller competitors to Meritor in the European CV brake market, although Haldex does hold larger market shares in America, Brazil and parts of Asia. Alternatively, Brembo's primary business is high performance and race car brakes, justifying its low market share in the CV EBM.

There are five OEMs currently operating in the EBM available to the brake suppliers to trade with. Having such a limited number of customers intensifies market competition as all the suppliers will be pitching to secure the same clients. A breakdown of the market share of the five OEMs is presented in Figure 2.3. Volvo-Renault holds the largest market share with 33%. Interestingly, during an interview with Thibaut Grosdemouge, Programme Manager of the EPB project at Meritor (Appendix A), it was revealed that 85% of Meritor's European brake sales were to Volvo-Renault. High risk is associated with a customer portfolio heavily geared towards a single customer with the possibility of losing them to a competitor. Also, in the case of Meritor predominately selling to Volvo-Renault, there remains 67% of the total EBM which they hold very small presence, presenting a large opportunity for growth. Indeed, this is the reason why Meritor is aggressively trying to enhance its standing within the EBM (Meritor 2010).

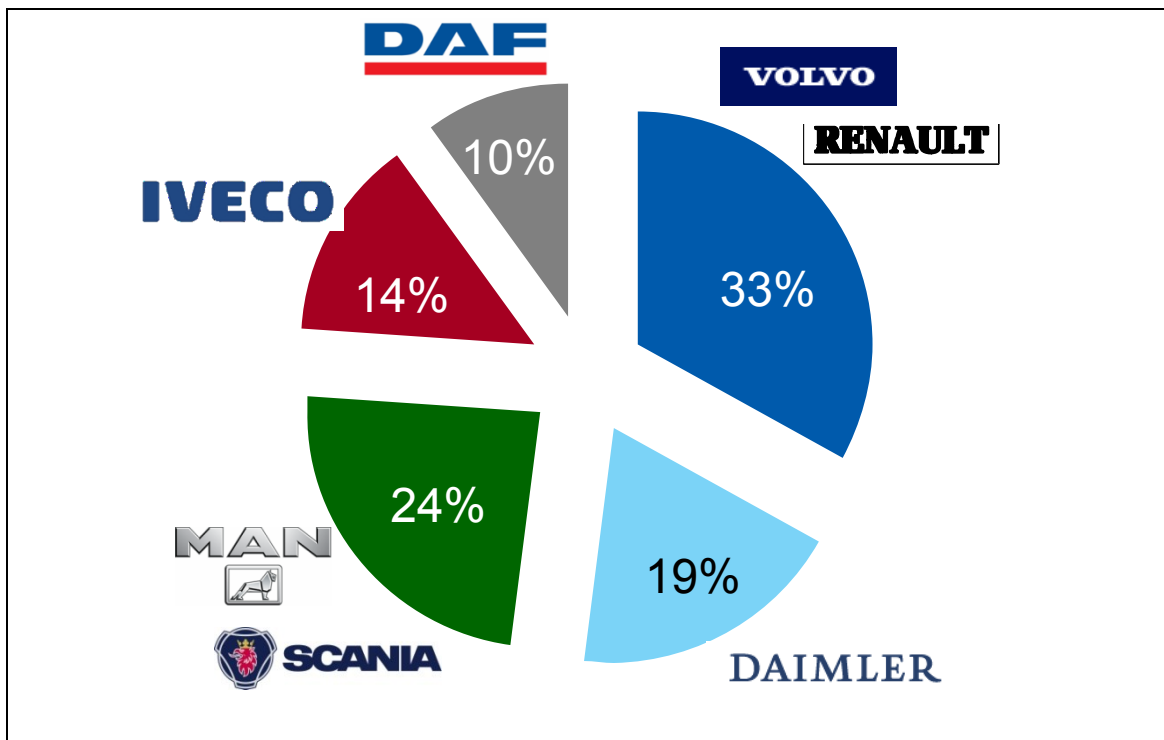


Figure 2.3: OEM market share 2010.

To define the size of the EBM, the EU foundation market share statistics (presented in Figure 2.2) will be used in conjunction with published data in the ArvinMeritor 2010 Annual Report. Total revenue for the company during the financial year of 2010 was reported to be \$3,590m. Of which, 24% was attributed to brake and braking systems sales; making their global braking sales figure \$861.6m. Unfortunately, the breakdown of regional sales percentages were not given in the most recent annual report, however, it was stated that 22% of ArvinMeritor's 2009 global

sales were recorded in Europe (ArvinMeritor 2009). In the absence of updated information, it will be assumed that this proportion remains consistent year on year. Subsequently, it can be calculated that revenues totalled \$189.4m from the brake and brake systems segment within Europe during 2010, provided that the proportion of brake sales also remains relatively constant around the world. Extrapolate with the market share value presents an estimated total market worth of approximately \$700m.

Potential sales volumes can also be approximated. Estimated European CV production in 2010 was 265,000 according to values given by Meritor (ArvinMeritor 2010). From Figure 2.2, it is known that 27% of the EBM is supplied with Meritor brakes, meaning of the newly produced vehicles 71,550 vehicles have brakes supplied by Meritor. Of which, approximately 60,800 units were supplied to Volvo-Renault.

Multiple vehicle configurations are present when looking at Medium- and Heavy-Duty CVs. For instance, a tractor unit can have either two or three axles, towing a single or two attached trailers. Parking chambers are always mounted to the rear axles in the tractor unit but sometimes, dependent on the operational climate of the vehicle, spring parking chambers are mounted on front axles too. Further parking chambers can be installed on some trailer axles as well. With the vast number of possible CV configurations, it becomes impossible to accurately estimate the volume of parking brake chambers without detailed information of company sales data, which unfortunately is often not disclosed. However, the “rule of thumb” estimation provided was that Volvo-Renault purchase, on average, three spring parking chambers per vehicle. In which case, Meritor sold 182,400 parking chambers to Volvo-Renault in 2010. Without individual supplier data for the different OEMs it has to be assumed that ratio of spring parking chambers per vehicle remains constant. Resultantly, an approximation for the total volume of parking chambers sold in 2010 to the EBM was 800,000 units.

All CV disc brake systems have a modular design, allowing the customer to select different components from any supplier and they will fit together to produce a fully functional brake assembly. Meritor can use this to their advantage by taking market share by marketing the EPB as a superior alternative to competitors’ spring parking chambers, subsequently fitting Meritor’s EPB onto competitors brake assemblies. Being first to market would vastly increase the chances of obtaining a leading market share by taking a larger proportion of the 800,000 brake chambers with the EPB than they currently hold with the regular spring parking chamber. Global trends presented earlier would suggest this is a real possibility as OEMs are looking for advanced technologies to help reduce emissions, which the EPB aims to do.

2.5 IAA Hannover Show 2010

The International Automotive Exhibition (IAA) is an exhibition showcasing current and upcoming products and prototypes for CVs, from Light- to Heavy-Duty. The show is located in Germany and is run on an annual cycle. All major CV OEMs present their most recent vehicles to a variety of exhibitors. In 2010 the IAA show was held in Hannover, the first since the 2008 global recession, where cost reduction and environmental issues were at the forefront of virtually every product on display. None more so than the MAN Concept S CV, which claimed that by using a radically improved combined aerodynamic truck and trailer shape, a 25% reduction in fuel consumption could be realised (Barrow 2010).

Meritor (or ArvinMeritor as it was at the time) was also in attendance parading a series of products. The exhibition presented an ideal opportunity for the announcement of a substantial sum of \$42m was to be invested into the European braking department to expand the popular ELSA pneumatic disc brake products, increase development in new braking technologies and to improve vehicle and lab testing equipment (Meritor 2010). The aim was to enhance the market position currently held by Meritor in the EBM.

More importantly for this project, it was the first occasion where people external to Meritor were made aware of the EPB project. As part of a general Meritor promotion of new technology developments, a working prototype of the EPB was shown to a limited number of people, primarily from OEMs. Instigation of discussion, based on new technologies, was the main priority for Meritor at the IAA show. Talking with their direct customers would help them understand what type of product(s) are desired and where they should focus both near and long term development efforts.

During the discussions with the OEM representatives, Meritor refrained from giving specific details about the EPB, i.e. what cost will be incurred/saved by the OEM with the EPB, nor were any explicit benefits outlined. As such, the EPB was not marketed directly on any specific benefit. This was a result of the strategic decision made to simply generate discussions with the OEMs, rather than to sell the product. With the meetings being held in an informal atmosphere, it is understandable that no recorded feedback was taken. However, Paul Roberts, Chief Engineer at Meritor, did summarise the verbal discussions by saying they did receive *“positive feedback to see we were working on some longer term technology developments, but concerns with the expected cost vs. benefit of EPB and overall braking system integration.”*

Although valuable information was likely to have been gained via this type of marketing, it is also relatively restrictive as the opportunity to receive feedback from the product's potential users and CV buyers is removed. Appreciating the opinions of the end users may not secure the short term economic certainty of the program, but it could uncover minor details or design improvements that could lead to successful product introduction. Development cost reduction would be the result of early discussions with the other beneficiaries of the EPB as design changes at the concept stage are much easier and cheap to make than at production stage of the product development cycle. An opportunity is therefore presented here to find opinions on the EPB, other than those of the EPB. This would give Meritor valuable information that they can use for design purposes and could strengthen the business case for the EPB, provided the responses are positive.

2.6 Benefit Analysis

As described by McDonald and Christopher (2003) "*when customers make a purchase, not only do they buy our product or service, but they also buy along with it a whole package, or 'bundle' of benefits.*" The bundle of benefits described by McDonald and Christopher refers to the mixture of benefits gained by both the core product (the physical product or service) and the products surround (the intangible benefits also realised by the purchase of the product or service). It is important to understand the mixture of benefits on offer for two primary reasons, firstly to ensure the benefits offered by the product meet with the needs of the customer and then to know how to market the product. Finding the former is not straightforward though, and can be both costly and time-consuming to accumulate this information. This section will identify in the benefit mixture on offer by EPB and what it is which would make it appealing to customers.

Segmenting the market into groups that require similar benefits is called Benefit Segmentation, developed and introduced in 1968 by Haley. Each group is assumed to purchase products on the potential benefits gained through their acquisition rather than the actual features offered by the product. However, Benefit Segmentation is a focused approach to understanding the various groups within a market, gained through questioning experienced people within the specific market, rather than extensive market research (Hooley *et al.*, 2008).

The brake market is schematically drawn in Figure 2.4 showing Meritor and its three separate customer tiers. Being a Tier 1 supplier, Meritor develops specific brake components and assemblies that are sold to OEMs and used in their vehicles. CVs are usually purchased as part of a fleet by companies who need to transport products to warehouses, shops and/or customers

and not generally by individuals. These companies employ specialist drivers to drive the CVs, who actually use the products developed by the Tier 1 suppliers. This is a typical scenario for sales in a business-to-business market. Subsequently, there are three separate sets of beneficiaries in the brake market, all requiring a different mixture of benefits. OEMs are under pressure to design vehicles that not only conform to European regulations, but they have to be technically superior to their competitors to prevent sales dropping whilst being competitive on cost. Resultantly, size and weight reduction with superior functionality, all for a similar or lower cost is the benefit mixture required to satisfy the OEMs.

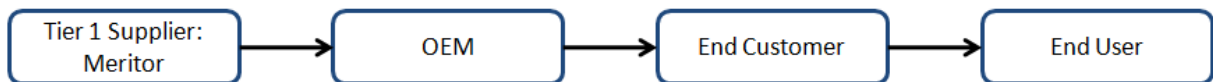


Figure 2.4: Tiers of the brake market.

It is accepted that an End Customer's primary requirement is cost reduction for their mix. Transportation of goods is an expensive procedure but essential for all product based businesses. To please this group of beneficiaries, components that reduce a firm's variable costs, to improve their profit margins, are needed. Safety is another important factor for End Customers as any accidents or collisions that involve the business's vehicles could produce a costly law suit or even damage the company brand. Comparing these needs to the final group, the End Users, discovers a completely different set of needs. Cost is no longer an issue as usability becomes the main focus. Although the product is being made smaller, lighter and more technically complex, it has to be usable for the people that actually drive the CVs.

Having dissected the brake market into three beneficiary sections, a benefit analysis was conducted based on the technical experience gained by the author. A benefit analysis is a practical procedure to determine the mix of benefits on offer from a particular product and is conducted via a four step process:

1. Firstly, the analyser must list what attracts the customer to product.
2. Identify the features offered which make the customer appeal a reality.
3. Discover the full range of advantages delivered by the product through its various features.
4. Finally, determine what are the fundamental benefits being received by the customer.

In each step, it is important to consider every customer segment within the market. In Figure 2.5, a simplified block diagram is shown representing the results for the undertaken benefit analysis. Interestingly, eight clear benefits have been identified through the author's market knowledge alone, from just two customer attraction factors.

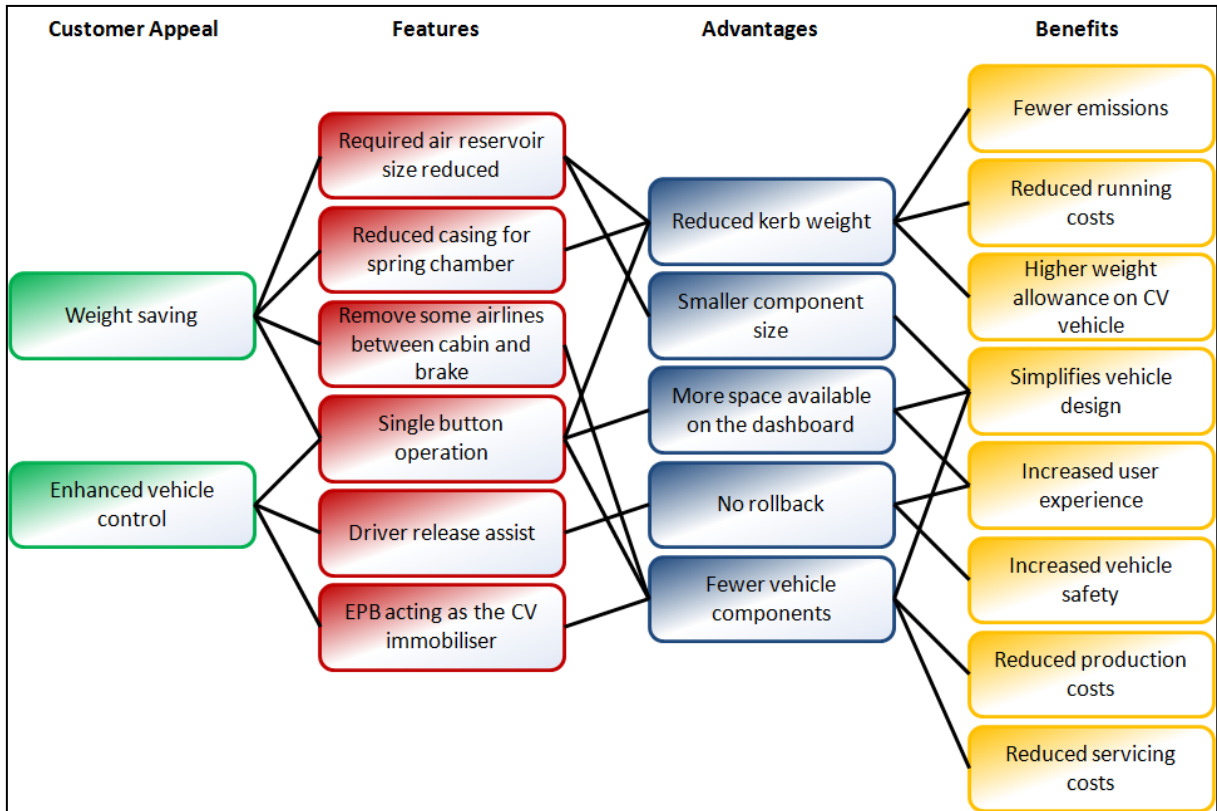


Figure 2.5: Benefit analysis for the EPB based on author's experience.

The first benefit has been discussed already; reduced vehicle emissions will be achieved with an EPB fitted to a CV. Weight reduction results in the engine using less fuel to deliver the same performance. This benefit is felt by the OEMs as their vehicles conform to the tough emissions regulations. Additionally, the End Customers can also receive this benefit as a firm can improve its brand reputation by seen to operate in a “green” manner. The coupled benefit of reduced running costs is also felt by the End Customer as a reduction in fuel expense reduces the variable running costs. A lighter kerb weight is the basis for the first three benefits with the third giving the End Customer the opportunity to increase the fleet efficiency as more cargo can be loaded onto a single CV.

By choosing to install the EPB, the design team has immediately gained flexibility. For instance, reducing the required space in the arch to allow greater space in between the wheels located on the same axle. With the engine and control components all mounted on the front truck axle whilst having to retain leg space for the driver and passengers, any component that eases the packaging difficulty will be beneficial to the OEM. A simplified design results in a double benefit for the End User; the potentially greater leg room will provide a more

comfortable vehicle to work in whilst the cab aesthetics may also be improved by replacing the larger spring parking chamber lever with a single button.

There are many aspects to the job done by End Users with the main focus on driving the CV. If the CV they have to drive is uncomfortable, it is feasible that the End User may decide to move to another company that have more luxurious CV. Recruiting new staff is a costly process for any firm, thus by purchasing more comfortable vehicles, they increase the chance of employee retention. Obviously, the End User also feels the increased user experience benefit.

All three beneficiary segments appreciate the benefits from increased vehicles safety. The driver release assist will prevent the drive from rollback when performing a hill start. The End User feels more secure in the vehicle, again helping the driver experience. With fewer road accidents, the End Customer does not have to go through the laborious claims procedure as often, enabling man power to be focused on improving the business, not saving it. Finally, by producing a safer vehicle, the OEM brand reputation improves and hopefully a corresponding knock-on effect will increase sales.

The ability of the EPB to function as the vehicle immobiliser also helps reduce the number of components on the vehicle. Having fewer vehicle components greatly helps the OEM, delivering them the final two benefits. Firstly, without a dedicated immobiliser unit CV production costs are reduced whilst the End Customer save on servicing costs as there are less components on the CV to malfunction.

The results of the benefit analysis bring to light some very interesting findings. To start, the core product offers the beneficiaries some real advantages to the way the parking brake will operate, in comparison to the conventional spring parking chamber. Single button operation makes the procedure of applying the parking brake extremely easy whilst offering a significant overall vehicle weight and CO₂ emission reduction, at a potentially cost neutral price; further in service cost savings may also be realised. However, it is the product surround which seems to have the largest positive influence on all the beneficiary segments. Perceived benefits included a greater driving experience felt by the End Users, giving them greater control of the vehicle and helping to make their job more enjoyable. Likewise, both the OEMs and End Customers can help improve their brand images by promoting an environmentally friendly attitude.

Having undertaken the benefit analysis and analysed the results, four key questions emerge for EPB success, they are:

1. What is the beneficiaries' current perception of potential benefits derived from EPBs installed in CV?

2. Do the benefits meet the needs of the three groups of beneficiaries?
3. Is technical experience adequate for discovering all the benefits offered by the EPB?
4. What is the best strategy to create demand for the EPB and break the spring chamber lock-in?

Consequently, results of the benefit analysis generated four distinct investigation sections are required to fulfil the set objects, which will be the focus of the work presented in Chapter 3. Identifying whether the beneficiaries truly understand the benefits on offer is of utmost importance. A selective questionnaire was constructed and sent out to various people in the three identified beneficiary segments. Identifying the individuals to complete the questionnaire is a comprehensive task in itself, as explained by Hooley *et al.* (2008). Finding relevant people in each segment with both sufficient knowledge of the subject and importance in the buying/selling process was required. Buyers working for OEMs and End Customer companies may not have been Engineers or they could have little influence in the brake buying decision, making it difficult to find an appropriate person. However, finding a sample of End Users was more straightforward as any CV driver has experience using a braking system.

Once an adequate set of questionnaire subjects had been established, a series of questionnaires were sent out in two stages. Firstly, an open style questionnaire to assess the current state of beneficiary opinions based on existing knowledge. A secondary questionnaire was then carried out, which provided more information about the EPB and its features to the respondent prior to asking questions, to explore what advantages and consequential benefits the individual beneficiaries segments believe could be achieved. The methodology undertaken and the results of these questionnaires is the focus of the next chapter.

3 Obtaining an EPB Route to Market

An appreciation of the current state of the braking market and the financial performance was obtained from the previous chapter. It was identified that the spring parking chamber holds a position of technical lock-in over CV parking units. To break this monopoly, one or more of seven identified previously identified impact factors that disrupt the market, must be found. By investigating the opinions of people in the various benefit segments, not only were relevant impact factors found, but a suggestion of how to exploit them was also provided in the form of a marketing strategy. To maximise the number of opinions received, the method of self-questionnaire was used. Discussion in Chapter 3 is based around the fabrication and analysis of the questionnaire investigation.

3.1 Questionnaire Objectives

Questionnaire analysis is a well-researched and practised topic, becoming the standard method deployed when the data required is based on opinion. A questionnaire can be described as a structured interview, defined by Brace (2004) as being “...one in which each subject or respondent is asked a series of questions according to a prepared and fixed interviewing schedule...”.

Yet, questionnaire design is not as straightforward as simply putting a list of questions together. If it were that simple, the compiled mass of research would be redundant. Care needs to be taken to avoid bias in the questionnaire, whilst generating results that fulfil the research objectives. A three stage planning process was proposed by Brace (2004) that should be adhered to when designing a questionnaire, increasing the chances of obtaining the required data. The first step is to define the principle information required by the questionnaire, which are dictated by the research objectives. When the questionnaire and research objectives are not aligned the questionnaire should not be conducted to prevent meaningless results from being generated. The second step is state any further information that may be requested from the survey. Once identification of all desired data is complete, the final step is to generate a general flowchart of how the questionnaire is going to read before an attempt at writing any questions is made.

Brace’s three stage questionnaire planning tool was used to in this investigation. Conducting the benefit analysis generated a series of research objectives that the questionnaire aims to resolve; these were:

1. What is the current perception of the EPB in the separate benefit segments?
2. Does the EPB meet the needs of the beneficiaries?

3. Are there any further benefits on offer from the EPB?
4. Which benefit is most important to each separate benefit segments?
5. What is the best for marketing strategy for Meritor to take with the EPB?

With the EPB being available on passenger vehicles for almost 10 years now, there is a good chance that knowledge of its existence has spread to the wider community. The first research objective is to explore these opinions currently held by the market. Alternatively, with the EPB being introduced primarily on more executive vehicles, the larger population could still be generally unaware of its existence. This questionnaire presents a good opportunity to test whether people have generally become aware of the EPB and if so, how they feel towards the product. This will be an important finding as it should help determine how the product is marketed.

The second research objective is to explore and identify the current needs of the customer. If the product does not fill a need, it will not sell. Therefore, it is vastly important to identify what the current needs of the customers are and see if they align with what is on offer from the EPB. Remember here that there are three separate beneficiary groups for the EPB, so there is a distinct possibility of three separate sets of needs will be identified.

A benefit analysis was conducted on the EPB, leading to eight benefits being defined. Information used to populate this list was based exclusively from the author's technical experience, which limits the potential number of benefits discovered. Asking the End Users and End Customers, who may have little technical experience, could extract additional benefits that are thus far unidentified; the third research objective. Finding these benefits would open possibility of using an alternative marketing strategy to promote the EPB. The fourth objective is a logical continuation from the third. Once all the EPB benefits have been identified, the most important benefit for each segment will need to be distinguished. Finding out what appeals to which customer segment will not only provide valuable data for the EPB, but for all products Meritor sell. Understanding customer needs and preferences can bring focus to a company's product development, whilst highlighting a marketing direction for both new and current products.

When the first four research objectives are complete, sufficient data will have been collected on the market needs and its opinions to recommend a marketing strategy to Meritor. In turn, this will achieve the fifth research objective.

On review of the five questionnaire objectives, it was decided that the research would be split into two separate questionnaires. The first was to be an exploratory questionnaire (EQ) focusing on the first three key questions that emerged from the questionnaire in section 2.6, making it a reflection on the current perceptions and providing the market an opportunity to further populate the benefit analysis. Only at this point would it be possible to determine the fourth key question. Also, with a large amount of information previously obtained, the second questionnaire would also be able to test an initially suggested marketing strategy.

3.1.1 Further Information

Historically, new products innovated by component suppliers in the EBM are typically pushed through the supply chain, as depicted in Figure 2.4. Direct interaction between Meritor and the End Customers and End Users is largely restricted in this arrangement, preventing market stimulation for their products. Since 1990, the general trend for firms implementing the marketing push strategy has been to use trade marketing techniques (McDonald and Christopher 2003). Here, both the suppliers and the distribution channels (OEM's) jointly market the product to the End Users and Buyers.

Asking questions to all three benefit segments could provide enough information to test whether the current marketing push model can be broken, allowing a demand pull system to be established. Demand pull strategies remove the marketing attention from direct selling and places it on stimulating demand from the End Users and Buyers. Companies that can successfully operate such a strategy can dominate the market share by utilising the power in their brand alone.

Intel is a fine example of a successful demand pull marketing strategy. In 1991 Intel launched their "Intel Inside" campaign. Intel produces a range of microprocessors for computerised devices. The Intel Inside campaign promoted the Intel brand to end users of personal computers and alike equipment, via multiple channels such as television adverts. The advertising campaign made use of '*product focused*' marketing throughout, to show power in the brand rather than the individual products (Norris 1993). Product focused marketing does not emphasize the particular product being advertised like its name would suggest, but uses other products or items that symbolises their brand image. For example, in 2006 Intel released their "It's time to Multiply" advertisement, which had a single dancer split into four, before being replaced by a second dancer, who in turn also splits into four. Both dancers were dancing the quickstep routine, signifying the speed of Intel's microprocessors whilst the switch from the first dancer to the

second illustrated the ability to use the two separate processors in their Core 2 Duo range (D'Souza 2010).

The result of Intel's strategy was that their microprocessors are perceived to be superior to rival products. In response to the generated public demand for Intel powered computers, OEM's put the Intel logo on their computers, making it clear that an Intel chip was in the computer. In essence, they were using product focused marketing techniques to gain the perceived advantages of the Intel brand for themselves. This point was one of the key factors to Intel's success, their products had the backing of the OEM's (Abdul).

In recent years, Intel has moved away from product focused marketing strategies and replaced it with a people centric strategy to show how the technology can improve individual people lives as well as the society. With their market dominance and the created perceived quality differential between them and competitors, Intel no longer feel they need to demonstrate their advantage points (D'Souza 2010). Creating such a strong brand image has enabled Intel, a Tier 1 supplier, to use people centric advertising. Parry-Husbands *et al.* (2010) have described "*People-centricity is at the heart of marketing, as opposed to sales which is never about the customer*", sending messages that people can believe, rather than trying to sell products to them.

The power of the brand image is clearly demonstrated here in the Intel example. A unique opportunity was offered by this questionnaire to find out the how strong the Meritor brand is amongst the various market segments, due to interacting with people not usually targeted directly by Meritor.

3.2 Explanatory Questionnaire

Up until now, the focus of chapter 3 has been on the questionnaire study as a whole. It is appropriate at this stage to focus the attention of section 3.2 exclusively on the development of the explanatory questionnaire (EQ). With the first two stages complete, step three of Brace's three stage planning process is completed first before the questionnaire writing procedure was done. Successful completion of section 3.2 will satisfy the first three research objectives.

3.2.1 Explanatory Questionnaire Flowchart

To complete step three, a simple flowchart of the question sections within the EQ was created. When identifying the types of questions to deliver the research objectives, three identifiable groups of questions were found. The first group was called New Products, questions within this group were directed towards discovering the respondents' opinions and how they view new CV

products. For example, what do they perceive to be a new CV product and how often do they think new products are put in CV's; it would be interesting to see how innovation is perceived across the individual benefit segments. The second group was Current Needs, devoted to finding out what the different beneficiary groups need from today's CV's. Finally, a section of questions would then be asked specifically on CV braking and the EPB technology. Ideally, being the most important section of the questionnaire it should be placed earlier. It is possible that a respondent may not find the time to complete the whole questionnaire, by placing the braking section earlier would increase the chances of the most important questions from being answered. However, by asking the braking questions early, the respondent will be biased to thinking more about the brake system when answering the other sections questions, which would introduce a source of bias. It was for his reason that the section referring to the braking specific questions

Figure 3.1 shows the three identified question groups in the order they are to be asked, along with two additional groups. The final group was Brand Awareness, already identified as additional information that may be useful. In contrast with the braking section, questions focused on brand awareness were low priority, due to being supplementary information and were therefore placed last in the questionnaire. To have a complete the questionnaire, the Personal Information section was placed at the beginning to capture some basic statistics. The planning stage is now complete so the remainder of section 3.2 will now centre on the questionnaire fabrication process.

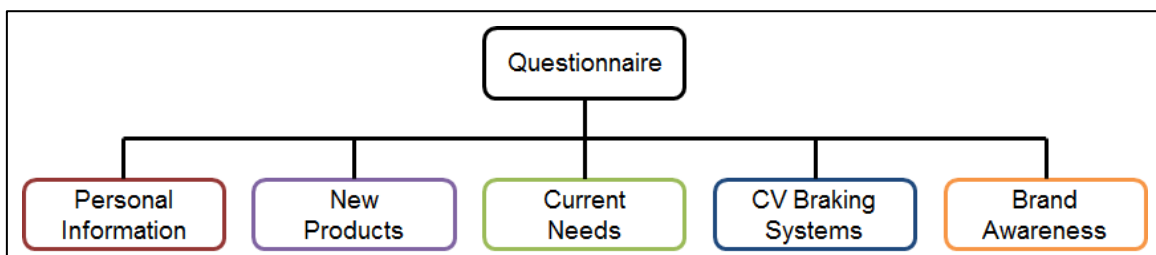


Figure 3.1: General questionnaire flowchart.

3.2.2 Population and Questionnaire Sample Size

The questionnaire population can be defined as the total number of people for whom the results represent. However, defining the people who make that group is very much discretionary. Often these populations are extremely large, making it impossible to question everyone within it. In these scenarios, a smaller 'sample' of people is selected to represent the full population. Inherent errors are incurred using this process because the reduction in data creates a loss of

confidence in results. For example, with a population of 100 people, if 95 people are asked a set of questions, how is it known what the other 5 people would respond? The obvious answer to this conundrum is that it is impossible to know. Statistical analysis is used to determine the level of confidence with a set of recorded data from a specified sample, which is representative of the actual population. The fundamental approach to statistical analysis will briefly be described before defining the population of each of the three beneficiary groups. Boone stresses the importance of defining the questionnaire population size before starting the design phase as the questionnaire style is very much dependent on the how many people it needs to reach.

Statistical significance is simply defined as a result occurring in the absence of chance. The calculation to whether a result occurred by chance, otherwise known as the observe significance level (or p -value), takes the form of a hypothesis test (Mendenhall and Sincich 2007). The magnitude of disagreement between the null hypothesis (H_0) and the p -value demonstrates the degree of test significance, resulting in a rejection of the null hypothesis if it is sufficiently large, dependent on the confidence level required. History has shown numerous examples of statistical significance testing being interpreted mistakenly. Daniel (1998) points to six common misconceptions that often lead authors to making inaccurate statements about their results. These misconceptions are:

1. Being statistically 'significant' does not mean the results are important to real-world situations.
2. The ability to get duplicated results from a survey using a different sample is not implied by significance.
3. Chance may have had little impact on the obtained results.
4. Being statistically significant has no bearing to whether the sample size used is representative of the population.
5. Statistical significance testing may not be the optimum method of analysis.
6. Validity coefficients and statistically significant reliability may be different from one sample to the next.

Considering the constant misuse, it is of no surprise that the method of statistical significance testing has its adversaries. For instance, Hoem (2008) encourages researchers to publish work even when no significance is achieved, for two main reasons; a non-result can draw a valid and interesting conclusion as well as understanding behavioural aspects of just a few can be an important finding in itself. Carver (1978) went further by actively calling for researchers to abandon statistical significance tests and use other scientific methods instead. A caveat was

made to researchers though as Carver stated that researchers continuing to use statistical analysis should only produce results once all other analysis have been interpreted and be accompanied by the statistical power of the test.

There are two types of error associated with statistical testing, type I error and type II error. The former is a result of rejecting a null hypothesis when it is in fact true, with χ being the probability of making such an error. The reverse is true for a type II error, accepting a false null hypothesis and the probability of making this error is denoted ψ ¹. The probability of actually discovering a difference as a result of any conducted procedure is known as the power of the test (Mendenhall and Sincich 2007), calculated by $(1 - \psi)$. Tests resulting in low statistical power “cannot reliably discriminate between H_0 and the alternative hypothesis...” according to Faul *et al.* (2007).

A population size will be estimated for each of the three benefit segments, allowing both power analysis and statistical significance test to be conducted after the results have been analysed. A software package called G*Power has been used to calculate the power values, which should only be accepted if they are equal to or above 0.8 (i.e. $\varphi \leq 0.2$), or alternatively written, the chances of a difference found in statistical testing is real and not a Type II error. Required variables needed to be inputted into G*Power for a power value to be calculated are the error probability, effect size and required power. Using values of 0.3, 0.05 and 0.8 respectively, as suggested in Faul *et al.* (2007), the calculated minimum required sample size necessary to ensure of a Type II error not occurring is 64.

3.2.2.1 End Users

Defining the number of End Users was not a straight forward process. The market in consideration is the whole EBM. Even if accurate numbers for the total population was found through government statistics, being able to find a creditable sample size would be virtually impossible. Written questionnaires would have to be translated into every language that is spoken within Europe, to prevent biasing the sample to respondents who only speak English; the responses would also need translating back into English. Even without the language difficulties, surveying the entire EBM population would be vastly difficult to achieve; multiple samples would have to be found in each country for a truly representative sample to be achieved. For these reason, the choice to limit the questionnaire to only residents within UK was made and will be deployed for all three segments.

¹ α and β are more commonly used but are defined for other parameters later in this report.

With the population now spatially defined, obtaining the sum people in the population was easy. The Labour Force Survey is a government survey conducted by the Office of National Statistics, aiming to find key statistics about the national workforce and their conditions (Office of National Statistics 2011). For the period of April to June 2011, a total of 100,286 people responded to the Labour Force Survey, allowing accurate estimates to be made for the entire population. Respondents who indicated they were currently a CV driver (End User) was estimated at over 468,000 people. The breakdown of different CV driver types is given in Table 3.1. Interestingly, it is estimated that only 36,000 professional female drivers in the UK, of which 10,000 drive vans (not shown in Table 3.1), excluding them from the population. Therefore, the total female proportion of the population is approximately 26,000, or alternatively described as only 5%. Female drivers were not be excluded from the survey but a representative sample would be predominately male participants.

Table 3.1: Breakdown of CV End Users in the UK (taken from the Office of National Statistics 2011).

Standard Occupational Classification	Total in employment ^{1,3}	Employees ³			Self-employed ³		
		Full-time	Part-time	Total	Full-time	Part-time	Total
8211 Large goods vehicle drivers	299,112	258,495	11,894	270,389	27,125	*	28,723
8213 Bus and coach drivers	116,278	91,366	17,229	108,595	*	*	*
8223 Agricultural machinery drivers	10,284	*	*	9,549	*	*	*
8229 Mobile machine drivers and operatives n.e.c. ⁴	42,869	35,714	*	36,208	*	*	*
Total	468,543	385,575	29,123	424,741	27,125	0	28,723

¹ Includes unpaid family workers and persons on government-supported training and employment programmes.

² Includes those who did not state their occupation.

³ Includes those who did not state whether they worked full or part time.

⁴ Not elsewhere classified

* Sample size too small for reliable estimate.

3.2.2.2 End Buyers

Once again, the ability to define the population size of the End Buyers segment was complicated. In comparison to the End Users, the segment is not as concisely defined; it is difficult to know which registered companies based UK use CV's, and out of those that do, who is the person/people that make the buying and/or leasing decisions? Unlike with the End User category, there are no readily available data sources to provide this information to ease the process.

It is easy to assume that all logistics based companies will have some CV's, based on the fact that their business is dependent on the transportation of goods. Yet, this may not be the case as a proportion of the 18,426 UK based logistics companies (found using the Fame database) use purely shipping or air transportation vehicles. Logistics companies are not the only users of CV's. Look at the retail industry for example, products have to be delivered to warehouses and then on to their shops or directly to customers' homes. Large companies such as John Lewis, who have 74,800 employees, will have several CV fleets to meet their operating needs, all over

the country. They also have numerous sales, administration and legal staff members as well. Dedicated fleet managers who make decisions on the specific CVs to buy/lease will only be a very small percentage of the total amount of employees, with no way of easily finding this number.

In comparison, small companies like Hockley Trading UK Limited, with a total of two employees, are more likely to use a logistics company to complete their logistical needs as this will be an easier and more economical solution for them. It would be impossible obtain which of the 101,263 UK based retail companies will have their own CV fleets and those who use logistics companies. The complexity increases when other industries are considered.

Subsequently, assumptions were made to enable an estimate of the population size. The first was that only companies earning annual revenues of at least £100k would be sufficiently large enough to have their own CV fleet. Also, only the retail, agriculture and logistics industries were used in this calculation. It was assumed other industries were more likely to use logistics based companies for their reduced transportation operations, for example, the medical profession will have nearly no CV usage, except for the supply of equipment. A further complication is added to the scenario, considering that not all of these companies deal with their logistical needs in-house and use a logistics company such as DHL to manage it for them. No data is universally available stating which companies do their own logistics and which ones outsource it. Therefore, it will be assumed that half of the companies that produce an annual revenues of £100k is made.

For the selected companies, both a minimum and maximum number of knowledgeable people were calculated. The minimum assumes there is only a single person in each company that has sufficient knowledge about the physical CV aspects and is the solitary individual when deciding which CV to buy/lease. Alternatively, the maximum assumes there is a team of 10 people who make the CV buying decisions, creating a possible population range between 4,187 to 41,870 people in the UK End Buyer segment (Table 3.2), when all assumptions have been applied.

Table 3.2: Estimated number of people with sufficient CV knowledge in the End Buyer segment.

Industry	Number of companies with more than £100k turnover	Minimum estimated number of people in population	Maximum estimated number of people in population
Retail	4,698	2,349	23,490
Logistics and Transportation	1,441	1,441	14,410
Agriculture	397	397	3,970
Total	6,536	4,187	41,870

3.2.2.3 OEM's

Defining the number of people in the final beneficiary segment is a much simpler task in comparison to the previous two segments. As described in Figure 2.3 there are only five groups competing in the EBM, which can be broken down into a total of nine OEM's. OEM's have hundreds of people in their design and technical division, but only a small team will be dedicated to braking. Because of this, the same assumption that this division could range from a solitary person to a maximum of 10 people was made once again. Thus, the OEM population range was from only nine people, up to a possible 90.

3.2.3 Administering the Questionnaire

Continuing the questionnaire design process, the next consideration was how the questionnaire should be administered. A thought process into what type of data was desired and how it should be collected had to be completed. With the aim of obtaining personal attitudes, open style questions were to be used, to generate qualitative data. Finding such qualitative data is never easy because of the required interactions with various people needed to extract the necessary data. By administering a self-completion type survey or conducting interviews are the two possible methods of acquiring such data.

Face-to-face interviews have historically been the primary mode of data collection, but its dominance over the past decade has declined (Brace 2004). This method involves an interviewer travelling to the respondents place of work (or any another desired destination) to administer the survey. It is not only the travel costs that make this research method the most expensive, but often the respondent will charge a fee for their time. Another downside to face-to-face interviews is that it spawns an opportunity for the interviewer to introduce bias into the data taking process by allowing their personal opinions to be portrayed to the respondent. Despite

these negatives, face-to-face interviews do extract the greatest amount of information from a respondent as the interviewer can delve deeper into a given answer, whilst being able to read body language. Any ambiguous questions could be better explained to the respondent also, resulting in a meaningful response rather than a skipped question.

Telephone interviews are personal, one-to-one discussions conducted over the telephone. Costs involved are subsequently less as travel expenses are obsolete, speeding up the survey time and allowing a geographically wider sample to be interviewed. Both Keller (2004) and Basi (1999) explain that the lack of a physical meeting between the interviewer and interviewee generally leads to more honest response to sensitive subjects, reducing the social desirability bias in the survey. The obvious disadvantage of telephone interviews is that pictures and prompt cards cannot be used as stimuli, whilst a long list of response options should be avoided to prevent the options being forgotten.

Self-completion questionnaire surveys remove the human interaction between the interviewer and interviewee; this is the fundamental difference between the self-completion and interview methods. Removal of the human interaction does bring certain benefits to the data collection process. A major source of bias is eliminated and the response levels of sensitive questions further increases. The traditional way of completing a questionnaire survey is to send out paper copies to respondents. Unlike in an interview situation, the respondent can take their time before answering a particular question. This can be seen as both an advantage and a disadvantage; taking extra time could lead to a fuller response with a greater amount of detail, but negative if the intension of the question was to get an instinctive reaction. The questionnaire administrator now has no control over the time taken on each question, removing the spontaneity from the response. Implementing pictures into the questionnaire is straightforward for question stimuli, likewise with written descriptions. Complex routing issues are found with paper questionnaires as it is impossible to prevent the respondent from investigating the questionnaire before he/she completes it. Efforts during the writing stage to prevent bias in the question order could be undone by this.

Using a web-based self-completion method fixes a lot of the problems with paper questionnaires as the program used to conduct the questionnaire can be 'clever' by ensuring the question routing is as the writer intended (Brace 2004). Also, time limits can be embedded into a question when instinctive responses are required. However, both paper and web-based questionnaires suffer dramatically from the main disadvantage of self-completion surveys: low response rates. Difficulties can arise when finding and identifying people within a population

that will create a representative sample size, leading to poor statistical significance. It is not uncommon to find the desired respondents identified are too busy to complete a questionnaire. For instance, Wu (2010) received only a 1.5% response rate from a sample of approximately 2,000 people.

Bradley (1999) investigated the different ways to conduct a web-based self-completion questionnaire. Six separate approaches were summarised and are listed below.

- Open web
- Closed web
- Hidden web
- E-mail URL embedded
- Simple e-mail
- E-mail attachment

Both the Simple e-mail and E-mail attached options are the least desirable methods to use as the option for complex routing, the main advantage of web-based self-completion questionnaires, is removed or cannot be enforced. In addition, the attachment option requires the respondent to download a file, complete it, save a new file then return the completed file. A large amount of cooperation is being asked of the respondent in these two methods so they often result in modest response rates (Brace 2004).

Consequently, the remaining four methods are frequently used. Determining the correct method to use is dependent on the questionnaire type and desired results. Open web questionnaires are constructed on a website that is freely available for anyone to locate and answer. This is ideal if sheer data quantity is wanted but there is no control to whom, or to how many times an individual can answer. No specific knowledge of a particular population can be guaranteed. Closed web questionnaires improve the data quality as the website can be restricted to invitees only. Hidden web questionnaires are often used as internet “pop-outs” when triggered after a certain criteria is met. Finally, embedding a URL link to the questionnaire within an email, is the method most suited to getting a focused sample of people to respond. As the link is put in an email, personalisation of the email can help persuade the recipient to complete the survey. The main disadvantage is the amount of time it takes to complete each invitation, especially if a list of names must be found first. For this reason, this web-based self-completion method is only feasible for small, but specific sample sizes.

A dual approach was decided upon with both the E-mail URL embedded and paper self-completion methods for survey conduction were used. The advantages of the former outweigh the negatives for reaching a specific sample so was implemented when contacting both the OEM and End Customer segments. Qualtrics is an online questionnaire writing and analysis package which was used to prepare and collect the relevant responses. Alternatively, the large population size of the End User segment determined that the self-completion method should be used in this final case. Practical reasoning also lead to the same conclusion as the End Users spend the majority of their day in a CV rather than on a computer; having a paper copy they could take and complete in their downtime would produce a greater response.

3.2.4 Constructing the Questionnaire

Having produced a plan, estimated the population size and determined the method of administration, the procedure of writing the questionnaire could begin. However, prior to any questions being written, a decision of what data was required and in what form the results should be in had to be made. A discussion of the different types of questions and response types is presented.

3.2.4.1 Question Types

All questions boil down to one of two types of questions, it is either open or it is closed. It is important to understand the difference between these two as the gathered data from them is very different, needing different types of analysis to be conducted on the results. With open questions, in no way are potential responses are implied or suggested, requiring the respondent to think about and describe their answer in words. When a question needs to extract information on personal attitudes from the respondent then open questions are the preferred question type. Brace (2004) outlines the difficulty experienced by a lot of people when expressing their feelings during surveys. Help is often required to produce viable data, especially to get the description in an analysable form. Verbal responses will have to be recorded if face-to-face or telephone interviews are conducted; otherwise open text boxes are used to allow the respondent to write their answer.

Closed questions are those that have a finite number of possible answers and they therefore tend to be predominately pre-coded, ideal for probing behavioural attitudes. These are easier to complete than written answers as the respondent only has to mark the correct answer (for them) from a list, whilst a person's memory and/or their willingness to answer are the only barriers

preventing data extraction. Brace (2004) does warn that to maintain user interest, and ultimately their participation, a mixture of both open and closed questions should be used.

3.2.4.2 Response Types and Scales

With the questionnaire being explanatory, the aim was to discover personal attitudes and opinions. Consequently, the majority of questions were of the open form, although the advice offered by Brace was adhered to by using closed type question in combination with open type, to retain user engagement. The inherent problem with open questions is the sheer amount of time required to examining each response and transferring it into a more usable form. Questions with pre-coded answers can be a used for open questions too, either when the answer is simple or when a complex answer needs to be categorised (Brace 2004). The ability to scale the pre-codes allows simple techniques to be applied at the analysis stage. Possible answers have to be determined beforehand with an additional “Other” option needed for when the answer list fails to provide an adequate response. When it is impossible to predetermine what the response may be then a standard textbox must be used.

Pre-coded lists themselves come in two forms. Multiple choice lists are used for closed questions, where the answers are behavioural based; a single or multiple responses can be checked dependent on the question style. Each possible response has no relation to the other, resulting in no definable scale between them.

Alternatively, using a scale based pre-coded list allows the user to give a rating to their answer, indicating their attitudes towards that particular topic. For this reason, itemised rating scales are often used in questionnaires to simplify open questions answers. It is essential that the scale has evenly spaced points, although there is no obligation to use numerical scales. A descriptive scale can be better suited to an answer than a set of numbers in many cases. Balanced scales have the same amount of positive responses as negative responses, with a mid-point answer usually placed in the middle (although can be off-centre), representing an uncertain or undecided attitude. A five point scale is most common but higher insight into respondents’ feelings can be gained with a greater number of points. Unbalanced scales can be used on specific occasions but awareness of how much bias is placed on the question must be documented and accounted for in the analysis stage.

A special type of balanced scale has become a standardised technique in questionnaire writing. With a Likert scale, the respondent is asked to state whether they agree or disagree to a set of statements. By having at least five points on the scale, the strength of the respondent’s agreement (or disagreement) can be scored, allowing statistical analysis. To make full use of the

Likert scale, a summation of all the responses from a single respondent should be made, although Albaum (1997) found that commercially, this process is rarely completed.

Order effect is a type of bias that is present in Likert scales, as well as other pre-coded type questions (Brace 2004). When scales are laid out horizontally, the human brain has a tendency to choose the left-hand answers. Acquiescence, the inclination to agree rather than disagree (Kalton and Schumen 1982), is a second bias that can counterbalance order effect if the agree option is located on the right-hand side.

If a respondent reaches their boredom limit, when asked to rate statements with a Likert scale, they are likely to fall into a trend known as pattern answering (Brace 2004). When pattern answering, a respondent will pay little attention to the statement and simply respond in a straight line down, horizontally or diagonally across the page/screen. Once again, keeping the respondent engaged in the questionnaire is paramount for quality data acquisition. By simply reversing the question into a negative statement, the respondent is forced to think about what they will reply. Randomly applying question negativity reversal was the advice offered by Brace to prevent a respondent falling into the pattern answering routine.

3.2.5 Pilot Questionnaire

With the information found in the literature acknowledged, the EQ was written (see Appendix B). Before it went live and the data collection process began, it was necessary to conduct a pilot questionnaire. Conducting a pilot scheme is of high importance during the questionnaire planning stage. It has a number of functions, which include:

- The questions are understood clearly and without ambiguity
- Pre-coded lists are sufficient in length, capturing the majority of possible answers
- The routing procedure can be followed (on paper versions)
- The length of time it takes to complete
- Whether any general mistakes have been made

Five trialists were chosen to complete the pilot study, one for each beneficiary segment and two further academics. The two academics were Stamatis Angelinas and Dr Marko Tirović, both of whom specialise in the braking department at Cranfield University. Being the first participant, Angelinas concentrated on basic grammatical and spelling errors. Conversely, a more detailed review was taken by Tirović, providing three main points. The first was a reflection of the questionnaire flow and how easy it was to follow the Qualtrics online weblink. Feedback was

pleasing as Tirović declared the question flow to be good, with the online interaction straightforward to use. The comment was that the length of the questionnaire was acceptable, although only “*just*”, implying any alterations made to the questionnaire should not lengthen it.

Finally, Tirović recommended changing the section of questions targeting an opinion on how the additional CV weight would be used. Originally, there were three questions placed here, with the first two looking for a reaction on a weight reduction of specifically 10 and 100 kg, allowing a comparison. The third question was multiple choice, asking the respondent to check the weight reduction range they believed a CV had to achieve before they had a realisable benefit. In response to Tirović’s comments, the three questions were reduced to two, the range question followed by an open question for a description of how it would be used (as seen in Appendix D).

Christopher Calvert was the third trialist to complete the pilot questionnaire. As he is a CV driver (End User), the mentality behind the feedback was of an alternative nature to that given by Tirović. The major source of concern came in question “*Q7 In your opinion, which of the following OEM's produces the best CV's?*” Calvert rightly voiced that not every driver will have experience with all the different manufacturers’ CV’s, making this an impossible question to answer. In response, the question was rephrased to give the same essence behind the question, but making it appropriate for everyone. Calvert also highlighted that clarity to question Q14, ranking the CV features, was needed; again, the question was rephrased. The final suggestion from Calvert was that Q25 appeared to be a simple yes or no question. Q25 was modified accordingly with another question following it asking for the respondent to describe their issues.

Representing the End Customers segment was Malachy Maginness, a researcher at Rolls Royce. Although not an ideal candidate to complete the questionnaire, Maginness did provide an excellent opportunity to examine the questionnaire feasibility on an individual from the End Customer segment. Several questions that should have had “Don’t know” options were initially missed but thanks to the diligence of Maginness, this was rectified. Likewise, the phrasing of both questions Q27 and Q28 had a degree of vagueness to them so they were also rewritten. One further suggestion given by Maginness that was adopted was to have a direct question asking what the respondent job title was. Initially, it was believed that it would be inferred from the answers to the personal information section, yet there is no guarantee this is the case, so a direct question was added. One suggestion from Maginness that was rejected, was to clearly state the objectives and the specific market segment the questionnaire is based on. By adding

this information, bias would be put into the questionnaire as the braking system would be placed into the respondent's subconscious before they answer any questions.

After the suggested modifications were made, the pilot questionnaire was completed by Andreas Sundqvist, a manager within the OEM Volvo. Because Sundqvist worked for an OEM, he considered himself to be working in the "Logistics and Transportation" industry. Due to the design and manufacture aspects of OEM's product output, it was expected that the "Engineer" option would have been ticked instead. Consequences of this meant that the questionnaire logic dictating what questions to respond to directed the Sundqvist to questions not appropriate for OEM's. Changes were made such that both the "engineer" and the "logistics and Transportation" options would continue the filtering process to confirm whether the respondent is or is not an employee within an OEM.

3.2.6 Explanatory Questionnaire Results

The explanatory questionnaire was distributed using both an online web-link taking the respondent to the self-completion questionnaire, and an identical paper copy, as shown in Appendix D. The former was used to contact primarily for OEMs and End Customers whilst End Users were given the latter. In total there were 42 responses to the questionnaire, with 33 people fully completing it. Achieving a completion rate of 79% is pleasing, although the total number of completed responses is heavily under the 64 people per segment calculated to be sure no Type II errors will occur. Nevertheless, a sufficient number of responses for meaningful analysis to be conducted was received and was examined.

Of the 42 respondents, 41 were male, meaning there was only one female respondent to the questionnaire. The breakdown of responses was five OEM replies, increasing to 13 from the End Customers, with the remaining coming from the End Users, at a total of 23; completed questionnaire breakdown figures are one, seven and 22 respectively. Summing the number of completed questionnaire by segment shows that there were only 30 respondents who fully finished it, a difference of three from the total completed questionnaires. Two respondents decided to withhold information by not answer some questions in the opening section, making it impossible to determine which benefit segment their results should be accredited to. Subsequently, these two results were omitted when divulging into specific benefit segment results only. Likewise, the final completed questionnaire was done by an employee of a Tier 1 supplier, so was also omitted from the results. In the interest of not sharing biasing the results, by removing Tier 1 suppliers, it reduces the chances of an employee from a competitor company from dishonestly answering it, leading to incorrect conclusions being made.

Identifying people in the various segments proved, on the whole, to be less difficult than originally expected. A list of 17 people, from eight different OEM's, was provided by Meritor. The difficulty was increased slightly when finding relevant people in the End Customer segment to invite to complete the questionnaire. Specific people were contacted in DHL, Tesco and John Lewis and asked to complete the questionnaire, as well as 20 people making up the Logistics Carbon Working Group, ran by the Freight Transport Association. Ceva Logistics is one example of the type of companies represented by the Logistics Carbon Working Group. A selection of End Users' was taken from Waitrose and DHL.

3.2.6.1 SECTION 2: Attitudes to New Products

With section 1 of the EQ dedicated to identifying which segment the respondent is from, as well as removing any unwanted respondents, the analysis begins from section 2. The aim was to understand the attitudes behind new product introduction for each of the benefit segments, and whether there is any commonality between them. A total of 11 questions were asked in section 2 but only those that produced meaningful results will be discussed.

With questions 2.1 and 2.2 proving ineffective in discovering the opinions of the End Customer and End User segments (results from OEMs would have been biased so they were not asked these questions) towards the frequency of new product introduction into CVs, the analysis begins with question 2.3, which was:

“Q2.3 Please read through the list of CV features below then rank their importance to you; where 1 is the most important and 9 is the least important. (You should use each number between and including 1 to 9 once only)”

This question was designed to determine what the important CV features are to the respective benefit segments. Respondents were asked to rank the importance to them of nine CV features. Because a ranking system was used, it is appropriate to use statistical analysis to evaluate this question. Figure 3.2 shows the averaged value given to each feature, with one being the most important and nine being the least important. On first glance Figure 3.2 provides a peculiar result as features that improve the driving experience are shown to be the most important.

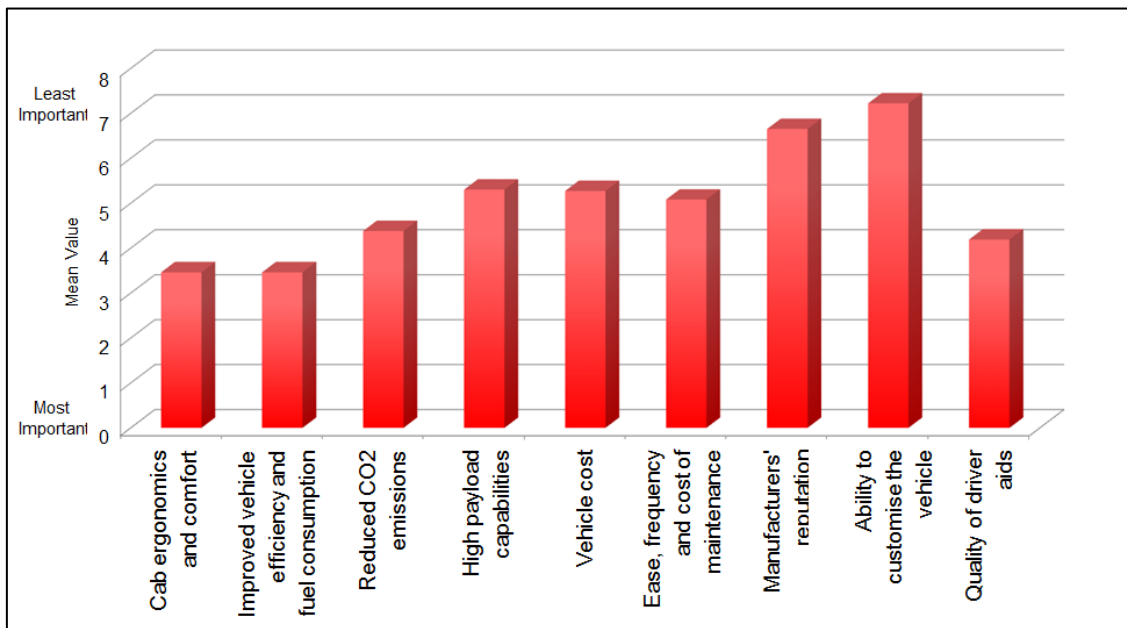


Figure 3.2: Q2.3 All Results - driver features appear to be the most important.

Out of the 33 completed questionnaires, 66% of respondents were End Users, introducing a heavy bias in their favour. To counter this bias, Table 3.3 presents a breakdown of the three most important CV features to each of the benefit segments. Immediately, this bias is confirmed as the features designed to increase driver satisfaction is shown to be a function of End User results only, being their two most important considerations as to what makes a good CV. However, there is some harmony between the three segments as *'Improved vehicle efficiency and fuel consumption'* was rated as one of the three most important CV features by all three segments. As the current trend of rising fuel price continues throughout the continuing economic downturn, increasing variable costs are a major concern for End Customer businesses, whilst increasingly stringent emissions legislations dictate a certain level of CV design capability OEMs have to adhere to. Justification is therefore given for the first two benefit segments.

End Users showing concern for the overall vehicle efficiency is harder to justify as this feature has little impact on their working life. The effects of recent social trends are influencing people's attitudes, with environmental issues now being a driving factor (European Social Survey 2012). The Triple-Bottom Line model presented by Bernon (2008) outlines that sustainable development should be based on environmental and social factors, in conjunction with economic profits. Results presented in Table 3.3 would support Bernon's model and tells us that the EPB offers Meritor a product capable of satisfying two of the three requirements for sustainable development, a platform for long-term profitability if it can be produced for a

neutral system cost compared to the current spring parking system. The latter point is highlighted by the fact that *‘Vehicle cost’* was highly important for both the OEM and End Customer segments; there is little point developing a product that will cost too much to buy, making it impossible to recover any development costs incurred.

It can also be derived that *‘Improved vehicle efficiency and fuel consumption’* is an important selling point of the EPB. All segments see vehicle efficiency as a highly important factor, so any marketing campaign Meritor undertake must clearly demonstrate the improvement in vehicle efficiency as one of the key selling points.

Another very interesting point discovered from Table 3.3 is that the *‘Ease, frequency and cost of maintenance’* of the CV is only considered highly important to the End Customers. The more difficult it is to repair a CV, the higher the maintenance cost will be, resulting in the lifetime cost of the CV to rise. By reducing the frequency and/or the cost of maintenance of the CV, the value of sunk costs spend by logistics companies will reduce. It could have been expected that the End Users feel this as an important CV factor. Broken down vehicles can lead to expensive repair costs and a reduction in output from the fleet with fewer vehicles operating.

Table 3.3: Q2.3 – Segmented results for the most important CV features.

	OEM	End Customer	End User
Most Important	Improved vehicle efficiency and fuel consumption	Vehicle cost	Cab ergonomics and comfort
	High payload capabilities	Improved vehicle efficiency and fuel consumption	Quality of driver aids
	Vehicle cost	Ease, frequency and cost of maintenance	Improved vehicle efficiency and fuel consumption

At the other end of the scale, the least recognised features by the three segments were the *‘Ability to customise the vehicle’* and the *‘Manufacturers’ reputation’*. However, contrary to the End User opinions, the OEMs see *‘Ease, frequency and cost of maintenance’* low on the importance to the CV design, in comparison to the other stated features. A contrast in opinions is clearly shown here with the OEMs and the End Customers and is perhaps somewhat surprising. Repeated vehicle failure will aggravate the End Customers and ultimately tarnish the brand. However, this result does not state that maintenance is unimportant to the OEMs, just

they are relatively less important than regulatory constraint criterion (like the Euro VI legislation).

Table 3.4: Q2.3 – Segmented results for the least important CV features.

	OEM	End Customer	End User
Least Important	Ease, frequency and cost of maintenance	Quality of driver aids	Manufacturers' reputation
	Manufacturers' reputation	Manufacturers' reputation	Vehicle cost
	Ability to customise the vehicle	Ability to customise the vehicle	Ability to customise the vehicle

Moving onto question 2.4, participants were now asked to specifically state up to three new CV features they “*have found to be the best or most useful, and why?*”, where new was defined within the past five years. This question was in the open format, allowing the respondent to give a more detailed answer. No statistical analysis was conducted as a consequence, although where possible, similar responses were grouped.

Starting with the OEM segment, with only a single respondent it is impossible to claim the view of the entire population has been sufficiently captured. Nonetheless, the answers provided by the solitary OEM respondent will still bestow some interesting information. The first two new features suggested were both brake related, with the introduction of “*ESP as mandatory*” and the “*Emergency brake system*” both being cited for their improvement in CV safety. The third was the launch of an “*Electronic air processing unit*” as it provides a weight saving advantage, delivering fuel efficiency and emission reduction benefits.

Encouragement for the EPB introduction can be gained from this as benefits offered by these new products are the same as those offered by the EPB, as the benefit analysis discovered. Coupling these comments gives further inspiration as it appears a braking solution that provides weight and emission advantages are desired by the OEM segment. It should be stated that there is a chance of bias in the answer as the list of contacted OEMs was produced by Paul Roberts of Meritor. Considering Meritor are a brake supplier to various OEMs, there is a high probability that the contacts provided are part of the OEMs braking team and therefore consider braking improvements as important. With the questionnaire being anonymous, it was impossible to find out who completed it whether they were indeed part of a braking team.

In contrast, eight End Customers in total gave an answer(s) to question 2.4. Results were generally based around four themes, which were:

- Fuel saving/efficiency
- Driver control functions
- Braking aspects
- Driver behaviour monitoring

In light of the answers to question 2.3, fuel saving or efficiency improving features being frequently described as the best or most useful feature is understandable. Yet, the '*Quality of driver aids*' was one of the least important CV features for the End Customers but was repeatedly mentioned as the one of the best new CV features. Clearly, although driver aids are relatively unimportant to the End Customers, a level of appreciation for what they offer exists. For example, one comment made was that advanced features "*...takes decision away from bad drivers.*" By offering support to drivers with limited ability, the End Customer can mitigate some of the risk of potential accidents. With braking functions, such as ESP, becoming more integrated into the CV control, the scope for the braking systems to capitalise on the risk mitigation is large. The assisted hill start advanced driver feature offered by the EPB does indeed give this advantage.

Finally, driver behaviour monitoring was also another fascinating result, although it has no relation to the EPB development. Technology is allowing businesses to track their CVs during service, providing critical safety enhancements by always knowing where the drivers are as well as deterring drivers from acting in a manner that is detrimental to the company.

Responses given by 17 End Users were surprising similar to those from the End Customers, with the same four response categories being present once again, but with an added fifth category: driver comfort. Considering the drivers spend multiple hours per day in their CV, their need for a pleasant cabin is reasonable. Replacing the braking lever arm with a push button will generate a little more space in the cabin compartment, allowing more room for the driver to feel comfortable in.

Types of products that have recently been released on CVs and been well received by the End Customers and End Users have been highlighted in question 2.4. There is a big acceptance of products that can deliver fuel saving/improve vehicle efficiency whilst offering enhanced driver functionality. Braking technologies have also been singled out as particular areas of pleasing recent progress. This all leads positively for the potential EPB introduction as the market would

appear ready to accept it, due to sharing many of the characteristics with the recently successful introduced products.

Question 2.5 was the reverse of question 2.4 as it asked the participant to provide their opinion on which recently (within the past five years) introduced CV feature was the worst or least useful. Understandably, the OEM respondent decided to withhold an answer as it would have been inappropriate to make negative comments about their own company's products. Six responses were received from the End Customer segment, having a single specific theme. Reliability of new products appears to be a serious problem, with maintenance costs increasing as a direct influence of the new technologies added to CVs. Numerous respondents pointed to electrical issues as the main cause of failure. A challenge is subsequently presented to Meritor as the End Customer segment may have a degree of hostility towards the EPB due to previous products not necessarily related to the braking system. During the EPB product introduction stage, Meritor will have to deliver a message through their marketing that the EPB will improve the CV performance and reduce the maintenance costs, not increase them.

A total 12 of replies were received from the End User to question 2.5, with two response categories that were independent from those of the End Customer. As with the previous question, in-cabin features have proved highly important to the End Users, with a number of newly installed cabin compartments showing to be more of an aggravation rather than an improvement. For example, one response points out that an ashtray was fitted to their new CV when they are no longer allowed to smoke in the cabins, taking up unnecessary space. Another points out that the sun visors fail to block sunlight as there are too many gaps between panels. Simple issues such as these can prevent the successful introduction of new products. Care during the design phase will be needed to ensure the operation of the EPB will not suffer from these seemingly minor issues, like where the operating button is placed. Studies into the optimum button position have been carried out by Peter (2012) but has yet to identify a best practise solution.

The second category of features the End Users repeatedly pronounced their dislike of was features that removed vehicle control from the driver. This was seen to devalue their skill set, rather than aiding them for better performance. A conflicting set of desired features has ultimately been shown here as the End Customers clearly want the improved control features to minimise risk but the End Users find them undermining. The proposed EPB will be situated directly in the middle of this conflict, as features such as Aided Hill Start will remove control

from the driver, but increases vehicle safety. A situation has presented itself here to Meritor and their OEM partners as to how to introduce such a component without infuriating the End Users.

The final question in section 2 that provided useful results was question 2.6, which had the aim of finding out if the respondent had issues with the idea of an electric actuation mechanism for the brake system. To reiterate, the respondents were unaware that the basis of the questionnaire was braking systems, so to prevent biasing the latter questions, the same question was asked for a number of different CV systems that are either hydraulically, pneumatically or mechanically controlled. Because these results have no interest to the EPB project, they will be ignored. Question 2.6 produced a very positive outcome for electric brakes, of the 34 respondents 79% did not express any concerns towards an electric actuation system, seen in Figure 3.3.

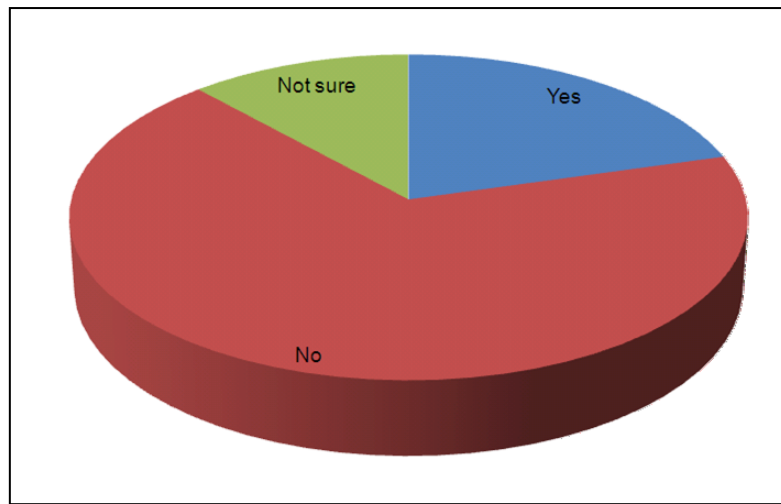


Figure 3.3: Question 2.6 shows little resistance to an electric actuation method.

The remaining 21% of respondents pointed to the possibility of electric reliability and/or failure as the reasoning behind their apprehension towards electrification the braking system, along with the known issues that plagued the passenger vehicle EPB introduction. The former is a serious issue for the EPB, but can be overcome by proving to the relevant benefit segments that the software and hardware behind the EPB is reliable through extensive testing. Unfortunately, the legacy of the passenger car EPB will be more difficult to overcome. With it being impossible to erase memories of past experiences, the doubts will remain over the CV EPB. Replacing the bad experiences with good ones is one of the best methods to overcome this problem, requiring a selection of End Customers and End Users to test-drive a CV with an EPB fitted. Fears should be alleviated by this, providing a path to successful introduction.

3.2.6.2 SECTION 3: Customer Needs

Defining needs for the different customer segments was the aim of the third section. Government policy, business objectives and operational performance were the types of needs this section was intending on exploring, along with other specific issues a particular segment/company/person may have. By understanding their needs, Meritor can better focus their marketing EPB efforts to help increase the chances of a successful EPB introduction. To do this, seven questions were asked with either a pre-coded set of answer offered or left open for detailed responses.

Out of the seven questions, it was only question 3.6 that gave a response of note. One of the main selling points of the EPB is that it will deliver a weight saving to the CV. Understanding how the different segments would benefit from the additional weight saving could lead to a segmented marketing messaging. However, before asking this question (which was question 3.7), participants were asked how much weight, they believe, needed to be removed from a CV before that benefit was realised. Pre-coded answers were given in 20 kg increments, up to 200 kg.

Figure 3.4 pronounces that the general consensus across all three benefit segments is that it is actually unknown as to how much physical weight needs to be removed from the CV before a benefit is realised. A small percentage did suggest the weight reduction had to be in excess of 200 kg to be useful. When comparing this result to that of question 2.3, we can see that weight saving and fuel economy is majorly important to all three segments, yet the actual physical advantage needed to deliver this benefit unknown. Being able to quantify the weight saving gives the distinct advantage of providing to the customers an accurate cost saving they would provide and also the amount their carbon footprint would reduce by. Yet, in the case of the EPB, this would be a pointless exercise as there is clearly a lack of knowledge on the market to understand how this information could be used. By simply stating the advantage in a marketing campaign will be enough for the customer to understand what the EPB offers, allowing them to stipulate the degree of benefit for themselves.

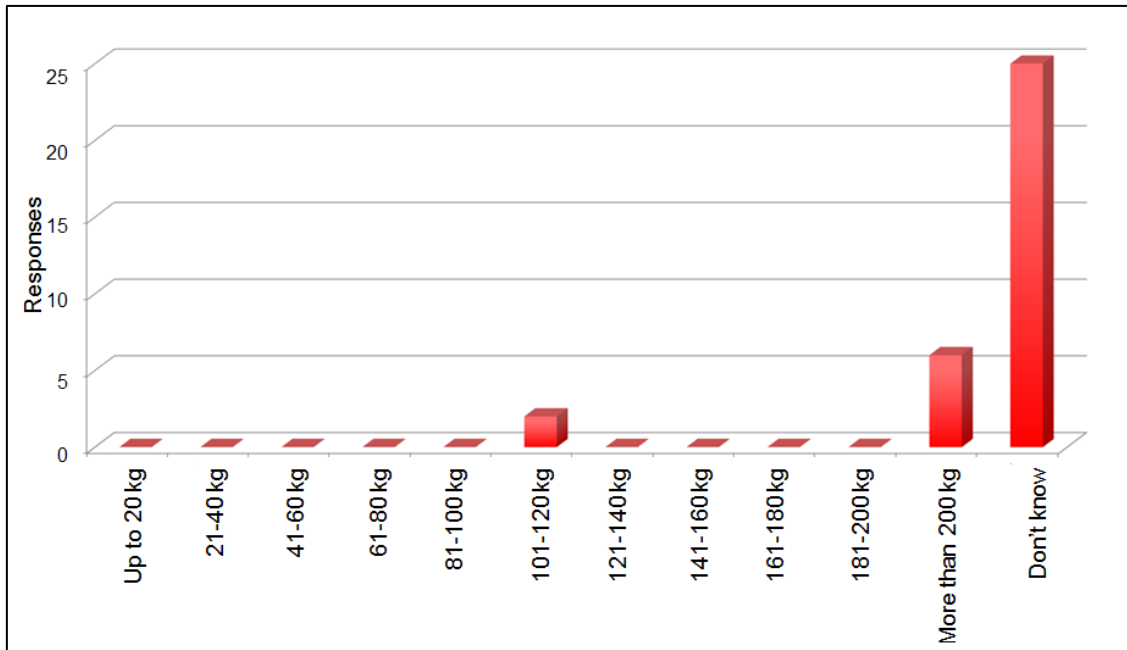


Figure 3.4: Question 3.6 shows the benefit segments don't know the amount of weight loss needed for them to realise a benefit.

3.2.6.3 SECTION 4: Braking and EPB Specific

Until section 4, the questionnaire had been carefully written, not allowing the respondent to know it was for a braking product, in an attempt to keep bias out of previous questions. With complex routing options in the Qualtrics software package, the respondent was forced to complete the questionnaire in order of the questions, whereas it was impossible to control this for those who completed the paper questionnaire. This was an unfortunate result of using this distribution method but was done to maximise the amount of respondents.

Now with the general questions were complete, specific braking questions could be asked without fear of impairing the quality of other questions. A total of 11 questions were asked in section 4, with a combination of pre-coded and open questions once again used. Questions 4.1 and 4.2 were coupled, asking the respondent if they “...ever had, or are aware of an in-service pneumatic brake failure?”. Question 4.1 was pre-coded, allowing those who answered “Yes” to give further details of the failure in question 4.2. In total, four instances of pneumatic brake failure were described by the respondents. One response said the failure as a function of an overheating disc brake/friction pad friction pair. Insufficient cooling or a prolonged braking application would have caused this fault, both of which should have been prevented by design. It should be noted that no date was given, or asked for, with these responses, making it possible that the problem suffered here may have already been overcome.

The last three responses were very telling in that they all highlight the same fundamental issue with the pneumatic system. These responses were:

- “Air leakage”
- “Air loss”
- “Failure of front brake hose, causing lock-up”

Pneumatic systems use compressed air to provide a force that actuates a particular system. If that air was to escape, although it would not be hazardous like hydraulic systems, the system develops a fault and subsequently breaks down. Two responses given to question 4.2 specifically state that they have suffered pneumatic braking issues as a result of air escaping the brake system. The third response may not be loss of air, however, the brake hose pipe is a component of the pneumatic system so if it fails, the pneumatic system fails.

Questions 4.3 and 4.4 were in the same form as 4.1 and 4.2, but specifically ask for parking brake failures, rather than the whole system. Five responses this time were collected, giving a very similar story. Issues with the air delivery either directly to the parking spring chamber or with a secondary pneumatic problem, was shown to be problematic for the parking brake system. The comment *“The air in the tank was low and the parking brake was jammed on”* vividly demonstrates this point. Here, either the compressor unit was faulty or there was a leakage in the air supply, producing an end result that causes the brake system to fail. A second comment stated that the *“Brake would not release. Had to drain out all the air before building pressure up again before brake would work.”* Having to drain the air pressure and building it back up again may not be an expensive problem but it is an annoyance that takes time away from the End User, reducing their daily efficiency. Again, the fault here is not the brake units themselves but with the components the brakes are dependent on.

Brake manufactures’ like Meritor are exposed to the risk of a damaged brand reputation as a consequence of being dependent on products developed by an alternate company. For example, when a leakage is found in an airline, it is a failure in the brake system that gets detected, causing a negative impression towards the brake system. Questions 4.1 to 4.4 have shown a major concern for Meritor but also an exciting area to exploit in the future. From section 2, it is clear maintenance costs are a big factor in the buying decisions for the End Customers and section 4 thus far, has determined that the majority of brake related issues are a result of the pneumatic system. Therefore, if Meritor can market the EPB as a maintenance reducing item, as well as delivering all the outlined performance and weight saving benefits, the probability of a successful introduction is increased.

The fundamental difference between the parking spring chamber and the EPB is that the actuation method is shifted from pneumatics to electrics. It is proposed here that independence from the pneumatic system should be one of the key selling points of EPB, as it will reduce CV maintenance costs. In doing so, Meritor (in conjunction with their OEM partners) will need to prove to the End Customers and End Users that the electric system is more reliable and less prone to failure. They will also have to retrace the passenger vehicle EPB introduction and see what problems it had and ensure the same issues do not present themselves again. By finding this additional benefit provided by the EPB, the conducted benefit analysis chart produced required updating, which is shown in Figure 3.5.

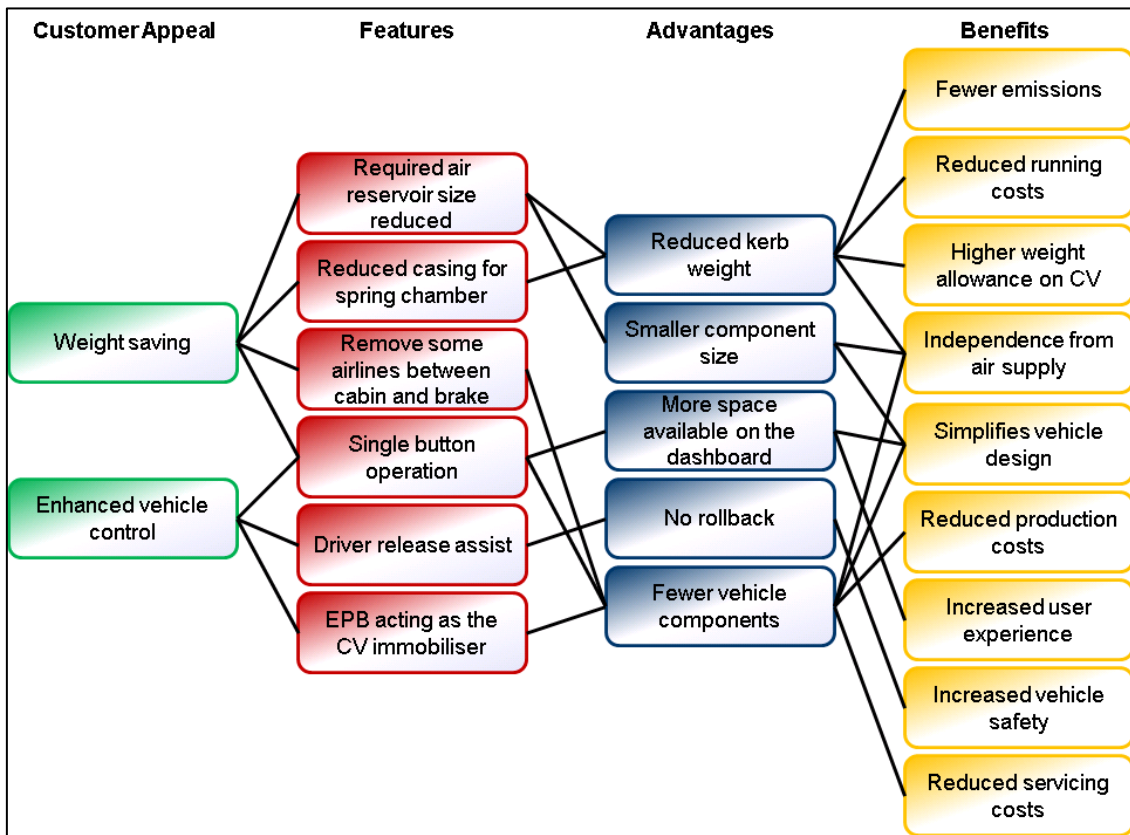


Figure 3.5: Improved Benefit analysis to include independence from air.

Question 2.5 had a dual purpose, firstly to discover the approximate proportion of people aware of the EPB, with the second being to filter out those unaware, due to the remaining questions in section 4 being opinion based on the EPB. To prevent the introduction of bias, like with the restraint of mentioning brakes in the questionnaire, this was the first time the EPB had been mentioned. Being nearly 10 years after it was first introduced, Figure 3.6 shows that the EPB is still relatively unknown as approximately only 1/3 of respondents recognised the technology. Evidence gathered here would suggest that the general public are still mostly unaware of the

EPB, an unfavourable situation for the technology. Demand for the product cannot be stimulated if people do not know about it, let alone understand the benefits it can bring. Therefore, one of the key focuses of Meritor's marketing must be simply to promote the EPB and develop the awareness of its existence.

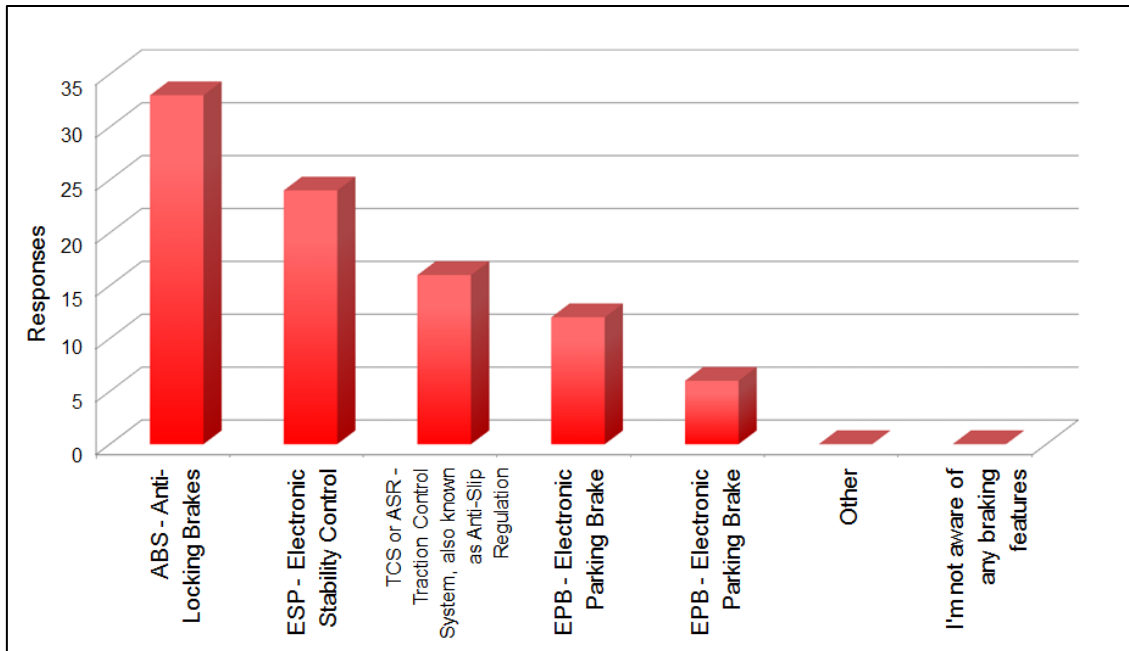


Figure 3.6: Only 1/3 of respondents knew of the EPB component.

Results of the following questions do not portray a more attractive picture for the EPB either. Starting with the four received responses to question 4.7, from the End Customers who said they were aware of the EPB. No positive responses were received, when asked whether they believed the EPB would be a beneficial enhancement to CVs based purely on their current knowledge of it. There was a mixed response from the End Users, showing a level of ambiguity towards the EPB from within the segment. Although there was only a single respondent from the OEM segment, they did hold a more positive view of the EPB and expressed they did believe it to be a beneficial addition. Overall though, considering the End Customers are the most critical segment in terms of deciding what CV to buy/lease, the market generally needs informing of its presence and what benefits are on offer by the EPB.

Associated fears with the EPB introduction, according to the results of questions 4.10 and 4.11 are electrical failure, a result matching that of question 2.6. It was previously suggested that Meritor need to prove the reliability of the electric system to their customers' as part of the introductory marketing to elevate these fears; questions 4.10 and 4.11 only enhance the necessity for this suggestion to be acted upon. As part of the product development and

certification, Meritor will have to conduct a series of test to prove the EPB is safe. The suggestion being made here is to incorporate these results into the marketing.

3.2.6.4 SECTION 5: Brand Awareness

Brand awareness was not the main topic of this questionnaire but a short investigation was decided to be conducted as it may generate some interesting additional information. This section consisted of only four questions, with no specific results being generated by the first question, leaving three remaining for analysis.

Question 5.2 used a five point Likert scale and asked the respondent to state whether they agree or disagree to two separate statements, and by how much their agreement/disagreement is. The first statement read *“The brake system is highly important to the overall CV performance.”* Figure 3.7 presents these results and a very strong agreement is present, meaning the brake system design is highly important aspect of CV design. In fact, the agreement was so strong that 88% of the responses selected either “Agree” or “Strongly Agree” with only 6% choosing to disagree with the statement.

The second statement investigated the market opinion as to whether there was any product differentiation from the various brake manufacturers’. The statement read *“There is little difference in quality between brake systems from the various brake manufacturers.”* Negativity reversal was used here in an attempt to prevent pattern answering, as advised by Brace (2004). Unfortunately, 66% of the respondents did agree with this statement, as shown by Figure 3.8. Such a result would suggest that the braking industry does little to distinguish their own products from competitors, thus companies compete on cost rather than quality. These two results are misaligned, with the braking system seen as highly important to the CV design but manufacturers’ compete on a cost basis rather than quality.

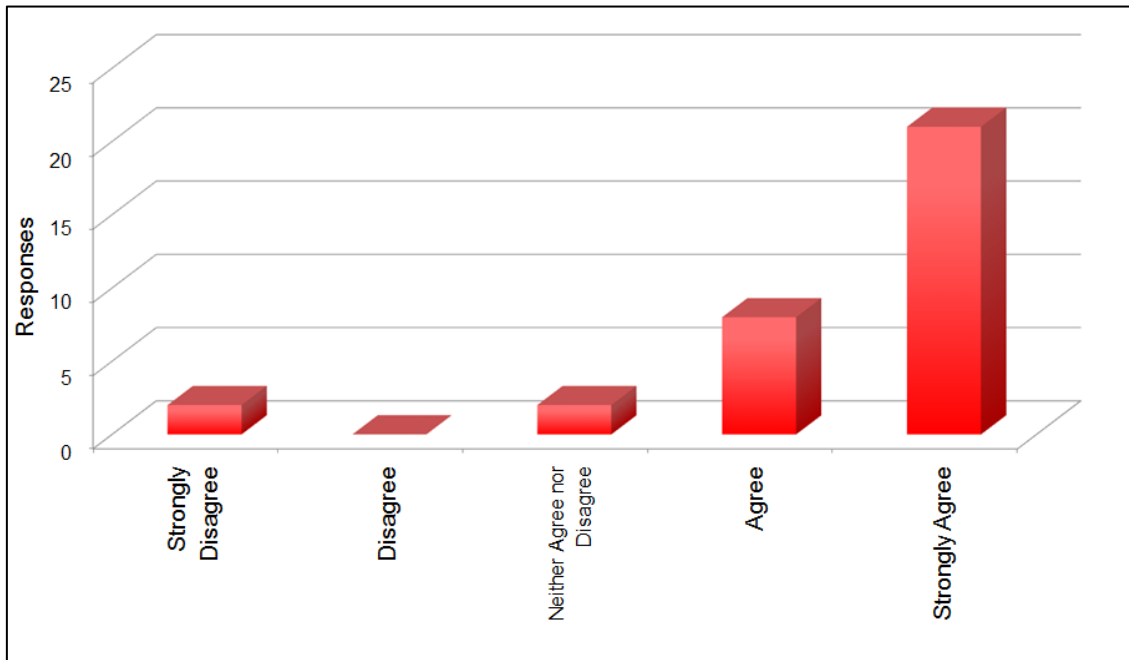


Figure 3.7: People strongly agree with the statement *“The brake system is highly important to the overall CV performance.”*

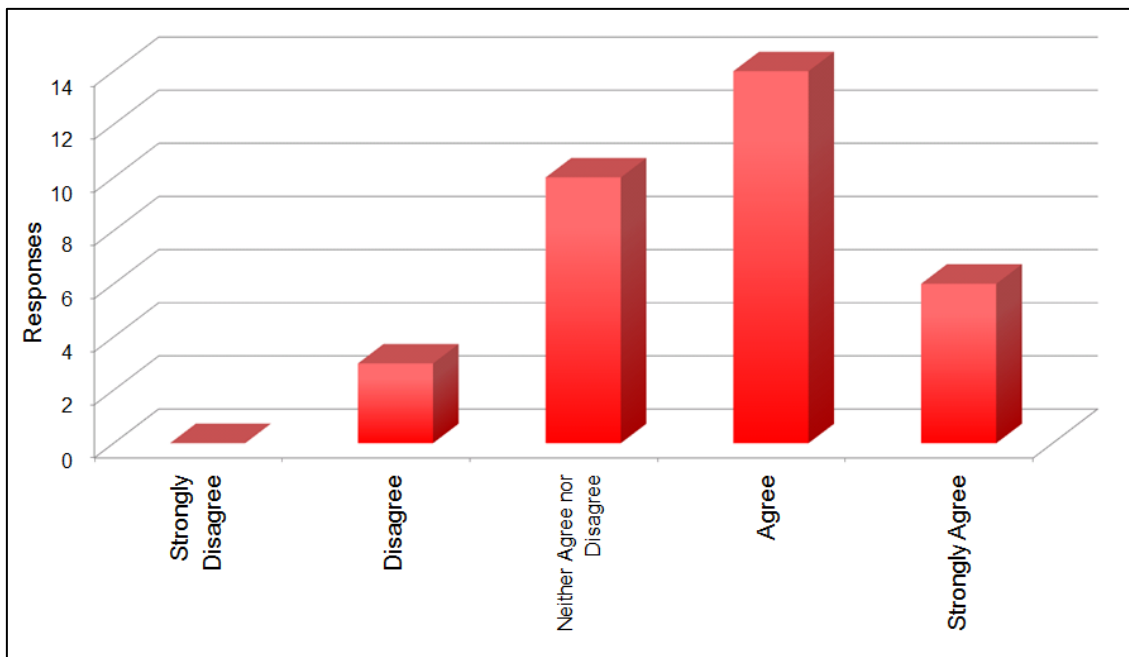


Figure 3.8: People generally agree with the statement *“There is little difference in quality between brake systems from the various brake manufacturers.”*

With the lack of differentiation within the CV braking market, it was unsurprising to see the results of question 5.3 show that 49% of respondents weren't aware of any CV brake manufacturers'. Of those that did, a worrying result for Meritor was achieved as their brand was

shown to be the least recognisable of all, as only 24% of respondents said they had heard of the Meritor brand.

Section 5 has highlighted a huge opportunity available for Meritor to bridge multiple issues with the EPB introduction. By delivering a high quality product first to the market, combined with a targeted marketing campaign, Meritor can distinguish their products from those of the competitors. For example, the previously discussed IAA show, held in Hannover in 2010, gave Meritor an excellent opportunity to showcase how good their products are first-hand to the End Customers, not just to the OEMs but this was not taken. The next opportunity would be the IAA Frankfurt Motor Show in 2013 then the IAA Hannover show in 2014. Demand for the product might begin to generate as a result. A similar result can be achieved with the End Users by advertising in selected CV driver magazines and alike, detailing the specific benefits to them. With a higher perceived quality, Meritor could potentially justify a more expensive price for their products.

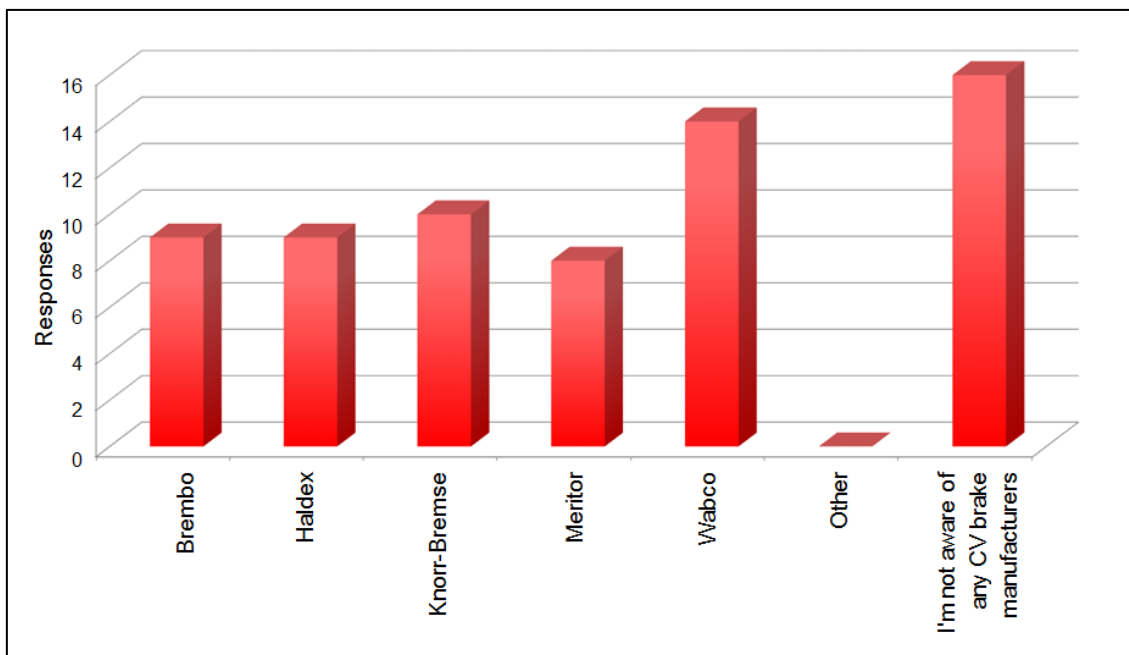


Figure 3.9: Meritor is the least known brake brand of brake manufacturers.

3.2.7 Explanatory Questionnaire Discussion

By deploying the self-completion questionnaire via both paper copies and an E-mail URL embedded version, opinions of 33 people were successfully obtained towards the first three questionnaire objectives, set out by the benefit analysis. To reiterate, the research aims where to find:

1. What is the current perception of the EPB in the separate benefit segments?

2. Does the EPB meet the needs of the beneficiaries?
3. Are there any further benefits on offer from the EPB?

Initial power analysis showed that the End Customer and End User segments required a minimum of 64 responses each to prevent Type II error from occurring in statistical analysis. Unfortunately, the actual number of responses received was below this figure, making the calculations of ψ values of 98%, 96% and 83% for the OEM, End Customer and End User segments respectively. Converting these ψ into the more useful form of the power of the test, it is seen that the probability of an actual discovery from these samples investigated are 2%, 4% and 12%. Little reward will be achieved from conducting significance testing on the EQ results as the results are likely to be statistically erroneous. Yet, taking the advice of Carver (1978), results have been presented and used regardless, even with no statistical relevance.

The first research aim was to determine what the current perception is of the EPB. Reactions of the initial questionnaire towards that the EPB were very negative as only 36% of the respondents recognised the product, and of those aware of it, only 25% believed that it would be a useful introduction on a CV. Two separate issues are identified here; firstly, knowledge of its existence has not spread, with the public in general oblivious to it, and secondly, barriers to successful market entry are in place as a result of current perception of the technology. Marketing based on promoting the EPB and outlines the benefits received by its installation on a CV should be the underlining message delivered by Meritor.

These issues are unfortunate because the evidence would suggest the market is ready to accept the EPB, based on the benefits offered match those desired by the benefit segments, braking technologies developments are seen as important and the low resistance to an electric actuation method. Current trends have shown recent CV products, which have been widely accepted by the various segments of the braking market, offer very similar benefits to those of the EPB. Furthermore, braking improvements were also singled out as new CV features that have made vehicle improvements. The conclusion that the market is ready for the EPB was based on these combined results.

One of the most important findings of the EQ was the reliability of pneumatic components is actually hampering the overall braking performance of Meritor products, in both the dynamic and stationary states. Multiple examples of pneumatic failure were disclosed, causing additional maintenance costs to the End Customers and undue frustration to the End Users, whilst damaging the Meritor brand. Removal of the pneumatic reliance was therefore shown to be a key selling point of the EPB, a benefit previously undiscovered prior to conducting the EQ.

3.3 Knowledge Based Questionnaire

Five research objectives were defined during the questionnaire planning stage, with answers for the first three provided by the EQ. In fact, from the results a marketing strategy based on improving the knowledge of the EPB was suggested, which is actually the fifth research objective.

A secondary questionnaire was conducted with two purposes, firstly with an intent on finding which benefit is most important to the segments and secondly, to provide an opportunity to validate whether a knowledge based marketing is correct to use. Examples of alternative methods are the product focused and people-centric marketing strategies, which were successfully deployed by Intel.

To test which benefit is seen as more important to the relevant segments, the respondent was individually given a description each EPB feature (see Figure 3.5), followed by a simple closed type question asking whether this was ‘useful’ to them. A pre-coding answering system was used, allowing the respondent to answer either “Yes,” “No” or “Don’t know”. When a “Yes” answer was given, the respondent was asked to further explain why they believed it was useful. By giving the respondent the EPB features, it was intended to see if the respondents understood how the feature would be useful to them and ultimately, if they subconsciously produced the same end benefits as those identified in Figure 3.5. Greater benefit importance will be attributed to the number of times the benefit is cited, in the absence of any prompting.

With the same individuals asked to complete a secondary questionnaire as the first, it was clear from the outset that the questionnaire had to be much shorter in length. The questionnaire administrator is reliant on the cooperation of the respondent, by asking them to complete another lengthy questionnaire is likely to irritate them. It was subsequently decided that target a questionnaire completion time was set at five minutes, hence why a simple pre-coded, closed questions were asked.

To test the validity of a knowledge based strategy, the second questionnaire provided the respondent with information about the EPB, such as what it was, how it worked and what product it was replacing. All respondent opinions therefore had a known anchor, ensuring each individual was able to provide a response, if they so desired. Strategy validation is then possible by asking the educated respondent whether they believed the EPB to be useful and compare back to question 4.7 of the EQ.

Thus far, six questions were identified by default whilst deciding what information was required from the questionnaire. A seventh was also found when investigating whether there was any additional information to be subtracted from the analysis. Independence from the pneumatic system was found to be a benefit offered by the EPB from the EQ, as well as being suggested as a key selling point. Conformation was sought to whether it is actually seen as a benefit, so a question was added to the questionnaire. For the sake of the questionnaire flow, the pneumatic independence question was asked in the same manner as the features questions. Likewise, a further question for whether the respondent believed the EPB itself would be useful (as described above) was also written in this style. One other question was added and written in the same style simply asked if the respondent could think of any more advantages.

Almost all the information required for the second knowledge based questionnaire (KBQ) was defined, completing the first stage of Brace's three step planning process. The only other information required from this questionnaire was who the respondent was and what benefit segment they belonged in, fulfilling the requirements of stage two. The generalised questionnaire flowchart is shown in Figure 3.10, completing Brace's planning process.

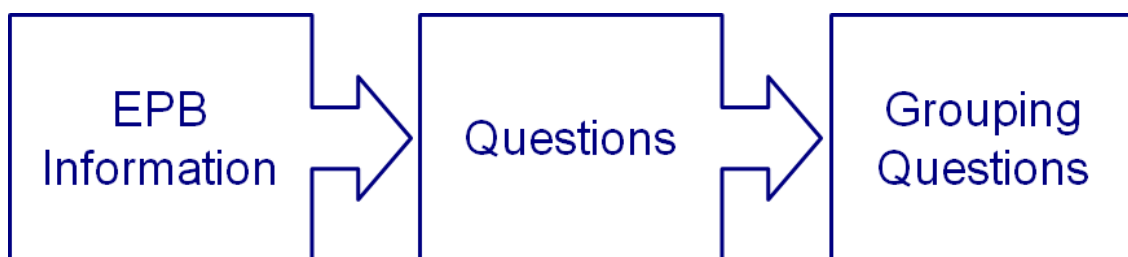


Figure 3.10: Knowledge based questionnaire flowchart.

A trial questionnaire was once again sent out to three different sources before going live with the final questionnaire. Apart from minor grammatical errors, no major changes were suggested. Therefore, the questionnaire shown in Appendix E went live, collecting responses for two months before results were analysed. The same method of using both a self-completion web-link and paper questionnaires was used once again to collect data from the different segments.

The KBQ was started on 42 occasions in total. After reading through the introductory sections where the respondents were given information on the EP, only 31 people remained and participated in the questionnaire. In total, 29 people filled out the questionnaire to its conclusion, giving a completion rate of 69%. With 11 participants not answering a single question, the results statistics were be skewed unfavourably.

Removing the 11 respondents who failed to answer any questions increases the completion rate to 94%, which is arguably a fairer representation. Reasoning behind using this latter value is that if the respondent failed to answer a single question then it is argued the questionnaire was never actually started. It is feasible that the respondent clicked on the link by mistake, opening the questionnaire in the Qualtrics software, recording the response. Alternatively, after reading the introduction, the respondent may have thought the questionnaire was irrelevant to them, hence why they chose not to continue.

Section two of the KBQ was the most important as this is where the detailed EPB questions were asked; 30 respondents completed this section in full, with one respondent answering only four questions before stopping. Unfortunately, one respondent failed to answer questions in the third section, making it impossible to identify a total of two respondents' respective segments. These two incomplete results were ignored only when individual segmented results are being discussed. OEM participation to the KBQ improved from only one in the EQ to four second time round. A further 16 questionnaires were completed by End Users, leaving the remaining nine responses coming from the End Customer segment.

Increasing vehicle fuel efficiency has been shown as one of the key benefit the EPB should be sold on. The first EPB feature described to the respondent was the decrease in both size and weight of the parking chamber, which realises the aforementioned benefit. An encouraging result to the first question is show in Figure 3.11 as 58% of respondents did see this as a useful CV feature, with only 23% rejecting this implication.

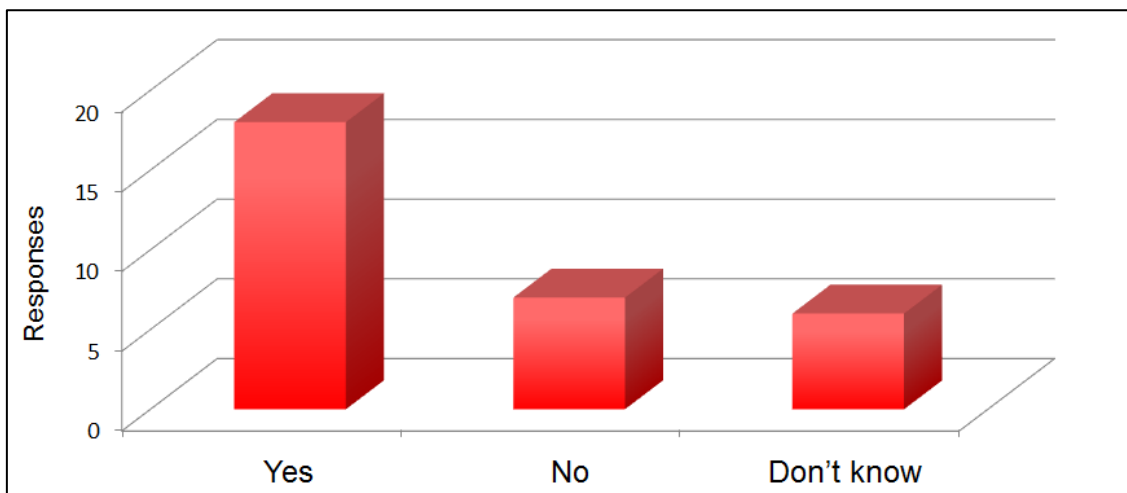


Figure 3.11: 58% believes reducing size and weight of the parking chamber is a useful feature.

OEM's understand the benefit of weight saving on vehicle components, demonstrated by all the OEM responses to the first question being positive, with two opting to comment. Reducing the

unsprung mass will decrease the loads exerted on the axle was the first, with the second pointing to the space saving benefits on the tight packaging constraint advantages it would have on rear axles. The former is an example of the expertise held in the OEM segment, allowing a more detailed explanation as to how the feature will provide the benefit.

End Customers also recognised the advantages of reduced weight as the ratio of positive to negative responses was 6:2, with one undecided. All six positive respondents chose to comment on their beliefs, with increased payload being the overwhelming reason as to why this feature would be useful to them. Two specific reasons were given why weight reduction was generally seen as advantageous; direct mention of the impending Euro VI emissions legislation was one, with the other being to counter balance some of the additional CV weight introduced by other new CV features, such as the Adblue system and its required additional tanks. Although it is asked directly in question seven, one respondent made reference to the freedom from pneumatic parts by saying “...I assume there are less air components to go wrong and less air required as the parking brake is electronic.” This demonstrates the importance of removing the pneumatic system and indeed identifies it as an important benefit.

The least interested segment for this feature was the End Users. Only 50% of the responses said they believed it to be a useful feature with efficient fuel economy described as the greatest benefit from it. Once more, the independence of pneumatic parts was commented on, saying “...with air brakes, pipe could get frozen and brakes not being able to move.” Fuel economy has been shown to be important but the issue of air supply appears perhaps holds larger implication on the success of the EPB introduction. Again, it is this benefit that has had a direct mention to rather than vehicle efficiency. However, 25% of End Users answered “No” to question one, showing there is still some scepticism as to whether the amount of weight saved by the EPB actually does make a difference to a CV. Looking more generally at the supply chain, the level of positivity towards the size and weight saving benefits reduces moving downstream, i.e. the End Users are the least positive about the EPB compared to the OEMs. Yet, with an overall 67% “Yes” response, it can be concluded that the weight saving advantages is seen to deliver a benefit.

The second and third questions found similar results to the first, which is unsurprising considering the three features that give a direct weight saving were grouped together by design. Replacing the pneumatic airline with copper cables (question 2) was described as useful by 52% of respondents (Figure 3.12); increased reliability was cited as one of the greatest advantage offered by the feature. Furthermore, it was said to reduce maintenance costs, due to air loss no

longer being an issue, matching the conclusions drawn from the EQ. Easier packaging of the components was another common statement and it was made at least once in each of the three benefit segments.

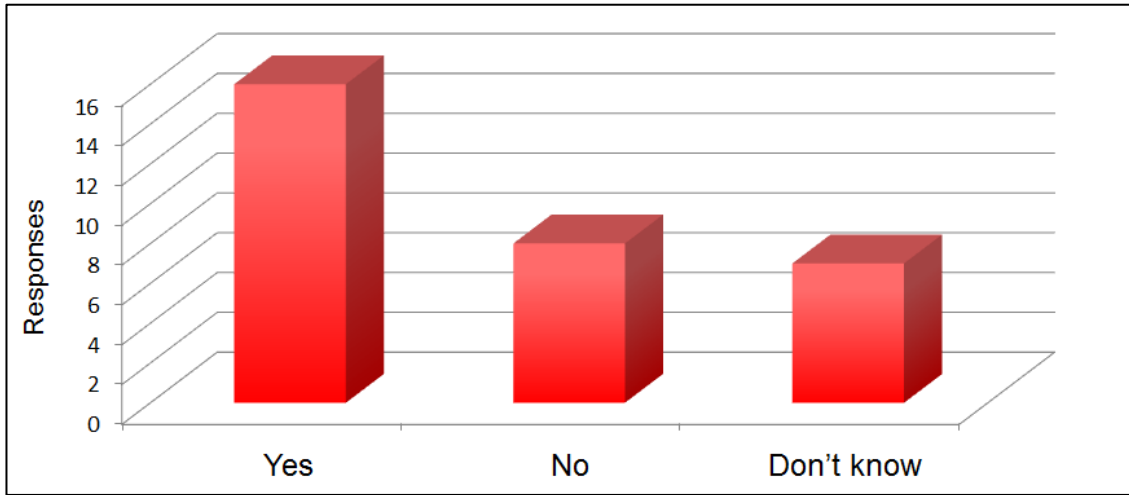


Figure 3.12: 52% of respondents agree that removing pneumatic parts is a useful CV feature.

Responses to question 3 were indistinguishable between benefit segments. Overall, a response of 58% believed that reducing the air reservoir was indeed a useful CV feature for all segments (Figure 3.14). Reducing the compressor size was seen to ease packaging issues, aiding the OEMs design process. Interestingly, the End Customers and End Users both saw this feature as an advantage because it creates more space for other technologically advanced products to be installed on the CV as well as making the vehicle cheaper, if only marginally.

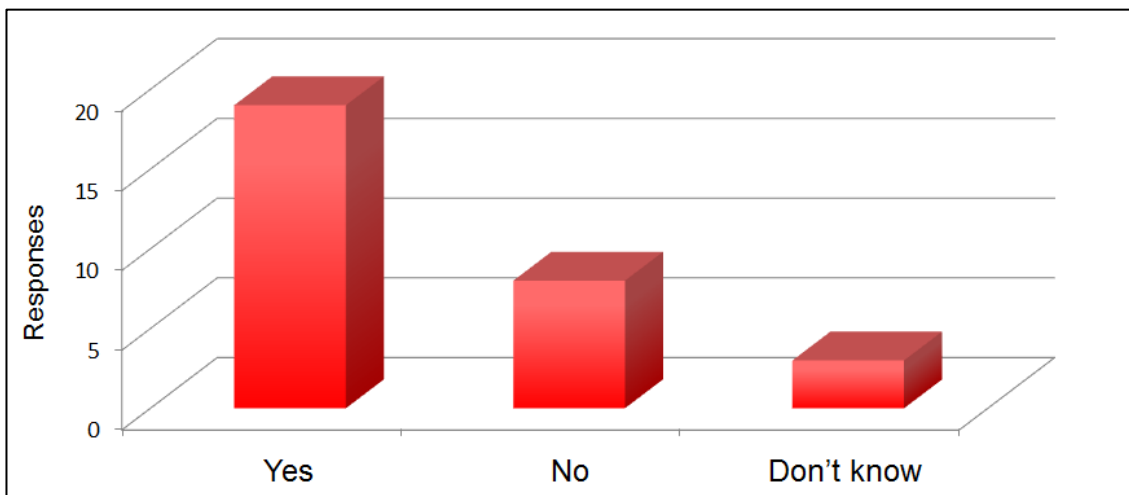


Figure 3.13: Reducing the compressed air reservoir was described as a useful CV feature by 58% of questionnaire respondents.

Question four takes the KBQ focus away from weight removal and places it on advanced driver features that the EPB offers. A brief description of how the EPB could interface with the CV electronic control unit (ECU) was presented to the respondent before describing the ability to prevent rollback during a hill start. A noticeably high, favourable response was given by both the End User and OEM segments with 12 out of 16 and three from four respondents respectively agreeing that the aided hill start feature is useful (Figure 3.14). End Customers were only slightly less optimistic about this feature as the “Yes” response fell to 67%, itself still an optimistic result.

Open responses towards the aided hill start feature described, for the most part, produced the same advantages and benefits pointed out during the benefit analysis. However, there was one advantage described which was overlooked in the benefit analysis stage. By allowing the brakes to hold the vehicle stationary whilst on a gradient, the driver will not be tempted to hold the CV via the clutch. A reduction in clutch wear will be the result of this, benefiting the End Customers mostly as it will be another source of reducing maintenance costs.

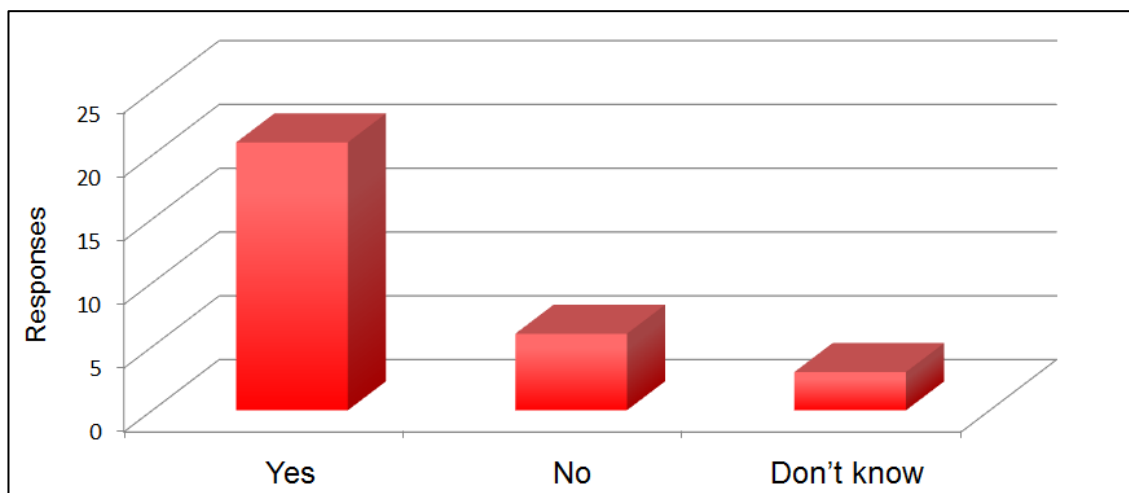


Figure 3.14: Aided hill start functionality is useful according to 70% of respondents.

Figure 3.15 displays 63% of respondents like the additional security benefits received by an EPB. However, unlike the previous questions, this figure does not tell the full story. The question specifically states the use of the EPB as a secondary or replacement immobiliser, yet one End Customer and five Ends Users perceived the feature to be an automatic braking function, applying the brake when the vehicle stopped or if the driver was to leave the cab without manually applying the parking brake; other responses were generic increased vehicle safety replies. In light of the comments made, it is more appropriate to replace the EPB immobiliser feature description with “Automatic brake application.” By making this change, not

only is the Immobiliser feature captured, but also all the additional features suggested by the respondents as well.

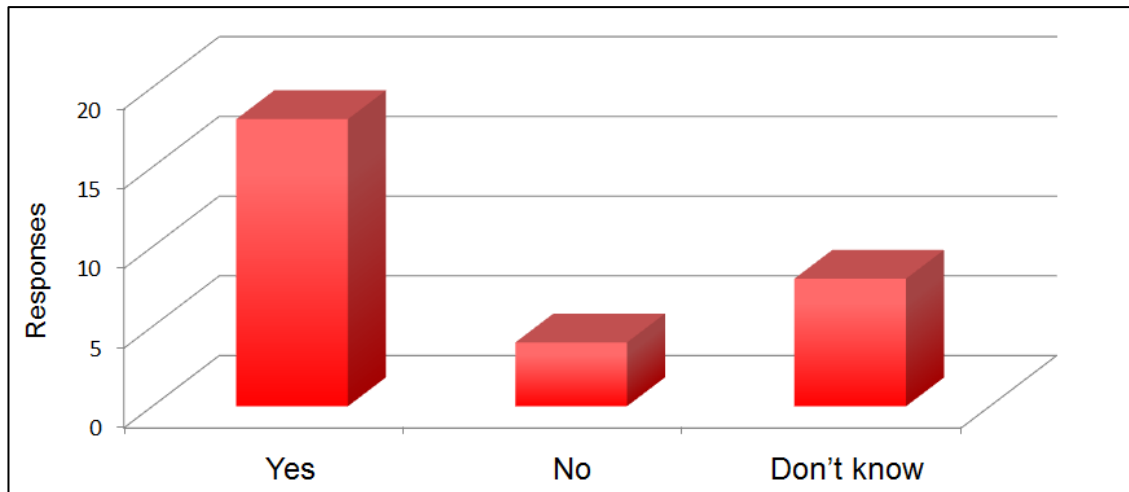


Figure 3.15: Use of the EPB as an Immobiliser appears

Question six brought about the final EPB features question, derived from the benefit analysis. Replacement of the operating lever arm, located in the driver cabin, with a smaller electrical push button was the feature in question. Again, a large proportion of the responses were positive towards the feature with 50% stating they believed the simple push button to be a useful addition to the CV (Figure 3.16). Installation of the electric button rather than the pneumatic valve combined with the complexity of the required airlines was cited by one of the two OEM respondents who commented as the greatest use of this feature.

The most scepticism of any of the EPB features was also shown with the push button installation as question six received the highest volume of “No” responses than any other question, at 30%. It was the End User segment that showed the greatest amount of dissatisfaction as the ratio of Yes to No responses was 7:6. Although it was stated to only describe how the feature was useful if a Yes answer was given, reasons behind these negative responses were given anyway. For instance, one comment stated that *“incidents of falsely applying the brakes are extremely dangerous in certain circumstances...,”* which is feasible if the button is located in an area where the driver often places his/her hands, i.e. close to the indicator switch. Another common concern was that the lever position gave a visual indicator to the driver that the parking brake was applied, as well as having a ‘Check’ position when coupling a trailer unit to the truck. A simple light system on the dashboard would overcome both these issues, at a minimal cost. As digital display units are become common place in vehicles, these visible signals may even come at no extra cost.

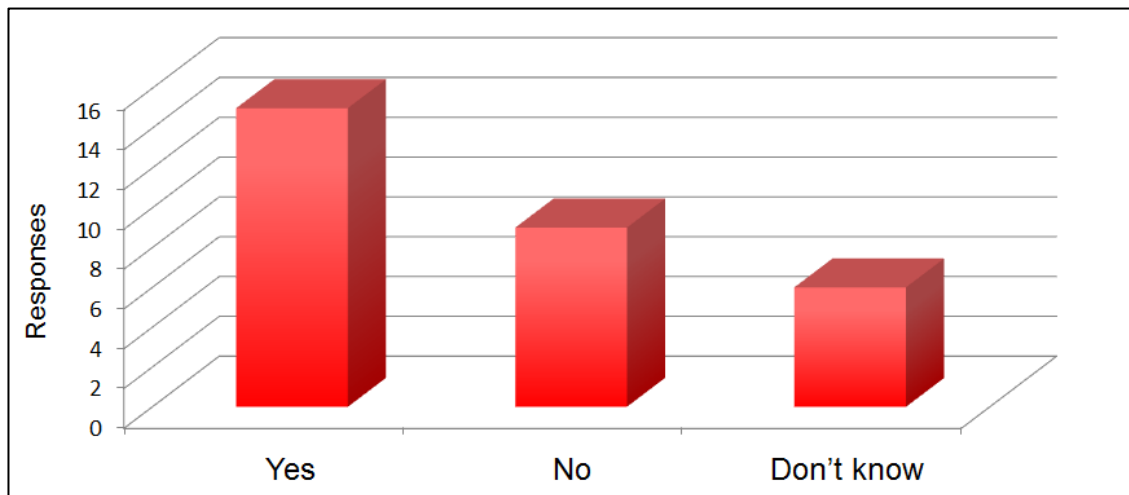


Figure 3.16: Single button operation is seen as useful, but with more scepticism than other features.

Results from the KBQ thus far, have shown all the features do undoubtedly provide recognised advantages to all three of the benefit segments. Many of these described advantages had already been discovered during the benefit analysis process. It was important that these results were generated as they represent a validation to the conducted benefit analysis. Knowing that all the segments of the braking market realise how the EPB can provide benefits to them, delivers a significant amount of confidence, with respect to the long-term success of the product. A few novel suggestions to the advantages on offer were also offered, strengthening the marketability of the EPB.

The remaining questions were no longer focused on the derived benefit analysis features. From the EQ, the idea of the brake system being independent from the pneumatic air supply was identified as a real advantage, predominately to the End Customer segment, and should be used as a key selling point of the EPB. Question seven directly investigates this hypothesis by asking respondent whether they believed the removal of air supply from the parking chamber was useful. A negative response to this question would have resulted in the rejection of the proposed marketing plan suggested in section 3.2.7. Thankfully, Figure 3.17 shows that, of the 19 respondents who had an opinion, 15 answered “Yes” to the question, which equates to 79% of respondents whom expressed an opinion.

Furthermore, in the End Customer segment, the positive “Yes” responses outweighed the adverse “No” replies five to three, with only a single person undecided. The argument was previously made that this segment should be targeted with the reduced maintenance cost benefit. Comments, such as there is *“less to go wrong and less air required...”*, confirms the End Customers have an understanding of the benefits on offer, making this a viable tactic.

Interestingly, of the 11 undecided people eight were from the End User segment, accounting for half of this segments responses, with the remaining all selected “Yes”. Therefore, not a single End User believed removing the air supply from the parking chamber would be detrimental to CV performance. However, with half of the responses being ambivalent towards pneumatic removal, a degree of hesitancy is clearly still present amongst CV drivers. In an attempt to find reasoning behind the high “Don’t know” response, question seven was subdivided even further with respect to the respondents’ age and also gender. No correlation was found between older and younger respondents as there was a relatively even split between the “Yes” and “Don’t know” answers for all the age ranges provided in question 10. As there was only one female driver, it is impossible to make a legitimate conclusion about the opinions of female CV drivers, due to a lack of evidence. It will be noted however that the female respondent was indeed one of the eight people who selected “No” for question seven. Ultimately, based on the evidence of the KBQ, attitude anchors for the End Users appear random.

Combining the results from question seven with results from the previous questions in the KBQ, the evidence is quite resounding. Removal of pneumatic parts and/or systems has shown vitally important and should be in tandem with the increased efficiency benefit, for marketing purposes.

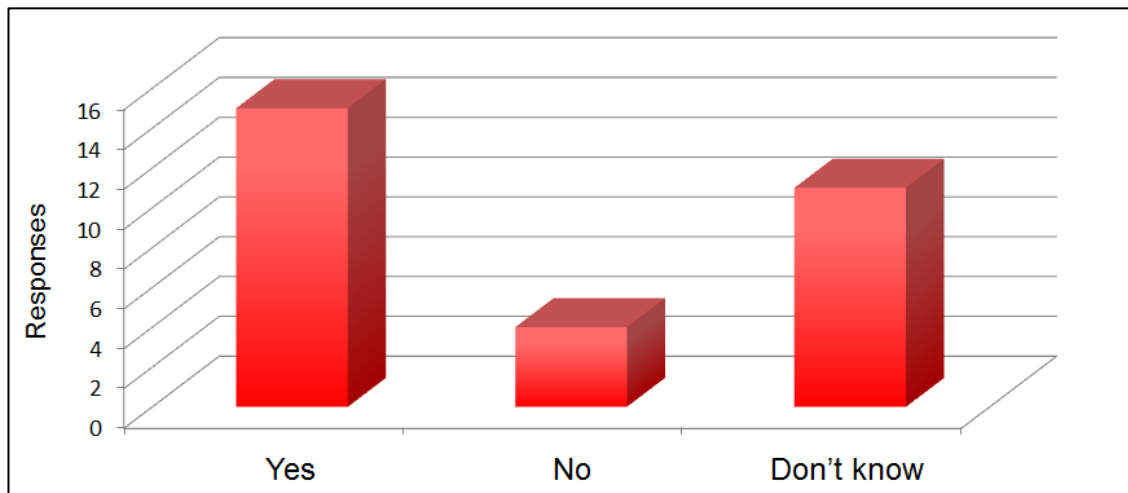


Figure 3.17: The parking chamber will no longer need an air supply to operate is useful according to 50% of respondents

The penultimate question simply asked the respondent whether there were any further advantages of the EPB which had thus far, been disregarded. In total, there were five additional advantages suggested; no suggestions came from the OEM segment, three came from the End Customer segment and two from the End Users. The first of the End Customer suggested advantages was that the EPB would allow quicker response times, both in general use and in

secondary braking. Pneumatic systems suffer from lag and compliance issues, resulting in a delay between the driver pressing the brake pedal or moving the parking lever to the brake being fully applied. By replacing the pneumatic system with an electrical system, the reaction time between driver application and brake application is limited by the sampling rate of the ECU. Considering it is common for processors to run in the mega samples per second region, brake application will appear virtually instantaneous to the driver, minimising the rollback feature experienced when parking the CV.

Coupling trailer units to the truck requires various connections between the units. The second End Customer suggestion was that making the parking brake connection electric, utilisation of a single connector to unite the parking brake and lighting systems can be achieved. Workforce efficiency will be improved, if only slightly, as the time taken to couple the units together is reduced. Also, the packaging issues are subsequently eased with fewer components on both the truck and trailer.

The third and final End Customer suggested feature would increase the safety of the CV by eliminating slow speed, reversing collisions. Being connected to the vehicle ECU, the braking system now has the ability to communicate and interact with other vehicle sensors, as described with the aided hill start feature. Rear parking sensors are becoming more standard on vehicles, indicting to the driver, either by a visual and/or a sound stimuli, if they are getting too close to an item/person behind the vehicle. If the driver chooses to ignore the alarm, the vehicle will still impact whatever is behind the vehicle. By allowing the EPB to communicate with the rear parking sensors, it would be possible to override the driver and force the vehicle to stop, preventing a collision and saving potential repair costs.

The first End User suggestion also stems from the removal of the pneumatic system, as there will no longer be a need to dump air when applying the parking brake, making the process much quieter. Noise issues are currently the greatest problem in the braking industry with vast amounts of the research effort being exhausted on understanding the brake squeal issue, as will be discussed further in Chapter 4. Yet, as this respondent highlighted, brake squeal is not the sole noise issue related to braking. Air dumping is short in duration, but can be considerably loud and startling for close pedestrians and cyclists. In city buses consistently apply the parking brakes, making them a particular problem. By using the EPB system, the parking brake application noise will be significantly reduced, with the noise source being a much quieter electric motor.

The ability to “future proof” the CV was the final advantage offered by the End Users. New technologies are being developed for vehicles all the time, with the vast majority having an ever increasing reliance on computer control. Like with the rear parking sensor suggestion, by allowing the EPB to communicate with the ECU, new components can be designed for a CV that can integrate and improve the EPB functionality.

Improvements have been made to the original benefit analysis and are shown in Figure 3.18. All the suggested advantages made by the respondents of KBQ have been added. These suggestions also led to a ninth benefit being added, which is the ability to meet legislative requirements. Clearly this is important to any CV with regards to the impending Euro VI regulations, but this also refers to future regulations on noise as well. Being able to offer a solution now to a future problem saves on the long term costs of the company.

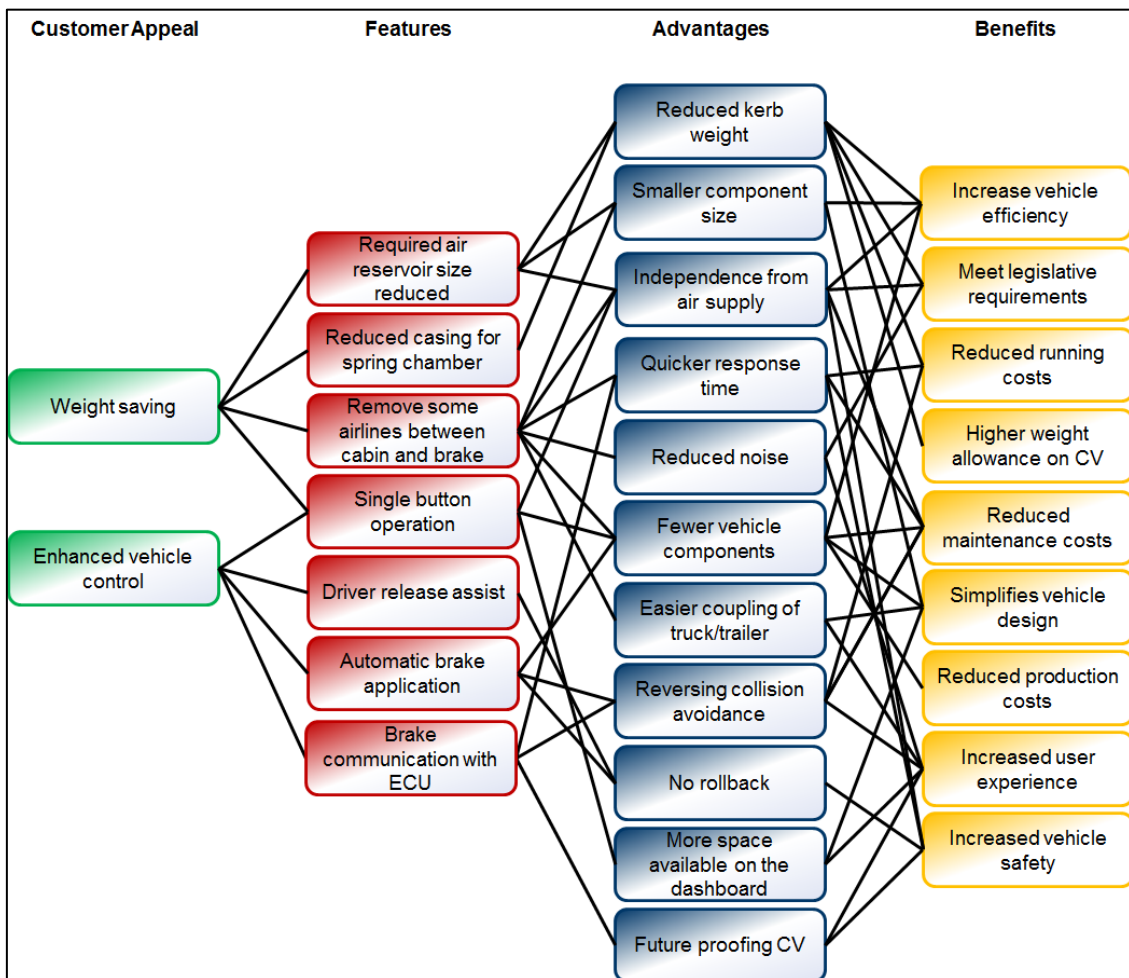


Figure 3.18: Final benefit analysis

To conclude the second and main section of the KBQ, the most important question of all was asked. At this point, the respondent had read through all the EPB advantages, and possibly

making a few suggestions of their own, as well as reading the educational information supplied in the first section. To test the effectiveness of the knowledge based marketing strategy, the final question asked simply whether the respondent believed the EPB would be a beneficial product on a CV.

A large amount of optimism should be taken from the results of question nine as, of the 30 received responses, 66% indicated that they did believe the EPB to offer CV benefits, shown in Figure 3.19. These results can be directly compared to question 4.7 in the EQ, where the same question showed that only 25% of uninformed respondents believed this. A huge improvement in the attitude towards the EPB has been demonstrated merely by educating the audience on the products functionality and the resultant advantages they will receive. Subsequently, based on the results presented from both the explanatory and knowledge based questionnaires, it is advised that Meritor deploy an informative approach to their EPB marketing, for the greatest chance of maximising the EPB success.

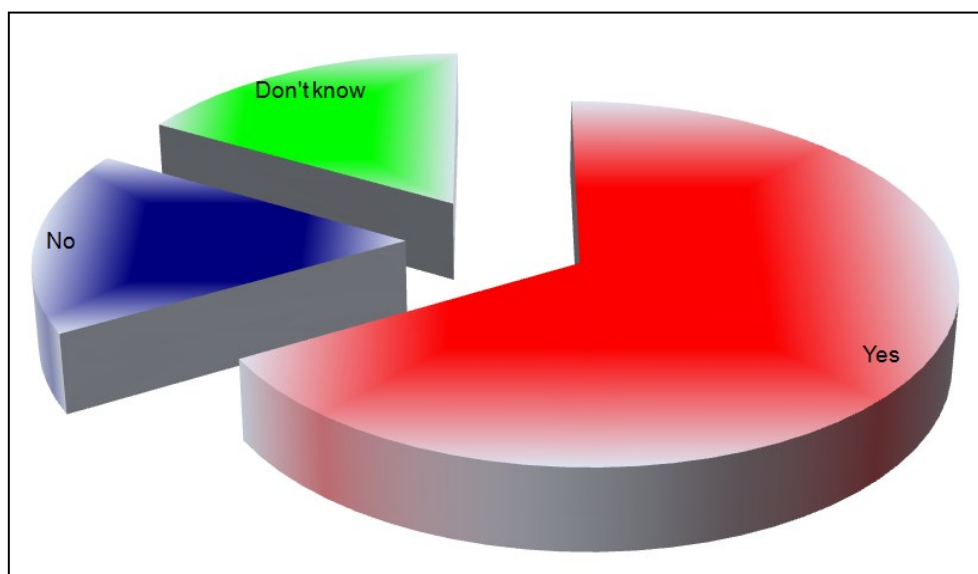


Figure 3.19: 66% of respondents believe say the EPB would be beneficial to a CV.

3.3.1 Discussion

The aim of Chapter 3 was to establish whether there is an opportunity for the EPB to break the stranglehold held by the pneumatic spring parking chamber, on the CV parking unit market. To do so, at least one of the impact factors must be exploited to break the current technical lock-in. By completing two questionnaires, two of these impact factors have been identified as modes to bring about change. Firstly, it has been shown that there is a real CV issue whilst in operation with the pneumatic systems. Air leakage causes the brake system to malfunction, immobilising

the vehicle. In an era where the economy is recovering from the global recession, company profits are generally low, with cash reserves heavily depleted from the past couple of years. Therefore, having to constantly pay-out for CV maintenance is problematic for many. Meritor could manipulate the situation by highlighting how pointless these payments are and create a “crisis in the existing technology”, one of the impact factors that can force change.

Furthermore, it was also shown in the EQ that features that deliver improved vehicle efficiency and/or vehicle safety are the style of product that is currently being accepted by the braking market. Thankfully, both these features match the characteristics of the proposed EPB. As a consequence, a second impact factor can be exploited to break the technical lock-in, which is the “Changes in taste” factor.

Two definite routes available to break the current status quo have been identified, but the question still remained as to what is the best method of making happen. After completing the finalised benefit analysis, Figure 3.20 illustrates the presented suggestions made to Meritor as to how to market the impending EPB. With a high percentage of people found to still be unaware of the EPBs presence, the idea of using a knowledge based (or informative) approach to the marketing was made. Verification came when the educated second sample demonstrated more enthusiastic opinions on of the EPB and the benefits it will deliver. With increasing knowledge being the underlining message used in all aspects of future marketing, it is depicted in Figure 3.20 by the large rectangle in the background, due to everything else needing to be built on upon this foundation.

Currently, Meritor entertains discussion predominately only with OEMs. By widening the conversation to the entire downstream benefit segment, it was possible to identify further benefits, which ultimately lead to finding the most important EPB selling factor: independence form pneumatic systems. Meritor should therefore continue with this this broadened approach with their market campaign. Targeting the downstream segments in conjunction with the OEMs may lead to greater demand, improving the chances of successful product introduction. Therefore, each of the three benefit segments are represented in Figure 3.20. As the messages given each segment must be specific to the targeted segment, they all have their own individual horizontal lines.

Illustrated quite vividly throughout this chapter, there are three key messages that need to delivered; the EPB delivers a definite (although quantitatively undefined) vehicle efficiency advantage, removes some of the braking reliance on pneumatic systems and additional driver aids will improve the standard of driving. Again, the separation of these messages is portrayed

by the three individual vertical lines in Figure 3.20. The layout is of a matrix structure, with an overlap being a representation of the specified message (vertical line) should be given delivered to that benefit segment (horizontal line), which should be made in an informative manner.

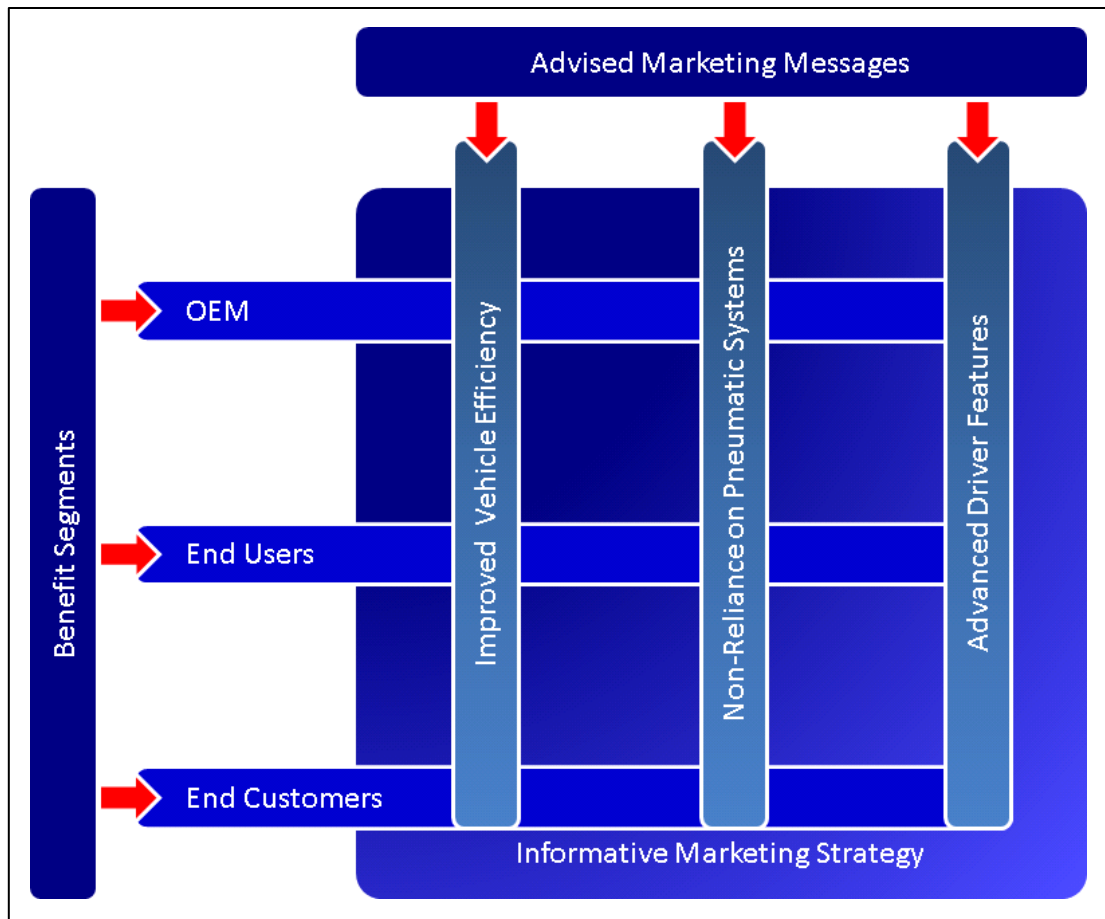


Figure 3.20: An illustration of the suggested marketing strategy made to Meritor.

Finally, it should be restated that the sample sizes used in this research were too small to statistically confirm any findings made. Small sample sizes results in only a small chance that the produced results are representative of the intended population. However, the conclusions made were based on collected data received from questionnaires. By minimising bias in the questionnaire itself and making the responses anonymous, the gathered data is reliable and therefore meaningful.

4 Literature Review

The study of brake design dates back to at least 1902 when Louis Renault designed the first drum brake, with Daimler fitting them on the first vehicle in 1903. A drum brake operates by applying a braking force to a pair of brake shoes located inside a rotating drum. With each pad pivoted at the same end, the actuating cylinders supply an input force that pushes the linings into the drum, generating the retardation force. There are generally two types of brake drum configurations, leading/trailing and twin leading. The former has only a single force input to the brake resulting in single pivoting position. One shoe will ultimately be pressing into the drum with the rotation (leading shoe), generating maximum braking force with this self-applying effect whilst the trailing shoe will be kept on the drum by the input force only. The clear advantage of this is that in the reverse direction, at least one shoe is creating maximum braking torque. Twin leading brakes are pivoted in opposite edges to ensure the self-applying effect from both pads in the forward direction but are limited in their use for parking applications as the force generated whilst in reverse is comparatively low, providing a high chance of rollaway. However, by the 1920's vehicle speeds had increased so much that greater braking performance was required, which brought about the introduction of four wheel braking. Duesenberg introduced the first hydraulic system delivering a braking force to each wheel in 1921 (Freudenberger 1999).

Nowadays, disc brakes have become more popular as the torque to friction coefficient, μ , relation is virtually linear, unlike with drum brakes providing the driver with a consistent and reliable braking performance. Also, as the brake mechanism is not enclosed, air flow around the brake is able to provide superior cooling characteristics compared to drums. Lanchester patented the first disc brake design back in 1902, but the lack of a better freely available material other than copper meant that the design was withdrawn until 1951 where it was displayed once more at the International Motor Show. Two years later, the Jaguar C-Type won the Le Mans whilst fitted with Dunlop disc brakes. Virtually all vehicles today use disc brake fitted to on the front axle with an increasing trend for placing disc brakes on all four wheels.

During a braking application, the energy transfer taking place converts the vehicles kinetic energy to thermal energy via the frictional interface between the disc and pads. A high proportion of that heat energy enters the disc brake with the remainder going into the pads. Disc distortions through thermal affects, or "coning" as it is commonly known, has led to three altering designs of disc brakes to be made in attempts to counter the deformation, shown in Figure 4.1; a) standard outer hat design, b) outer with neck, c) inner hat, d) inner hat with hole.

Passenger vehicles regularly use the standard disc as the small disc mass available for thermal distortion is low compared to larger CV and train disc brakes.

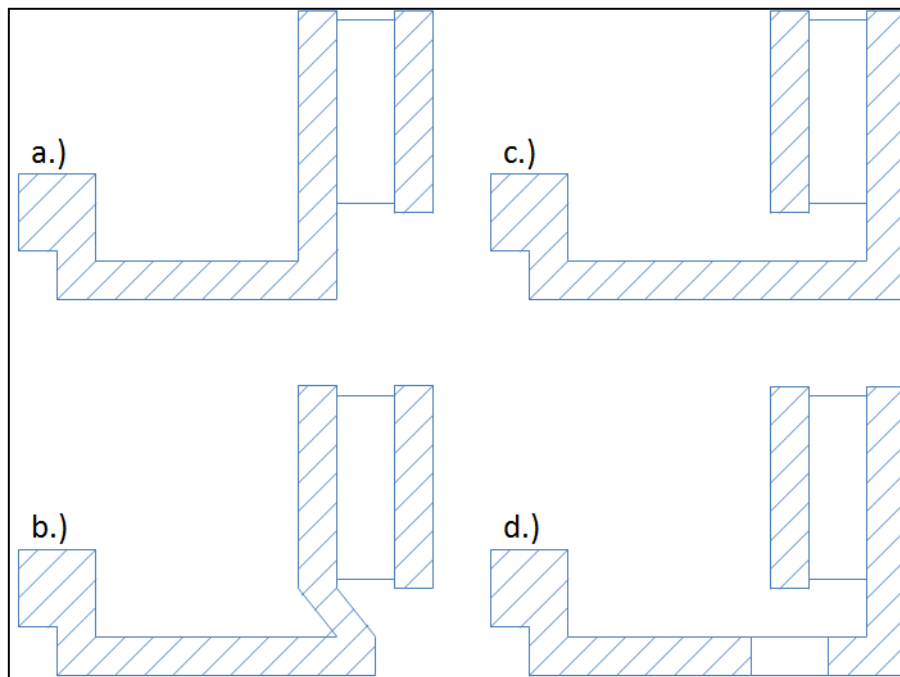


Figure 4.1: Common types of disc brake design a) standard outer hat design, b) outer with neck, c) inner hat and d) inner hat with hole.

4.1 Electric Parking Brake

Securing any vehicle in a parked situation is extremely important in preventing a vehicle from moving without the presence of a driver. When parked on a hill, this occurrence is called rollaway. Rollaway is not a common problem in vehicles, but can be catastrophic especially with CV if it was to happen in a largely inhabited village or city. If a 44 tonne lorry was to gain movement rolling uncontrollably down a hill, very little would be able to take the impact on collision, let alone the human body.

Large amounts of thermal mass in CV disc brakes results in a large volume of thermal expansion, leading to large thermal contraction as the brake system cools down once the vehicle is parked. Thermal contraction could influence the clamp force levels enough for the vehicle to rollaway on a hill under its own weight. The cause of rollaway in passenger vehicles on the other hand, is only likely to be if the driver failed to apply enough force to the handbrake lever as the thermal mass available is far smaller. As explained in Chapter 1, there is no regulation in for “hot” parking; provided the brake system can hold the CV on an 18 per cent incline

regulations have been met (ECE Regulation No. 13 2008). Therefore, it is feasible a brake system could conform to ECE Regulation 13 and still suffer from rollaway.

In passenger vehicles, a mechanical linkage from a cable with one end connected to the handbrake located in the driver compartment and the rear brakes to the other, has historically been the typical method to secure a passenger vehicle. As tension is applied to the cable, the pads are clamped against the disc to create the parking torque. CVs differ slightly as the connection in the passenger compartment is an air line running to the brakes, with the driver input releasing the air from the spring chamber, allowing the spring to apply the braking force.

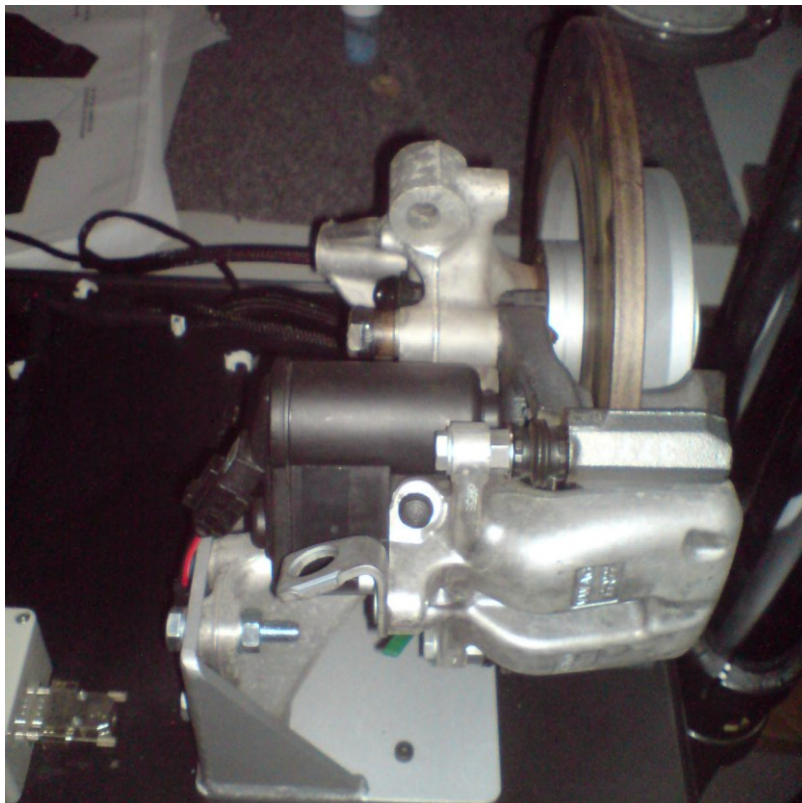


Figure 4.2: Passenger vehicle EPB

In recent times, weight reduction has been a high on designers' priorities with brake assemblies not escaping this trend. As a result, the conventional hand brake is in the process of being replaced by the EPB. A typical EPB uses a small motor to deliver a torque to a gear set via a belt drive transmission. The gears operate a spindle which applies the pistons, generating braking force. Figure 4.2 shows a passenger vehicle EPB attached to a sliding caliper where the black plastic casing contains the EPB components.

Alternatively, the original cable method of applying the pads can remain with the EPB controlling an actuator for the brake cable located towards the rear of the vehicle, shown in

Figure 4.3. The first EPB was released by TRW in 2002, meaning the technology is still in its infancy. Published research on the product is therefore scarce. An overview of what has been carried out to date is presented.

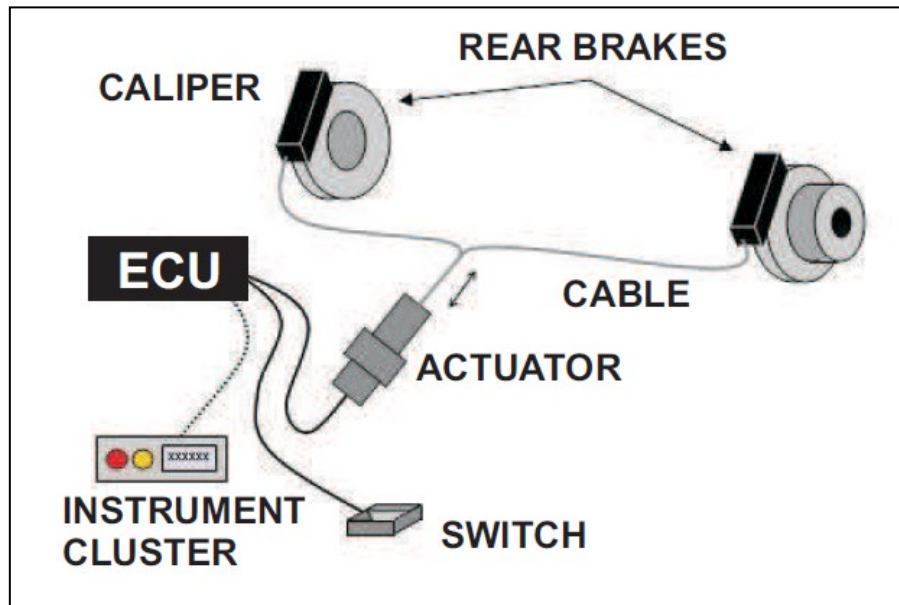


Figure 4.3: Electric brake cable type EPB (Slosarczyk *et al.* 2008).

With the EPB being a motor-gear system, noise is inevitably produced when the EPB is operated. Griebel *et al.* (2004) investigated the nature of the noise in an attempt to reduce the ‘annoying’ sound heard by people outside the car. The housing of the motor-gear was identified as the greatest noise source with the caliper housing providing very little. Gear teeth meshing and the belt drive are also large sources of noise. Helical teeth and an optimised belt drive vastly reduced the noise generated. These EPB developments are designed to improve the public perception of EPBs and help improve the desire for them in passenger vehicles. CVs already produce large amounts of noise so the addition of an EPB would make very little impact to consumer perception, removing that problem in the case of larger vehicles.

Additional functionality is capable with the installation of an EPB. Drive Away Release (DAR) is a function to control the release the EPB at the moment the driver wishes to start driving, preventing the vehicle from rolling backwards when setting off on a hill. Investigations into the DAR safety implications by Slosarczyk *et al.* (2008) lead to a new control system being designed that uses the throttle and steering angle sensors to detect driver presence. Also, a better estimation of vehicle mass was developed as underestimations results in the EPB releasing too early whilst too heavy estimates cause the EPB not to be released at all, eventually stalling the engine.

Another feature the EPB is able to offer is the functionality of an immobiliser. If the engine is started without the required key or keycard present then the EPB will not release the brake. Subsequent attempts to move the vehicle by the driver will fail. Cost saving will be created as a separate immobiliser will not have to be fitted to the engine.

Minseok Jang *et al.* (2009) have further developed the EPB control system by integrating a clamp force measurement into the brake ECU, which is independent of both clearance distant and force sensors. Force sensors can be difficult to install in tight spaces and come at a cost whilst pad wear will mean a continually changing pad clearance distance, thus force reading measurements will remain accurate throughout the pad lifecycle. The control software operates in a three step process; detection of the initial point of contact through changes in the motors angular velocity, estimating the clamp force and then consider the inertia effects of the motor delivering a little extra torque whilst it slows down once the motor is switched off.

A standard EPB control signal delivered to the motor is in the form of a PID controller; Peng *et al.* (2009) developed a fuzzy type controller as a replacement for the standard PID controller. Fuzzy controllers provide a faster response time compared to PID, delivering a better experience for the driver. However, the developed fuzzy controller has only been proved theoretically thus far, so still requires full vehicle testing before it is introduced on commercially available EPBs.

Finally, Lee *et al.* (2010) increased the safety of the EPB system by implementing a fault detection system. With the parking brake doubling up as the emergency brake in the event of hydraulic, pneumatic or any other brake failure, a fault detection method is necessary to alert the driver. Mechanically sensorless estimation of individual faults was used in this process by comparing ripples in the current, generated by the motor, to a simulated current load. Faults were reported when residual values calculated between the measured and simulated current exceeded a specified threshold.

The success of the EPB is emphasized by TRW alone with the announcement made in 2009 that they had manufactured their 10 millionth EPB unit. However, these units are all destined for passenger vehicles. As seen above, research in the field of EPB has improved the performance of the current EPB systems and enhanced the driver experience with the technology whilst mechanical capabilities of the EPB have been ignored. Implementing an EPB into a CV is an innovative procedure which thus far, has not been fully achieved. A hybrid system has become available, similar to the design shown in Figure 4.3 where the same spring parking chamber is used to generate the braking force with the electronic controller regulating the airflow to/from the brake. For a fully integrated system, removing heavy brake lines and other common

components, significant research is needed to ensure the EPB will be reliable under far harsher loading and thermal conditions than the passenger vehicle.

Meritor are not the sole developers of the CV EPB. Peter (2012) presents work on another aspect of the EPB system, the driver feel and interface. A study was completed as to where the on/off switch should be placed, and to the nature of the button itself. Three key positioning factors were identified, and they were:

- The location must intuitive to the driver, making fast activation possible
- Position of the button must not lend itself to unintentional activation by the driver
- Unauthorised users (passengers) must not be able to activate the parking brake

Pushbutton suggested locations were mounted on the dashboard, close to the steering wheel for quick activation. Furthermore, it must be mounted high enough that it is not accidentally pressed by the driver's knee/leg. Optical lighting of the button was also recommended to ensure it is intuitively recognisable to the driver, allowing for fast activations times.

4.2 Heat Transfer

4.2.1 Conduction

Heat conduction is the mode of heat transfer that describes the interaction between excited molecules and their bordering, less excited molecules. Heat conduction in solids is caused by two separate effects; lattice vibrational waves and the energy carried through the molecule by the flow of free electrons (Çengel and Boles 2007). The former effect occurs in a lattice, a series of molecules which are approximately fixed in position with a constant separation distance. As one molecule gains energy it begins to vibrate causing its neighbouring molecule to begin vibrating at a similar rate. This pattern continues throughout the material in a wave from until all the molecules are vibrating at a uniform rate and hence, have a uniform thermal energy distribution. Free electrons in a solid pass from one atom to another, with an energy transfer occurring when they collide with the new atom. An electron originally from a warmer atom will conduct energy in this way to a cooler atom. Conduction modes are slightly different for liquids and gases due to the random motion of the molecules as well as the vibrational and rotational motions. It is collisions between molecules, rather than free electrons, which allows the energy transfer from the highly excited to the less excited molecules.

The rate at which heat can be conducted, \dot{Q}_{cond} , through a layer of material with a regular thickness, Δx , is directly proportional to both the temperature difference across the layer, ΔT , and the cross sectional area normal to the direction of heat conduction, A , giving:

$$\dot{Q}_{cond} = kA \frac{\Delta T}{\Delta x} \quad (4.1)$$

where k is the thermal conductivity of the material. As $\Delta x \rightarrow 0$ the differential equation known as Fourier's law of heat conduction is created:

$$\dot{Q}_{cond} = -kA \frac{dT}{dx} \quad (4.2)$$

Because heat always flows from the warmer heat source to the cooler heat sink, the temperature gradient, $\frac{dT}{dx}$, will always be negative. A negative sign was added to equation (4.1) to make the conductive heat transfer in the positive x direction proportional to the temperature gradient across it. At the interface between two components or molecules, thermal contact resistance, R_{cond} , is present, preventing 100% of the heat being passed to the lower energy level component. Figure 4.4 demonstrates the effect of thermal contact resistance where material A is conducting heat from the heat source at the zero position into material B. A proportion of energy is used in the transfer of heat energy resulting in the temperature gradient seen, not a constant temperature. At the interface there is a sharp drop in temperature between the two surfaces (depicted in red), which represents the thermal contact resistance. Contact pressure has the largest effect on thermal contact resistance, with an inversely proportional relationship. Surface roughness of both contacting components, at the microscopic level, prevents perfect contact between the two, which also reduces the heat flow across the interface.

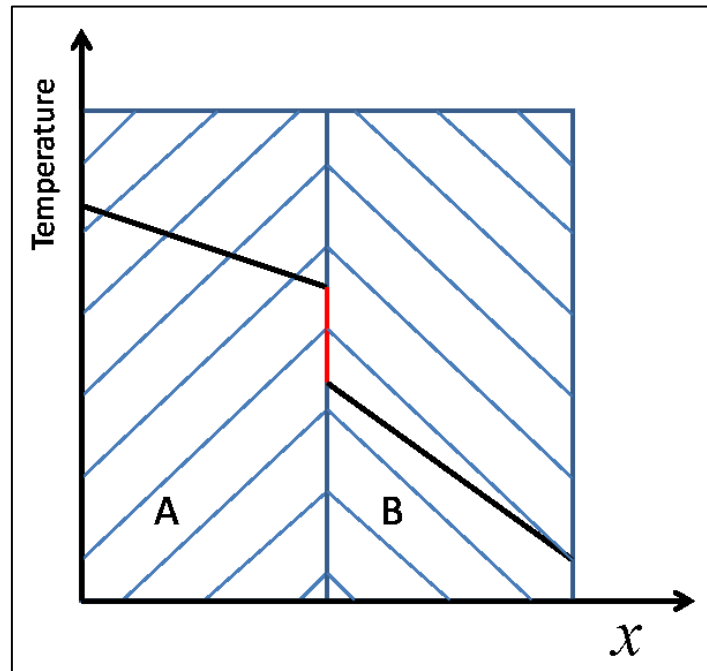


Figure 4.4: Thermal contact resistance example.

Thermal contact resistance can be calculated by:

$$R_{cond} = -\frac{\Delta T_{int}}{Q_{cond}/A_{int}} \quad (4.3)$$

where ΔT_{int} is the difference in absolute temperature at the interface of the disc and pad and A_{int} is the contact area at the disc/pad interface. A more useful quantity than R_{cond} is the conductive heat transfer coefficient, h_{cond} , as it describes the heat transfer through the material per unit area and temperature. It can be calculated by:

$$h_{cond} = \frac{1}{R_{cond}} \quad (4.4)$$

Substituting equation (4.4) into equation (4.3) gives equation (4.5); the amount of thermal energy dissipated conductively across two surfaces in contact.

$$\dot{Q}_{cond} = h_{cond}A\Delta T \quad (4.5)$$

4.2.1.1 Thermal Conductance

Thermal conductance is a material property that can be defined as the amount of energy transfer through the material thickness per unit area and absolute temperature difference. Being an unmeasurable property, determination of it can be troublesome. Through the years, four main

procedures have been developed to calculate the value of k ; each method will be outlined individually.

4.2.1.2 Harman Technique

The Harman technique is a fairly straightforward way of determining the thermal conductivity. It makes the most of the Peltier effect (the heat absorbed across a junction) by applying a current to the sample, producing a voltage across it (Tritt 2005). Recording temperature rise and the current applied the thermal conductivity can be calculated. The main problem with this method is that it is sensitive to heat losses. Savvides and Goldsmid (1972) successfully measured the thermal resistance, and hence published a value of conductance for Silicon using a modified experimental technique first developed by Harman in 1958.

4.2.1.3 Parallel Thermal Conductance

The parallel thermal conductance (PTC) method was developed by Zawilski *et al.* (1999), allowing k values to be determined for relatively small sample sizes; length and surface area measurements of approximately 2 mm and 0.05 mm² respectively. The PTC method is conducted on crystalline structures at very low temperatures, from 10 to 310 K. The method involves raising the temperature of one surface steadily by a heater, whilst the other end is held constant by a cooling plate to artificially create a temperature gradient through the specimen. The main advantage of this method is that the value of \dot{Q} does not need to be known to get the value of k . Orendacova *et al.* (2007) have more recently applied this method successfully on single crystal specimens.

4.2.1.4 3 ω Technique

Wang *et al.* (2007) outlined the 3 ω technique. An AC current of constant amplitude is passed through a single carbon fibre located in a vacuum, causing a rise in temperature that fluctuates at different frequencies at multiples of ω , i.e. ω , 2ω and 3ω with the frequency being a direct representation of the material's k value. This method has been developed because of the demand from the racing and high performance passenger vehicles, as well as the aeronautical industry, for a greater understanding of thermal properties rather than just the mechanical carbon fibre properties.

4.2.1.5 Laser Flash

The first pulse method can be dated back to 1961 where Edward Woisard presented his work on the measurement of thermal diffusivity, α , by supplying heat into a test specimen in a short pulse. Thermal diffusivity is a measure of a material's ability to absorb the heat from its

surrounding substance, calculated by dividing the thermal conductance by the volumetric heat capacity (product of the specific heat capacity and the material density).

$$k = \alpha C_p \rho \quad (4.6)$$

Woisard used an electrical current as the pulse source into a long rod with a thin diameter. Later that same year, Parker *et al.* evolved the pulse method to what is now known as the laser pulse method. As the name suggests, a laser replaced the original electrical current as the heater source. The method works by heating the front surface of the test specimen with the laser and recording the time taken for the heat to flow through the material, such that the rear surface is half that of the front. Calculations for thermal diffusivity and specific heat can be conducted from the data collected and used in equation (4.6).

Advantages gained by using the new method were that the test specimen sizes can be substantially reduced, measurements can be taken at higher temperatures, little energy is required by the laser and values for the diffusivity, thermal conductivity and heat capacity can all be calculated from a single experimental procedure. Although the specimen size can be reduced, considerations regarding the specimen thickness still need to be considered as Parker *et al.* conclude that too thin a thickness will produce a low diffusivity value, whilst too thick will allow radiation and convection heat losses to manifest in the results, reducing the accuracy.

In more recent times, Kim (2006) applied the laser flash technique to record the thermal diffusivity of various disc materials, allowing their thermal conductivity to be measured. A general assumption is that the beam exiting the laser is of uniform nature although this is not true in reality. Measures can be taken to reduce the scatter from the beam, as performed by Kim, by shining the beam through an optical tube, producing even distribution of energy. To successfully use the obtained thermal diffusivity results in the calculation given in equation (4.6), a known value of specific heat capacity, C_p , and density are needed. Kim conducted this test on well know materials such as aluminium and iron as a C_p value could be well estimated although it was proposed by Parker *et al.* that the C_p values could be determined by the technique.

Kim *et al.* continued their research with the laser flash method in 2008. The same five material specimens were used except this time the C_p values were measured using a differential scanning calorimeter (DSC) and thermal expansion values measured by push-rod transducers. Thermal diffusivities were shown to decrease with an increase in temperature, attributed to the thermal carriers (electrons in metals) having greater resistance at higher temperatures. Thermal

expansion of the material will increase the internal friction between the molecules, restricting ability for electrons to flow. Iron discs proved to have a linear drop in diffusivity whilst the aluminium disc was a little more irregular. On the contrary, C_p values increased linearly with a temperature rise, again with iron discs producing a linear relationship. As thermal conductivity is proportional to thermal diffusivity, the same patterns will be repeated.

4.2.1.6 Fourier Number

Modelling of conduction is characterised by the Fourier Number (Incropera *et al.* 2006), shown in equation (4.7). Essentially, this is a dimensionless ratio of heat conduction rate to energy storage. When performing thermal modelling, it is important to consider the Fourier number as larger values ($Fo > 1$) results in the material struggling to reach a thermal equilibrium, causing extended calculation times, whereas low Fourier numbers ($Fo < 0.1$) means heat is insufficiently conducted through the material in the desired time frame, leaving only the skin heated.

$$Fo = \frac{\alpha t}{R^2} \quad (4.7)$$

4.2.2 Convection

Convective heat transfer takes place between a solid surface and adjacent fluid surrounding the solid. Convection is made up of both conduction and fluid flow affects (Çengel and Boles 2007). The rate of fluid flow around a solid surface is the governing variable determining the effectiveness of the convection process. Stationary fluid in contact with the heated solid surface, in accordance with the zero slip condition, will conductively gain heat energy from the solid. A thermal gradient is between fluid particles at the surface and a distance away from it. The heat energy is dissipated from the wall particles to the bulk fluid particles, reducing the thermal gradient, and hence reducing the rate of heat dissipation from the surface. The flow of the fluid results in the now warm bulk fluid being replaced by cooler fluid, restoring the high thermal gradient and rate of convection. The velocity of the fluid flow is therefore directly proportional to the rate of convective heat transfer, so the higher the flow rate, the greater the convective heat transfer from the surface.

When the solid surface is in stationary liquid or gas the type of convection is known as pure convection. Pure convection is therefore the worst case for cooling as the only fluid flow is a result natural convection where the flow is created through buoyancy effects.

In natural convection, the fluid flow forms naturally from buoyancy effects around the solid surface. Alternatively, forced convection is when the fluid flow is described as forced when the

solid is placed in a region of flowing fluid from a source, such as a pump or fan. In forced convection the buoyancy effects can be neglected.

Newton's law of cooling can be used to determine the convective heat transfer, \dot{Q}_{conv} , given by:

$$\dot{Q}_{conv} = h_{conv}A(T_{surf} - T_{\infty}) \quad (4.8)$$

where h_{conv} is the coefficient of convective heat transfer, A is the surface area the heat transfer is taking place, T_{surf} is the solid surface temperature and T_{∞} is the bulk temperature of the fluid at a distance from the solid surface.

4.2.2.1 Boundary Layer Theory

The concept of the hydrodynamic and thermal boundary layers is important to understand in any heat convection study. The former describes the physical motion of the fluid as boundary layer is created between the wall and free stream. In this part region, viscosity has a large influence of flow properties. Molecular forces exerted on the air particles close to the wall cause the zero slip condition, causing a zero velocity for the molecules directly adjacent to it (Allen 1982). Moving away from the wall, the passing fluid increases velocity until it reaches the free stream, V_{∞} , creating an interface between it and the hydrodynamic boundary layer. Fluid viscosity effects determine the thickness of the hydrodynamic boundary layer, with higher internal fluid shear effects making thicker boundary layers. Figure 4.5 shows the velocity profile in a typical hydrodynamic boundary layer.

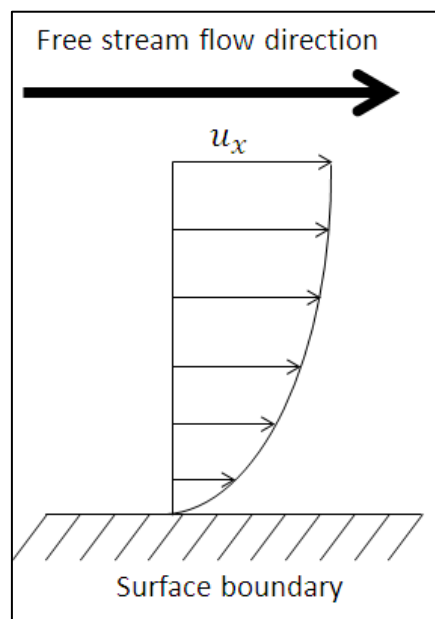


Figure 4.5: Typical velocity profile in hydrodynamic boundary layer (turbulent).

A laminar boundary is the initial state of all boundary layers as a fluid first interacts with a solid surface at the leading edge. The velocity profile increases approximately linearly from the wall, where it is zero, to that of the free stream. Differences in velocities between adjacent flow layers cause molecular viscous forces without the presence of vortices (Allen 1982 and Fox *et al.* 2004).

Further downstream surface friction effects slow down a greater volume of air. Generally, thick boundary layers cannot maintain laminar flow and therefore transition into a turbulent boundary layer via a transition critical point, x_{cr} . Where this transition point is located is sensitive to a number of factors, which include surface shape, temperature, roughness and upstream flow characteristics as well as many other intricate flow properties. Uncertainty in fluid modelling can be driven by not knowing the transition point, causing erroneous results (Anderson 2007).

Turbulent boundary layer thicknesses grow at a faster rate than laminar due to having a greater amount of friction within it. The source of friction comes from rotational velocity caused by the greater absorption of flow energy resulting in internal eddy currents. Turbulent boundary layers consequently increase thickness rapidly and create greater heating effects. A typical boundary layer formed when an airstream interacts with a flat plate, causing at a sufficient speed for the boundary layer to pass through the laminar state and into turbulent is shown in .

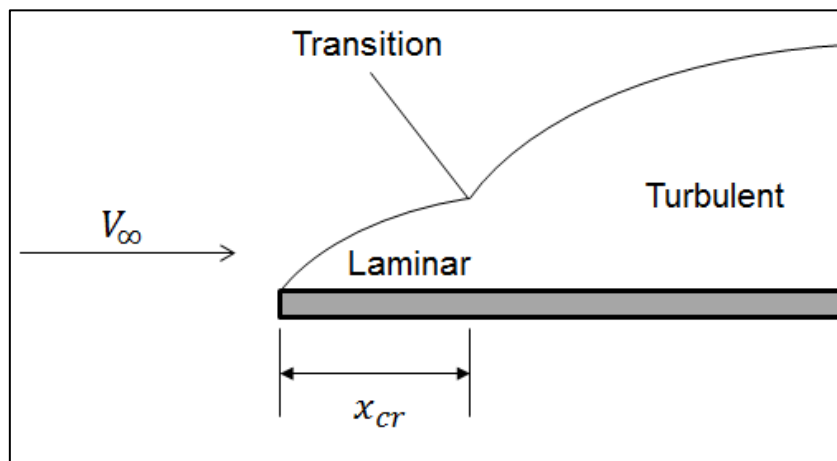


Figure 4.6: Transition from laminar to turbulent flow. The boundary layer thickness is not to scale (Anderson 2007).

A thermal boundary layer is formed when a temperature gradient is present between the solid surface and the free stream with heat transfer occurring from the surface to the fluid. With fluid velocity equalling zero at surface, it is commonly assumed that the fluid temperature is equal to the surface temperature. Conduction transfers heat through the fluid until a point (boundary layer interface) where the temperature is equal to the bulk free stream temperature. A close

relationship is formed between the thermal and hydrodynamic boundary layers but their relative thicknesses are often dissimilar. Heat transfer capabilities are highly dependent on the flow regime, found by exploring a set of dimensionless numbers. A discussion of each is offered before being used as part of the variable h_{conv} investigation.

4.2.2.2 Reynolds Number

The Reynolds number, Re , is one of the most significant and important parameters to understand in fluid flow theory. It is a dimensionless value that calculates the ratio of inertial forces to viscous, it is calculate using equation (4.9).

$$Re = \frac{\rho v L}{\mu} \quad (4.9)$$

where ρ is the fluid density, v is fluid velocity, L is the characteristic length (or diameter if a cylinder) and μ is the dynamic viscosity.

High Re values signify viscous forces are negligible resulting in turbulent flow, whereas low values demonstrate significant viscous forces and therefore the flow is in a laminar regime. Understanding the Re values around a cylinder can be used in this study as the hat region of a CV disc brake is essentially a cylinder. Research into flow regimes around circular cylinders is not scarce, leading to a high level of understanding. Six flow patterns exist when a fluid flows around a cylinder, dependent on the Re value (Anderson 2007):

1. Very low values of Re , $Re < 4$, the flow is characterised by Stokes flow, where the velocities are so low inertia effects have little influence. Streamlines consequently, are almost symmetrical with the flow remaining attach to the surface the entire way around.
2. Increasing the Re value range to $4 < Re < 40$ sees flow separation at the trailing edge of the cylinder. Two stable vortices are created and occupy the space directly downstream of the cylinder.
3. Further increasing the Re above 40 makes the flow behind the cylinder unstable as the stable vortices now regularly shed in an alternate pattern, known as a Karman vortex street.
4. Increasing the Re still results in the Karman Vortex Street to become turbulent and thus, transition into a full wake region behind the cylinder. Separation from the cylinder now

occurs on the leading edge of the cylinder, approximately 80° around from the stagnation point. This flow is demonstrated in the region of $10^3 < Re < 3 \times 10^5$.

5. When the flow is between $3 \times 10^5 < Re < 10^6$ a double separation effect occurs. Initially, the laminar boundary layer continues to separate on the forward face, with the free shear layer above the separated region tripping into a full state. The turbulent flow then reattaches to the cylinder before separating once again at approximately 120° , causing a thinner wake than before.
6. Flows with Re values above 10^6 transitions to fully turbulent on the forward cylinder face but remains attached until the some point on the back face.

By making the assumptions that air will travel at 1 m/s under natural convection and with a diameter of approximately 0.2 m, it was possible to use equation (4.9) to generate an initial understanding for the expected flow pattern around the hat region of a CV disc brake during a parking application. A calculated value of 1.4×10^4 would suggest the unsteady flow behind the hat section, in the form of a wake.

4.2.2.3 Prandtl Number

The Prandtl number describes the relationship between the momentum dissipation of the fluid to the heat diffused to the flowing fluid. High Prandtl numbers are often found in oils where momentum diffusion is stronger than the thermal diffusion; consequently, thermal conduction is the predominant mode of heat transfer. On the contrary, Prandtl numbers are small in substances such as liquid metals, where convection is dominant (Necati Özisik 1985). The thicknesses of the velocity and thermal boundary layers are both dependent on size of the Prandtl number, with small hydrodynamic boundary layers correlating to primarily convective cooling. The Prandtl number is independent of the surface interaction as it is a fluid only property.

$$Pr = \frac{C_p \mu}{k} = \frac{\mu \rho}{k / (\rho C_p)} = \frac{v}{\alpha} = \frac{\text{Molecular diffusivity of momentum}}{\text{Thermal diffusivity}} \quad (4.10)$$

4.2.2.4 Grashof Number

The Grashof number is a very important dimensionless parameter in buoyancy driven flow. Like the Reynolds number in force convection flow, the Grashof number describes the ratio of fluid inertia forces to fluid viscous forces. When viscous forces are dominant, the flow is said to be in a laminar state, damping out potential eddy currents in the flow. As the inertial forces increases in significance, the flow goes through a transitional state before tripping into a fully

developed turbulent flow. Inertia forces are now too strong to be dampened by the viscous forces. Small hydrodynamic boundary layers are present with turbulent flows, resulting in high convective heat transfer coefficients as the cooler fluid replenishment can occur more rapidly.

The Grashof number can be calculated by using equation (4.11) where g is the gravitational acceleration, ζ (often termed β) is the coefficient of thermal expansion (Necati Özisik 1985), L represents the characteristic length of the body surface (Richardson 1963), T_w is the wall temperature of the solid and ν is the kinematic viscosity of the fluid.

$$Gr = \frac{g\zeta L^3(T_w - T_\infty)}{\nu^2} \quad (4.11)$$

4.2.2.5 Rayleigh Number

When investigating heat transfer from a body subjected to buoyancy driven flow, the Rayleigh number is used in place of the Grashof number; calculated by multiplying the Grashof and Prandtl numbers (equation (4.12)). It represents the ratio of conductive heat transfer to convective heat transfer. Below the critical value conduction is the dominant mode of heat transfer and reversing to convection thereafter. Depending on the situation and shape of the solid surface, the critical value of Ra varies. For example, McAdams suggests the critical value for a flat horizontal plate is as low as 10^7 whilst Necati Özisik (1985) proposes a value up to 10^9 for vertically placed cylinders in free air.

$$Ra = Pr \cdot Gr \quad (4.12)$$

4.2.2.6 Nusselt Number

Where the Prandtl number looks at the flowing fluid and the relationship of heat dissipation through it, the Nusselt number considers the ratio of convection to conduction energy transfer from the solid surface boundary to the flowing fluid and across its thickness, in a direction normal to the surface. Nusselt numbers at unity show an even distribution of conduction to convection heat dissipation from the surface, characteristic of laminar type flow. In convection dominant turbulent flow, values of Nu will rise above 100 (Necati Özisik 1985). It is important to note that the parameter L in equation (4.13) is the characteristic length of the body's surface.

$$Nu = \frac{h_{conv}L}{k} \quad (4.13)$$

Finding the Nusselt number is not always as straightforward as inserting values into equation (4.13), usually because they are not all known. Small changes in geometry impacts the intensity

of the buoyant flow and subsequent parameter values (Corcione *et al.* 2011). With the Nusselt number, it is often preferred to use approximation equations found by gathering experimental data and performing a correlation analysis on them. Necati Özisik (1985) demonstrates the correlation method produces values closer to experimental results compared to theoretically derived equations. Various correlations have taken place for different solid surface configurations within buoyant fluid flowing over it. Churchill and Chu (1975) provided a correlation equation for a vertical wall (equation (4.14)), valid for Rayleigh numbers between 10^{-1} and 10^{12} and when isothermal wall conditions are assumed.

$$Nu_m^{1/2} = 0.825 + \frac{0.387Ra_L^{1/6}}{[1 + (0.492/Pr)^{9/16}]^{8/27}} \quad (4.14)$$

A second equation proposed by McAdams (1954) has been said to match experimental data more accurately by Necati Özisik (1985). The later equation takes the form:

$$Nu_m = cRa_L^n \quad (4.15)$$

where c is a constant and n is the exponent of Ra . Values of these two parameters are dependent on the Ra ; they are shown in Table 4.1.

Table 4.1: Parameters for the McAdams relationship for Nu_m (McAdams 1954)

Flow Type	Range of Ra	c	n
Laminar	10^4 to 10^9	0.59	$1/4$
Turbulent	10^9 to 10^{13}	0.10	$1/3$

Considerable research has also been devoted to buoyant air flow around cylindrical shapes. The considerable length and diameter of the cylinder shaped hat region of a CV disc brake allows a significant amount of convective heat dissipation to occur from this surface, so it was therefore important not to neglect it. As with flat walls placed vertically in free air, Churchill and Chu (1975) correlated a trend in Nusselt numbers from experimental results. Their correlation equation (4.16) is valid for isothermal surfaces only, for Rayleigh numbers falling within the range of 10^{-4} to 10^{12} .

$$Nu^{1/2} = 0.60 + \frac{0.387Ra_D^{1/6}}{[1 + (0.559/Pr)^{9/16}]^{8/27}} = \left(\frac{h_{conv}D}{k}\right)^{1/2} \quad (4.16)$$

Morgan (1975) also provided a correlation equation, it has the same form as the McAdams equation for vertical walls, but with the coefficient values shown in Table 4.2 corresponding to the relevant Ra value range.

$$Nu = \frac{h_{conv}D}{k} = cRa_D^n \quad (4.17)$$

The Morgan equation, not only has the same form as the McAdams equation but its coefficient values also have the same magnitude. Consequently, the dimensionless numbers are expected to have the same profile, varying only its scale because of the change in characteristic length.

Table 4.2: Values for the Morgan equation with ranging Ra (Morgan 1975)

Ra_D	c	d
$10^{-10} - 10^{-2}$	0.675	0.058
$10^{-2} - 10^2$	1.02	0.148
$10^2 - 10^4$	0.850	0.188
$10^4 - 10^7$	0.480	0.250
$10^7 - 10^{12}$	0.125	0.333

4.2.3 Radiation

Radiation is the final mode of heat transfer. As a body increases its temperature, its electronic compositions alter, resulting in electromagnetic waves being given off, emitting thermal energy from the body. This process happens to any substance that has a temperature greater than absolute zero. Radiation is actually volumetric phenomenon, however, due to the radiation given off inside a solid never reaching the surface as it gets absorbed within the body, it can be considered to be a surface phenomenon for opaque solids (Çengel and Boles, 2007).

The Stefan-Boltzmann law determines the maximum rate of thermal energy that can be emitted from a surface, which is:

$$\dot{Q}_{rad,max} = \sigma AT_{surf}^4 \quad (4.18)$$

where σ is the Stefan-Boltzmann constant, A is the surface area and T_{surf} is the absolute temperature of the surface. Equation (4.18) assumes blackbody radiation, an idealised situation where a body perfectly accepts all the electromagnetic waves. In reality this is not possible as the matter reflects some of the radiation. Emissivity, ε , is a material property that approximates how close the material replicates a blackbody. The range of values for emissivity is from 0, where the material reflects all the electromagnetic waves, to 1, a blackbody. Applying the emissivity property to equation (4.18) leaves the radiation emitted by a real surface to be:

$$\dot{Q}_{rad} = \varepsilon \sigma AT_{surf}^4 \quad (4.19)$$

In the case where a substance, at an absolute temperature, is surrounded by a gas such as air, the radiated energy is proportional to the temperature difference between the fourth powers of the absolute surface temperature and the bulk gas temperature, T_{∞} making equation (4.19):

$$\dot{Q}_{rad} = \varepsilon\sigma A(T_{surf}^4 - T_{\infty}^4) \quad (4.20)$$

Like with conduction and convection, Newton's law of cooling can be applied, creating:

$$\dot{Q}_{rad} = h_{rad}A(T_{surf} - T_{\infty}) \quad (4.21)$$

where h_{rad} can be determined by equating (4.20) and (4.21), leaving:

$$h_{rad} = \varepsilon\sigma(T_{surf}^3 + T_{\infty}^3 + T_{surf}T_{\infty}^2 + T_{surf}^2T_{\infty}) \quad (4.22)$$

4.3 Heat Transfer Coefficients

The need to understand heat transfer coefficients in greater detail was realised many years ago, demonstrated by the early FE modelling conducted by Newcomb (1969). Sisson (1978) was another early user of the FE methodology and realised the importance of generating an accurate understanding of heat transfer coefficients. Whilst exploring the possibilities of combining basic FE analysis with numerical modelling for a tool to calculate disc brake temperatures, Sisson demonstrated that the simulation accuracy is bounded most significantly by the heat transfer coefficients used. The importance of residual torque in disc brake cooling simulations was also shown, as the cooling factor is significantly altered with additional heat flux putting thermal energy into the disc whilst having a negligible effect on the deceleration rate.

Thermal effects in a dynamic situation were investigated by Naji and AL-Nimr (2001) by numerically modelling an entire braking system. The mathematical model tested three different braking applications at differing sliding velocities. Only the brake application representative of an emergency stop showed to have a dramatic effect on thermal behaviour. More significantly, Naji and AL-Nimr proved convective heat transfer coefficients, located at disc OD and at the disc/hat junction have the biggest effect on thermal behaviour. Naji and AL-Nimr failed to separate the individual heat transfer coefficients into individual dissipation modes. Clearly, at the disc/hat interface the coefficient will be completely conductive whereas at the OD a combination of convection and radiation will be present.

Voller (2003) progressed the work of Naji and AL-Nimr by proving that at high rotational speeds, convective cooling is the most dominant heat transfer mode from the disc. The faster the disc rotational velocity, the faster air is pumped through the vanes, quickly recovering the

thermal gradient between the stationary air at the wall boundary and the adjacent flowing air. The convective heat transfer coefficient will resultantly increase with the rotational speed, shown in Figure 4.7. To confirm this, Voller performed cooling tests from 140°C down to room temperature, with rotational speeds of 150 min⁻¹ and 450 min⁻¹. A secondary finding also showed that shrouding the disc had little effect of the rate of heat transfer compared to increasing the rotational velocity. Stationary cooling tests were neglected by Voller. By extrapolating back a convection coefficient of 2.5 W/m²K can be found if a linear relationship is assumed. However, experimental reliability is question here as only four rotational speeds were physically measured. With such a low number of experiments, error within any of the measurements will have significant impact which could give a false outcome.

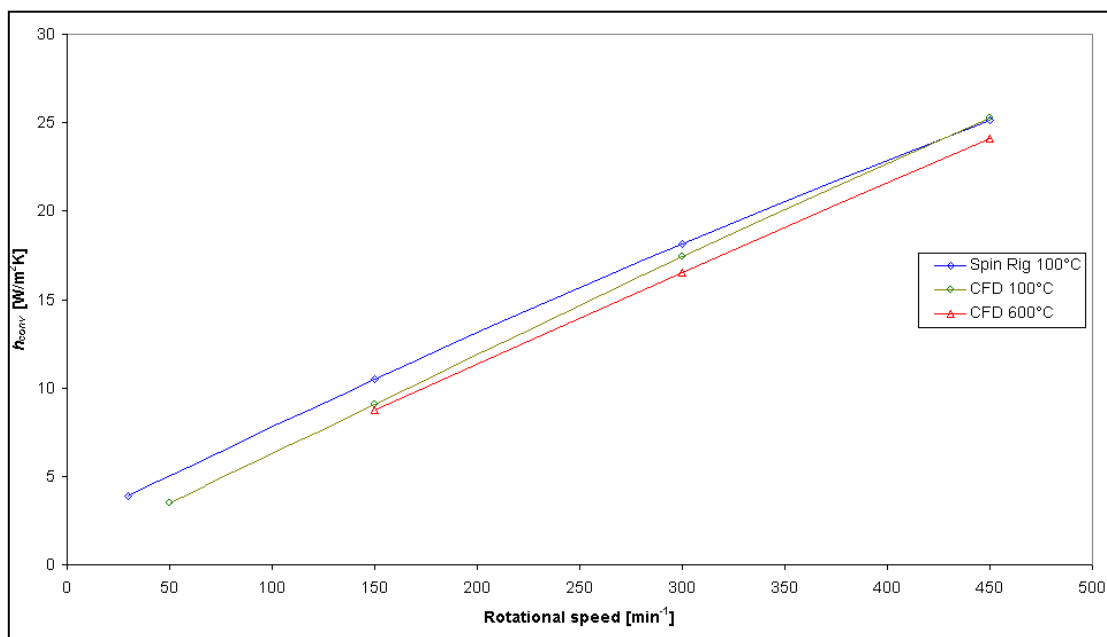


Figure 4.7: h_{conv} vs rotational speed for CV disc (Voller 2003).

As the rotation declines, the pumping of air also reduces allowing the speed independent dissipation modes to become more important. Voller *et al.* (2003) observed that after the rotation speed drops below 170 rpm radiation becomes the dominant dissipation mode, with a further decline in speed reduces the contribution of convection to the total disc dissipation even more (Figure 4.8). Note, the investigation was conducted at a temperature of 600°C. A different critical rotational speed will be seen when cooling from a different temperature, changing the characteristics of Figure 4.8. Again, zero speed was ignored so the dissipation division between the three modes is uncertain for parking applications.

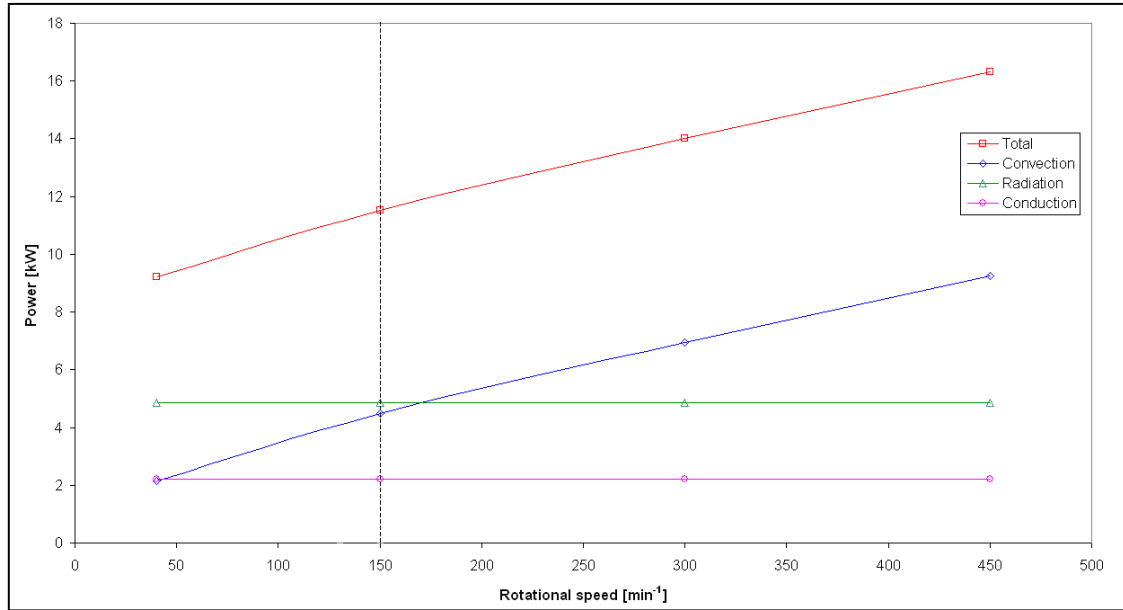


Figure 4.8: Influence of dissipation modes against rotational disc brake speed (Voller *et al.* 2003).

Voller *et al.* (2003) continued their work on heat transfer coefficients by examining the variation in the conduction pattern at the disc brake flange face and a wheel carrier for CV brakes. Both the disc and wheel carrier had a slightly corroded surface, representing the condition a disc would spend the majority of its operational life in. The presence of bolts, tightened to a nominal torque of 300 Nm, produced a contact pressure between the two surfaces that ranged from 10 to 50 MPa. An average of this interface pressure, P_{avg} , can be calculated from equation (4.23).

$$P_{avg} = \frac{n_b F}{A_{int}} \quad (4.23)$$

Where F is the individual bolt clamp force and n_b is the number of bolts. Higher localised pressure values were generated close to the bolt holes and at the ID. A linear relationship was found between increasing the friction surface pressure and h_{cond} values. Using equation (4.24), Tirović and Voller (2005) calculated high h_{cond} values, approximately 5,000 W/m²K in between the bolts which raised to 10,000 W/m²K at the bolt hole perimeters.

$$h_{cond} = 80P_{avg} + 2300 \quad (4.24)$$

Emissivity values of h_{rad} in the current literature vary greatly. This was expressed vividly by Voller *et al.* (2003) when values gathered from various literature sources (see Table 4.3) were shown to differ from 0.15 to 0.90. Using these values, Voller *et al.* (2003) calculated h_{rad} values for a range of temperatures up to 670°C, shown in Figure 4.9. The lowest emissivity

value produced heat transfer coefficients ranging between 2 and 12 W/m²K whilst the highest emissivity value range was between 6 and 52 W/m²K. The latter describes an 88% drop in radiative energy dissipation as the disc cools down to ambient. The importance of obtaining an accurately value of emissivity was demonstrated in the experiment, even more so with applications having low rotational speeds.

Table 4.3: Emissivity values used by Voller *et al.* (2003)

Author	Emissivity
Limpert (1975)	0.55
Noyes and Vickers (1969)	0.8
Grieve <i>et al.</i> (1998)	0.4
Eisengraber <i>et al.</i> (1999)	0.15-0.9

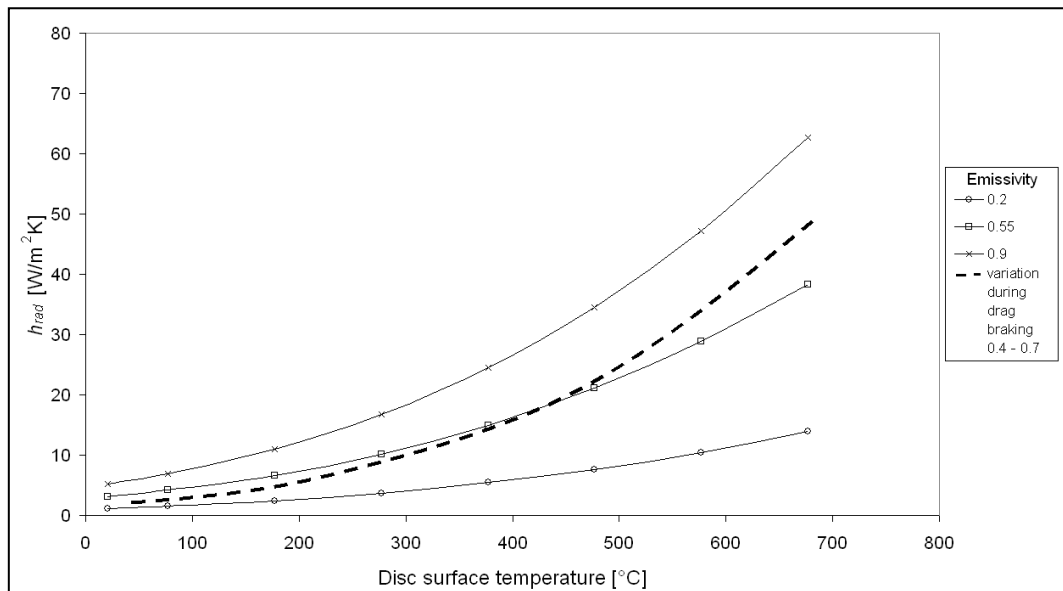


Figure 4.9: Varying emissivity values (Voller *et al.* 2003).

Furthermore, the condition of the disc impacts heavily on the emissivity value. Voller *et al.* measured the emissivity of newly machined disc as 0.2 whilst a disc with corroded surface had a far greater emissivity of 0.9. The IR camera method of comparing measured thermocouples surface temperatures to the IR image and adjusting the emissivity until a match between the temperatures was achieved. Disc conditioning is therefore also an important factor in low speed investigations considering the disc has the largest surface area emitting energy.

Liang *et al.* (2005) used a numerical method to calculate h_{conv} values which were used in an FE model. Liang *et al.* recognised that the rate of convection will be different at the external disc surfaces to the values seen within the vanes, resulting two separate h_{conv} values being

calculated to represent the two areas of heat dissipation. The numerical model was to investigate disc brake temperatures during repetitive braking for different speeds. Values for h_{conv} at the external surfaces, h_{outer} , were calculated with equation (4.25) when the flow is not fully turbulent, defined by $Re \leq 2.4 \times 10^5$. Alternatively, fully turbulent flows, $Re > 2.4 \times 10^5$, used equation (4.26).

$$h_{outer} = 0.7 \left(\frac{\lambda_a}{D_o} \right) Re^{0.55} \quad (4.25)$$

$$h_{outer} = 0.04 \left(\frac{\lambda_a}{D_o} \right) Re^{0.8} \quad (4.26)$$

By making the individual convective heat transfer coefficients a function of Re , the coefficient is variable with air speed, thus agreeing with the work provided by Voller (2003). Similarly, for in-vane convection coefficients with low Re values of equal to or less than 10^4 , equation (4.27) with equation (4.28) for when $Re > 10^4$.

$$h_{vane} = 3.72 \left(\frac{Re}{Pr} \right)^{1/3} \left(\frac{d_h}{l} \right)^{0.83} \left(\frac{\lambda_a}{D_h} \right) \quad (4.27)$$

$$h_{vane} = 0.046 \left[1 + \left(\frac{D_h}{l} \right)^{0.67} \right] Re^{0.8} Pr^{0.33} \left(\frac{\lambda_a}{D_h} \right) \quad (4.28)$$

where l is the length of the disc brake and D_h is the hydrodynamics diameter.

$$l = \frac{(D_o - D_i)}{2} \quad (4.29)$$

$$D_h = \frac{2BD_i \left(\frac{\theta D_o}{360} - A_c \right)}{D_o \left(B + \frac{\theta D_o}{360} - A_c \right)} \quad (4.30)$$

These equations will be able to model a parking application because the equations are independent of the disc rotational speed, with fluid characteristics being the only variables needed. These equations are complex with many sub calculations needed to compute each h_{conv} value. It is unrealistic to use such equations for a vast number of nodes at every time step as the computational time to completion would be enormous, limiting this method to calculating general initial convection values only.

During the investigation into the different fundamental designs of a disc brake, Okamura and Yumoto (2006) recorded discs fabricated with holes in the hat section produce lower hat flange face temperatures than their solid counterparts. Subsequently, it can be concluded that

conduction is a volumetric process, the greater the amount of mass in the hat, the more heat can be passed to it from the friction contact faces.

A lumped heat transfer coefficient, h , was found by Heffernan (2006) through experimental procedures which was then used in numerical modelling. The single value of h incorporated conduction, convection and radiation effects rather than finding them individually. The aim was to produce a simple design tool through numerical modelling. Heffernan stated predicted results from the model matched well to the measured temperature data. For one set drive cycle this was true, however, two other reported drive cycles show inaccurate cooling rates; after half an hour of cooling, in Run 1, there was approximately 40% difference between the measured and predicted temperatures. The lumped method was shown to be a useful tool in the initial design stages only, thereafter a more complete understanding of the heat dissipation modes and thermal interactions are needed, challenging the views of Heffernan.

McPhee and Johnson (2008) proved that external convective cooling is as important to disc brake design as internal convective cooling. By completing cooling tests with and without blocked vanes, and with an asbestos plate between the disc mounting hub and the wheel carrier interface to restrict the conductive effects, the effect of external convective cooling was separated from the total amount of convective cooling. For a moderate rotational speed of 342 rpm it was found that only 45.5% of h_{conv} was due to the internal vane flow, rising to 55.4 % at 1,025 rpm, resulting in the vane flow becoming more significant with an increasing speed. The results suggest that in-vane air flow will be less significant than external surface flow in parked situations. Buoyancy driven flow is expected to be strongest within the vane the air will be hottest here due to having less surrounding air particles to pass the heat onto. Therefore, the in-vane dissipation would have a larger impact than the external flow, contrary to the finding by McPhee and Johnson.

Numerical modelling can be used to inspect the conductive capabilities of both the disc and pad. By applying the two common contact pressure distribution assumptions, uniform pressure and uniform wear, Talati and Jalalifar (2008) showed that a uniform pressure distribution causes greatest disc temperature with the presence of a thermal resistance situated between the disc and pads. A temperature gradient is created at the disc/pad interface. Conduction effects were the predominant dissipation mode responsible for heating the caliper and its internal components to that of the discs after a finite amount of time. Furthermore, convective heat transfer coefficients of 48.4, 63.8 and 88.2 W/m²K for vehicle speeds of 71.5, 101.0 and 151.4 km/h respectively, were recorded and matched well with equation (4.31), which is:

$$h_{conv} = CV^{0.8} \quad (4.31)$$

where C is a constant to be determined and V is the vehicle speed. Equation (4.31) gives a good approximation to h_{conv} values at high speed. However, it is demonstrating a non-linear relationship between h_{conv} and vehicle speed, contradicting the work of Voller *et al.* (2003). Neither experiment conducted enough tests to produce conclusive evidence for argue either way.

FE analysis produced by Wawrzonek and Bialecki (2008) reinforced the knowledge that emissivity changes with temperature. FE results were compared to the contactless temperature sensors which proved to match poorly. Erroneous results were found more in the contactless temperature sensor readings rather than with the FE simulation. Contactless temperature sensors have a high degree of sensitivity to emissivity, directly impacting any h_{rad} calculations based on their results. Importance of understanding the emissivity change was therefore shown by Wawrzonek and Bialecki.

4.4 Natural Convection

As stated already, natural convection differs from forced convection as the air flow does not have a source, rather driven purely from buoyancy effects. Cooler stationary air molecules are heated from the solid surface, which reduces their density and causes them to rise starting a convection current. Having a small air inlet and large air outlet for brake vane shapes causes pumping of air through the disc when it is rotating. When the brake is parked, a lack of the pumping effect means buoyancy driven flows can no longer be neglected. This section outlines the work conducted by researchers related to the field of natural convection in and around the disc brake.

Buoyancy driven air flow through a partially open cavity has been numerically simulated by Desai and Vafai (1992) using the Galerkin formulation of the Finite Element method. The simulation was of a hot inner cylinder placed inside a cold outer cylinder with an air medium between them. Two simulations were run, firstly with the air having an Ra value equalling 10^4 then secondly matching 10^6 ; both surface temperatures were kept constant throughout. Importance of the Rayleigh number on heat transfer was evident when moving from the smaller Ra value to the larger as higher flow velocities are coupled with higher Ra values, thus generating a stronger buoyancy-driven flow dissipating more heat through convection rather than conduction. Likewise, areas of recirculating flow causes increase the heat transfer between the walls and passing fluid as the recirculating air has a high flow rate.

Das and Reddy (2006) were interested in the 2D flow field and heat transfer within a square enclosure where a smaller square located centrally within the outer square acts as a heater. Adiabatic boundary conditions were placed on the walls. Within the closure, the critical Ra value was shown to be 10^3 . Comparing the results of Das and Reddy to Desai and Vafai (1992), it can be seen that for a square enclosure over a cylindrical enclosure, the critical Ra value is a full order of magnitude less.

Das and Reddy furthered their research by investigating the effect on the buoyancy flow by inclining the square. It was found conduction driven heat transfer, low Ra values, inclination has little effect on the heat transfer. However, a non-linear rise in Nusselt number was recorded with inclination angle. This finding can be related to brake research as a disc brakes have many open channels rotated at various angles from the horizontal. This result could affect the dominant heat transfer mode from one vane to the next during a parked application and as the disc temperature cools.

Azwadi *et al.* (2010) also presented similar work to Das and Reddy (2006) as to the effects of an increasing inclination angle on the flow of fluid. Again a square cavity was used, but with two opposite walls acting as a heat source and heat sink with the perfectly conducting boundary conditions set to the remaining walls. A finite difference numerical model of the situation was creating with the Boussinesq approximation being made (all densities assumed equal). Increasing the gradient of inclination gives rise to a secondary vortex manifesting in the centre of the flow somewhere between the 60° and 80° gradients. The average Nusselt number, based on this work, peaked an inclination angle of 65° . Presence of the secondary vortex is having adverse on the convective heat transfer. Again this result can be related to individual vanes in a disc brake when in a parked situation; is there a presence of vortices in the flow hampering the heat transfer.

4.5 CFD Modelling and Forced Convection Cooling

Jerhamre and Bergstrom (2001) were interested in the flow field within the wheel arch and through the disc. CFD techniques were used to estimate the tangential and radial flow velocities for two separate vehicle equivalent velocities, 70 km/h and 100 km/h. Due to the pumping effects within the vanes the flow will be turbulent. The reasonable assumption that all flows, both in-vane and external, were turbulent. Consequently, the $k - \varepsilon$ model was used throughout. Wall interactions can have large effects on flow characteristics, especially in confined areas such as disc brake vanes. Both the 2-layer model and the law-of-the-wall model were used in separate simulations to predict flow velocities; the former gave typical Y^+ values in the range of

one to three, but never exceeded six whilst the latter gave a substantially larger range of values, from of 40 to 70. When comparing the law-of-the-wall model to measured flow velocities, a small underestimation of the tangential velocity of 4% was seen using prism cell elements only. Tetrahedral cells were showed inferior accuracy by delivering an underestimation of 15%. Furthermore, the 2-layer model provided to be ineffective at describing the internal vane flow.

A two-stage disc brake performance analysis was conducted by Damodaran *et al.* (2003). Stage one was to perform a CFD Analysis on a straight vane rotor. Generated results gave a lumped heat transfer coefficient, taking the effects of all three modes of heat dissipation into a single figure. Disc cooling performance characteristics where provided in the form of pressure against volume flow rates. Combining the two outcomes enabled Damodaran *et al.* to describe an inversely proportional relationship between air pressure and lumped heat transfer coefficient for a given constant rotor velocity. This finding only refers to the convection abilities of the disc as radiation is an electromagnetic phenomenon which occurs regardless of the medium it is in with conduction occurring at the interface between to molecules. Therefore a better conclusion is that air pressure is inversely proportional to convection. Increasing density will decrease the kinematic viscosity of the fluid, which ultimately decreases the Pr value. Reducing in the Pr value shows the fluid diffusion rate strengthens against the convection, hence the inverse relationship.

The second stage of Damodaran *et al.* investigation was to input the performance characteristics from stage one into a second, more ambitious quarter car CFD model consisting of over 2 million cells. It was shown that for discs mounted on the rear axle, removal of the dust shield had little effect on brake temperatures whilst its presence on the front axle leads to higher disc temperatures as air flow is restricted.

Sakamoto (2004) used numerical techniques to examine disc brake cooling of underground train disc brakes in response to a series of thermal crack failures. Numerical calculations were based on the total convective heat transfer coefficient being a summation of the separate convection coefficients from the external surfaces and within the vanes; both were calculated as a function of the Pr number, thermal conductivity, dynamic viscosity and the length of the convective surfaces. Using this assumption, the cooling rate parameter, φ , was derived and gave realistic estimates to the maximum disc temperatures under braking cycles that decelerated the train to stationary from an initial vehicle speed of 128 km/h. High values of φ gives lower disc temperatures, delivering a better cooling efficiency. Railway disc brakes were used to verify the model with experimental comparisons. Three discs with varying distance between the vanes

were used. A second finding was made that the air inlet area restrict air flow into the vanes if it is too small, reducing the heat transfer.

$$\varphi = \frac{hA}{C_p m_d} \quad (4.32)$$

Sun (2006) executed a study on the sensitivity of many factors on a car disc brake by performing CFD analysis to acquire h_{conv} values and then used them in an FE model to predict the rise in disc temperatures after 80 braking and acceleration cycles. CFD analysis showed that a pillared vane design produced large areas of flow recirculation within the vane, reducing mass flow rate by a third and consequently, reducing the h_{conv} values by 25% compared to the standard radial vane configuration. Secondly, there is an optimum gap length between radial vanes to achieve the highest h_{conv} value, reported to be 16.02 W/m²K for a 45 vane rotor at 24 km/h and 32.96 W/m²K at 64 km/h. Other discs tested produced values of 15.82 and 15.60 W/m²K for 36 and 54 vane rotors at the lower speed and 32.65 and 32.36 W/m²K at the higher speed. Air flow was shown to separate at the entrance with a larger gap between vanes causing a larger recirculation area for greater air speeds in the wider entrances, developing the finding of Sakamoto (2004). However, larger inlet gaps also increases the average in-vane air temperature. Subsequently, the most favourable trade off for the highest h_{conv} value was the 45 vane rotor. To manufacture more discs to further increase the amount of possible vane channels per disc would be expensive. CFD analysis could have been conducted cheaply to find the optimum number of vanes to achieve the highest h_{conv} values was not completed. Surprisingly, the convection heat transfer coefficient was shown to be insensitive to another disc geometric property, vane length.

Palmer *et al.* (2006) simulated a 27° segment of a passenger vehicle disc brake, rotating at 1,140 rpm and compared the results to measured data taken from a front axle brake during operation. Disc friction surfaces were uniformly heated at 500°C and considered smooth whilst conduction effects to the hub and radiation were both ignored. Air flow tumbles at the vane inlet at the trailing edge of the vane. This tumbling effect has significant consequences on the flow as vortices are formed, which cause areas of recirculation to reduce in size because some of the separated flow rejoins the main air stream. Average heat transfer coefficients were calculated for CFD and for the vehicle testing, which were 128.2 and 104.5 W/m² K respectively. The presence of the wheel was solely attributed for the over-estimation of the cooling rate. Indeed the presence of a wheel will have an impact on the cooling rate, however, the inaccurate initial temperature of 500°C is an unlikely assumption, as the rotational velocity at the OD will cause

more friction here generating temperature gradient along the friction surface. From equation (4.8), the convective cooling power is proportional to the temperature difference between the heated surface and passing fluid. Palmer *et al.* drastically overestimated the temperatures towards the ID resulting in the CFD analysis to over-predict disc temperatures.

Further convective cooling tests were carried out by Tirović and Galindo-Lopez (2008) via CFD analysis. Four different discs were tested, a base type disc having 30 straight vanes and three modified discs housing a short vane in between the longer 30 straight vanes, which are positioned radially close to the ID, the OD and one in the middle. It was found that the air vane inlet speed is higher than inside the vanes themselves due to localised effects. An exaggerated wheel velocity of 800 min^{-1} was used to amplify the effects of flow and heat transfer differences. The generated results are therefore also unrealistic, demonstrated by the highest h_{conv} value of $168.7 \text{ W/m}^2\text{K}$. Although the results cannot be compared directly, the distribution of h_{conv} is relevant. Unsurprisingly, the maximum is on the front face of the vane, where the air velocity is greatest, dropping gradually on the trailing vane face as the air reaches the OD. Recirculation of the air flow on the leading vane face causes the drop in h_{conv} to be severe. Again, the conductive effects were restricted with the installation of a Bakelite plate.

Barigozzi and Perdichizzi (2008) assessed the confidence from CFD results by comparing numerical results to experimentally gathered data. Exit vane air velocity, from a disc rotating at 750 rpm, was captured via Laser Anemometry whilst air temperatures were recorded with cold wire thermometry. Exit air temperature were constantly underestimated by the numerical CFD program. The standard quadratic k- ϵ turbulence model was used for flow conditions. It was the use of this model that was contributed to the error as too much heat was dissipated. Boundary layers towards the wall are ignored with the k- ϵ model, resulting in cooler air replenishing the thermal gradient from the solid surface to the air flow faster than in reality, creating the high convection rates. In addition, the presence of the inlet separation bubble consistently caused the flow to exit the vane channel on the opposite side of to what it entered.

4.6 FE Modelling Investigations

Abbas *et al.* (1969) was one of the earliest adopters to implement computer methods for calculating heat transfer characteristics of the disc brake system. They realised the importance of conduction effects with hub temperatures being important. A one-dimensional numerical simulation was devised that calculated the heat conduction to the hat from the disc; Figure 4.10 is a graphical representation of the model calculations. A reason able accuracy was achieved by

Abbas *et al.*, which showed a thermal gradient from the disc to the hat and the potential power of computer in thermal investigations.

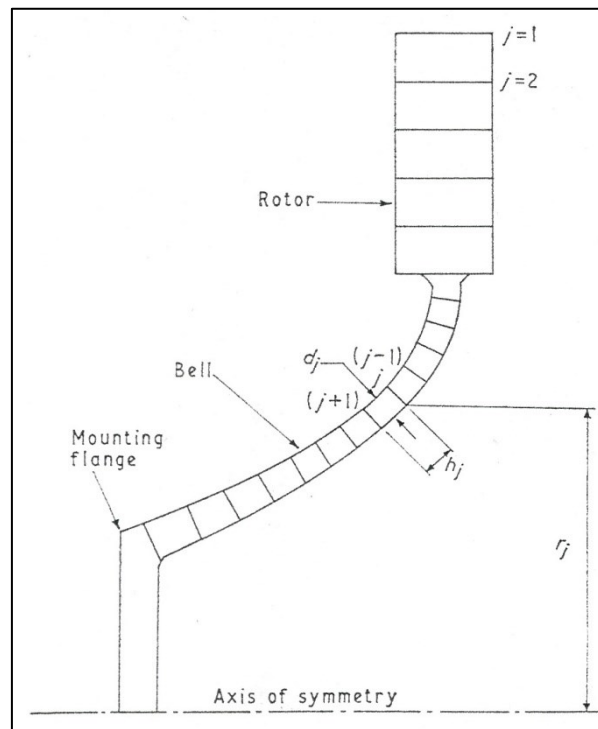


Figure 4.10: 1D model to calculate hub temperatures (Abbas *et al.* 1969)

Limpert (1975) used computer processing with an early FE simulation. A simple 2-dimensional finite-difference model of a solid disc brake was created, consisting of only 36 nodal points; 12 of which were through the centre line of the disc and 12 on either friction surface. This elementary model was run twice with two independent assumptions, firstly the pad pressure was uniform to represent new or bedded pads and then with a non-uniform pressure for the faded pad condition. Limpert showed that with a uniform pressure distribution the temperature increases radially from the ID to the OD so it is acceptable for the heat flux to be uniformly spread across the friction surface. Conversely, with non-uniform pressure the disc brake temperatures became independent of the radial position. Rubbing thermocouples measuring maximum disc temperatures matched well with the thermal numerical analysis, although the measured data had a lag of approximately one second in comparison.

As technology improved, the modelling complexity moved with it. Sheridan *et al.* (1988) took advantage of the improved technology to create a series of models that analysed the disc temperature distributions during multiple stops. A 2D model on a standard disc demonstrated conduction effects with the hat section pulling heat from the outboard disc surface, leaving the inboard disc surface to be warmer. A lack of reliable conductive heat transfer coefficients was

said to be responsible for the mismatch in measured and FE pad temperatures. Indeed, this is emphasized by the use of a single heat transfer coefficient, not individual values for the three modes of heat dissipation; shown already to be insufficient in many modelling application but commonly used in early simulations. The advancing technology was demonstrated further by the creation of a 3D model pie section of a straight vane car disc brake, consisting of 750 hexahedral elements. A basic assumption was made that the heat transfer coefficient at disc flange/wheel hub interface was double that on the contact face with radiation ignored as calculations showed only 5% of the energy is dissipated by radiation. Temperatures reached were approximately 450°C. Segment modelling produced relatively well matched results although Sheridan did concede that full disc brake modelling would be needed for more accurate temperature distribution predictions.

A numerical simulation was conducted by Eppler and Klenk (2002) allowing designers to import improved brake data into the model during the design phase for increasingly more accurate disc brake temperatures. All four brakes on a passenger car were included in this model. For a full system simulation, the energy distribution into the individual brakes was shown to be critical. Conditions of the brake linings were shown to affect the energy input with the fade condition being the most significant as the braking factor reduces once the temperatures reach 200°C but recovers after 400°C.

The use of hydraulic systems is often deployed as the brake actuation method in cars, trucks and small vans. Temperatures in the fluid lines are critical for braking performance as temperatures that are too high will vaporise the liquid, which is a concern as vaporised brake fluid is highly compressible. Compressible fluid in the brake lines will mean force applied by the driver compresses the vaporised fluid rather than transferring the force to the caliper and ultimately prevents the vehicle from decelerating. During the braking application the high fluid pressures will prevent the vaporisation process, resulting in the process occurring when the driver releases the foot pedal. This is extremely dangerous as the only time the driver will be aware of the problem is when they press the pedal and getting no response. An FE model was constructed by Emery (2003) to investigate this very problem. In doing so Emery showed that using an iterative approach to finding the energy input percentage at the disc/pad interface is adequate for matching FE results to measured temperatures. Although the brake temperatures from the model matched well, the cooling rates between stops differed considerably. Convection coefficients were originally selected from values in Limpert (1999) but ultimately increased them by 150% to match the measured values. The increased value of h_{conv} was equal to 35 W/m²K.

To model a realistic braking application, it has been shown various times that numerous parameters and effects must be modelled. Dufrénoy (2004) attempted such a task using FE with a macroscopic model that included thermomechanical disc brake behaviour, friction surface variations, distortions, pad wear and an introductory attempt at modelling thermoelastoplastic disc material. Disc emissivity was set to a constant 0.75, thermal conductance at the disc/pad interface was evaluated at $17,500 \text{ W/m}^2\text{K}$ with a pad wear calculated as function of energy input of 0.8 g/MJ . Comparisons between FE results and an IR camera showed a relationship between the number of heating zones reduces as disc velocity increases. Heating zones are caused by the real contact area created from surface irregularities. Having a Young's modulus that varies with temperature allows surface variations to be modelled, which is stimulated from pad wear. Surface variations can differ from one disc cycle to the next, compared to disc distortions that tend to focus the contact zones into a single area progressively more with increased disc velocity. Using this advanced FE model, Dufrénoy successfully replicated the temperature and position of hot rings, or "fire rings," by assuming the temperature varies in the radial and axial directions only.

The 3D FE model of a drum brake and pad assembly presented by Liang *et al.* (2005) in section 4.3 was modified to produce a "fast" 2D FE model simulating the same application. A reduction from 59,884 nodes down to 953 nodes was seen by the use of a 2D model. Computational time was vastly reduced from 48 hours for the full 3D model down to just 3 minutes. Surprisingly, the results of the significantly simplified model showed very good agreement to measured data, with the highest error being less than 6%. To reiterate, the use of a single heat transfer coefficient may prove restricting for full cooling braking applications, limiting the use of the fast FE model.

Another example of FE modelling being utilised to generate disc temperatures and thermal stresses was done by Apte and Ravi (2006). The purpose of the work was to generate disc brake thermal stresses during the early design phase for a car. Both conductive and convective heat transfer coefficients were kept constant to simplify the model as well as non-temperature dependent material data. Disc geometry such as bolt holes and slots were also ignored. Reasonable accuracy was delivered, within 20% of measured data, concluding that such assumptions are adequate for initial stage models.

Distribution of the surface contact pressure has a large factor on the temperatures reached at the friction interface. FE modelling conducted by Qi and Day (2007) compared well to measured temperatures obtained by probe type thermocouples placed through the pads, once the real

contact ratio, R , was set to 0.536. The real contact ratio is defined as the ratio of actual pad surface area in contact with the disc, A_r , against the whole pad surface area, A_a . Decreasing the value of R causes the maximum surface temperature to increase as a result of the heat flux into the pad increasing. Decreasing R shows a linear increase in maximum temperature until an undefined threshold is reached, where Qi and Day showed further reduction in R will have a more dramatic effect on maximum temperature.

Disc brake temperature variation was model by Amin *et al.* (2007) by using the Order-of-Magnitude method for numerical analysis. A 1D model was made to investigate the heat flow in the axial direct with a second 2D model for both the axial and radial heat flows. Unsurprisingly, heat energy was shown to flow in the axial direction mostly, with very little motion in the radial direction, so it was concluded that the Order-of-Magnitude method of numerically modelling thermal heat flows is viable.

Hassan *et al.* (2008) used FE analysis to model a passenger vehicle disc brake and pads to understand the frequencies brake squeal occurs. A fully coupled 3D thermomechanical contact analysis was created featuring slow disc rotational speed, equivalent to a 10 km/h vehicle speed. Contact stresses increase circumferentially from the leading contact edge to a maximum at the pad centre before reducing. Rising heat increases the stability eigenvalues, demonstrating the importance of thermal studies in mechanical studies. Separate friction coefficients were used and held constant during braking. High frictional coefficients caused unrealistically high temperature to be reached during the braking cycle, showing that a varying temperature dependent μ value should be used when modelling contact and not constant values.

Ouyang *et al.* (2009) constructed a full brake system, excluding only the seals, for the purpose of investigating thermal effects on contact pressure and brake squeal. Their model contained an assembly with 8,350 solid elements for the caliper, pads and disc from a passenger vehicle, which was capable of combining heat conduction with contact analysis. To reduce computing time, a boundary condition assumption was made that no heat transfer occurs from the rear backplate surface as conduction through to the backplate is slow when compared to the sliding friction heat generation process. This assumption is only valid when looking at the actual braking application in dynamic situations as large amounts of energy are conducted through to the pistons, and subsequent caliper components. Pad friction surface temperatures demonstrated different heat distribution patterns between the inboard pad, pressed by a piston, and the outboard pad, pressed by the bridge. Contour plots showed the hottest surface temperature is located just off the leading edge on the bridge pad and more centrally located on the piston pad.

The same patterns are seen for higher vehicle velocities, but with a non-linear temperature increase with sliding speed increase. The contour plots are noticeably distorted, suggesting the mesh used at the points of contact were too coarse to capture the surface interactions precisely. Using a finer mesh would help the quality of the results, although would increase the stated large 3 week runtime.

Nowadays, computational power and the volume of available memory are far superior to any other time in history. A typical crash investigation using FE will consist of approximately 3 to 4 million elements (Pavlidis and Siskos 2010). Current software improvements are now being developed, not to optimise calculation but to improve the ease of post-processing large quantities of data generated by the FE analysis. Pavlidis and Siskos discussed the capability of their μ ETA software, with respect to the model they developed containing over 10 million nodes (see Figure 4.11). The μ ETA software reduces the memory usage by only loading specific test data into the memory storage, allowing real-time video analysis to be compared simultaneously with the FE animated results. This is a very powerful tool as results FE results can be validated as soon as they are outputted from the solver. Other computational difficulties overcome by the μ ETA software were the post-processors ability to read the FE data and the graphical performance, both as a direct result of the data reduction in the memory. Regardless, the improvement made in computer aided analysis since the early simulations is seen when comparing the model made in 1961 by Abbas *et al.* in Figure 4.10 to the full vehicle crash model by Pavlidis and Siskos seen in Figure 4.11.

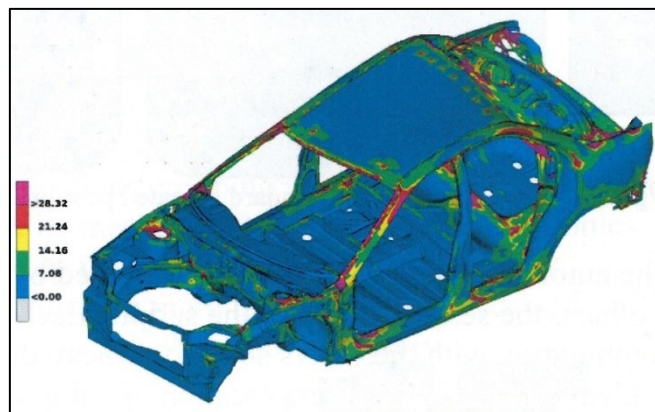


Figure 4.11: Full car model (Pavlidis and Siskos 2010).

4.7 Thermal Stresses

Valvano and Lee (2000) used a combination of FE analysis and a numerical model as tools to study the thermal stresses induced in the disc brake and the resultant coning. The numerical

program was used to determine the brake system temperatures, which were used as boundary conditions in the FE thermomechanical model. Both conductive and convective heat dissipations were modelled as constant for the duration of the simulation, but radiation was ignored. Another assumption made was that the both the disc and pad friction surfaces were equal in temperature throughout. Compressive stresses during the braking applications were recorded, which turned to tensile stresses during the cooling phases. Discrepancies between measured and the predicted coning angles, defined as the angle of rotation of the outboard disc contact face from its initial position, were attributed to the lack of data points outputted in the FE simulation. However, it is argued here that the incorrect assumptions made a larger impact. During a brake application the rotational velocity decreases, reducing the volume of air pumping through the vanes, which in turn reduces the convective heat transfer coefficient. As cyclic braking was used for the test procedure, disc cooling in between the braking applications would cause the cooling rates to decrease and not stay constant like Valvano and Lee assumed. This would cool the disc too much, reducing the amount of coning seen, better explaining the coning discrepancies.

During a short braking period, the generated heat goes into the disc section whilst the hat section remains temporarily constant, creating a thermal gradient at the interface of the disc and hat regions. Mackin *et al.* (2002) have shown that the presence of this thermal gradient causes compressive thermal stress at the interface. As conduction transfers heat from the disc to the hat, the disc brake generates a uniform temperature some time after the braking application. The increasing hat temperature causes the direction of stress to change during the cooling phase, but not to the levels seen during the dynamic brake application. Subsequently, measuring hat region temperatures for modelling validation was shown.

A comprehensive study conducted recently by Okamura and Yumoto (2006) into which factors stimulate the coning process most by combining Taguchi methods and a sequentially coupled thermomechanical FE model. It was found that increasing the axial length of the hat section reduced the induced thermal stress at the disc/hat interface shown by Mackin *et al.* (2002). Temperature factors were looked at during the same experimental procedure with only the pad ID length having a major impact on disc temperatures. This result seems surprising as the disc rotates faster at the OD, thus creating a greater heat flux as more friction is present. It would seem then that the OD geometry would be of more significant to disc temperature than the ID.

The cause of thermal cracking on grey cast iron CV disc brakes was also studied by Bagnoli *et al.* (2009). The discs under investigation came from fire fighting trucks that were not anti-

coning in geometry. A fully coupled thermomechanical FE model produced von Mises stresses in the centre of the disc which reached 360 MPa whilst small areas on the OD saw stresses approaching 450 MPa. Presence of brown/blue coloured regions on the used fire fighting disc brakes, caused by oxidation, indicates that real service temperatures are likely to be in the region of 400-500°C. The cracks were a result of thermal fatigue as the high thermal gradients are combined with compressive stresses from the braking mechanism.

Numerical modelling of the stress distributions conducted by Yevtushenko and Kuciej (2010) showed compressive stresses to occur at both the disc and pad friction surfaces due to the thermal stresses induced. Tensile stresses are also generated simultaneously in both the pad and disc about 2 mm in from the friction interface. These regions quickly disappear in the braking application with a tensile stress region developing at the interface towards the end of the braking simulation; no further change of stress signs occur during the cooling phase. These patterns were measured using numerical calculations of a cast iron disc in contact with a metal-ceramic pad segment, braking from 30 m/s. The aim of the Yevtushenko and Kuciej experiment was to assess the sensitivity of pad boundary conditions on the interface temperature and corresponding thermal stresses by applying a constant zero temperature on the boundary of the pad material, located 5 mm away from the friction interface, then compared the results to a fully insulated boundary. Normalised stress distributions showed very similar patterns despite a near 200°C difference in calculated maximum surface temperatures. The zero boundary condition grossly underestimated the interface temperature compared to measured value, whilst the insulated condition was much closer, matching the measured well. The model only predicted the stress distribution for 11 seconds after the initial brake application leaving patterns unknown during the entire cooling phase.

4.8 Hot Spotting and Third Body Layer

Lee and Barber (1993) were early investigators into thermoelastic instabilities of an automotive disc brake by using numerical analysis. During low speed, an antisymmetric mode of deformation become unstable for any forced vibratory wavelength generated at the friction interface. This mode of deformation creates a buckling affect around the disc, allowing hot spots to be generated on alternate sides of the disc. The findings hold true for deformation waves that have a length at least equal to that the pad, otherwise the pads will dampen any deformation waves smaller than its length. Furthermore, the critical speed for thermoelastic instability was predicted to be in the region used typically experienced on motorways.

Dufrénoy and Weichert (1995) used a thermomechanical FE analysis to model the radial temperature distribution of a train brake during braking cycles. As decelerations rates of trains are relatively low, the assumption of constant angular temperature was made to reduce computational time. An IR camera was used to confirm the hot bandings predicted by the FE, due to a non-uniform pressure distribution. Continuous hot spotting in a single circumferential plane was actually observed with the IR camera, not a hot banding. The constant circumferential temperature assumption is therefore inaccurate when modelling the effects of contact pressure and temperature. However, the temperature gradients on the disc friction surface were shown to be greater in the radial direction than in the circumferential direction. FE analysis proved the most sensitive to the friction materials Young's modulus and thermal expansion coefficient. The former drastically impacted the maximum temperature reached whilst in the range of 0.5 GPa to 2.5 GPa; higher values gave less significant variations and lower values produced results matching a uniform pressure distribution test.

Lee and Dinwiddie (1998) conducted research on the friction coefficient and thermal instabilities whilst investigating brake judder for passenger vehicle disc brakes. With the use of a IR camera capturing the disc temperatures when subjected to drag brake loading, they showed that below the critical speed hot bands (or fire rings) are present around the effective radius with a uniform temperature distribution in the circumferential direction. The hot bands are caused by the brake pad bulging due to the thermal expansion, meaning contact will be more localised towards the centre radial position. However, above the critical speed, antisymmetric hot spotting occurred on either side of the disc due to the thermal instabilities created, shown by Lee and Barber (1993). Temperatures between individual hot spots and their adjacent cooler areas, within the same circumferential plane, showed differences of over 200°C. The finding by Dufrénoy and Weichert (1995) that the radial thermal gradients are more important than the circumferential thermal gradients appears to be inaccurate in the light of Lee and Dinwiddie's work. For the friction pair tested, the critical speed was 95 km/h (60mph), suggesting a high possibility that drivers are frequently experiencing brake judder whilst driving on both rural roads and motorways.

Detecting hot spots can be difficult. A spot on a disc spinning with high rotational velocity will merge into a single ring of high temperature with the human eye. Hartsock *et al.* (2000) compared two methods of capturing hot spots with contactless technology, the first being the standard IR camera used by many authors. This piece of equipment is expensive, difficult to use during post processing and has accuracy errors associated with the emissivity. Although, it does provide real-time visual results showing varying disc temperatures that can be recorded as still

pictures and/or films for future use. The second method was an IR sensor system which included an array of fibre optics correlated with a two-colour IR detector. Advantages of this second system are that the variability of the emissivity has a reduced factor as a ratio of the logarithms of the IR detectors has a near independence from emissivity, the instrumentation is cheaper and data matrices recorded make outputted data easily transferable to other programs such as EXCEL and MatLab for post-processing purposes. The setup of the fibre optics would be far more complex and time consuming, plus any data taken cannot be used until the experiment was finish as results are not given in real-time but do deliver less error in the results.

Panier *et al.* (2004) used experimental investigation, by means of a IR camera using a constant emissivity of 0.75, to explore the emergence of microscopic hot spots (MHS). It was shown that MHS transpire most frequently in a three stage process; firstly a ‘hot’ band forms around the disc with a relatively uniform angular temperature distribution, then the band acquires its own thermal gradient across it that leads to the development of microscopic hot spots, seemingly due to thermoelastic instabilities and dynamic brake loading. Additionally, MHS emergence was observed simultaneously with the thermal band but this was less frequent. The observations made by Panier *et al.* gave rise to the conclusion that it is the amount of energy dissipated into the pads that give rise to the formation of MHS. In total, five classification for hotspot formation was proposed by Panier *et al.* based on this work and previous findings by Dufrénoy and Weichert (1995); captured in Figure 4.12. Type 1 is the Asperity type hotspot where only small areas of rapid temperature rise are seen; type 2 have gradients across a hot band rings due to small contact areas from a single rubbing path. Hot bands are then formed from pad expansion causing a larger contact patch in the circumferential plane (type 3). Buckling effects cause the fourth type of MHS with regional hotspots being the final type generally seen at the end of a braking application.

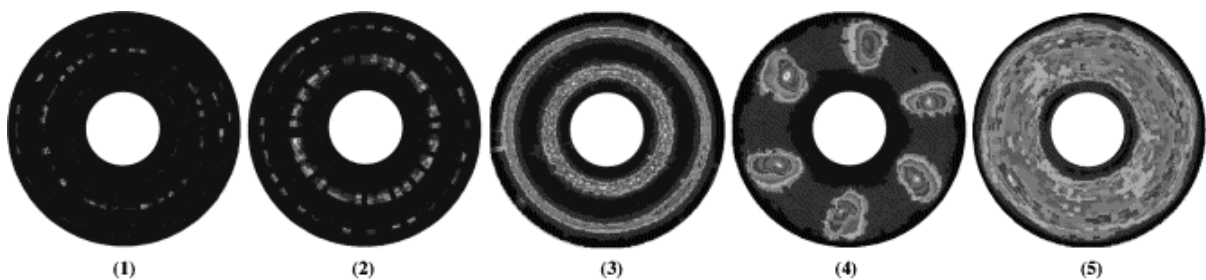


Figure 4.12: Hotspot classifications (Panier *et al.* 2004)

Further investigations by Panier *et al.* (2004) found a softer pad material will produce larger areas of MHS at lower temperatures, suggesting that the interface pressure distribution is more uniform with a softer pad material, which in turn will produce a reduction in thermal stresses.

Previously, FE modelling will generally use either one of the two common techniques when modelling the sliding contact at the disc/pad interface. Perfect contact assumes the temperature at the disc and pad friction surfaces are equal, whilst imperfect contact says there is a temperature gradient across the friction interface caused by TCR. Recent developments by Majcherczak *et al.* (2005) question the precision of either of the two aforementioned modelling techniques. The introduction of a thin layer between the disc and pads revealed that not all the thermal energy is dissipated into the disc and pads with some being stored in this layer, known as the third body. Third body modelling proved highly dependent on the layer thickness and thermal conductivity values used. Too thin a thickness will lead to over estimating the pad surface temperatures, values around 0.05 mm seems reasonable, whilst a value of 0.07 W/mK was reported to agree well with the literature. Effusivity is a material's ability to share heat with its surroundings. Majcherczak *et al.* found that the maximum temperature reached was actually in the third body rather than on either surface, closer to the pad surface than the disc. Effusivity values are lesser for brake pads compared to disc effusivity. Therefore, the disc pulls the heat from the third body layer better than the pad.

$$\xi = (k\rho C_p)^{1/2} \quad (4.33)$$

Majcherczak *et al.* (2007) continued their investigations on the occurrence of hot spotting and the third body theory by utilising thermocouples and infrared camera technology on controlled steel and Sapphire cylinders in sliding contact. Two types of third body were identified; compact and smooth micro-plates and granular micro-plates. The former is a result of real contact area between the disc and pad, supporting the work of Qi and Day (2007). Numerical modelling suggested that the real contact area varies during a single brake application between the 1/1000th and 1/2000th of the disc friction surface area. Heating zones detected around the disc surface had a direct correlation to surface depressions. Surface depressions leave open areas for wear debris to cluster and create granular micro-plates above the disc surface meaning contact between the pads and the disc occurs on these micro-plates, increasing the thermal loading at a single points, which consequently increase surface temperature. According to the work of Panier *et al.* (2004), this type of hot spotting corresponds to asperity or focal hot spots.

The conductive effects through the disc and pads were studied by Talati and Jalalifar (2009). A mathematical model was derived to predict the distribution of the generated heat energy into the disc and pads. Two distinct pressure distributions at the disc/pad interface were modelled; uniformly distributed pressure and a pressure to give uniform wear of the pads. The former is representative of new pads whilst the later portrays the pressure distribution seen after numerous

braking cycles, therefore it is more characteristic of the pad performance seen for the majority of a pad lifecycle. It was found that uniformly distributed pressure at the disc/pad interface will cause considerably greater temperatures in both the disc and the pads. With the uniform pressure distribution, the friction force increases with radial distance meaning more work is done towards the OD. Greater work done towards the OD gives rise to the additional temperatures not seen from the uniform wear pressure distribution, due to the frictional force not being dependent on radial distance. Additionally, a thermal gradient of approximately 600°C was calculated between the disc and pads; pad temperatures were the reason for the gradient as temperatures reaching above 800°C for uniform wear and over 900°C for uniform pressure whilst. Such a gradient is unrealistic, giving further evidence to support the third body layer theory.

4.9 Friction Pair Materials and Friction Coefficient Studies

The effects of friction coefficient during sliding has been studied for many years, for example the known stick-slip relationship which occurs from a difference between static and dynamic friction coefficients. Gao and Kuhlmann-Wilsdorf (1990) evolved this theory further with the introduction of the negative stick-slip phenomena; once the static friction force has been overcome, the μ level drops significantly before increasing with relative slip velocity until the dynamic friction coefficient is reached. Thereafter the μ is independent of relative sliding speed as described in Figure 4.13. Minor changes in density and/or chemical compositions were observed to impact the μ level with the dynamic and static μ values typically varying by 10%.

Grey cast iron is the general material of choice to fabricate a CV disc brake. High thermal conductivity characteristics enable the disc to remove thermal energy away from the friction interface and into the disc quickly whilst having a good level of damping properties to weaken the braking force vibrations. Hecht *et al.* (1999) looked at the former characteristic with respect to the diffusivity and how graphite flakes affect it. The flash laser method was used to measure the thermal conductivity of various samples of disc brake material with consisting of varying graphite flake lengths. A general observation that the diffusivity decreases with temperature was seen. It was also found that at low temperatures, the different alloys tested showed large differences in diffusivity but they became more aligned with a rise in temperature. Large graphite flakes within the structure increased disc diffusivity but they also increase the surface area where oxidation to occur and penetrate the disc.

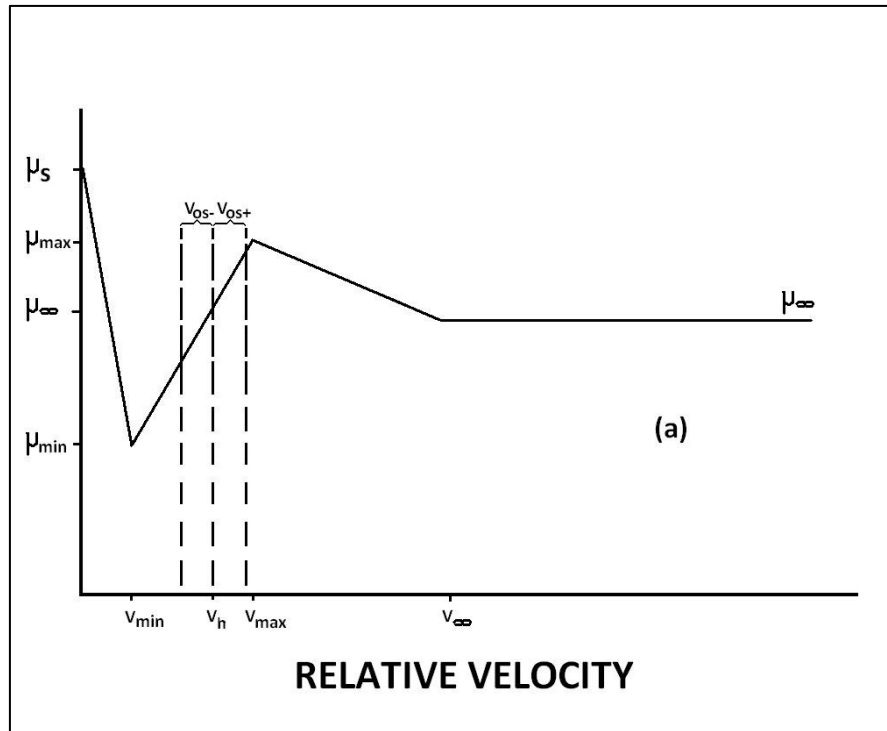


Figure 4.13: Negative stick-slip phenomenon (Gao and Kuhlmann-Wildorf 1990).

Metallic materials such as Copper, Aluminium, Steel, Brass, Iron, and Bronze have become common in brake pad materials. Brake pad properties can be modified depending by inclusion/removal of metallic fibres. Generally, there are two types of friction material compositions used in CVs, a low-steel (also known as low-met) friction material that can have up to 15% steel fibres whilst the other is a non-asbestos organic (NAO) material that uses a small mixture of the metallic fibres dependent on the braking duties they will be subjected to. Kim and Jang (2000b) demonstrated that the introduction of a mixture of metallic fibres in CV brake pad materials can give a more stable μ level during a brake application compared to the low-met material, which has a negative $\mu - v$ gradient; as speeds increase, the braking force reduces. Resultantly, vibrations are created and exerted to the driver through the chassis. Torque stability is also a source of vibration. Friction surface pressure was also proved by Kim and Jang to be insignificant on the μ level.

Kim and Jang (2000a) continued their investigation into the performance characteristics of friction material components with respect to the resin properties by replacing a small volume of the phenolic resin with aramid pulp. It was observed that a stronger resin material produces superior wear resistant properties compared with a softer equivalent. Interestingly, it is the softer resin which produces better heat resistance and friction stability, signifying a trade-off between these braking aspects. The ability to maintain the μ level at high temperatures for the

duration of a braking application means the pad is exposed to higher stresses for longer as friction force maintained. Porosity was also linked to heat resistant properties of the friction material with a lower porosity giving a better thermal stability and heat dissipation, preventing brake fade; brake force (μ level) decreasing with a temperature rise. Replacing some of the resin mixture with aramid pulp improved the stability of the friction force generated up to a certain, undetermined point. Further increases only increased the μ level without altering the friction stability further.

Friction materials can be manufactured with an excess of 20 separate constituents to find the balance between the desired μ level performance and wear rate. Lu *et al.* (2002) used the golden section principle of optimisation on a base line CV brake pad consisting of seven materials (plus the phenolic resin) to increase the friction coefficient from 0.357 to 0.419 whilst drastically reducing the wear rate by a factor of 2.16 for only a small 20% manufacturing price increase. Benefits are consequently delivered to the user as brake pads will need changing less often, for only a small increase in price. During this process, Lu *et al.* were able to show steel wool reinforcing metal material delivers a greater μ level and wear rate than its iron powder alternative, resulting in the optimised friction material having approximately six times the volume of steel wool to iron powder. Table 4.4 ranks the seven materials used in the CV pad (excluding the phenolic resin) for their abilities to decrease the wear rate and increase the friction coefficient. A trade-off between wear rate and μ level is well demonstrated by the material Coke, as it has the greatest effect on reducing pad wear but generates the poorest friction coefficient.

Table 4.4: Order of wear rate and μ level influences for CV brake pad materials (Lu *et al.* 2002).

	Wear Rate	Friction Coefficient
	Coke	Steel Wool
Strong Influence	↓	↓
	MgO	Iron Powder
	↓	↓
	Styrene-butadiene Rubber (SBR)	BaSO ₄
	↓	↓
	Steel Wool	Graphite
	↓	↓
	Graphite	SBR
	↓	↓
	BaSO ₄	MgO
Weak Influence	↓	↓
	Iron Powder	Coke

The effects on the μ level and stability at high temperatures with the inclusion of Copper, Aluminium and low carbon steel fibres was investigated by Jang *et al.* (2004). Brake pads were fabricated with 15% volume of one of the metallic fibres; the full pad makeup is shown in Table 4.5.

Table 4.5: Brake pad makeup (Jang *et al.* 2004).

Function	Material	Volume (%)
Organic Fibre	Aramid pulp	15
Binder	Phenolic resin	20
Solid Lubricants	Graphite	7
	MoS ₂	4
Abrasive	ZrSiO ₄	4
Friction Modifier	Cashew dust	5
Fillers	BaSO ₄	26
	Ca(OH) ₂	4

At low temperatures, a negative relationship was presented between the friction level and sliding disc/pad velocity when both the copper and steel fibres exist in the pad matrix, whereas aluminium fibres cause μ levels to remain constant with various rotation velocities. Temperature investigations also proved interesting with steel fibres keeping the μ level relatively constant with an increasing temperature. Copper also showed good thermal characteristics as only a

relatively small drop in μ level, for a lower wear rate, compared to steel. Finally, Jang *et al.* recorded wear rates with both aluminium and copper fibres remain constant when thermally tested against both grey cast iron and aluminium discs.

According to Abu Bakar *et al.* (2005), brake pad surface topography has a major importance when considering pressure distribution. A number of brake pads were examined and found to have a unique surface topography, slightly altering the pressure distribution from one pad to the next; new pads having rougher surfaces than worn pads. Greatest pressure was constantly observed towards the OD of the pad regardless of the condition. A method of validating the contact pressure was suggested by Abu Bakar *et al.* which is to compare the FE static distribution before attempting dynamic FE analysis as they successfully attached their FE results to experimental. Smooth surface assumptions have therefore been shown inaccurate to use when modelling with FE.

Another trend in brake research presently is to do with brake squeal. Consumer perception is the driving force behind this trend as brakes are commonly assumed faulty if brake squeal is detected, resulting in the user having the brake pads replaced. If the car is still under warranty then the OEM is obliged to pay for this replacement. Work carried out by Majcherczak and Dufrénoy (2006) has shown that the friction coefficient increases with the presence of brake squeal, showing the consumer perception to be mistaken. However, it is difficult to change the perception of the consumer in safety critical systems. Huge levels of research is being undertaken to eliminate brake squeal.

4.10 New Technologies

For many years annular disc brakes have been utilised in the aerospace industry. Recently, Erlston and Miles (2005) have attempted to apply this braking structure to automotive applications. With an annular brake pad, the pad contact area spans the entire disc friction surface. Advantages gained are a full 360° uniform pressure distribution around the disc/pad interface, a reduction in actuation force is needed to generate the equivalent braking force leading to longer pad life and better conductive heat dissipation through the pad material to the backplates and surrounding caliper components. Complex design of such a system (Figure 4.14) would surely increase manufacturing costs, although Erlston and Miles claim otherwise. Another disadvantage would be the weight gain from such a substantial caliper design, diverging from the current trend of weight reduction in the automotive industry.

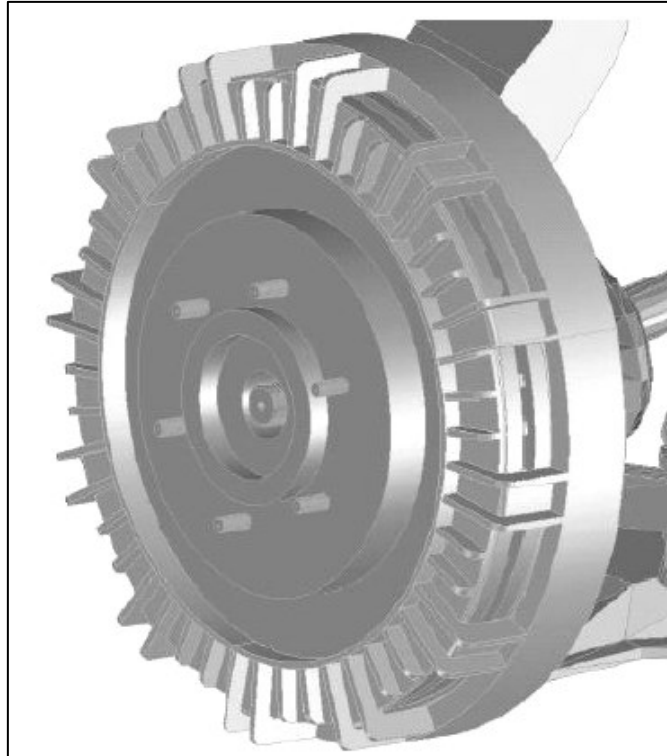


Figure 4.14: Annular disc brake design for automotive use (Erlston and Miles 2005).

Tretsiak and Kliuzovich (2006) have examined the possibilities of using self-boosting disc brakes on CVs as ‘intensifying plugs’ are inserted in the pad/carrier interfaces to prevent the pad’s motion in the circumferential direction. The effort which is usually used to move the pads whilst in contact is directly used as braking force instead, increasing the brake performance. A design like this enables less air pressure to be put into the service chamber for the same level brake torque, resulting in a smaller air reservoir being needed, consequently reducing the vehicle weight.

To maximise the returns on investment, many companies are using common components across entire product ranges to capitalise on economies of scale. ArvinMeritor gain economies of scale by using 80% of common products in all-but-one of their brake assemblies (Thomas and Jackson 2007). Current development of an auto adjuster is also planned to be used across the ArvinMeritor product line. Significant gains can be achieved through the auto adjuster as the brake pedal feel will always be the same with the clearance gap being kept constant for every braking application. Also, the thermal expansion of a pad will become less significant in the design as residual braking effects can be eliminated whilst making it quicker and easier to maintenance during pad changes. Parked braking will still be affected as the opshaft input from the mechanism will be the same.

Seglö and Svendenius (2010) demonstrated the capability to decrease the braking distance of a CV by implementing an electro-mechanical brake system. The traditional service chamber, as seen in Stevens (2009) was replaced by a motor actuator coupled with a self-enforced mechanism to reduce the power requirements from the motor. Such a design is excellent for reducing vehicle weight as the need for pneumatic air lines and pressure reservoirs are minimised. Seglö and Svendenius claim an EPB is implemented in such a brake system without mention to the thermal effects or the secondary brake actuation in the event of electrical failure. Courtesy

Traditional design methods are now under threat with the introduction of commercially available optimisation software. Tirović and Sergent (2010) optimised the topology of a high performance racing car brake caliper using the OPTISTRUCT software package. The standard and optimised calipers were structurally tested for deflections under loading via FE modelling. A 29% weight reduction was achieved whilst delivering a similar structural rigidity. The importance of boundary conditions in such a technique can determine the effectiveness of the procedure, with incorrect information leading to high levels of error and a poor design. Due to the optimisation process only being set to minimise the volume for the same structural rigidity with no thermal analysis incorporated, the true stress and deflections from the new caliper design are unknown under operating conditions. Nevertheless, the power of optimisation software for the speed of design was shown.

Digital image correlation (DIC) is a new process recently developed which can be implemented for to measure structural displacements without contact. Two separate cameras are placed at different angles around the test specimen that has a white base coat with randomly applied black paint spots over the top. Displacement is calculated by measuring the relative movement of the spots. Tirović *et al.* (2012) demonstrated the capability of such a technique, as a validation tool for FE modelling by comparing results for a CV brake caliper when the user defined boundary conditions are correct. Results of a static experiment at ambient temperature and without torque were presented showing good agreement between the two. A demonstration of the possibilities of the DIC method was successfully achieved, however, meaningful results, such as the displacement with thermal affects and/or when a brake torque is applied, are yet to be investigated. The possibility for future work involving such a method is therefore obvious.

Electro-mechanical braking systems are fast becoming a hot topic in brake research due to their ability to be incorporated into a brake by wire (BBW) system, saving on vehicle weight faster response times. The potential of BBW systems is being explored. Integration of the brake ECU

with the main vehicle ECU gives the opportunity for information such as vehicle speed and weight to be available to the BBW ECU, enabling accurate calculation of the brake force necessary for a desired deceleration. Hirose *et al.* (2010) have capitalised on this to produce a system of warning the driver that they are close to a collision via a light in the driving compartment, before applying the brake automatically 0.8 seconds later. A time to collision of 2.3 seconds was found to give a good deceleration from 30 km/h to stationary, without unacceptably interfering with the majority of drivers' braking action.

4.11 Literature Review Summary

A detailed search of the literature has been presented here which spans a large proportion of the braking topic, focusing principally on the thermal aspects. Brake simulations have become common place amongst brake designers with maximum temperatures and cooling performance showing to have a high importance. Heat transfer coefficients have frequently been considered constant for these calculations to reduce computational time and in some cases a lack of reliable data. Lumped coefficients only seem useable when dealing with early stage designs to get a feeling of the temperature distribution as their inaccuracies hamper their precision. With the exception of the natural convection studies investigated, authors are interested in the dynamic effects of the brake during applications to evaluate the performance characteristics or structural integrity whilst the brake is retarding the vehicle. Parking applications have previously been ignored but the introduction of an EPB has generated a need to understand the thermal interactions during the stationary brake applications.

Breaking the three heat dissipation modes down into their individual factors, each has been shown to have significant effects on the brake temperatures in certain conditions. Convection is widely seen as the greatest contributor to brake cooling with the vehicle speed being proportional to the convection rate. Historically, CFD and numerical modelling have been used to find h_{conv} values with the former recently becoming the most favourable with increasing ease of usability. More air flowing through the vane will positively impact on the convective cooling rate, whilst any rise in air pressure has a detrimental effect from the conservation of mass law. Fluid recirculation within the vane also hampers the cooling rate although tumbling fluid from formed vortices can reduce the recirculation area minimising the impact. Thus far, little to no work has been published regarding the fluid flow properties through and around a disc brake with the flow being driven by buoyancy affects only. In this scenario, fluid interactions with the wall will be critical. For dynamic modelling, the k- ϵ model has been shown to insufficiently predict the heat transfer properties with a heavily turbulent flow. Natural

convection flows will be much closer to laminar flows in comparison, resulting in a more complex model being needed. Also, the inclination angle influences the number of vortices present, how this discovery relates to the individual in-vanes flows during the cooling phase is undetermined and is a potential area of research for this project.

Determining the rate of conduction has also been proved difficult. Accurate material property data is needed to determine the thermal contact resistance, which is used to find the conductivity coefficient. Four methods to measure thermal conductivity has been presented with the Laser Flash method appearing to be the most useful for finding friction material data although the technique is complicated. Contact pressure is said to have a linear relationship the h_{cond} but his observation has only been shown at room temperature. How conductivity changes with both temperature and pressure for various friction materials and disc brake conditions is a research opportunity for this project.

The amount of thermal energy dissipation via radiation is dependent on the emissivity of the material. Where conduction and convection are usually kept constant for heat dissipation modelling, radiation is often overlooked completely as it is insignificant compared to convective cooling during high speed testing. Even when it is included, the variability in the literature values is considerable. For low speed and stationary testing, whilst the disc is still extremely hot, the radiative effects will potentially be having the largest effect on the disc cooling as well as caliper component heating. Emissivity variations with temperature are needed to fully understand the role of radiation for the entire cooling phase with an IR camera commonly used to capture such data.

Different friction material matrix compositions produce differing pad and friction pair interaction characteristics. Metallic fibres are used to change the wear rate and thermal stability of a pad to suit the drive conditions the particular pad will be used in. A negative stick-slip relation was observed to drop the level of friction drastically before recovering back to the dynamic μ level when a force is applied. In parking, the temperature at the disc is consistently cooling over time. If the weight of a CV was to reach the static μ level under its own weight on a hill, the sudden drop would allow the CV to start rolling uncontrollably down the hill. Dependant on the material composition, friction can alter with temperature. The need to understand the static friction level variation is important in the design of the EPB.

Finally, modelling complexity has increased dramatically with newer technology advancing the computing power. FE simulations have been useful at predicting hot band developments, maximum temperatures and the direction of heat flow amongst others. A common feature of all

the models made is that heat transfer coefficients, friction data and material properties are kept constant for the duration of the simulation. A few exceptions are presented (for example the work of Dufrénoy (2004) where the modulus was a function of applied force) yet no model has attempted vary all three simultaneously. Duration length of the dynamic brake application gives little chance for some properties to significantly change. Parking applications present an opportunity to model variations with temperature and contact pressure.

5 Experimental Equipment and Procedures

Any investigation into a brake system will require an element of experimentation to validate numerical models produced. Common brake testing is conducted on inertia brake dynamometers, giving friction and dynamic brake characteristics. This project is different, in the respect that it is exclusively looking at heat transfer in parking scenarios. Large inertia wheels are not necessary as the simulation of CV inertia under braking loads is not being investigated. Therefore, the much simpler Thermal Rig located at Cranfield University, used by Voller (2003) and Culierat (2008), was used successfully. Details of the Thermal Rig, the instrumentation used on it, material properties of the brake assembly and the uncertainty associated with the instrumentation will all be discussed in this Chapter before describing the experimental procedures used, with a discussion on their development and some initial findings.

5.1 Laboratory Equipment

A standard² 434/234 mm straight radial ventilated disc brake and the Elsa 225 caliper assembly described in Figure 1.2 were mounted on the modified Thermal Rig. The disc brake was heated and left to cool, simulating the cooling phase of a parking application. Various instrumentation was required to capture the brake assembly's cooling performance, such as a displacement transducer and multiple types of thermocouples. This section discusses all apparatus used in the laboratory in conjunction with the Thermal Rig.

5.1.1 The Thermal Rig

The Thermal Rig installed at Cranfield University is an inline arrangement, consisting of an ME 415 V 7.5 kW motor outputting to a dual speed and torque sensor, then to a bearing unit, which then delivers the torque to the disc brake via a splined shaft, as shown in Figure 5.1. The ME motor is controlled by a Eurotherm CFW 08 7.5 kW, 3 phase inverter, enabling a disc brake rotational speed of up to 1,500 rpm, with at a 50 Hz supply. The Eurotherm inverter had the desired property of external remote control, allowing improved control over the motor. Clearly, such a low power setup has many disadvantages when compared to a full scale brake dynamometer as no dynamic friction braking applications can be tested. Yet, the simple setup does offer advantages too. For example, with the absence of friction braking, there is also the lack of pad wear. Wear particles on the surface are a cause of surface hot spots, which can make

² It should be noted that the terminology "standard" disc brake is used within Meritor and throughout this thesis. It refers to this particular disc brakes ability to mount onto either side of the vehicle and onto any current brake configuration.

experimental repeatability difficult to achieve. A constant emissivity is able to form across the disc brake friction surfaces also without the presence of surface hot spots. To get the disc brake to operating temperature, an induction heater coil was used in the absence of friction heating, which is described further in section 5.1.6.

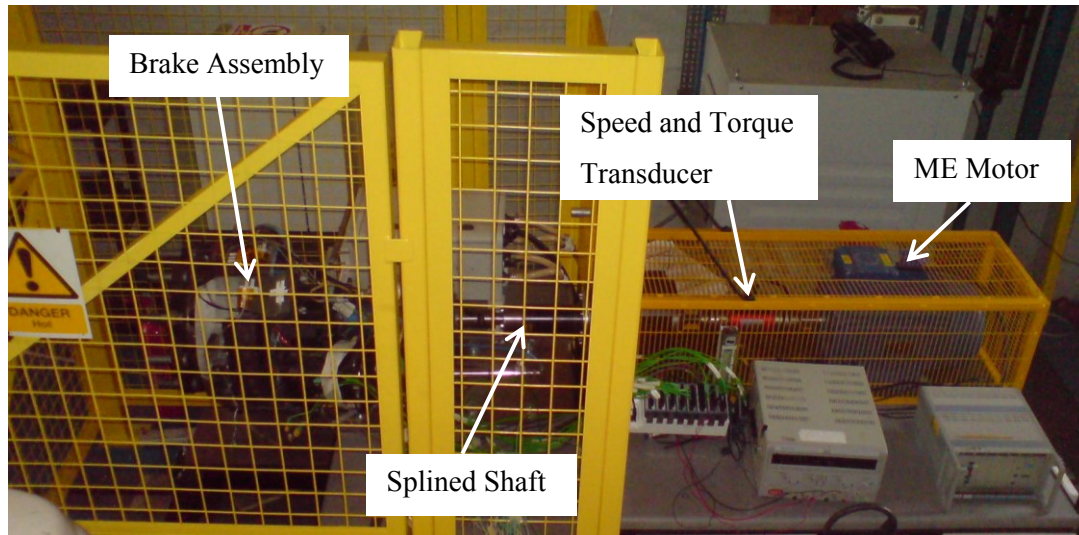


Figure 5.1: Full Thermal Rig

The Thermal Rig has evolved over a number of years. It was initially used by Voller (2003), where the disc brake mounted directly on the output of the bearing unit. Modifications made by Culierat (2008) improved the Thermal Rig's capability by implementing a frame to mount a full caliper assembly. After Culierat's development, the Thermal Rig was not commissioned at the start of this project. The remainder of section 5.1 outlines the equipment sourced (with the exception of the safety cage) to enable Thermal Rig commissioning for full thermal analysis testing of a CV brake assembly.

One final modification was planned to which would have seen the installation of a pneumatic ram designed to introduce static torque. The design of the modification is shown in Appendix F but it was not implemented due to the change of project priorities.

5.1.2 Temperature Measurements

To measure the temperature of the disc brake, pads and caliper temperatures a range of thermocouples were used. All of the contact thermocouples used were K type, which are suitable for measuring a large range of temperatures, from approximately -200°C to 1300°C . Two different Nickel based alloy wires are used to make K type thermocouples; one with 90% Nickel, 10% chromium and the other with 94% nickel and the remaining 6% a mixture nickel alloys that include aluminium, manganese, iron, cobalt and silicon, discussed in detail by Davis

(1997). For experiments conducted in this thesis, the temperature range thermocouples will be measuring is from 0°C to a maximum of 500°C, producing a voltage output from 0 mV to 20.6 mV (NIST ITS Thermocouple Database 1999).

There were three different styles of contact thermocouples on the test rig: welded tip PTFE, probe and rubbing thermocouples. The welded PTFE thermocouples were placed at individual points around the brake assembly and held in place by heat resistant tape. Probe thermocouples were placed inside three holes drilled in the brake pads, to enable the transient temperature difference to be measured through the pads. The three holes had a 1.6 mm in diameter and 10 mm in depth, two in the friction material and the other in the backplate. Likewise, various holes were drilled in the hat section of the disc brake and the wheel carrier. Finally, rubbing thermocouples were positioned against the disc brake's friction surfaces. Rubbing thermocouples were used as they enable temperature readings to be taken whilst the disc brake is rotating and during the stationary cooling phase.

The uncertainty associated with thermocouple measurements was investigated in depth by Nakos (2004). It was found that for uncalibrated thermocouples, the uncertainty in the measurement was the largest of either $\pm 2.2^\circ\text{C}$ or $\pm 0.75\%$. For temperatures below 293°C the former value shall be used with the latter used for hotter temperatures. Measurement uncertainty will be returned to in section 5.3.

5.1.3 Measurement and Data Logging Equipment

To collect data from the experiments various measuring instruments were used on or around the test rig. To collect and control these instruments, a variety of National Instruments (NI) products were used. The specification sheets for all the NI products can be found in Appendix G, with the individual modules and their characteristics explained below.

5.1.3.1 CompactRIO

The CompactRIO is an embedded controller which allows real-time data acquisition and instrumentation control. By combining the CompactRIO with the NI cRIO-9112 chassis, eight individual modules could be used simultaneously for data logging or control purposes. Utilisation of on board FPGA processors enables the CompactRIO to sample at multiple frequencies.

5.1.3.2 Thermocouple Modules

Three different types of module were used to capture the temperature readings from the thermocouples in the CompactRIO; they were the NI 9211, NI 9213 and the NI 9214. The generated signal produced by thermocouples actually follows a 9th order polynomial pattern (NIST ITS Thermocouple Database 1999). All three thermocouple modules are controller by the LabVIEW program described in section 5.1.3.5. The linearization of the thermocouple signal is conducted within LabVIEW, providing an accurate reading of the temperature.

The NI 9211 is the simplest of the three thermocouple modules. It is a straightforward analogue voltage reader, sensitive enough to detect the small voltages changes generated by the dissimilar materials in the thermocouple wire. The voltage range for the NI 9211 is ± 80 mV, making it incapable of detecting voltage signals from the majority of laboratory instruments, due to these generally having a voltage range two orders of magnitude larger. Up to four thermocouples can be logged simultaneously with this module, at a maximum sampling rate of 14 Hz, with a resolution of 24 bits. According to the specified data sheet, the NI 9211 has a maximum uncertainty of on 1.3°C (National Instruments NI 9211 Datasheet).

The NI 9213 was the next thermocouple module used in conjunction with the CompactRIO. Essentially, it is very similar to the NI 9211 but the number of available channels to record is increased from four to 16. The ability to sample at a higher frequency was also added, 75 Hz if all 16 channels are being used or 100Hz if 12 or less are used (National Instruments NI 9213 Datasheet). An increase in the uncertainty was also quoted for the NI 9213 to be 1.8°C.

Finally, the improved NI 9214 thermocouple module was also used in the CompactRIO. Like the NI 9213, the NI 9214 offers 16 channels of instrument recording with a high degree of accuracy. According to the NIST ITS-90 Thermocouple Database, a K type thermocouple will output 20.6 mV when heated to 500°C. A stated accuracy range of ± 36 μ V (National Instruments NI 9214 Datasheet) is representative of an uncertainty 0.85°C, at 500°C.

5.1.3.3 Universal Module – NI 9219

As the name indicates, versatility is the greatest attribute of the NI 9219. The primary function of the NI 9219 is to detect changes in analogue voltages. The main difference between NI 9219 and the NI 9211 is that the NI 9219 cannot detect extremely low voltage changes outputted by thermocouple but it does have the ability to operate in the range of ± 60 V, vastly greater than the NI 9211. There are four ports on the module allowing four simultaneous voltages to be recorded at once. Each port is constructed with six pins; two for the input signal, the remaining

four pins allow the module to supply a maximum excitation voltage of 2.5 V in a quarter, half or full bridge circuit.

5.1.3.4 Output Voltage Module – NI 9263

The NI-9263 can is designed to deliver a simple analogue output voltage. The operating range that it can deliver is ± 10 V, with an accuracy of 1.1%. The NI-9263 has the capability to control four individual components at once.

5.1.3.5 High Speed Digital I/O Module – NI 9401

A digital pulse signal is transmitted by a speed sensor placed on the Thermal Rig's driveshaft. To read such a signal, the NI 9401 digital input/output (I/O) module was acquired. Eight digital signals can be either read or sent with this unit, at frequencies up to 30 MHz.

5.1.3.6 LabVIEW Program

LabVIEW is a software program developed by National Instruments, which can be used simultaneously with their own instrumentation and equipment produced by other manufacturers. It was used exclusively in the laboratory for data acquisition and control. The software interface utilises two separate screens called the front panel and the block diagram. A simple graphically user interface enables the user to easily write a deployable script file from the block diagram, whereas the front panel is a real time screen that allows the operator to view measured data and control systems present in the experimental setup.

Having the CompactRIO in the system enables real-time programming, which is advantageous when accurate transient measurements are necessary. In preliminary experiments it was found that as the bearings became warm, the rotational speed delivered by the motor varied as the resistance in the system reduced, for no change in motor setting. By using Real-time programming, in conjunction with a speed sensor (located on the driveshaft) connected to the NI 9401, a closed-loop motor controller was created to ensure the rotational speed was kept at the set target. An inbuilt PID control block was used to automatically calculate change in output signal. Tuning the PID controller was done by the trial and error method. This was acceptable as the matching speed was not critical for heating the disc brake in a control manor. If a fast response matching time is important, other methods such as Ziegler–Nichols method are available (Haugen 2010).

The closed-loop motor control is displayed in Figure 5.2. Being a digital device, the signal delivered by the speed sensor is in Boolean form. LabVIEW is set to decode the signal into a frequency reading, which is then averaged before converted into a speed. After a conversion

into voltage, the signal is passed into the PID controller, with the output voltage sent to the motor inverter via the NI 9263 (block AO1). All this occurs inside a “while” loop, depicted by a grey rectangle, and would continue until the “Stop” button was pressed on the front panel.

A case structure, which acts like an “if loop” in standard programming language, was placed within the while loop. The motor inverter is unable to work from a zero but from a minimum speed. Inclusion of this case structure ensures that when the required speed is zero, i.e. no rotation, the motor is switched off. A 5 V transistor, situated in between the CompactRIO and the inverter, switches on/off the supply voltage to the inverter. If the requested rotational speed is zero, or a negative value, the output voltage from the NI 9263 (block AO3) would be zero. Otherwise, the output voltage from the NI module was large enough to switch the transistor and allow the inverter to operate.

A second while loop was set to run in parallel with the motor controller loop for data acquisition. This loop was much simpler, requesting the channels for data collection, the file they were to be stored in and the sampling rate the second while loop was to run at. The latter was set to 0.5 Hz (or sample every 2,000 ms), much slower than the motor control loop, set to sample every 15 ms.

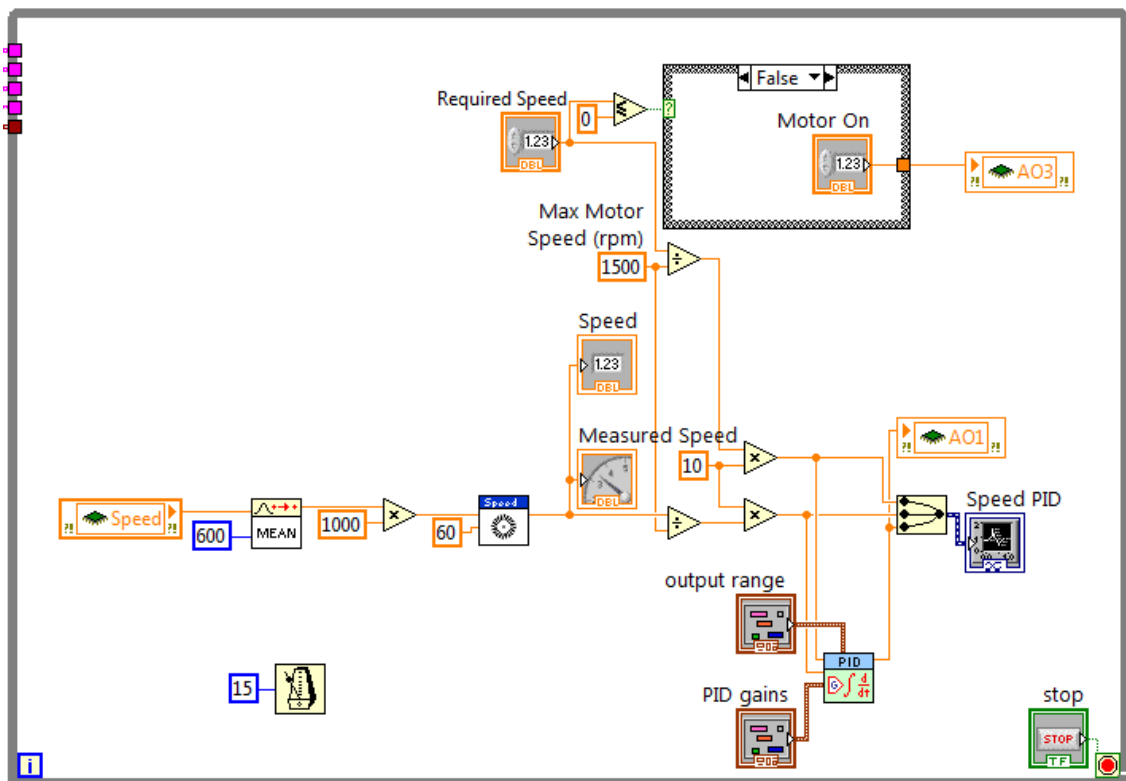


Figure 5.2: LabVIEW closed-loop motor controller.

5.1.4 Displacement and Input Force Transducers

Capturing the amount of brake pad displacement is the key measurement in determining how much thermal contraction is seen in the braking system during the coolback phase. Ideally, a sensor would be placed inside the pad to measure its movement directly, however, this was not possible. Subsequently, the amount of pushrod displacement was recorded via a Sensonics LVDT *sr* series transducer mounted on the rear of the service chamber; the displacement transducer provides a voltage of ± 10 V. When air pressure is supplied to the rear of the service chamber, the rubber membrane pushes against the pushrod, delivering an input force to the system. The displacement transducer is located in such a way that it measures the amount of membrane displacement, and hence the pushrod travel; the pushrod travel is referred to as actuator displacement. Applying the opshaft ratio to the measured actuator displacement will give a calculated pad displacement. The pushrod was strain gauged to measure the input force delivered to the brake system when the air pressure is supplied, again giving a voltage output of ± 10 V. Such an arrangement has previously been developed and proved reliable by Meritor.

The output signal from the displacement transducer is not actually a function of displacement but of velocity instead. To integrate the signal from velocity to displacement, the displacement transducer was connected to an integration (signal processing) box and then into the NI-9219 CompactRIO module. It was possible to connect the transducer directly to the CompactRIO system and integrate the logged signal however this option was not taken for two reasons: the integration box is also able to deliver the excitation voltage of 10 V to the transducer and it also has a drift reduction feature built in. The strain gauge was also connected to the integration box before connection to the NI-9219 as it too needs an excitation voltage of 10 V.

5.1.5 Pressure Transducer

The input pressure is measured via a HBM P8AP pressure transducer. It is located at the inlet to the service chamber. When connecting to the NI-9129 module for the purpose of logging the data, a full bridge configuration was used to supply an excitation voltage of 2.5 V; Figure 5.3 displays the wiring diagram used. For more information on the workings of the pressure transducer and the mounting position see Culierat (2008).

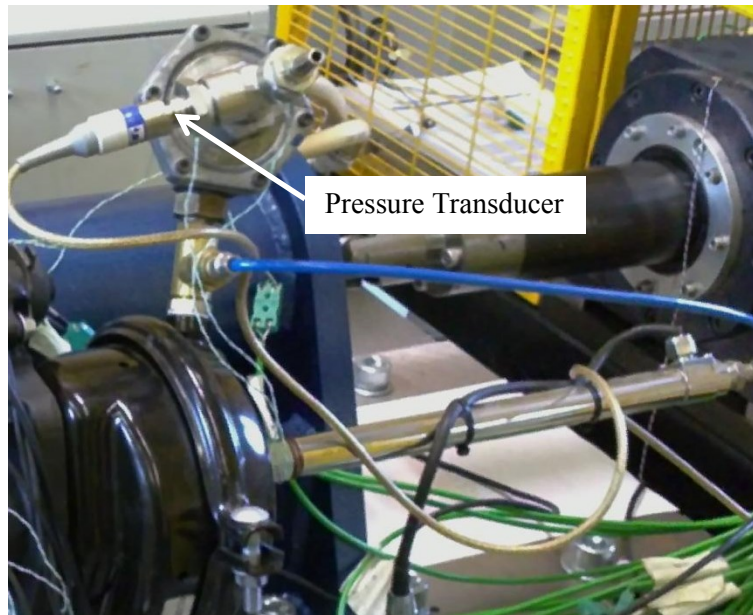


Figure 5.3: Connection between the pressure transducer and the NI-9219

5.1.6 Induction Heater Coil System

The main purpose of a braking system is to convert the vehicle's kinetic energy into thermal energy. Ideally, to simulate this situation in the laboratory a high powered motor and/or large inertia wheels are needed to overcome the frictional torque when the pads are applied to a rotating disc. However, as discussed in section 5.1.1, the motor on the Thermal Rig produces only a very small amount of torque, preventing the employment of the drag braking technique to generate heat into the system. Induction heating was therefore chosen as the alternative heating method, similar to the methods used by McPhee and Johnson (2007). The advantage of induction heating is that it is a contactless procedure, reducing mechanical wear of the disc brake and pads with a quick heating time.

Induction heating works by placing a piece of metal (in this case, the disc brake) inside a coil. A high voltage and current are passed through the coil at high frequency (100 Hz), causing the heat generation in the metal components. Modifications made to the Thermal Rig (see Culierat 2008) prohibited the ability to use the simple coil originally used by Voller (2003), meaning a specialised heater coil shape had to be designed. Furthermore, the ability to experiment with the wheel shrouding the complete brake assembly was also desired, adding complexity to the coil design. The induction coil shown in Figure 5.4 was the final coil design produced and installed on the test rig. This design is improvement on the original design (Culierat 2008) as it benefits from a smaller inner diameter of 70 mm, leaving only a 12.5 mm gap between the coil and

surface area of the disc. Using such a small gap reduces the amount of lost energy from the coil, producing quicker disc heating times.

Both the coolant (deionised water) and electrical current are supplied to the induction coil by the induction box. It was therefore imperative to decide on the location of the induction box before designing the coil, see Figure 5.4. The centre of the induction box was installed 259.2 mm away from the disc ID. A 5 mm gap was left from the edge of the coil to the nearest point on the ID in an attempt to prevent directly heating the disc bearing. Powder coated copper piping with an OD of 8 mm was used to fabricate the coil.

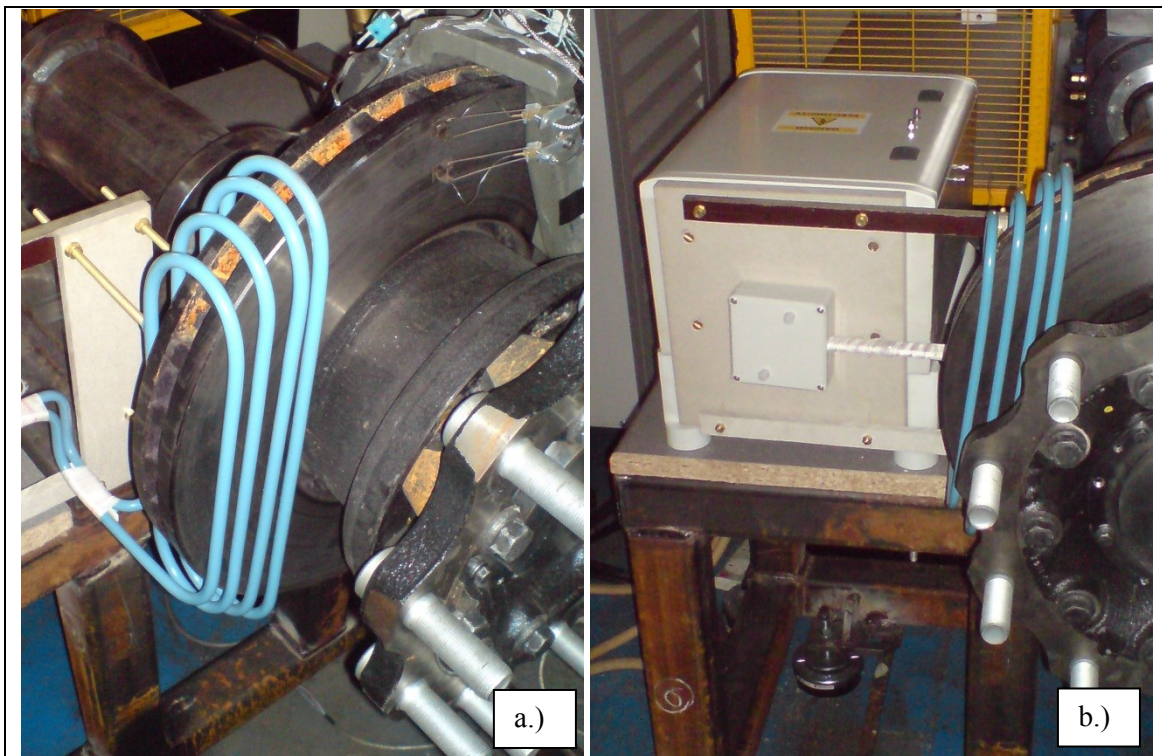


Figure 5.4: a.) Installed induction heater coil and b.) the induction box

5.2 Material Properties of Brake Assembly Components

Material properties are crucial to any modelling process. Meritor provided a data sheet comprising of values for various material properties, these values are given in section 5.2 and used in all relevant models within this project.

5.2.1 Brake Caliper

The brake system is made up of many parts (Appendix H), however, the main areas of interest are the caliper, disc brake and brake pads. The caliper used was an Elsa 225 Service caliper (Figure 1.2). The caliper is constructed by three separate parts; the pad carrier, the bridge and

the off-centred operating shaft and gearing system housing. The pad carrier locates the assembly as it is fastened to the vehicle axle and houses the brake pads. Two tappets connect the bridge to the carrier, allowing the sliding motion in the axial direction. The operating shaft and gear housing is attached to the bridge such that it moves axially with it. Finally, the service chamber, with the parking brake, is fixed to the operating shaft and gear housing (see Appendix H for a section view of the whole brake system). All the properties of the pad carrier, the bridge and the operating shaft and gear housing are given in Table 5.1.

Table 5.1: Spheroidal Graphite Iron material properties for the pad carrier, bridge and housing components (from Meritor HVBS).

	Value/range	Unit
Density	7150	kg/m ³
Young's modulus	170	GPa
Poisson's ratio	0.275	-
Specific heat capacity		
20-100°C	515	J/kg K
100-200°C	530	
200-300°C	550	
300-400°C	570	
Coefficient of thermal expansion		
20-100°C	11.2	10 ⁻⁶ /K
100-200°C	11.8	
200-300°C	12.4	
300-400°C	12.9	
Coefficient of thermal conductivity		
100°C	34.2	W/m K
200°C	34.1	
300°C	33.9	
400°C	33.8	

5.2.2 Disc Brake

The disc brake design used for the thermal investigations was on a grey cast iron straight vane ventilated disc brake of anti-coning configuration. It has an OD of 434 mm and an ID of 234 mm, leaving an effective working radius of 100 mm. There are 30 vane channels between the two friction surfaces, which are vital for cooling. Including the hat section the discs total mass is 35.3 kg. Known disc brake material properties are presented in Table 5.2 and further design details given in Appendix I.

Table 5.2: Material properties for the disc brake (from Meritor HVBS).

	Value/range	Unit
Density	6900 – 7100	kg/m ³
Young's modulus	120	GPa
Poisson's ratio	0.26	-
Specific heat capacity	470	J/kg K
Coefficient of thermal expansion	11.7	10 ⁻⁶ /K
Coefficient of thermal conductivity	48	W/m.K

5.2.3 Friction Materials

Thermal effects of two contrasting friction material, T3016 and FER 4567, were studied in this investigation. The friction material T3016 is a softer, more compressible pad material designed for use in vehicles that do numerous stops from low speeds, such as buses. FER 4567 friction material is a harder material used for driving cycles that are much less frequent compared to buses but from higher speeds, therefore, they more demanding braking applications, such as coaches and lorries operating predominately on motorways. Table 5.3 displays the known pad properties for the T3016 friction material whilst the known FER 4567 friction material properties can be seen in Table 5.4.

At the beginning of the project, consideration of these two friction materials was deemed important in order to understand the performance characteristics of the two possible extremities of brake pad material properties on the EPB. However, in the course of the project, the research focus shifted from EPB and towards generic heat transfer within and dissipation from a stationary disc brake assembly. Both friction materials attach onto a generic backplate design, with steel being the material it is made from. Material properties for the backplate are given in Table 5.5.

Table 5.3: T3016 friction material properties (from Meritor HVBS).

	Value/range	Unit
Density	2500 – 2700	kg/m ³
Young’s modulus	8 – 10	GN/m ²
Poisson’s ratio	0.29	
Specific heat capacity	800	J/kg K
Coefficient of thermal expansion at 190°C	90	mm
Expansion at 260°C	0.33	%
Coefficient of thermal conductivity		
100°C	3.10	W/m K
200°C	3.00	
300°C	2.60	
400°C	1.90	

Table 5.4: FER 4567 friction material properties (from Meritor HVBS).

	Value/range	Unit
Density	3000 - 3100	kg/m ³
Young’s modulus	610	MPa
Poisson’s ratio	0.2	

Table 5.5: Brake pad backplate material properties (from Meritor HVBS).

	Value/range	Unit
Density	7820	kg/m ³
Young’s modulus	207	GN/m ²
Poisson’s ratio	0.29	
Specific heat capacity	490	J/kg K
Coefficient of thermal expansion	11.7	10 ⁻⁶ /K
Coefficient of thermal conductivity	43.6	W/m K

In addition to investigating the difference between two friction materials, seven pairs of brake pads have been supplied for each material with different levels of wear, replicating different stages of the pad lifecycle. For example, pad sets 1/2 and 3/4 have both been through a fade tests, which is termed as the “faded state” throughout, whilst sets 5/6, 7/8 and 9/10 have been through just a bedding in test; two set of brand new pads have also been supplied, termed a “bedded state” throughout. It should be noted that the numbering convention for each pair of brake pads is that the inboard pad is given an odd number, with its corresponding outboard pad given the following even number.

A bedding test exerts a pair of pads to 200 brake applications at low speed and temperature on a dynamometer. Brake pads in the bedded state represent new pads recently fitted to a vehicle. Surface imperfections would not have been removed leaving the friction material thermally unstable.

Two sets of dummy pads were also fabricated, one set from steel and the other from aluminium. The dummy pads will have constant known properties throughout so will be used for control experiments and comparisons.

5.3 Uncertainty analysis

Many laboratory experimentation was conducted throughout this investigation. During the testing procedure, a variety of measurements were taken, including temperature, pressure and speed. However, it is inevitable that the measured values for variables were not the “true” value as an amount of error is always associated with experimentation. As described by Moffat (1988), “*the error in a measurement is defined as the difference between the observed value and the true value of the intended measurand.*” This definition can be defined mathematically by equation (5.1).

$$X = X(\textit{measured}) \pm \delta X \quad (5.1)$$

The true value is represented by the term X , the measured reading is $X(\textit{measured})$ with δX being the difference between the two. Calculation of equation (5.1) delivers a precise value of a specific reading, yet the value of δX is often never known, making it impossible to find the true value. A large part of the problem is the correct identification of the type of error.

The meaning of the term “true” value is not as straightforward as one may think, as described previously by Moffat (1985). Examining the result an instrument produces will highlight the issue. For instance, taking the use of a thermocouple as an example, the reading at the junction of the thermocouple and the solid surface can be said to be the estimate of the true value (T_1); this is an intrinsic error. However, there is usually an amount of gas flowing over the surface, cooling the thermocouple junction slightly. Even though the cooling may be small, the second estimate of true temperature (T_2) should account for this. Interaction with of the measuring equipment and non-experiment specific conditions (i.e. with the surrounding air) is known as sensor interaction. Further refinement is made if the amount fluid of air passing over the surface is calculated as if the thermocouple was not there (T_3). At some point a judgement is needed to say what the true value estimation is being taken as. In the case of this investigation, intrinsic

errors only for any of the measuring systems will be used as the true value estimation; as seen for (T_1).

Uncertainties during experimentation are generated generally in two forms, random uncertainties and systematic uncertainties. Systematic uncertainties are functions of the experimental process, producing an element of bias to the results, whereas random errors occur, as the name suggests, in a random manner. Statistical analysis can be conducted on random errors, allowing an element of correction or justification to their reading. Conversely, systematic errors cannot be detected by statistical means and therefore present the danger of generating conclusions based on inadequate data. Efforts must be taken to ensure all experimental procedures minimise any systematic uncertainties. Systematic uncertainties that can be measured are those of created from the experimental instrumentation. For example, if a thermocouple is measuring the temperature too low, it will under predict the temperature by the same proportion for every experiment.

With temperature measurements being the predominant experimental reading taken in during this investigation, it is important to understand the uncertainty associated with thermocouple system. As stated previously, there uncertainty for individual thermocouples is known. However, the thermocouple system comprises of more than just the physical thermocouple, with uncertainties propagating though. The total uncertainty is calculated by addition of the uncertainties at each stage of the process, generating an overall system uncertainty. In the case of the thermocouple, there is a junction box coupling connecting the thermocouple and the cable, δX_{junc} , a connection between the cable and the thermocouple module in the CompactRIO, δX_{conn} , the thermocouple module itself located in the Compact RIO, δX_{NImod} , as well as the thermocouple, δX_{thermo} , to consider.

$$X = \bar{X} \pm (\delta X_{thermo} + \delta X_{junc} + \delta X_{conn} + \delta X_{NImod}) \quad (5.2)$$

Two of the uncertainty terms displayed in equation (5.2) are known from earlier work discussed in section 5.1; δX_{thermo} and δX_{NImod} . Through experimentation, Nakos (2004) found that provided there is no temperature gradient through the thermocouple/cable junction then the uncertainty in the recorded measurement is so small it can be neglected, due to the connector pins being of lesser quality material than the thermocouple cable. By assuming that this is the case for the experiments conducted in this investigation, the δX_{junc} term in equation (5.2) can be disregarded. This assumption is valid to make as there is sufficient length of thermocouple wire, enabling the junction boxes to be kept out of the range necessary to produce sufficient heat

transfer that would cause a gradient across it. Nakos also investigated the uncertainty for the connection between the cable and a National Instruments terminal block. A conservative uncertainty value of $\pm 0.8^{\circ}\text{C}$ was suggested. Although the equipment used was different to that used here, the same value will be used as the connection from the various modules from National Instruments are very similar, which will cause the uncertainty to be fairly similar. In addition, as the value was described as conservative anyway, it can account for a potential slight increase with different modules. The uncertainty in a thermocouple reading can therefore be calculated as

With three thermocouple modules used in the CompactRIO, there were three different values of thermocouple uncertainty that needed to be calculated. Starting with the NI 9211, values of 2.2°C , 0.8°C and 1.7°C for δX_{thermo} , δX_{conn} and $\delta X_{NI mod}$ respectively, were put into equation (5.2).

$$X = \bar{X} \pm 4.7^{\circ}\text{C} \quad (5.3)$$

A total uncertainty of $\pm 4.7^{\circ}\text{C}$ was found for the thermocouple system, using the NI 9211. Unfortunately, this value seemed to be too conservative, which could potentially lead to valid results being rejected on the basis on uncertainty. Thankfully, there was a set of results to compare to that will clarify whether this uncertainty estimate is indeed too conservative. Figure 5.5 displays the overall thermocouple system error when using K type thermocouples with the NI 9211 module (taken from the NI 9211 datasheet). Instrumentation used in the production of this graph were calibrate to a high level. It was shown that the uncertainty range for the temperatures in this investigation was considering between 2.2°C and 2.5°C , approximately half the value calculated. Consequently, it is confirmed that the calculated value in equation (5.3) is too conservative. Therefore, the values shown in Figure 5.5 were used.

It is a similar case for the other two thermocouple modules. An uncertainty value of $\pm 4.8^{\circ}\text{C}$ was calculated for the NI 9213 module, with the NI 9214 generating an uncertainty of $\pm 3.8^{\circ}\text{C}$. Figure 5.6 shows the former configuration has an uncertainty range between 2.5°C to 3.0°C , somewhat lower than the calculated value. A big difference is found with the final thermocouple as the uncertainty range displayed in Figure 5.7 is between only 0.35°C and 0.45°C . A discrepancy is presented here as this value is much lower than what Nakos found for the thermocouple uncertainty by itself, let alone for the full system.

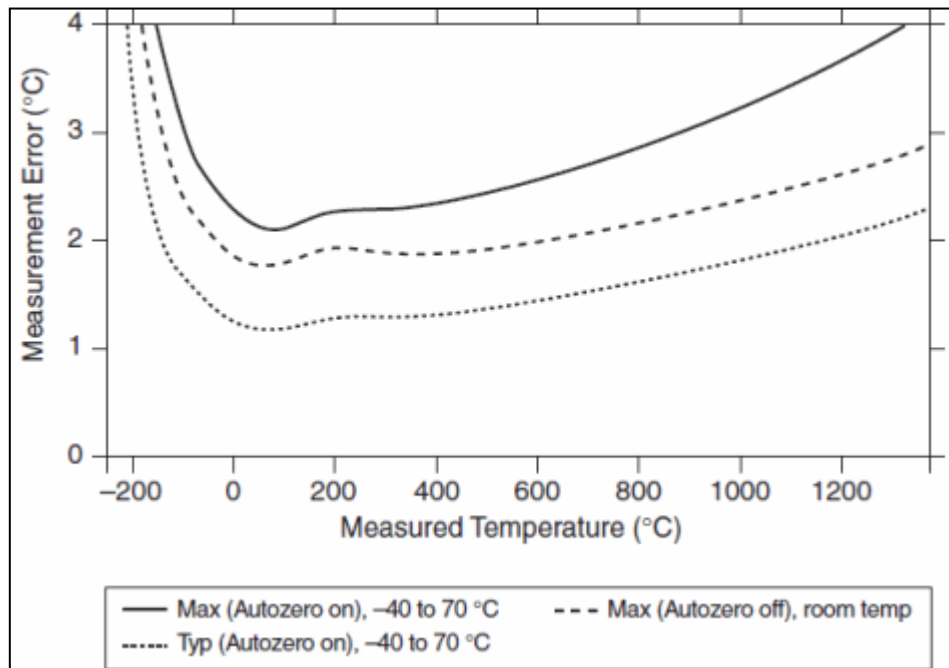


Figure 5.5: Thermocouple system error when using the NI 9211 module (National Instruments NI 9211 Datasheet).

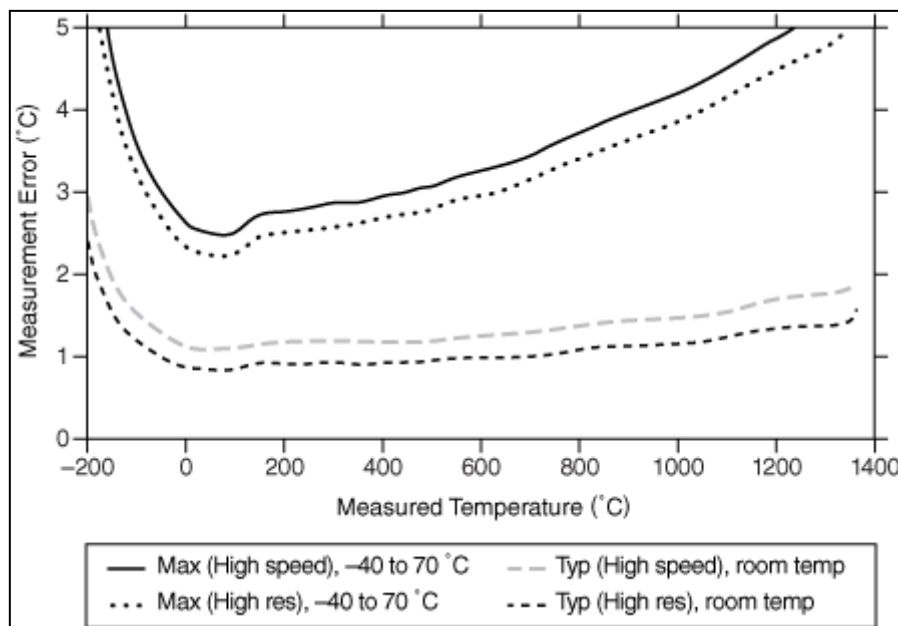


Figure 5.6: Thermocouple system error when using the NI 9213 module (National Instruments NI 9213 Datasheet).

Taylor (1982) describes the benefit of using multiple readings where possible to minimise the overall uncertainty in the data. In nearly all cases, where multiple data points have been

collected, taking the mean of the data produces the best estimate of the true value³. Equation (5.1) has to be altered slightly to accommodate the change to multiple measurements rather than a single reading. Therefore, $X(\text{measured})$ can be replaced with \bar{X} , which represents the best estimate of the true value that can be made from the data.

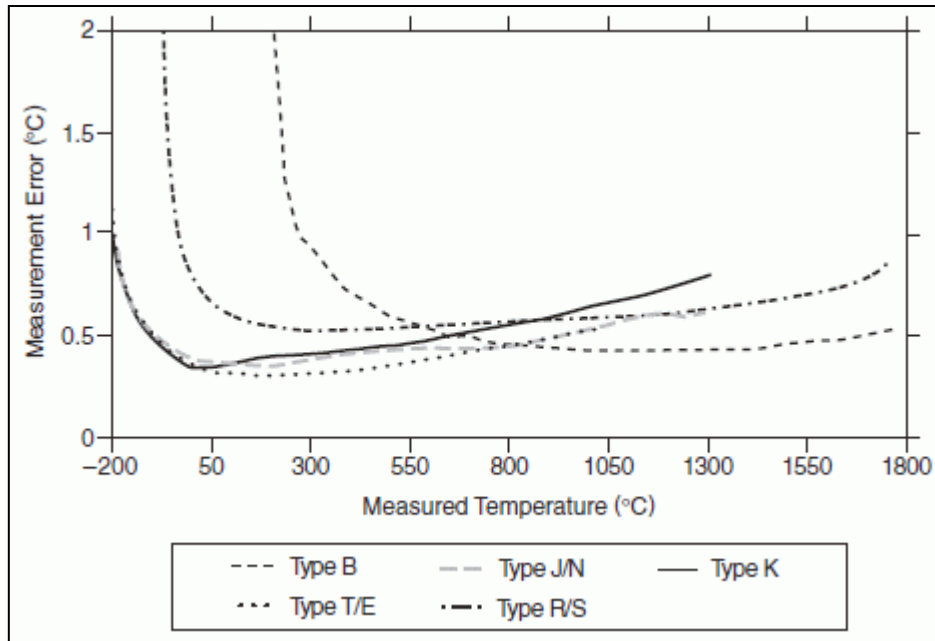


Figure 5.7: Thermocouple system error when using the NI 9214 module (Instruments NI 9214 Datasheet).

Likewise, a change in the uncertainty term is also needed. The standard deviation, σ , is calculated from the differences each measurement in the set is from the mean, thus characterising the average uncertainties. Small values of σ show the experiments are precise whilst large values are obviously not precise. The uncertainty term in equation (5.1) is now replaced with the σ , giving a 70% statistical confidence that the true value lies within this range. Equation (5.1) therefore becomes (5.4).

$$X = \bar{X} \pm \sigma_X \quad (5.4)$$

Increasing the uncertainty term to $\pm 2\sigma_X$ improves the confidence that the true value has been captured, from the measurement set, to 95%. Therefore, the final uncertainty equation for a multiple data set is outlined in equation (5.5), provided the value of systematic uncertainties is much lower than this.

³ Taylor has numerically justified this statement in Chapter 5 of the 1982 book '*An Introduction to Error Analysis The Study of Uncertainties in Physical Measurements*'. The reader is directed to this reference if they are interested further.

$$X = \bar{X} \pm 2\sigma_X \quad (5.5)$$

The discrepancy between the work produced Nakos (2004) and the NI 9214 datasheet previously discussed will be countered by using the $\pm 2\sigma_X$ method of uncertainty calculation. High confidence in the obtained results is obtained without over or under predicting the experimental uncertainty.

5.4 Static Testing Method

To attain a fundamental understanding of the underlining properties of the CV braking assembly, and more specifically within the brake pads, static tests were carried out. The term ‘static test’ refers in this report to the process of applying an input force, controlled by a pressure regulator, when incrementally increasing the actuating pressure from 0 to 7.5 bar and then return to 0 bar. The aim of these tests was to discover the compression properties of the friction materials.

Before the Static testing method can be explained, it is necessary to have an appreciation of the opshaft ratio. Both the actuator displacement and input force were measured from the relevant pieces of instrumentation. However, the transfer of actuator displacement and input force are applied through the opshaft (see Figure 1.3), which does not deliver a linear relationship with the brake pad contraction/expansion or clamp force respectively. Accordingly, they were calculated by the relevant factor (or opshaft ratio), determined by the amount of actuator travel. Figure 5.8 shows the non-linearity provided has a third order nature and is calculated by equation (5.6).

$$\alpha_{opt} = 2.23E - 05x^3 - 1.989E - 03x^2 + 0.1181x + 13.54 \quad (5.6)$$

Where the amount of pushrod displacement is x and the opshaft ratio is α_{opt} . By using this equation, pad displacement can be calculated from the pushrod displacement. The clamp force can also be calculated by relating the opshaft ratio to the recorded input force.

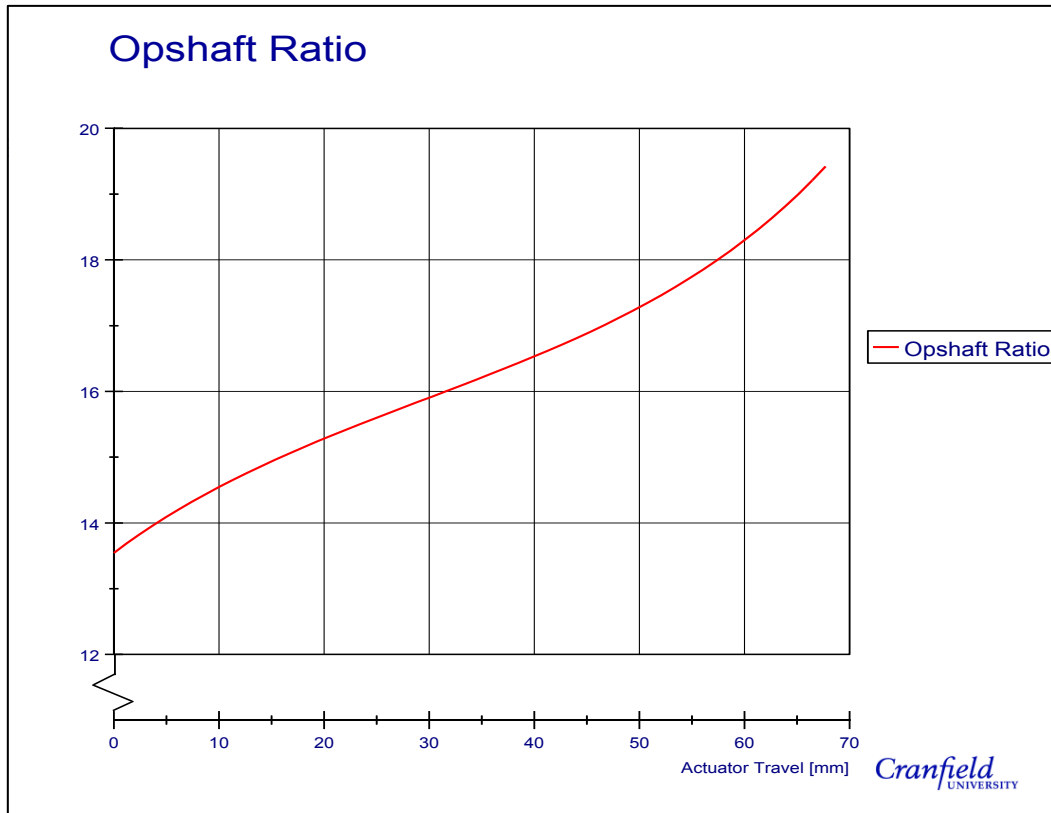


Figure 5.8: Internal caliper output ratio as a function of pushrod travel

The compressibility of the friction material can be investigated with this testing method, by comparing the calculated total brake assembly displacement of the two friction materials and compensate against results produced for the steel and aluminium dummy pads. As part of the experimental setup, a technique for setting the initial pad clearance, known as “the clearance gap”, was conducted. It starts by applying a small input force to the caliper, which presses the pads against the disc brake. Actuating pressure is then removed, leaving the pads in contact with the disc brake when the pistons retract, resulting in a large gap being then left between the inboard backplate and the pistons. This distance created between the inboard backplate and the piston surface is the clearance gap. It represents the total running clearance of the brake system necessary for the disc brake to rotate without residual drag.

The pistons were then closed by turning the control screw until enough contact was made to feel friction when attempting to rotate the disc brake, but not enough to completely prevent rotation. It was important that the same operator conducted this step due to the level of judgement needed when determining the set point, as different operators will sense the set point differently, causing a large source of systematic error. To measure the clearance gap, metal plates with a defined thickness were manufactured and inserted in between the inboard backplate and the

pistons, as in Figure 5.9. Once the set point had been achieved by the operator, the plates were removed to leave the defined clearance gap. A digital vernier caliper, with a measuring accuracy of 0.005 mm, was used to confirm the thicknesses of the setting plates.

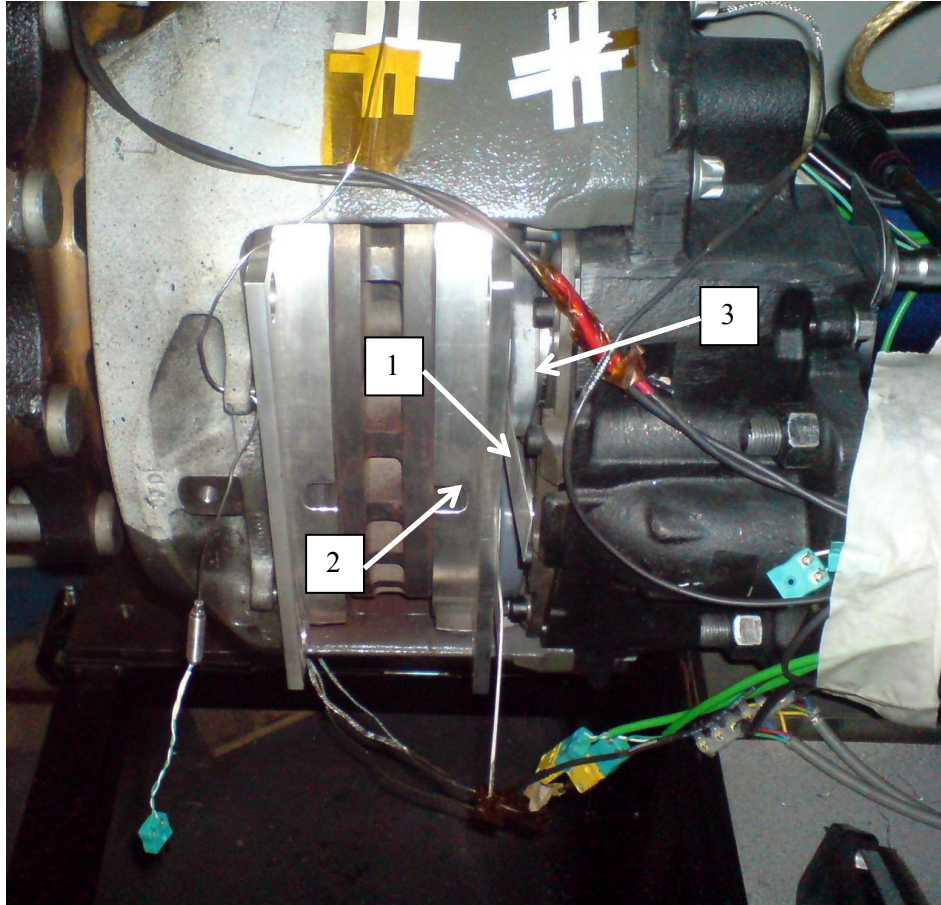


Figure 5.9: Correctly fitted plates (1) between the brake pads (2, steel dummy plates in this instance) and the pistons (3), to create the gap clearance.

5.5 Equipment Calibration

All readings for force, displacement and pressure were taken with transducers, with output readings in the form of voltage changes. To reliably convert the delivered voltage signal into an accurate physical value a suitable calibration technique was needed. This section describes the techniques used and how they were verified.

5.5.1 Displacement Transducer Calibration Method

To calibrate the Sensonics LVDT *sr* series transducer, the hydraulically actuated Instron machine, available at Cranfield was utilised. It is able to control its displacement to within an uncertainty range of ± 0.005 mm and therefore, could generate an accurate calibration curve. A

fixture had to be built to enable the service chamber and transducer combination to work in the Instron machine, shown in Figure 5.10a. Connection between the pushrod and the Instron head unit was done via a locating pin with a cone-shape milled into its lower surface. Subsequently, the pushrod was able to self-locate in the pin (see Figure 5.10b).

The pin was lowered onto the end of the pushrod with no pressure supplied to the service chamber until there was just enough force acting on the pushrod for a reading to be measured by the strain gauge; this position was deemed the zero displacement position. In increments of 5 mm, the pin was raised to 75 mm, resulting in defined actuator displacements. Displacement readings were taken only once the pressure within service chamber had settled and returned to 2 bar.

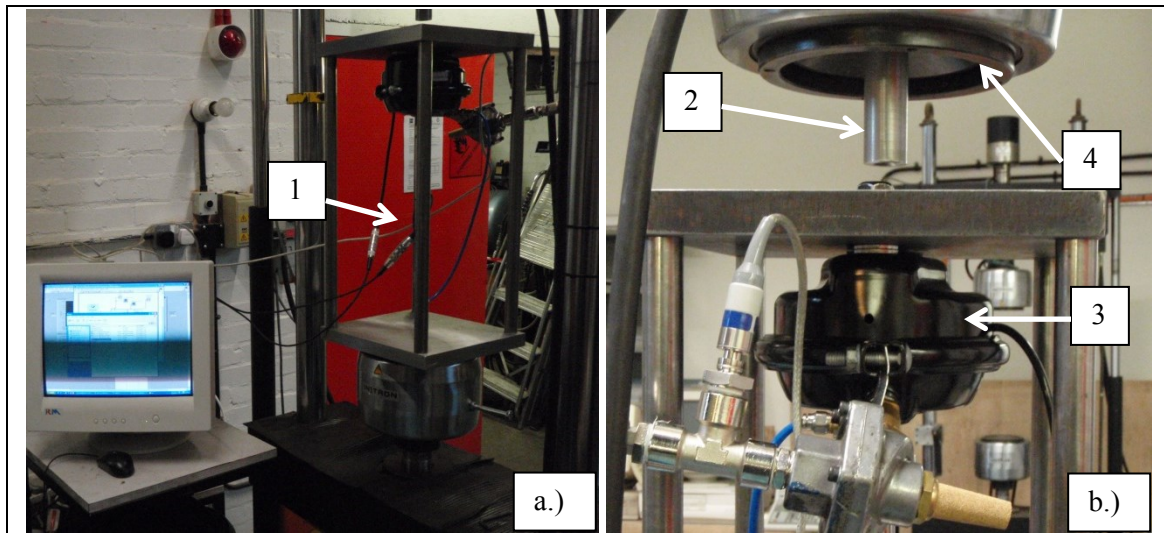


Figure 5.10: Displacement transducer (1) calibration equipment, incorporating a self-locating pin (2) to locate the pushrod from the service chamber (3) in the Instron machine head unit (4).

It can be seen in Figure 5.11 that there is a positive linear trend between the displacement transducer output voltage and the known actuator displacement. The calculated gain from the calibration procedure determined that for every 1.00 V increase in displacement transducer voltage signal, represents a 15.24 mm of actuator displacement. Due to the mounting position of the transducer on the chamber, a drift of 46.12 mm was observed.

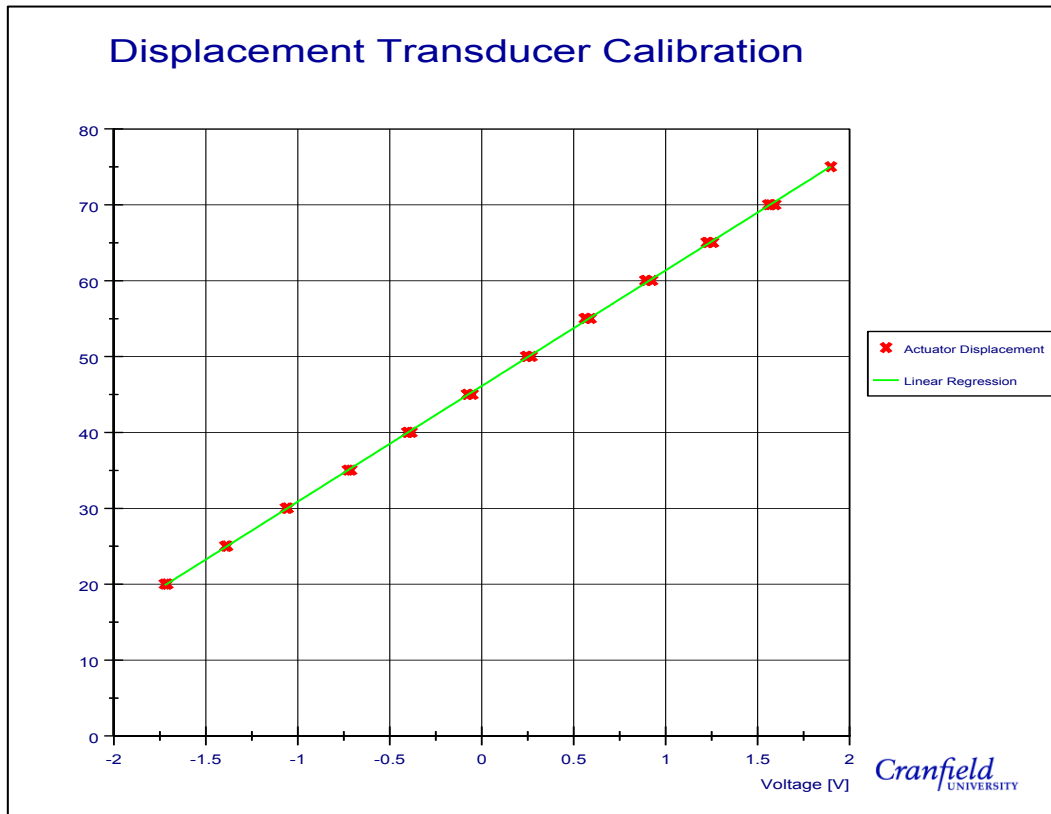


Figure 5.11: Calibration results of the displacement transducer

5.5.2 Strain Gauge Calibration Method

Calibration procedure of the load cell installed on the service chamber's pushrod is now discussed. Ideally, the same Instron machine would have been used for calibration purposes but at the time of experimentation, the load cell in the machine was faulty. Therefore, a simpler two-stage method using a load cell was derived. First, calibration of a 2.5 kN load cell would be conducted, then would itself be used as the calibration tool for the pushrod strain gauge. A simple tension/compression load cell, with a maximum load rating of 2.5 kN, was used to measure the input force delivered by the service chamber. The load cell was connected to the CompactRIO system for excitation and for voltage logging.

Seven weights varying in mass, ranging from 1.00 kg to 10.00 kg, were compression loaded on the load cell to mimic the loading condition the service chamber would apply to it, as shown in Figure 5.12. The output voltage from the load cell was linear, illustrated in Figure 5.13. A 1.00 V change in the output load cell voltage signal represents a decrease in force of 1,740 kN. The sensitivity of the load cell readings was tested by two separate sets of weights having just 0.02 kg difference in mass between them, both small changes are evident and lie on the best fit line in Figure 5.13.

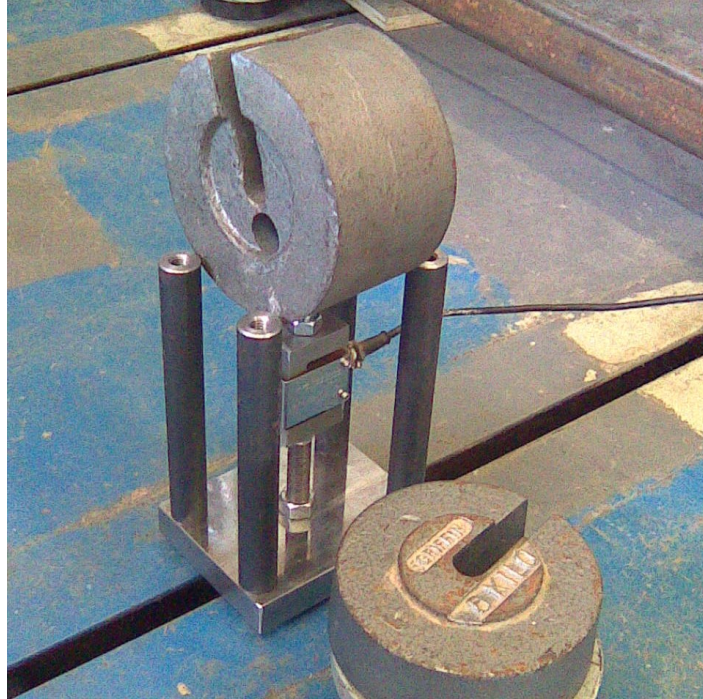


Figure 5.12: Use of weights to exert a known compression load on the load cell

Even with the maximum 10.00 kg weight the maximum force exerted on the load cell was only 0.098 kN. Considering the operating input force from the service chamber is approximately of 10 kN, the calibration was dramatically out of the operating range by three orders of magnitude. Unfortunately, due to a deficit of larger weights, more realistic load cell comparisons were prevented. By making the assumption that the linear trend seen at low loads would remain linear at higher loads, allowed a calculated gain value for the load cell to be made.

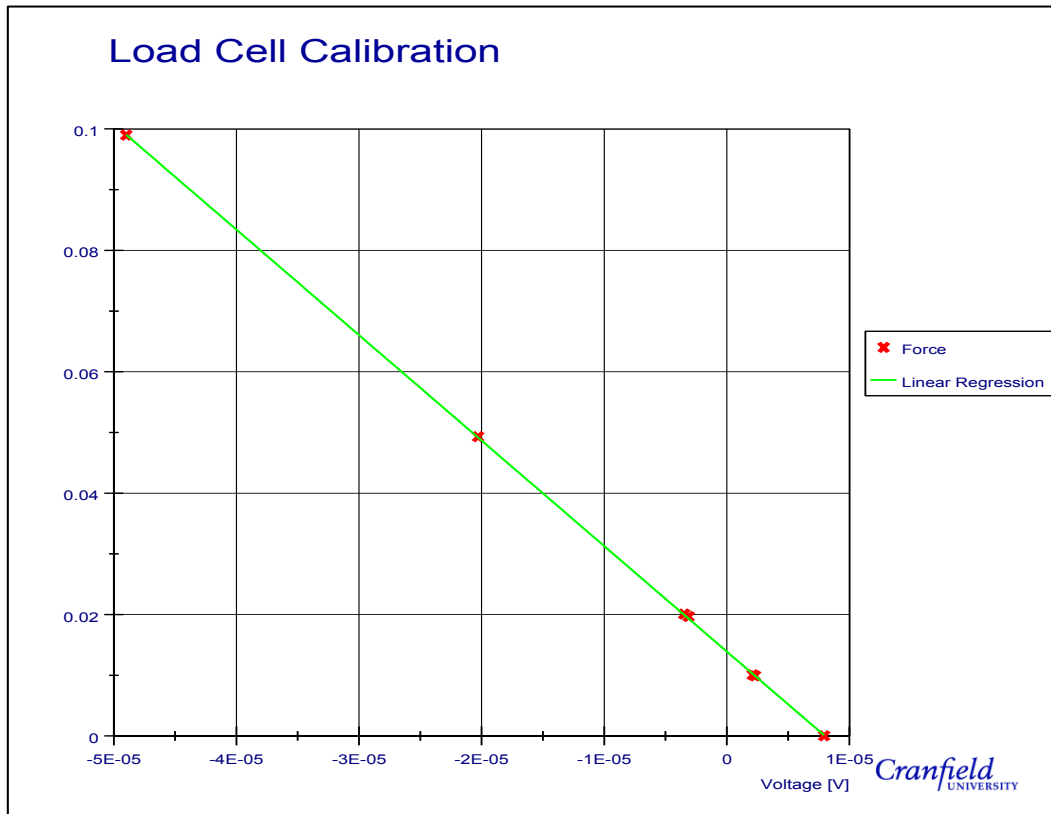


Figure 5.13: Calculated gain from the load cell

Now with an appreciation of the load cell output signal, it could be used in conjunction with the service chamber to calibrate the pushrod strain gauge. To do so, an additional part to the fixture was manufactured to house the load cell, shown in Figure 5.14. An M16 bolt runs through the top surface to locate the centreline of the load cell with the service chambers. Using a bolt in this manner makes changing the distance between the load cell and pushrod straightforward, as bolts above and below the top plate are loosened, allowing the load cell height to be adjusted manually. A vernier caliper with an error of ± 0.005 mm was used to measure the change in height between the load cell top surface and the top plate lower surface.

Location of the load cell was achieved by an M12 screw, therefore a modification to one end of the M16 screw was needed. In the opposite end of the load cell was a hex head M12 screw. Like with the locating pin used in the Instron machine, a cone shape was milled into the screws head for the purpose of pushrod self-location. To calibrate the equipment, the load cell was lowered until the M12 screw was placed on the pushrod and locked in place by the two bolts on the upper plate; this was the zero position. A height reading was taken before the actuating pressure was increased. In total, four heights were used and at each position the actuating pressure was raised to 1.0, 2.0 and 2.5 bar.

Figure 5.15 demonstrates that the strain gauge has a linear relationship between the output voltage signal to an increasing load, with a gain value of 4.02 kN/V. In total, this calibration method was conducted three times, with a variance of less than 1% from the quoted gain. The experimental equipment was now calibrated and ready for testing.

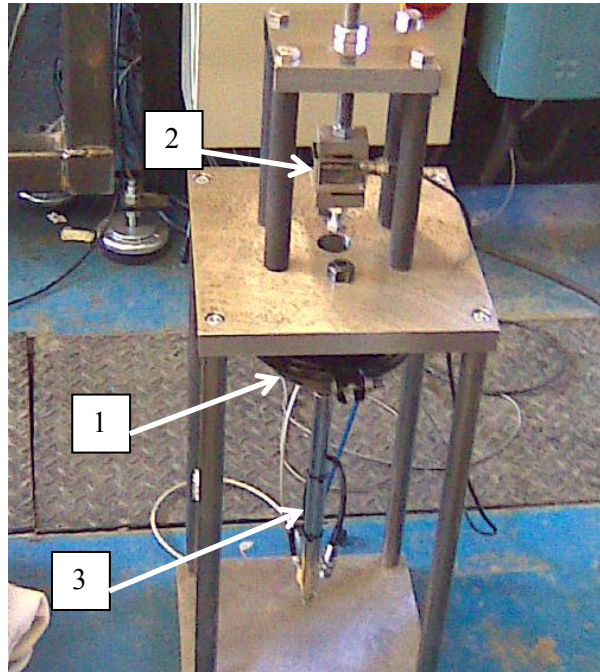


Figure 5.14: Fixturing used to calibrate the strain gauge located on the pushrod, housed in the service chamber (1), using the load cell (2) and displacement transducer (3)

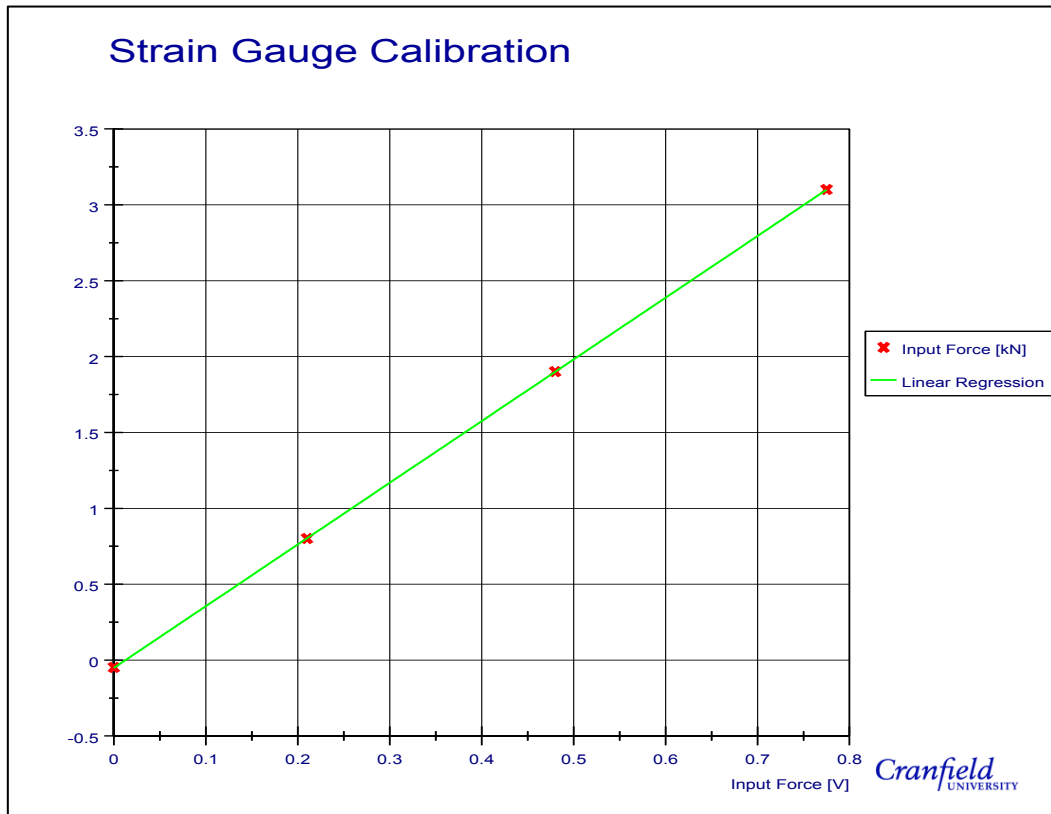


Figure 5.15: Calibration graphs used for the second set of static tests

5.5.3 Calibration Validation

To test the validity of the calibration, the static test procedure described in section 5.3 was performed. Both friction materials were tested as well as both pad conditions, as well as the steel and aluminium dummy pads. The validation procedure was a comparison between the experimental results and a results set provided by Meritor for the same procedure. Calibration would be deemed acceptable if there is a match between the two sets of data.

Measured gradients for the static tests are displayed in Table 5.6, with Meritor's results shown in Table 5.7. These gradients represent the amount of total brake assembly deflection generated for a given force. Clearance gap sizes of 0.0 mm, 0.4 mm and 1.0 mm were used to match the procedure conducted by Meritor. By changing the clearance gap, the position the system is on the opshaft ratio changes also, modifying the amount of system deflection. The 0.4 mm was used instead of the 0.5 mm clearance gap, as per the Meritor results, as there was no readily available material that could be used to fabricate the setting plates. To save on experimental time, 0.4 mm thickness plates were made as there was an abundance of this available.

As the Steel dummy pads were used as a reference, discussion will start with this material. With a nominal elastic modulus of 210 GPa, the dummy steel pads could be considered infinitely stiff in comparison to the friction material pads. As a consequence, the measured deflection when the steel dummy pads are inserted can be considered as the elastic deformation of the caliper. Being a stiffer material than the others, the recorded gradient values considerably lower than those for the friction materials. With no clearance gap, the lowest gradient is produced, a finding common amongst all results, due to being lower on the opshaft ratio and therefore the actuating force is amplified less. Although difficult to claim from only three points, the increase in gradient appears linear, starting from 1.30 mm/kN at a 0.00 mm clearance gap to 1.49 kN/mm with the maximum 1.00 mm clearance. The former value is 10% smaller than Meritor’s result and rises to an 18% difference for the 1.00 mm clearance. Both friction material results show a contrary story as all 0.00 mm and 1.00 mm clearance gap results fall within 4% difference, inside the calibration acceptance limit.

Table 5.6: Experimental results of the static tests.

Clearance Gap (mm)	Steel (mm/kN)	Aluminium (mm/kN)	FER 4567 Fade (mm/kN)	T3016 Fade (mm/kN)
0.00	1.30	1.45	2.26	2.54
0.40	1.39	1.52	2.34	2.67
1.00	1.49	1.65	2.56	2.94

Table 5.7: Meritor’s static test results.

Clearance Gap (mm)	Steel (mm/kN)	FER 4567 Fade (mm/kN)	T3016 Fade (mm/kN)
0.00	1.43	2.27	2.55
0.50	1.57	2.57	2.81
1.00	1.78	2.66	2.87

Gradient values for the middle clearance values, although cannot be directly compared, indicate that there is a slightly bigger difference between them. Figure 5.16 and Figure 5.17 show the comparison graphs for the friction materials FER4567 and T3016 respectively. It can be seen from these figures that the relationship between input force and actuator displacement is actually nonlinear, although a linear approximation would still be valid as the degree of nonlinearity is small. Since the two middle clearance gap were different, measurements would have been taken different points on the opshaft ratio, causing the greater difference between the

gradients. Still, the differences were only 9.8% and 5.2% for the FER 4567 and the T3016 measurements respectively.

Strain gauge calibration results have been shown to be fairly accurate, with like-for-like measurements comparisons to Meritor's results having only a 4% difference. Large differences were present between the Steel dummy pads however. With the closeness of the friction material results, the difference in steel experiments was attributed to likely surface flatness issues. To reduce cost and speed up the manufacturing time required to produce the dummy pads, no flatness requirement was placed on the manufacturing drawing. The effect of this is that control has been lost over the contact regions between the disc brake's friction surfaces and dummy pads, as well as with the pistons/bridge. Consequently, it can be concluded that the results obtained using the static testing method with the load cell method of calibration, achieves good correlation with the Meritor's results and therefore, the results obtained are of sufficient accuracy to continue the experiments.

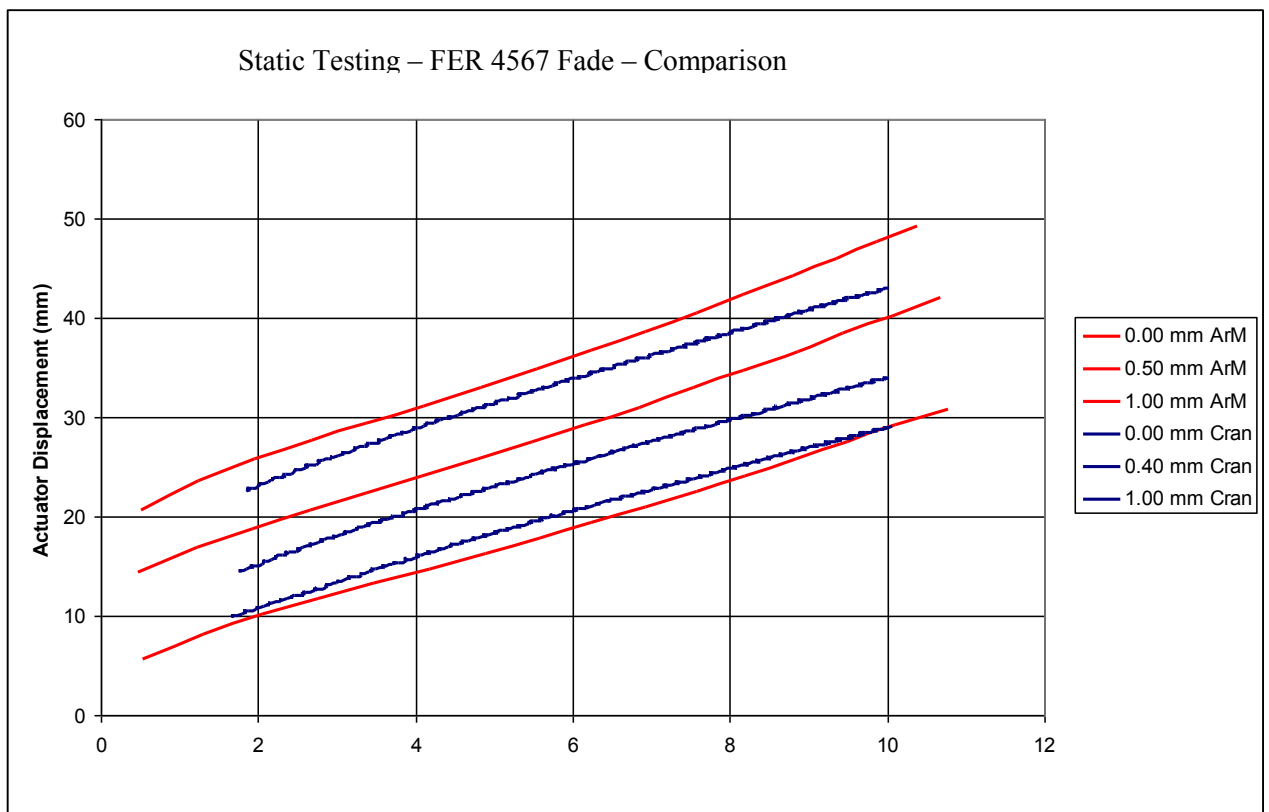


Figure 5.16: Third static test comparison of FER 4567 friction material

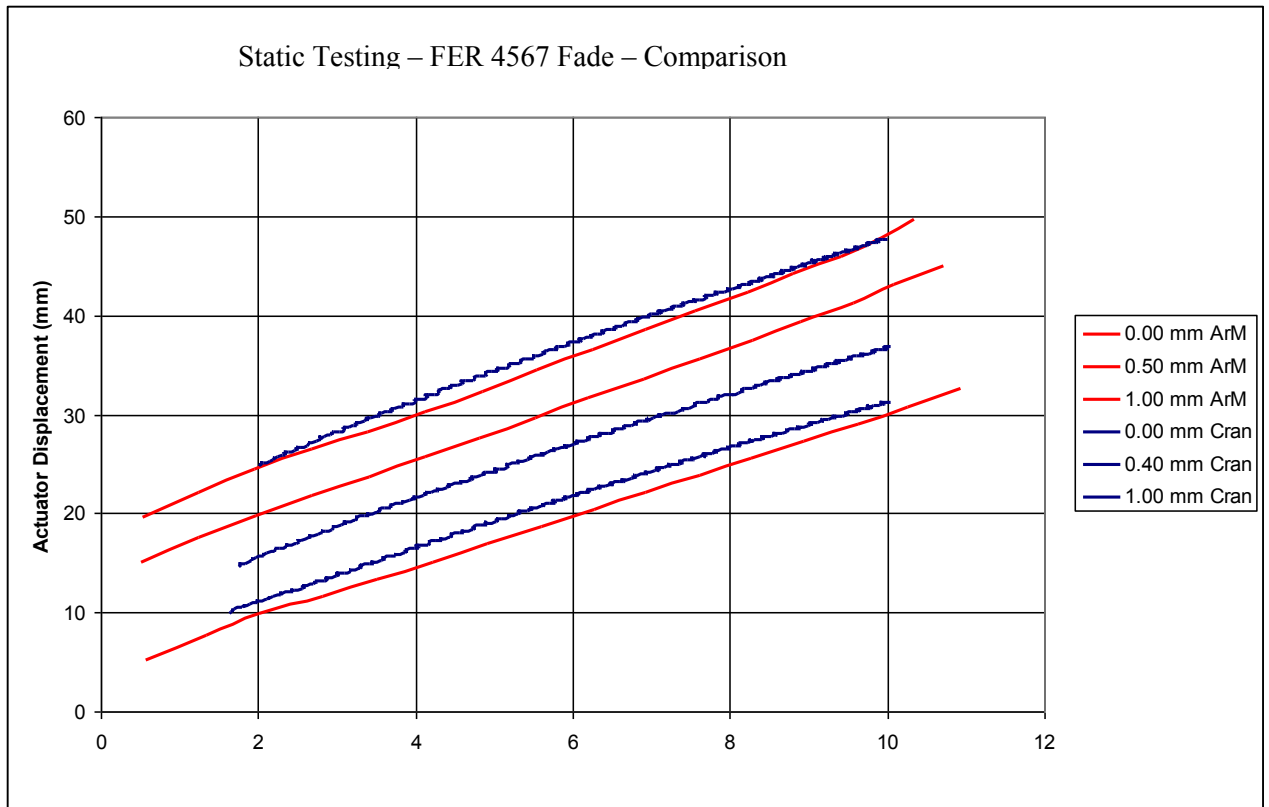


Figure 5.17: Third static test comparison of T3016 friction material

5.6 Cooling Test Methods

The primary aim of the cooling tests was to simulate the thermal effects within the disc, pads and caliper once the parking brake has been applied and left on for a long period of time. As the current specification for the EPB allows a maximum of 1 mm actuator displacement during the coolback phase, the cooling tests will help to determine whether this is enough to sufficiently prevent roll away.

Data taken by thermocouples attached on a CV, which was driving on demanding hill roads within South Wales are presented in Figure 5.18 (data supplied by Meritor). This unique data set gives the opportunity to understand temperatures reached during a challenging operation. It is seen that disc brake temperatures can reach in excess of 500°C after heavy brake applications although it is very unlikely that a CV is parked after such an application. Less severe braking applications, on the other hand, frequently reach and exceed 400°C. Consequently, it was decided that a parking application simulation would begin with a disc brake surface temperature of 400°C, representing a realistic but harsh case.

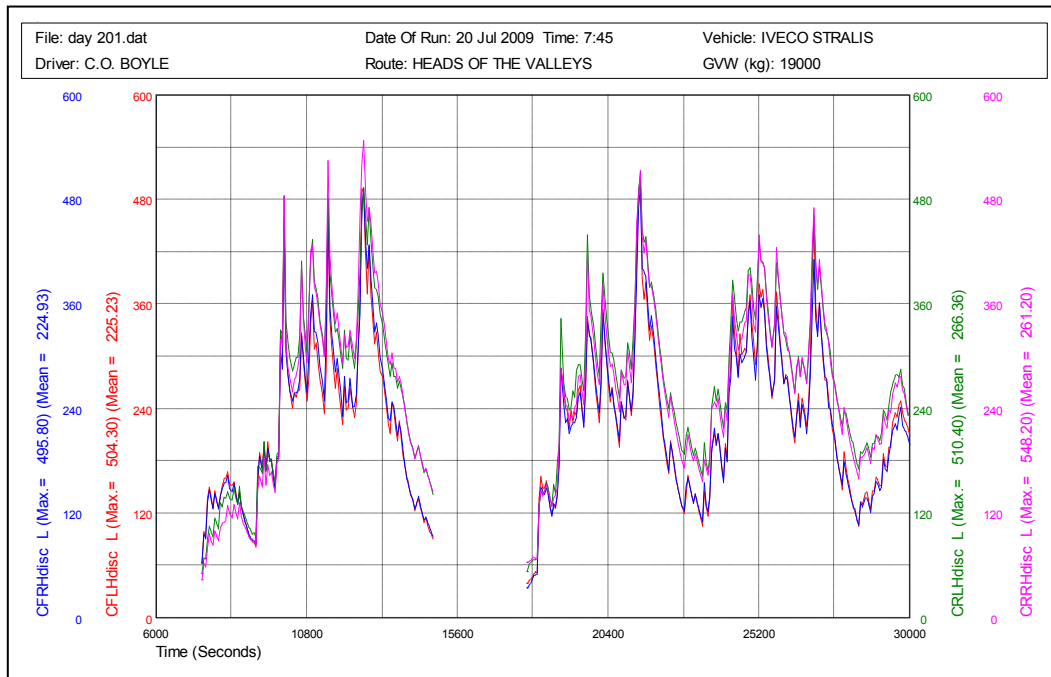


Figure 5.18: Disc Brake temperatures taken from an actual drive cycle (Data provided by P. Gibbens, Meritor H.V.B.S)

Replication of this braking application was to be carried out on the Thermal Rig. To capture surface temperatures,

A total of 28 thermocouples could be measured for any one experiment, limited by the space available in the CompactRIO⁴. Initially, nine rubbing thermocouples were attached to measure the disc temperatures, six on the outboard side split with three high and three low, all positioned as centrally as possible (Figure 5.19), with three probe type thermocouples were placed in each brake pad (Figure 5.20). Multiple caliper temperatures were also be recorded to generate realistic boundary conditions to input into the predictive model and to detect the heat flow path through the caliper. Eight welded PFTE thermocouples were located on the caliper, as shown in Figure 5.21 with a further eight in the reciprocal positions on the lower half of the caliper. The final two thermocouples were used to measure the temperature of the pushrod within the actuator and the ambient air temperature.

⁴ At the time of these experiments, 16 channel thermocouple modules were not available from National Instruments. This value was increased at a later date once new modules had been acquired.

Disc Out High Top

Disc Out Mid Top

Disc Out Low Top

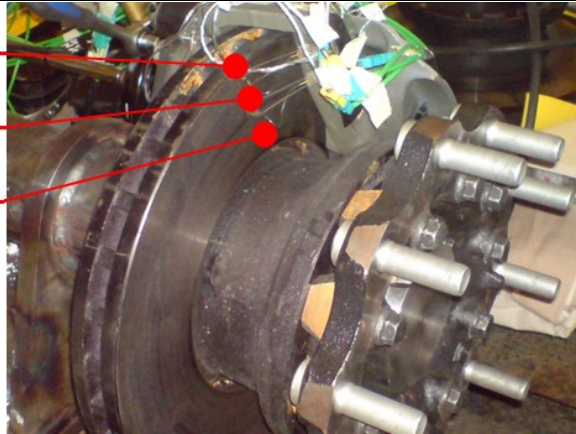


Figure 5.19a: Three rubbing thermocouples above the horizontal centreline on the outboard side

Disc Out Low Bottom

Disc Out Mid Bottom

Disc Out High Bottom

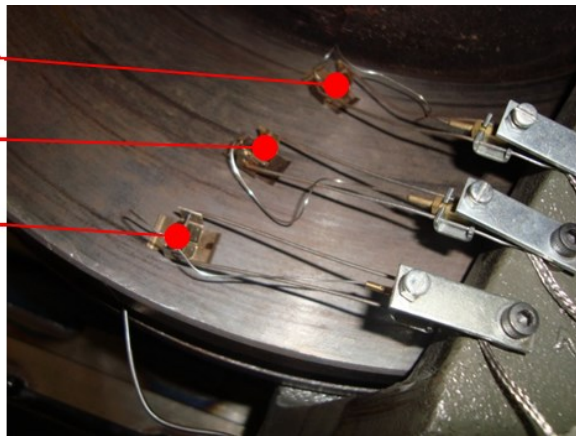


Figure 5.19b: Three rubbing thermocouples below the horizontal centreline on the outboard side

Disc In High Top

Disc In Mid Top

Disc In Low Top

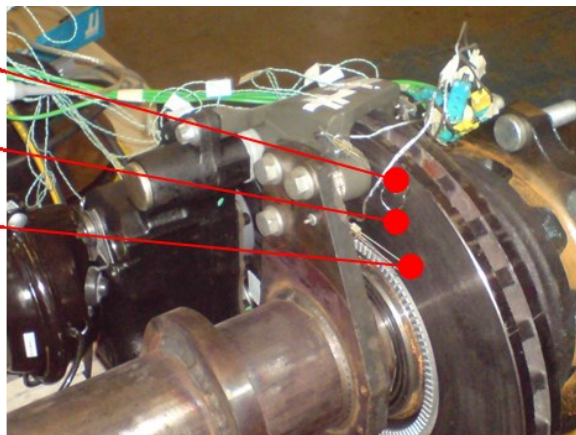


Figure 5.19c: Three rubbing thermocouples above the horizontal centreline on the inboard side

Figure 5.19: Rubbing thermocouple placement on the disc brake.

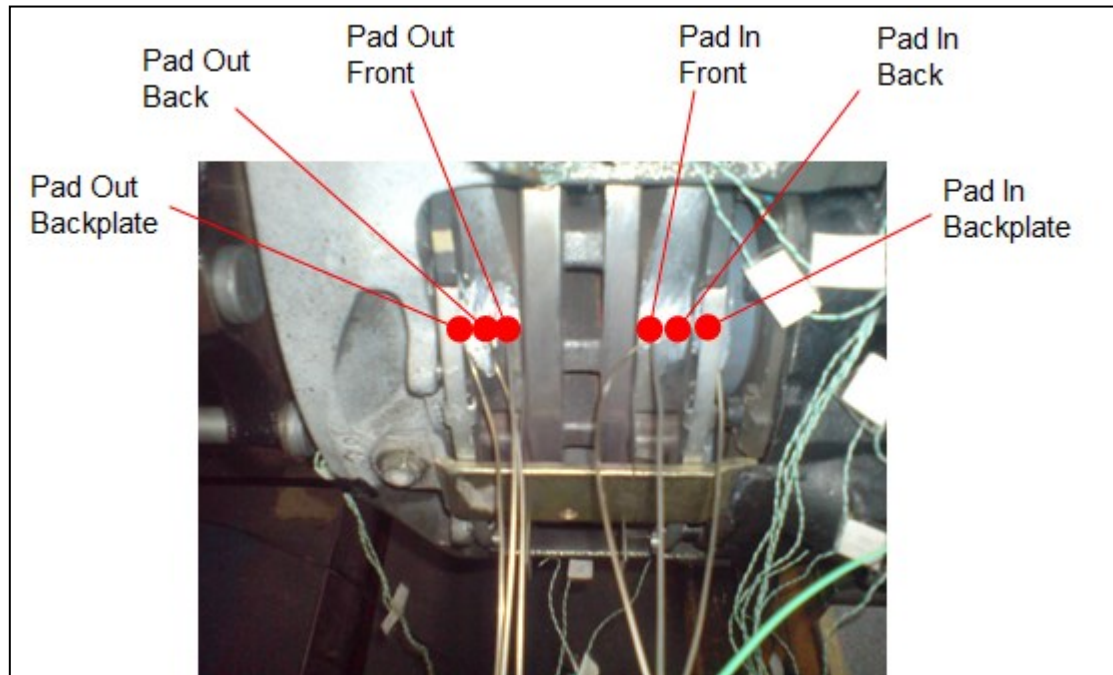


Figure 5.20: Positions and labels of thermocouples in the pads

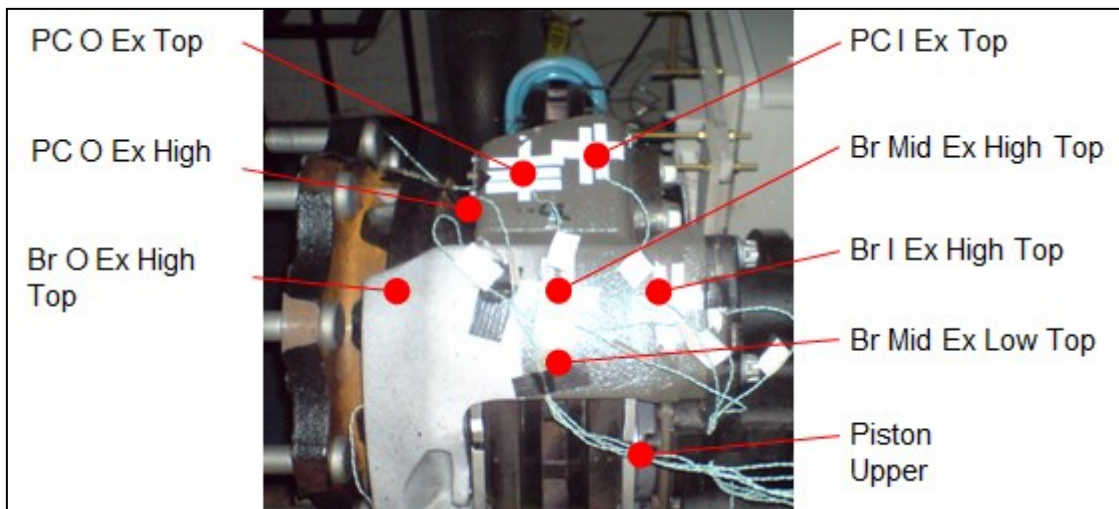


Figure 5.21: Positions and labels of thermocouples on the caliper

In order to heat the disc uniformly the motor was set to rotate at a low rotational speed of 50 rpm, such that all the disc mass was exposed equally as possible to the inductive field generated by the heater coil. Rotation also prevented a single segment of the disc brake being over-heated whilst the rest of the disc still cool. Due to conductive properties, a temperature gradient will be present over the friction surfaces. It was decided therefore that a reference thermocouple would be used for experimental control. Once this reference thermocouple (chosen to be the Disc Out

High Top thermocouple position) had reached the prescribed 400°C temperature, the induction heater and the motor were turned off.

Simply applying an actuating pressure at this stage would not provide reliable results because both the pads and caliper were at room temperature. Preheating clamps were necessary to transfer heat into the rest of the assembly. A preheating clamp is an application of the brake once the induction heater and motor have been turned off, to promote conduction effects from the disc brake to the pads. Each clamp was held on for five minutes to allow the heat to penetrate through the pads then removed. The motor and heater coil were then switched on again to reheat the disc back to the desired temperature. Initially, two preheating clamps were used, both at 6 bar input pressure. After the second release of the pads a final reheat of the disc was completed, the pads were clamped with a 6 bar parking pressure and left to cool; at this stage the cooling test began.

5.7 Experimental Methodology Development

The classification of the cooling test experimental procedure was set out in the previous section. A sequence of preliminary tests was conducted to refine the procedure before detailed disc brake cooling experimentation started. Section 5.7 discusses the development procedure and some initial conclusions found during this process.

5.7.1 Influence of the Wheel on Disc Brake Cooling

When attached to a CV, the LM 120 Offset D-Elsa brake assembly is mounted within the wheel, shrouded from the open air. Whilst the wheel is in motion, the shrouding prevents the flow of cool ambient air into the disc vanes, reducing the convective cooling capability. When parked, assuming the wheel is sufficiently shrouded from the wind, any resulting air flow around the brake will be from buoyancy effects only.

Initial investigations tested whether the wheel affected this natural air flow and if there was significant amount of heat reflection back to the disc brake from the wheel, using the instrumentation set out in section 5.6. The disc brake was heated by the induction heater until all rubbing thermocouples read at least 300°C⁵. Two preheating clamps were then applied, allowing heat to soak into the pads. After which, the actuating pressure was set to 7 bar and left to cool. Both the preheating and coolback phases are presented in Figure 5.22 for the thermocouples present in the experiment, which were Disc Out High Top, Pad Out Surface, Pad Out Back and

⁵ Note that this experiment was conducted before the experimental data shown in Figure 5.18 was collected, therefore the 400°C target had not yet been set.

Pad Out Backplate. As a CV will undergoes many low torque braking cycles during operation, the pads will not be cold when the parking brake is applied, making these preheating section vital for generation of realistic experimental conditions.

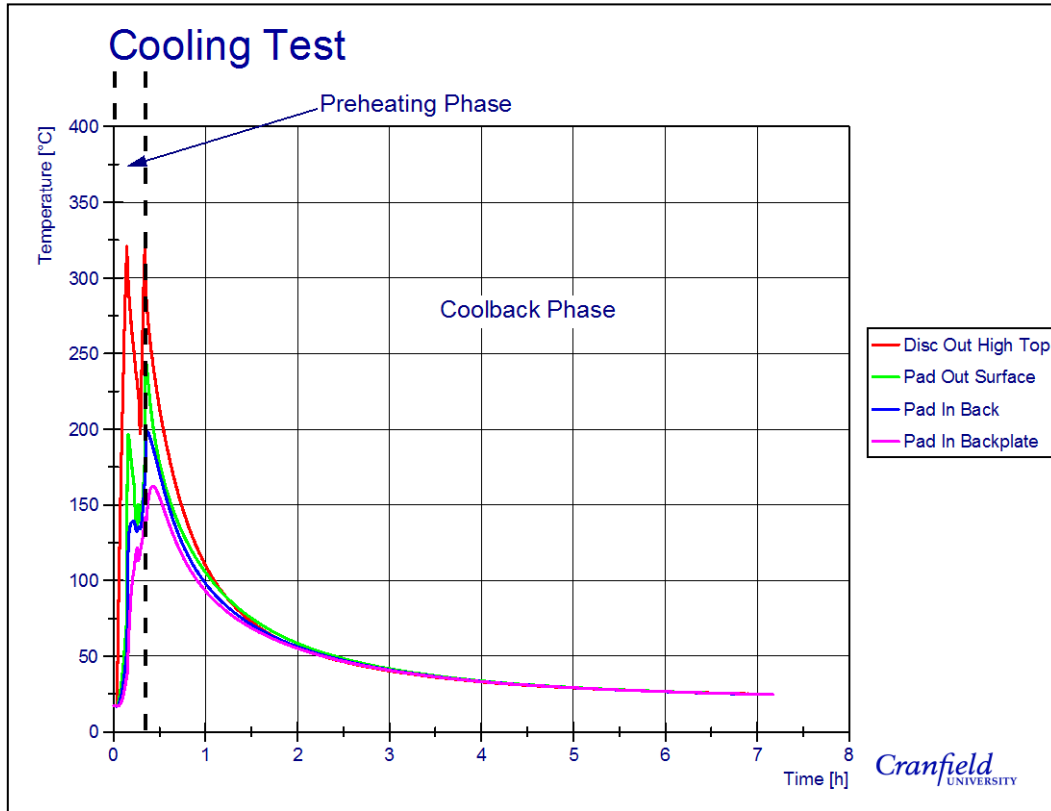


Figure 5.22: The full cooling test time cycle with two preheating clamps and the wheel present

Angelinas *et al.* (2012) showed the wheel strongly affected the disc brakes cooling characteristics by blocking air from entering into the wheel cavity whilst in dynamic (driving) conditions. By conducting two cooling tests, one with and one without the wheel attached to the wheel carrier, a comparison between the results should detail whether a similar effect occurs whilst under stationary conditions or whether the wheel could be removed from the experimental procedures.

Results of the two cooling tests are shown in Figure 5.23. Only the Disc Out High Top thermocouple reading is shown for the two test, with the red curve representing the no wheel experiment and green for when the wheel was present. The graph shows the temperatures as soon as the thermocouple readings had dropped below 300°C and for the following eight hours. Little difference between the two sets of data is seen as they lie approximately on top of one another. It can be concluded then that the wheel has little effect on the disc brake cooling on the Thermal Rig. Therefore, future cooling tests were all conducted without its presence. As only

one experiment was carried out for each test the results will not have statistical significance. It was deemed acceptable in this case as the experiments were devised to simply to understand if the wheel significantly impacts on cooling, with further tests planned if this result emerged.

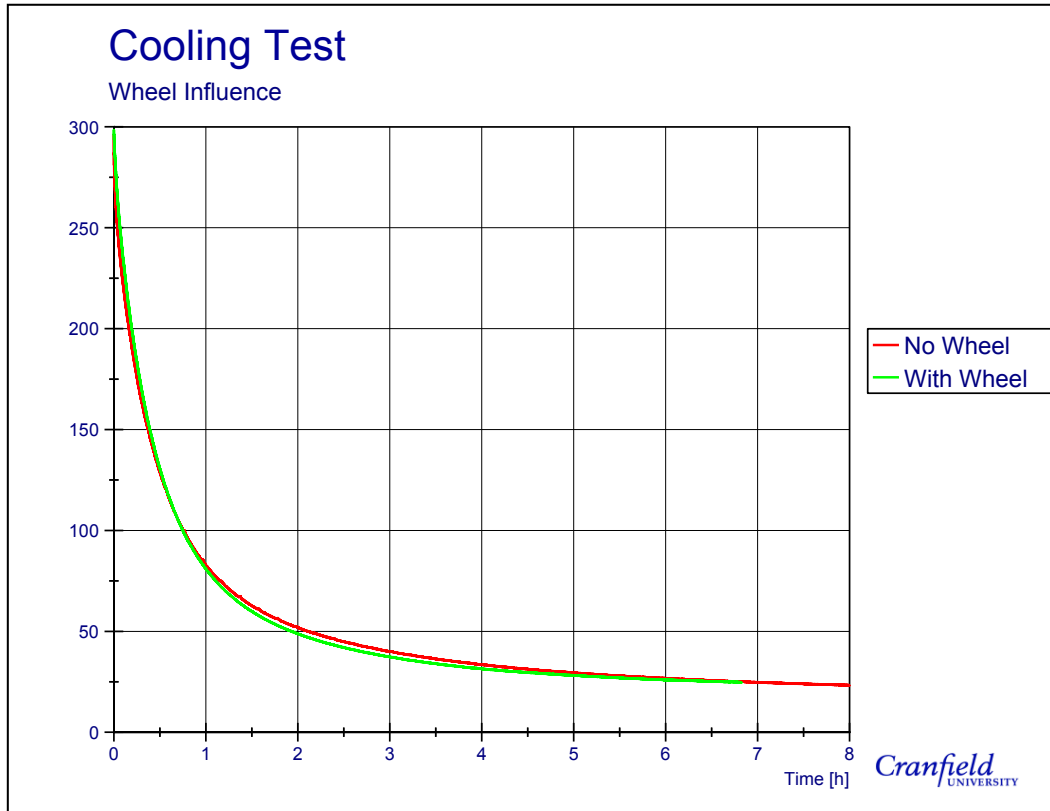


Figure 5.23: There is a negligible difference in the cooling phase when the wheel is attached and when not attached

5.7.2 Input Force Readings

A set of cooling tests were conducted with the three separate actuating pressures, to test the effect of various input forces on the disc brake cooling rate. During these cooling tests, a record of the actuating pressure supplied to the service chamber was taken; the results for the 7 bar experiment is displayed in Figure 5.24. A slight drop in pressure of approximately 0.1 bar can be detected over the first hour of the cooling phase. Interestingly, this pressure drop was a common feature in all three experiments. The manually operated pressure regulator was used during these experiments and it was this piece of equipment that was attributed to the pressure drop. As a consequence, an electro-pneumatic pressure regulator was later sourced and installed to eliminate this effect. Unfortunately, air leakage in the pneumatic supply line caused the pressure built-up by the compressor to drop over time. The compressor automatically turned back on once the pressure drop was greater than 0.5 bar. This continual change in supply

pressure is the reason for the pressure reading in Figure 5.24 appears to have noise within the signal.

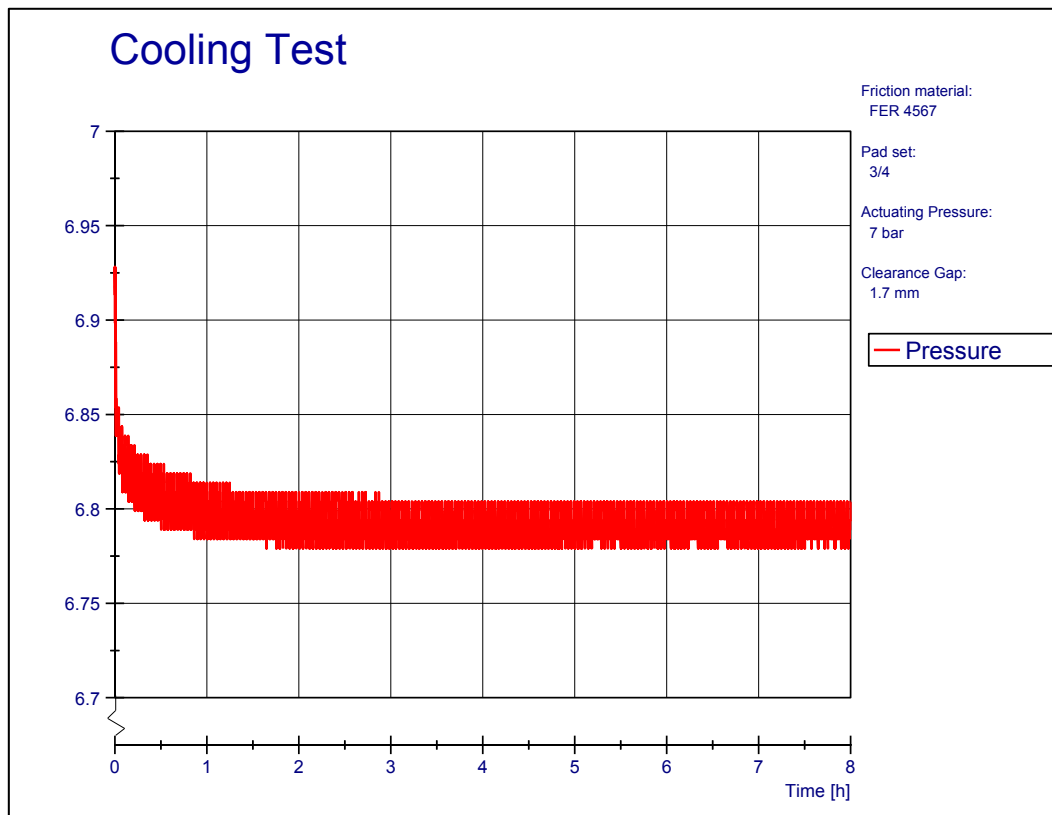


Figure 5.24: Presence of a pressure drop during the cooling tests

During the coolback phase, the total displacement of the disc brake and pads should reduce as the thermal expansion effects begin reduce. For the cooling test run with 7 bar input force, a clearance gap of 1.70 mm and with the FER 4567 friction material, the total amount of contraction in the disc brake and pads caused the actuator displacement to increase from 51.7 mm to 56.1 mm, a total of 4.4 mm (see Figure 5.25).

According to the nonlinear relationship of the input force to actuating displacement, described in Appendix J, the service chamber should have delivered a reduction in input force for the entire measured range of actuator displacement. A reduction of input force can be distinguished initially in Figure 5.26 lasting approximately 30 minutes before the input force increases steadily for an hour towards a peak, before decreasing again for the remainder of the coolback phase. There were three possible reasons that could help explain the increasing input load; firstly, heat input into the caliper had reached a maximum, resulting in the caliper starting to contract as well as the disc brake and pads. As the Elsa 225 caliper utilises a sliding mechanism, whilst the caliper contracts it actually pushes harder against the outboard pad, creating a greater

clamping force at the disc/pad interface. Secondly, there could have been a problem with the instrumentation causing the increased input force. Finally, thermal soaking through the caliper, via conduction, could have increased the pushrod temperature. With the strain gauge fixed to the pushrod, its readings would have altered and therefore could require compensating. All three of these possibilities are investigated.

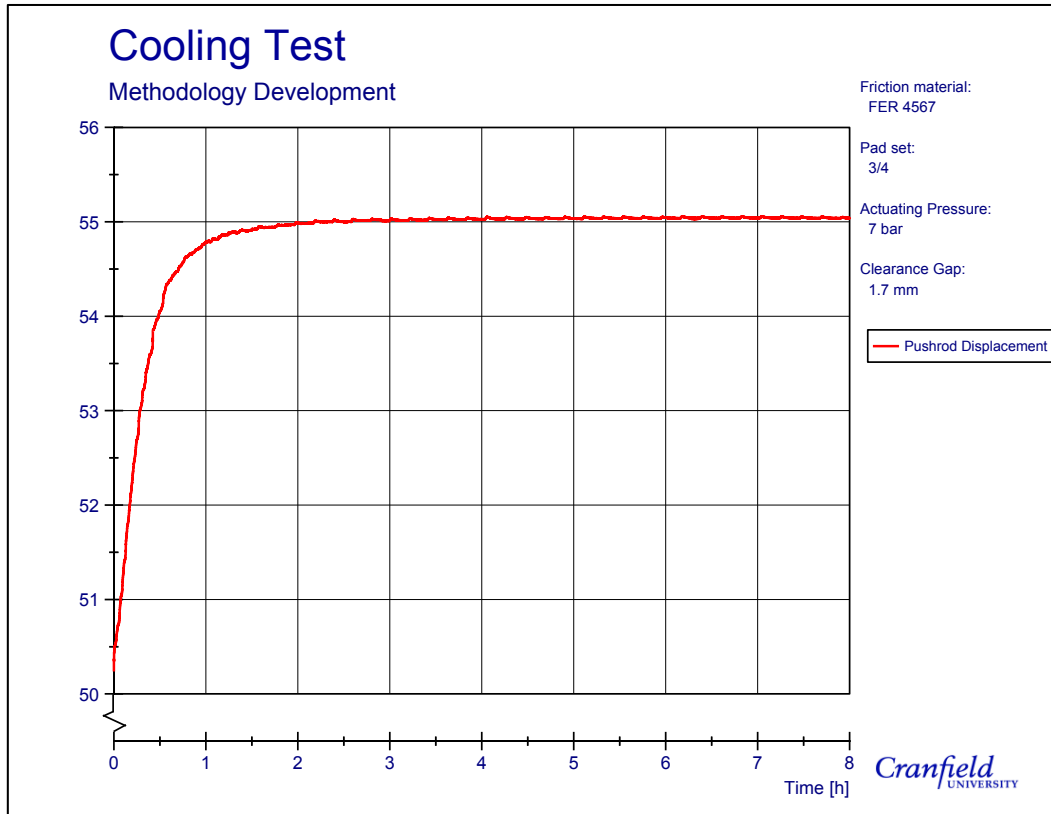


Figure 5.25: Measured actuator displacement during the coolback phase of the cooling test for FER 4567 pads, total initial clearance gap of 1.70 mm and an input pressure of 7 bar

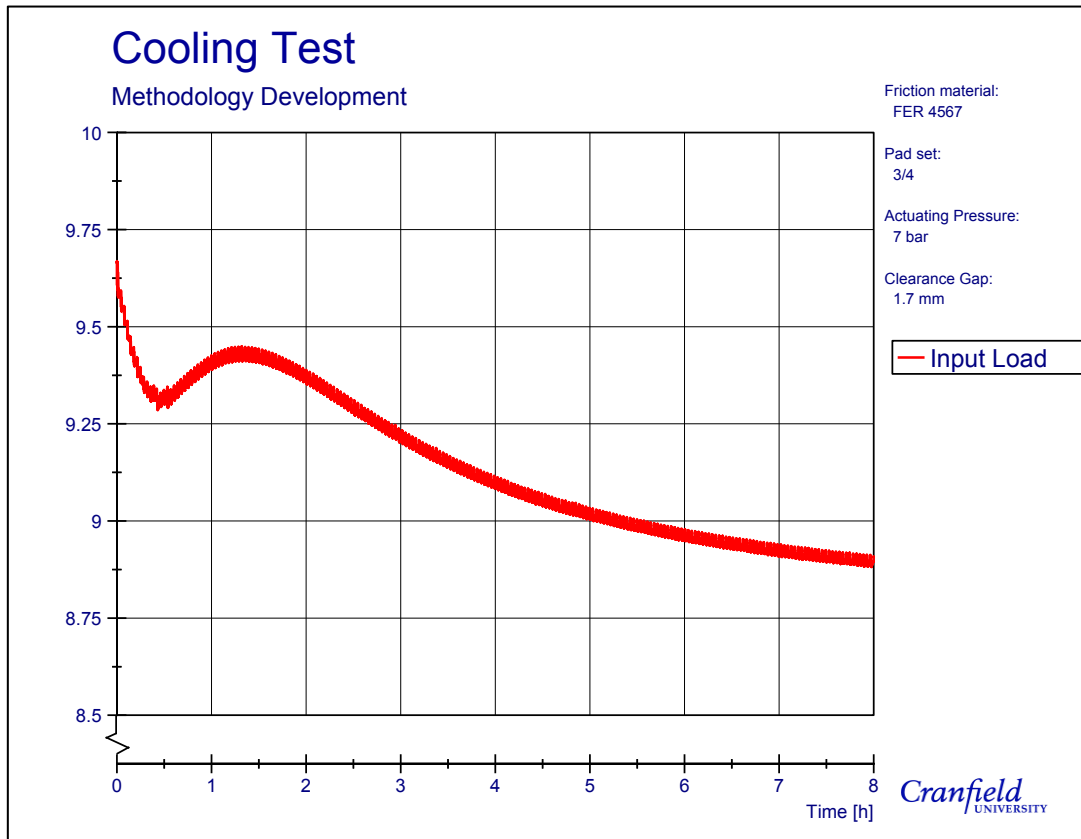


Figure 5.26: Measured input force during the coolback phase of the cooling test for FER 4567 pads, total clearance gap of 1.70 mm and an input pressure of 7 bar

Additional thermocouples were placed on the on the pad carrier, bridge and piston components. By monitoring their temperatures during the cooling phase, especially the bridge, the first possibility for the increasing input load could be tested. Figure 5.21 shows the position and the reference names given to the newly added thermocouples, on the top half of the caliper only; reciprocal thermocouples were also placed on bottom half of the caliper.

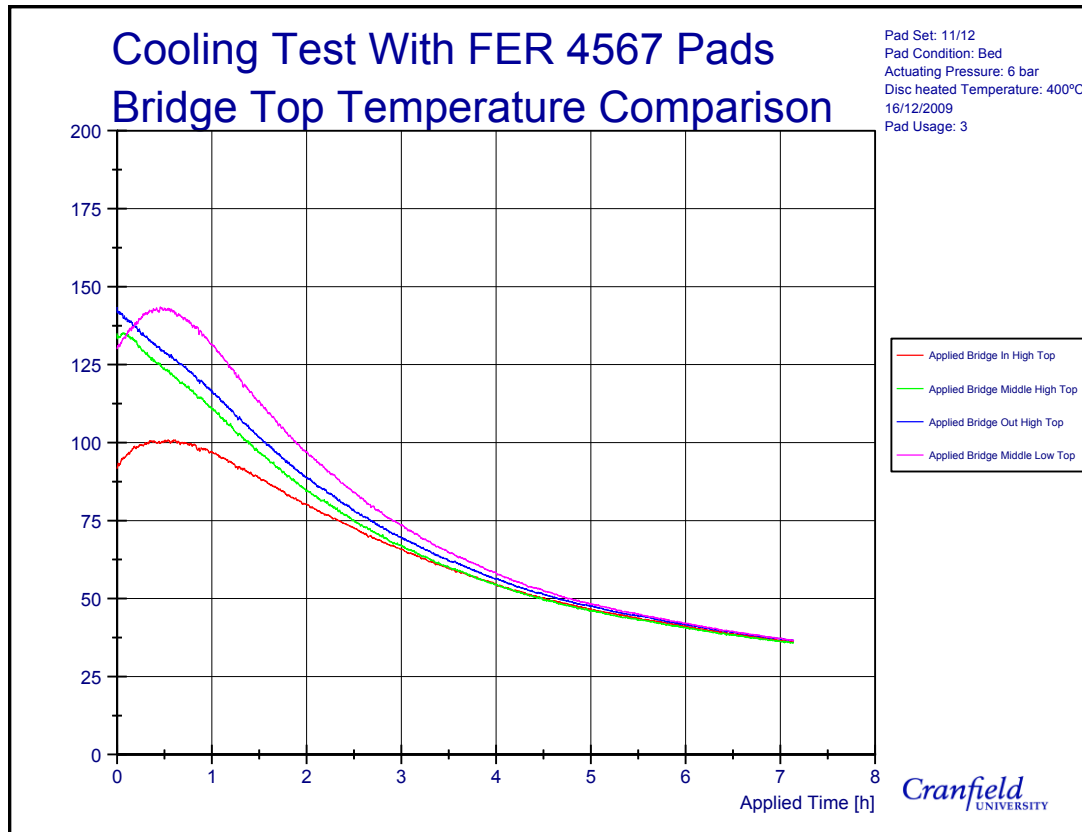


Figure 5.27: Bridge temperatures during the cooling phase.

5.7.2.1 Thermal Loading of the Caliper

Figure 5.27 shows contrasting evidence to both support and deny the first possibility. Two thermocouples do indeed show that the bridge does increase in temperature for approximately 30 minutes. Whilst the temperature increases, the bridge would be expanding, causing a reduction in clamp force as some of the generated input force will be used to counter this expansion. After the temperature peak, the bridge cooling will have the opposite effect, increasing the clamp force.

Alternatively, the Br O Ex High Top and Br Mid Ex High Top thermocouples show a continuous decrease in temperature throughout the cooling phase. This evidence suggests the caliper would be contracting throughout the whole period, only increasing the input force. Having such vastly different temperature profiles existing in a single component exposes the complex nature of the thermal loading and its interactions. The bridge's impact on clamp force change is therefore inconclusive. Recently, Tirović *et al.* (2012) demonstrated the ability to use the DIC method to measure the displacement over a large area of a CV caliper. A similar technique would be needed to prove or disprove the coolback of the caliper has an effect on the clamp force.

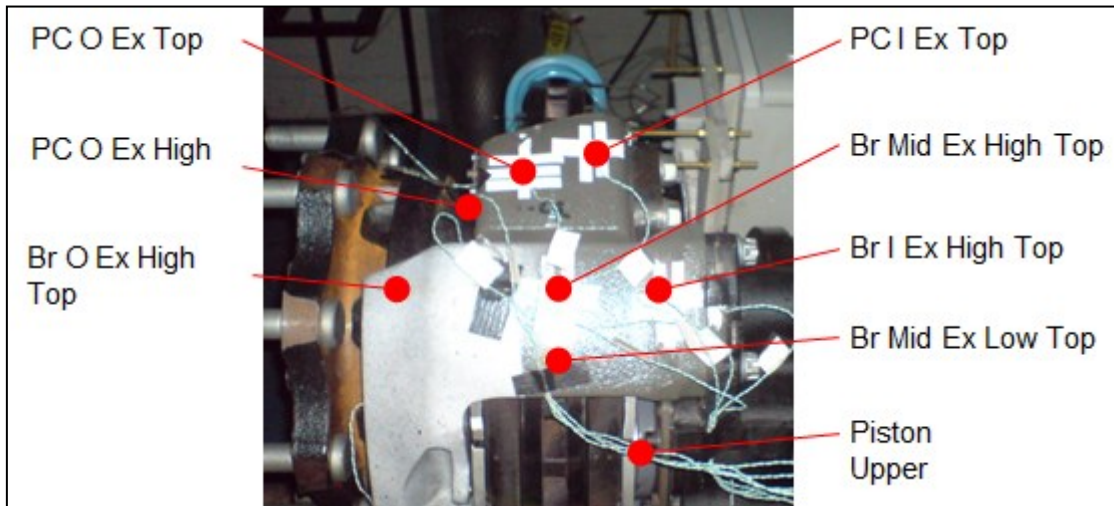


Figure 5.28: Positions and labels of thermocouples on the caliper

5.7.2.2 Integration Box Reliability

Suspicious about the integration box's ability to keep a zero value over a sustained period of time arose during testing. A simple experiment was conducted to see if this was the case. A log of the output voltage from the integration box was kept when no actuating pressure is applied to the service chamber. As this was a static situation, no voltage change should have occurred.

Figure 5.29 shows a vast amount of unwanted zero shift. For the hour period indicated on the graph, the amount of zero shift recorded can be calculated as much as a 0.9 kN reduction in clamp force. Using the opshaft ratio on the recorded input force for the results shown in Figure 5.26 calculated that there was a 7 kN drop in clamp force during the cooling phase, from 168 kN to 161 kN. Consequently, the recorded zero shift could have accounted for up to 12.8% of the change in clamp force, presenting an unacceptably large amount of uncertainty into the results.

A second zero shift test was done, to confirm the repeatability of the zero shift, with results shown in Figure 5.30. A dramatic change in nature is evident between the two experiments as the second experiment showed a more variable zero shift change, compared to a more common decreasing pattern like originally recorded. Unfortunately, the lack of similarity between the two sets of results signifies that the shifting pattern is random and therefore cannot be accounted for. It becomes impossible then to discount the increase in input force shown in Figure 5.26 being a function of instrumentation error.

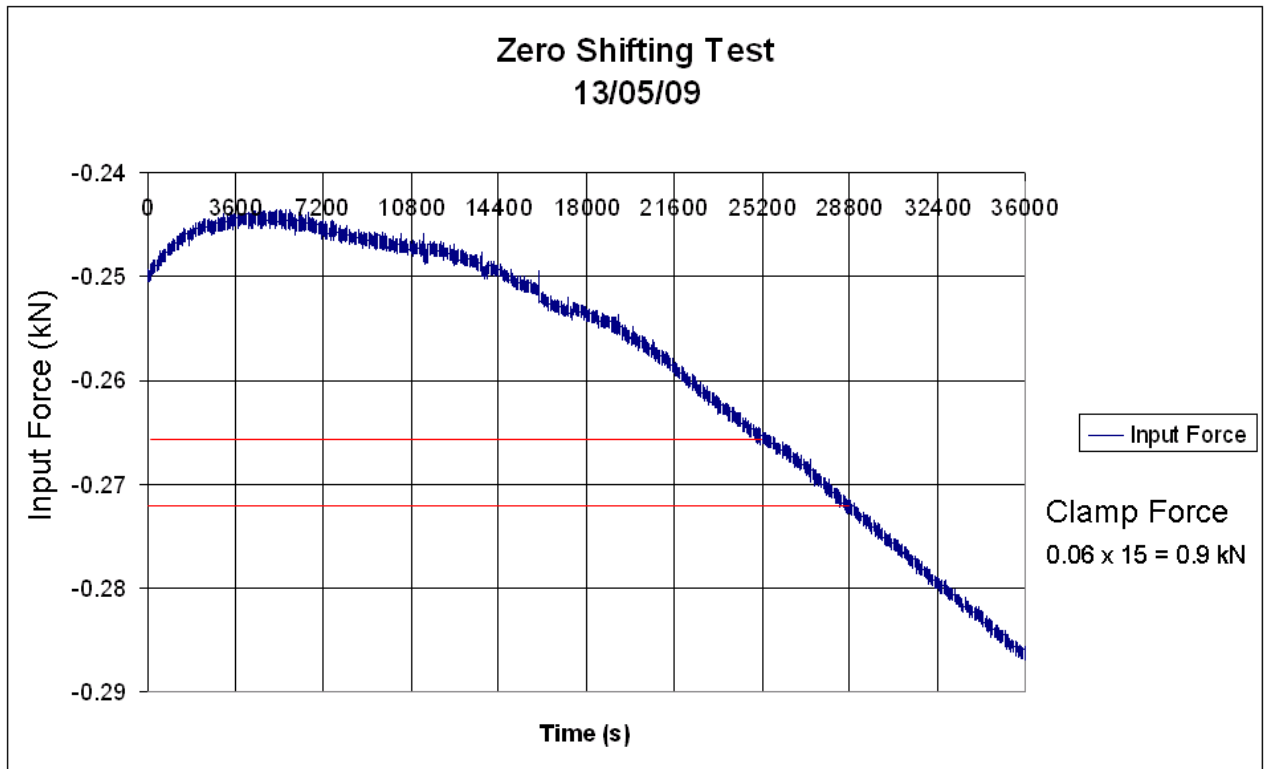


Figure 5.29: Zero shift from the integration box produces a large effect on the calculated clamp force

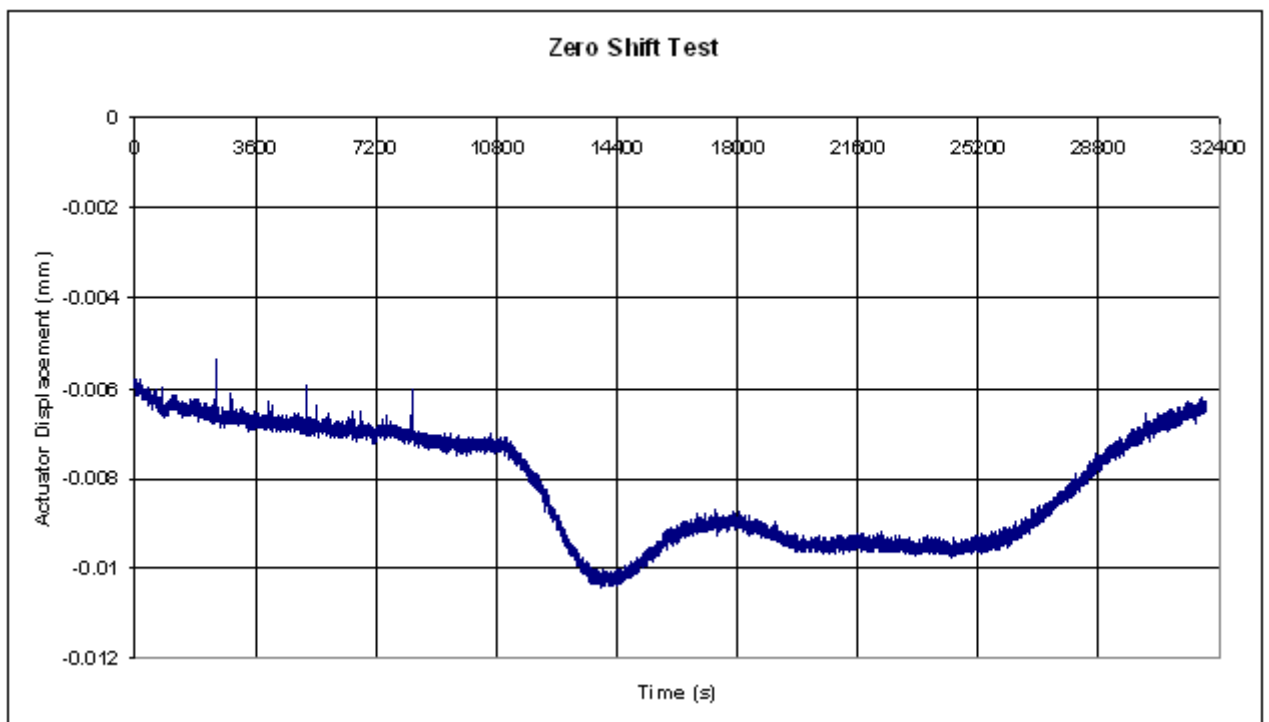


Figure 5.30: Second zero shift test confirming randomness of the shifting

5.7.2.3 Strain Gauge Temperature Correction

A final possibility was that after 30 minutes heat had reached the pushrod by conduction, increasing its temperature. As the strain gauge transducer is fixed on the pushrod, its temperature will also increase. A temperature increase in the pushrod will cause a change in resistance within the strain gauge, due to it gaining heat via conduction. Additional strain is therefore placed into the strain gauge as a direct consequence of heat. The thermal output function, $\varepsilon_{T/0}$, can be calculated by equation (5.7) and can be used to determine the correct the strain reading.

As the additional strain is purely a factor of temperature, it is known as thermal output. The thermal output can be calculated from the thermal resistance from the equation:

$$\varepsilon_{T/0} = \frac{\left(\frac{\Delta R}{R_0}\right)_{T/0}}{F_I} \quad (5.7)$$

where F_I is the gauge factor of the measuring instrument, usually given a value of 2.0 for Vishay instrumentation (Vishay Micro-Measurements 2007) and $\left(\frac{\Delta R}{R_0}\right)_{T/0}$ is the amount of thermal resistance. The change in thermal resistance due to the thermal output can be calculated by:

$$\left(\frac{\Delta R}{R_0}\right)_{T/0} = \left[\beta_G + F_G \left(\frac{1 + K_t}{1 - \nu_0 K_t} \right) (\alpha_S - \alpha_G) \right] \Delta T \quad (5.8)$$

Where β_G is the coefficient of temperature resistance, F_G is the gauge factor of the stain gauge, K_t is the transverse sensitivity of the strain gauge, ν_0 is the Poisson's ratio taken as 0.285, $(\alpha_S - \alpha_G)$ is the difference between the thermal expansions of the substrate (pushrod) and the grid (strain gauge), and ΔT is the change in temperature.

By substituting equation (5.7) into (5.8), the amount of additional strain due to temperature effects is calculated by (5.9).

$$\varepsilon_{T/0} = \frac{\left[\beta_G + F_G \left(\frac{1 + K_t}{1 - \nu_0 K_t} \right) (\alpha_S - \alpha_G) \right] \Delta T}{F_I} \quad (5.9)$$

It was possible to find values of β_G and α_G values in the literature, however, this was not possible for the F_G . The gauge factor is a ratio of electrical resistance to mechanical strain. A change in temperature alters the electrical properties of the strain gauge, making calculation of the F_G value difficult. As the focus of this thesis was to investigate thermal properties, it was decided that no further effort would be spent attempting to find this value. Consequently, the third reasoning for the increasing input force could not be confirmed or denied. Figure 5.31 is taken from the technical support document supplied by Vishay Micro-Measurements; it indicates a large potential for additional strain to be recorded by the strain gauge transducer, severely altering the results. Thermocouple readings in Figure 5.32 show that the temperature of the pushrod does not exceed 40°C, rising less than 20°C. Figure 5.31 would suggest that only a small temperature induced strain should be present for such low temperature rises. However, it was after approximately 30 minutes that the pushrod temperature increased sharply, coinciding with the rise in input force. Perceivably then, the additional strain induced by temperature rises is having greater effect on the strain gauge readings than Figure 5.31 would suggest. Before any further force reading are taken the three unknown strain gauge properties must be found to dispose of the thermal output effects, enabling accurate clamp force calculations.

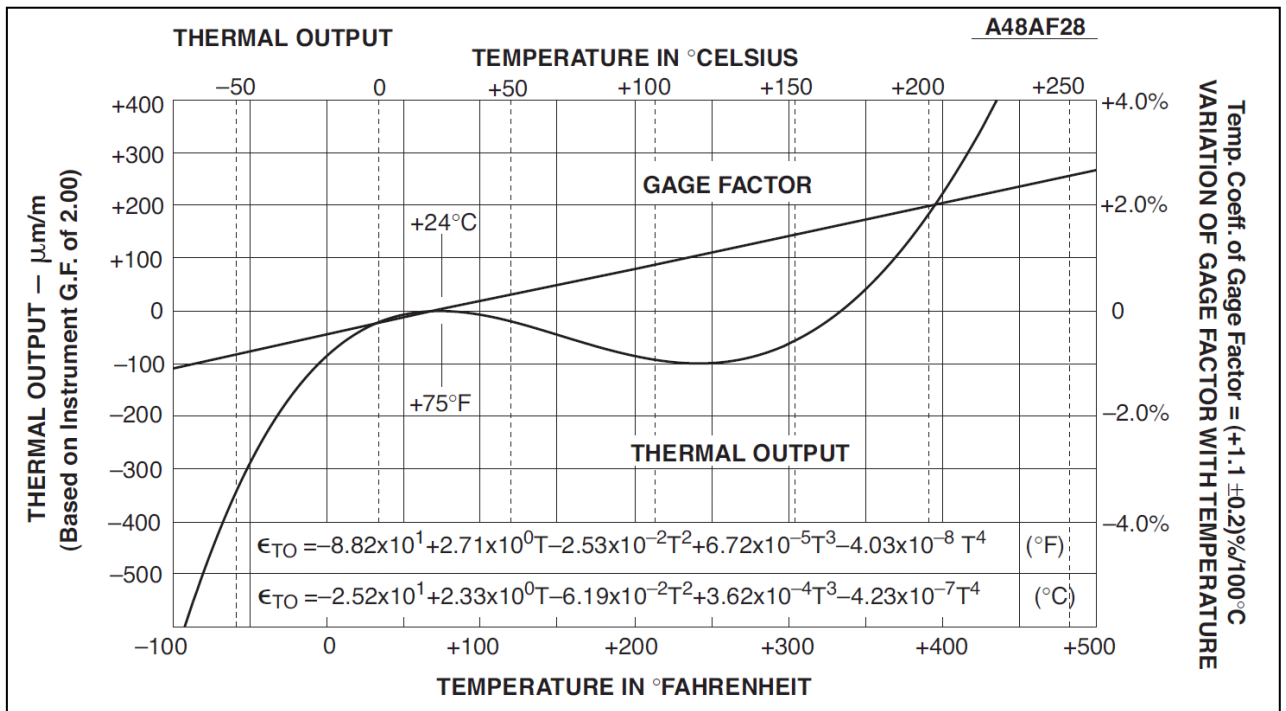


Figure 5.31: Graph taken from the Vishay technical support document Tech Note TN-504-1 displaying the amount of additional strain generated in the strain gauge from the effects of temperature (Vishay Micro-Measurements 2007)

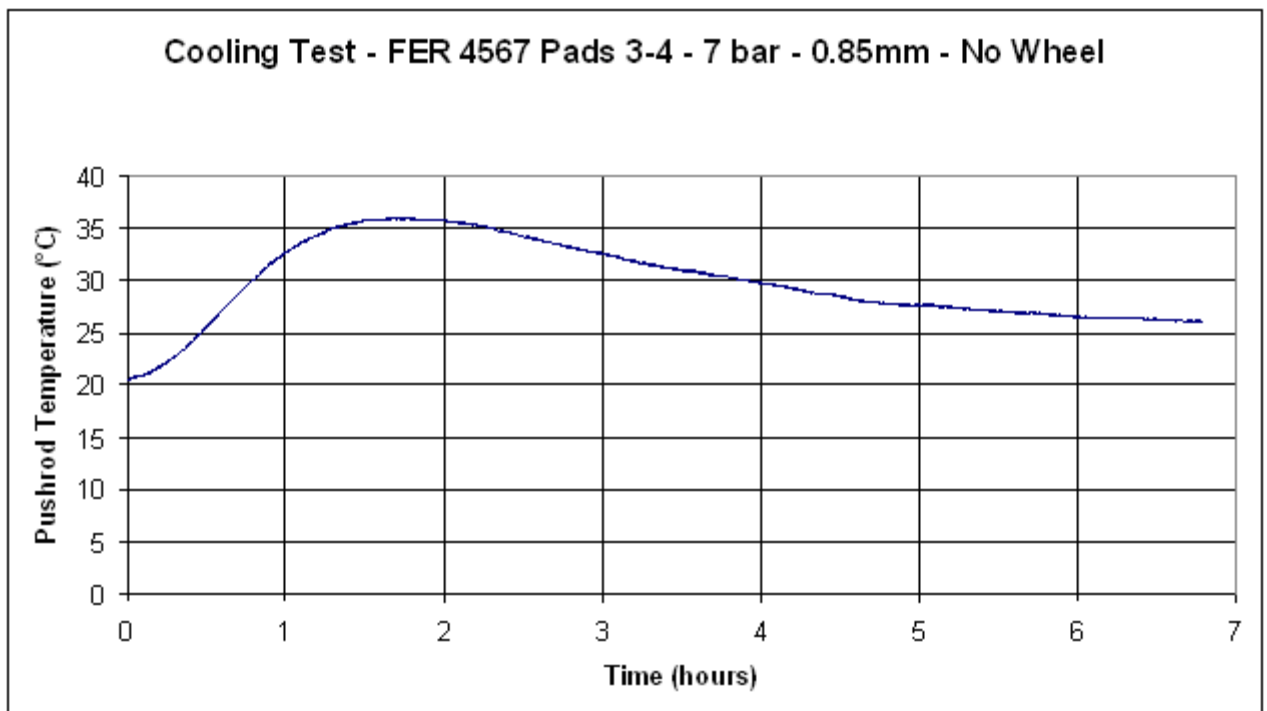


Figure 5.32: Temperature rise of the pushrod during the coolback phase.

Experimental results have shown that input force varies during the coolback period. However, these results were proven inconclusive due to potential apparatus errors in the form of a random zero shift, which suggests differing force patterns would have been measured for individual experiments. This was not what happened in reality as the increasing input force was consistent. The effect of thermal output is still a mystery as missing material properties prevented suitable analysis. Furthermore, new techniques are available to measure the coolback caliper displacement to understand if this is having an effect on the input force. It is a necessity to eradicate these areas of uncertainty related to the strain gauge measurements before a torque mechanism is introduced to the cooling tests to distinguish the EPB capabilities to prevent roll away.

The main aim of this investigation is to understand the thermal aspects of the disc brake assembly during the cooling phase of a stationary parking application. The issue surrounding the input force measurements impacts any testing related to mechanical effects and therefore the erroneous measurements had little impact to this research. Consequentially, a decision was made to concentrate effort on determining the thermal effects on the brake system rather than finding a solution to the apparatus issue. New equipment and validation techniques could have procured to accurately calculate the input force yet, it has been shown already that there are very complex thermal interactions occurring in the brake system during a stationary parking

application that currently unknown. By investigating these interactions, a full understanding of the heat paths through the brake assembly can be achieved and used to develop a full brake assembly FE model. Having a fully functioning thermal FE model is advantageous as it will allow a sequentially- or a full-coupled thermomechanical FE model to be produced, which will act as a key design and analysis tool for the EPB development.

5.7.3 Thermal Set in the Brake Pads due to Preheating Input Pressure

In contrast to the measured input force measurements, it was possible to take accurate contraction readings as the confidence level in the displacement transducer was a lot higher, due to no instrumentation issues being detected. Conformation is shown in Figure 5.25 where the actuator displacement measurement showed clean and repeatable results. Initially, when the temperature difference between the disc brake surface and the surrounding ambient air was large, there was a sharp increase in displacement, leading to 75% of the total pad movement occurring in the first 30 minutes. Afterwards, the contraction rate falls drastically.

During a typical CV journey a driver will repeatedly use relatively low speed, low deceleration braking applications to reduce the vehicle speed. For example, a typical in-city bus journey has a maximum speed of only 30 mph but constantly braking the vehicle back down to stationary, for the purpose of picking up and dropping off passengers. The deceleration rate must be low to accommodate the standing passengers, meaning the braking application will be conducted with low actuating pressures and consequentially, low input forces.

The current test procedure uses the same actuating pressure for the preheating and cooling phases. A typical parking input pressure is 6 bar, which is described in Appendix J to deliver an input force greater than 8 kN. Evidently, there is a contrast between the pad heating procedures seen in the laboratory to how they are heated in operation. To test whether the preheating cycle affects the cooling rate of the pads, three separate preheating cycles were used on a cooling test. The FER 4567 friction material pads, in the faded state, were used for three experiments, with a clearance gap set to 1 mm and a parked input pressure of 6 bar. The preheating cycles were:

1. As in section 5.6 above, a 6 bar input pressure was applied for two preheating clamps.
2. A 1 bar input pressure was applied for two preheating clamps.
3. A 1 bar input pressure was applied for five preheating clamps.

The aim of the experiment was to determine whether the disproportionately high preheating pressure caused a semi-permanent thermal setting effect in the pads, and if so, what was the best procedure to use in future cooling tests. As the temperature in the friction material increases, the

molecules within the pads will want expand. However, a high compression level generated by the high input force prevents natural expansion. An unnatural contraction ultimately transpires, causing a temporary alteration in the thermo-mechanical characteristics of the material until the pad cools back to normal. As the alteration is usually temporary, the process is known as semi-permeable set.

Figure 5.33, Figure 5.34 and Figure 5.35 display the full range temperature results, including the preheating and cooling phases, for the conducted cooling tests with preheating cycles 1, 2 and 3 respectively. An important observation is made that there was a larger temperature difference in the backplate between the start of the cooling phase and the previous preheating clamp when only two preheating clamps are used. Pad temperatures were much closer to reaching an equalised state when using five preheating clamps, increasing the experimental repeatability. Temperatures are also more likely to match those found during operation as the bus operation example outlines, the pads can be used frequently, absorbing large amounts of heat.

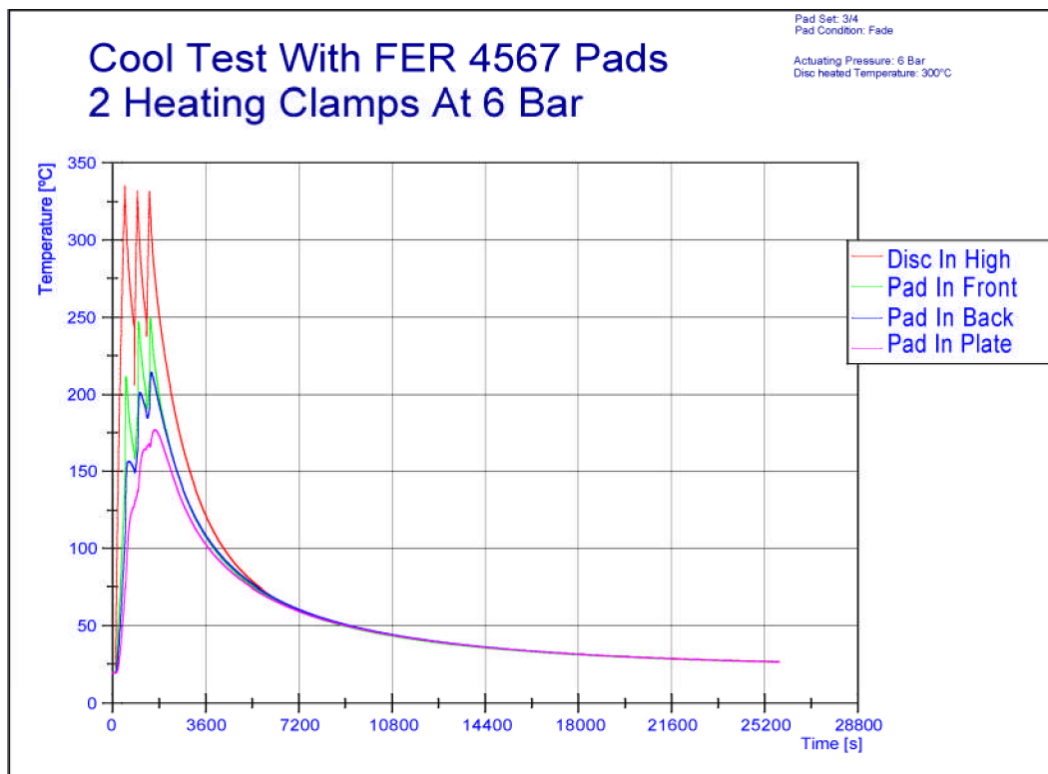


Figure 5.33: Cooling test with 2 preheating clamps at 6 bar

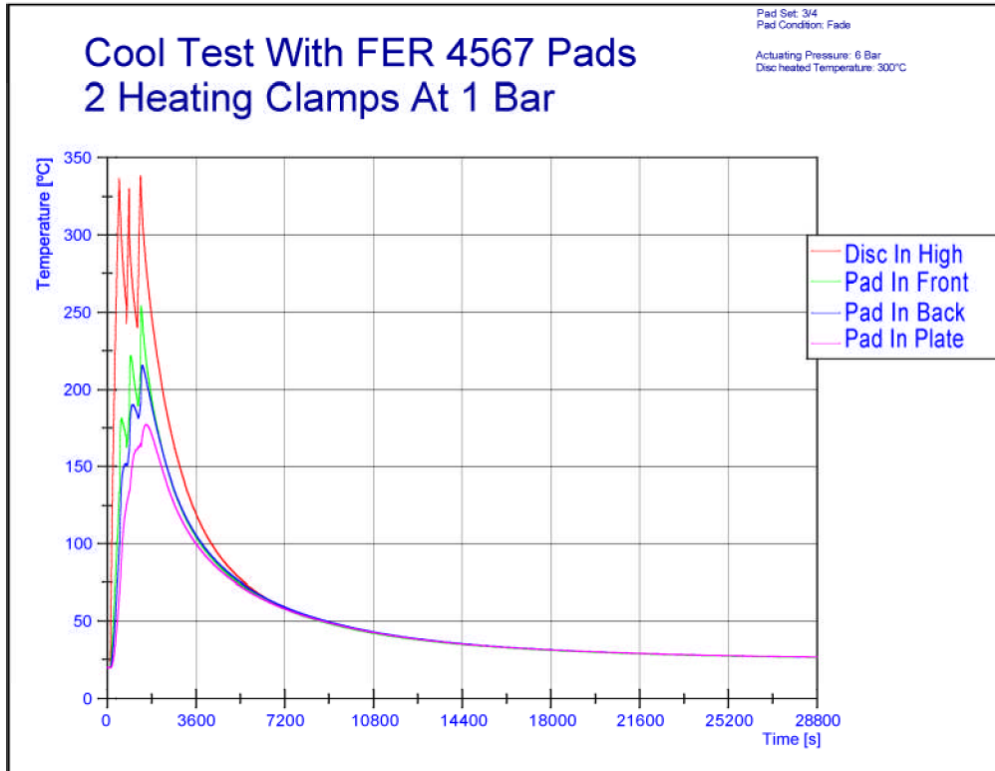


Figure 5.34: Cooling test with 2 preheating clamps at 1 bar

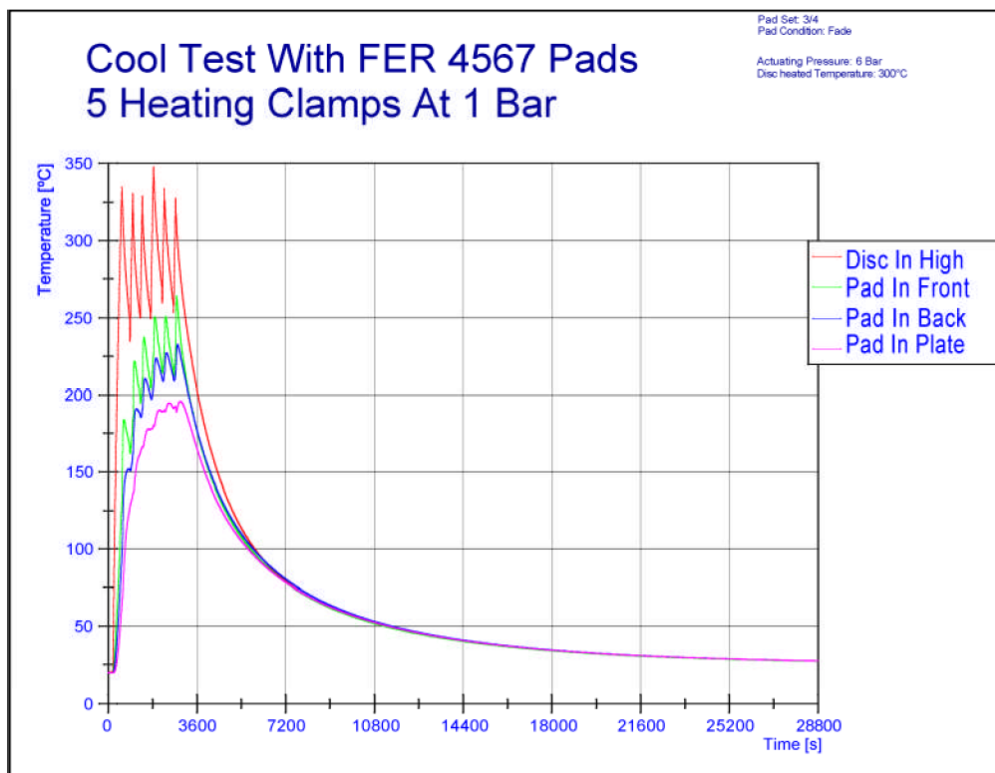


Figure 5.35: Cooling test with 5 preheating clamps at 1 bar

Figure 5.36 looks closely at the cooling rates at the Pad Out Backplate thermocouple position (see Figure 5.20), from 150°C down to 50°C, for the three different preheating sequences. A large distinction can be made between procedures using two preheating clamps to the procedure that used five preheating clamps. A slower rate of cooling is the result of more realistic energy storage in the brake pads, taking the backplate 15 minutes longer to cool from 150°C to 50°C. This pattern was common amongst all thermocouple reading through the pads. Obviously, more energy in the system will lead to a longer amount of time to dissipate the energy from the same geometry.

However, by comparing preheating sequences using 6 and 1 bar actuating pressure for the 2 preheating sequences, evidence of thermal setting is presented in the form of the cooling rate being slower for the higher actuating pressure. By using the lower actuating pressure, faster cooling rates are achieved, which is an advantageous result for EPB design as it reduces the amount of time rollaway is possible for once a parking application is applied. Modelling procedures and prototype testing are therefore somewhat simplified. An opportunity for an investigation into the changes in friction material molecular structure and/or properties under various thermal and mechanical loads is presented. However, the suggested research is outside the scope of this investigation so was not pursued here as this thesis concentrated on thermal aspects, in relation to stationary cooling rather than material properties and EPB aspects.

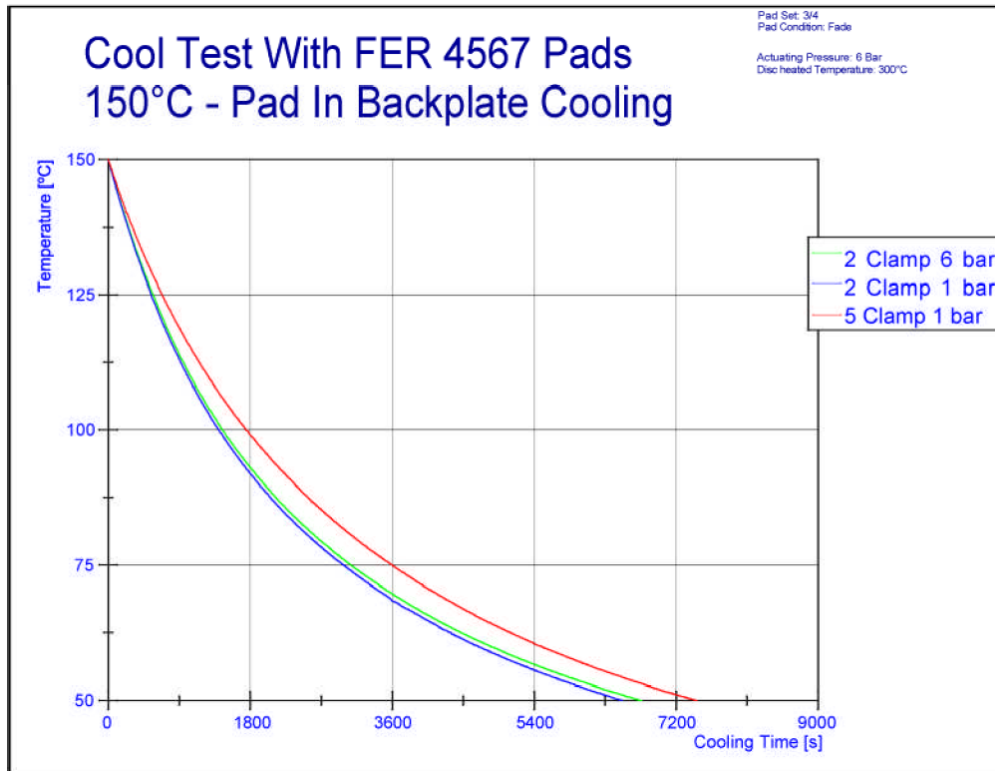


Figure 5.36: Cooling rates in the backplate from 150°C.

From the results of all the experiments discussed, the final cooling test procedure used for all subsequent cooling tests had the more realistic five preheating clamps at 1 bar actuating pressure, before using a constant 6 bar during coolback. Even though full equalisation did not fully occur with five preheating clamps, this is the number that was used to allow good results to be achieved without elongating the time necessary to complete a single cooling test. Furthermore, the pads used a standard total running clearance of 1 mm and the wheel was disconnected from the brake assembly (as shown to have very little influence on stationary cooling).

5.7.4 Worst Case Pad Conditioning Testing

A total brake system expansion of 0.198 mm was previously measured in Figure 5.25, after applying the opshaft ratio. Meritor's current design requirement specified a maximum brake assembly contraction of 1.00 mm. Although these results clearly show the total assembly contraction was comfortably inside the set criteria, it cannot be said that the EPB will successfully hold a CV under all conditions as this particular test was conducted under the best case set of conditions i.e. the pad material used was the less compressible FER 4567 friction material, in the thermally stable faded condition. It was therefore necessary to conduct a set of

experiments that investigated brake assembly contraction with both friction materials, with differing thermal conditioning.

To test the maximum pushrod displacement condition, experimentation using the newly defined cooling test procedure was conducted with both friction materials at various thermal loading states. Red lines in Figure 5.37 represent the results using the FER 4567 friction material with green lines for the T3016 material. In both cases, sets that were in the brand new, faded and bedded states were used. The latter were subjected to three full cooling tests, for the purpose of finding how the thermal loading affects the contraction properties experienced by the friction material. Continuity between the two friction materials is shown in Figure 5.37, as each subsequent cooling test with a set of bedded pads reduced the total amount of brake assembly contraction. This result is a function of the friction material behaviour rather than any other part of the caliper as no other component changes made between experiments. As the caliper components had all been subject to many thermal applications prior to starting the cooling test, they were all in a thermally stable condition. Therefore, any changes in the actuator displacement measurement, and hence the total brake assembly contraction, can be attributed to changes in the friction material.

The largest amount of brake assembly contraction was calculated at 0.65 mm from the displacement transducer measurement when using the FER 4567 friction material, in the freshly bedded condition. Interestingly, there was nearly 5% more total contraction than the equivalent brand new pad, a result echoed with the T3016 friction material, although there is only a 1% in this case. This is an interesting result as it details that the most severe case is not with a brand new set of pads, but once the pads have been through an initial bedding in process, putting the material through a defined number of heating cycles. Consequently, the worst case scenario will occur once the CV has left the maintenance unit with new pads and is an uncontrolled number of miles away. The maximum recorded contraction was 0.35 mm less than the design limitation, allowing up to a further 50% contraction before the restriction is reached. A large safety factor is therefore presented.

It should be stressed that these results do not show that the EPB design will prevent a CV from rollback, they show that the current design has sufficient compliance for the amount of possible contraction before losing all input force. Further development work is necessary to determine the change in friction force during a parking application before stating rollback will not occur. For this, an in-depth study into the variability of μ (and therefore the change in clamp force) during the cooling phase of a parking application. This package of work will focus on the

mechanical aspects of the brake assembly rather than the thermal aspects, which are outside the scope of this investigation and, as discussed previously, remains as further work.

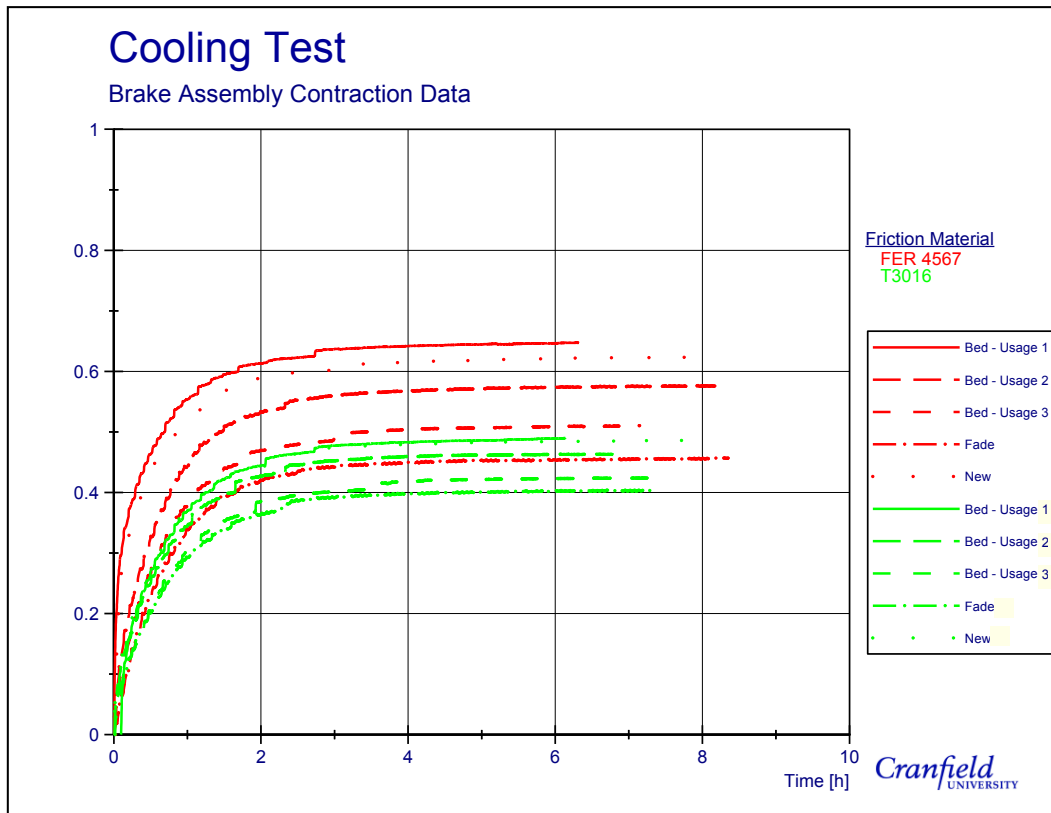


Figure 5.37: Total measured brake assembly contraction using various pad materials, in various thermal states.

Another interesting result was that the FER 4567 showed more cooling contraction than the softer T3016 friction material, which has a 10% lower density. However, compressibility can be defined as the change in volume with pressure, or stress. This result would appear to show the thermal stresses induced in the FER 4567 friction material are larger than in the softer T3016, allowing for more thermal expansion during heating, and thus, more contraction during coolback.

This result is something of a self-safety feature of friction materials as the majority of hot parking applications are likely to be in the faded state, which contract least. Provided the CV does not rollaway on after the first few applications, the pads will contract less, reducing the chances of vehicle rollaway. By designing the EPB to hold the CV with new or just bedded pads, the risk of rollaway will be reduced.

Figure 5.37 shows the full cooling data taken during the 10 experiments. The amount of time the experiments were allowed to run for varied lengths of time, dependent on how long the

operator was available for. Remembering the five preheating clamp sequence was used, which adds nearly an hour on top of the shown cooling time to each experiment, the total duration for the cooling test took approximately 9 hours (a whole day including setup time). Measured actuator displacement (total assembly contraction) was negligible after 6 hours, with the majority of the cooling and contraction happening in the primary 2 hours of the cooling phase. Similarly, the temperatures of the disc brake also returned approximately back to ambient after 6 hours of cooling (Figure 5.23). Consequently, the final adaptation to the cooling test was to limit the cooling time to 6 hours.

6 FE Thermal Modelling of a Parking Application

One of the key research objectives for this project was to produce an FE model capable of accurately predicting temperatures throughout the cooling phase of a parking brake application. An incremental approach was taken to achieve this objective, as there is high complexity in such a system, requiring further understanding of all the thermal interactions between components. This section discusses the construction of a simplified disc brake and pads only FE model, before presenting results generated from it. Ultimately, Chapter 6 demonstrates that the standard method of brake modelling commonly used within the industry is unsuitable when simulating stationary parking applications.

6.1 FE Model Creation

To model a stationary parking brake application, the FE programme ABAQUS was used. The full CAD brake assembly was provided by Meritor in the widely used data exchange step file format, to allow the files to be opened by all CAD and FE programmes. Figure 6.1 shows the complexity of the disc brake geometry is maintained using such a file. However, creating an FE mesh capable of preserving all the intricate geometric detail would need an element size so small that the simulation runtime would become practically unacceptable. Consequently, modelling simplification was a necessity for the majority of brake assembly components before FE analysis could be run.

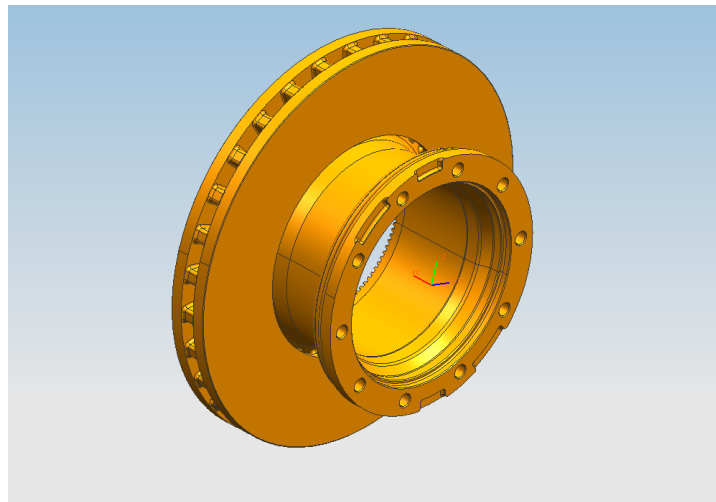


Figure 6.1: CAD model of the disc brake provided by Meritor

6.1.1 The Disc Brake

Getting an accurate representation of the disc brake, close to the geometry depicted in Figure 6.1, was important as this was the most significant component in the brake assembly. Typically,

over 90% of the generated thermal energy enters the disc brake before being transferred to other components and dissipated because of the higher effusivity in the disc brake pulling heat from the third body layer (Majcherczak *et al.* 2007). The closer the geometric approximation, the more accurate the result will be to reality, but with the longer computer runtimes.

Figure 6.2 shows the simplified 3D disc brake model created in ABAQUS. A major omission in the FE model was the removal of the bolt holes that attach the disc brake to the wheel carrier. Indeed, the presence of holes will amplify the stresses in this vicinity, but with clamp loads approaching 160 kN at the disc brake/pad interaction, which will generate vastly greater stress levels, significant stresses will be present elsewhere in the model. Yet, as structural significance is not an issue in thermal modelling, this simplification will cause minimal effect on the results by increasing the bulk material slightly. For the same reason, all small fillets located inside the hat section, towards the flange face, were replaced with a single step from the hat ID to the flange ID. Likewise, all small radii located on the transition of the friction surfaces were also replaced with sharp corners for modelling simplicity.

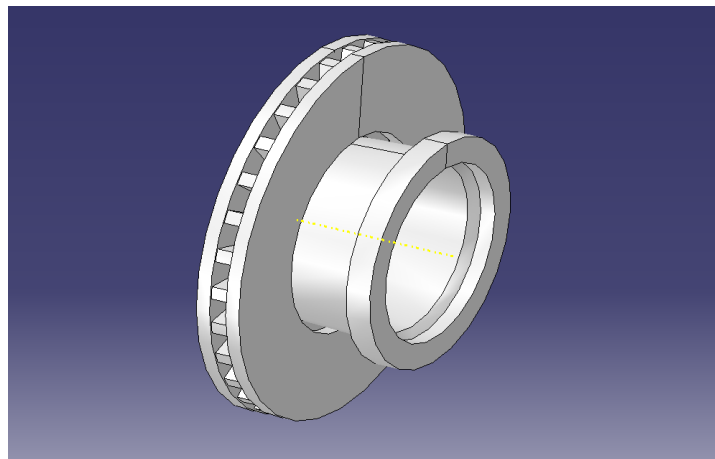


Figure 6.2: Fully simplified disc geometry used for FE analysis – ID side.

It is important to consider the type of mesh required for the assembly at an early stage as different elements require differing techniques to be performed. In three dimensional FE analysis, it is common for continuum elements to be used. Structured, sweep and bottom-up meshing techniques can all be used to create continuum elements. Considering the disc brake is not a continuous shape in the circumferential plane (due to the vanes not being in the pure radial plane), the sweep technique was rejected. With the relative ease associated with using a structured technique, it was preferred over bottom-up meshing; it places a defined arrangement of elements on a surface and extrudes the pattern through the cell volume, creating a series of

elements. Hexahedral elements were used in the assembly for their stability when modelling contact.

Even for the simplified disc brake, the geometry was too complex for ABAQUS to automatically generate a structured mesh. By sectioning the disc brake into smaller, simpler geometry segments, localised structured meshes could be generated. Figure 6.3 demonstrates the sectioning of the disc brake's friction surfaces with the internal vanes. A common edge was generated between the friction surfaces and the vanes, where shared nodes are placed automatically. Strategic placement of the segment boundaries like this increases the mesh efficiency as fewer nodes are required, keeping computational time to a minimum. For this reason, each vane was projected onto the friction surface to ensure that nodes within the vanes would be aligned to those on the friction surface. Furthermore, three sectioning cuts were made on the rotor section, being representative of the outer vane edge, inner vane edge and the friction surface ID, shown in Figure 6.3.

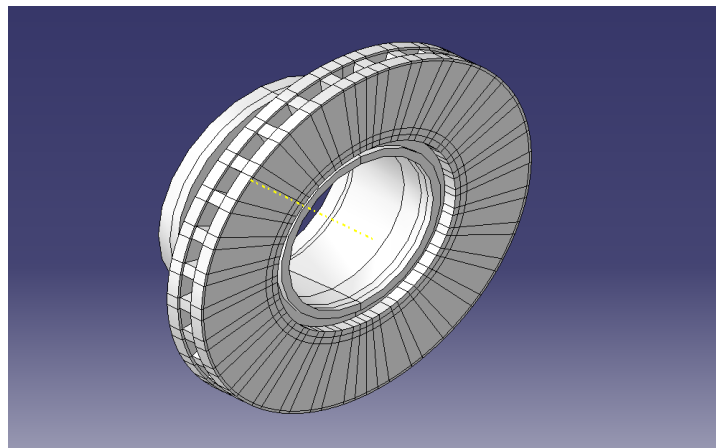


Figure 6.3: Disc segmented by simplified vane shape.

6.1.2 Brake Pad Friction Material – T3016

As explained in Chapter 5, there were two different friction materials being used in this research; the FER 4567 and T3016 materials. Initial FE modelling was conducted using T3016 pads despite them contracting less during cooling, due to having more known information (thermal properties, from Table 5.3). The part was made from a 22 mm extrusion of the friction material shape. Generally, braking simulations require contact analysis between the disc brake and pads. High importance was placed on obtaining node-to-node contact when modelling multiple components, as it ensured the forces and temperatures are exerted by one element are completely received by the other. When nodes are misaligned, ABAQUS uses a lumped model technique to interpolate the proportion of the force/heat going into the nearest nodes.

Computational time is consequentially increased with additional mathematical operations, as well as errors being introduced to the simulation.

Figure 6.4 demonstrates the measures taken to create node-to-node contact between the disc brake and friction material. As discussed, the vane shape had to be imprinted on the friction surfaces to control node locations. By precisely drawing the vanes, and other disc brake geometry, on the friction material surface, nodes created on the disc brake would also be generated on the friction material in exactly the same location.

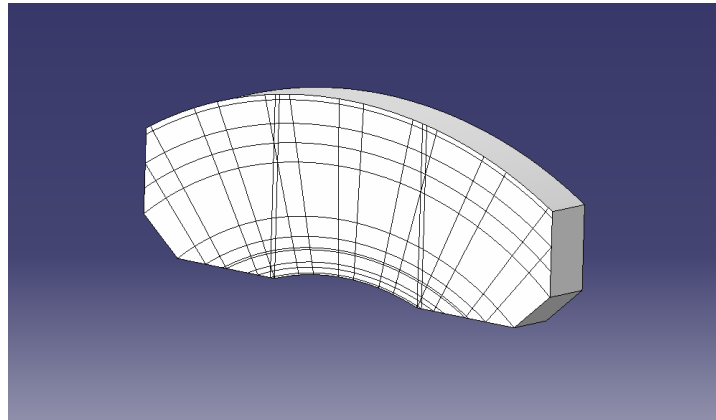


Figure 6.4: Sectioning pattern placed on the T3016 pad friction material.

An iterative approach was taken when developing the friction material shape. The extruded shape had subtle modifications to that in the design drawing but remained within the allowable manufacturing tolerance limits, to enable edges in close proximity to share a common node. For example, the two pad grooves were moved slightly inwards, towards the centre of the pad to intersect the inner radius.

The presence of both the grooves and vanes resulted in triangular shaped segments being created. By default, hexahedral elements are rectangular in shape. By creating triangular segments, deformation (or skewing) of the hexahedral elements must occur to fit them within the cell. Small levels of skew have little impact on result reliability, however, the analysis can become unstable with large amounts of skew. The skew angle is calculated by ABAQUS, with a warning outputted when it reaches a designated figure. The generally accepted value of 20° was used throughout, according to the ABAQUS User's Manual (2004).

A total of 6,176 elements were used to construct the friction material, of which none had errors and only 420 (6.8%) elements produced skew warnings. If mechanical modelling were being conducted, it would be advisable to use wedge elements in triangular regions. The additional

level of mesh complexity was not justified for thermal analysis FE simulation, therefore tetrahedral elements were used to ease the model creation.

It is important in contact analysis that the two surfaces in contact are meshed correctly, ABAQUS uses a master-slave relationship for the surfaces. It has already been said that node-to-node contact is necessary for accurate results but the same importance is also put on defining the master-slave relationship correctly. The master surface is typically selected to be the component that is the stiffer of the two. The slave surface must have a finer mesh than the master, or at worst match on a 1:1 ratio. This ensures that the master surface can protrude into the slave surface and not the reverse, because the contact algorithm used by ABAQUS only uses the master as a surface. The slave is seen as a series of nodes, with the associated surface area assigned to each node but without a normal. By imprinting the friction surface sectioning pattern directly on the disc brake, as shown in Figure 6.5, node-to-node contact could be guaranteed.

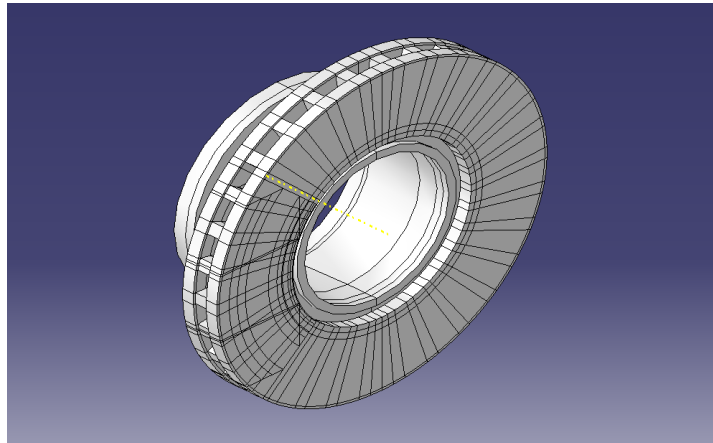


Figure 6.5: Pad section put into disc as well.

The grey cast iron disc brake has an E value approximately 10 times greater than the friction material. Coupling the difference in the two materials Young's moduli with the fact that the thicknesses of the friction material and the disc brake friction surfaces are similar, resulted in the disc brake being made the master surface. With the friction material being the slave surface in the disc brake/pad interface, a finer mesh was used (where possible) than on the disc brake. There was predominately a 2:1 ratio for pad to disc brake elements, with only a small section towards the OD where the ratio was reduced to 1:1

On the left-hand side of Figure 6.6 is the fully meshed disc brake. It can be seen that a fairly course mesh was used in these preliminary simulations, with 11,195 elements. As described above, the hexahedral elements were the main type of element used to fabricate the mesh, depicted by the green cells on the right-hand side of Figure 6.6. Cells coloured pink illustrate

where a free mesh was necessary to join two dissimilar mesh patterns together, with tetrahedral elements used in these sections. Triangular segments formed during the sectioning process fortunately did not cause any meshing errors, meaning the model would run, although 730, or 6.5%, of the disc brake's elements were skewed.

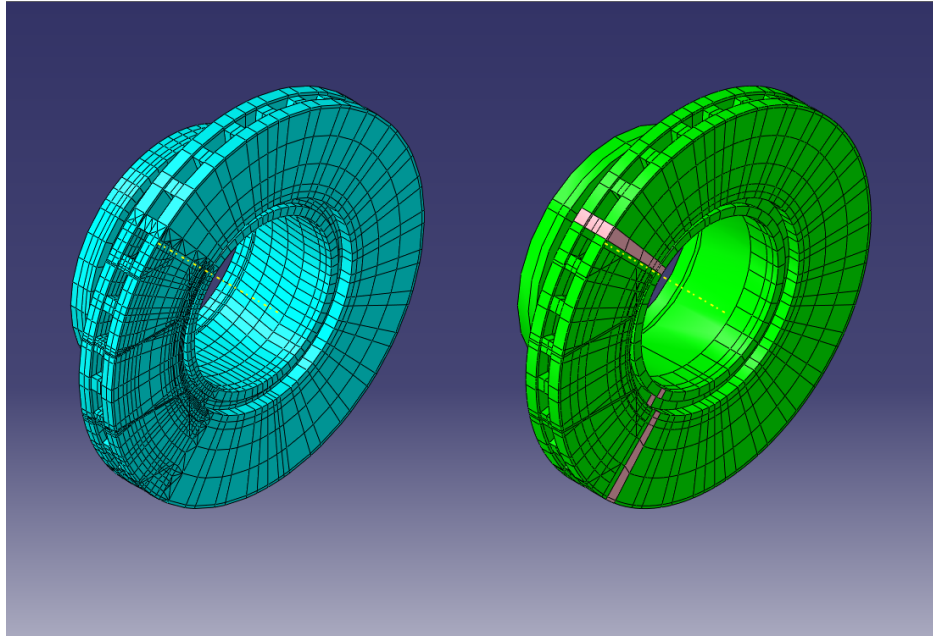


Figure 6.6: Fully meshed disc

6.1.3 The Backplate

The meshing of the backplate component in ABAQUS was more straightforward than the previous two parts. An 8 mm extrusion of the backplate shape, obtained from the CAD file provided by Meritor, was used to generate the 3D volume. A perfectly flat backplate was the result of this procedure, a slight change to reality as the backplate was slightly curved at either end. Contact between the backplate and friction material dictated the same sectioning pattern seen on the disc brake and friction material be placed on the backplate as well, shown in Figure 6.7.

Depending on whether the backplate was located on the inboard or outboard side of the disc brake, contact would occur either with the pistons or bridge to the backplate respectively. As a result, a similar sectioning procedure was needed on both backplates to maintain the node-to-node mesh assembly. This required imprinting both shapes through the both backplates, the friction material and disc brake. Due to the complexity of the segmented geometry of the disc brake and pads already, it was decided to split the backplate up into three sections instead, reducing the amount of triangular elements. The division closest to the disc brake had the same

sectioning as the friction material, as in Figure 6.7a. Surfaces contacting either the bridge or pistons were the third section, with Figure 6.7b demonstrating the latter. Two circles represented the piston contact area, which were sub-sectioned further to help ABAQUS with meshing a circular pattern with hexahedral elements. A secondary, intermediate section was located between the two backplate extremities that acted as a joining layer.

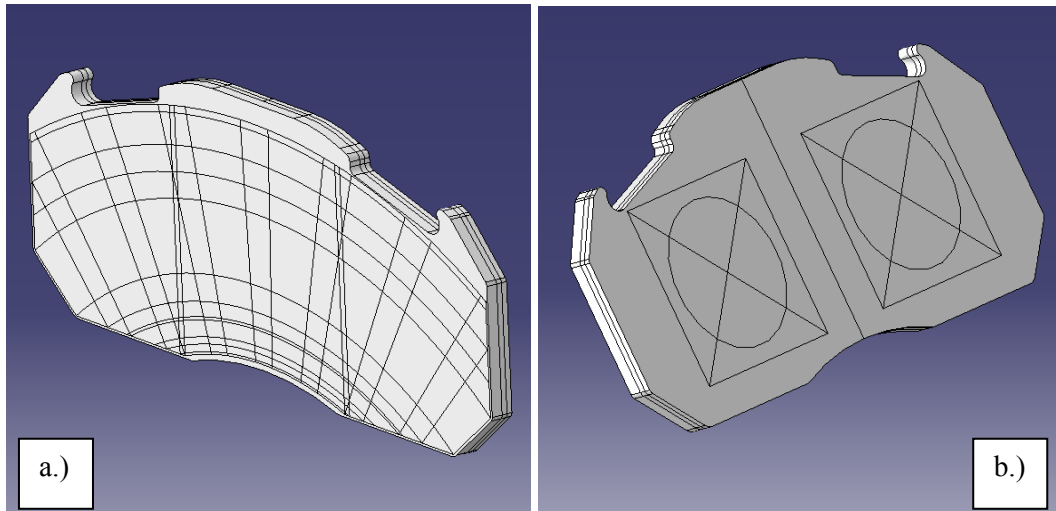


Figure 6.7: a.) The brake pad and disc sections put into front side of backplate, and b.) piston rings located on the rear of the backplate

To complete the assembly mesh, a combination of hexahedral and tetrahedral elements was used to mesh the backplate; the former for areas of contact and the latter used everywhere else. Figure 6.8 shows the meshing techniques used to create the backplate's mesh. A higher proportion of elements in backplate produced skew warnings, compared with previous components; 1,209 (14.1%) out of 8,562. Differences in the first and third division caused distorted elements in the joining segment.

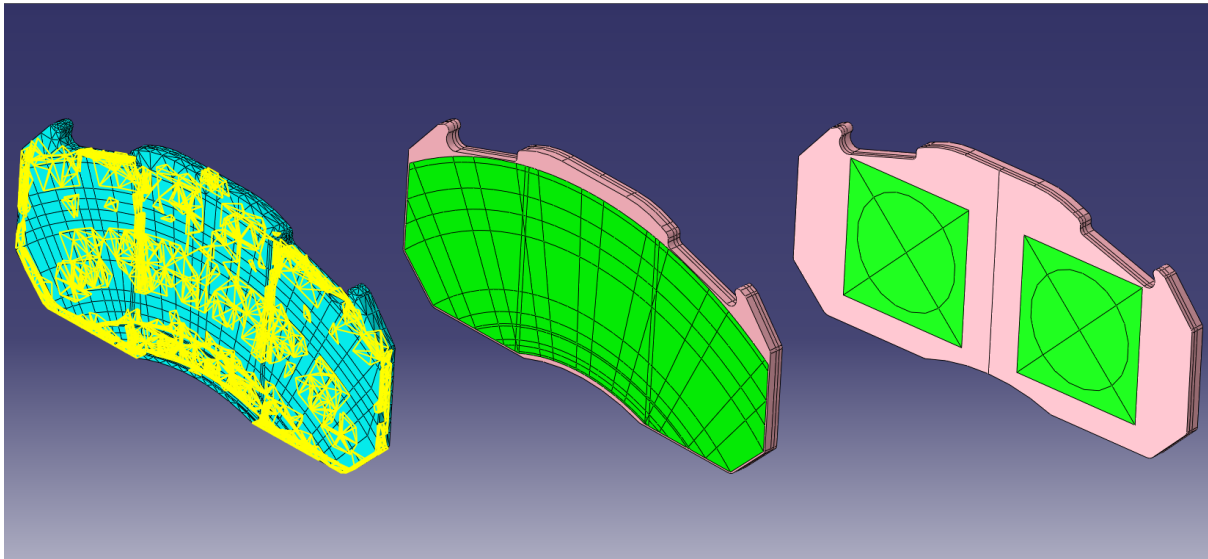


Figure 6.8: Mesh techniques for various backplate divisions.

6.2 FE Model Preparation

Confidence was gained in ABAQUS's ability to accurately simulate thermal models prior to creating the simplified assembly model by conducting a simulation and comparing results to theoretical bulk temperature rise. With confidence in the FE program, setup of the constructed brake assembly model could happen. Before any simulations, the initial temperatures of the assembly components and any relevant boundary conditions were inputted into the model. Section 6.2 details the model setup process.

6.2.1 Initial Parking Application Conditions

To perform a cooling test simulation, an estimation of the heat distribution at the start of the parking application was first made. Two methods were used to generate high initial temperature distributions, either by inputting a single temperature for each component, like in Robinet (2008), or to generate the temperature distribution via a primary, heating simulation. The former is unquestionably the easier method and reduces computational time. However, the assumption that every part of a component is at the same temperature is unrealistic. It was therefore decided that the brake assembly's initial temperatures would be achieved via the second, more complex heating method. Preheating data was collected during the cooling experiments conducted in section 5.7.3, so modelling of the full preheating sequence was conducted, due to the actual experimental data being readily available.

Figure 6.9 and Figure 6.10 each show three measured thermocouple temperatures located on the outboard disc brake friction surface and in the outboard pad respectively, during the preheating

sequence. Initial temperature modelling objectives are to match the temperature profiles within the standard $\pm 20\%$ limit. The acceptance range is large as thermal experimentation often causes variability, even under the controlled conditions of the Thermal Rig. Small changes in ambient temperature, air flow conditions plus others all impact experimental conditions making it extremely difficult to create perfectly repeatable results.

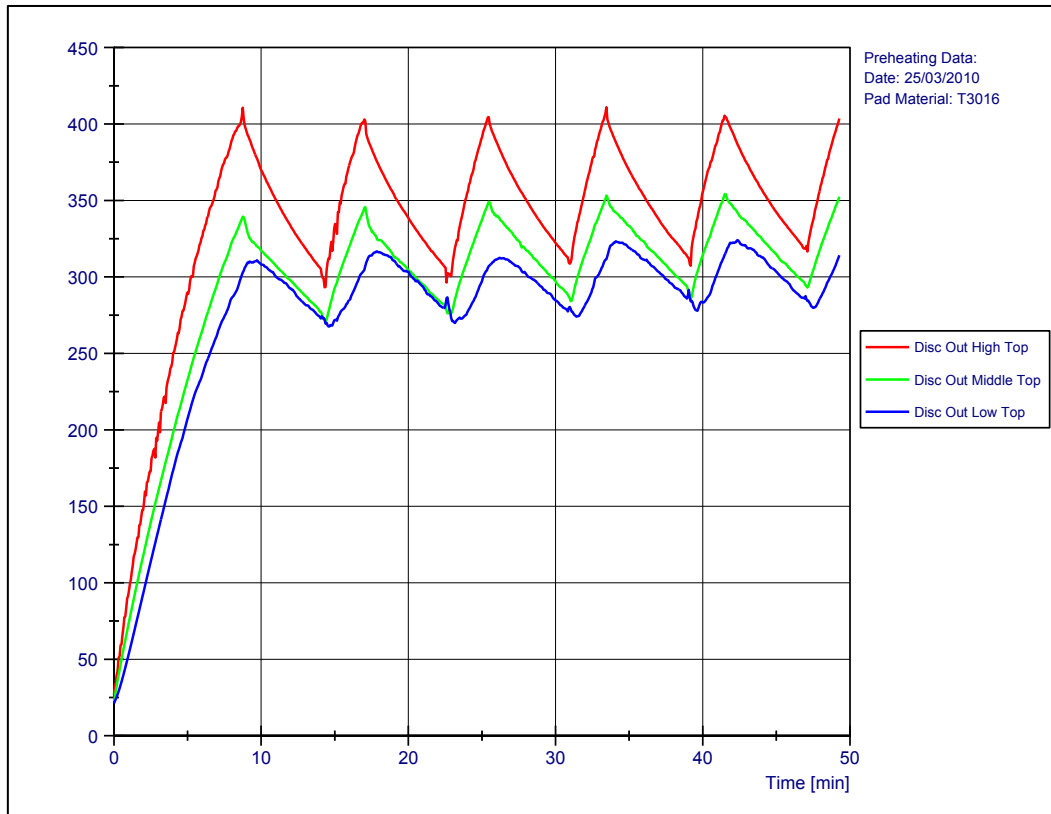


Figure 6.9: Outboard disc friction surface temperatures during the preheating sequence.

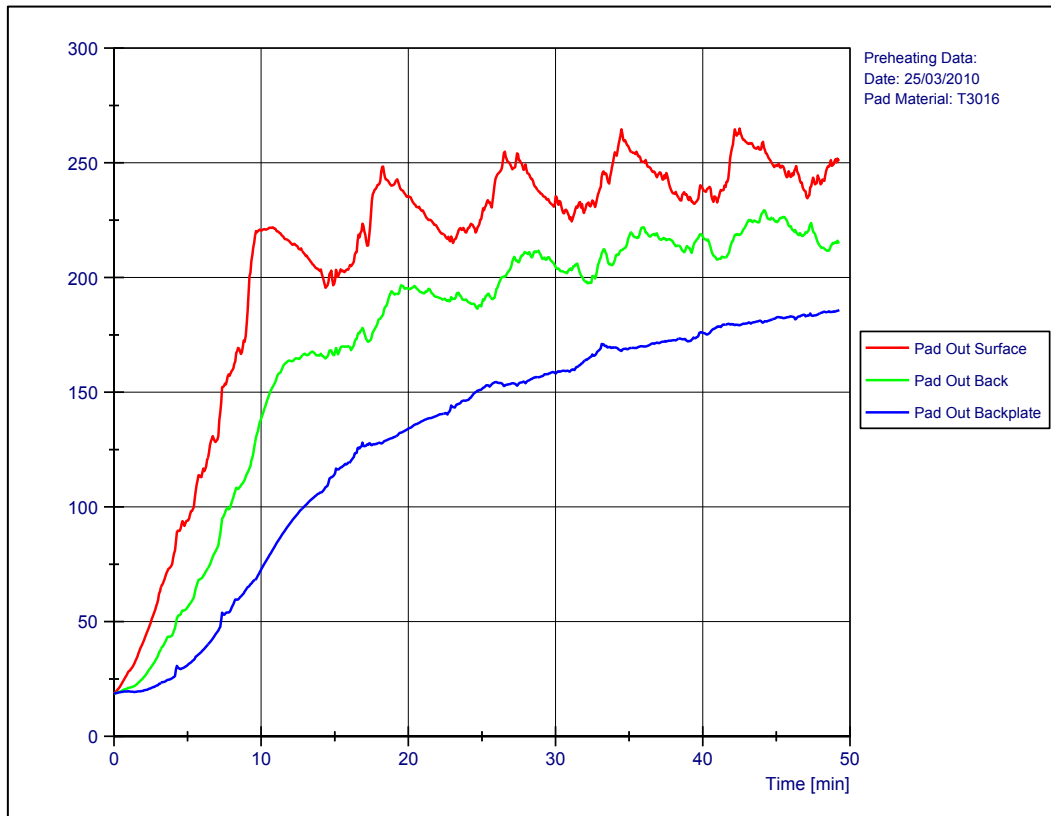


Figure 6.10: Outboard pad temperatures during the preheating sequence.

At the beginning of the simulation, the temperature of every element in the model was set to ambient temperature, taken to be 20°C. Heating on the Thermal Rig was done via the IHC. To replicate, a surface heat flux was used on the contacting disc brake and pad surfaces, like in Figure 6.11.

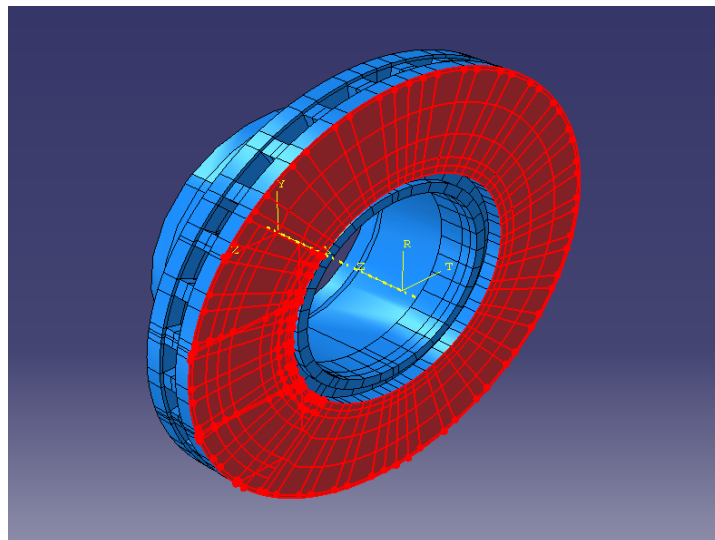


Figure 6.11: Uniformly distributed heat flux into the disc friction surface.

According to Callebaut (2007), 87% of the energy delivered by the IHC penetrates into the disc brake down to a depth of δ , which diminishes in intensity away from the surface. For grey cast iron, this value is typically around 9 mm. Body heat flux simulations can be conducted in ABAQUS but it was rejected. Grey cast iron is a good conductor of heat, having a high C_p value, resulting in heat energy to quickly penetrate through the disc brake, making the more complex body flux unnecessary.

From Figure 6.9, the disc brake heating time from ambient to 400°C was approximately nine minutes. After numerous iterative thermal analysis, a heat flux value of 55,000 W/m² gave a close approximation to this. Figure 6.9 also demonstrates the presence of a thermal gradient radially across the friction surface of approximately 80°C.

Simultaneous to the heating input, all three modes of heat dissipation will be occurring. To get the correct temperatures in the disc brake, pads and caliper, correct simulation of the heat flows in both the preheating and cooling phases were necessary. It is discussed below how each heat dissipation mode was setup in ABAQUS with corresponding heat transfer coefficients, followed by other boundary conditions placed on the assembly that were related to thermal interactions. ABAQUS uses a standard notation with regards to the degrees of freedom (d.o.f), with number 1-3. In a purely thermal simulation, d.o.f 1-3 are all set to zero allowing for no displacement within the assembly. The flow of thermal energy within brake components can be investigated with only the temperature d.o.f (number 11 in ABAQUS) free.

6.2.1.1 Radiation

Being able to consider radiation purely as a surface phenomenon drastically reduces FE computational time as only nodes on the external surfaces need calculating. The amount of radiation at any one surface is governed by the emissivity value. From Voller *et al.* (2003), a disc brake fabricated from cast iron, in the fully oxidised condition, has an emissivity value in the region of 0.9; this will be validated later in Chapter 9. As this condition matches the disc brake used on the Thermal Rig it was used in the simple assembly FE simulations. The same emissivity value was used for the friction material and the backplate, due to both being black in colour, so are expected to produce radiation levels approaching those of a black body.

There are two types of radiation modelling interactions used in an FE simulation; “To Ambient” radiation and “Cavity” radiation. As the name suggests, To Ambient radiation is where surface temperature is lost directly to the ambient air as no other components are in the vicinity of the emitting surface to accept this heat. Cavity type radiation is a three-dimensional interaction as where one surface emits energy to another surrounding surface. The amount of absorbed energy

by the receiving surface is a function of temperature difference between the emitting and receiving surfaces, the view factor and the distance between them. A view factor calculates the percentage of energy emitted by a surface which can be accepted by the receiver. For example, two perfectly parallel plates of the same size will have a view factor of 1 (100%) as all the energy emitted can be absorbed whereas, if one is at an angle, a percentage of that radiation will be lost to the environment, leaving a reduced percentage of the energy being absorbed.

Both types of radiation interactions have been used in the FE model assembly. A number of To Ambient radiations are present with the omission of the wheel around both the disc brake and the pads. Only two examples are presented in Figure 6.12.a and Figure 6.12.b, with the circumferential disc brake edge (located at the OD) in the former and the friction surfaces (minus the actual pad contact area) in the latter.

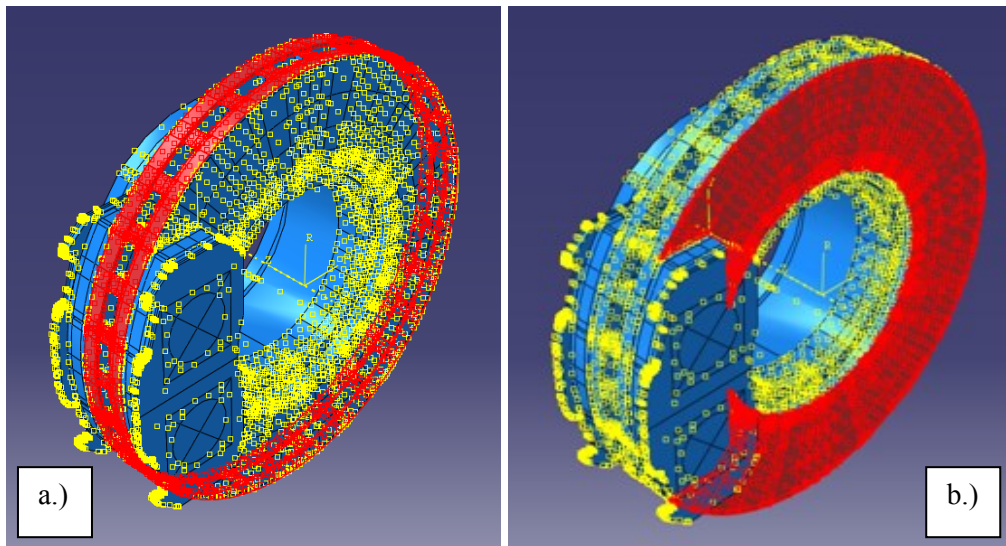


Figure 6.12: Surface radiation boundary conditions set on the disc brake a.) OD axial surface and b.) disc brake friction surface

The exclusion of the pad contact area in Figure 6.12.b was important because energy here is not being radiated to the atmosphere but to the friction material, until the pads are pressed against the disc brake. Therefore, during heating stages only, a Cavity type radiation was used between the disc brake and pads. By default, ABAQUS calculates the view factor from the normal of the master surface (disc brake) to the slave surface (friction material). With no deformation in a heat transfer model, the surfaces are perfectly parallel, creating a view factor equal to one.

6.2.1.2 Convection

By inputting a h_{conv} value, ABAQUS calculates the convective heat dissipation from the surface nodes, by using equation (4.8). Prediction of h_{conv} is found through CFD analysis,

experimental testing and/or taken from the literature. As no CFD work has been conducted thus far, values of h_{conv} were taken from Figure 4.7. During the heating phase, the disc brake was rotated at approximately 50 rpm, corresponding to a h_{conv} value being assigned to the surfaces highlighted in Figure 6.13, of approximately 5.0 W/m²K (taken from Voller 2003). In the absence of experimental value, the extrapolated 0 rpm speed of 2.5 W/m²K was used when simulation the stationary cooling. The same heating and cooling stage h_{conv} values were used for the internal vane channels surfaces, as those used on external surfaces.

The values of h in all these areas will be studied later in great detail in Chapter 8. However, some initial values had to be adopted at this stage. It should be noted that accuracy of the h values during the heating phase actually had very little influence on temperature predictions since heat input was higher by many orders of magnitude. Additionally, heating times were much shorter, typically only 10 minutes long and therefore, not allowing inaccuracies due to incorrect h values to manifest.

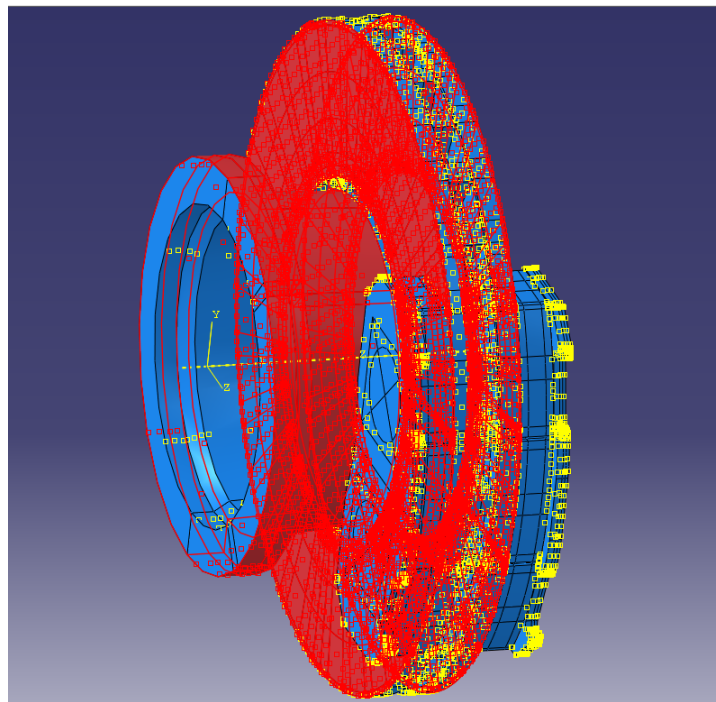


Figure 6.13: Standard convection from highlighted surfaces.

6.2.1.3 Conduction

Thus far, there were only two sources of conduction in the model; between the disc brake/friction material interface and the friction material/backplate interface; Figure 6.14 a.) and b.) respectively. Gap conductance usually refers to the microscopic gaps left between two surfaces in contact. However, as Lang (1962) states, a gap smaller than 6 mm will demonstrate

the occurrence of gap conductance with the absence of convection, providing the surface is much larger than the gap. A total pad clearance of 1 mm was used as a test standard for cooling tests, meaning an ideal clearance gap of only 0.5 mm was seen between both disc brake/pad interfaces. Table 6.1 presents the h_{cond} used in the simulations, found by an iterative approach. For the purpose of initial modelling, the same value was assumed for the friction material/backplate interface.

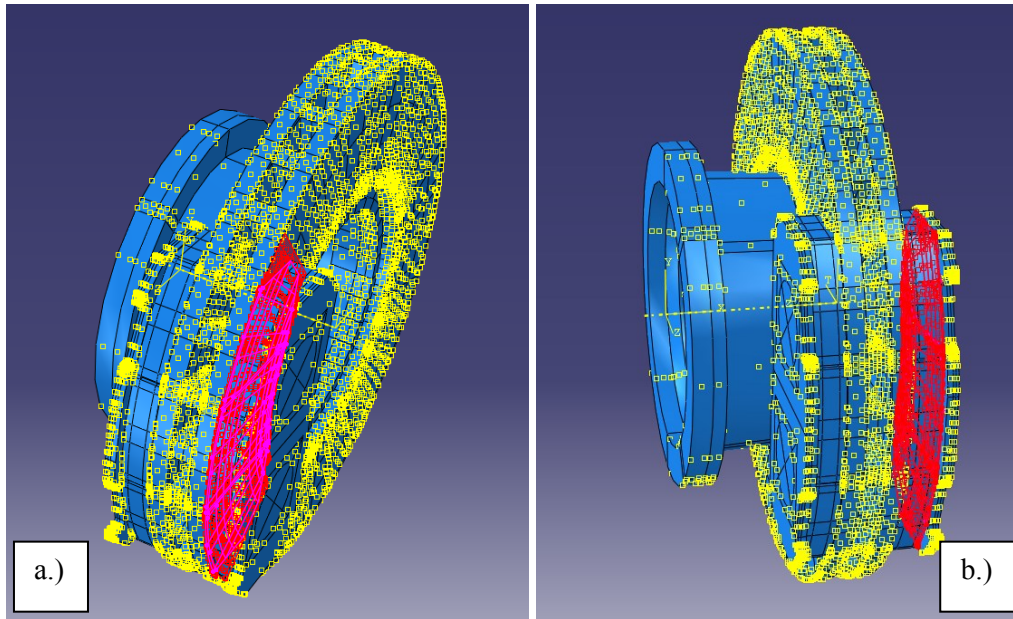


Figure 6.14: Conduction interaction at the disc/friction material interface

Table 6.1: h_{cond} values for the disc brake/friction material interface

h_{cond} (W/m ² K)	Gap (mm)
250	0
150	0.5
0	1000

6.2.2 Preheating Results

Construction of the simple brake assembly FE model was now complete. As previously stated, prior to cooling test simulations the preheating sequence had to be modelled to calculate realistic initial temperatures within the assembly. Section 6.2.2 looks at the preheating and the validation of the model.

On the Thermal Rig, the positions of the thermocouples were previously shown in Figure 5.19. For direct comparisons between the two sets of data, nodes had to be created in ABAQUS in the

approximate locations of these thermocouples. ABAQUS gives each node a number, with Figure 6.15 displaying the node numbers closest to the equivalent thermocouple positions.

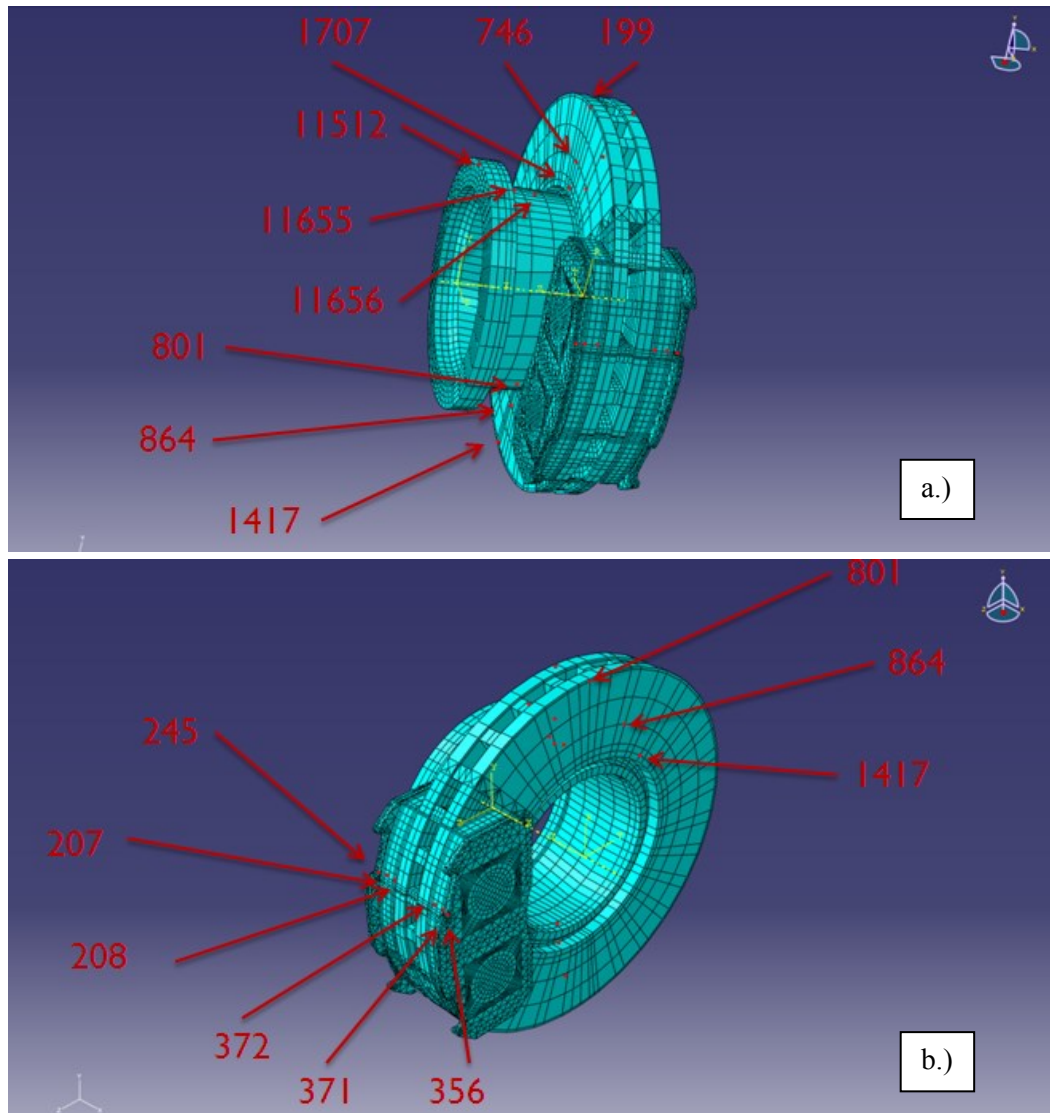


Figure 6.15: Approximate thermocouple node positions in ABAQUS

The FE results of a full preheating sequence are given in Figure 6.16. A good match is seen qualitatively between the FE results and the measured data presented in Figure 6.9. There is a noticeable difference between the two sets of results though, which is the time taken to complete the preheating sequence, with the FE under predicting by approximately five minutes. The difference is due to experimental error as additional time is taken to physically retract the pads off the disc brake after air pressure is released. The electric motor does not produce sufficient torque to overcome the static friction, unlike a CV engine, forcing the process to be done manually. Further time is taken to move between the brake, IHC control and air supply as they are located in different areas of the laboratory. Whilst all this is occurring, the disc brake

temperature drops more than the FE prediction, meaning the IHC must heat the disc brake for a little longer than the predicted FE results. All these incremental time differences sum to the additional five minutes seen during experimentation. It is the summation of all these small but incremental physical actions that are partially attributed to the difference in times.

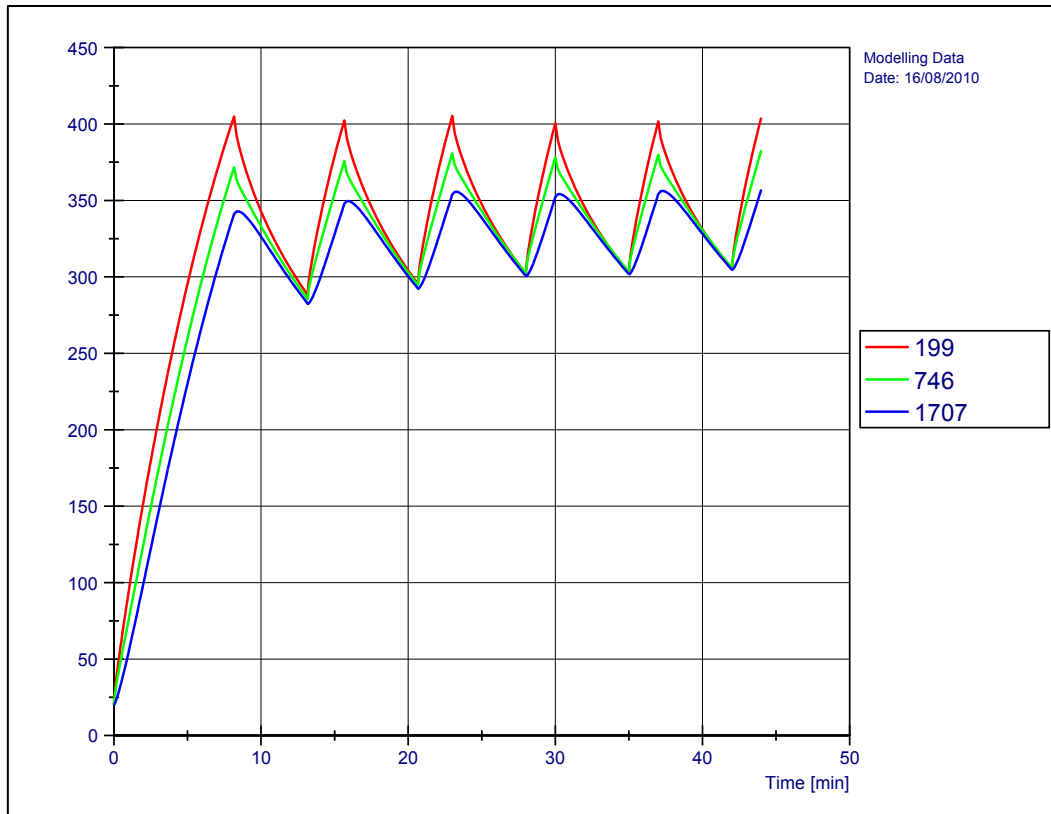


Figure 6.16: FE model results for the preheating sequence for the thermocouple position Disc Out High Top (see Figure 5.19 and Figure 6.15)

To further investigate the accuracy of the FE model, data were compared for the first heating cycle during the preheating sequence. Modelling accuracy was evaluated by comparing the thermocouple temperatures to the comparative FE node temperatures directly. Usefulness of the data comparison at the DOHT thermocouple position was somewhat limited as this was the position of control in the experiment, with both the FE and physical heating procedures being stopped once 400°C was reached in this location. The remaining two Disc Out Top positions were not controlled so their temperatures were functions of the energy input and heat flow from around the disc brake, making the comparison much more useful.

Figure 6.17 shows the temperatures reached by the Disc Out Top thermocouple during the preheating sequence, with the purple lines indicating the temperatures reached at the end of the first heating cycle. In this particular experiment, the final DOHT temperature reached was a

little over 400°C, whilst the DOMT and DOLT thermocouples measured temperatures were 339°C and 305°C respectively. Cooling temperature predictions are the key focus of this project, with modelling of the preheating sequence to generate a realistic temperature distribution. Therefore, provided the temperatures matched within an acceptable tolerance, taken to be $\pm 20\%$ then the model was accepted and considered reliable. For early modelling simulations, Apte and Ravi (2006) demonstrated that a $\pm 20\%$ range was adequate and therefore was deployed.

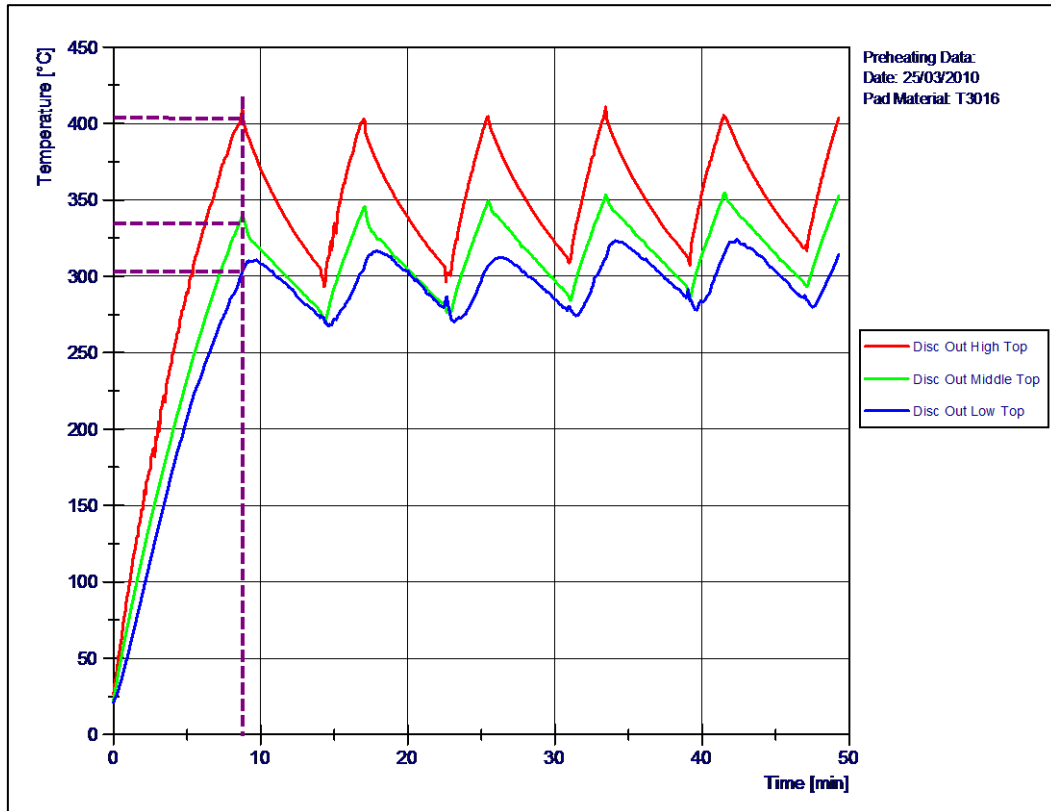


Figure 6.17: Predicted temperatures reached at the end of the first heating sequence (see Figure 5.19 and Figure 6.15 for thermocouple positions)

Figure 6.18 compares the FE results for the duration of first heating procedure to those recorded by the Disc Out Top thermocouples. Initial inspections show a high level of similarity between the two sets of results with very little difference between DOHT temperatures. Likewise, the FE results match the measured data well at the ID but the middle values have been slightly over predicted by the FE to a temperature of 371°C, although this prediction is an increase of 9.4%, which is considered to be within the acceptable range. However, the results are potentially masking errors in the FE model. Looking more closely the three comparisons in Figure 6.18, the FE model does not follow the same heating curve as the experimental data. At higher temperatures, by using a constant heat transfer coefficient, the FE prediction does not diminish

as strongly as the experimental results. It is expected that the total heat transfer coefficient is too low towards the end of the heating cycle, with insufficient energy being dissipated from the disc brake/pad assembly, explaining the lower cooling rate. Additionally, considering the cooling rate diminishes with temperature would suggest that varying heat transfer coefficients should be used rather than constant values.

Figure 6.19 shows calculated temperatures from the FE modelling were higher than the measured results. Temperatures 5 mm from the pad surface (thermocouple position POS) were 167°C and 194°C for the measured and FE respectively; a 16% over estimation was predicted. Interestingly, an over estimation of 16% was also calculated for both the POB and POBp positions. Sufficient evidence is therefore presented to claim the simple FE model is accurate throughout the preheating stage.

Considering the generated FE values were within the acceptable limits, the FE analysis can be considered of sufficient accuracy for modelling of the heating phase. However, the possible sources of error that have been identified may prove to have greater significance during the cooling experiments, due to having a longer time to manifest and becoming increasingly pronounced throughout.

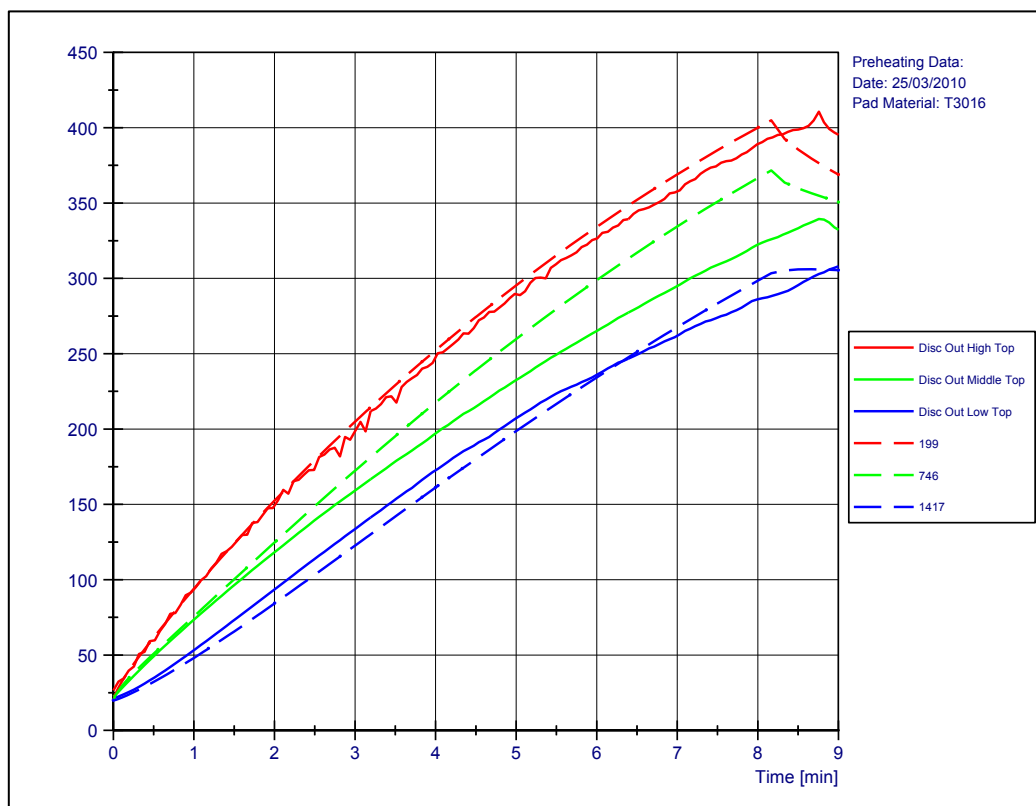


Figure 6.18: First heating procedure comparisons for the Disc Out Top positions (see Figure 5.19 and Figure 6.15)

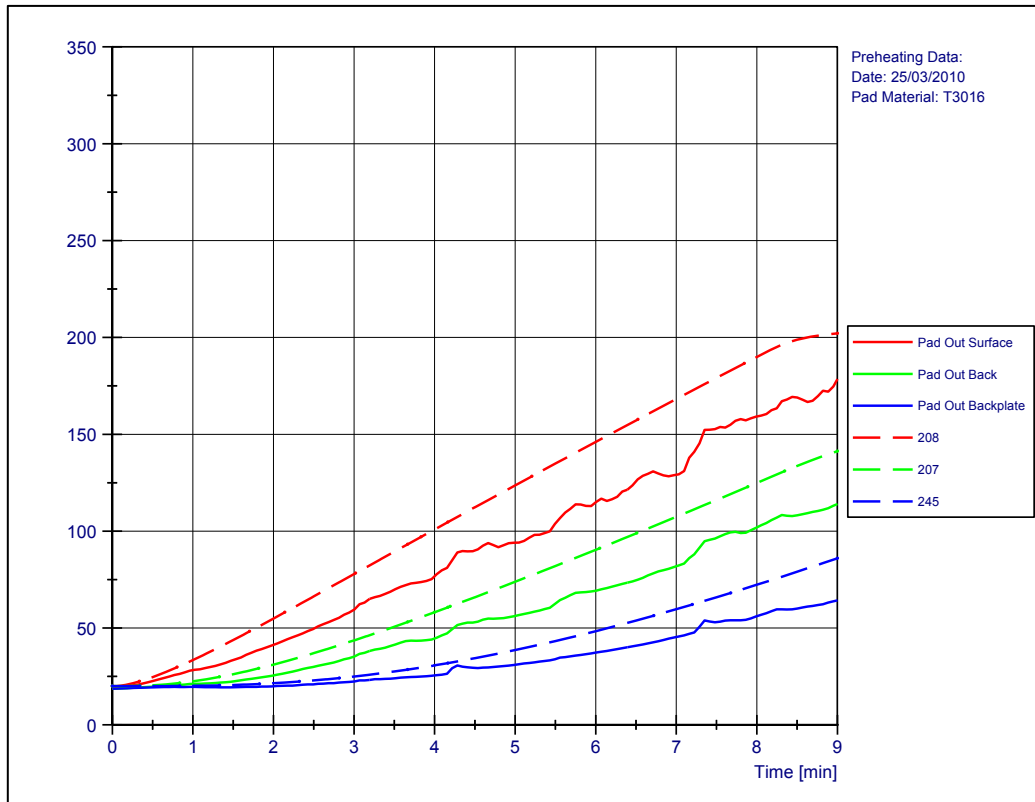


Figure 6.19: First heating procedure comparisons for the Pad Out positions (see Figure 5.20 and Figure 6.15)

6.3 Cooling Test Simulation Results

With realistic initial temperature values achieved and heat transfer characteristics inputted for boundary conditions, full cooling tests simulations could commence. No changes were made to the model from switching to the cooling simulation from the preheating sequence, other than completely removing the heat input.

Figure 6.20 shows the predicted temperatures for the six hour cooling FE simulation. Only three minutes pass before the FE simulation predicts all temperatures on the top half of the outboard disc friction surface become uniform. Hereafter, the temperature gradient across the contact disc surface is negligible. The fact that FE modelling does not support buoyancy driven flow, this outcome is unsurprising. Nonetheless, comparison with cooling test data will still be made. Furthermore, the time taken to return to 50°C was calculated to be two hours 22 minutes.

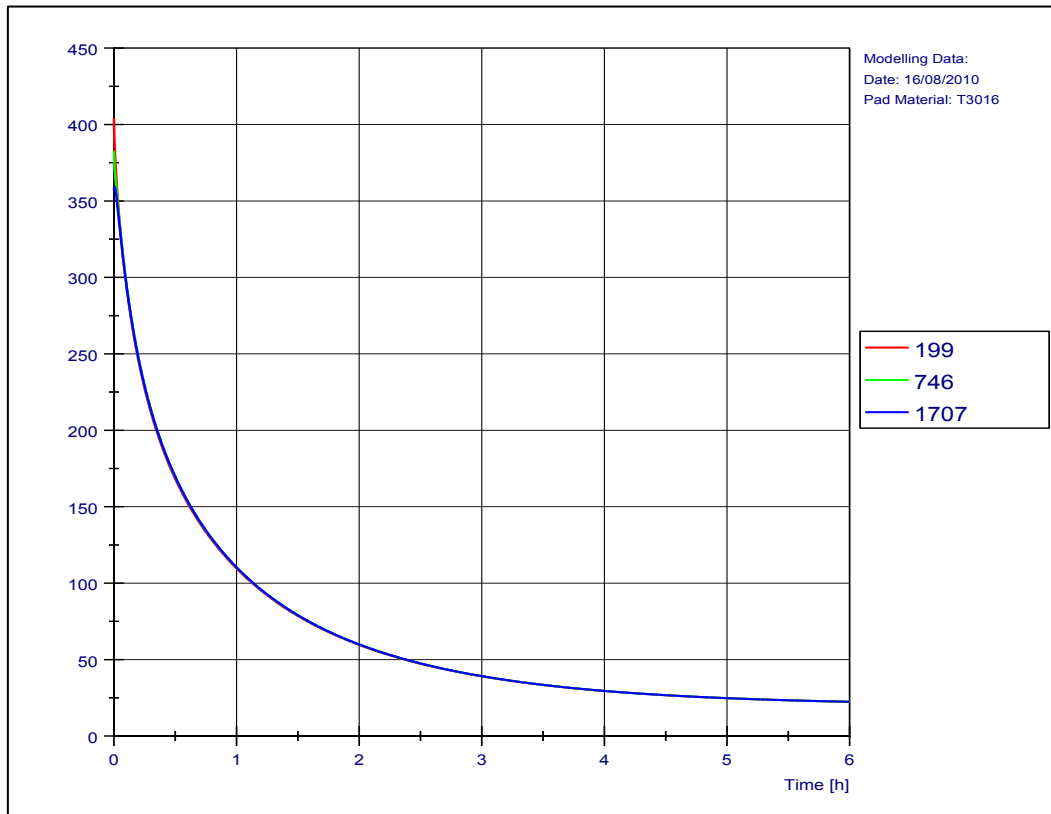


Figure 6.20: Outboard disc cooling results from FE (see Figure 6.15 for thermocouple positions)

Predicted outboard pad temperatures are shown in Figure 6.21. A large difference in cooling rates was predicted for the two nodes situated within the friction material. Initially the warmer of the two, the node closest to the friction surface (node 248) cools faster than its counterpart positioned towards the backplate, taking the same amount of time to cool down to 50°C as the friction surfaces. With all the thermal energy entering the pads comes from the disc brake, it is unsurprising the cooling rate of the surface node matches this. In contrast, the back friction material node matches the slower cooling rate of the backplate, taking an additional 22 minutes to return to 50°C.

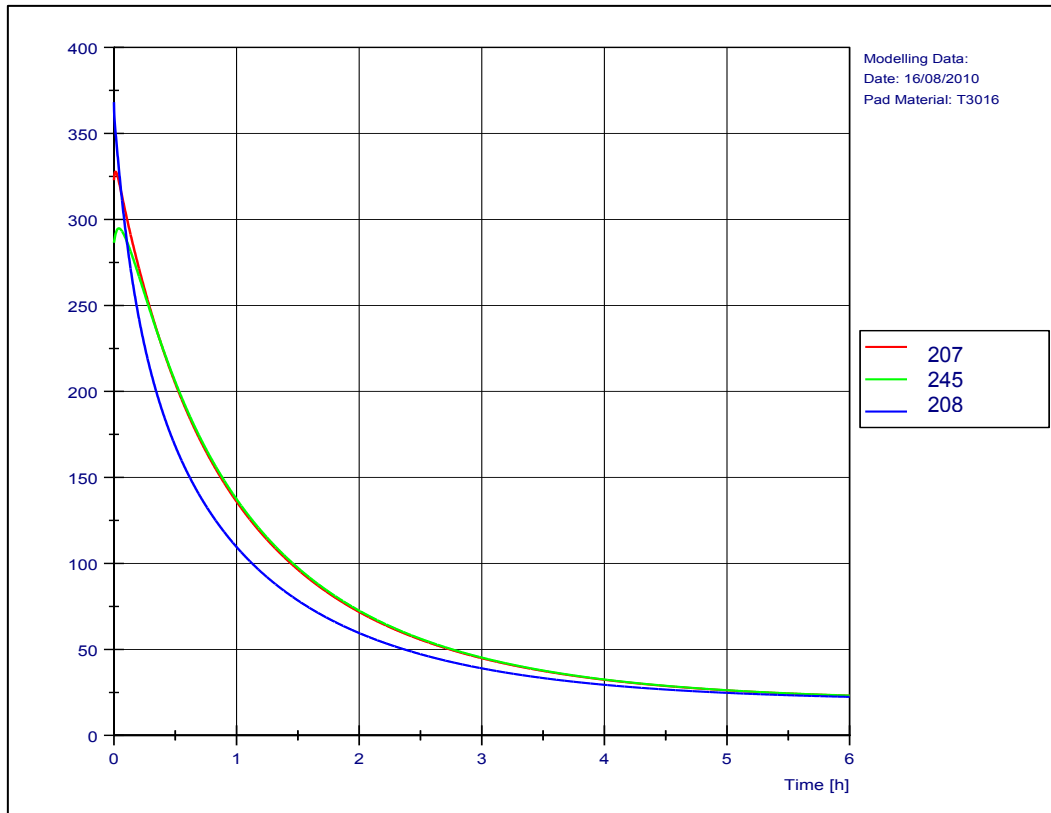


Figure 6.21: Outboard pad cooling results from FE (see Figure 6.15 for thermocouple positions)

To test the accuracy of the FE results, a series of 10 cooling tests were conducted, with temperatures taken by the 32 thermocouples placed around the brake assembly. The aim was to develop a temperature range representative of a typical brake application that could be used to validate the FE simulation. During the cooling phase, temperatures at 10 points in time, in addition to the initial temperatures, were found and used to generate the FE validation band. To reduce the amount of data displayed, only the maximum, minimum and an average temperature (from the 10 experiments) are given in Table 6.2, for the DOHT thermocouple.

Table 6.2: Average, maximum and minimum temperatures for the Disc Out High Top thermocouple

Time (h)	Disc Out High Top		
	Max (°C)	Min (°C)	Average (°C)
0.00	408	394	401
0.25	299	282	288
0.50	240	226	232
0.75	202	189	193
1.00	172	162	165
1.50	133	120	126
2.00	108	96	102
3.00	80	70	75
4.00	65	55	61
5.00	56	45	51
6.00	50	38	45

The average temperatures calculated for each thermocouple became the target temperatures to which the FE simulation needed to match to be considered reliable. Figure 6.22 displays the average DOHT thermocouple temperatures with the arbitrarily set $\pm 20\%$ band. Disappointingly, when adding the FE simulation temperatures to the graph (green line), it is clear that the match is poor as they remain inside the $\pm 20\%$ boundary for only the first 15 minutes. Although the temperature differences may not appear too large, there is a difference in cooling times. FE predictions suggest it should take the disc brake 2 hours 22 minutes to cool down to 50°C , which is less than half the time taken for the average thermocouple reading, recorded at 5 hours. Over-predictions of this nature was not a onetime occurrence as every node in the FE simulation produced the same outcome.

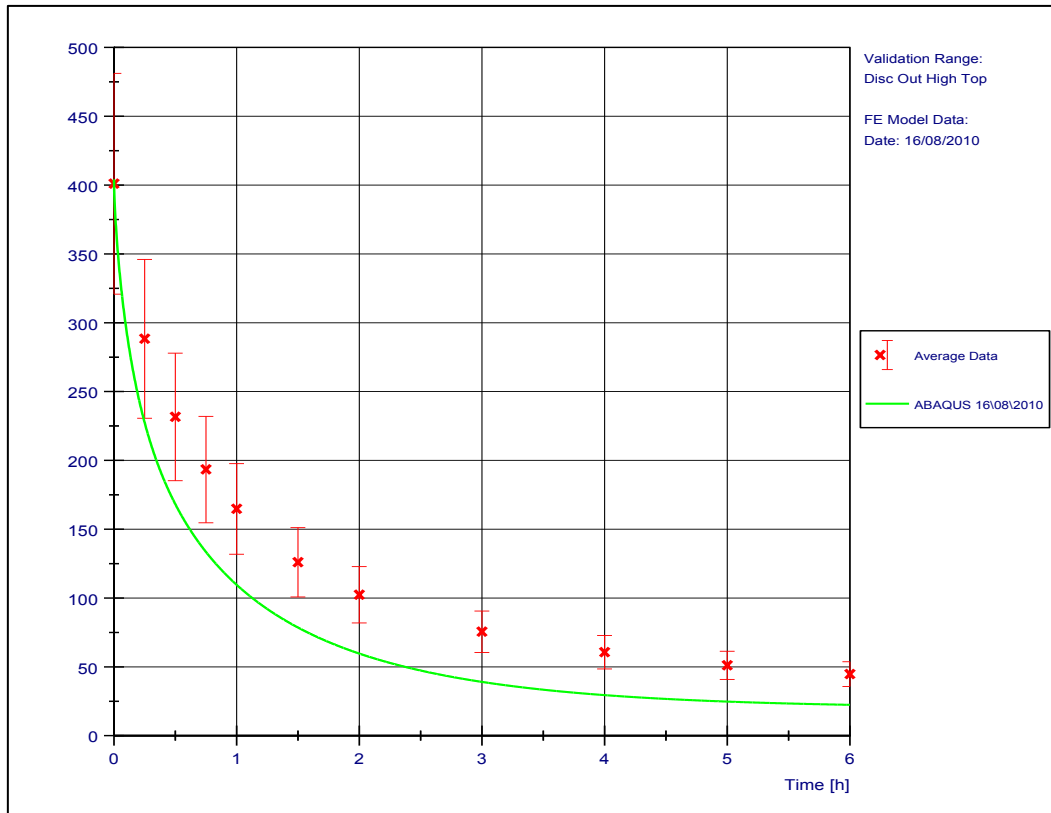


Figure 6.22: Average friction surface experimental data with the corresponding FE predictions

With temperatures being accurate at the start of the cooling phase but quickly drops out of the acceptable range, there was evidence to suggest that the used heat transfer coefficients were inappropriate for the scenario being modelled. Heat Transfer coefficient values were deduced from previous experimental data (Voller 2003) that were not representative of a parking situation. Instead of a forced convection, the flow was buoyant around the brake assembly, resulting in natural convection values of h_{conv} vastly changing with temperature.

To improve the accuracy of the FE model, an investigation was needed to find the representative values. The importance of this work is highlighted by Figure 6.23 as inaccurate disc brake cooling characteristics is the root cause of inaccurate pad temperatures to also be predicted. Due to the greater thermal mass of the disc brake, it influences largely on the cooling rates of all assembly components. Without an advanced understanding of the buoyant cooling characteristics of the disc brake, it will be impossible to generate an accurate full brake assembly FE model, as demonstrated here by a simplified FE model. For this reason, subsequent chapters focus on the thermal aspects of a stationary parking application.

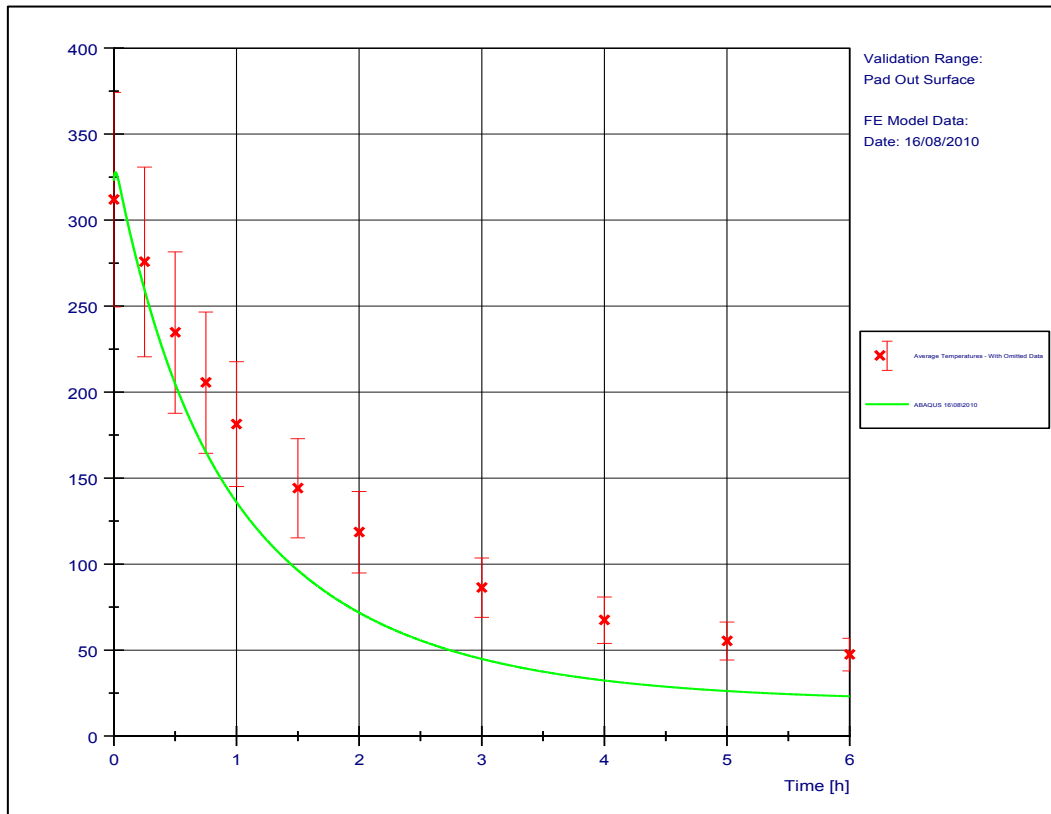


Figure 6.23: POS average temperature with erroneous results omitted.

6.4 Chapter Summary

In Chapter 6, the fabrication of a simplified FE model was described with details of the boundary conditions used. Within the braking industry, it is common for brake application modelling to be conducted using constant heat transfer coefficients. This is acceptable when the braking times are short and the amount of heat inputted into the system far outweighs what is being dissipated. Matching FE temperature predictions with experimental data were achieved during the heating stage, with short cycle times. However, poorly matching predictions for the parking applications provided substantial evidence to conclude that these common assumptions are inappropriate to make for the much longer scenarios. Further work is required to find more suitable heat transfer coefficient values that will allow more accurate predictions to be made.

7 Analytical Investigation into Disc Brake Cooling

Thus far, modelling of heat transfer from stationary disc brakes has proven a more complex task compared to modelling a dynamic scenario. In the latter, symmetry about each vane channel and constant HTC's are valid assumptions to make with disc rotation and short braking times. However, because airflow is driven purely by natural convection and cooling times are much longer in stationary parking applications, heat transfer coefficients can no longer be assumed constant. Having previously investigated the global heat transfer between brake assembly components, Chapter 7 aims to understand the variability in convective heat transfer from the disc brake.

To achieve this aim, analytical modelling of a simplified disc geometry was conducted to find the local convection heat transfer coefficients across segments of the surface. These values were then averaged across the whole surface area to generate an equation for the average h_{conv} over the specific temperature range relevant to CV parking applications. Using the energy balance equation, three cases were inspected numerically with the modelling assumptions increasing in complexity; section 7.2 discusses only the more difficult case where convection is allowed to vary with temperature alongside radiation, by using the previously derived h_{conv} equation. It was found that by allowing both of these heat transfer modes to vary, a more representative cooling profile can be determined. Chapter 7 is concluded by applying the same analytical method to the hat region by replacing vertical wall theory with the theory of heat dissipation from horizontal cylinders, to complete a full disc brake analysis.

To simplify the process, the work presented in this chapter assumes all cooling transpires on the two friction surfaces, without conduction passing heat to the wheel carrier. These assumptions mean the equations derived directly relate to the results presented in section 9.2.1, where the disc brake vane channels were blocked and had a gasket acting as a thermal barrier between the disc and wheel carrier. Subsequently, validation and accuracy testing will be conducted by comparing the analytical results with these measured results.

7.1 Analytical Modelling of a Vertically Positioned Disc

Heat transfer research on natural convection has throughout history been completed on bodies with simple geometry. For example, McAdams (1954) showed the generation of the thermal and hydrodynamic boundary layers of free air from a flat plate placed vertically and horizontally whilst Morgan (1975) conducted similar work but with cylindrical geometry in free air. Despite all the research, there is still no defined way of calculating the heat dissipation from a CV disc

brake in stationary conditions, where buoyant flow will be affected by the intricacies of the complex geometry.

It would be very convenient to model the disc brake as a series of concentric cylinders placed in free air as equations are already available to find the heat transfer properties. The thickness of the rotor section is much smaller than the OD, meaning the majority of convective cooling transpires from the vertical friction surfaces. Therefore, it would be a more reasonable to assume the disc is two vertical plates in free air. Using standard equations proposed by both McAdams (1954) and Churchill and Chu (1975) would be difficult to justify as they calculated their equations based on rectangular plates in free air, where their characteristic lengths are considered constant.

Considering the friction surfaces of the disc brake are essentially hollow circles, using the straight vertical wall equations would also be inappropriate as the characteristic length changes continuously around the disc. Simplified disc geometry was necessary to enable an estimate of the heat dissipation patterns from the disc brake, with section Figure 7.1 outlining the generation of the simplified geometry, followed by the subsequent flow analysis. The assumption that the friction surfaces could be separated into the four separate regions was made and demonstrated in Figure 7.1. On either side of the disc, an area is made by an arc starting and finishing directly above and below the ID, located on the horizontal centre line (black centreline in Figure 7.1). The height of the arc above the horizontal centre line, y_{arc} , was found using equation (7.1), based on Pythagoras's theorem.

$$\frac{dA_{arc}}{dx} = y_{arc} = (r_o^2 - x^2)^{1/2} \quad (7.1)$$

To find the area of the arc section, integration of equation (7.1) was completed. Limits of the integration were in the x direction, along the horizontal distance from the inner radius, r_i , to the outer radius, r_o . Obviously, the total arc area is the summation of the area above and below the horizontal centreline but equation (7.1) only calculates the height from the horizontal centreline. As the areas are symmetrical above and below, a doubling compensation factor has been added to the integration in equation (7.2). Integration was conducted by using the trapezium rule with a step size of 1 mm. Figure 7.2 shows the area for each segment of the arc as equation (7.2) is integrated. Summation of the individual areas gave the total arc area of be 0.0258 m².

$$A_{arc} = 2 \int_{r_i}^{r_o} (r_o^2 - x^2)^{1/2} dx \quad (7.2)$$

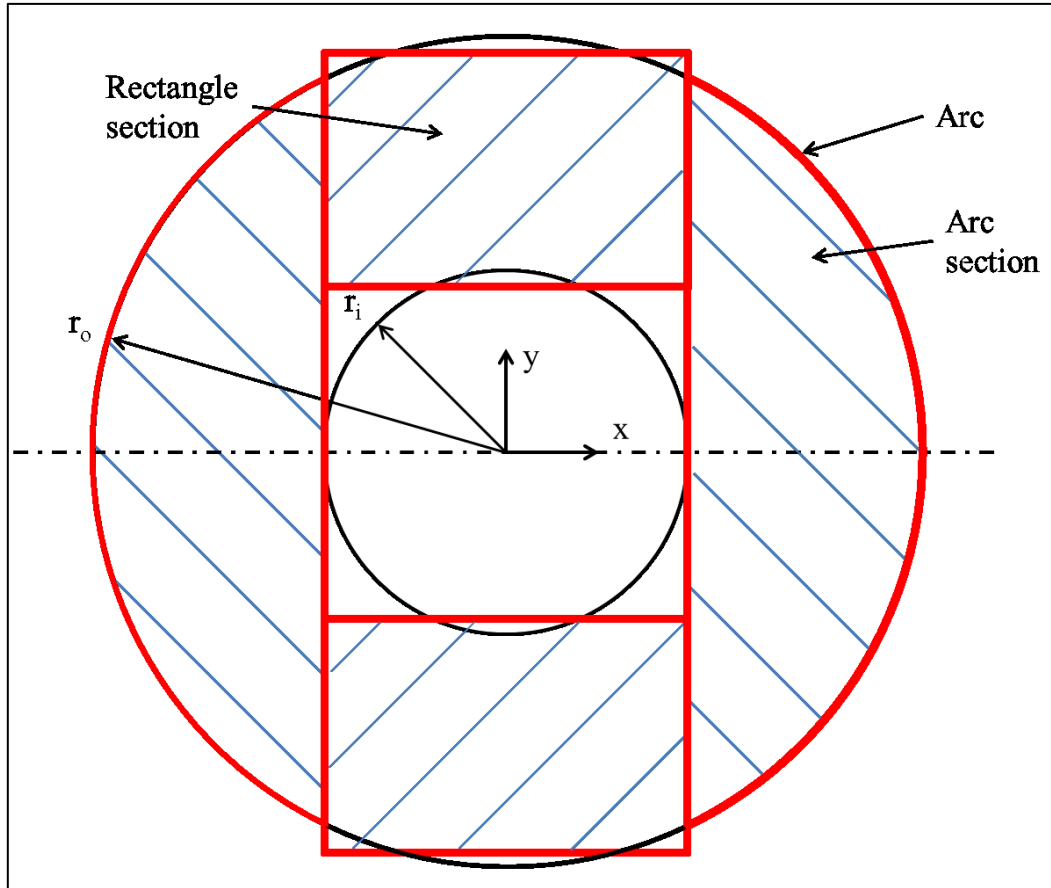


Figure 7.1: How the contact face surfaces area was broken down into simplified geometry (not to scale).

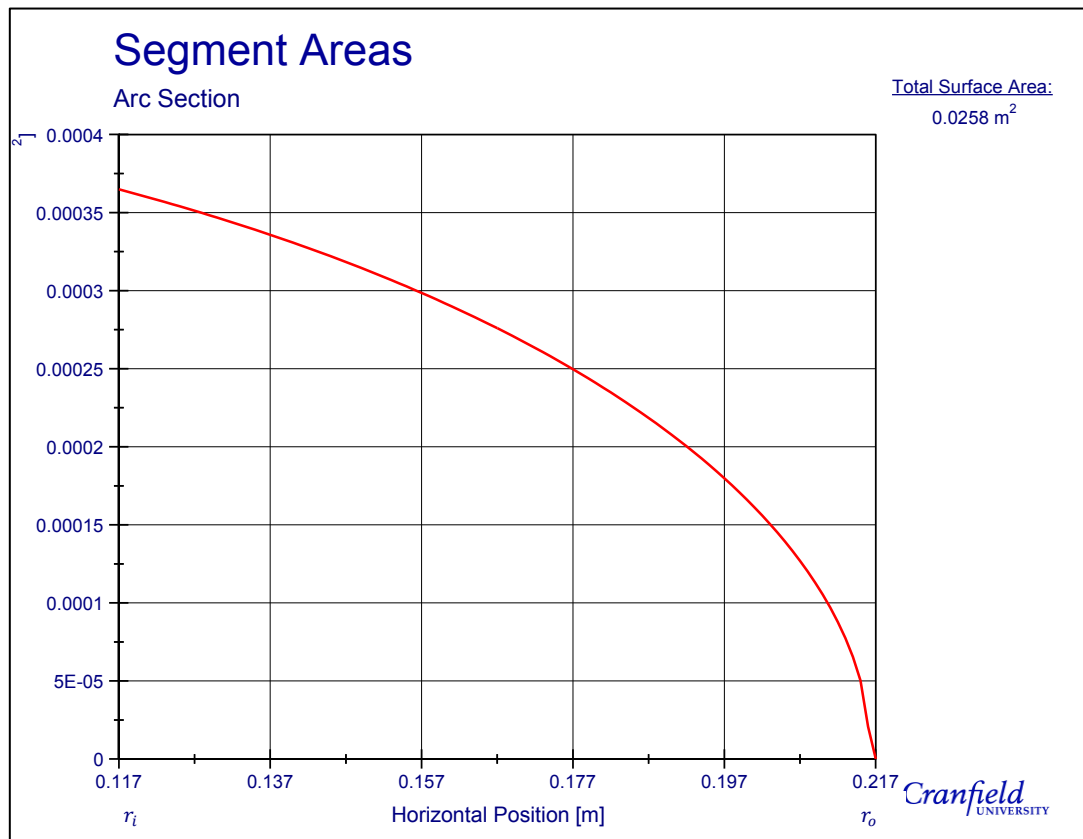


Figure 7.2: Arc area integration results.

With arc geometric properties now known, attention turned to the airflow patterns and heat dissipation across the arc, the first action was to access the heat transfer mode within the fluid. Figure 7.3 shows that the Pr value remains constant across the wall surface. This is unsurprising as it is function independent from any wall interaction. Increasing temperatures do however decrease the Pr value. It should be noted that the fluid used throughout was air with the properties outlined in Appendix L. The highest Pr value was generated at a temperature of 20°C equalling 0.703, with the lowest value of 0.688, a 2% drop at the maximum 400°C air temperature. These Prandtl numbers are below unity and is therefore considered a low value, specifying that convection is the main heat dissipation mode within the air passing over the solid disc brake.

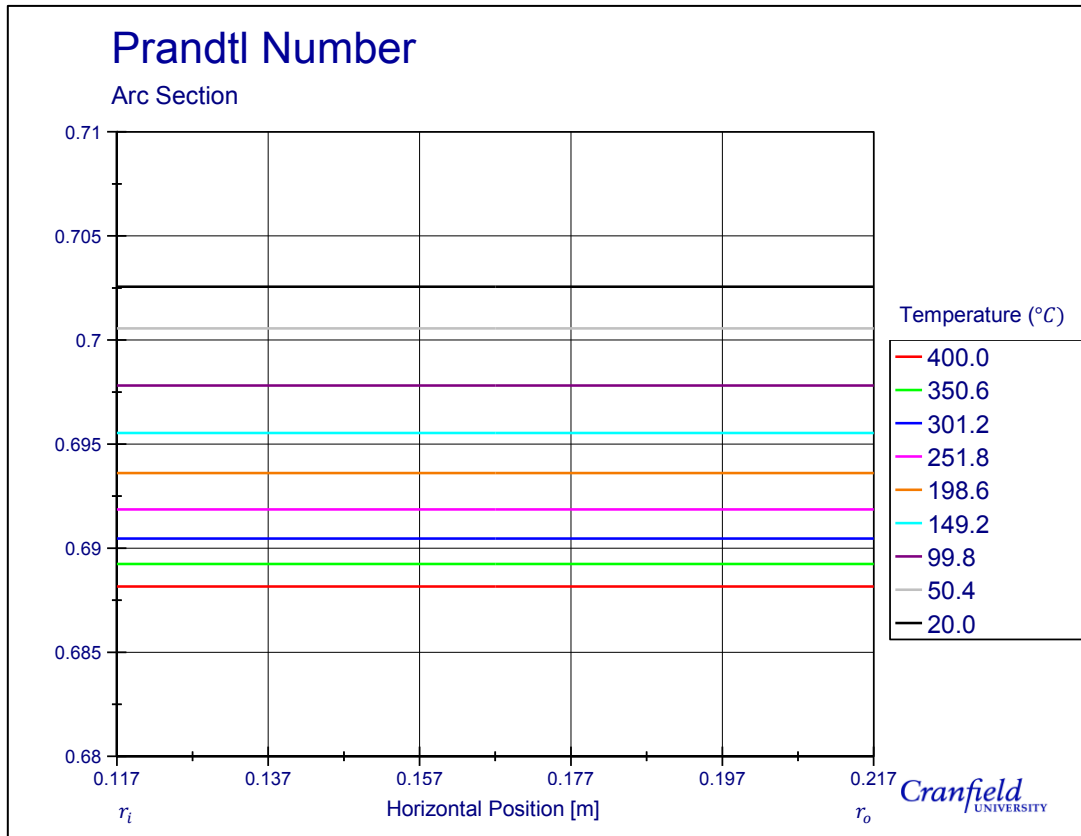


Figure 7.3: Prandtl number across the arc section at different temperatures.

The next dimensionless number investigated was the Grashof number. Unlike the Prandtl number results, a significant change is seen across the horizontal centreline (Figure 7.4). At the r_i , where the local characteristic length was greatest, a value 5.08×10^8 was calculated. This figure reduces in the x direction across the arc, down to zero at the r_o because the characteristic length is zero. This is a very interesting result as it shows that airflow over parts of the arc could have transitioned into fully developed turbulent flow, or at least into the transitional phase, whilst laminar flow is existing further towards the OD.

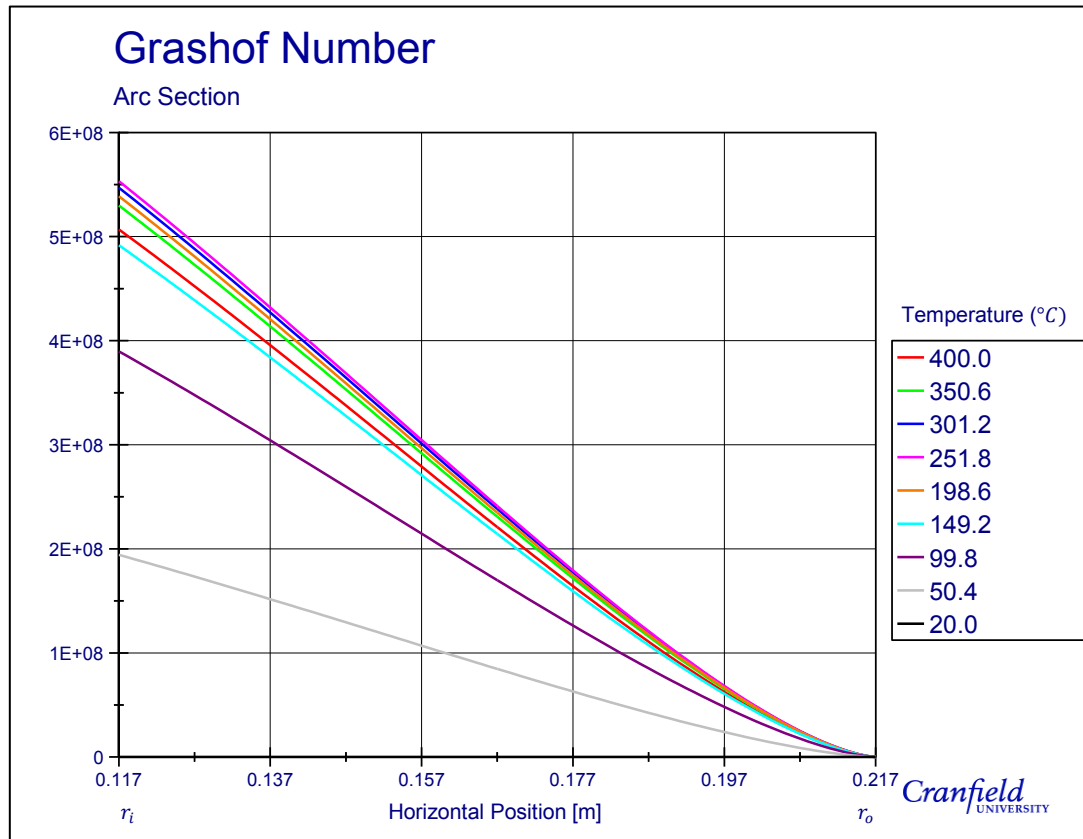


Figure 7.4: Grashof number across the arc section at different temperatures.

The values of Gr assume the flow over the local vertical surface, with a specific characteristic length are independent of the flow horizontally adjacent to it. Eddy currents created by the perturbing flow towards the turbulent r_i cannot be expected to be only influencing the air perpendicular to the surface. Perturbations will create some lateral flow motion, affecting some of the laminar flow regions towards the laminar r_o . Without CFD analysis this effect cannot be investigated further due to the added difficulty in the mathematics and the time constraints associated with the project. For now, the assumption that the any flow turbulence will be confined perpendicular to the horizontal position on the disc brake surface will remain.

Interestingly, looking at a single point on the horizontal centre line, as the temperature drops the magnitude of the Grashof increases until a maximum is reached at the temperature 255.6°C. Afterwards, the Grashof number falls until it reaches zero at ambient temperature when there is no thermal gradient present. This result is somewhat a surprise looking at equation (4.11) as the change in temperature is directly proportional to the Grashof number. The occurrence of the peak Gr value is attributable to the change in kinematic viscosity as Gr is inversely proportional to its square. As the temperature of a fluid increases, its density drops as thermal expansion occurs. Lower density fluid results in reduced friction within the flow, lowering the kinematic

viscosity. Above the critical temperature of 255.6°C, the changing kinematic viscosity effects surpass the thermal gradient, thus and reducing the Gr value hereafter.

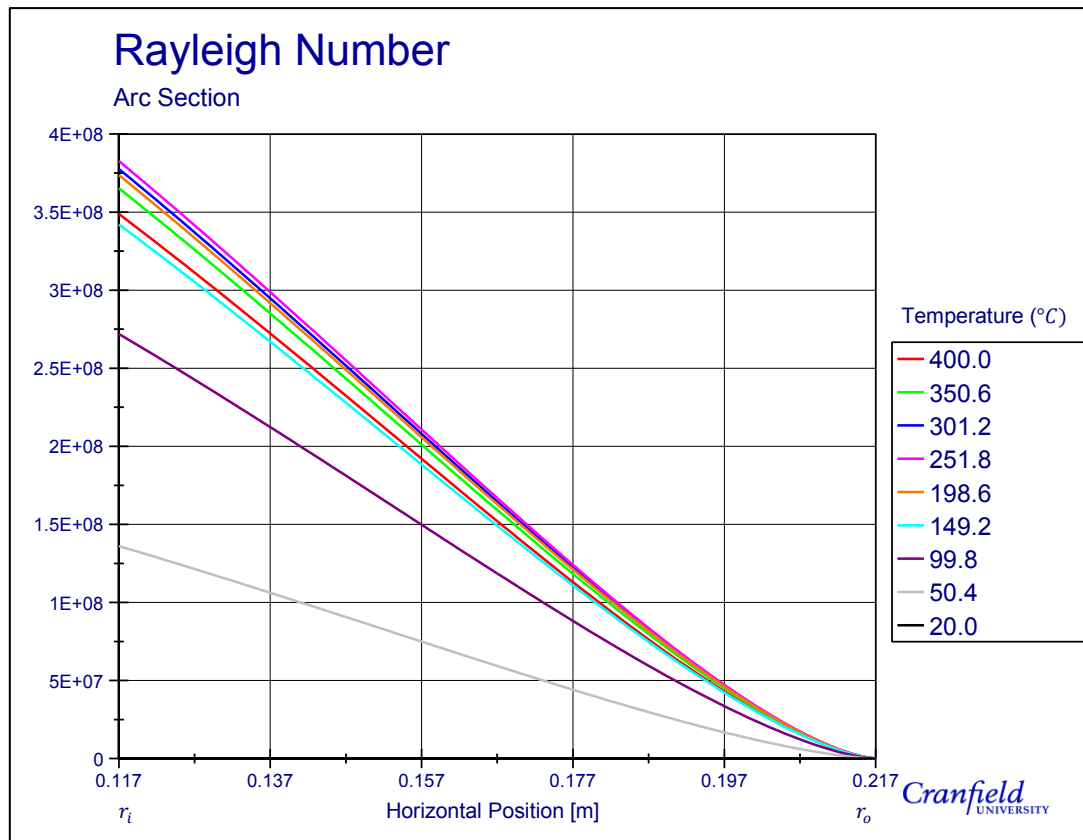


Figure 7.5: Rayleigh number across the arc section at different temperatures.

Considering the Rayleigh number is a function of the Grashof number, it is unsurprising that the results seen are of the same nature. A value of 3.49×10^8 at 400°C corresponds to turbulent flow according to McAdams (1954). The results show the flow trips into a turbulent state just 8 mm from the OD. In contrast, the critical Ra value proposed by Necati Özisik (1985), albeit for a different geometry, would suggest that the flow perpendicular to arc surface would be in a laminar regime throughout. Neither value derived was for the same surface geometry as the arc, making it impossible to tell by numerical calculation whether the flow has fully tripped into a complete turbulent regime. Ambiguity with the airflow state has made definite heat dissipation conclusions impossible to state, although the evidence would suggest the flow, at very least, will have reached the transitional period in between laminar and turbulent flows when the disc brake is at its hottest.

Having completed the study into the fluid properties flowing over the arc surface, focus was placed on understanding thermal interaction from the wall to the fluid. Determination of the Nusselt number over the arc region will help describe the dominant mode of heat transfer. Two

separate correlation equations have been presented by Churchill and Chu (equation (4.14)) and McAdams (equation (4.15)) to calculate the Nusselt number; both were used and compared.

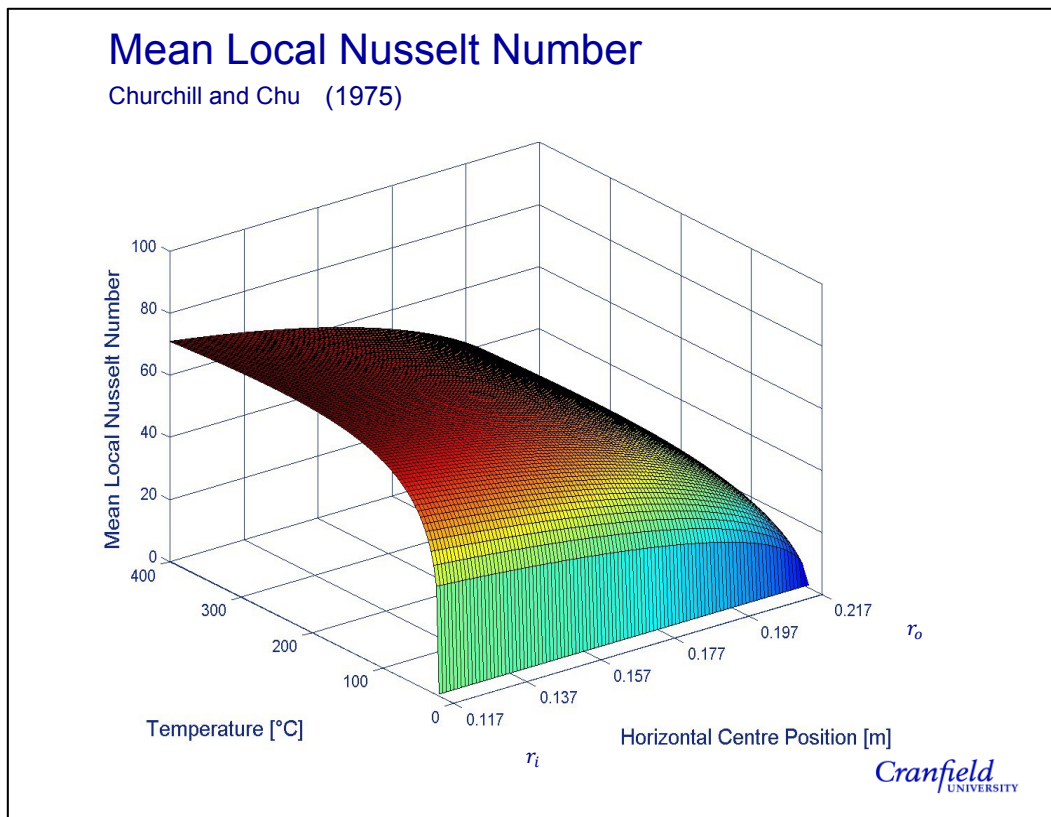


Figure 7.6: Mean Nusselt number for temperature and horizontal position for Churchill and Chu (1975) relationship.

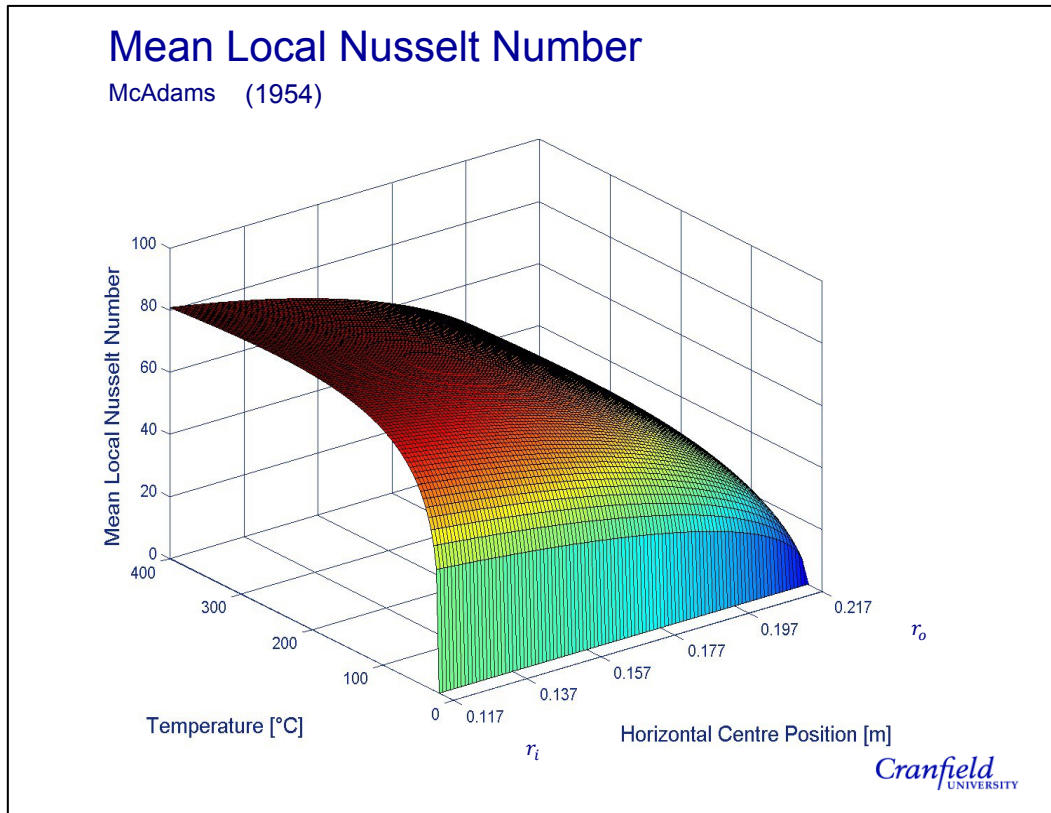


Figure 7.7: Mean Nusselt number for temperature and horizontal position for McAdams (1954) relationship.

Two ways of calculating the Nusselt number given in section 4.2.2.6, one from McAdams (1954) and the other by Churchill and Chu (1975). Both methods produce a mean Nusselt numbers across the thermal boundary layer. A comparison of the two methods was completed, with the Churchill and Chu method examined first. Nusselt numbers above 100 relate to a surface to fluid regime dominated by convection, whereas it can be said that conduction through the fluid and away from the surface is represented by values of one and below. It can be seen in Figure 7.6 that the Churchill and Chu equation predicts a value of 70.7. Keeping with previous patterns, this value is somewhere in between the two critical values, demonstrating a transitional state. However, the value is still high, signifying that convection dissipates the majority of heat from the arc surface but with conduction still having an influential effect. The maximum calculated was 72.4, located at the r_i where the characteristic length is greatest and when the temperature dropped to 251.8°C. This nonlinear characteristic fall shows that the Nusselt number is dependent on both the temperature and the location.

In comparison, the correlation equation derived by McAdams (1954) produces a similar looking Nusselt number pattern across the arc surface (see Figure 7.7). However, with Nu values

calculated to be 80.6 at the maximum temperature, with a maximum of 82.5 at 251.8°C show the McAdams equation produces values 14% higher. Even with the large increase in Nu , the heat transfer process from the arc surface still cannot be characterised as convection dominated. With both equations being based on experimental data, it was expected that a closer alignment between the generated results than what was actually achieved. According to Necati Özisik (1985), the McAdams equation is a closer approximation to actual value so will be used in all further calculations regarding vertical wall heat transfer calculations.

Having established that convection dissipates the majority of heat from the arc surface to the air, calculation of the convective HTC could transpire. Firstly, it must be stated that any calculation of h_{conv} will encompass the conduction effects from the surface to the air. In Figure 7.8 the locally calculated mean h_{conv} values, established from equation (4.13), are presented for different locations across the disc brake arc section. High variability is seen for h_{conv} values, ranging from zero to a maximum of 14.4 W/m²K at the maximum temperature.

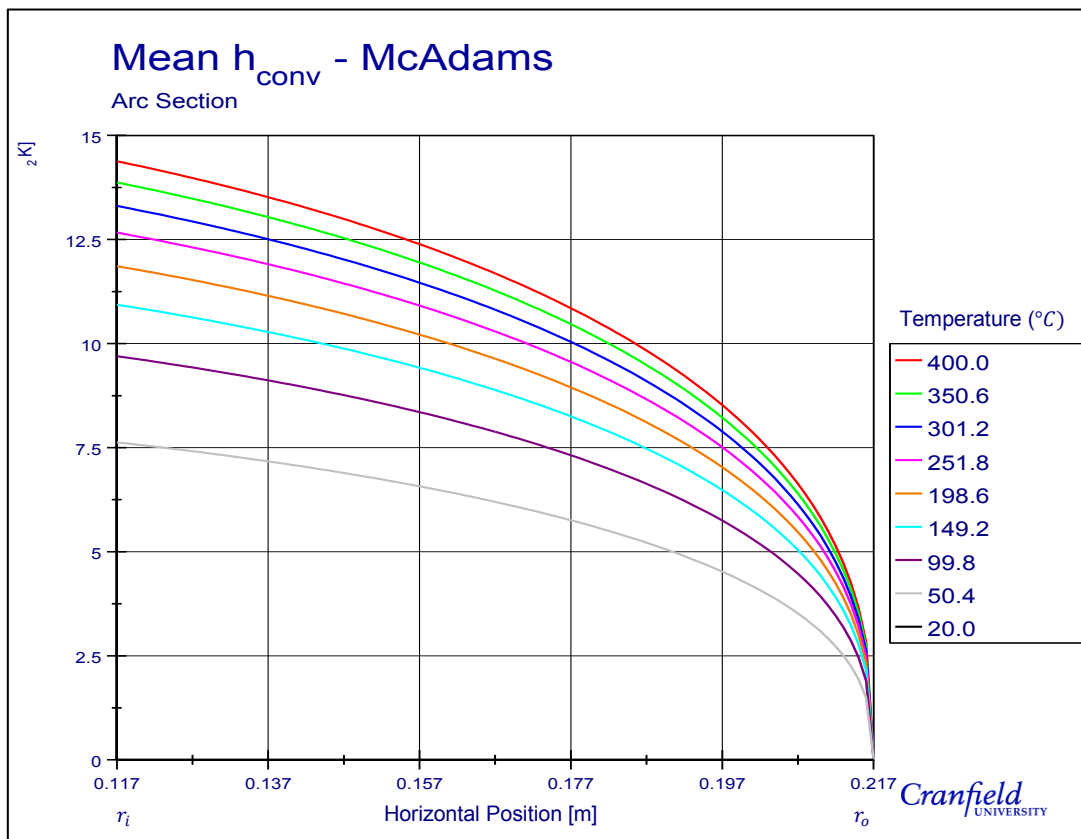


Figure 7.8: Calculated h_{conv} values for the arc section - Churchill and Chu relationship.

An increase in the thermal conductivity with temperature prevents the occurrence of a peak h_{conv} value as seen of the Nusselt number, at least within the region this project is concerned about. One pattern that is equivalent is the magnitude reduction as the characteristic length

(height from centreline to the arc) decreases towards the OD. This is an expected result because the characteristic length of the thermal boundary layer shortens, reducing the amount of heat transfer taking place.

With the data shown in Figure 7.9, it was possible to derive an equation relating to convective HTC with both temperature and location. It was unnecessary to develop such a complex equation as the aim was to produce a total surface relationship for a convective HTC. A single average h_{conv} value spanning the entire arc section was found through the use of equation (7.3).

$$h_{conv} = \frac{\sum_{i=r_i}^{r_o} h_{conv_i} A_{arc_i}}{A_{arc}} \quad (7.3)$$

Results of equation (7.3) were plotted against temperature in Figure 7.9, showing a highly nonlinear reduction in h_{conv} . A regression analysis was conducted on the results, using the post-processing program DIAdem, to obtain a relationship relating h_{conv} to temperature. A quadratic relationship, with a natural logarithm correction term, was found to deliver the optimum estimation as nearly 98% of the data was captured (see (7.4)).

$$h_{conv} = a_1 + a_2 T_d + a_3 T_d^2 + a_4 \ln(T_d) \quad (7.4)$$

The natural logarithm term was required to account for the decay as temperatures approached ambient. A regression equation describing over 99% of the data was achievable when ten higher order terms were included but it was decided the added accuracy was not justifiable considering the additional computational time that would be needed. Coefficients for equation (7.4) have been determined for the arc section and given in Table 7.1. The only caveat when using this equation is that it does not pass through zero at exactly at the point of ambient temperature. Therefore, for the purpose of future FE modelling, the user must manually input a zero h_{conv} value for the ambient temperature and then allow equation (7.4) to predict thereafter.

Table 7.1: Coefficients relating to equation (7.4)

Coefficient	Arc Area	Rectangular Area	Disc surface	Mean Cylinder
a_1	-10.65	-10.22	-8.07	-7.37
a_2	-0.0251	-0.0240	-0.0189	-0.0100
a_3	3.42E-5	3.28E-5	2.56E-5	1.22E-5
a_4	4.56	4.37	3.45	3.13

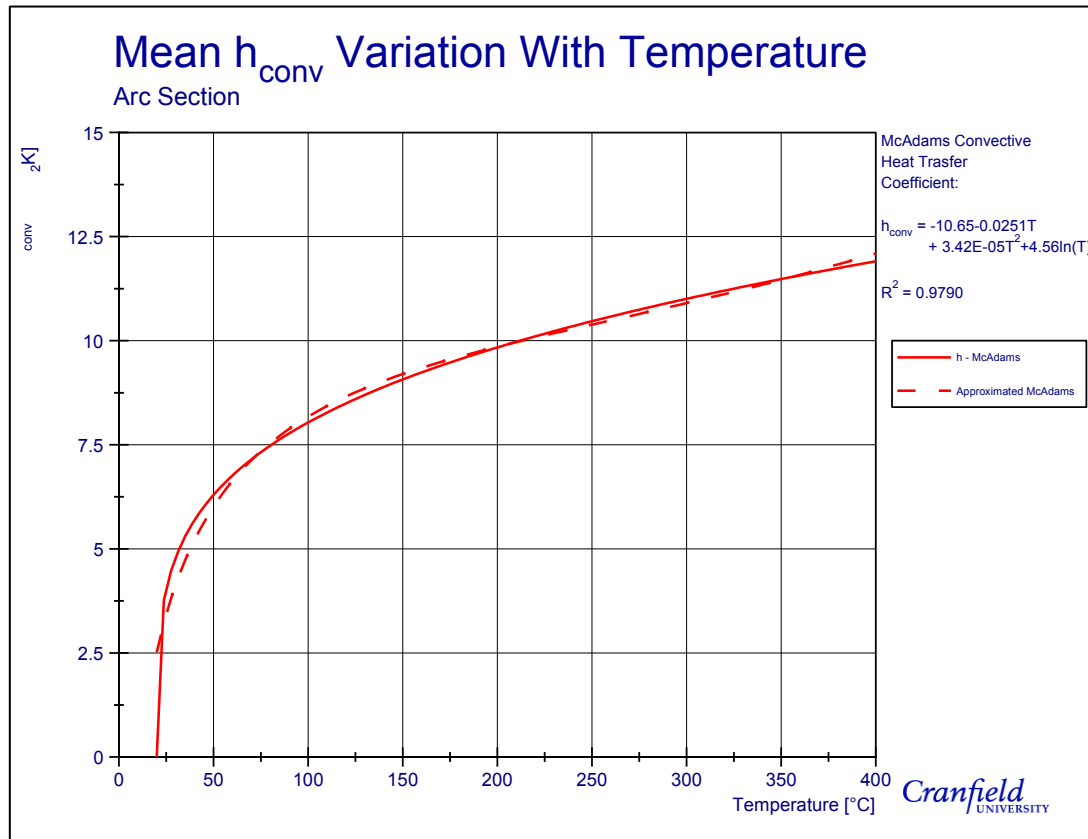


Figure 7.9: Mean h_{conv} values across the arc for various temperatures

7.1.1 Rectangle Section Properties

Of the four sections on the simplified disc brake friction surface geometry, convective heat transfer from the two rectangular sections remained undefined. By completing a similar procedure for the rectangular sections as for the one just completed for the arc sections, a disc brake friction surface h_{conv} equation could be made. An advantage of being able to assume a rectangular shape is that the boundary layer on the surface normal would develop evenly across the surface, in the horizontal direction. Consequentially, the airflow and hence, the heat transfer properties across the section would be constant; this lack of dependency on local horizontal position greatly simplified the process.

Due to the construction of the simplified geometry, the base length of the rectangles were equal to the r_i dimension. Rectangle height, y_r , would be analytically calculated by equating the whole disc surface area to the four sections then rearranging for y_r . By doing so, the area of the simplified geometry was equal to the standard geometry, making them equivalent. Through the use of equation (7.5), the rectangle height was found to be 114.1 mm. A resultant rectangle surface area, A_{rec} , was calculated to be 0.0267 m^2 .

$$A_{surf} = 2A_{arc} + 2A_{rec} \quad (7.5)$$

$$y_r = \frac{\left(\frac{\pi(r_o^2 - r_i^2)}{4} - 2A_{rec}\right)}{2r_i}$$

Dimensionless numbers were calculated for the rectangle using y_r as the characteristic length of the wall. The temperature range being investigated will remain from 20° to 400°C with the air properties changing described in 0. Figure 7.10 shows the change in Prandtl, Grashof, Rayleigh and Nusselt numbers with temperature. Prandtl values decrease with an increasing temperature; as air remains the fluid, the values match those given for the arc section. The Grashof, Rayleigh and Nusselt numbers all show the same fundamental characteristics as they started at zero and raised in a nonlinear fashion to a peak value before falling away thereafter; peak values were 1.68E7, 1.16E7 and 34.5 for the three varying dimensionless numbers respectively. Dimensionless values are much lower than those realised for the arc section as the maximum characteristic length is much smaller. In contrast to the arc, flow representative of laminar conditions is suggested for the air flowing over the rectangle surface. Larger hydrodynamic boundary layers would be present here, resulting in lower HTC's than for the arc.

It was no surprise to find the convective HTC result demonstrating the same pattern seen for the arc section, because the same equations and fluid properties used. The variability of the mean convective HTC with temperature is shown in Figure 7.11. Indeed, with a maximum value of 11.4 W/m²K at 400°C, the h_{conv} value was lower than the arc section by a difference of 4.1%. The regression equation that predicts the h_{conv} values was in the same format as equation (7.4), with its coefficients also given in Table 7.1.

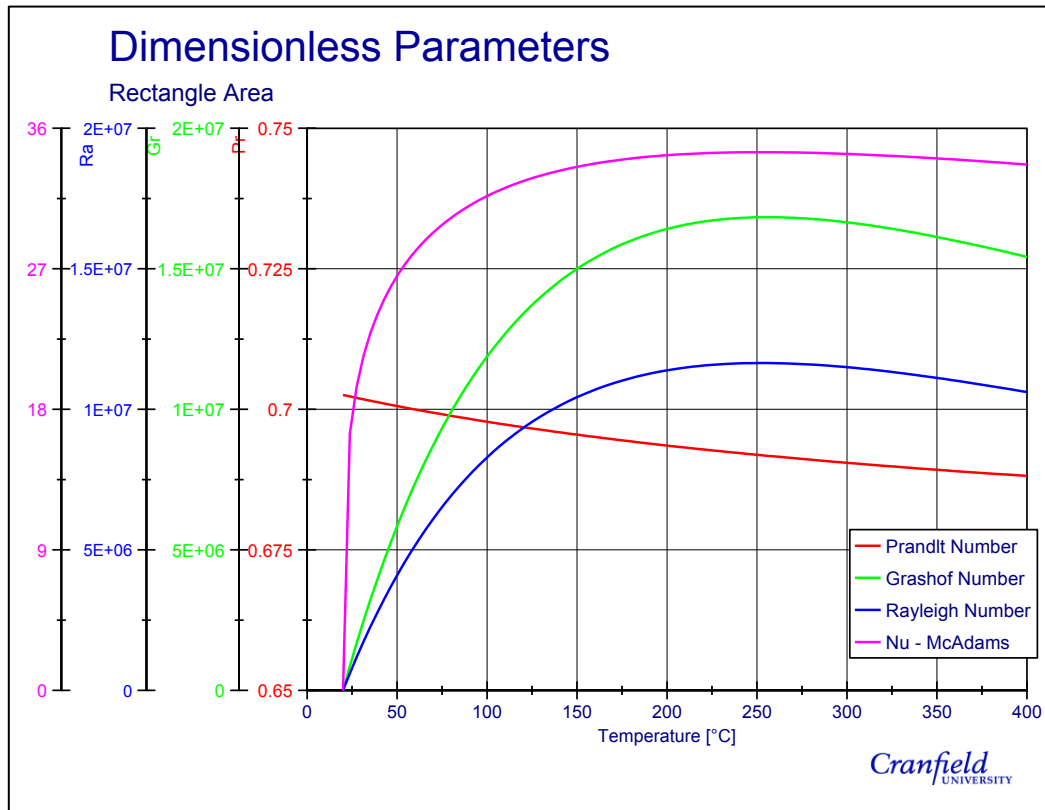


Figure 7.10: Calculated dimensionless parameters for a rectangular section.

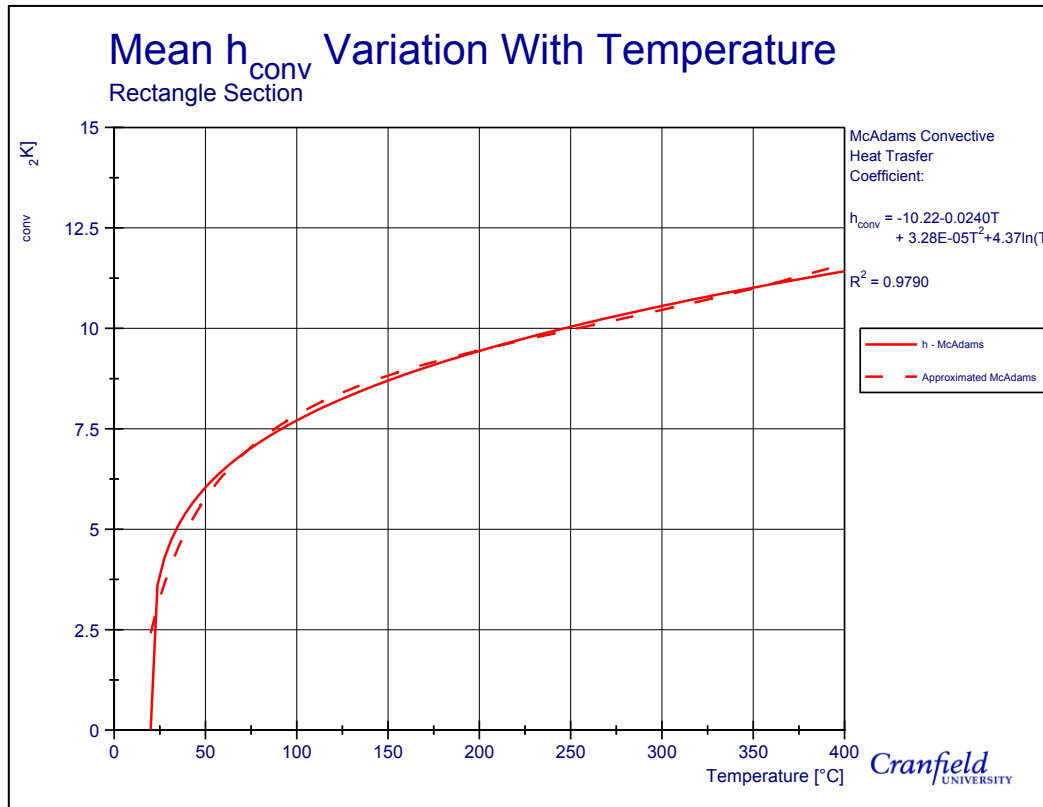


Figure 7.11: Mean h_{conv} values for the rectangle area against various temperatures

7.1.2 Disc Brake Friction Surface Convection Heat Transfer Coefficient

Simplifying the disc brake geometry allowed two separate heat transfer investigations to be conducted for the disc brake surface. By taking a weighted average of the equivalent h_{conv} values, a generalised appreciation of the heat transfer variation with temperature was realised for the whole disc brake surface. The contribution of the arc surface area to the whole surface contact face area is 51%, making its weight function 0.51 with 0.49 being the resultant rectangle weighted function. A final disc surface regression equation is presented in Figure 7.12. Again, nearly 98% of the data is represented by the corrected quadratic equation; coefficient values available in Table 7.1.

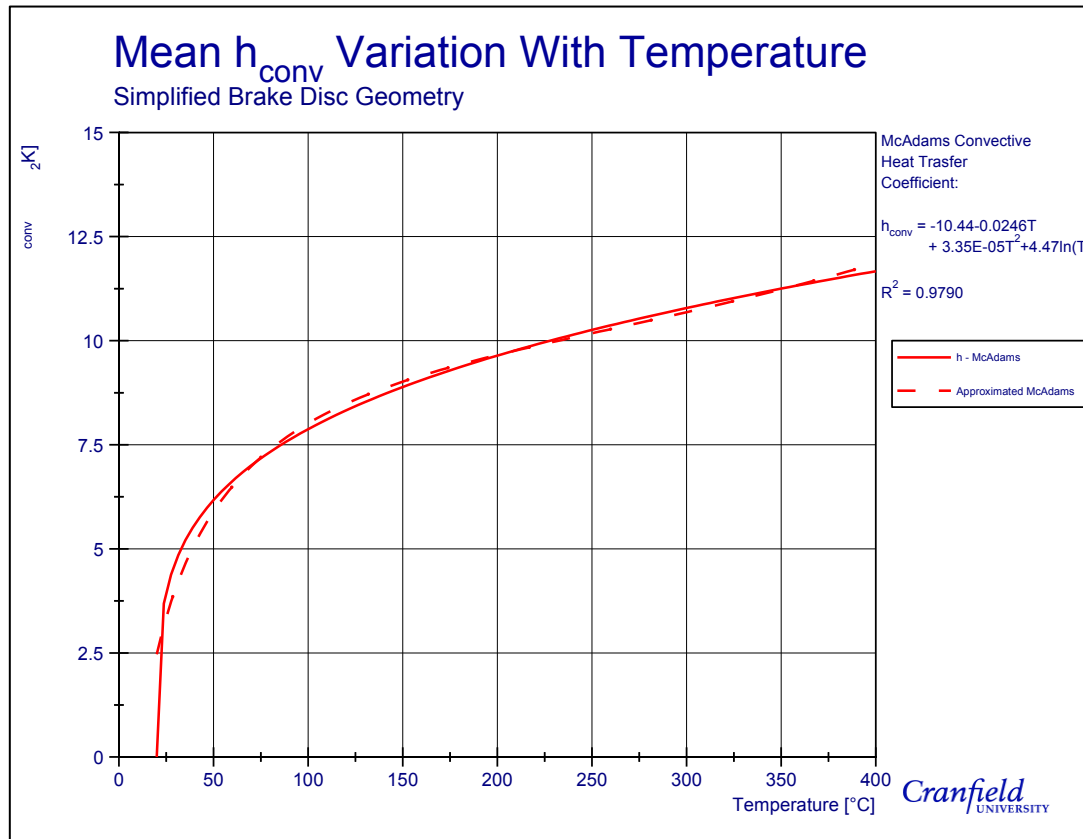


Figure 7.12: Mean h_{conv} values for the full simplified geometry with various temperatures

Section 7.1.2 was successfully devoted to achieving an equation that describes the convective heat transfer from the disc brake friction surfaces but the need for four terms in the h_{conv} equation describes the relative complexity of the behaviour. Many factors that influence the h_{conv} value were overlooked to produce the relationship. For example, it was mentioned that relative position on the surface was ignored. The presence of the hat section on the outboard side has been shown to affect the flow over the surface. Incorporating this effect would have dramatically increased the mathematics difficulty. A final effect that was neglected was the air flowing over the top rectangle would be hotter than the bottom rectangle. Identical figures were used to calculate the top and bottom rectangle heat transfer values. Clearly, the symmetrical results generated will not be true to nature. Because all the simplifications made and interactions ignored, the h_{conv} equation made should be used for relatively crude calculations of heat transfer. However, this approach is much improves the cooling temperature prediction processes currently used for disc brakes under parked conditions. Furthermore, the convective heat transfer properties have been investigated from a generic disc shape geometry thus far in Chapter 7, orientated vertically in free air. Consequently, this technique can be used

to find the h_{conv} value for the free end surface of all thin, hollow cylinders placed horizontally placed in free air.

7.2 Numerical Modelling

To build on the information gained from the analytical modelling, section 7.2 generates a numerical model to predict the heat dissipation from the full brake disc. Modelling of three individual cases was conducted, all of which were for the scenario of the disc brake only. For each case, the initial differential equation started from the energy balance equation (equation (K.1)). Different assumptions were then applied to create three separate cooling cases. Case 1 used the standard brake assumptions as a baseline result, i.e. the heat transfer coefficients for all modes of dissipation were held constant. Case 2 increased the analytical models complexity by allowing the radiation to vary with temperature of the cooling range, whilst Case 3 allowed variability in radiation and convection.

Using MatLab to solve the derived 1st ODE for Case 1, it became apparent that constant HTC's did indeed lead to inaccurate results (see Appendix K) as predicted in Chapter 6. Predicted cooling profiles, from the differential equation, failed to accurately recreate the experiment data profile. By integrating the differential equation, an exact solution was able to be generated for the cooling profile. Temperature predictions under-estimated the convection HTC from the disc brake during the cooling phase, making the derived equation not useful to the design Engineer.

Allowing radiation to vary with temperature did produce an improvement in Case 2 as the rate of heat dissipation was be increased at the higher temperatures. However, the ability to integrate the improved cooling equation was eliminated by the increased equation complexity, which prevents a mathematically exact solution. Alternatively, an approximation equation was derived instead (equation (K.30)) of an exact solution by using an asymptotic expansion. This assumption equation was found useful only for a specific temperature range, much lower than what was being investigated in this project.

Due to the demonstrated importance of convection variation throughout the cooling phase, only the results of Case 3 are presented in section 7.2; the reader is directed to Appendix K if they are interested further in the mathematical derivations and results from Cases 1 and 2.

7.2.1 1st ODE Generation

Permitting radiation to vary achieved greater accuracy from the numerical analysis. It was then predicted that by having variable convection coefficient simultaneously with variable radiation

coefficient would further increase the accuracy of the analytical analysis (Appendix K). Having found a relationship for convection with temperature above, it was now possible to test this hypothesis.

The energy balance shown in equation (5.1) was used as the starting point for determining the differential equation for the third case. Differences between Case 2 and 3 emerge when equation (7.4) is substituted in rather than holding h_{conv} constant. The corresponding 1st ODE was:

$$\begin{aligned}
 m_d C_{p,d} \frac{dT_d}{dt} &= -[h_{conv} A_{surf} (T_d - T_\infty) + h_{rad} A_{surf} (T_d - T_\infty)] \\
 m_d C_{p,d} \frac{dT_d}{dt} &= -\left[\left(a_1 + a_2 T_d + a_3 T_d^2 + a_4 \ln(T_d) \right) A_{surf} (T_d - T_\infty) \right. \\
 &\quad \left. + \sigma \varepsilon A_{surf} (T_d^4 - T_\infty^4) \right] \\
 \frac{dT_d}{dt} &= -\gamma \left[\left(a_1 + a_2 T_d + a_3 T_d^2 + a_4 \ln(T_d) \right) (T_d - T_\infty) \right. \\
 &\quad \left. + \sigma \varepsilon (T_d^4 - T_\infty^4) \right]
 \end{aligned} \tag{7.6}$$

Figure 7.13 shows a comparison of the three numerical analysis results to the experimental data; 10% error bars have been inserted to represent the desirable accuracy level. In Cases 1 and 2, where convection is being held constant, a value of 10 W/m²K was chosen as it gave a reasonable relationship to both low and high temperatures.

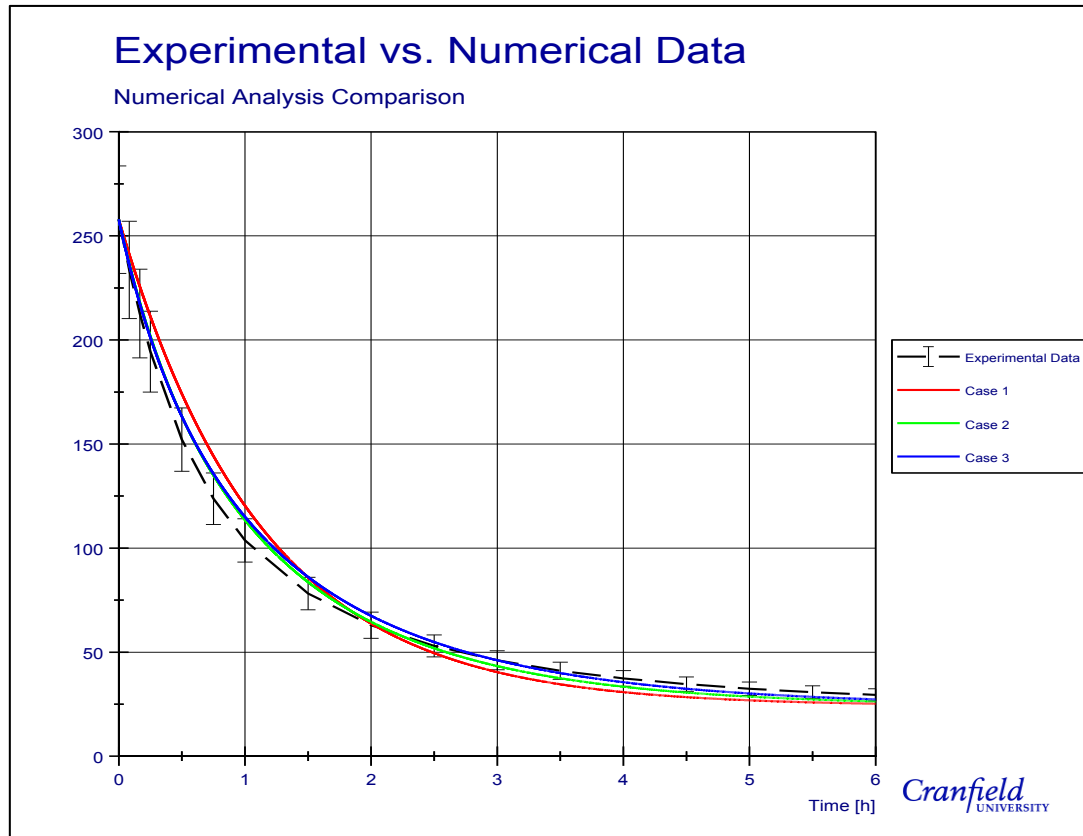


Figure 7.13: Comparison of the three different cases shows the fully variable case to be superior.

For the first hour very little difference between the predicted temperature profiles was seen for Cases 2 and 3, whereas the lumped case clearly over predicts the temperature by more than the required limit. The main difference between Cases 2 and 3 occurs after the hour mark, when the two profiles separate. For Case 2, using a constant h_{conv} forced the temperature profile gradient to change less quickly than Case 3 once the disc brake had fallen below 125°C. Both methods remain within the 10% error limit but the ability to vary the convection made Case 3 qualitatively match the cooling profile better than Case 2. It can be concluded that having a variable convection coefficient is important for maintaining the surface temperature cooling profile integrity during the transition from hot to cold temperatures. To reiterate, the geometry used in this study was for disc brake analysis, but it is also representative of any generic hollow disc in free air and therefore this method can be used for alternative applications.

7.2.2 Inclusion of Hat Section

To complete the convection study on the CV disc brake, the same dimensionless number investigation, undertaken for the disc brake friction surface, was repeated on the hat section. Numerical analysis was not performed on the hat section however, due to its temperature being

dependent on the rotor temperatures. An FE modelling solution would be required for this type of temperature prediction, conducted later in Chapter 10. An FE model boundary condition will be the h_{conv} values over the hat, section 7.2.2 aims to determine appropriate values to use over this surface.

Starting with the hat geometry, Figure 7.14 shows the cross section of the disc brake. The hat was assumed to be constructed of two separate cylinders located in free air allowing convective HTC values to be found by using the Morgan equation (equation (4.17)). Cylinder 1 has a diameter of 220 mm and a length of 73 mm whilst Cylinder 2 has a diameter and length of 283 and 32 mm respectively.

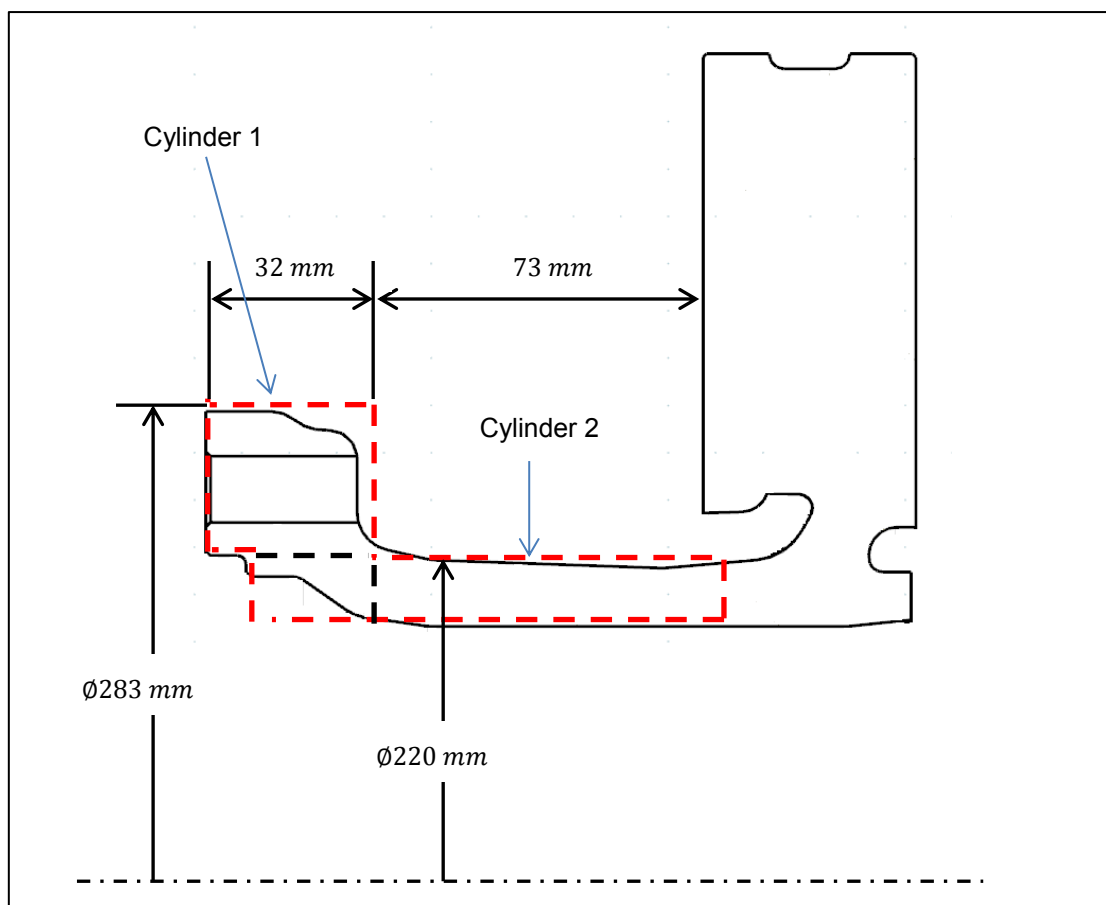


Figure 7.14: Simplified hat geometry.

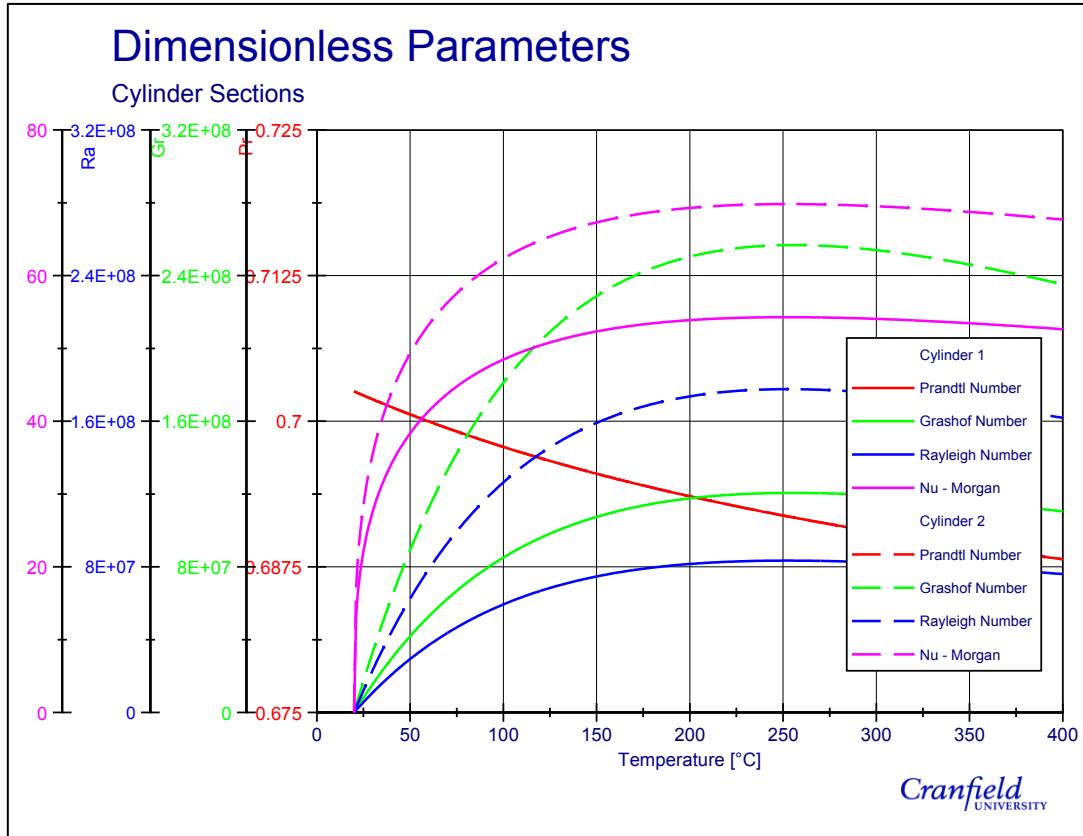


Figure 7.15: Dimensionless parameters for both cylinders representing hat geometry

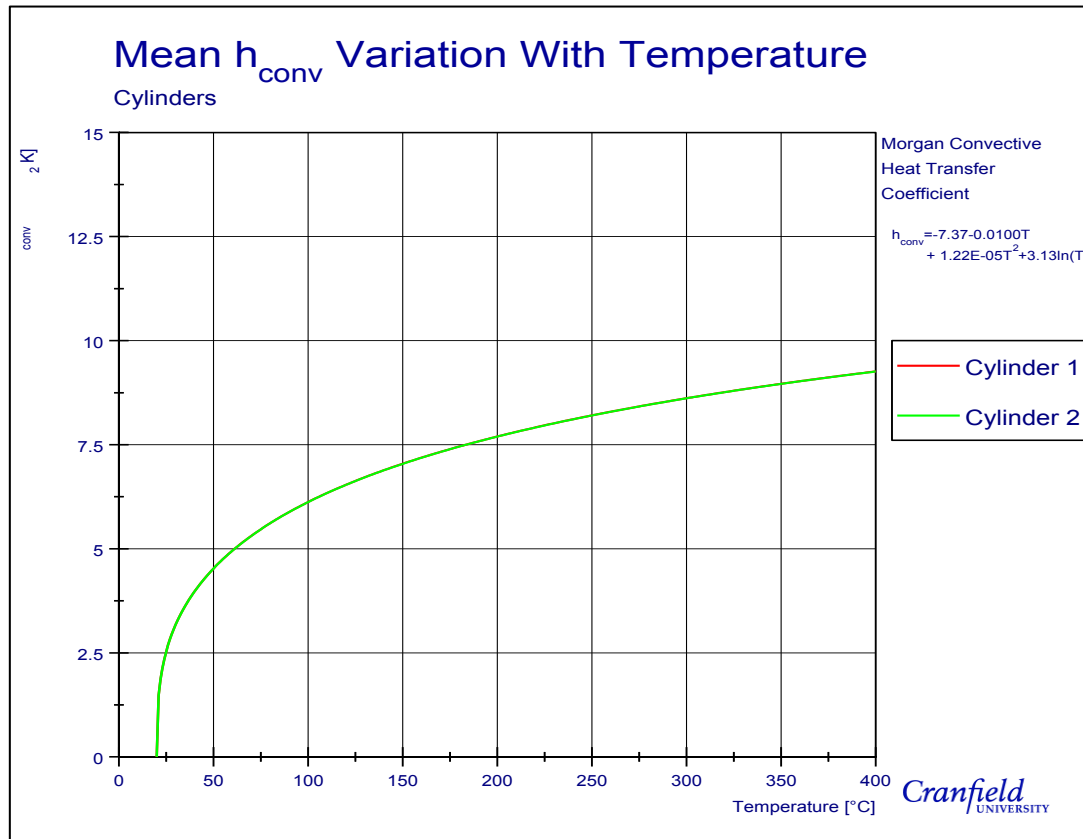


Figure 7.16: Variable convective HTC over both cylinders.

Calculated values for the four dimensionless numbers for both cylinders are shown in Figure 7.15. The larger diameter of the second cylinder causes greater magnitudes for each of the dimensionless numbers except for the Pr number due to being a function of fluid properties only, independent of surface interaction. The larger diameter is offset by the long length of the first cylinder when calculating the convective HTC as Figure 7.16 shows virtually no difference for the two. Only a single h_{conv} equation was created by averaging the Figure 7.16 results. Continuity was kept with the equation format as it once again matches equation (7.4); cylinder coefficients are shown in Table 7.1.

7.3 Chapter Summary

Analytical modelling of a disc brake in a stationary parking application was conducted in Chapter 7. From first principles, three 1st order differential equations were created that calculated the heat transfer rate from the surface. The first simulated the reference model, where all HTCs were held constant, the radiation was permitted to vary with temperature in Case 2 with convection also varying for Case 3. The inability to integrate the 1st ODEs, for Cases 2 and

3, made it impossible to develop a tool that produces an exact solution, which could be used by a designer in the early design stages.

To enable the 1st ODE to vary with temperature in Case 3, a method of calculating h_{conv} was established, which was based dimensionless analysis. This involved using simplified friction surface geometry, making the results generic to any disc positioned vertically in free air. A non-linear relationship was found for a vertical disc surface h_{conv} with temperature. Numerical solutions were calculated in MatLab, which demonstrated that having this fully variable boundary condition produces not only accurate results, but also generates a cooling profile of the right qualitative nature as well. Temperatures investigated in this chapter were for average surface temperatures only. Although this method has its uses, localised deviations in h_{conv} values are not explored. To enhance heat dissipation knowledge from a CV disc brake, the following chapter utilises CFD technology to explore h_{conv} variation over the whole disc brake surface area.

8 CFD Modelling of Airflow and Heat Transfer from a Stationary Ventilated Disc Brake

Convective dissipation in a 2D plane was the focus of the previous chapter, finding average surface values of h_{conv} over the disc brake. Chapter 8 aims to progress the knowledge previously acquired by focusing on the 3-dimensional flowfield generated around the disc brake subjected to natural convection. The standard CFD modelling approach to such problems was utilised, with airflow and h_{conv} distribution results presented. A qualitative validation procedure was developed to confirm the predicted results.

8.1 Validation Equipment and Procedure

In order to validate the CFD work, practical experiments were undertaken on the Thermal Rig. A common technique to validate CFD modelling is the hot wire anemometry method, which measures air speeds and compares them to the CFD calculated speeds, as used by many previous authors such as Galindo-Lopez (2008). In buoyant conditions, the air speeds will be a whole order of magnitude lower than in dynamic applications so it was not possible to use the hot wire anemometry validation technique. Alternatively, a method based on air temperatures rather than speeds was devised.

Numerous thermocouples were installed into the Thermal Rig and situated around the disc brake. Rubbing type thermocouples recorded the friction surface temperatures whilst 7 probe type thermocouples recorded air temperatures. The position of the probe thermocouples along with their corresponding reference names used in this report are identified by red markers in Figure 8.1. The air thermocouple naming convention starts with the circumferential angle the thermocouple is positioned relative to the vertical centreline, when looking from the outboard surface. Positive angles represent a clockwise position from the vertical centreline, whilst negative values are anti-clockwise positions. The relative angle is followed by AO (standing for Air Outside) with the final value describing the thermocouple radial distance from the disc brake OD surface.

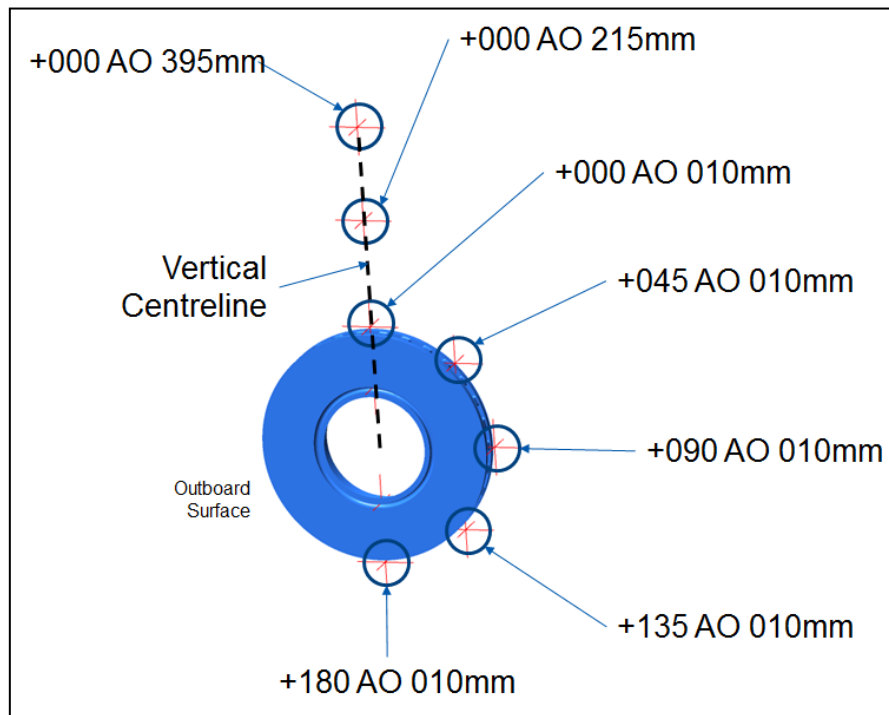


Figure 8.1: Thermocouple names and positions.

As the IHC was located on only the one side of the disc, to ensure an even distribution of heat, the disc was rotated at 100 rpm through the induction field during the heating phase. Thermal equilibrium was achieved by holding the disc brake friction surfaces at 400°C for 30 minutes, allowing the conduction process to heat the entire disc brake volume to a uniform temperature. After this time period, the IHC and motor were turned off to replicate the stationary disc brake cooling scenario.

To detect the airflow movement, neutral buoyancy smoke was introduced to the air. An ATE Smoke Generation unit was used to control the flow of smoke via a swan-neck probe. As the oil passed through the probe it was inductively heated beyond its flash point to vaporise it, which for the used Ondina EL oil was 159°C. Consequently, the smoke exiting the probe was hotter than the ambient but cooled quickly due to it being relatively low in volume in comparison to the surrounding air. Being low in volume prevents the storage of thermal energy so it is dissipated quickly. Provided the probe tip was sufficiently far away from the surface when introducing the smoke then the elevated smoke temperatures had minimal effect on the flow patterns.

To aid the smoke visualisation process, a low power constant beam laser was used in conjunction with a beam splitter to create a plane of light, as demonstrated in Figure 8.2a. For greatest effect, the light plane needed to be in the same direction as the particle flow, giving

maximum photon exposure to the flowfield – vertically positioned in this case. The laser was placed in three subsequent positions, allowing a large amount of data to be captured and analysed. As seen in Figure 8.2b, two of these light planes are parallel to the friction surfaces and above the midpoint of the disc brake, the first was on the flange surface (A), with the second light plane located at the centre of the vane channels (B). The final light plane was rotated through 90° , such that it captured the airflow through the disc brake's centreline, in the axial direction and below the midpoint (C).

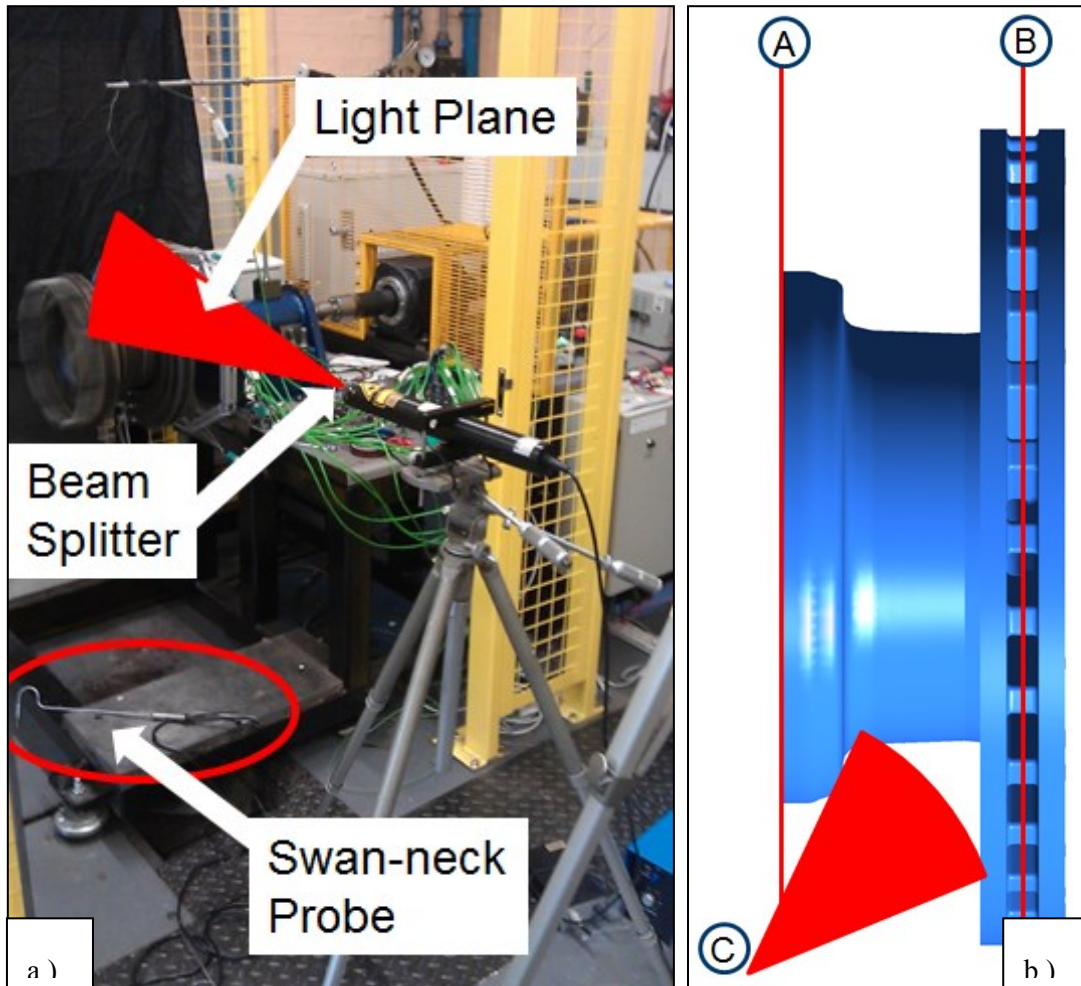


Figure 8.2: Smoke machine testing with light planes to aid flow visualisation.

8.2 CFD Model Construction

CFD has been developed and used for many years now, becoming common practice when conducting airflow analysis. The greatest asset of CFD for this study is the ability to produce flow predictions within channels, where it would be otherwise impossible to see the effects of geometry on temperature and airflow patterns. From the literature, it appears Olphe-Galliard (2011) is the only author who has attempted to use a generalised CFD program to predict

airflow around a stationary passenger car disc brake. A discussion on the CFD model generation process is presented before the results of a test into the relative effectiveness of four generalised CFD turbulence solutions are examined.

8.2.1 Volume Mesh Generation

Initial modelling of airflow around a complex shape, such as a ventilated disc brake, driven purely by buoyant affects has proven difficult. Olphe-Galliard (2011) found that a much larger volume has to be considered, compared to the axisymmetric models often used in dynamic braking simulations, such as Voller (2003) and Galindo-Lopez (2008). Furthermore, a much finer volume mesh was required, including prism layers close to the surface boundaries, giving greater near-wall shear stress evaluation. Building on the previous work, Figure 8.3 shows the rectangular geometry encased around a standard 434/234 mm radial vane CV disc brake, making the CFD volume mesh. The geometry extended 1.0 m downwards in the negative Y direction and in both the positive and negative X directs from the origin (located on the flange face plane, on the disc centreline), 0.5 m from both the flange and the inboard contact faces (Z directions), whilst extending a further 2.5 m above the disc brake (positive Y). The consequence of such a large area is that the CFD solver had to make calculations for a total volume of 3.795 m³. Having to use a relatively fine mesh over such a large volume will inherently cause the computational time until convergence to rise.

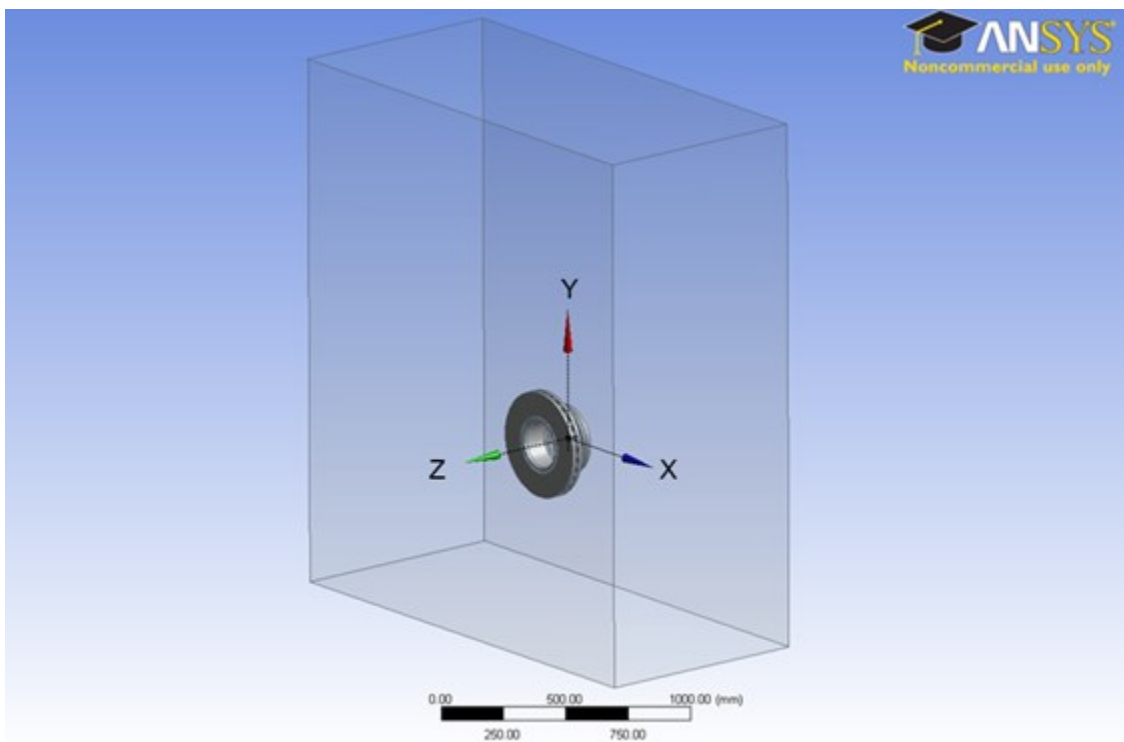


Figure 8.3: CFD model domain.

The mesh used for the duration of the CFD investigation is presented in Figure 8.4; a cut through the centre of the YZ plane is shown for all three sections. Figure 8.4.a displays the full volume mesh that was created by a total of 9.2 million elements. Of these, 6.3 million were tetrahedral, 2.8 were wedges and the final 0.1 million were the near-wall prism elements. As seen in Figure 8.4.b, the mesh density gets finer towards the disc brake surface boundary, with a part of the prism mesh displayed in Figure 8.4.c. Olphe-Galliard (2011) conducted a grid convergence study to show the mesh quality generated was adequate; this investigation used the same meshing strategy and therefore also generated an adequate mesh quality.

The prism layer itself was extended around the entire disc boundary surface. There are two methods of creating a prism (or inflation) layer, the first is to set the thickness of the first layer only and the other is to set the total thickness of the prism layer. With the former, there is a smooth transition between the prism layer and the tetrahedral elements and has superior capabilities when meshing with complex geometries, but does have the disadvantage that the number of layers used does vary. Alternatively, the constant layer thickness option keeps the same total thickness the inflation layer thickness around the surfaces but can change the number of prisms in the layer. To understand why this might be an issue, the y^+ term is discussed.

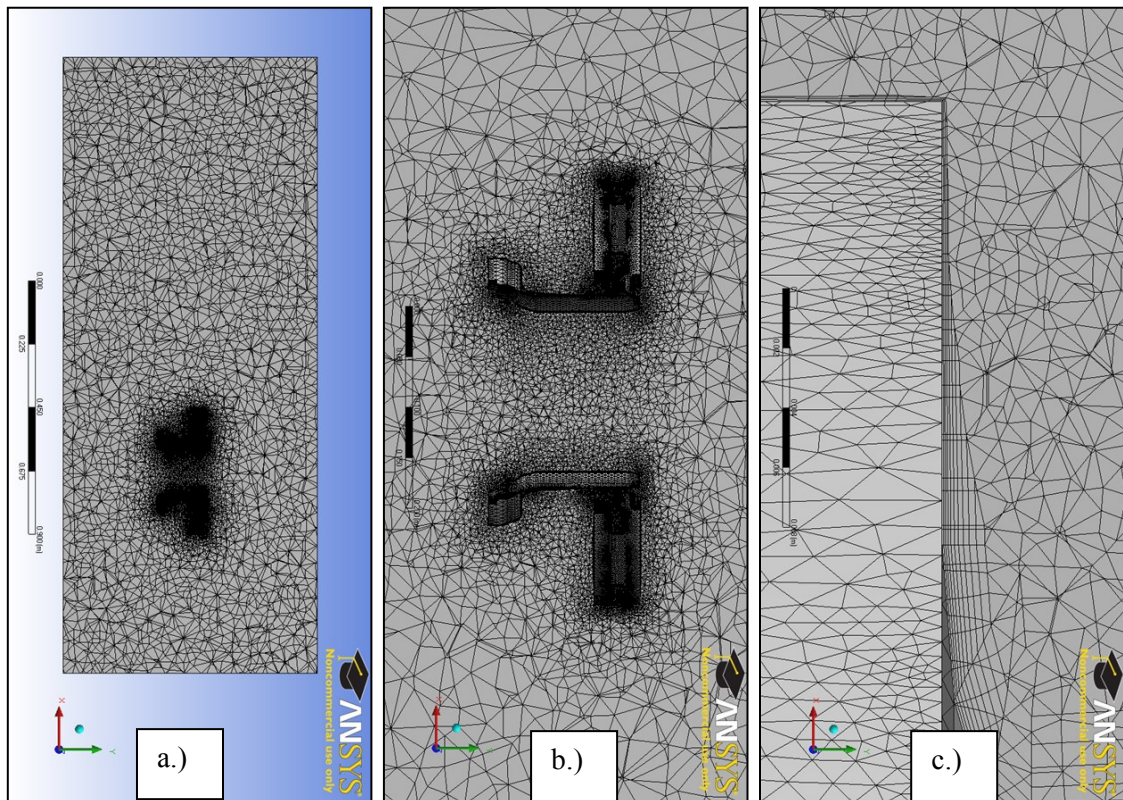


Figure 8.4: Mesh generated for CFD investigation, with a.) the full volume mesh, b.) finer mesh around the disc brake and c.) prism layer close to the surface

Near wall interactions are always important, however often in turbulent flow the near wall interaction is less important than the free stream flow because of the small boundary layer. In these cases, the first element in away from the wall is treated as the laminar near wall region with the remaining elements in the turbulent region. Special near wall functions are built into CFD programs to deal with these laminar regions differently than in the turbulent regions. To calculate the distance the first node needs to be away from the wall, Δy , the follow equation is used.

$$\Delta y = Ly^+ \sqrt{(74Re_L^{-13/14})} \quad (8.1)$$

Where L is the flow characteristic length scale, Re_L is the Reynolds Number based on the flows characteristic length and y^+ is the desired value of y^+ . Using equation (8.1), taken from Release Notes for FLUENT 6.3 (Fluent Inc. 2006), the thickness of the first prism layer can be determined by using a desired value of y^+ , which is a non-dimensional distance. High values, above 100, are for turbulent flow, it can be into the thousands for high speed aerofoils. A high value of y^+ describes laminar flow is present throughout the first wall element, with no laminar flow in the following element. Having a too high a y^+ value will result in the first element being placed too far outside the boundary layer and subsequently using laminar wall functions on regions of turbulent flow. Conversely, by using a value that is too small a value under predicts the size of the boundary layer, introducing errors into the simulation; values smaller than 11 are generally deemed as too low (Jerhamre and Bergstrom 2001).

However, wall functions are only important when the flow regime is turbulent. In the previous chapter it was concluded that the flow regime will be in a transitional phase over the disc brake. This lower velocity flow driven under natural convection, will require a small y^+ value to capture the more significant shear stress factors associated with natural convection flow all the way through the boundary layer, resulting in y^+ values below 11 are likely to be needed. Standard wall functions therefore cannot be used. Scalable wall functions allow the flow to be resolved all the way through the boundary with a finer near wall (prism layer) mesh and consequently, one was used throughout this investigation.

With the flow not expected to be fully turbulent, a smaller first layer thickness of 0.075 mm was used with an exponential growth rate to ensure the laminar effects were captured; this relates to an estimated y^+ value of five. A maximum of 10 layers was set but as the first layer thickness prism layer meshing scheme was used, this number was able to reduce in complex geometry regions. The advantage of a smooth transition from the prism layer and the tetrahedral elements

was one reason for using first layer thickness meshing scheme, but it was the guaranteed smaller size of first layer thickness which was the main factor behind the using the scheme. The software used to produce this mesh was ANSYS Mesh version 12.1 solver.

8.2.2 CFD Model Setup

With a completed mesh, attention turned to setting up the CFD model. Parameters that needed defining were the open surfaces temperatures, disc brake surface temperatures, which turbulence model would be used in the solver and what was the desired convergence target. Starting with the temperatures, the open type boundary surfaces (displayed in Figure 8.5) were set to an ambient 20°C. As the disc was heated to 400°C initial temptation was to match the disc brake surface boundaries with temperatures. However, as the disc brake had to rotate during heating, air temperature measurements were recorded after the disc brake friction surfaces had been allowed to cool to 350°C, ensuring no rotational effects remained from the heating process. All resultant airflow was then a function of natural convection. CFD surface temperatures were therefore set at 350°C on the rotor. Conduction to the hat section of the disc brake would cause its temperature to rise, but dissipation by radiation and convection will result in the temperature being less than the friction surfaces; the hat was assumed to be at 200°C.

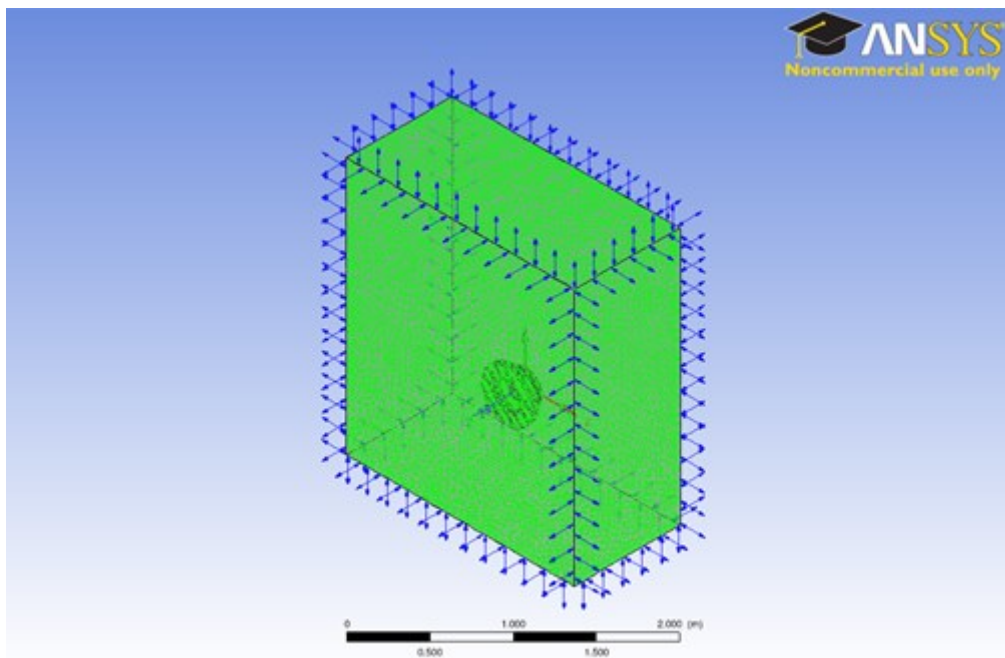


Figure 8.5: Open surfaces set to 20°C.

Convergence levels from a CFD model is determined by the size of the residual values produced from the solver compared to a predetermined target value. A model is said to be complete once all the governing equations have reduced to the specified value. The residual values are a

resultant of the truncation error generated in the solver when truncating the numerical approximation series equations. Convergence analysis has been covered in-depth (Galindo-Lopez 2008) and was found that to achieve good agreement between CFD and experimental results, for both momentum and heat transfer, a convergence target of $1e^{-5}$ should be used, which was subsequently selected and used in this investigation.

Selecting the turbulence model was somewhat less straightforward. The amount of work readily available in the literature on natural convection airflow around a stationary disc brake is minimal. Subsequently, there is little advice readily available as to which turbulence method is most suited for stationary braking applications. Numerous authors have published work using the $k - \varepsilon$ model in dynamic scenarios because of its robustness and quick convergence times associated with it, whilst $k - \omega$ models have been used for wall-bounded flows. As Figure 8.4 and Figure 8.5 demonstrate, the volume is partially wall bounded (in the vane channels) and partly free stream so either of these turbulence models could be used. Also, with the flow regime possibly transitional, a simple laminar model may well prove to be the most appropriate to use.

In response to the lack of published work, CFD predictions were generated with four separate models. Each simulation used a different turbulence, with the purpose of determining which turbulence model is most appropriate to use when modelling stationary braking applications. A short discussion is offered first about the three mentioned turbulence models, as well as a fourth (being the Shear Stress Transport (SST) model), before the results are presented.

8.2.2.1 Laminar Model

In all CFD generalised code, the fundamental equations that are being calculated are the unsteady Navier-Stokes equations, which is given in the general form in equation (8.2).

$$\rho \left(\frac{\partial \bar{v}}{\partial t} + \bar{v} \cdot \nabla \bar{v} \right) = -\nabla p + \nabla \cdot \tau + \bar{f} \quad (8.2)$$

Where \bar{v} is the flow velocity vector, τ is the stress tensor and \bar{f} is a single representation for other forces that may be acting in the system. For simple laminar flow, the Navier-Stokes equation breaks down into the continuity equation and the conservation of momentum. The former calculates properties related to the mass within the system whilst the latter calculates the 3-dimensional flow properties. This process requires four equations to be solved for each node. If heat transfer is present in the simulation, a conservation of energy is also calculated. In this case, diffusion is the mechanism for energy transfer within the fluid. The laminar model can be

used for high Reynolds Number flow but with additional terms are required as there are no mathematical terms to deal with the added energy components.

8.2.2.2 $k - \varepsilon$ Model

The $k - \varepsilon$ turbulence model is by far the most common model used when conducting CFD analysis. To aid the governing Navier-Stokes equations with the presence of flow turbulence, the $k - \varepsilon$ model calculates two additional equations, or transport equations, at every element. The first is to calculate k , the amount of turbulence kinetic energy. The second ε equation is for the turbulence eddy dissipation rate. One disadvantage of this model is that it was derived for purely turbulent models only so will produce inaccurate results if used for any other flow regime. Robustness is achieved when using the two additional equations that generates reasonable accuracy (provided in turbulent conditions), for economical computation times. These factors are the source behind why it is commonly used throughout research and industry.

8.2.2.3 $k - \omega$ Model

Like with the $k - \varepsilon$, the $k - \omega$ turbulence model uses two transport equations to calculate the additional turbulent energy; the turbulent kinetic energy, k , equation remains with the specific dissipation rate, ω , replacing the turbulence eddy dissipation rate. Terms in the ω equation allow molecular viscosity effects to be calculated, giving the desirable characteristic of accurately calculating near-wall boundary layer flow.

However, the main problem with the standard $k - \omega$ model is that it is extremely sensitive to free stream flow. The baseline (BSL) model is a slight derivation of the original $k - \omega$, it was established to give the robust and accurate near-wall region flow predicts generated by the $k - \omega$ but with the advantage of also delivering the free-stream properties of the $k - \varepsilon$ model. To do this, the $k - \varepsilon$ equations are transformed and added to the $k - \omega$ equations. By implementing a blending function, the BSL model differentiates between the two sets of equations with respect to each elements relative position. In near-wall regions, the blending function is one and zero in the free stream, the reverse is true for elements in the free stream region. Consequently, $k - \omega$ based models are widely used for simulations where the flow is constrained by walls.

8.2.2.4 SST Model

The SST turbulence model theoretically improves on the BSL models as it introduces terms to the transport equations that calculate the transportation of turbulent shear stress. The omission

of turbulent shear stress in the BSL model prevent accurate predictions of flow separation under pressure gradients and/or from smooth surfaces (Menter 1994).

8.2.2.5 Turbulence Modelling Comparison

To test the validity of the four discussed turbulence models, temperatures were recorded during the practical experiment from the thermocouples positioned in Figure 8.1 and compared to the four CFD models. Table 8.1 shows the amount of time each model took to reach convergence. Having to calculate the fewest number of equations per iteration, it was unsurprising that the laminar model was the quickest to complete. It transpired that the SST turbulence model is the quickest out of the remaining three to converge for a disc brake CFD simulation. The effects of having turbulent shear stress terms in the SST model greatly improve the time to convergence when compared to the other $k - \omega$ derivative as the BSL model took virtually double the amount of time, whereas the $k - \varepsilon$ model was approximately 11.5 hours longer than the SST.

Table 8.1: CFD model tests – convergence times.

Turbulence Model	Time to Convergence (days hr:min:sec)
Laminar	2 04:58:04
$k - \varepsilon$	2 21:24:02
BSL	4 05:39:36
SST	2 09:57:15

It should be noted here that none of the models fully converged to the $1e^{-5}$ limit set. Instead, this time was until the limit of 1,750 iterations was reached. In all cases, the mass and three momentum equations did indeed reach the residual limit in the allowable region (Figure 8.6a), what prevented full convergence was the heat transfer properties (Figure 8.6b). The residual values in each of the models quickly reduced to $1e^{-3}$ before plateauing and remaining constant for the remaining calculations. Clearly, limitations of the current solver capabilities for such a complex problem were reached. However, considering all the momentum equations successfully converged with the heat transfer residuals all converging to a similar satisfactory level, albeit not to the desired level, the results could still be acceptable if the predicted temperatures were close to the measured.

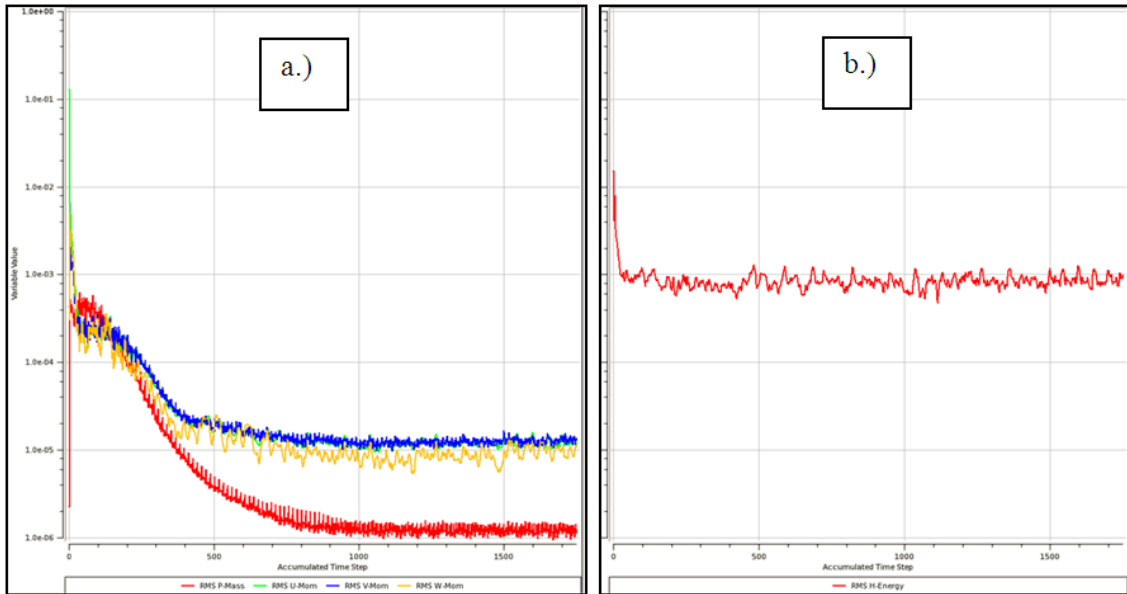


Figure 8.6: Typical convergence graphs for a.) mass and momentum, and b.) heat transfer.

The predicted air temperature values for the laminar and the three separate turbulence models under investigation are compared to the measured air temperatures in Table 8.2. It is interesting to see that no turbulence model can claim superiority over the others for all thermocouple positions. For example, at thermocouple +000 AO 010mm the SST model produced the closest match to the measured data with only a 4.1% overestimation, as well as being best matched at two other locations, whereas it was considerably poorer than the laminar prediction at position +045 AO 010mm. Little differentiation is seen from the results for the air temperatures on the lower half of the disc. Generally, the SST results approximately differ by 10% to the measured data in absolute terms, and less than 20% in when temperatures are converted into relative terms. With good agreement between the SST model and the measured data, the CFD modelling can be described as accurate even with the reduced heat transfer CFD convergence level.

It can be concluded from this investigation that the SST turbulence model was the most appropriate when simulating natural convection around a disc brake for both accuracy and computational time advantages. However, it should be noted that the laminar model results produced satisfactory values too. By using equation (4.9) an estimate of the Re value can be calculated at 2.2×10^4 , taking air property values from Appendix L at 100°C and assuming a velocity of 1 m/s. According to Allen (1982), this value falls within the unsteady laminar region, where the flow is transitioning from laminar to turbulent. This prediction matches well with the analytical modelling in Chapter 7. A laminar or early stage transitional period over the disc brake friction surfaces is detrimental to brake cooling as the additional turbulent energy helps to increase flow velocity, which in turn increases the amount of convection. It can be

concluded that of the four models used, it is the SST model that is the most appropriate to use in stationary parking applications to ensure the low energy inflow turbulence is captured.

Table 8.2: CFD model results compared to experimental results - % difference from measured.

Thermocouple	Measured Temperature K	Laminar $\Delta\%$	$k - \epsilon$ $\Delta\%$	BSL $\Delta\%$	SST $\Delta\%$
+000 AO 010mm	528	9.2	-9.8	8.4	4.1
+000 AO 215mm	391	-13.7	-18.5	-13.8	-12.3
+000 AO 395mm	340	-4.1	-8.7	-5.2	-3.8
+045 AO 010mm	322	1.9	-3.7	7.4	7.1
+090 AO 010mm	327	-10.3	-10.5	-10.3	-10.3
+135 AO 010mm	324	-9.6	-9.6	-9.6	-9.7
+180 AO 010mm	326	-10.2	-10.1	-10.1	-10.2

8.3 CFD Results

Having defined the CFD setup procedure in section 8.2, results of the CFD simulation are now presented. The results have been broken down into three subsections and discussed individually; they are an air temperature based validation technique, predicted airflow patterns and concluded by further CFD validation, this time via the qualitative smoke machine method.

8.3.1 Flange Airflow and Heat Plume Existence Testing

The first results discussed are at the flange position. Predicted air streamlines, which originated on this plane, are shown in Figure 8.7. A distinct velocity plume is clearly generated directly above the disc, which does not extend to the extremities of the disc brake width. As the air is accelerated around the hat section, gaining heat as it does so, a plume of this nature would be expected. Nonetheless, four further thermocouples were positioned on the Thermal Rig, located in accordance with Figure 8.8, to test the validity of CFD results.

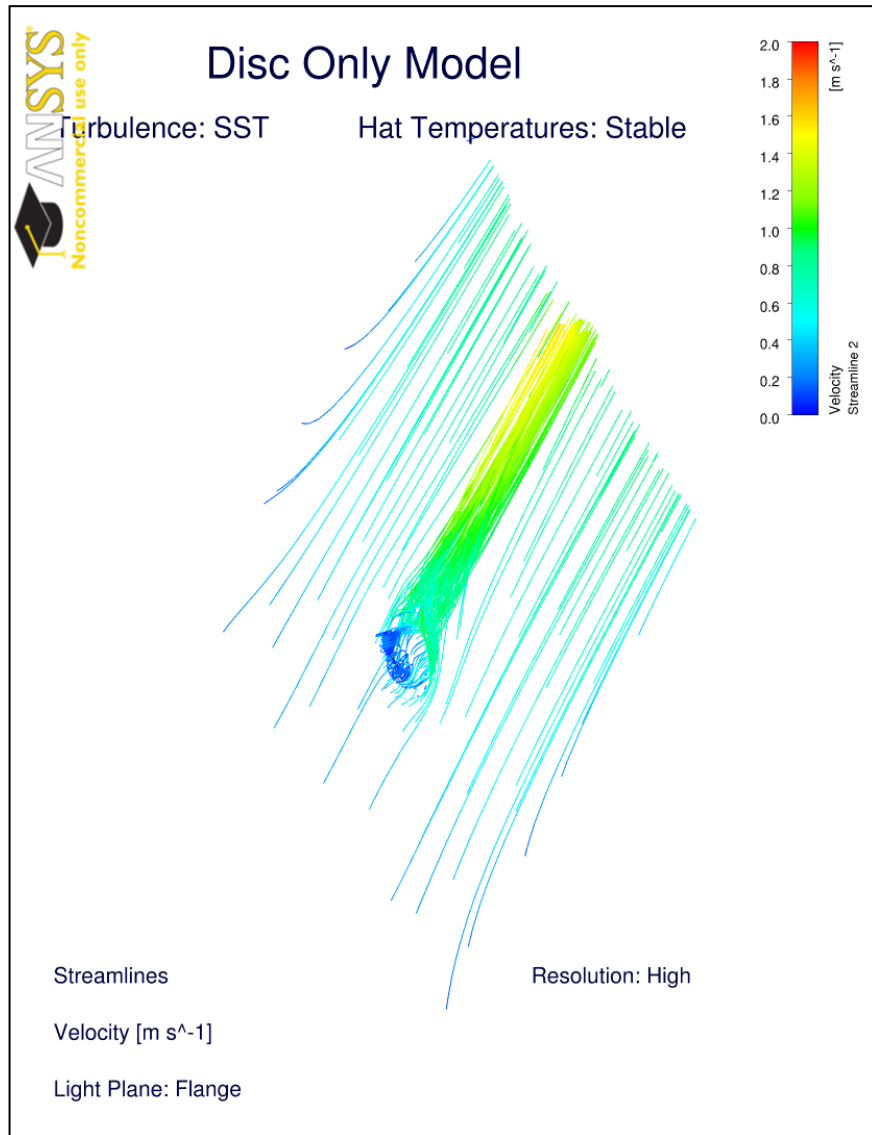


Figure 8.7: Predicted plume presence from CFD modelling located on the flange face

Results are displayed in Table 8.3. Once again, CFD predictions matched well to the measured data, showing the existence of the predicted plume. Air temperature remained at ambient for three of the four additional thermocouple locations with only the outboard side temperature rising by a marginal amount, which was not captured by the CFD simulation. This results was attributed to the fact that only the disc was in the model, whereas in reality the wheel carrier component was also attached to the fixture, increasing the length of heat source in that direction.

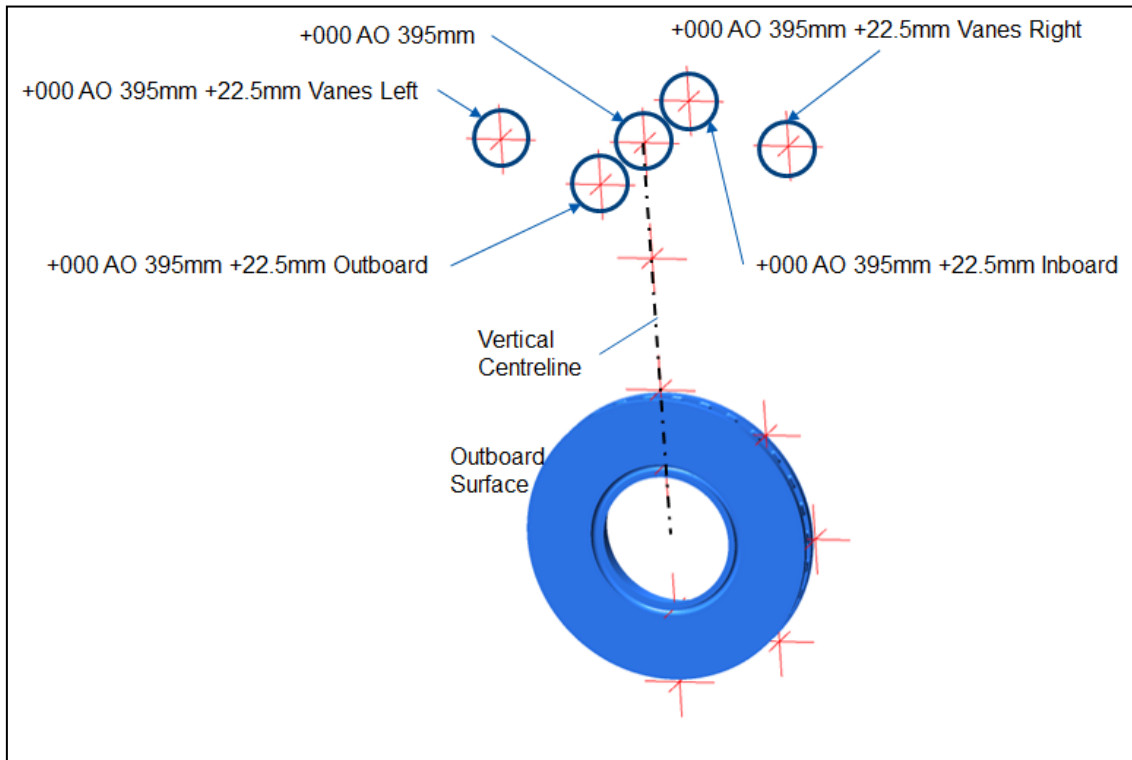


Figure 8.8: Additional thermocouple positions for plume existence test.

Table 8.3: Plume test results (Ambient temperature set at 20°C)

Thermocouple Position	Measured Temperature °C	CFD ΔT (°C)
+000 AO 395mm	67	-13
+000 AO 395mm +22.5mm Outboard	28	-8
+000 AO 395mm +22.5mm Inboard	21	4
+000 AO 395mm +22.5mm Vanes Left	20	1
+000 AO 395mm +22.5mm Vanes Right	20	1

Figure 8.9 depicts the airflow pattern around the hat region. Results show there is no Karman Vortex Street formation at this region, however, there are two weak vortices evident at the trailing side (upper half) of the hat section. Although it is not uncommon for vortices to exist in laminar flow, their presence is usually associated with turbulent flow, where the Re number is high, due to the high fluid velocity. Low airflow speeds have been predicted, with the maximum from the flange plane to be in the region of 1.3 m/s, indicating that brake cooling under stationary conditions does in fact produce the more uncommon low power vortices. Both points provide evidence that supports the idea that there is insufficient energy in the flow to trip into a fully developed turbulent regime.

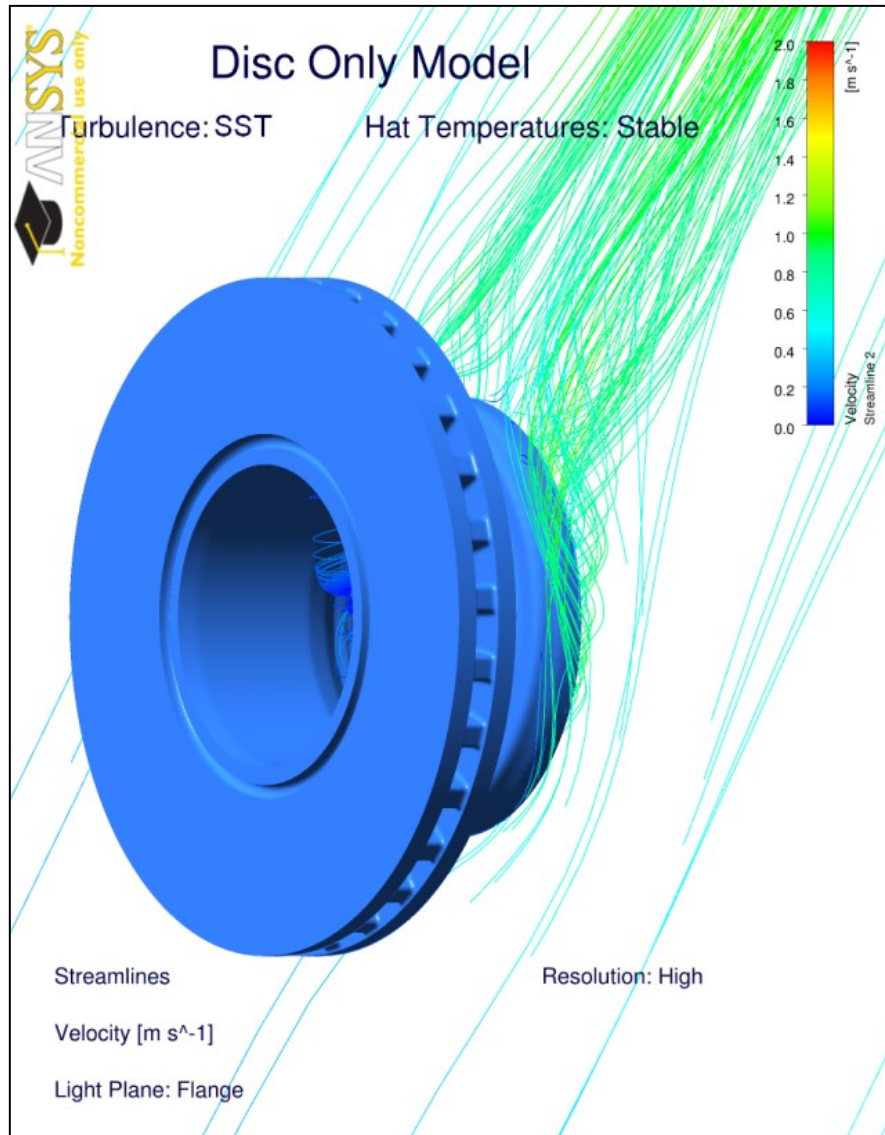


Figure 8.9: Close up view of velocity streamlines on the flange surface light plane

8.3.2 Airflow Results

Having analysed the CFD procedure in terms of temperature at specific points, results of the CFD simulation will now be presented. Results are given in the plane located at the centre of the vanes, parallel to the friction surfaces; the plane is depicted by the red surfaces shown in Figure 8.10.

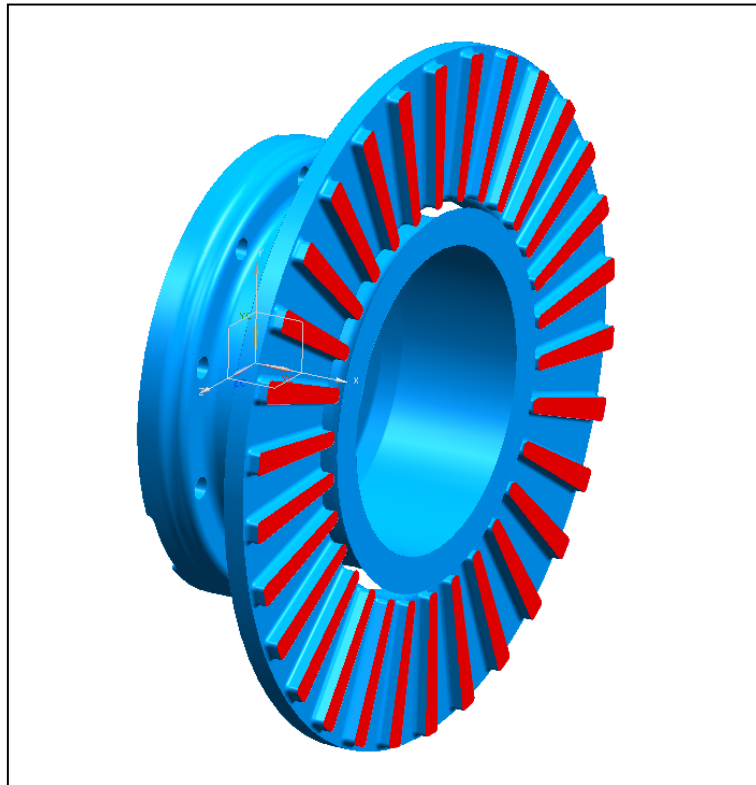


Figure 8.10: The plane used at the vanes centre to analyse CFD results.

The inspected plane was at the centre of the vanes, with the CFD results, in the form of streamlines, presented in Figure 8.11 and Figure 8.12. It is clear that only a limited amount of air that started on the plane remains on, or even remains close to the plane of origin. Deflection of the air streams happens in two forms, the first being the influence of the outer disc brake surfaces. Accelerating air below the disc brake rises vertically and is forced to deflect when it comes into contact with the relatively bluff circumferential surface. Considerably more air is deflected around the outside of the disc brake than what enters the lower vanes (90° to 180°). Air exiting from these lower vanes, at the ID, accumulates some axial momentum in addition to the vertical momentum, due to the disc brake geometry, providing the second source of airflow deflection. Exiting airflow subsequently travels over the hat section, producing the fastest predicted air speeds of anywhere in the domain, with values reaching 1.7 m/s.

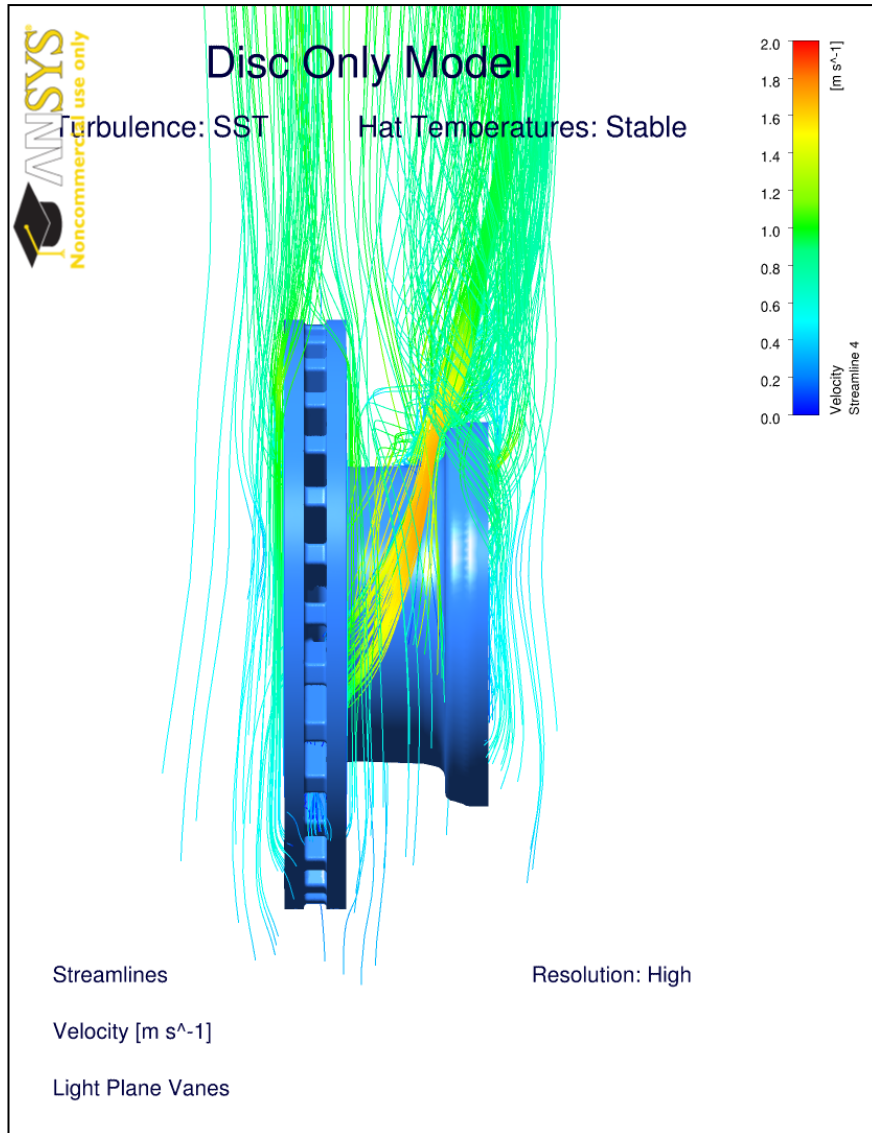


Figure 8.11: Velocity streamlines from the central vanes light plane

For analytical calculation purposes, buoyant airflow over a disc brake surfaces has historically been considered as two-dimensional. Using this assumption enables the friction surfaces of the walls to be treated as flat plates, allowing dimensionless analysis of Rayleigh and Nusselt numbers to provide an end convective heat transfer coefficient value. Coupling 2D flow with the ideal gas laws suggests that as the air gains thermal energy, the density drops and rises over the surfaces and through the vanes. CFD results in the form of streamlines present evidence in both Figure 8.11 and Figure 8.12 that only a small volume of air enters or exits the vanes at the OD, in the region between 45° and 135° from the vertical centreline, when compared to the amount exiting at the ID from the lower vanes.

As the highest air speeds are not seen at the highest point on the disc brake, a more sophisticated approach than the simplified 2D approach to disc brake cooling must be adopted. Subsequently, the traditional methods can be used successfully to predict basic flow properties, but do not have sufficient power to accurately predict the highly complex 3D airflow patterns for stationary, ventilated disc brake applications.

Figure 8.12 divulges a little more information to what was shown in Figure 8.11, as the walls of the disc brake have been removed, allowing visual access to the in-vane flow. The in-channel velocities are lower than on the outer disc surfaces, with the maximum channel speed being only 0.8 m/s. As flow recirculation is a function of low flow energy, the rate of thermal energy transfer to kinetic energy from the channel walls to the flowing air must be low for the occurrence of these recirculation regions to develop.

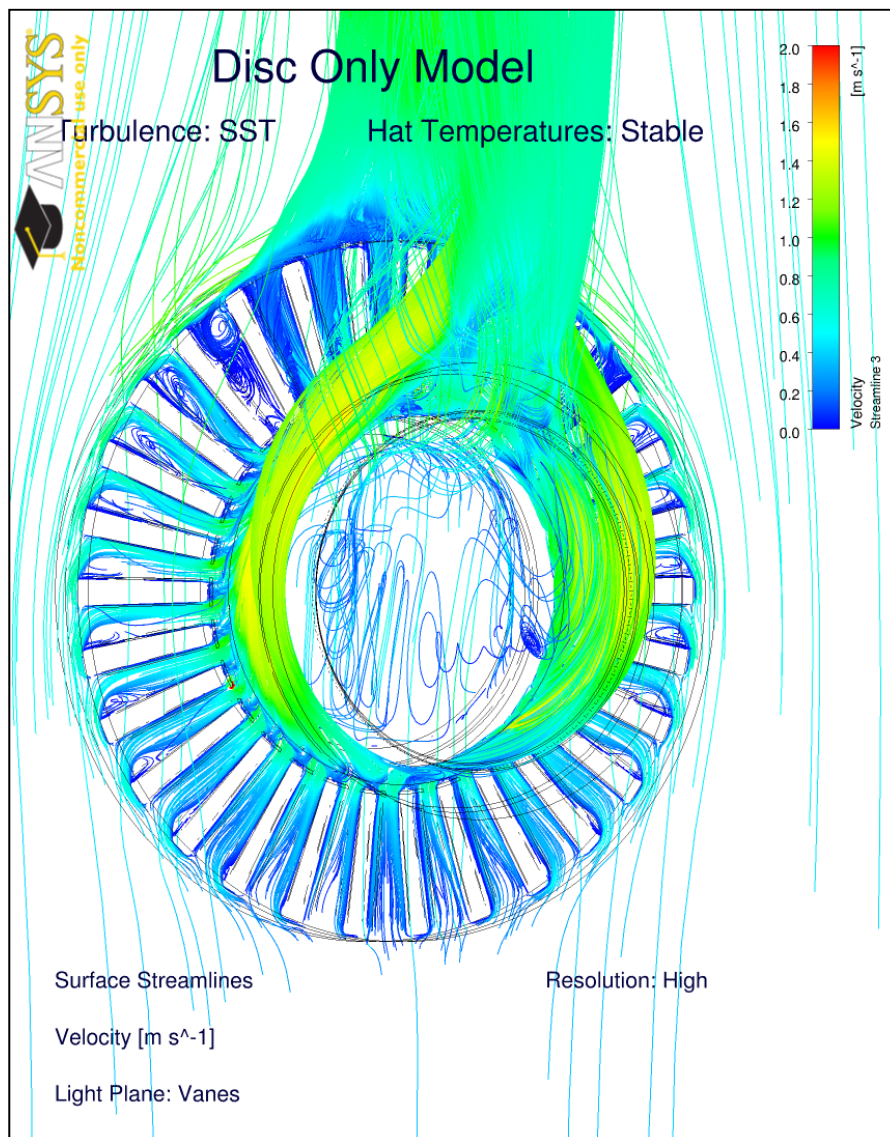


Figure 8.12: Velocity streamlines within the vane channels (surfaces have been removed)

Energy is conducted from the wall surface, through the boundary layer and into the free stream. As already stated in section 4.2.2, cooler upstream air then replaces the now hot air to re-establish a high thermal gradient. Greater flow velocity allows for a quicker replenishment of the cooler air, increasing the convective heat transfer, making convection highly speed dependent. Figure 8.12 shows that air replenishment is not happening in large channel areas, causing the air temperatures in the vanes to be high. Figure 8.13 offers further proof since there is little difference between the vane surface and in-channel air temperatures.

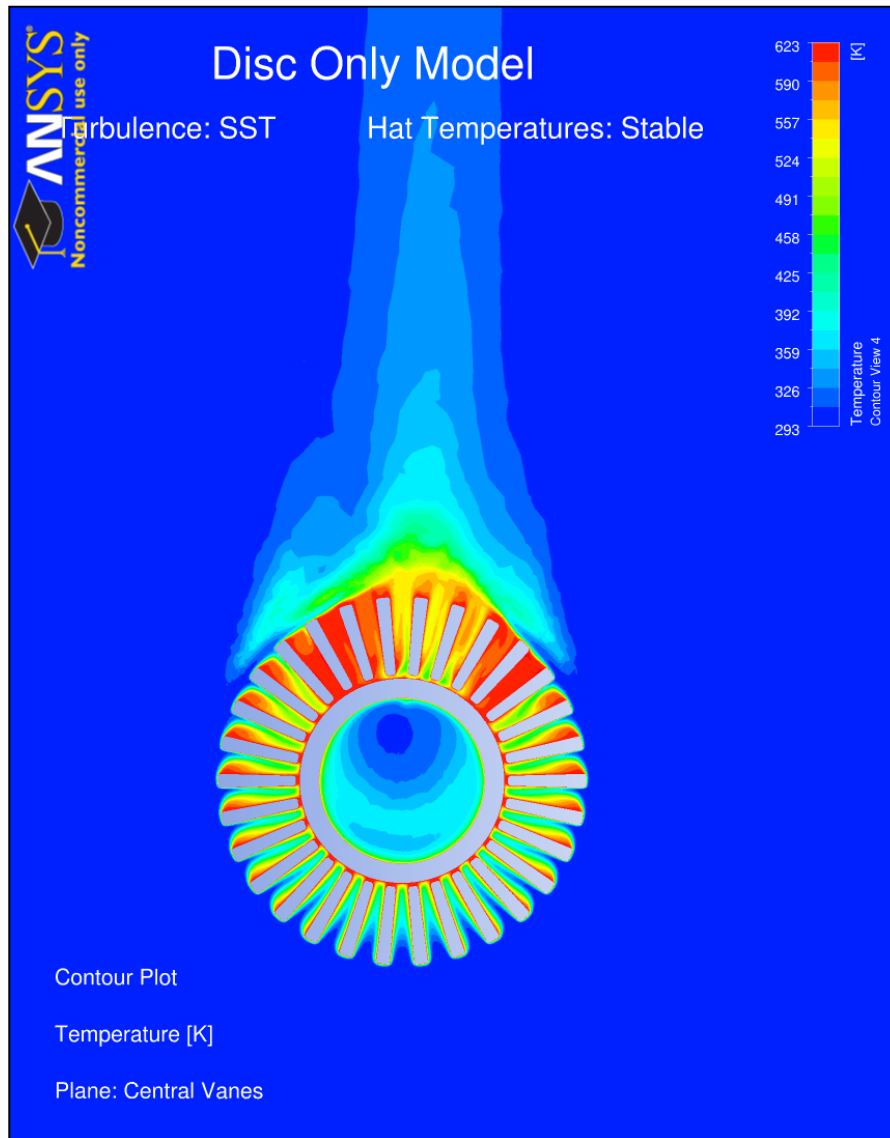


Figure 8.13: Central vanes located plane demonstrating high in-vane upper temperatures.

The disadvantageous effect of recirculating low density air at the channel OD is that these regions act as barriers for the free air entering the channels. A detrimental cycle arises where recirculating air is formed due to the low energy air flow, but the low density recirculation

blocks higher energy flow from entering the vane. Consequently, the cooling performance of the ventilated disc brake under stationary conditions is compromised.

Remarkably, dual recirculation is present in the vane channel located 36° from the vertical centreline, as blockages prevent air from entering or exiting the vane at either the OD or ID (see Figure 8.12 and Figure 8.13). Convective cooling in these channels is negligible with almost no airflow transpiring through it. External flow is the greatest cause for this, as the angle that the air has to deflect from the free stream and into the vane channel OD is now too great. External airflow has been shown to cause dual recirculation regions before (Angelinas *et al.* 2012) but only when the wheel is attached during rotational simulations. A simplified scenario is simulated here with no caliper components or a wheel, which are likely to further hinder the channel airflow, suggesting the anti-coning disc brake design may cool even worse than what is depicted.

The final streamline results discussed are in the axial (YZ) plane, on both the lower half (Figure 8.14) and the upper half (Figure 8.15) of the outboard friction surface. Starting on the lower portion of the disc brake, it can be seen that accelerated air within the vane turns 90° on exit and flows axially along the hat section, as previously stated. This exiting axial airflow entrains the air on the outside of the vanes, taking the main stream away from the ID. It is the effect of this entrainment process that prevents the airflow from entering the upper vanes ID, creating the entrance blockage.

An apparent flow characteristic that is also shown in Figure 8.14 is the propagation of an external recirculation region. The cause of this region is the axially moving air coming into contact with the bluff surface of the bolt fixing section. The kinetic energy after impact with the surface is not sufficient to re-join the main stream, resulting in the flow folding back in on itself.

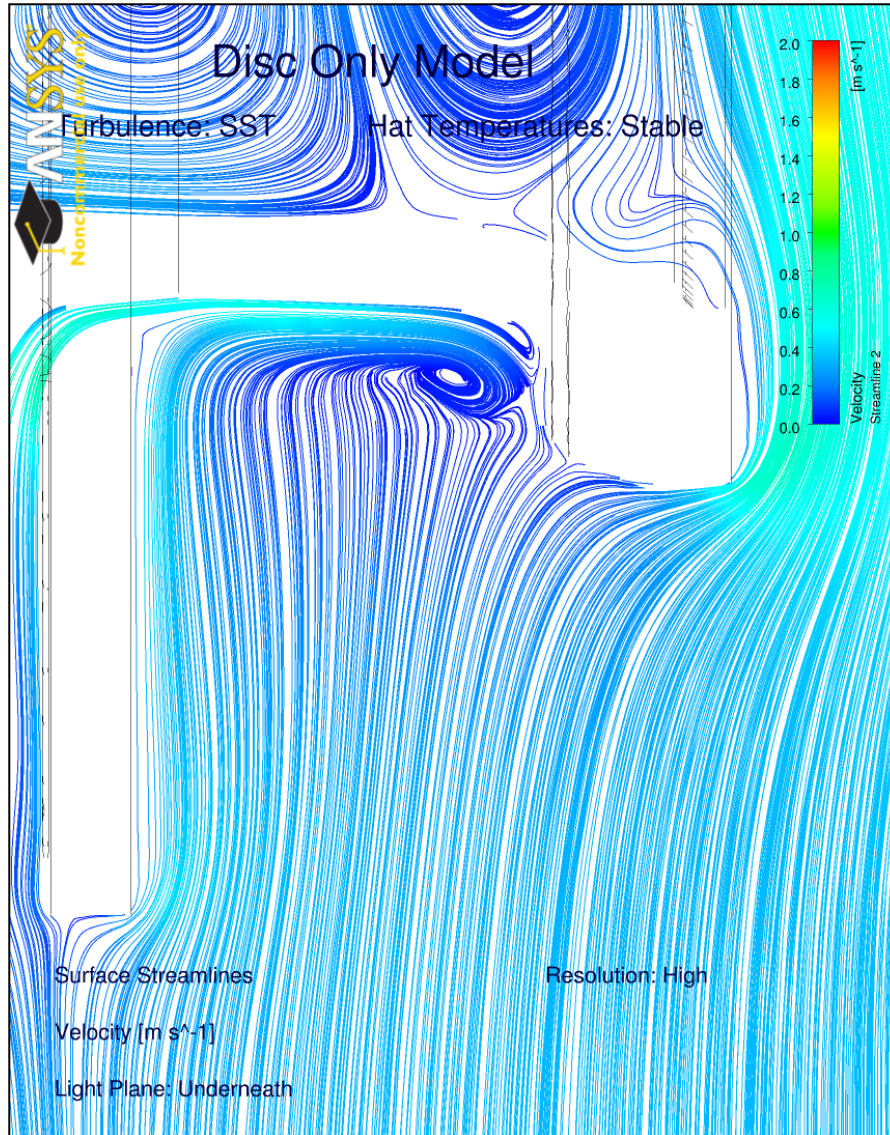


Figure 8.14: Airflow streamline CFD results in the axial plane at the outboard friction surfaces on the lower half of the disc brake (cross section view).

The airflow on the upper section (Figure 8.15) is the opposite of what occurs on the lower section. Airflow into the vanes now transpires at the ID, with the OD becoming the outlet, but the volume of entering air is much reduced. Airflow leaving the vane channels at ID is a clear differentiation between stationary and dynamic flows as this phenomenon does not occur in the latter. At the 0° position, air is drawn downwards off the outboard surface, towards the hat. A stagnation point is subsequently created approximately $\frac{1}{3}$ of the way up the upper outboard friction surface, with most of the downwards drawn flow moving away from the ID entry, due to flow entrainment by the fast moving air flowing around the hat. This only leaves a little volume of air to be taken into the 0° vane, reducing the in-vane cooling potential once again.

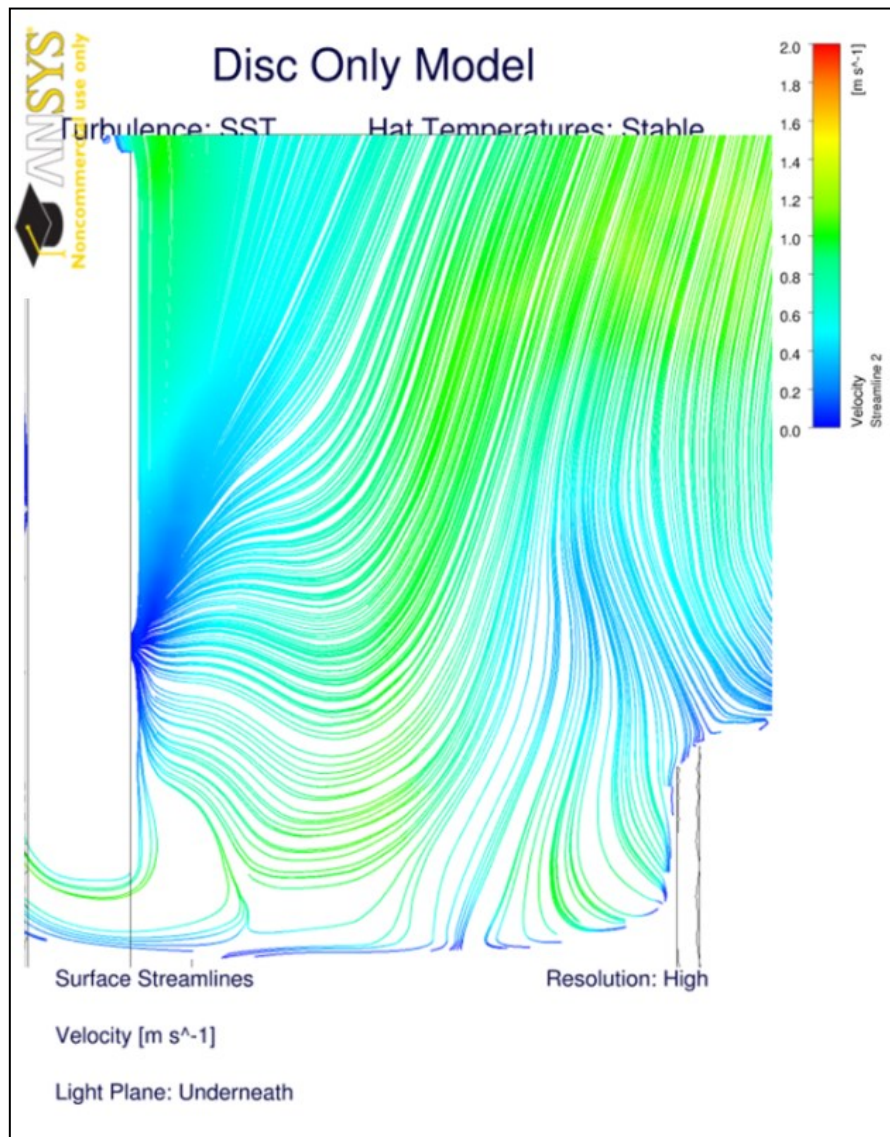


Figure 8.15: Airflow streamline CFD results in the axial plane at the outboard friction surfaces on the upper half of the disc brake.

Only a small amount of air is drawn into the ID of the 0° vane and its adjacent neighbours. Reasoning behind the low volume entering these vanes is similar to the 36° vane (with dual recirculation) as the suction from the vane is weaker than the entrainment by the free stream. With a lack of air in the vane channel, the in-channel pressure is also low, creating a gradient between the higher external and lower in-vane pressures. It is the formation of this pressure gradient that draws some airflow into the 0° vane, which creates the stagnation point on the friction surface. The reason a dual recirculation region is not present between the 0° and 30° vanes is that the airflow drawn down from the friction surface is now far enough away from the lower ID vane exit airflow, like seen in the 36° vane.

Figure 8.16 also illustrates why the exiting lower ID airflow had a greater amount of molecules passing through a smaller area. Heat energy transferred to the air via convection causes the air to increase in temperature. As it does it expands, reducing in density. However, the lower vane channels are shaped like a converging duct, causing a greater amount of air molecules to pass through a smaller cross-sectional area, which increases the in-channel pressure and ultimately the air velocity. Low pressure air external to the vanes are consequently not able to enter the vanes in this location, causing the blockage effect previously discussed.

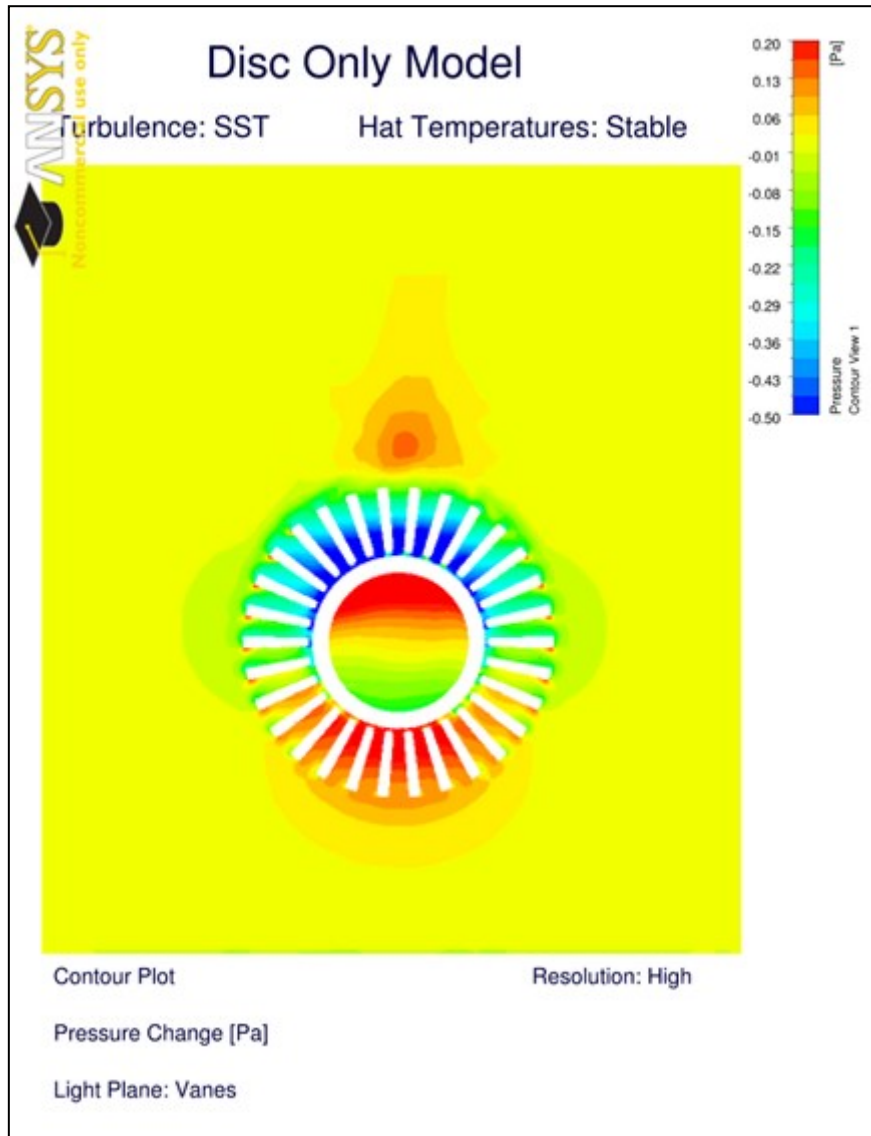


Figure 8.16: Pressure change from atmospheric conditions.

8.3.3 Qualitative Airflow Validation

Thus far, CFD results for a disc brake only model have been presented, with validation of air temperatures given and shown to fall within an acceptable accuracy tolerance. To confirm the

nature of the flow, hot wire anemometry experiments are usually conducted to find air velocities, which are then subsequently compared to the CFD. Although the hot wire anemometry equipment was available at Cranfield University, it was not used as there was no capability of calibrating the apparatus to such low speeds; within the region of 1 m/s. To install further confidence in the CFD results, a qualitative validation process was devised to confirm the airflow characteristics rather than the traditional quantitative approach. Firstly, this approach will be used to investigate the flow regime in operation before moving onto the validating the CFD results, with a final section investigating how the reinstallation of the caliper affects the buoyant airflow.

8.3.3.1 Flow Regime Around the Hat Section

A degree of uncertainty as to which flow regime the air is in over the disc brake surfaces, was generated by both the analytical work in Chapter 7 and the results in presented Table 8.1, where laminar and SST turbulent models predicted temperatures closest to those measured at different thermocouple positions. By combining a light plane, created from the low power laser, and the introduction of the neutral buoyancy smoke to the airflow, photographic snapshots were taken and compared with the CFD results. The light planes were orientated in the vertical position to maximise the photon exposure in it, maximising the potential for effective visualisation.

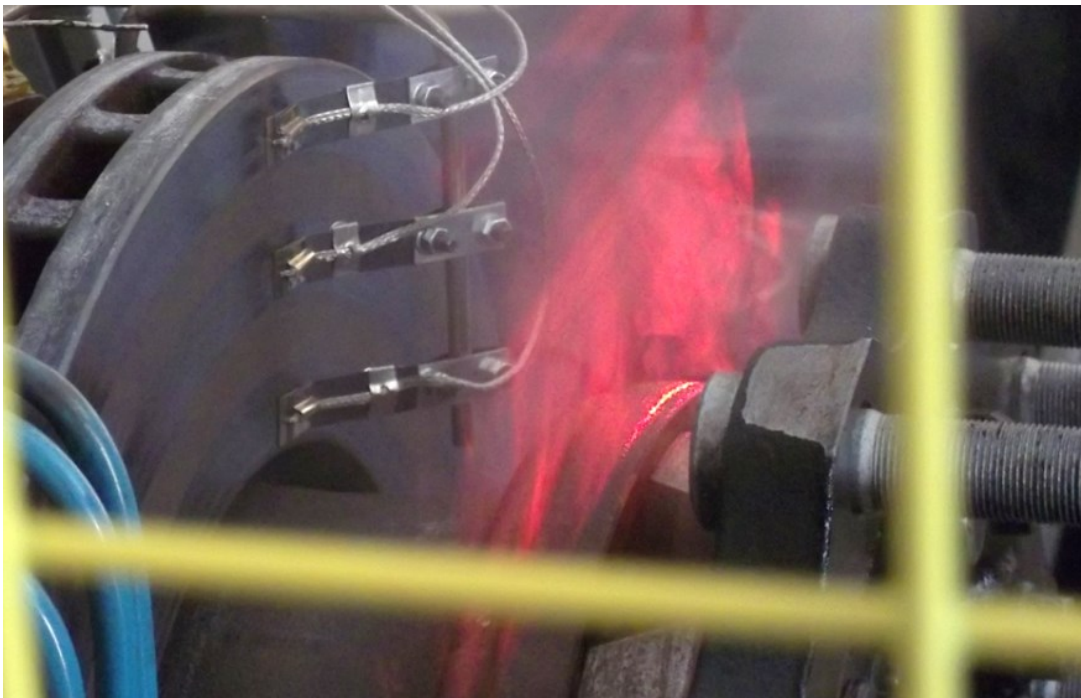


Figure 8.17: Light plane in the Flange location, suggesting flow over the hat is the laminar regime.

From Figure 8.17, it appears that a laminar flow regime is present over the flange/hat region. There are no large eddy formulations seen on the trailing side, which would be expected if fully

turbulent, with the flow streams appearing to smoothly converge. However, this finding was not permanent. Large periodic fluctuations within the flow were consistently seen, as per Figure 8.18. The presence of fluctuations describe the internal flow forces dominate the viscous forces, a typical characteristic of a turbulent regime. In low turbulent flow, fluctuations of this nature are can be the result of a Karman Vortex Street formation.

According to Çengel and Cimbala (2004), the formation of a Karman Vortex Street only occurs when the flow Reynolds number is between 40 and 400. Using equation (4.9), the flow over the hat region was calculated at approximately 19,000 when taking the maximum velocity predicted in Figure 8.11 (1.7 m/s) and the air properties values presented in Appendix L, taken at 100°C. Recorded flow fluctuations are consequently a function of flow turbulence rather than a Karman Vortex Street. Subsequently, both laminar and turbulent flow regimes were simultaneously recorded over the same geometry. This proved further evidence showing that the regime was in a transitional, unsteady laminar state between the two.

In light of this, it is no surprise that no CFD model proved more accurate than any of the other substitutes as they were derived for either the laminar or turbulent regimes, not specifically designed for a transitional period. Complications when attempting to model transitional flow regimes with general-purpose CFD code were shown by Di Pasquale *et al.* (2009). The problem is not the turbulence models used per se, but the inability of the CFD code to reliably calculate local operations. Further development by authors such as Menter *et al.* (2006) have improved the transitional modelling with general-purpose CFD codes, however these transitional models were not sufficiently advanced to be included in the software package used at the time on conducting the work. At this time, the required localised operation for buoyant flow could only be achieved via specifically written code, which is deployed in specialist subroutines.

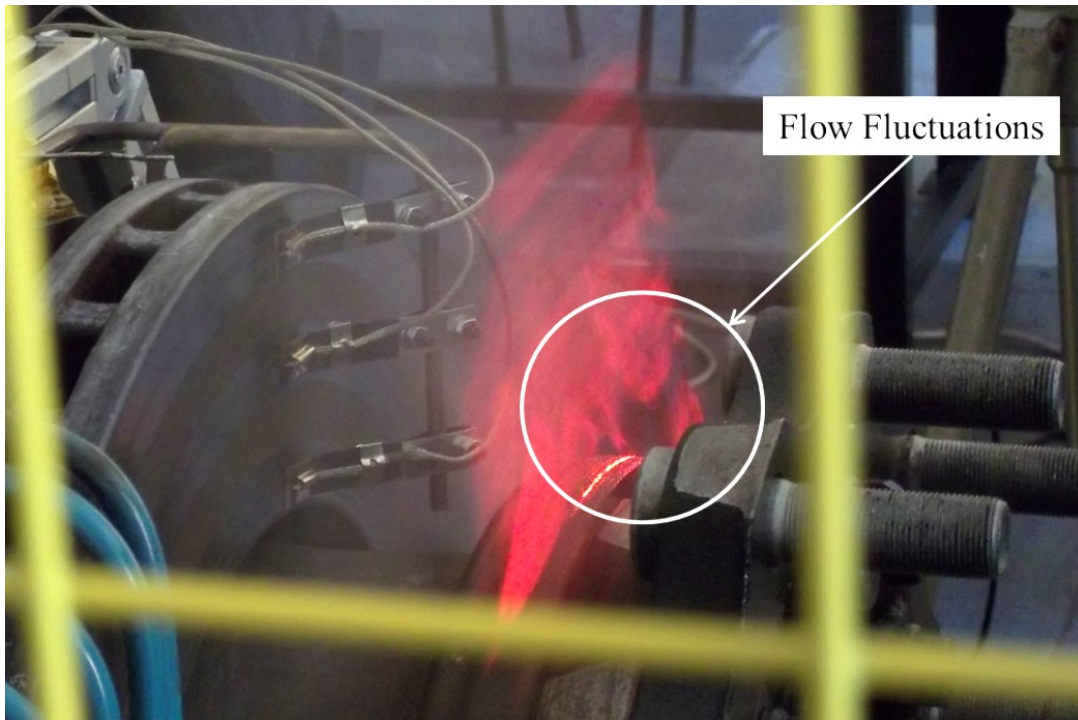


Figure 8.18: Light plane in the Flange location showing flow fluctuations.

8.3.3.2 CFD Qualitative Validation

Numerous flow features that are specific to the stationary CV disc brake were discussed in section 8.3.2. The aim of section 8.3.3.2 is to provide sufficient evidence to prove that general-purpose CFD is capable of defining the global flow field, even with the inherent transitional regime issues found by Di Pasquale *et al.* (2009) and hence, further validate the work presented in this Chapter. Further validation procedure will be performed by comparing the CFD results with photographs from the smoke machine testing.

Two ‘holes’ are evident in the light plane when the laser was positioned at flange position (light plane A), displayed in Figure 8.19. As the light planes have all been positioned vertically, results are limited to motion in the vertical direction only. These ‘holes’ were created by air having momentum in a non-vertical direction. Results from the CFD analysis predicted the presence of vortices in the same locations, clearly visible (Figure 8.9, Figure 8.11 and Figure 8.12), which does provide an adequate explanation of their presence. Circular momentum is hindering the light plane from detecting airflow in these regions, but providing further confidence in the CFD results.

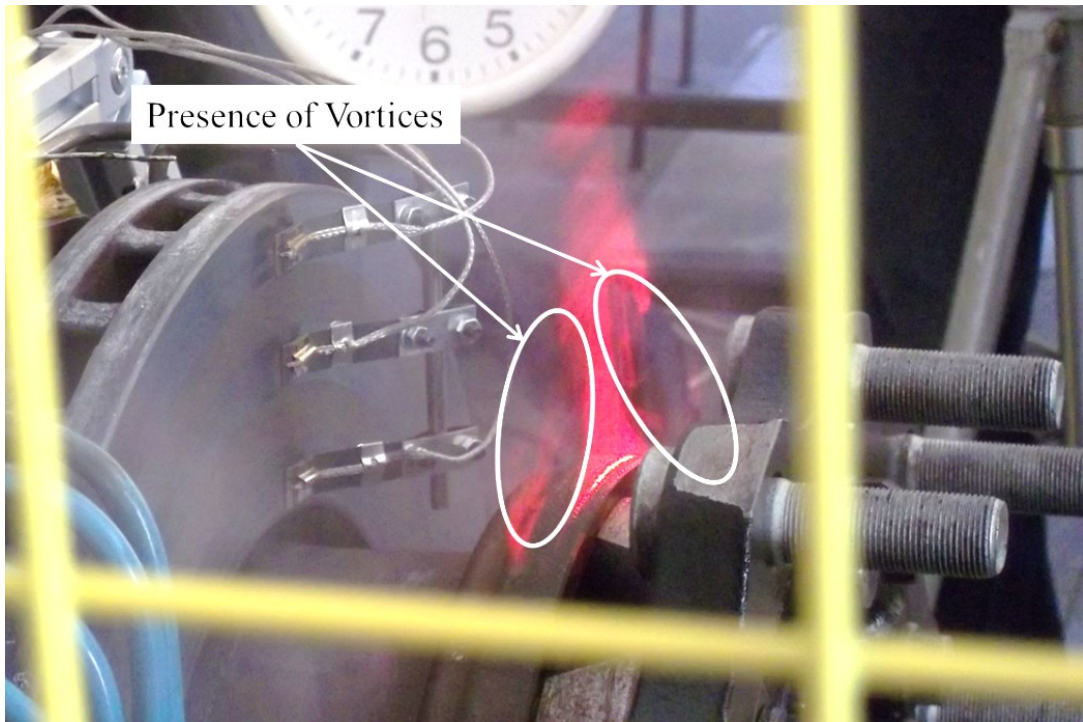


Figure 8.19: The presence of weak vortices creating holes in the light plane.

Figure 8.20 shows the results from smoke machine testing in the light plane B position (central vanes). To test whether the predicted deficiency of the upper in-channel convective cooling does indeed occur in reality, the smoke probe was positioned such that the smoke was channelled directly into the ID, at the mid (90°) position. The laser beam edge is visible on the disc brake but the lack of smoke leaving the channels prevents the light plane from being observed. Yet, smoke was deflected to an area outside the light plane in sufficient volume to demonstrate a clearly emerged airflow pattern. A blockage to the vane inlet was predicted by the CFD (Figure 8.11) and Figure 8.20 demonstrates that this phenomenon does indeed transpire in reality. The smoke was heavily deflected away from the vane inlet and pushed over the hat section.

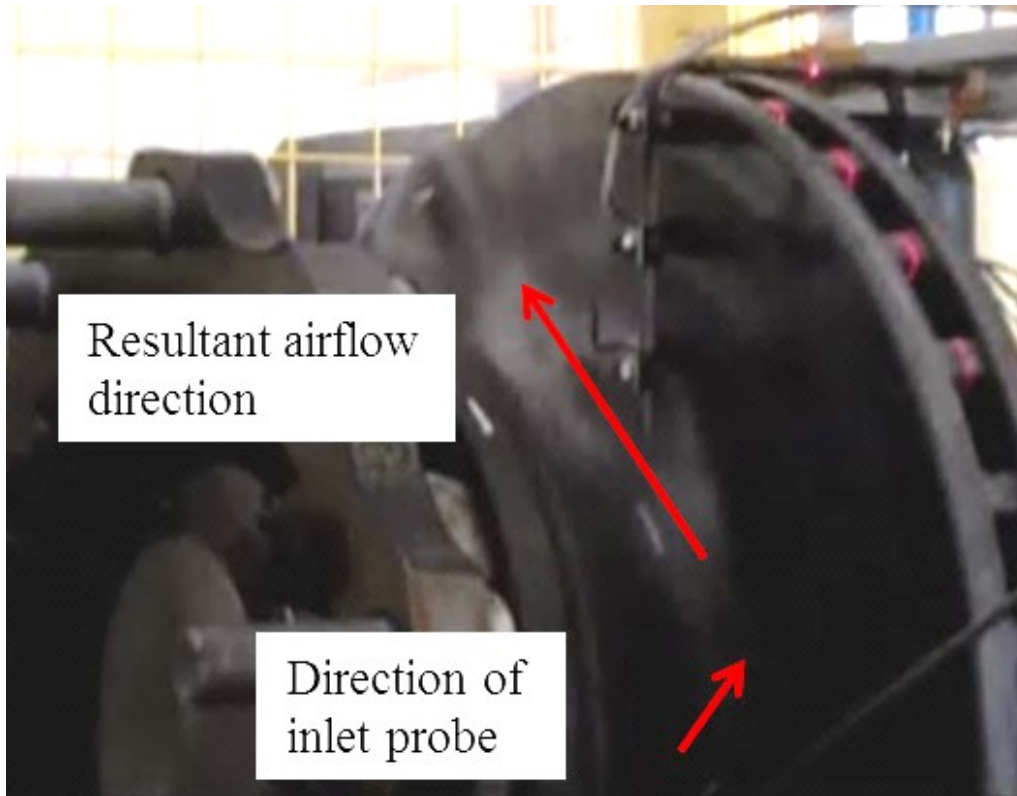


Figure 8.20: Airflow forced into upper ID regions does not travel through the vanes channels.

Remaining on the same light plane, Figure 8.21 captures the airflow when the smoke machine probe tip is positioned directly below the disc brake, at the 180° position. Some of the smoke is passed directly into the lower vanes, with the remainder deflected over the friction surfaces. On exiting the lower channels, the airflow is projected axially across the hat section, in the same fashion as the predicted in Figure 8.11, creating the blockage effect to the mid and upper vane channels described previously. Supporting evidence of the blockage effect has been achieved through the combination of evidence shown in Figure 8.20 and Figure 8.21.

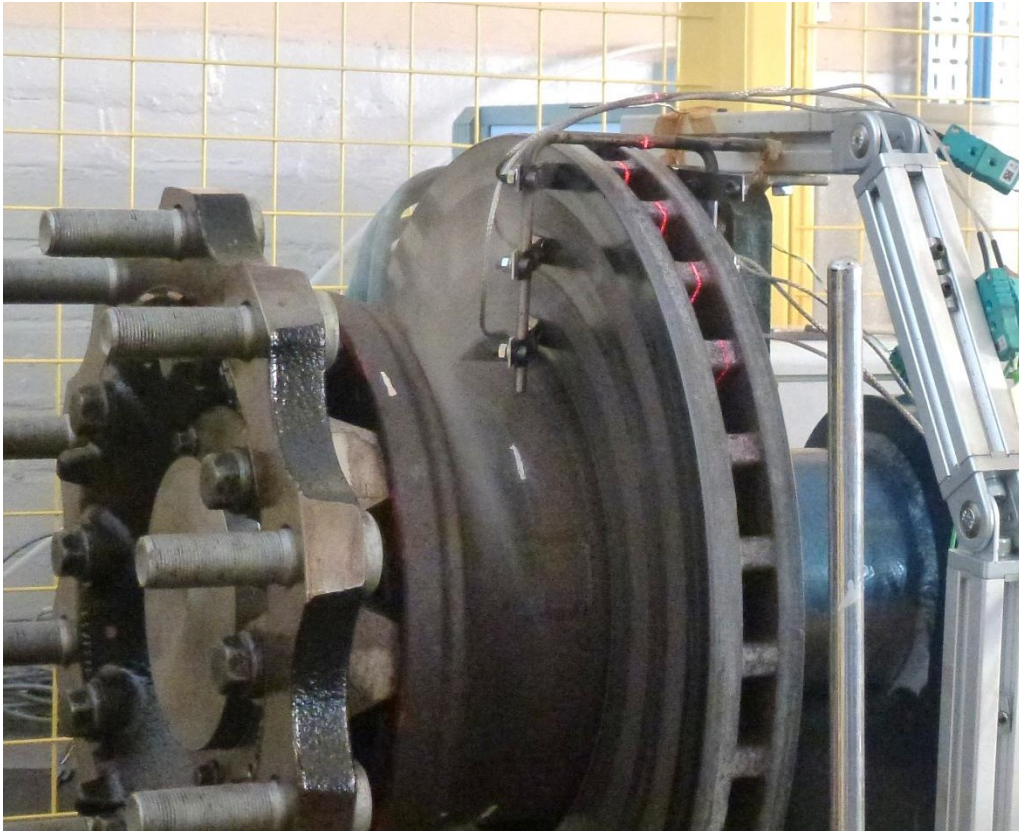


Figure 8.21: Evidence of exiting ID airflow causing the upper inlet blockage.

The final validation picture to be discussed is Figure 8.22, with the aim being to confirm the presence of predicted recirculation regions in slow speed flows. Obviously, it is impossible to observe the in-vane airflow, but the CFD analysis did predict multiple recirculation regions within them and this phenomenon needs evaluating. The presence of low speed, external recirculation region predicted by Figure 8.14 was investigated by smoke machine testing.

With the probe head again positioned directly below the 180° vane channel, smoke was forced to travel through it. Again, the majority of the smoke was dispersed around the sides of the hat with the quickly moving bulk flow, leaving no visible trace due to an insufficient volume in a signal region. Nevertheless, a small cloud was detected on the neighbouring bolt surface. The existence of the smoke cloud was constant for the entire time the probe head was positioned, signalling that the cloud was not an instantaneous occurrence. The reason why the cloud did not disappear was that it was a flow recirculation region, previously predicted in Figure 8.14.

In conclusion, the described recirculation region predicted by the CFD analysis has been shown to exist, confirming the coding within the CFD programme had the ability to accurately predict low energy level recirculation regions. Therefore, it can be concluded with a high confidence

level that the in-channel recirculation must also exist, creating the channel entry barriers, seen at the OD locations, resulting in the adverse flow characteristics described in section 8.3.2.

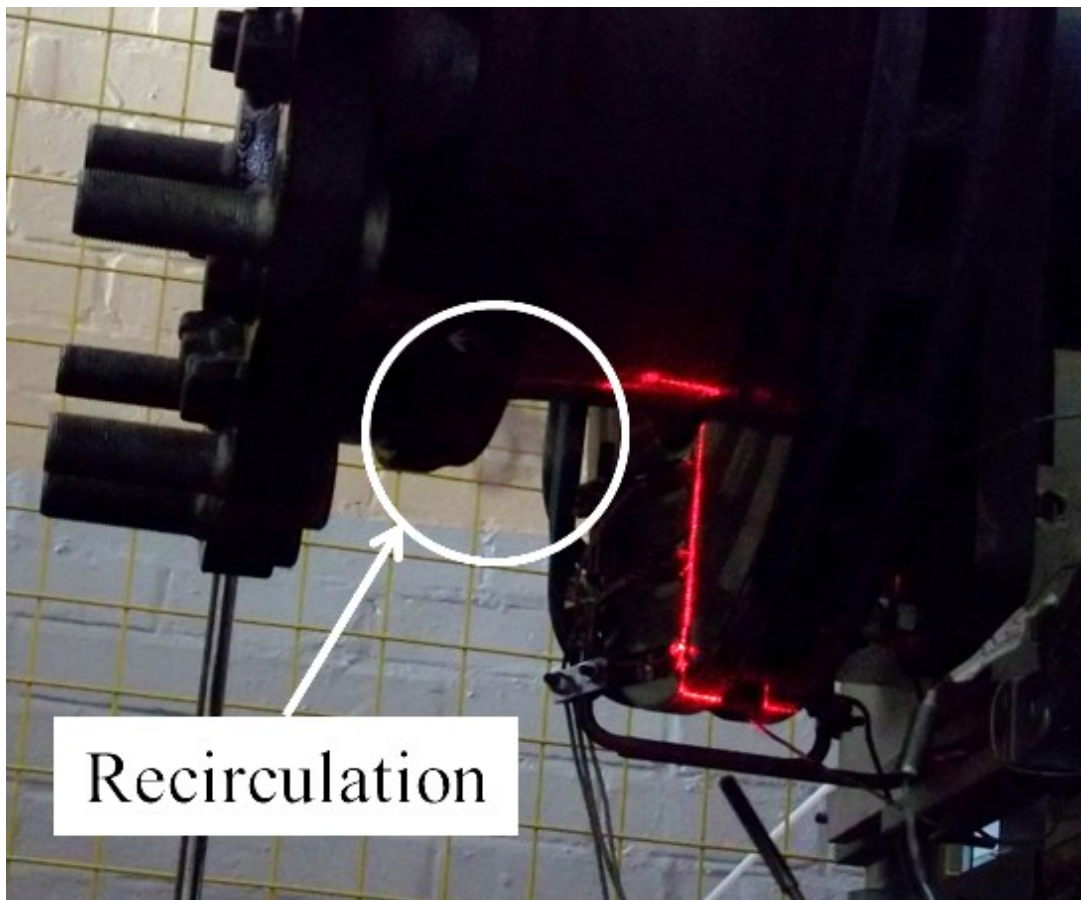


Figure 8.22: Existence of an external region.

A combination of CFD analysis and smoke machine visualisation testing has confirmed that the airflow around the stationary disc brake actually hampers the overall cooling capability. With the thermal mass of the disc brake being an order of magnitude greater than that of a passenger vehicle, the cooling time is significantly enlarged. The consequences of the presented results are that the unoptimised cooling design of an anti-coning, straight vane CV disc brake will keep the it is temperatures hotter for longer, which will resultantly increase the maximum temperatures seen in the caliper components. This is the real risk associated with poor disc brake cooling as potential overheating issues with seals and electrical components housed within the caliper may occur from these elevated temperatures. This fear is greatest on applications where the parking brake is consistently applied, for example bus routes where ambient temperatures are high, or parking after long gradient descents. Both of these scenarios will be very challenging for a CV EPB.

8.3.3.3 Effect of the Caliper on the Airflow

Having successfully generated and validated a basic disc brake only CFD model, the initial intention was to increase the modelling complexity by conducting a full brake assembly model. However, considering the basic disc brake only CFD model had over 9 million elements, taking more than two days to complete, it was decided the meshing process and the time to convergence needed to conduct the full simulation would not be justified by the generated results. Instead, the relatively quick smoke machine testing was conducted with the caliper attached to the Thermal Rig to allow more qualitative analysis to be conducted.

To begin, the volume of air passing over each side of the friction surfaces was investigated by again placing the smoke machine probe below the brake. Although it has not been shown here, when the caliper was not installed on the Thermal Rig, an approximately equal amount of smoke passed around either side of the hat section, causing an equal amount of airflow over both sides of the disc brake. A definition of the two sides of the assembly, termed caliper side and free side, is given in Figure 8.23. An equivalent degree of heat transfer therefore transpires from both halves of the disc brake. As seen by Figure 8.23, the symmetry is broken when the caliper is present. With the probe tip located underneath the caliper, air is entrained from the caliper side to the free side of the disc brake. Subsequently, the greater volume of air passing over the free side will increase its h_{conv} value, compared to the disc only CFD results.

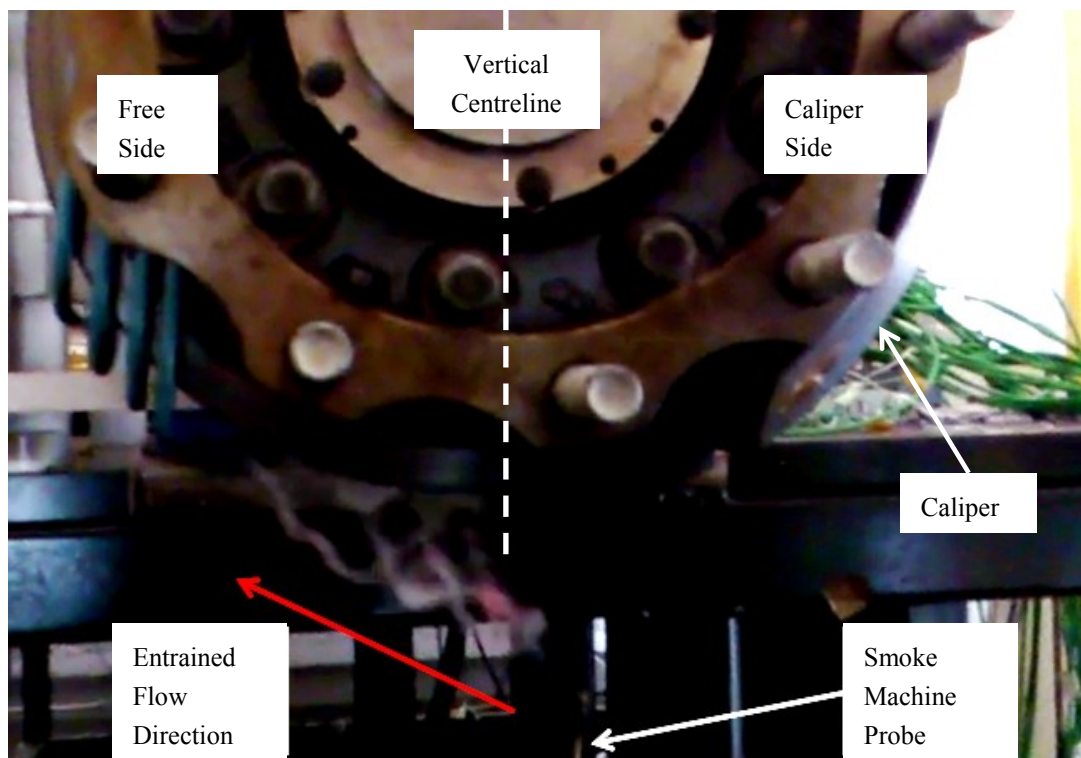


Figure 8.23: Caliper presence causes more air to be entrained over the free side of the disc.

The Elsa 225 brake caliper is of a sliding type configuration, constructed of multiple components. Small air passages are created between the gaps in caliper components in which the flowing air could take to help re-establish a small portion of the convective heat transfer from the caliper side of the friction surfaces. With the smoke machine placed below the pad carrier outer surfaces (Figure 8.24), it was possible to demonstrate that the majority of the airflow passed directly over these gaps rather than flowing into them. This has implications long term during the cooling phase as practically no airflow is reaching the caliper side friction surface, reducing the convective dissipation further and increasing the importance of the less proficient conductive cooling.

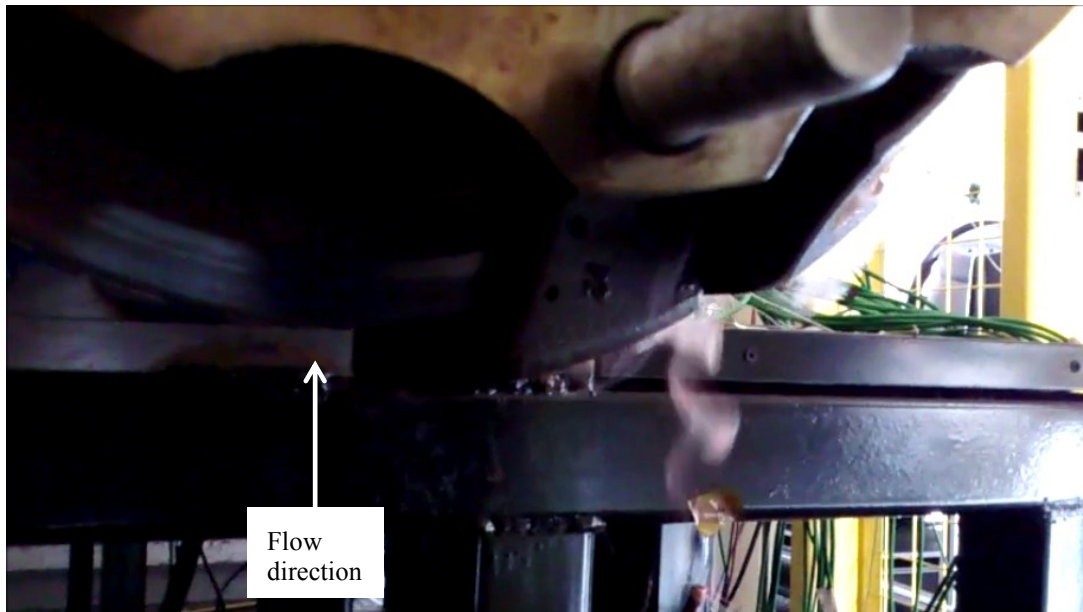


Figure 8.24: Passages between caliper not providing air passages to vane inlets.

By moving the smoke probe around to the side of the caliper, the influence of the caliper on the airflow was further investigated. In Figure 8.25, the probe was positioned such that smoke was projected towards the opening between the circumferential disc brake surface and the bridge. According to the predicted disc brake only CFD results, the inlet to the vane channels are on the OD. By introducing the caliper, the gap created by the bridge will have one of two potential effects. Firstly, it is feasible the bridge could act as an air splitter, forcing an increased amount of air into the upper OD channels. The increased amount of air would improve the airflow through the channels, increasing the convective heat transfer from the disc brake, which is a favourable outcome. Alternatively, the caliper could act as a barrier to the channel entrances. In this latter case, the airflow into the upper channel OD inlets was reduced from the presented CFD results, negatively impacting heat transfer capabilities.

As depicted in Figure 8.25, the result is that the bridge does not act favourably for heat transfer. Airflow passes straight over the bridge and not into the channels, which will cause low pressure recirculation regions to occur in these upper channels, on the caliper side of the disc brake. The realisation of this result is that the possibility of multiple dual-recirculation regions is high on the caliper side, when the caliper is attached. This differs significantly from the disc brake only CFD modelling results, where only a single dual-recirculation region was predicted. The presented evidence suggests that the caliper negatively influences the disc brake's cooling characteristics.

According to the CFD results (Figure 8.12) a small proportion of the smoke should be seen flowing into the disc brake, at the OD, before reaching the bridge. However, no smoke could be seen entering at the OD. Either the direction of the airflow through the channels had changed with the attached caliper or the dual recirculation regions are present as far round as the 90° vanes, possibly further. There is little chance of the former happening due to the existence of the axial airflow exiting the lower channels, at the ID. Subsequently, the results presented suggest that the cooling properties of the standard straight vane, anti-coning disc brake design are hampered further when the caliper is attached, with multiple dual-recirculation regions likely to be present in the caliper side.

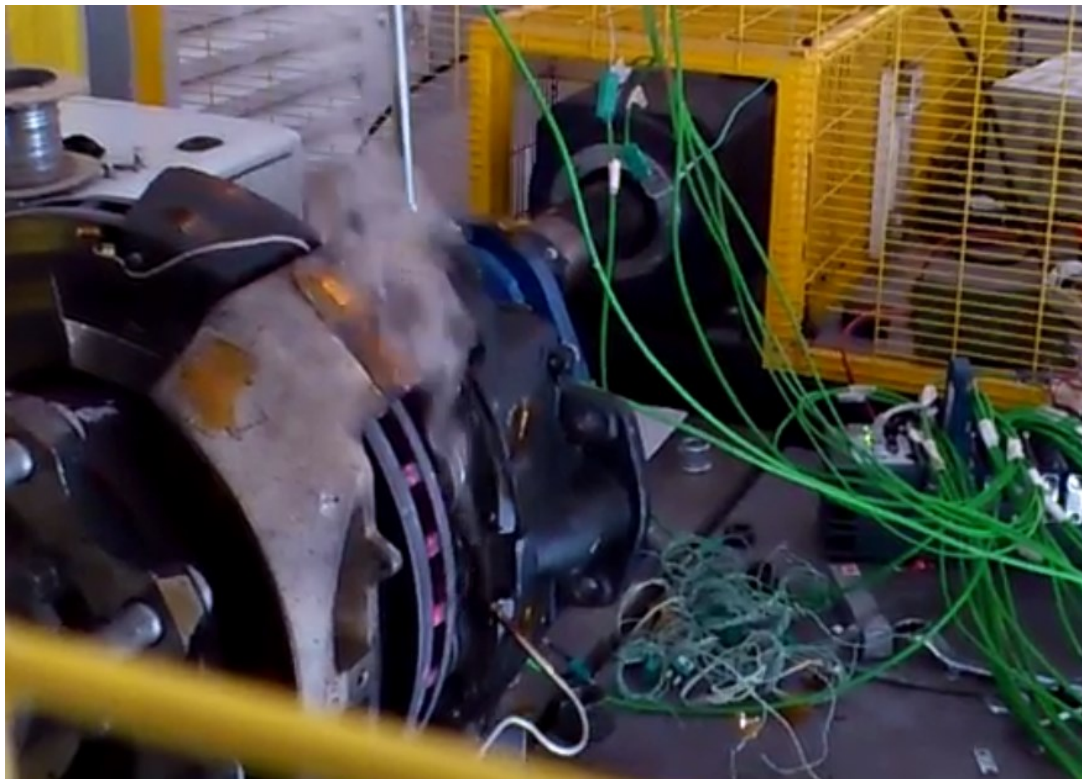


Figure 8.25: Bridge component acting as a barrier to upper OD vane channel inlets.

8.4 Distribution of Heat Transfer Coefficients

Presented here is the first attempt at understanding the distribution of the h_{conv} values in stationary conditions. The results are split into two sections, the first being the generated convective heat transfer coefficients from the CFD modelling. Section 8.4.2 develops the heat transfer distribution discussion further by investigating the change in h_{conv} values as surface temperatures drop.

8.4.1 Convective Heat Transfer Distribution at High Temperatures

Distribution of the h_{conv} values around the disc brake investigations shall begin at the vanes region. By removing the outer disc brake faces, Figure 8.26 shows the variability in convective dissipation from channel-to-channel. Wall effects aside, the largest values are seen on the lower channel walls, reaching 5 W/m²K. Reasonable values are maintained for the middle section (45° to 135°), except in the regions of recirculation, where heat transfer is reduced. Low heat transfer is also seen for in the vanes between 0° and 45°, attaining only 3 W/m²K at the OD. For the dual recirculating channel at 36°, the heat transfer via convection is negligible, as predicted by the velocity streamline results.

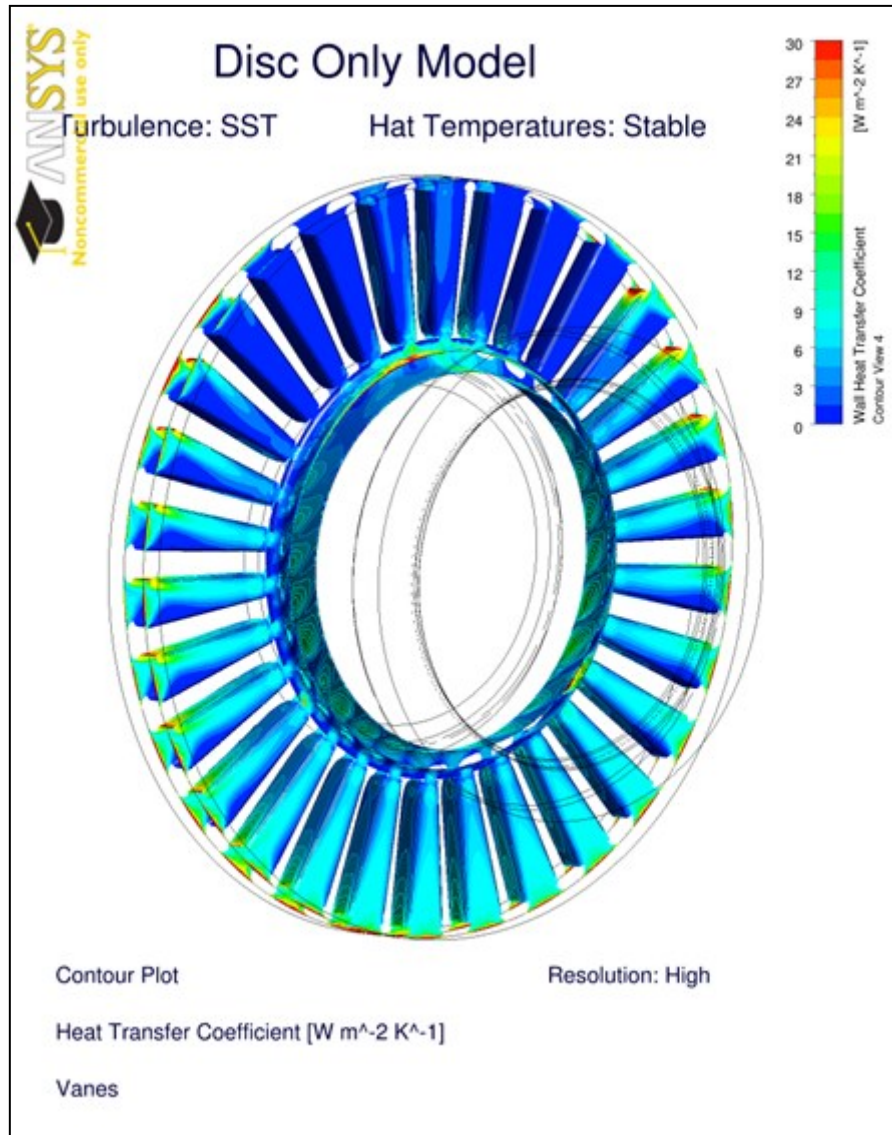


Figure 8.26: h_{conv} distribution of the in-vane surfaces when the friction surfaces are at 350°C.

Looking now at external surface heat dissipation, Figure 8.27 shows that there is only a small amount of variation in h_{conv} values between the upper and lower sections of the outboard friction surface. Values generally remain close to 11 W/m²K throughout the entire surface, increasing only slightly towards the OD. A sharp increase is evident directly at the OD, with exceptionally high values greater than 30 W/m²K displayed. Values of this magnitude are common when the disc brake is rotating at 500 rpm (Figure 4.7). The model was simplified at the disc brake edges by removing the chamfers and a finer mesh was not used in this region either. These actions were necessary to prevent the computational time from extending further, thus the high local values produced in Figure 8.26 and Figure 8.27 can be attributed to these actions. Indeed, high heat transfer coefficient values is a characteristic of a the start of a boundary layer, however these extreme values are present on both the beginning and ending

regions of the flow and are an order of magnitude larger than the average across the friction surface. For these reasons, it was correct to consider these values as erroneous. Since the total area where the error occurs is less than 2% of the total surface area, their influence on the global cooling pattern is minimal.

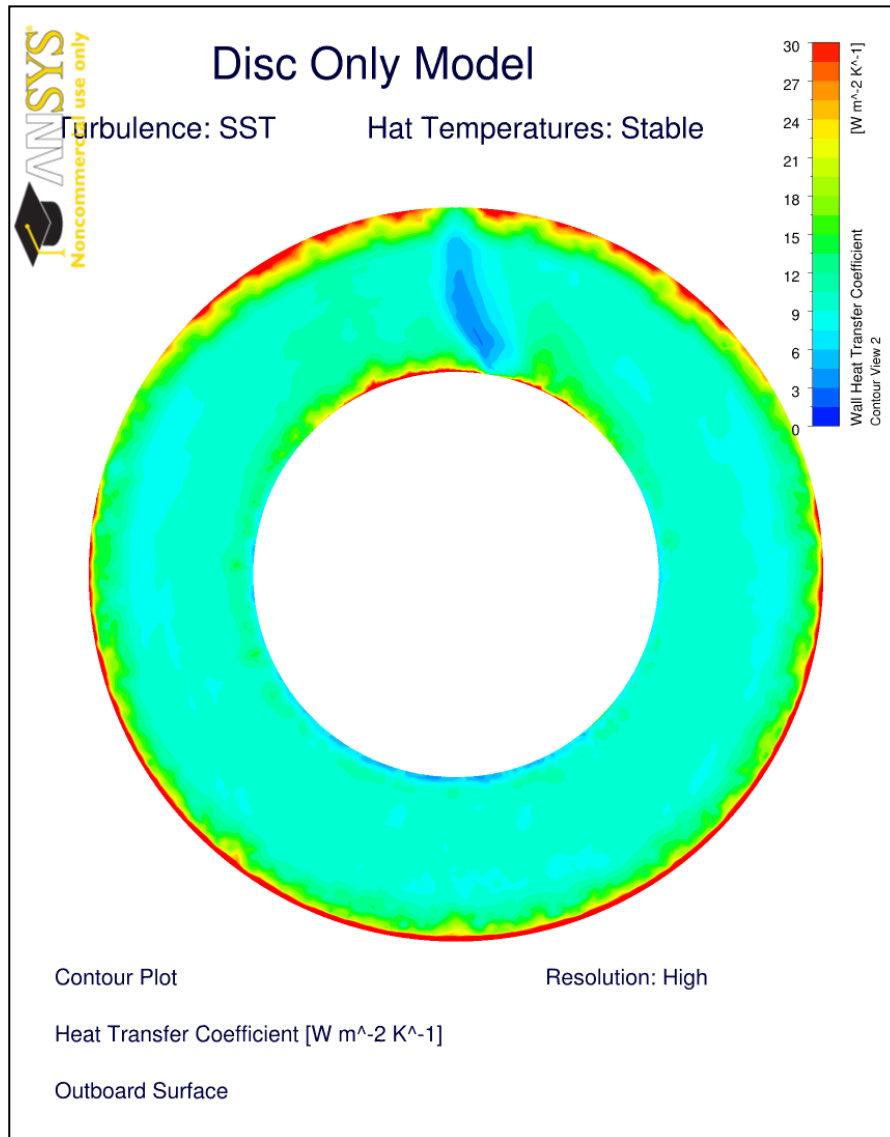


Figure 8.27: h_{conv} distribution off the outboard friction surface at 350°C .

There is an omission to the generalisation made of a relatively constant outboard h_{conv} value, and that is in the 0° vicinity. The stagnation point on the outboard friction surface, discussed in section 8.3.2, is the cause of this h_{conv} drop-off. The absence of air movement inhibits the convection process from occurring, hence the predicted low coefficient value. Interestingly, the same distribution pattern is seen on the inboard friction surface, but with a reduced area of low h_{conv} values. Being of an anti-coning configuration, the suction from the low in-channel air pressure cannot be the cause of the reduced h_{conv} region like on the outboard surface. Instead, it

is a simple function of geometry. Vertically travelling air comes into contact with the bluff ID surface, forcing it to dramatically change direction rather than having a smooth transition to the friction surface; the latter would eliminate the area of low convection.

To complete the HTC distribution study, h_{conv} values over the hat section are discussed. Setting the surface temperature across the hat section to a constant 200°C should result in reduced h_{conv} values when compared with the disc brake friction surfaces. Indeed, this is the case for the most part, shown in Figure 8.28; values are around 3 W/m²K. There is a sharp rise in h_{conv} towards the 0° circumferential position. Air flowing around the hat section, with an Re value approximately 19,000, detaches prior to this point to create a low pressure region. Air is resultantly pulled down off the outboard surface, forming the stagnation point displayed in Figure 8.15. This sucking effect increases the axial velocity component in the air, increasing the localised h_{conv} value. With the largest thermal gradient present between the friction surfaces and air, rather than between the hat and air, the greatest potential for convective heat transfer is away from the hat surface. The suction effect is therefore an undesired effect on disc brake cooling.

Interestingly, the discussed effect of axially travelling airflow, promoted by the exiting air at the ID of the lower channels, influences the highest predicted region of h_{conv} on the disc brake; at the outboard side of the hat. The effect of the axial airflow was that it leads to a larger volume of air passing over the increased hat diameter (Cylinder 1 in Chapter 7). Equation (4.13) states that the characteristic length (or diameter in the case of a cylinder) has an inversely proportional relationship with heat transfer. If everything remained unchanged, a drop in h_{conv} would occur. Conversely, a peak value of 17 W/m²K shows the dominance of the increased airflow volume.

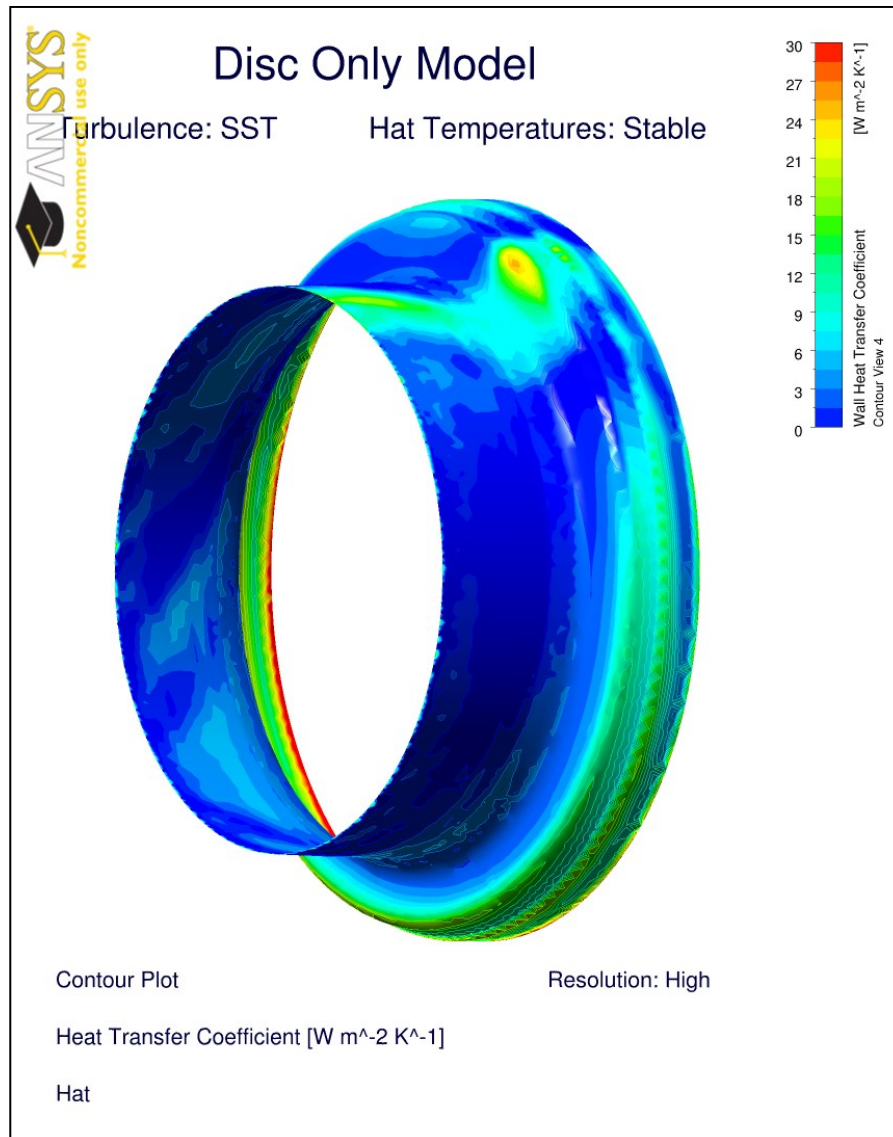


Figure 8.28: Convective heat transfer distribution over hat section outer surface.

8.4.2 Changes in Convective HTC Values During Cooling Phase

To conclude Chapter 8, the change in the predicted CFD h_{conv} values, as the friction surface temperature drops towards ambient, was investigated. An advantage of CFD utilised for this investigation is that the same CFD model, including the mesh, used previously could be deployed once again by simply modifying the disc brake surface temperatures. Three further friction surface temperatures were used, based on the bulk rotor temperature found experimentally, shown in (Figure 9.13); which were 213°C, 112°C and 49°C. An estimation of the hat temperatures could also be made from this graph, which were 175°C, 112°C and 49°C respectively. Noticeable changes in the airflow patterns and the distribution of convective dissipation will be discussed prior to making a comparison between the CFD h_{conv} values and

those predicted analytically in Chapter 7. The same modelling setup was used as before to allow direct comparisons of the results, i.e. the SST turbulence model was used throughout.

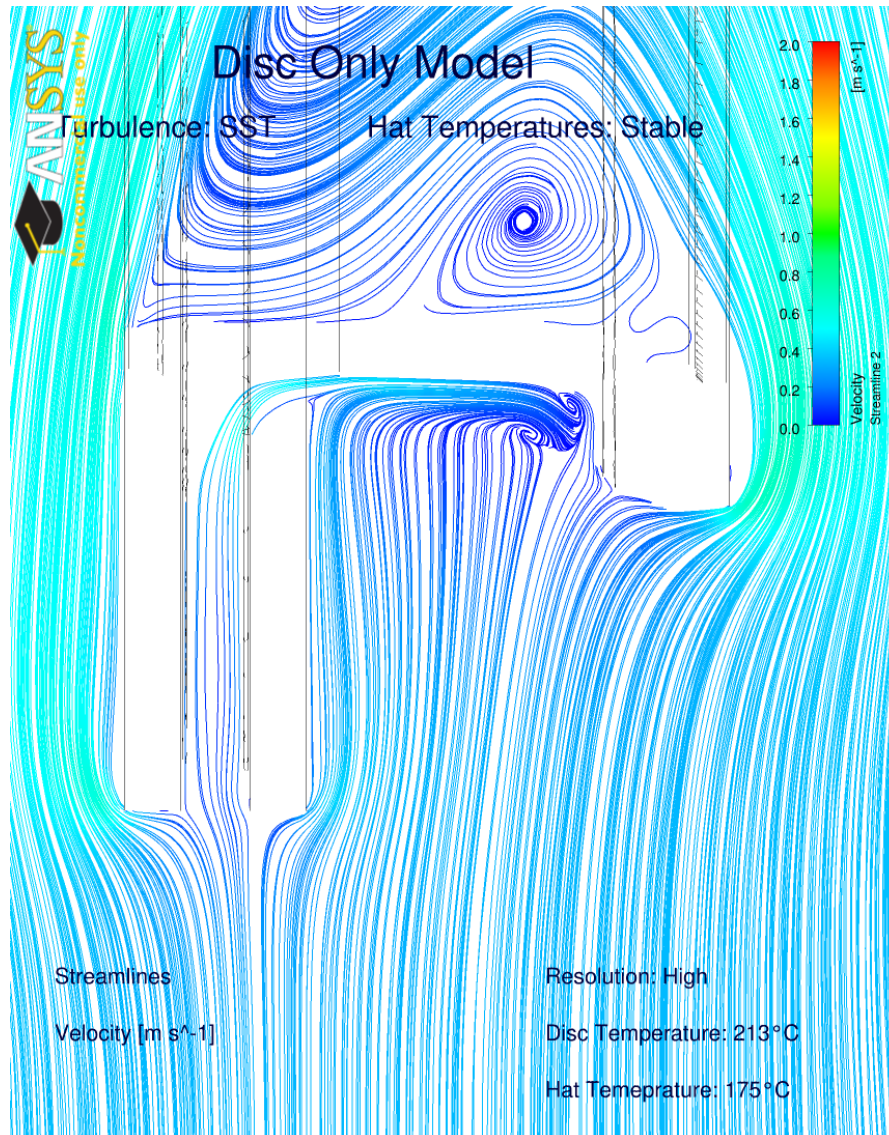


Figure 8.29: The recirculation region in the axial plane, on the lower half of the disc (Figure 8.14)

By looking at the new CFD results in descending temperature order a sense of how the airflow changes as the disc brake cools will be achieved, starting with the 213°C friction surface temperature simulation. Airflow in the axial plane, on the lower half of the disc brake is shown in Figure 8.29. A direct comparison can be made with the same airflow picture when the friction surfaces were set at 350°C (Figure 8.14). Previously, a large recirculation was present towards the bluff surface at the bolt fixing section. It can be seen that the reduction in temperature causes this region to be virtually eliminated. With the surfaces being cooler, the amount of energy transferred to the air is reduced, resulting in the exiting air at the ID having a reduced velocity. Ultimately, this reduces the amount of entrainment of the external airflow in the axial direction.

With air having less axial momentum at the bolt section, there is less energy in the free-stream flow to force the exiting ID airflow to fold in on itself after impacting the bluff bolt fixing surface, thus removing the potential for recirculation.

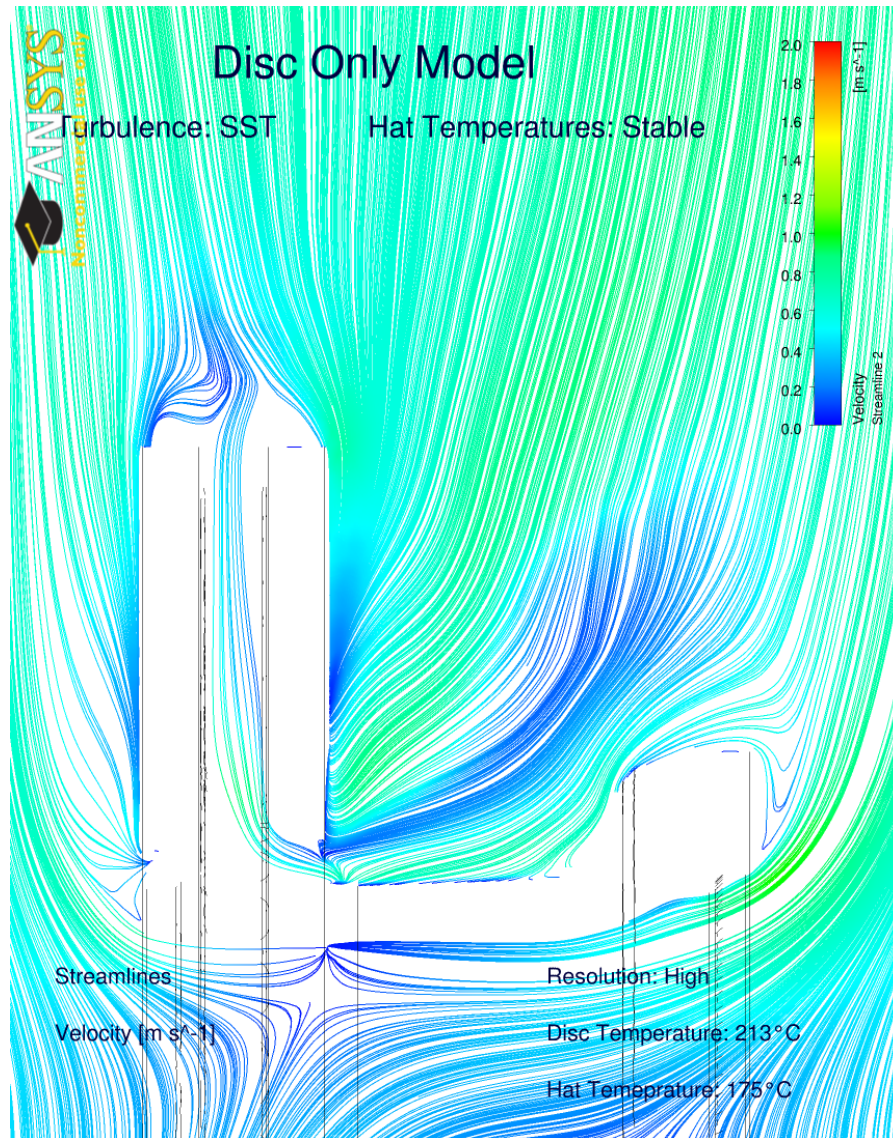


Figure 8.30: Upper velocity streamlines in light plane C at 213°C (can compare with Figure 8.15)

Further evidence of the reduced entrainment is seen in Figure 8.30. Airflow is again in the axial plane, but on the upper half of the disc brake. Comparisons with Figure 8.15 can be made, starting with the stagnation point still present on the outboard friction surface. Originally, low energy air near the stagnation point was pulled down, with a proportion going into the channel. The channel presented the low energy airflow an alternative route. At a lower friction surface temperature, the axial velocity is lower, enabling virtually all the air on the outboard surface to join the free-stream. Subsequently, there is a reduction in air flowing through the central, upper vane channels, which will reduce the h_{conv} value.

However, when the friction surface temperature reduces further to 112°C, the situation reverses. Figure 8.31 demonstrates air flowing around the hat section has little to no axial momentum. This is true until the air approaches the top of the hat (the 0° position), where it is drawn from the bolt section back across the hat and into the vanes. The pull from the in-channel low pressure is now stronger than the external flow entrainment.

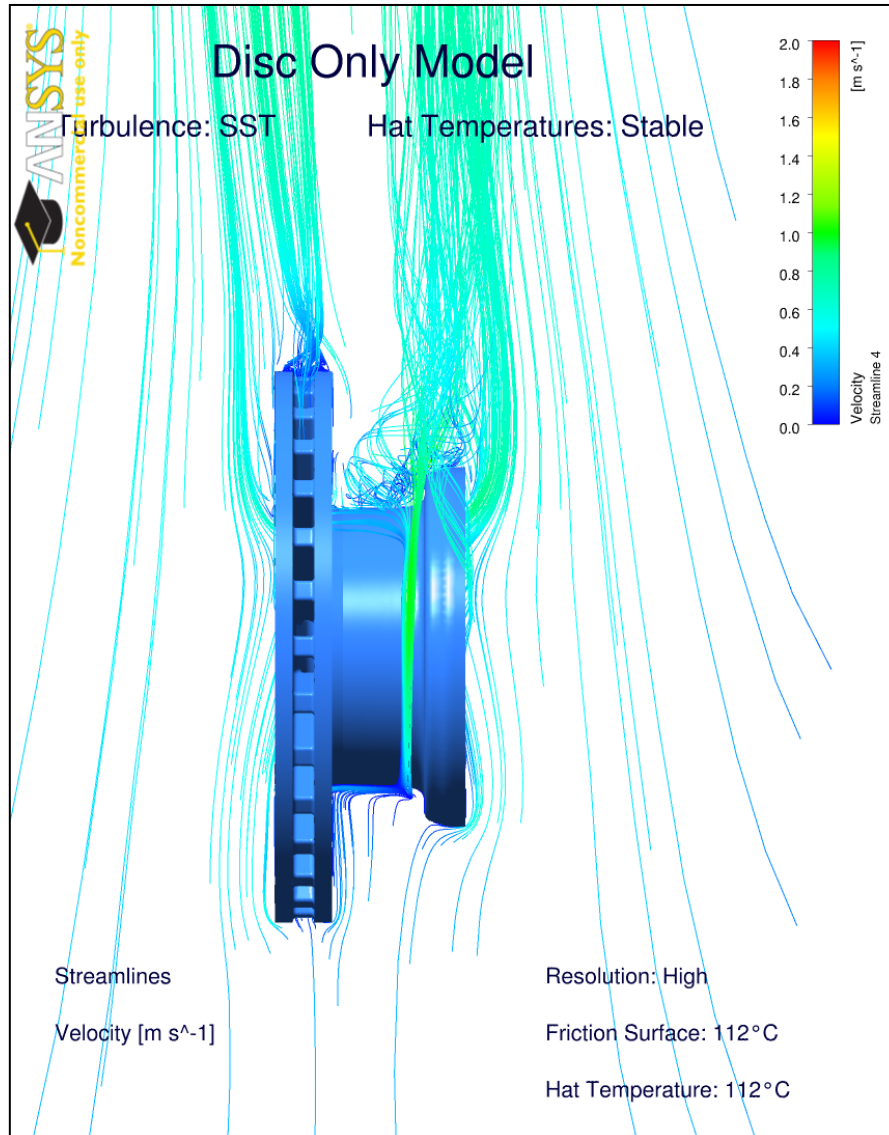


Figure 8.31: Velocity streamlines in light plane B at 112°C

Finally, airflow characteristics for the lowest friction surface temperature simulation (49°C) will be examined. Starting in the axial plane once again, Figure 8.32 shows a significant change to previous airflow patterns. The recirculation at the bolt fixing section has now completely disappeared, with a new recirculation appearing at the ID, in the vane channel exit. This has a hugely contrasting effect to previous temperatures because the external free-stream flow now has a higher amount of energy than the exiting airflow from the vane channel. In fact, instead of

the airflow having axial momentum away from the outboard friction surface, the reverse is seen with air flowing inwards, towards the rotor ID, although the predominant motion is vertically upwards.

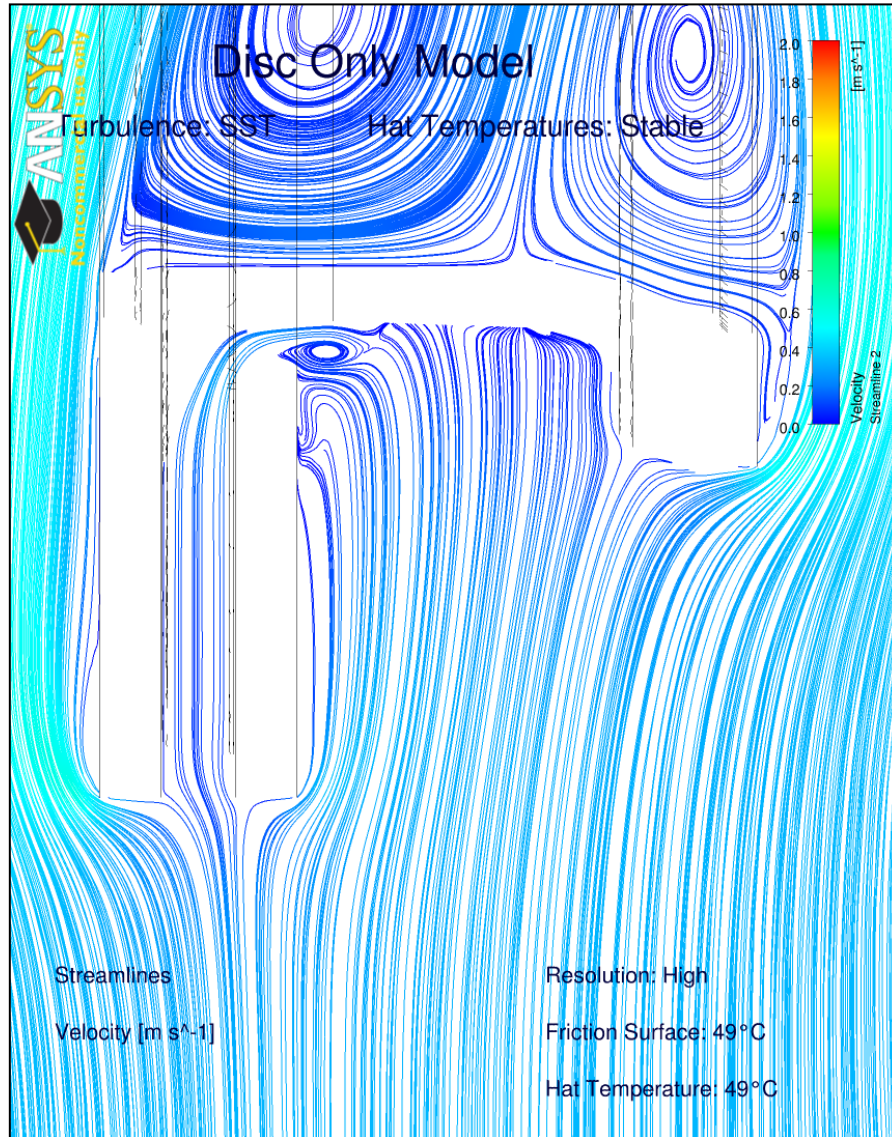


Figure 8.32: Lower velocity streamlines in light plane C at 49°C

Changes in the airflow around the hat also caused changes to the convective HTC surface dissipation patterns. Although air speeds are extremely low, approximately 0.5 m/s, Figure 8.33 indicates that the area of high h_{conv} values around the hat is much larger than for any other friction surface temperature. The lack of an axial momentum allows the airflow to be much more uniform across the hat rather than being pushed across to one side. The maximum h_{conv} is therefore somewhat reduced in magnitude to approximately 15 W/m²K. This is still higher than on the friction surface.

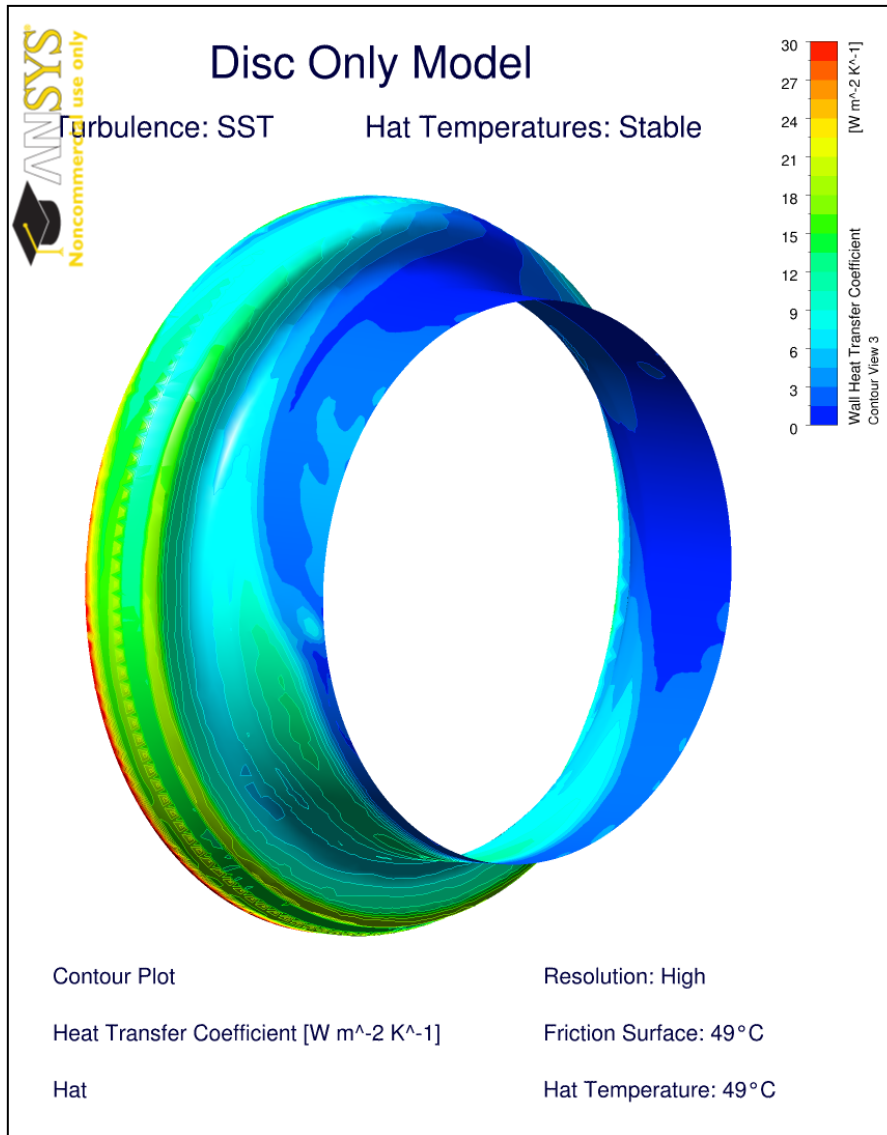


Figure 8.33: Increased area of high convective heat dissipation over the hat section, at 49°C

The large h_{conv} area is however, a local occurrence as it is restricted to the bottom half of the hat section. On the upper half, convective HTC values are close to zero, due to insufficient airflow in this region. With such a small volume of air flowing around from the bottom side of the hat, there is little air available to flow over the upper outboard surface. Resultantly, the stagnation point on the outboard friction surface, originally shown in Figure 8.15, shifts to the OD position at these lower temperatures (see Figure 8.34). A much larger area of zero convective HTC is produced when compared to Figure 8.27.

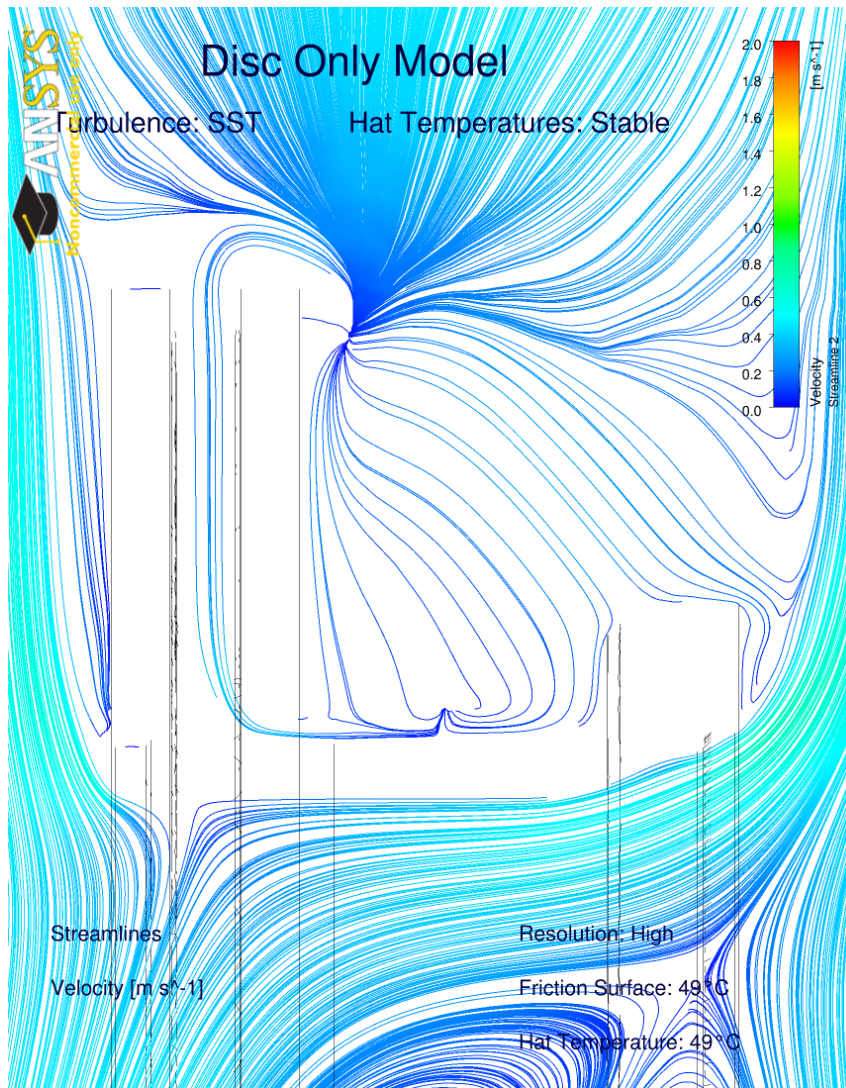


Figure 8.34: Upper velocity streamlines in light plane C at 49°C

To complete section 8.4.2, the predicted average values of h_{conv} produced by the CFD simulations for the inboard, outboard, hat and vane surfaces are presented in Figure 8.35. Predictions of the rotor values (inboard, outboard and vanes) are coloured in red whilst hat predictions are green. To begin, it can be seen that there is little difference between the h_{conv} values on the inboard and outboard friction surfaces when heated to 350°C, as there is only a small amount of additional dissipation occurring from the inboard friction surface. Decreasing the friction surface temperature to 213°C sees the outboard surface value of h_{conv} reduce at a faster rate than the inboard. This increased rate of h_{conv} reduction was common throughout. It has already been shown that as the temperature reduces, the axial velocity component of the air flowing around the hat reduces, pushing the localised outboard stagnation point towards the OD. Below the stagnation point, there is a volume of low energy air, which isn't joining the free-stream flow, causing an area of low heat convective dissipation. Hence, as the stagnation point

increases in height, the area of low dissipation increases and ultimately reduces the total outboard surface h_{conv} .

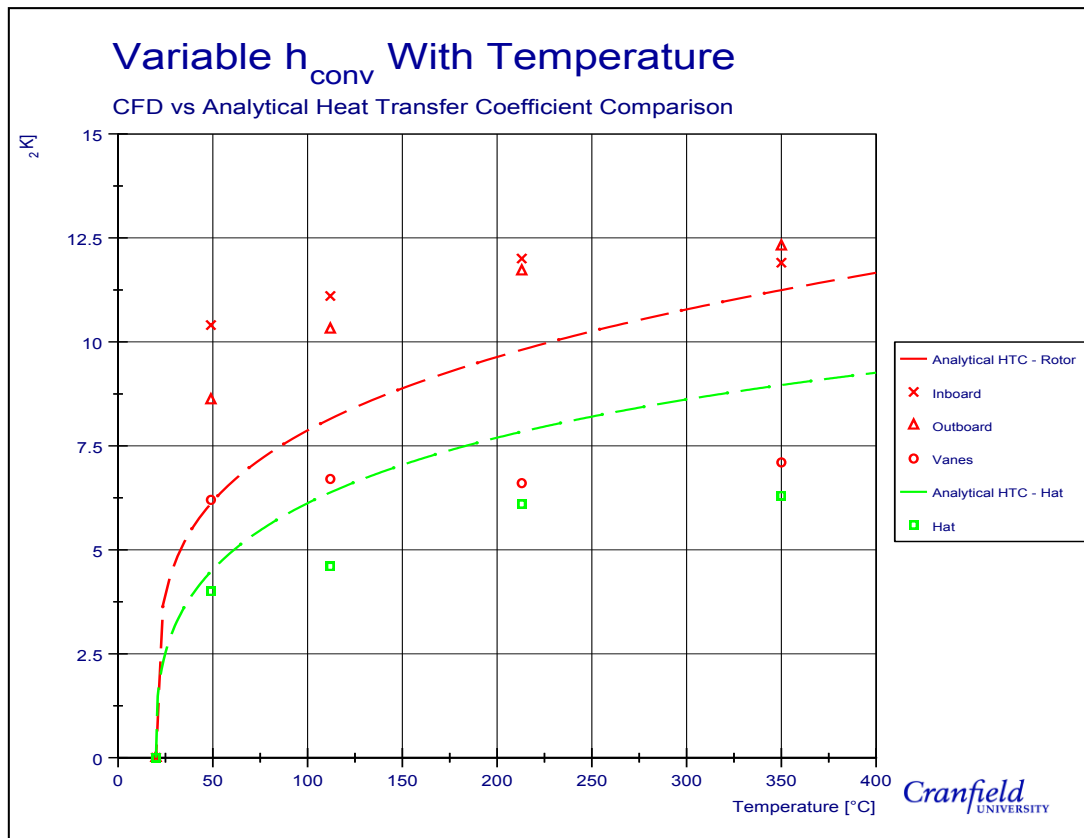


Figure 8.35: CFD h_{conv} values compared to the analytical values predicted in Chapter 7.

Another interesting observation that can be made from Figure 8.35 stems from the airflow through the vane channels. Analytical modelling was used to predict the average rotor h_{conv} value, based on idealised friction surface data leading to a smooth decrease in h_{conv} with temperature. Looking at the vane wall h_{conv} values, a decrease in h_{conv} was predicted between 350°C and 213°C, as would be expected. However, when looking at the next temperatures decrease, from 213°C to 112°C, an increase was predicted. This irregularity can be attributed to the phenomenon already discussed in Figure 8.31. Ejected air from the lower vane channels, at the ID, flows around the hat section close to the bolt fixing section before being sucked back into the central vanes ID, on the upper half of the disc brake. This favourably impacts the amount of heat dissipation as there is more air flowing through the upper channels. Having the ability to calculate the airflow in three dimensions, CFD has produced a more sophisticated result compared to the 2D analytical results, which was validated against experimental results. Only a few temperature points were investigated here. Further modelling would be needed to find the temperature where the air starts to get pulled back across the hat and into the upper channels.

Analytical h_{conv} values produced in Chapter 7 are also shown on Figure 8.35, allowing a direct comparison to be made. In a qualitative sense, CFD predictions match well with the analytically predicted values, demonstrating a similar form, with regards to the decrease in value with temperature reduction. CFD results plateau at higher temperatures slightly more than the analytical results, suggesting less h_{conv} variation with temperature. At low temperature there is a difference of approximately 70% at 49°C, for the inboard surface, which reduces to only 17% at 350°C.

The complex three dimensional flow predicted from the CFD ensured a difference between the two sets of values would be present, yet there were limitations in the simulation process preventing the result from matching better numerically. Two reasons have been identified as potential discrepancy sources. The first relates to the areas of extreme h_{conv} values consistently located towards the edges of the model. It was said originally that these areas will have little impact on the predicted airflow predictions because of their relatively low surface area. This still holds true for the predicted airflow patterns, as proved in the smoke machine validation process. However, calculations of the mean h_{conv} will be drastically hampered by the recorded edge errors as these localised values, in excess of 120 W/m²K, increased the total surface average somewhat beyond the analytical values. Again, the only feasible way to remove this error from the simulation process would have been to increase the mesh density at the geometry edges. This was not done due to the computational power and time constraints associated with making these changes.

The second source of error is more fundamental as it is an error built into the CFD coding. To calculate the h_{conv} , the temperature gradient between the wall surface and the ambient air must be found. Both the wall temperatures and the ambient temperatures are user defined values inputted during the CFD setup process. Like most CFD codes, Ansys CFX calculates the temperature gradient component of Newton's law of cooling, between the inputted wall and ambient temperatures. This is reasonable to do for external surfaces exposed to the fast flowing air. Within the channels however, the air speeds were shown to be extremely low and in a few cases, virtually stationary throughout. In turn, this caused the air temperatures within the channels to severely increase. In these cases, where the air in close proximity to the surface is flowing slowly and at a high temperature, it is argued here that the air temperature value taken should be the in-channel air temperature, not the ambient air temperature, a distance from the surface. In-channel h_{conv} values would therefore decrease significantly. To apply these changes, a separate subroutine would need to be written to bypass the standard CFD coding, so was not conducted during in this investigation.

8.5 Chapter Summary

In Chapter 8, the focus was to better understand the cooling performance of the disc brake when the flowfield investigation is enhanced to a 3-dimensional analysis. To do so, the popular CFD modelling technique was employed. As very little work of this nature had previously been conducted, there was little advice in the literature as to how to setup the model. Thus, an experiment to find the greatest compromise between accuracy and computational time was conducted. An air temperature based validation method was devised that numerically assessed the results of the CFD simulations by comparing them to measured data, achieved through the cooling test procedure. It was found that of the commonly used turbulence models, the Shear Stress Transport model is the most appropriate to use when modelling stationary parking applications.

Stationary braking airflows were proven to have a complexity level of at least dynamic braking application, if not more complex. Confirmation that an alternative modelling approach is required when investigating such an application, as discussed in Chapter 6. Fast moving air exiting the lower vane channels at the disc brake ID, travelling axially, creates a blockage to the upper channel inlets. With the lack of air entering the upper channels, heat transfer capabilities are vastly reduced. Air flow restriction was found so severe in one particular case that a dual-recirculation was predicted within a single vane-channel, stifling all the flow through the entire channel.

Predicted airflow patterns were backed up by the smoke machine testing, coupled with the light plane; the use of this technique was novel within the braking sector. A lack of detected smoke detected on the upper channel exit light plane proved the inability of the disc brake geometry to funnel airflow through these channels. Combining the smoke machine testing with the CFD flow simulations lead to the conclusion that the CV anti-coning, straight vane disc brake design does not cool optimally during a parking application. Consequences of this are that the disc brake remains at a hotter for an extended period of time, transferring surplus amounts of heat energy into the caliper. Elevated caliper temperatures can lead to secondary brake failure problems as thermally sensitive components, located within the housing, can be affected. Moreover, the smoke machine testing was able to capture both laminar and transitional flow regimes simultaneously on over the hat section, showing the flow is in a transitional state. Reynolds numbers were calculated above the known range for Karman Vortex Street, which indicated that the fluctuations in the flow are a function of turbulence.

CFD simulations also produced predictions of surface h_{conv} distribution. Inboard and outboard friction surfaces distributions were both relatively constant, at approximately $11 \text{ W/m}^2\text{K}$, at high

surface temperatures. In channel values were just under half of those predicted the friction surfaces. Coding of the CFD uses takes the temperature difference between the inputted wall and ambient temperatures rather than the localised air temperatures, leading to an overestimation of channel h_{conv} values. In reality, the disc brake is likely to cool worse than the predicted CFD modelling suggests as the caliper negatively impact airflow around the brake assembly, shown by smoke machine testing.

9 Detailed Thermal Analysis of Disc Brake Cooling

FE modelling in Chapter 6 predicted disc brake and pad temperatures which were different to measured values. Identification of the HTC values which should be used for convective disc brake cooling was the subject of the two subsequent chapters. Attention now focuses on developing a method for distinguishing the thermal interaction between components and determining appropriate coefficient values for the other two modes of heat dissipation. In Chapter 9, Thermal Rig modifications and the associated analysis technique for disc brake cooling and energy flow between it and the wheel carrier will be discussed.

9.1 Component Analysis Experimental Method

Experiments conducted as part of Chapter 9, termed Component Analysis Testing, were fundamentally the same as the cooling test experiments presented in Chapter 5, with disc brake heated to 400°C and then left to cool for six hours. The main difference lay in the heating process. In the cooling tests, the induction heater was turned off once the temperature at the disc OD had reached 400°C, whereas for the component analysis tests, it remained at 400°C until the disc had reached thermal equilibrium. The criterion for the disc brake to reach thermal equilibrium was that no thermocouple reading varied by more than $\pm 2^\circ\text{C}$ over a five-minute period.

To gather disc brake surface temperatures during the cooling tests, rubbing thermocouples were used, which were mounted to the Pad Carrier. By removing as many components as possible, including the Pad Carrier, modifications to the Thermal Rig were necessary to enable disc brake temperatures to be recorded. With the reduction in assembly components, an opportunity had presented itself to measure numerous surface temperatures at different locations, which would have usually been obscured by caliper components. Because of the disc geometry, monitoring temperatures in both the radial and circumferential directions was desirable. Yet, with the Pad Carrier removed there was nothing to mount the rubbing thermocouples.

After much iteration, a design to hold a maximum of 42 thermocouples against the disc was fabricated and is outlined in Figure 9.1 and Figure 9.2. A 30 mm aluminium profile frame, made of five straight profile sections with four 135° angles in between, was bolted onto the top and bottom of the caliper axle mount. Seven thermocouple holders were located in the frame, constructed from a yoke section and an attachment bar (both made from steel). Each yoke held six thermocouples, three on either side, placed at the OD, middle and ID positions. The attachment bars were braised to the yokes and go through the frame and held in place by grub

screws. The holes in the frame were positioned such that the rubbing thermocouples were aligned radially with disc brakes axis of rotation. Five were separated by 45° , starting from the 0° reference line; defined as being a vertical line, rising from the disc brake axis of rotation through the upper portion of the disc. Positive angles are those which are positioned circumferentially clockwise from the reference line when viewing the disc brake from the outboard side, round to an angle of 180° , whilst negative angles are those positioned in the reverse direction. Two further yokes are positioned either side of the 0° reference position by $\pm 15^\circ$ which would be used to test the assumption of symmetrical heat distribution through disc centreline.

The naming convention for the thermocouples starts with their circumferential position, followed by a series of letters to describe its position; the first letter (D) represents it is a disc temperature being recorded, followed by either I or O standing for Inboard or Outboard respectively. The final letter outlines the thermocouple radial position so the rubbing thermocouple. For example, the thermocouple positioned circumferentially 90° around the disc, located in the middle of the inboard surface has the name +090 DIM.

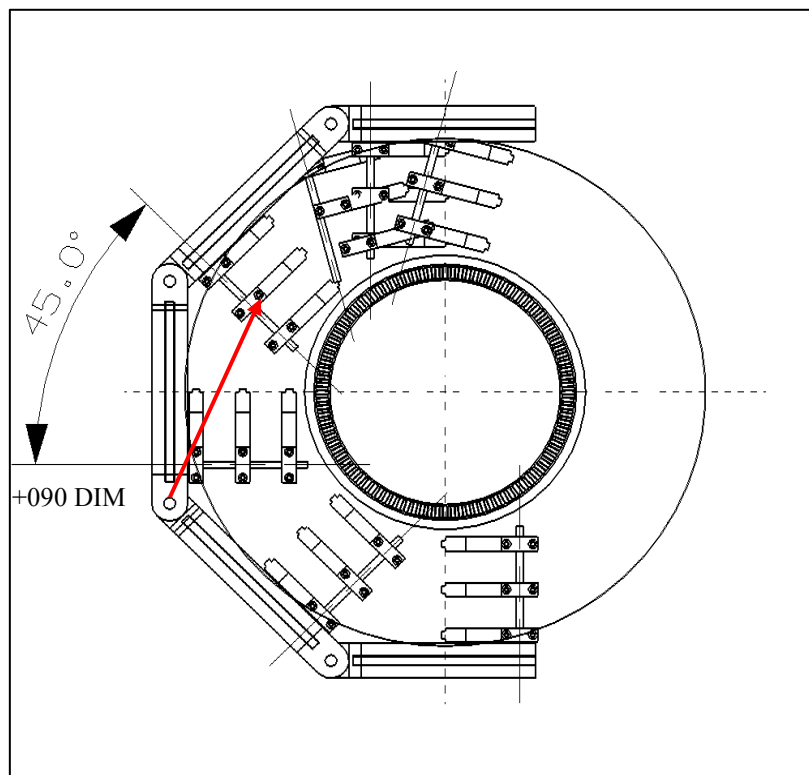


Figure 9.1: Position of the disc brake thermocouple holders

Keeping the speed constant for a prolonged period of time was a necessity if the component analysis tests were to be successful. As Angelinas (2009) found, the speed controller on the

Thermal Rig produces unreliable speeds that lead to incorrect results. During the experimental setup process, it was found that as heat passed through to the wheel carrier and into the wheel bearing, although the output of speed controller remained constant, the actual disc speed increased. Resistance in the bearings actually decreases with temperature.

A solution to the problem was found by using a closed loop control within the LabVIEW program. To adequately control a motor, a high frequency sampling and writing rate was necessary otherwise lag is produced in the system, potentially resulting in the desired speed to never be reached. The National Instruments NI 9401 module, used to measure the speed by counting the frequency of pulses generated by the IML speed sensor, was required to log data simultaneously as the thermocouples. Over the six hour period, the thermocouples were set to record data at a frequency of 0.5 Hz to prevent large amounts of unnecessary data from being logged. Unfortunately, this low frequency was too slow for acceptable speed control. Two separate “while loops” were therefore required to allow multiple data sources to be logged at different frequencies. The CompactDAQ system which was being used to record the data regrettably did not support multiple frequency logging. Consequently, a CompactRIO, with the ability to record data in real-time replaced the CompactDAQ and removed the speed variance issue. A 15 Hz sampling rate was used to record speed measurement.

An inbuilt PID controller preinstalled in LabVIEW software was used for the closed loop control system; the values 1.4, 0.3 and 0.015 for the proportional, integral and derivative terms respectively were used. These values were found experimentally through the trial and error method. Desired speeds were not reached instantaneously. For example, it took approximately 30 seconds for a stationary disc to speed up and remain steady at 100 rpm. Once the disc speed was settled at the requested velocity, deviation from the set value is no more than ± 2 rpm. This level of speed control was sufficient for the designed analysis tests so the more complex Ziegler–Nichols and the Cohen-Coon methods of setting the PID control values were unnecessary, as recommended by Svrcek *et al.* (2007).

In addition to the friction surface temperatures, probe type thermocouples were used to record a combination of six hat temperatures 5 mm from the surface, three temperatures in the wheel carrier and up to nine air temperatures to enable a full field temperature distribution understanding. Three slots in the CompactRIO were reserved for speed control and voltage readings, leaving five slots open for thermocouple readings. Deployment of the NI9213, NI9214 and three NI9211s meant a maximum of 44 thermocouples readings could be taken during every

experiment. Due to the space limitations not all thermocouple locations could be recorded for every experiment, resulting in a chosen selection being used.

In one set of experiments, five probe thermocouples could have been placed 10 mm radially away from the outside rotor edge, located centrally between the two contact faces and aligned to the rubbing thermocouples separated circumferentially by 45° . Also, two probe thermocouples were placed at the vane inlets at angles of 0° and 180° . A second set of air temperatures were taken by replacing the 45° and 135° probe locations with two points 210 mm and 395 mm from the disc brake OD, on the 0° reference (see Figure 9.2).

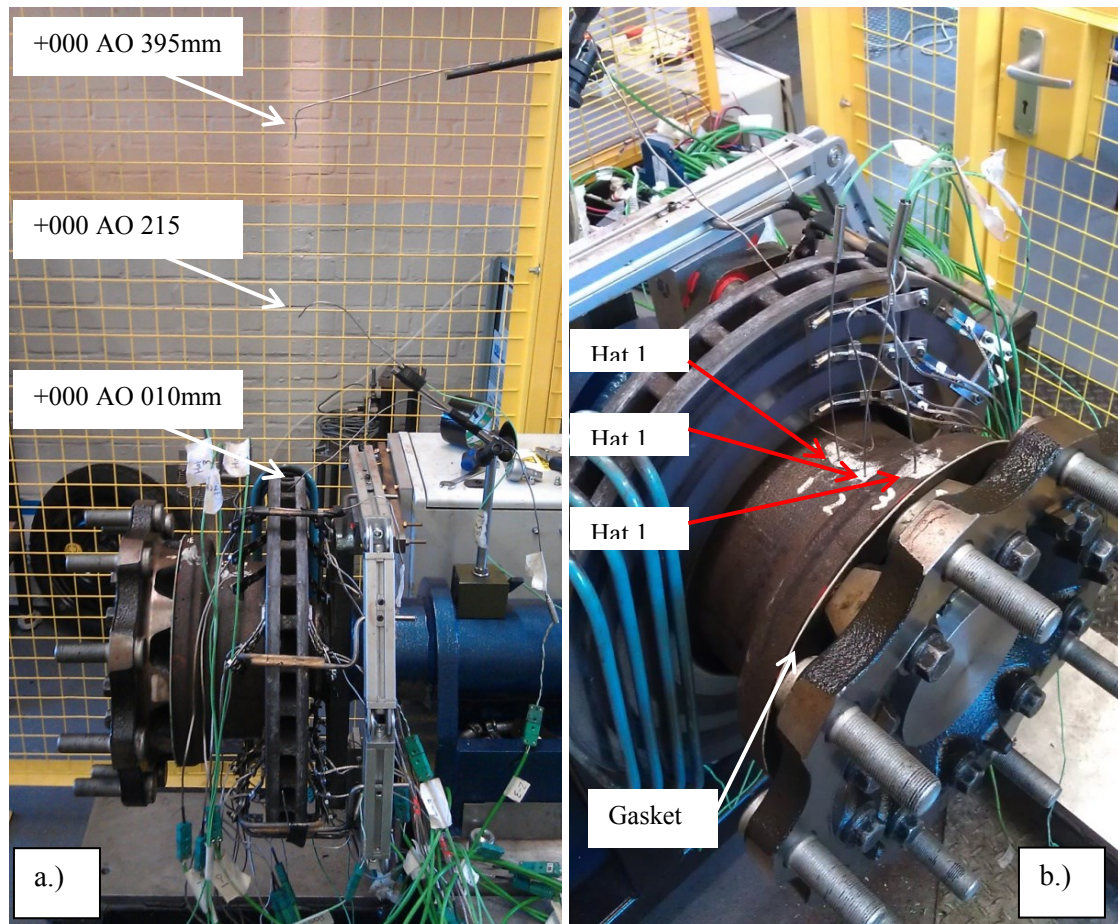


Figure 9.2: Thermal Rig modifications showing a.) the vertical air thermocouples and b.) the three hat thermocouples

9.2 Disc Only Experimental Cooling Temperatures

Energy transfer from the disc brake to other brake assembly components has already been attributed to being one of the main causes of error in FE modelling. Initial investigations were conducted on the disc only. Being the component that holds the greatest amount of thermal

energy, it is important to understand the cooling characteristics of this component in greater detail. As the IHC requires the disc brake to rotate, it was impossible to completely isolate the disc brake from other components (remembering the driveshaft is attached to the wheel carrier on the Thermal Rig). By inserting a gasket in between the flange face of the disc brake and wheel carrier (Figure 9.2), the assumption could be made that no thermal conduction occurred between the two components. Experiments were also conducted with the ventilation channels both open and blocked, with results from each scenario being discussed in turn. These experiments match the three cases explored analytically in Chapter 7.

9.2.1 With Gasket and Blocked vanes

Discussions on these “Disc only” experiments starts with the case where heat dissipation is limited to radiation and convection from the external surfaces only (gasket in place with blocked ventilation channels). The disc was rotated and kept at a constant 100 rpm throughout the duration of the heating process. Although situations where the disc brake is rotating are not so relevant to the EPB, an opportunity to discover the ratio of external convective cooling to in-vane cooling presented itself. An appreciation of the ratio of in-channel to external surface convective cooling at slow speed could subsequently be achieved. All the necessary data to complete the additional investigation was already being recorded as part of the Component Analysis testing.

From the differentiated energy balance, given in equation (9.1), disc brake thermal equilibrium is reached when the energy supplied by the IHC is equal to the total energy dissipated, creating a zero temperature gradient, $\frac{dT_d}{dt}$.

$$\dot{Q} = mC_p \frac{dT_d}{dt} \quad (9.1)$$

In the experimental procedure above, it dictates that thermal equilibrium is reached once each rubbing thermocouples vary its temperature by less than $\pm 2^\circ\text{C}$. Figure 9.3 shows the final five minutes of the heating stage, for the thermocouple located in the +000 DOO thermocouple, before the cooling phase begins (denoted as $t = 0$ in Figure 9.3). The average temperature (depicted with a dashed line) was measured to be 401.0°C over the five minute period with the thermocouple reading (solid line) not veering outside the $\pm 2^\circ\text{C}$ limitation. Although only a single thermocouple result is shown in Figure 9.3, all temperatures were monitored and complied with the $\pm 2^\circ\text{C}$ boundary limitation.

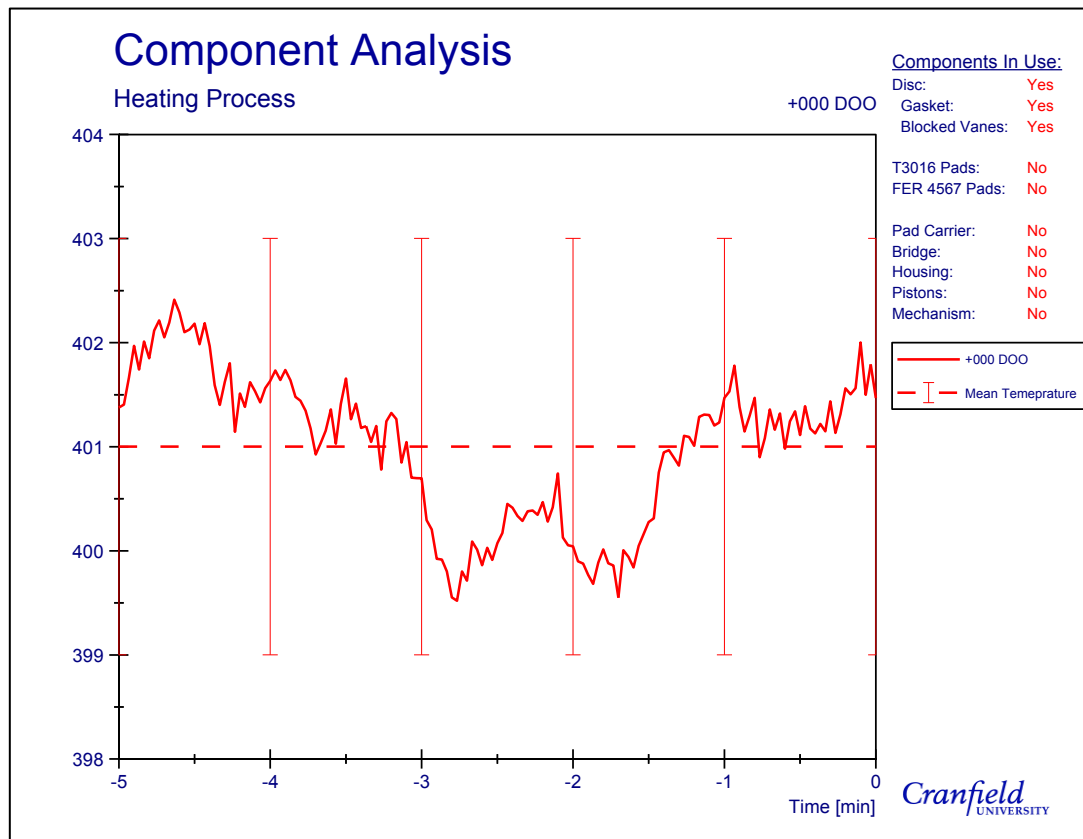


Figure 9.3: Temperatures varying less than $\pm 2^{\circ}\text{C}$ before cooling starts, thermal equilibrium conditions

Thermal equilibrium was reached for the external surfaces cooling scenario when the control unit of the IHC was set to deliver 177 V, at 100 Hz, corresponding to a power rating of 6.20 kW. From the work of Adloff (2007), the actual power delivered to the disc brake could be calculated to be 5.70 kW. Consequently, the sum of the radiation and external surface convection is equal to 5.70 kW, as expressed in (9.2).

$$Q_{in} = Q_{rad} + Q_{conv}$$

$$Q_{in} = 5.70 \text{ kW} \tag{9.2}$$

External convective power can be worked out by substituting the radiation Fourier cooling relationship in place of the Q_{rad} term in equation (9.2), forming (9.3). A total disc brake energy change is being investigated here, therefore a bulk temperature for the disc brake was needed. During heating only the disc surface temperatures were the only temperatures recorded as it was impossible for probe type thermocouples to be in place when the disc is spinning. Slip ring thermocouples are needed for this measurement type. In their absence, a bulk temperature was taken by averaging just the surface temperatures, producing a value of 385.2°C . An average

ambient temperature for the same period was 22.2°C and the disc brake external wetted area was 0.336 m².

$$Q_{in} = \sigma \varepsilon A_{surf} (T_d^4 - T_\infty^4) + Q_{conv} \quad (9.3)$$

Stevens *et al.* (2010) showed that the emissivity value of a grey cast iron CV disc brake varies insignificantly during long cooling periods so can be assumed constant at a value of 0.92. Consequentially, the amount of dissipation via radiation at thermal equilibrium was calculated to be 3.73 kW, leaving 1.97 kW of convection dissipation from the external surfaces at a disc rotational velocity of 100 rpm. The total change in disc brake internal energy by heating the disc up to 385.2°C, from the initial 19.2°C, was calculated to be 5.97 MJ using the internal energy balance equation (9.1).

The transition from the heating to the cooling phase is displayed in Figure 9.4 where the outboard, 0° thermocouple recordings are displayed. A 10 minute time period is shown; nine minutes before and the first minute after the full cooling phase began. All three thermocouples demonstrate an initial rise in temperature once the IHC and the motor were turned off. The peaks take two differing forms, the first being a sudden temperature jump and a second, much slower temperature increase. The former is common for all thermocouples located closer to the IHC as a result of electromagnetic interference (EMI) given off by it. The effect of EMI increases the readings by 2.0°C as soon as the motor and IHC are powered down. Considering 2.0°C is approximately 0.5% of the recorded temperature, it was anticipated that any investigation into the EMI effect would result in an insignificant outcome so it was therefore ignored.

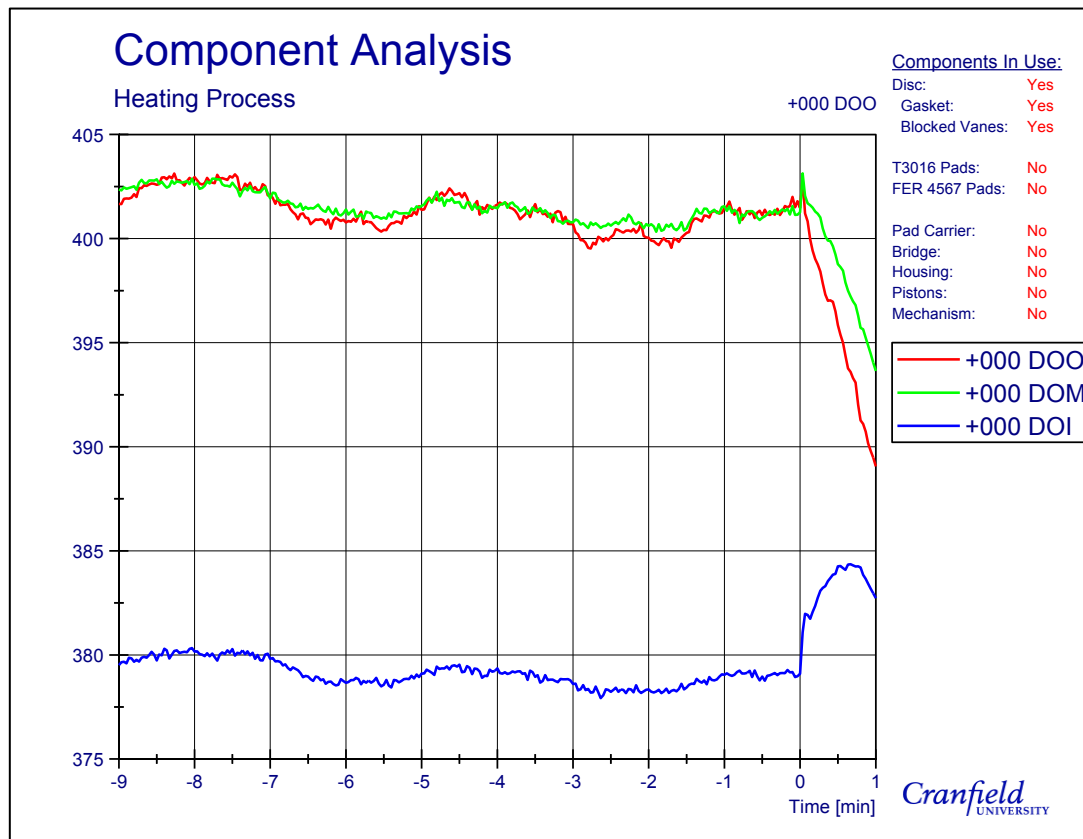


Figure 9.4: Temperatures prior to and including the start of the cooling phase

Whilst the EMI temperature increases were seen for thermocouples in close proximity to the IHC, the second peak type, seen only by the +000 DOI thermocouple in Figure 9.4, was mutual for the thermocouples positioned at ID only.

Whereas the first peak was a function of EMI, the second peak type is a conduction phenomenon. As the disc rotates through the IHC, the middle section of the disc has a continuous arc through the electromagnetic field, getting a large exposure time to the energy source. Likewise, the OD may not have a continuous path through the electromagnetic field but its exposure time is still large enough for substantial amount of heating to transpire. In contrast, the ID never enters the field as the IHC was designed such that it is position 5 mm away from the ID. A resulting temperature gradient is generated along the surface. Once the IHC is switched off, the source creating the surface thermal gradient is removed and conduction effects bring the disc to a natural state. A small period of time is required for both a buoyant air current to manifest and for the disc brake to come to a balanced thermal state. For this reason, and because additional probe thermocouples needed to be inserted into various places within the hat section, the cooling phase for all component analysis tests were started once the +000 DOO

reference thermocouple fell below 350°C. To differentiate the full cooling phase it shall be referred to from here on as the 350°C cooling phase.

Each component analysis cooling test was conducted five times with an average taken for the final temperature curve for each thermocouple. Five experiments were required to ensure there was experimental repeatability and to help remove subjectivity from the results as outlier visibility is enhanced. To save time during the analysis process, not every data point was used. Instead, 17 points in time were chosen and processed; these time points were the beginning of the 350°C cooling phase, five, 10, 15, 30 and 45 minutes after it, then on every hour and half hour from thereon. An accurate representation of the 350°C cooling phase was still achieved.

An example result is displayed in Figure 9.5 with temperature plots for all five experiments at the +000 DOO thermocouple position. In this case, all results show close alignment to each other. Examining all other graphs for the various thermocouple positions, it was clear that the rubbing thermocouples +135 DOO, +135 DIM and +135 DII generated erroneous data. All three recorded temperatures, when the disc was at its hottest, in the region of only 150°C. Reasoning for the unrealistic temperatures were that all three thermocouples made insufficient contact on the disc surface and consequentially, all recorded extremely low surface temperatures. When investigating the issue, it became clear that that the screw holding the +135 DOO thermocouple had untightened, presumably through vibrations being subjected to it from the disc rotating. The remaining two thermocouples were impeded by the fixings of the Thermal Rig modification frame that held the rubbing thermocouples, making it impossible to position the thermocouples correctly. All results from the three thermocouples were omitted from the analysis.

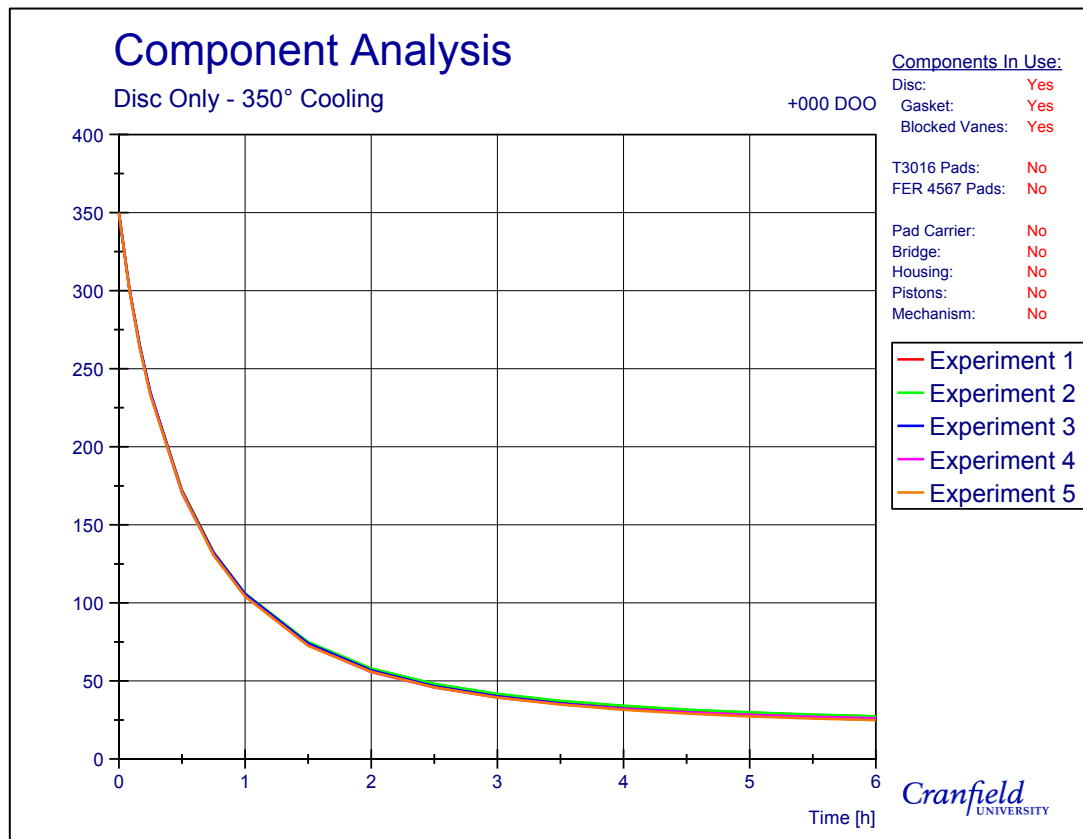


Figure 9.5: 350°C cooling profiles for all five experiments from the +000 DOO thermocouple - for case 1

Visual inspection of the five experiments is reasonable for determining whether a single experiment was invalid. What cannot be determined through inspection is whether there is too much variation within the recorded data, meaning the taken average is statistically representative of what is actually happening. Standard deviation, σ_{sd} , analysis is commonly adopted by technical disciplines when establishing the degree of dispersion within experimental data. Thermal experiments are difficult to control, even with apparatus such as the Thermal Rig. Rickard (2008) has shown that if all data points from a set of experiments fall within a $\pm 2\sigma_{sd}$ range from the mean, the averaged data can be considered representative for a 95% confidence interval. This approach was adopted, with any temperature measurement calculated outside the $\pm 2\sigma_{sd}$ limit was rejected.

Standard deviations for each of the experiments are shown in Figure 9.6, excluding the three erroneous thermocouples already identified. The maximum dispersion is seen for the thermocouple located in the +045 DOM position, having a standard deviation value of 3.0°C, making the allowed variation from the mean value (337.8°C) to be $\pm 6.0^\circ\text{C}$. All five temperature recordings fell within the confidence limit set, with the maximum difference being only 3.3°C, therefore the average data could be accepted. However, a more stringent test would be to

investigate the lowest standard deviation value because the allowable variation range will be greatly reduced. The smallest standard deviation was seen for the thermocouple position positioned +090 DOO, setting a 2σ limitation of $\pm 0.2^\circ\text{C}$ about the calculated mean of 162.8°C . Again, all measured values fall within the $\pm 2\sigma_{sd}$ constraint, representing good repeatability and generates confidence in the results.

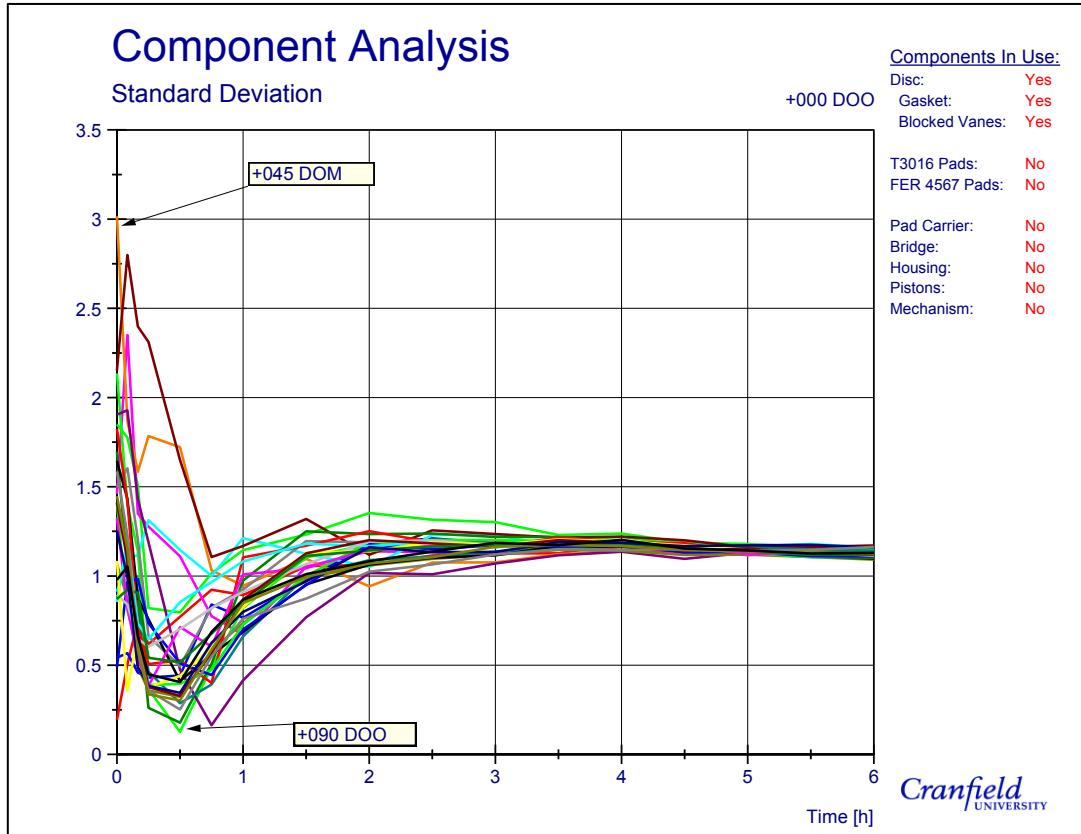


Figure 9.6: Standard deviation values for the average blocked vanes, with gasket experiments

Figure 9.7 shows the position of all 30 rubbing thermocouples (highlighted in red) with the corresponding averaged thermocouple recordings for the outboard side of the disc brake. These temperatures were recorded when the +000 DOO thermocouple dropped below 350°C for the first time in the cooling phase. Presenting the results in such a way helps develop a visual understanding of the thermal pattern present on the disc brake surface. Although not all shown, a series of these pictures were made and used as the base for further analysis; one for each of the 17 time samples, on either side of the disc. Empty boxes represent the locations of faulty thermocouples.

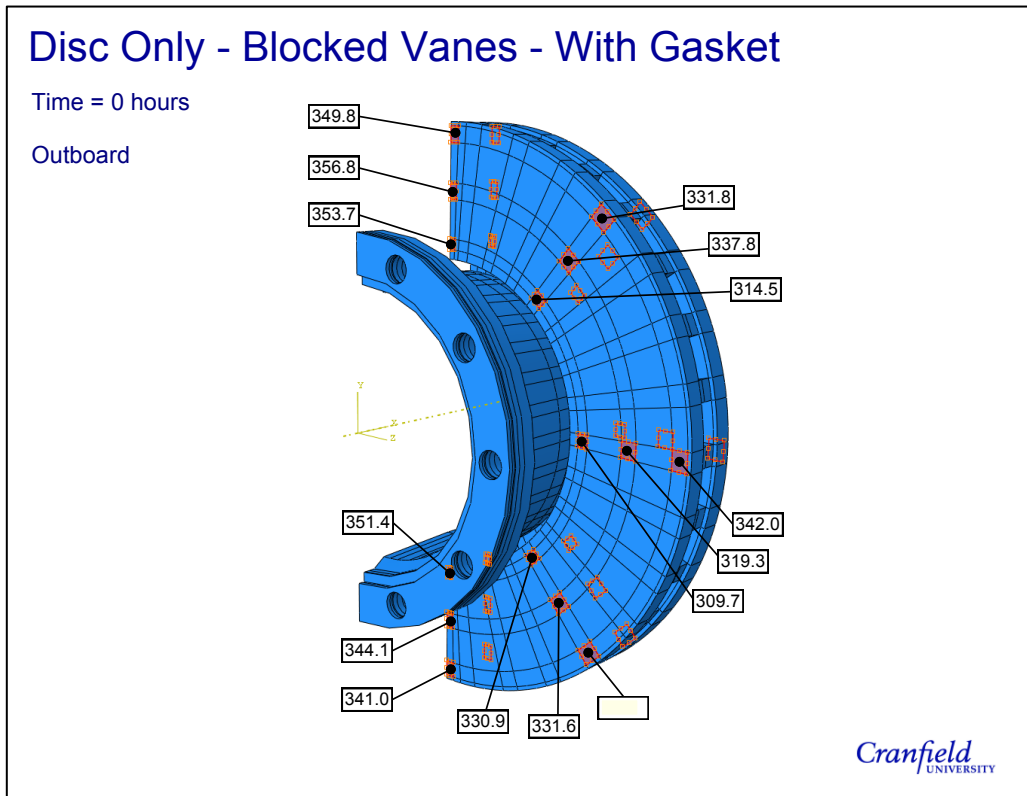


Figure 9.7: Averaged outboard disc brake surface temperatures, at the 350°C reference

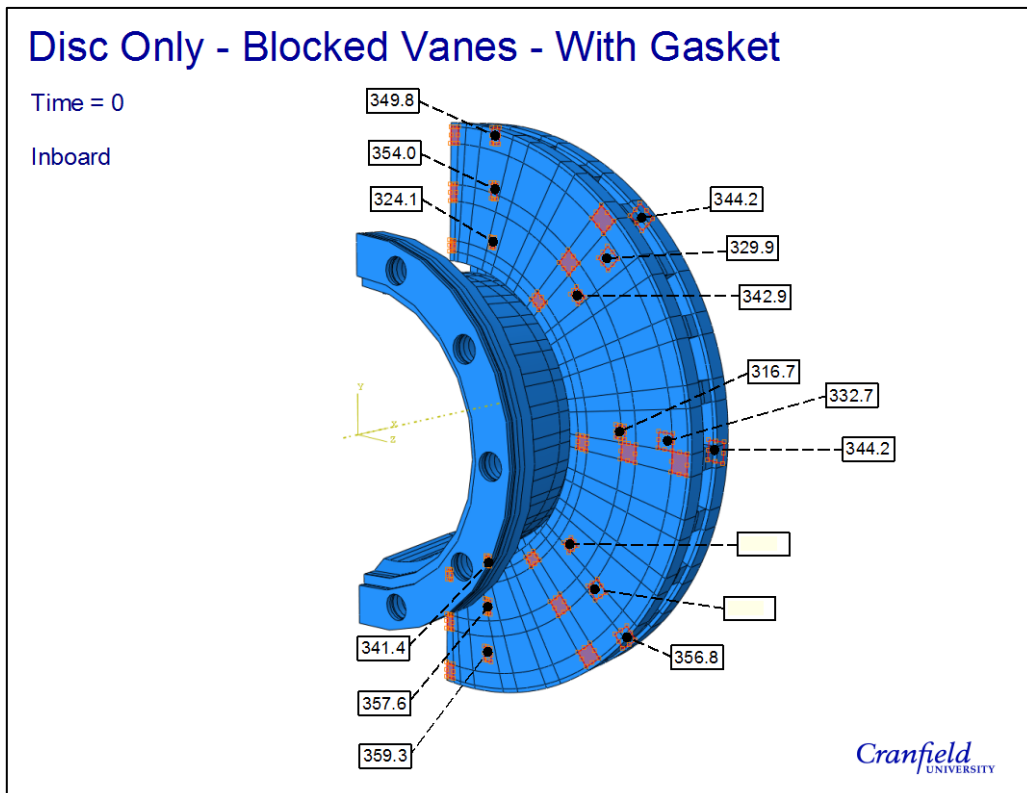


Figure 9.8: Averaged inboard disc brake surface temperatures, at the 350°C reference

A comparison between the inboard and outboard results (Figure 9.7 and Figure 9.8) can be made. With internal conduction effects pulling heat from the rotor to the hat section, it was expected that the inboard surface to be cooler than the outboard, due to being of anti-coning configuration. For all thermocouples positioned in the 0° radial plane this is true, but nearly all other temperatures show the reverse. For this finding to be true, the outboard surface must dissipate heat better than the inboard surface. Localised areas of high convective heat transfer from the friction surfaces are the cause of this phenomenon. Supporting evidence for this has already come been presented in the Chapter 8, in the form of CFD simulation results. High velocity air exiting the channels at the ID causes high convection rates on the outboard friction surface, around the 90° central position, with low velocity air at the 0° position causing a region low h_{conv} , causing a warmer outboard friction surface.

Circumferential heating patterns at the start of the cooling phase are better displayed in Figure 9.9; temperatures for the five thermocouples placed at the same radial location circumferentially around the disc are grouped together. Temperatures are generally high at the 0° position and decrease moving around the disc brake. Interestingly, the temperature starts to increase towards the lower half of disc brake, after the 90° position. Studying all the produced line graphs, the temperature increase was a common occurrence for all circumferential results. Again, the faster flowing channel exiting flow is the cause of this midpoint dip in temperature.

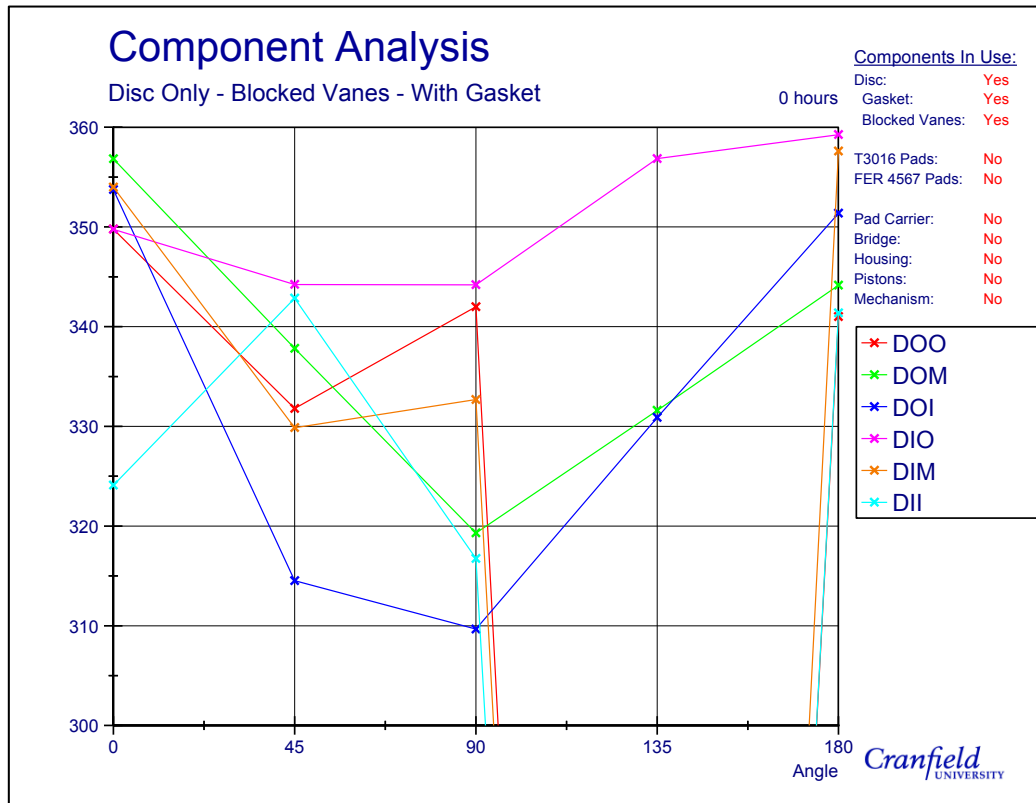


Figure 9.9: Averaged circumferential temperatures at the start of the cooling phase

9.2.2 Further Disc Only Experiments

Both the second and third disc only experimental cases (open vanes with the gasket and open vanes without the gasket) were conducted and analysed in the same manner as the first. Thermal equilibrium was reached before turning the IHC and motor off to let the disc brake to cool. Table 9.1 summaries the heating results generated for the disc only experiments. Removing the blockage from the vanes elevated the required actual input power from the IHC to reach thermal equilibrium by an additional 0.74 kW. With no other aspect of the experimental procedure changed, in-channel convection was attributed to the additional power increase.

A surprisingly low ratio of nearly 1:4 for internal to external convection cooling was achieved, for disc brake rotational speeds of 100 rpm. A comparison of this ratio can be made with the a ratio found by McPhee and Johnson (2008), on a passenger vehicle disc brake fabricated with straight vanes, which was 9:11 when the rotational velocity was 342 rpm. Increasing the rotational velocity raised the proportion of internal vane convection. Values calculated here would appear to match those of McPhee and Johnson well as lower speeds would produce a lower internal convection ratio, similar to that of the calculated ratio; experimental confidence was gained from this result. This was anticipated as McPhee and Johnson’s experimental

procedure was very similar the one presented and conducted for this project. Higher speeds create greater pumping through the vanes, making flow velocities higher and increasing the cooling properties.

Table 9.1: Summary of the rotational thermal properties at 100 rpm.

	Case 1	Case 2	Case 3
Gasket	Yes	Yes	No
Open Vanes	No	Yes	Yes
Bulk Disc temperature at thermal equilibrium [°C]	385	396	386
IHC power input (set / actual) [kW]	6.20 / 5.70	7.00 / 6.44	7.00 / 6.44
Total convective power output [kW]	1.97	2.71	2.71
In vane convective power output [kW]	0	0.74	0.74

A surprise result was found when exploring the power input from in the third disc only case with the removal of the gasket making little difference to the total disc brake dissipation. Without a gasket between the disc and wheel carrier a marked increase in conduction was expected, resulting in more power being needed from the IHC to reach thermal equilibrium. In fact, no increment from the 6.44 kW of power from the IHC was still sufficient to reach the specified criteria. What this result suggests is that conduction has little influence on heat transfer between these two components, making a different mode of heat transfer predominant.

Figure 9.10 displays the cooling profiles of all three cases for comparison. The first case does portray a lower cooling rate than the other two, confirming that airflow through the channels impacts the heat dissipation during the cooling phase. The difference between the cooling profiles of cases two and three was minimal, so they can effectively be perceived as equivalent to each other. Consequentially, it can be concluded the presence of the gasket had little impact on the flow of thermal energy.

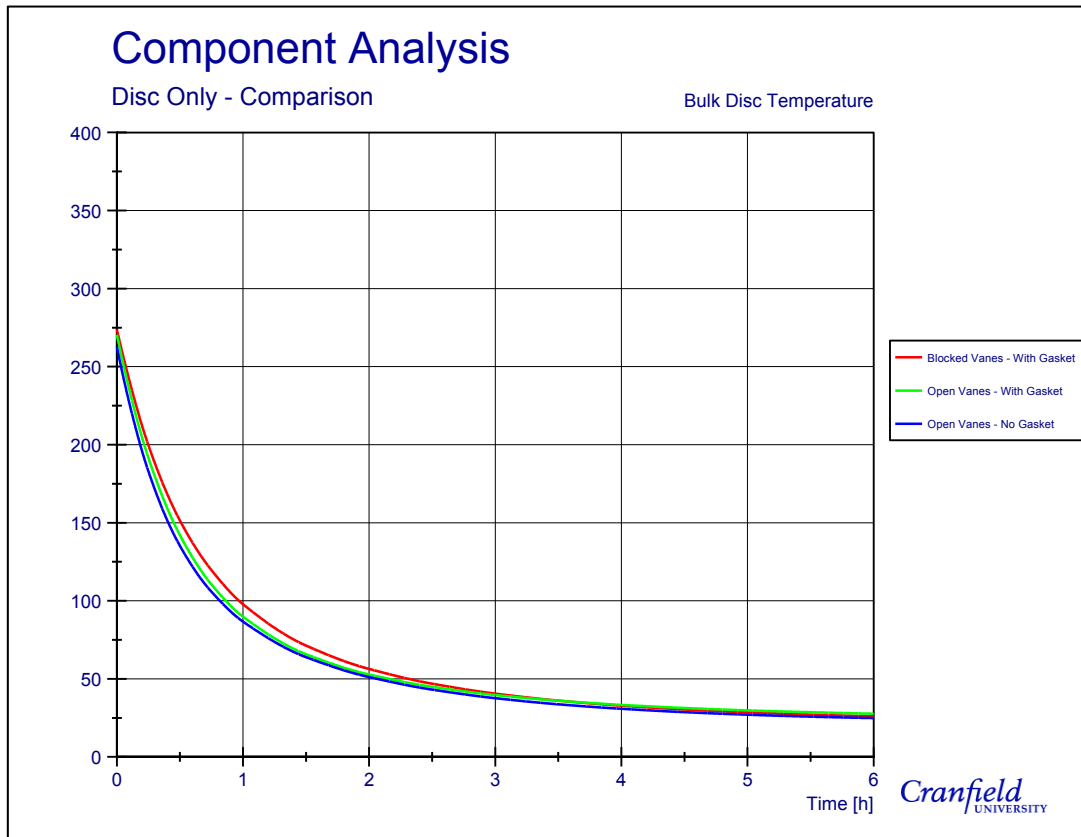


Figure 9.10: Comparing the averaged cooling data for the three disc only cases.

Temperatures in close proximity to the disc brake/wheel carrier interface were captured by placing three probe type thermocouples in each component; 2.75 mm, 5.85 and 9.22 mm away from the disc flange surface and 2.05, 3.88 and 6.10 mm from the wheel carrier interface. As temperatures couldn't be measured whilst the disc was spinning, cooling data was used. Like before, the average temperature from five individual experiments was taken for each of the thermocouples.

It was essential to get at least three temperature readings for both components to enable reasonable approximations of the heat profiles through them. From Figure 9.11, some interesting results were found for the experiments without the gasket. Heat profiles in both the disc brake hat section and wheel carrier could be assumed linear to a 90% regression confidence. The gradient of each line describes amount of thermal energy passing through the respective bodies, if the heat is assumed to travel in a single dimension only. By extrapolating the lines of best fit back to the interface, estimation of the friction surface temperatures could be made. At the start of the of the 350°C cooling phase, the disc brake was 11.5°C warmer than the wheel carrier.

A thermal flow through the grey cast iron disc brake material was calculated at $17,904 \text{ W/m}^2$, as per the calculation method set out in Voller (2003). Knowing the temperature drop across the interface was 11.5°C and the contact area between the brake disc and wheel carrier was $5.94\text{E-}3 \text{ m}^2$, the thermal resistance was $0.642\text{E-}3 \text{ m}^2\text{K/W}$, or more favourably $1,557 \text{ W/m}^2\text{K}$. It is argued that this method of finding an interface h_{cond} value is insufficient as only a single material is analysed and that there a lack of insulation is used, making it impossible to isolate the conduction affects from the other dissipation modes. For this reason, a separate method of calculating h_{cond} values was used and will be discussed in section 9.3.

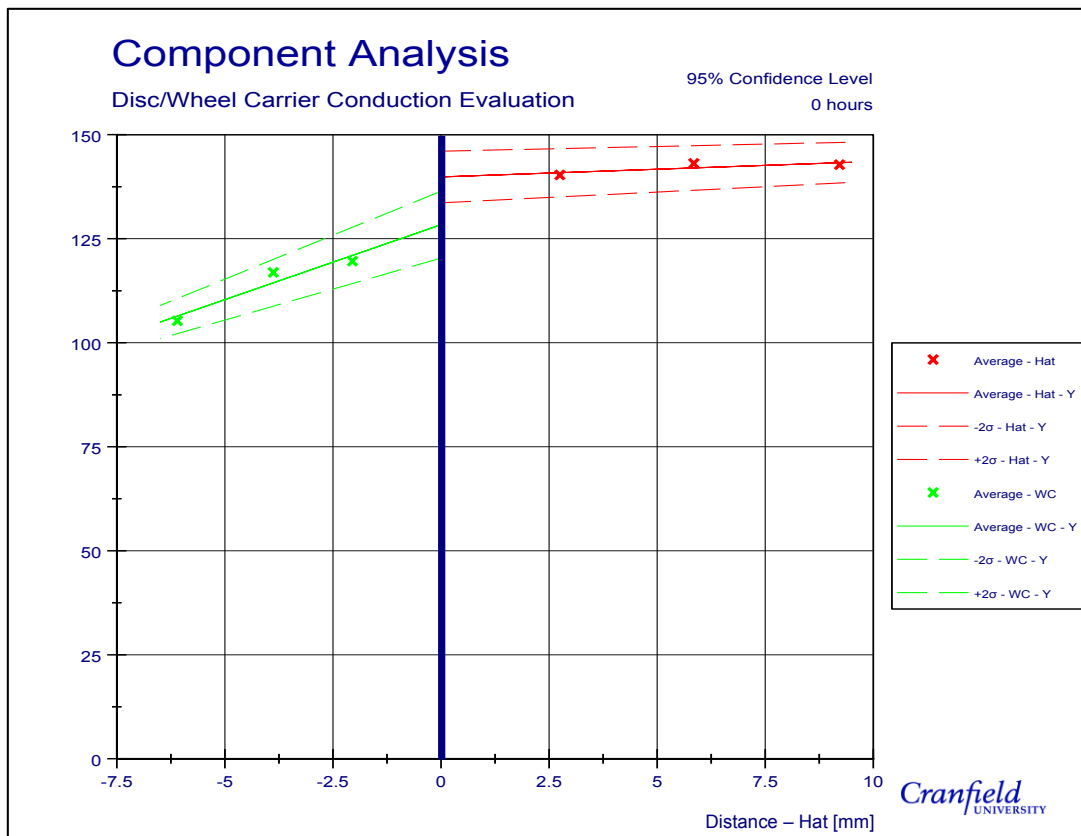


Figure 9.11: Thermal gradient across the disc brake/wheel carrier interface.

The temperature difference reduces with time and after 40 minutes, the gradient reverses as the wheel carrier becomes hotter than the disc. The greatest temperature differential whilst the wheel carrier was warmest was only 2.7°C , reached 2.5 hours into the 350°C cooling phase. It was not until a further 2.5 hours had passed before the disc brake becomes hotter than the wheel carrier. Significance of this result is that for the first time, the disc brake is no longer the most important component in the assembly, in terms of its thermal behaviour. As the disc cools, the warmer wheel carrier is pushing heat back into the disc rather than receiving it. The more

energy absorbed by the wheel carrier in the early stages of the cooling phase, the longer it will take for the full brake assembly to return to ambient conditions.

The findings produced in section 9.2.2 are very interesting and could have a significant impact on future design of relevant brake assembly components. Before this is implemented however, the results need to be clarified and confirmed that the measured temperature gradient is indeed present and is not just a function of experimental uncertainty. Uncertainty in each temperature reading, when taking the average of five or more experiments, was shown by Taylor (1982) that the true value of the reading is captured to within a 95% confidence level when the upper and lower temperature boundaries are defined by $\pm 2\sigma$ (see section 5.3 for more details). By using the upper and lower boundary values for each temperature reading taken, upper and lower boundary conductivity lines were found and drawn on Figure 9.11, extending back to the interface. Unfortunately, it can be seen that at the 95% confidence level, the lower boundary disc brake flange surface temperature is cooler than the upper boundary wheel carrier flange surface temperature, creating an overlapping temperature region. Consequently, there is a lack of evidence to disprove the results from being within experimental error.

Taylor also showed that by calculating the uncertainty bands within the reduced $\pm\sigma$ limits, a reasonable 70% confidence level is still achieved. Figure 9.12 again shows the averaged temperature readings for the three probe thermocouples located in each of the disc brake's hat section and the wheel carrier, with the associated average conductivity line and the upper and lower boundary conductivity lines calculated using the $\pm\sigma$ criterion. With the reduction in confidence level, it is shown that the measured temperature gradient is present.

A 70% level is not usually accepted within scientific and engineering disciplines due the large degree of error possible. However, only three temperatures points were taken on each component here, with a linear trend assumed. Although three points are the minimum amount necessary before a linear trend can be assumed, a better understanding is achieved when at least five point temperatures are taken. On the limited space available on the geometry, very fine thermocouples would be required to allow additional recordings to be made. At the time of experimentation, there were no finer probe type thermocouples available to repeat the experiment. By default then, the amount of experimental error will be larger, making it unrealistic to state 95% confidence in the experimental procedure. Resultantly, the 70% confidence limit is more appropriate in this case and therefore, it can be stated that the measured thermal gradient is a physical occurrence.

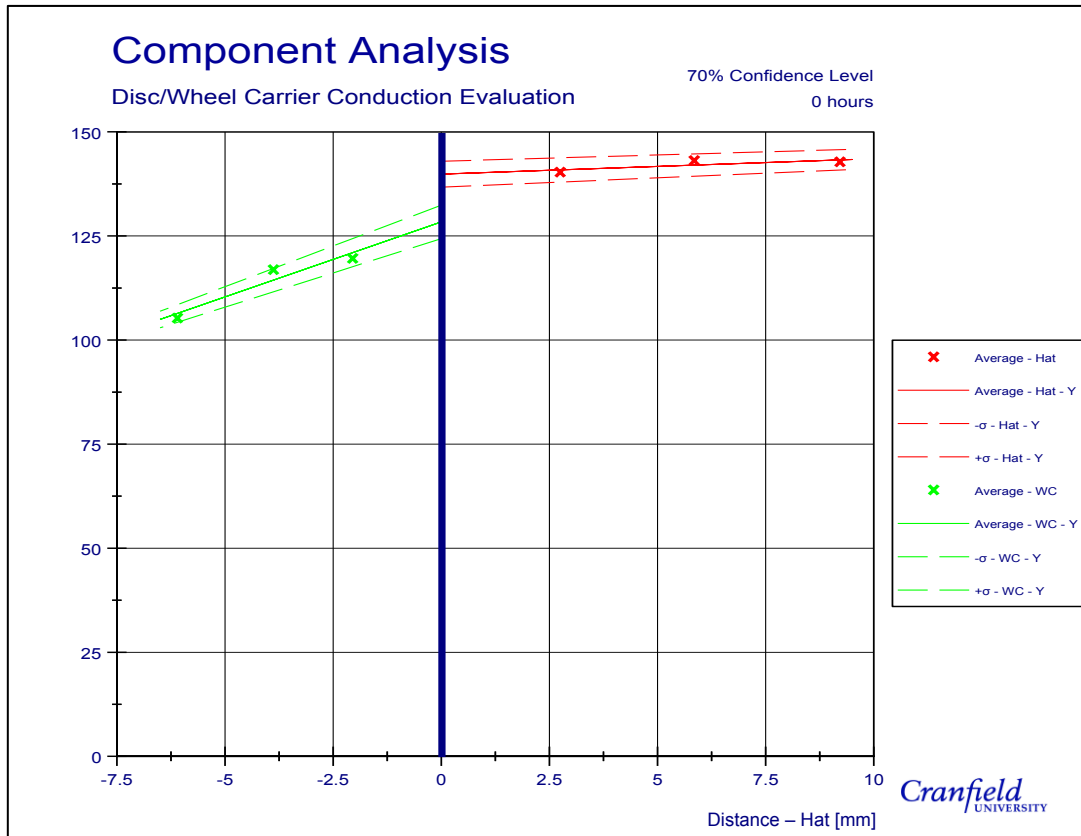


Figure 9.12: The results of disc brake/wheel carrier testing confirms the thermal gradient between the pair to a 70% experimental confidence level

Furthermore, even at the 70% confidence level, the gradient is only present for the first 15 minutes of cooling, before the upper and lower boundaries overlap once again. A deficient of evidence prevents the statistical conformation of the previously discussed phenomenon, where the wheel carrier becomes warmer than the disc brake.

9.2.3 Hat Temperatures

To complete the experimental study on disc brake temperatures, throughout the cooling phase, an examination of the hat temperatures was conducted. This was done by comparing the three probe thermocouples inserted into the hat to the bulk rotor temperature, found by taking an average of all the working rubbing thermocouples. In Figure 9.13, a sample result is presented. The rotor part of the disc always starts as the hottest but its increased energy slowly erodes and after a period of time, the rotor section becomes the coolest. This is a common characteristic for all three disc only cases.

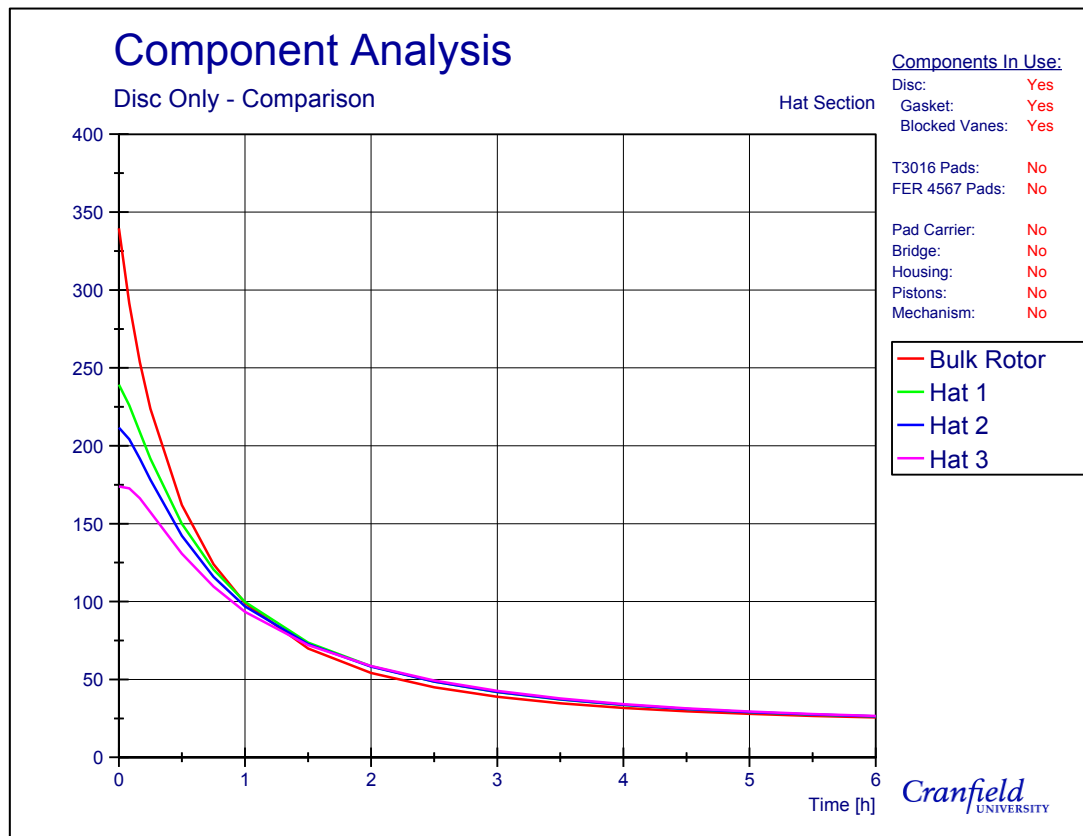


Figure 9.13: Bulk rotor temperatures drop below hat temperatures during the cooling phase (see Figure 9.2 for thermocouple positions)

For the rotor to become the coolest part of the disc brake, the temperature profile recorded by all three hat thermocouples had to intersect the cooling bulk rotor profile. Table 9.2 expresses the times when each thermocouple surpasses the bulk rotor and the temperature when it did so. Evidence of a temperature wavefront progressing through the hat is presented. The change transpires sequentially, starting with the thermocouple closest to the rotor (Hat 1) through to the outer brake thermocouple located close to the disc/wheel carrier interface (Hat 3). When air was allowed to flow through the vanes, the time until the outer Hat 3 thermocouple to become warmer than the rotor was just under an hour. In comparison, the blocked vane meant a further 19 minutes was needed for this to happen. If the significance of the airflow through the vanes had not fully been proven, the evidence here leaves no doubt; without the ability to dissipate heat to the flowing air in the vanes, thermal energy is blocked and retained in the rotor.

For the second experimental case, where the gasket was present, it only took 43 minutes for the first thermocouple to be hotter than the bulk rotor temperature. It was a further 16 minutes before the heat wavefront reached the outer hat thermocouple. Higher hat temperatures were a function of the inability to conduct energy out of the hat, causing the larger initial temperatures.

A shorter time was subsequently recorded as the Hat 1 section had to heat up less before matching the bulk rotor temperature. Although in the third experimental case it took longer for the Hat 1 thermocouple to match, the effect of conduction can clearly be seen as rate at which the heat wavefront moves through the hat section was much faster; it only took 9 minutes for the outer thermocouple to become higher than the bulk rotor temperature. Confirmation that the gasket did in fact reliably prevent conduction in the first two cases is gained, validating earlier results.

Table 9.2: Times and subsequent temperatures when the hat thermocouples become higher than the bulk rotor temperature

	Hat 1		Hat 2		Hat 3	
	Time (mins)	Temperature (°C)	Time (mins)	Temperature (°C)	Time (mins)	Temperature (°C)
Case 1	56	104.0	70	87.5	78	78.5
Case 2	43	116.0	51	102.0	59	91.0
Case 3	50	101.0	55	92.0	59	86.5

9.3 Conduction Coefficient Calculations

When two surfaces are in contact, thermal energy is transferred from one body to the other via conduction. As explained in section 4.2, the mechanism of the energy transfer is lattice vibrational waves and/or free flowing, highly energised electrons. Thermal contact resistance is the property that describes the resistance to energy transferring between the two mating surfaces, with its inverse being called conductance. Tirović and Voller (2005) conducted extensive research into the amount of energy transferred by conduction between two surfaces. On the back of this work, they were able to find equation (4.23), which calculates the average pressure distribution across mating surfaces being held together via a set of bolts. By using calculated P_{avg} values in equation (4.24), for surfaces either with or without bolts connecting them, will result in specific h_{cond} values to be found for each mating pair.

Tirović and Voller's method of finding h_{cond} values was used in this investigation to find relevant values to use in the full brake assembly FE model, shown in Table 9.3. Unlike the variable h_{conv} values found in previous Chapters, constant values of h_{cond} were used in the FE modelling process. Tirović and Voller's concentrated on finding the spatial h_{cond} variability rather than its dependency on temperature. With time constraints placed on this investigation, no theoretical or experimental testing was completed, to understand the feasibility of this possible source of simulation error. Therefore, the constant values shown in Table 9.3 were used throughout the heating and cooling stages of the following FE simulations.

Table 9.3: Calculated h_{cond} values for all assembly contacting surface, using equations (4.23) and (4.24)

Contacting Surfaces			Surface Area (mm ²)	P_{avg} (MPa)	h_{cond} (W/m ² K)
Disc	To	Wheel Carrier	739	4.06	2,625
Disc	To	FER 4567	14,764	10.16	3,113
Disc	To	T3016	20,989	7.15	2,872
FER 4567	To	Backplate	14,764	10.16	3,113
T3016	To	Backplate	20,989	7.15	2,872
Backplate	To	Pistons	3,019	24.84	4,287
Backplate	To	Bridge	3,119	24.04	4,224
Bridge	To	Housing	1,600	0.36	2,330
Housing	To	Mechanism	9,534	0.25	2,320
Piston	To	Mechanism	800	93.75	9,800
Pad Carrier	To	Chassis	5,038	0.18	2,314

Average pressure distribution on a surface is inversely proportional to the size of the surface in contact under a given force; the larger the contact region, the lower the average pressure. As the average pressure being one of the key variables in determining the h_{cond} value, it is important that accurate values of surface area were used. By using the surface area calculation feature within the CAD package NX 7.5, precise area values were determined for the mating pairs.

9.4 Emissivity

Heat dissipation by the mode of radiation, by definition, is highly variable with temperature, as there is a fourth order relationship between the surface and ambient temperature. By combining the Stefan-Boltzmann law with Newton's law of cooling, equation (4.22) was derived for the radiation HTC. Calculating the h_{rad} value is relatively straightforward as it is dependent on surface area, surface temperature, the Stefan-Boltzmann constant (σ) and the emissivity (ϵ) values only. A simple cooling test was conducted to experimentally determine surface and air temperatures to place into equation (4.22) for the entire cooling period. With the σ value being constant, the only outstanding property needed in the h_{rad} calculation is the emissivity of the disc brake. As previously shown, Voller *et al.* (2003) have demonstrated the large range of emissivity values used in the literature, for multiple disc brake materials and conditions. In this section, the procedure undertaken to identify the appropriate ϵ values to use for the fully oxidised, 434/234 mm grey cast iron disc brake, as used on the Thermal Rig.

Emissivity is a property that describes a body's ability to accept and radiate electro-magnetic waves. An indirect measurement technique was therefore used to generate reliable values for this property. By utilising a FLIR A320 infrared camera in conjunction with temperature measurements, the emissivity of the disc brake could be determined.

The FLIR processing software ThermaCAM Researcher was utilised for emissivity calculations, which required the physical temperature readings to be imported into the software. By using an iterative method of selecting a value of emissivity, the IR camera temperatures from the location SP01 (shown in Figure 9.14) could be matched to the recorded physical temperatures from the +000 DOO thermocouple. A limitation of the FLIR A320 camera and its corresponding processing software was that the temperature ranges it was capable of recording were from 0°C to 350°C and 200°C to 1000°C. Seeing as the temperature range under investigation throughout this project is from 20° to 400°C, the cooling test had to be conducted twice to capture data over the entire cooling phase.

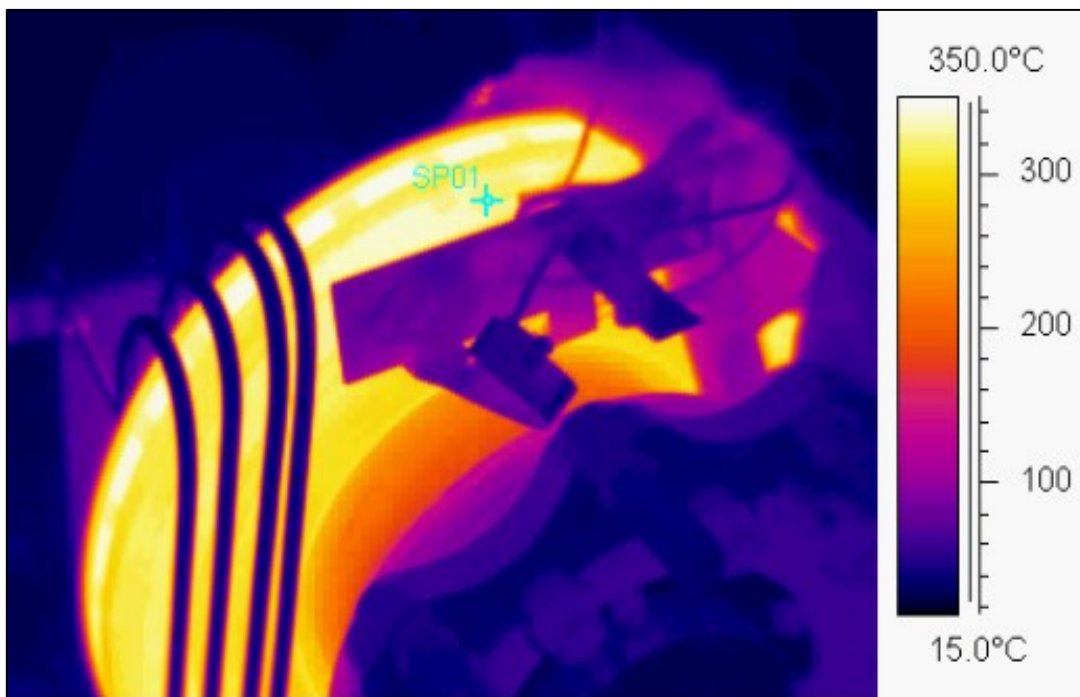


Figure 9.14: Thermal image of the initial parking application, showing the Spot temperature SP01 position (located on the outboard 0° friction surface) and the adjacent +000 DOO thermocouple

Figure 9.15 displays the results of the emissivity testing, with the red markers for the higher range and green markers for the lower. Emissivity changes with temperature as the potential to accept electromagnetic waves diminishes as a body gets hotter. Figure 9.15 does indeed show this pattern, but the decrease with temperature is so minor, the difference it will make for calculation is negligible. Therefore, it can be assumed that the emissivity of the grey cast iron

disc brake is constant throughout the stationary parking application. It should be noted that this test was only conducted on the one disc brake, which was in the fully oxidised state. Consequently, this assumption can only be made for disc brakes that match this condition. Emissivity values shown in Figure 9.15 were taken at 10°C intervals, starting from 50°C up to 400°C. By averaging all the values, a mean emissivity value of 0.92 was found. The minimum and maximum emissivity values calculated were 0.912 and 0.946 respectively.

ThermaCAM Researcher required a set of parameters to feed into the software to help it decipher the image taken by the FLIR A320 IR camera. For instance, the intensity of the light received by the camera is a function of how far the camera was away from the targeted surface. For the photo taken in Figure 9.14, the camera was positioned 0.9 m away from the outboard disc brake friction surface. Other important factors the software needed was the ambient temperature, relative humidity and the reflected temperature. Ambient temperature in the laboratory was approximately 20°C on the day of testing, so this value was used. It was also used for the reflected temperature value. From Chapter 8, it is known that the heat dissipating from the disc brake has little effect on the air temperatures away from the disc other than directly above it, allowing the same temperature assumption for the reflected temperature as that of the ambient to be made.

To test the importance of the humidity reading, the change in calculated emissivity readings was assessed when values of 50% and 90% were used. A difference of less than 0.5% in emissivity values were calculated for the 400°C surface temperature, indicating that calculations are insensitive to the humidity. A predicted value of 70% relative humidity was used in the end calculations.

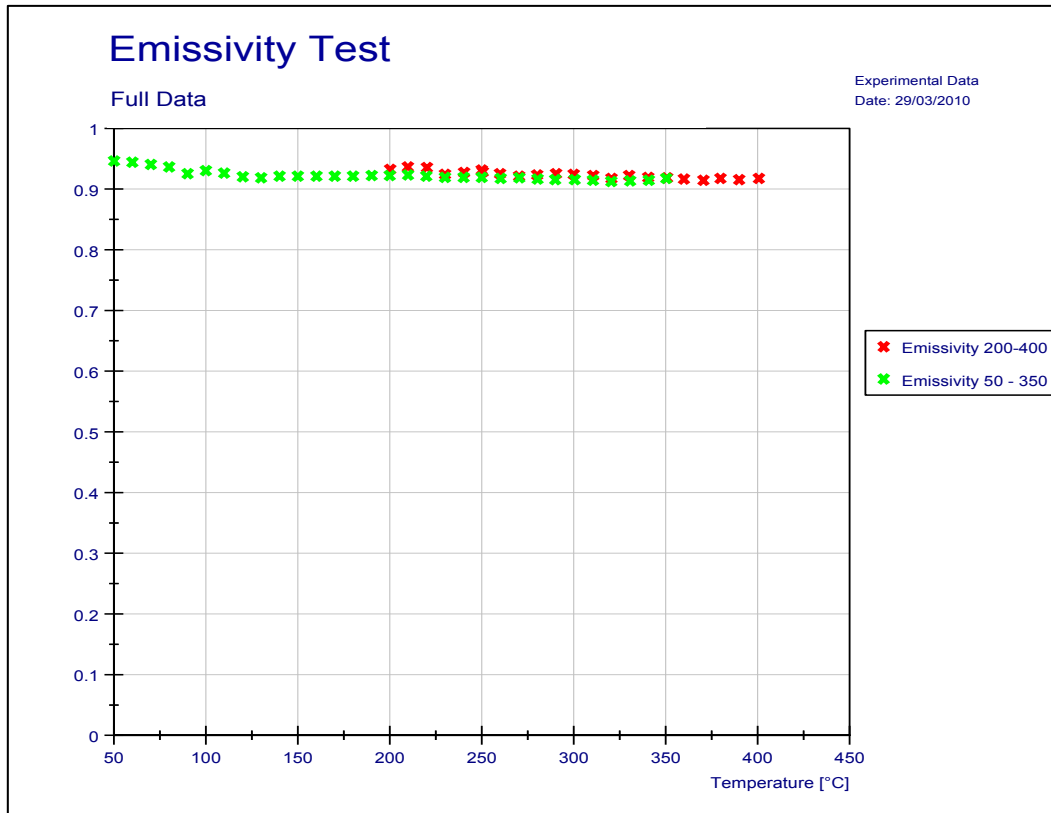


Figure 9.15: Emissivity results over the full cooling phase

9.5 Chapter Summary

Chapter 9 closely examined the manner of disc brake cooling after reaching a state of thermal equilibrium. It is common practice in brake FE modelling to ignore conduction to the wheel carrier as the applications times are short, preventing the heat from reaching the interface. For stationary parking applications, it was shown the wheel carrier impacts the disc brake temperature, discrediting this assumption. Consequently, this effect keeps the disc brake hotter for an extended period of time, making the inclusions of the wheel carrier essential when simulating the longer parking application. However, conduction is not the dominant mode of heat transfer to the wheel carrier. Regardless, values of h_{cond} were found for all contact interfaces within the brake assembly.

Radiation was the last heat transfer mode to be investigated. By employing the use of a thermal imaging camera, a technique was developed and used to find the emissivity value of the fully oxidised grey cast iron disc brake located on the Thermal Rig, over the entire parking application cooling phase. An assumption of a constant emissivity value throughout the cooling phase could be derived from the procedure, at a value of 0.92. Reliable radiation calculations are therefore possible as an outcome of this finding.

Furthermore, temperatures during the heating phase were also recorded. By comparing results from a disc brake with and without its vane channels blocked, at rotational speeds of 100 rpm, it was found that 80% of convective cooling is done on the external surfaces.

10 Full Brake Assembly FE Analysis

With a good understanding of the three modes of heat transfer found in the previous chapters, reliable boundary condition values can be entered into a full brake assembly thermal FE model. Starting immediately with a full brake assembly FE model would have been perilous though, as thermal interactions between the various caliper components were not well recognised, leading to probable erroneous results. Instead, the FE model was built slowly, adding only a single component (where possible) to the assembly, in an attempt to capture correctly all heat flow interactions.

The importance of getting the initial temperatures correct was demonstrated by the results produced by Robinet (2008) and in the previous FE modelling presented in Chapter 6. Incorrect initial settings can lead to unacceptable errors in temperature predictions. By repeating the experimental methodology conducted in section 9.2, it could be estimated how much energy enters each component and its corresponding surface temperatures, when in a state of thermal equilibrium. As the only source of energy entering the assembly came from the IHC, which entered the disc brake, any heat present in the other assembly components will be a result of heat transfer originating from the disc brake.

Five further heating tests were therefore planned, in addition to the brake “disc only” scenario presented in Chapter 9, to capture the thermal interactions. Components present in each experiment were:

1. Disc
2. Disc and FER 4567 pads
3. Disc and T3016 pads
4. Disc and Pad Carrier
5. Disc, Pad Carrier, Bridge and Housing
6. Disc, Pad Carrier, Bridge, Housing, Mechanism and Pistons

As the Wheel Carrier component was also present in every experiment by default, it was omitted from the list. Although it was planned to be carried out, experiment 3 three was abandoned due to the time restriction placed on the project. It was decided that having experimental data for a single brake pad friction material would be sufficient to demonstrate the reliability of the modelling process.

Discussion will be based on the experimental results produced from the six experiments outlined above, to find the initial surface temperature distribution at thermal equilibrium and how they were modelled. The presence of additional components has already shown to impact on the airflow around the disc brake during the smoke machine airflow testing. Inevitably, the disc brake cooling characteristics will change from those presented in section 8.3 when additional components are incorporated into the assembly. For this reason, the discussion will therefore transpire on a component-by-component basis, rather than for each individual test.

10.1 Disc Brake Temperatures

For two reasons, the disc brake is the most important component in the modelling process of the brake assembly, the first being that it has the highest thermal mass and secondly, it is where all the energy entered the system on the Thermal Rig. The experimental procedure conducted in the section 9.2 was not only used to find the surface temperatures during the cooling phase, but also during the heating stage. By using the data recorded when the disc brake was in the thermal equilibrium state, initial temperatures could be found and will be used to validate the FE modelling. A discussion on the physical temperatures recorded will be delivered prior to introducing the modelling techniques used to match the FE simulation results with the experimental data.

10.1.1 Experimental Disc Temperatures

Measured temperature data recorded by the rubbing thermocouples, located on the outboard friction surface, are shown in Figure 10.1. Red dots indicate the outboard thermocouple positions with the reciprocal inboard friction surface thermocouples and corresponding temperatures are shown in Figure 10.2. Many of the pictures displayed in Chapter 10 are in the same form as Figure 10.1, with each displayed thermocouple position presenting the average recorded temperature for each of the six scheduled experiments. A colour scheme is used in these figures to indicate when a significant change in temperature has occurred from the previous experiment, defined by a minimum of a $\pm 5\%$ temperature variation. In section 5.3 it was shown the worst case experimental uncertainty of the temperature measuring system can be considered as $\pm 2.2^\circ\text{C}$ at the 100°C . By making a significant change $\pm 5\%$, the recorded temperature change will always be at least double the experimental uncertainty and will therefore be a physical occurrence, not a function of experimental error. Values shown in red indicate that the temperature change from the subsequent experiment had significantly increased and blue values demonstrate a significant temperature reduction.

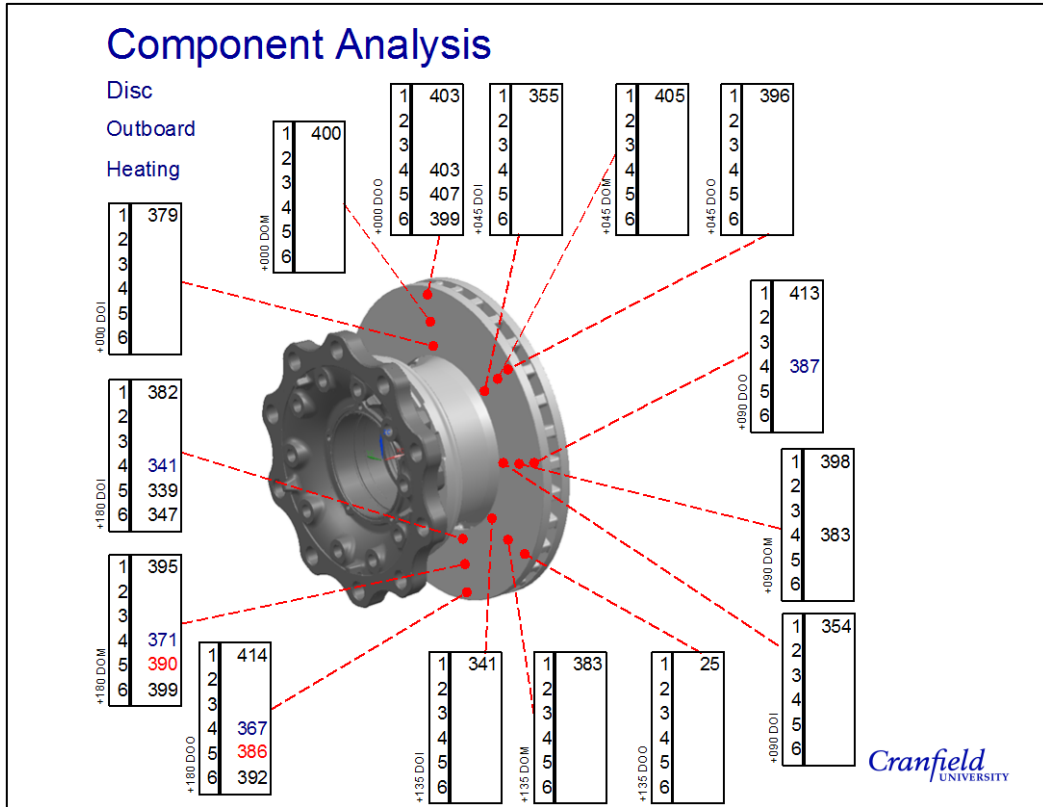


Figure 10.1: Outboard brake “disc only” thermal equilibrium temperatures

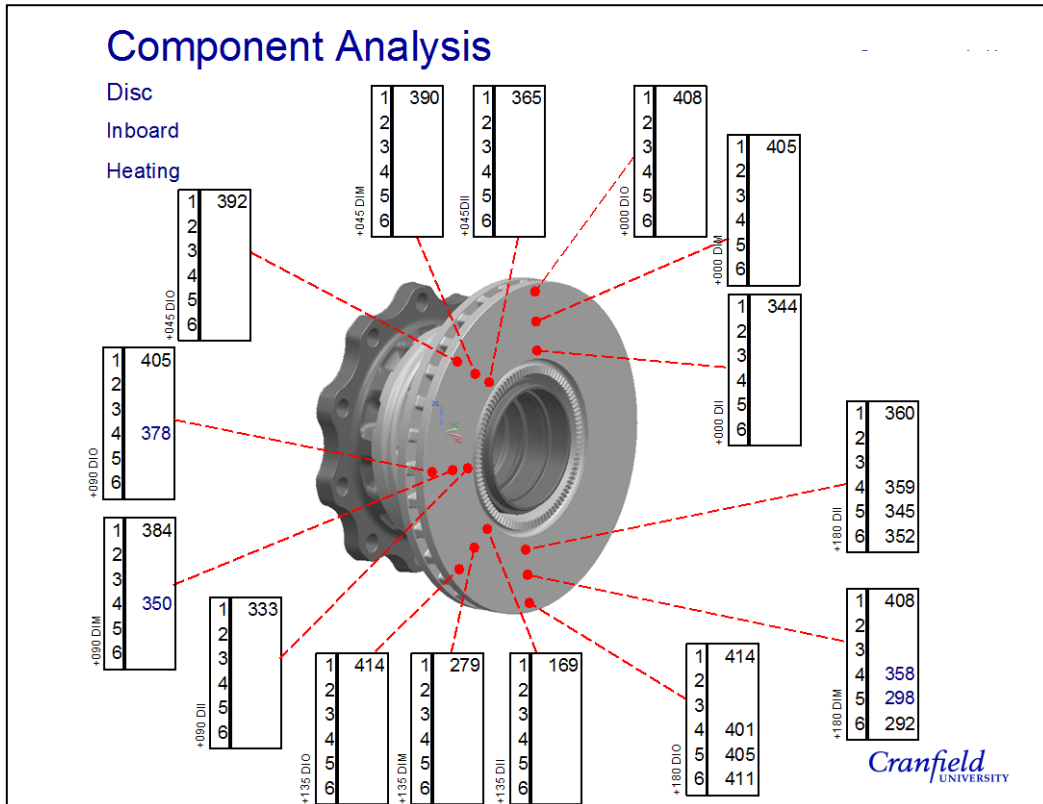


Figure 10.2: Inboard brake “disc only” thermal equilibrium temperatures

As six experiments were scheduled, each thermocouple had the potential to be used up to six times. Three spaces in the CompactRIO were dedicated to non-thermocouple modules for the purpose of the closed-loop motor controller. Consequently, only a selection of the thermocouples ran through every experiment.

Capturing the friction surface heat distribution pattern was obtained by deploying 30 rubbing thermocouples during the disc only experiment. From Figure 10.1 and Figure 10.2, a relatively even distribution of heat was seen whilst the disc was heating. The outboard friction surface was generally warmer than on the inboard, the difference typically staying within a 35°C range. A wider temperature difference was seen across the inboard friction surface, peaking at just over 80°C.

10.1.2 Initial Disc Only Modelling

The simplified CAD model developed in Chapter 6 was used again here and throughout the remainder of the project. The addition of the wheel carrier can be seen in Figure 10.3, along with 10 highlighted surfaces, to indicate the contact regions between the two components. Conduction therefore occurs through these surfaces in accordance with the h_{cond} value outlined in Table 9.3.

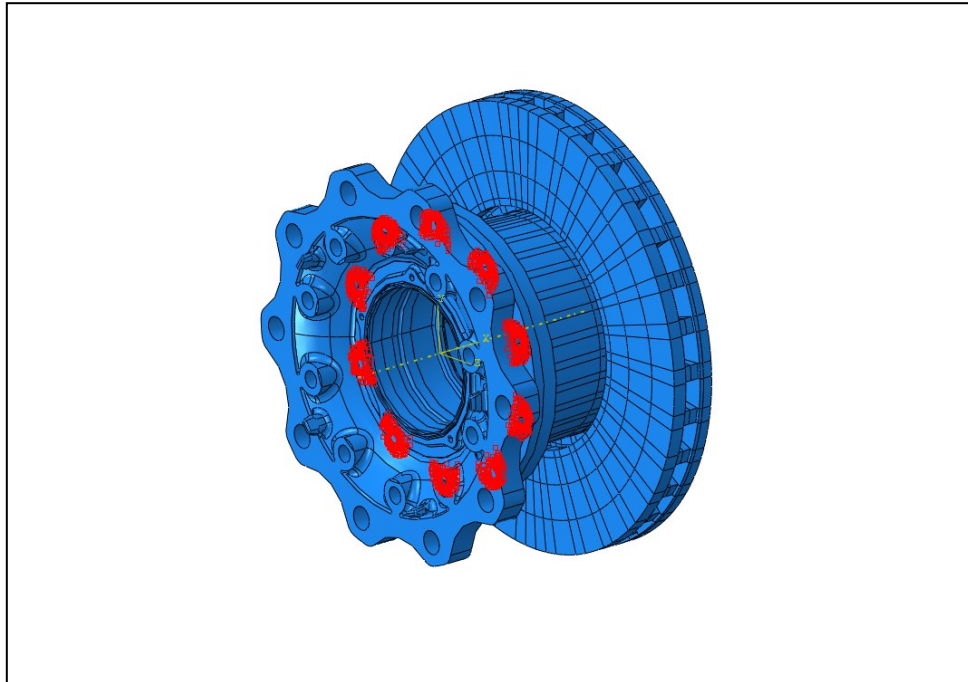


Figure 10.3: Highlighted conduction path for the simplified disc brake and wheel carrier model

Heating the disc brake was done, as previously mentioned, with the disc brake rotating at a constant speed of 100 rpm. As the IHC was set to input 7.00 kW of power into the disc brake,

efficiency losses resulted in the disc brake only receiving 6.44 kW (see Table 9.1). Calculations determined that the resultant heat flux into the each friction surface was 30,687 W/m², assuming it is spread evenly between the inboard and outboard surfaces and across the entire friction surface.

Air was be pumped through the vanes and over the external disc brake surfaces during rotation, causing a degree of forced convective cooling. Constant values of h_{conv} were used during the heating simulations for simplicity. The aim was to achieve realistic final heating temperatures (or initial cooling temperatures), not to necessarily match the heating profile making it possible to simplify the model in this manner. External h_{conv} values used during the heating simulation are shown in Table 10.1, based on the Voller (2003) for the friction surfaces and an iterative approach was used to find the vanes and hat values.

Table 10.1: h_{conv} values used during heating stage of FE simulation, based on 100 rpm rotational speed from Voller (2003) and iteration results

Component	Surface Region	h_{conv} (W/m ² K)
Disc Brake	· Outboard	10
	Friction Surface	
	· Inboard	10
	Hat	10
	Vanes	15
Wheel Carrier	All External	15

Being a large component itself, the wheel carrier will receive and then store a large amount of the heat energy from the disc brake. If the total amount of heat dissipation from the wheel carrier is lower than from the disc brake, there will be a reverse direction of heat flow; from the wheel carrier to the disc brake. Two cooling interactions were resultantly created in the FE model. Highlighted surfaces shown in Figure 10.4 are those chosen for both a radiation and convection purposes. Due to a lack of data, h_{conv} and h_{rad} values for the pad carrier, and all other caliper components coincidentally, were based on engineering judgement. An emissivity value to match that of the disc brake was also used. Although the surfaces were not corrodes, the did have a rough, dark coating that would be relatively close to the friction surface value, making this assumption viable.

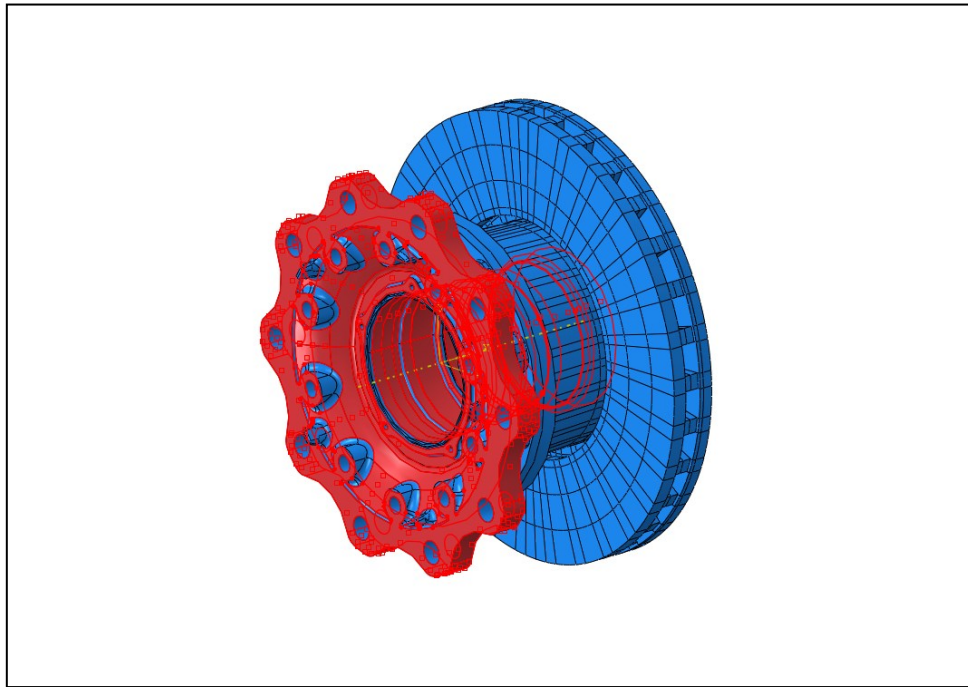


Figure 10.4: Cooling from wheel carrier external surfaces.

One final interaction required with the wheel carrier in the assembly was an open type cavity radiation interaction. Heat exchange in the form of radiation between the two components can therefore be captured. Energy will be emitted from the inner hat disc brake surface and accepted received by the cylindrical, bearing housing section of the wheel carrier (Figure 10.5).

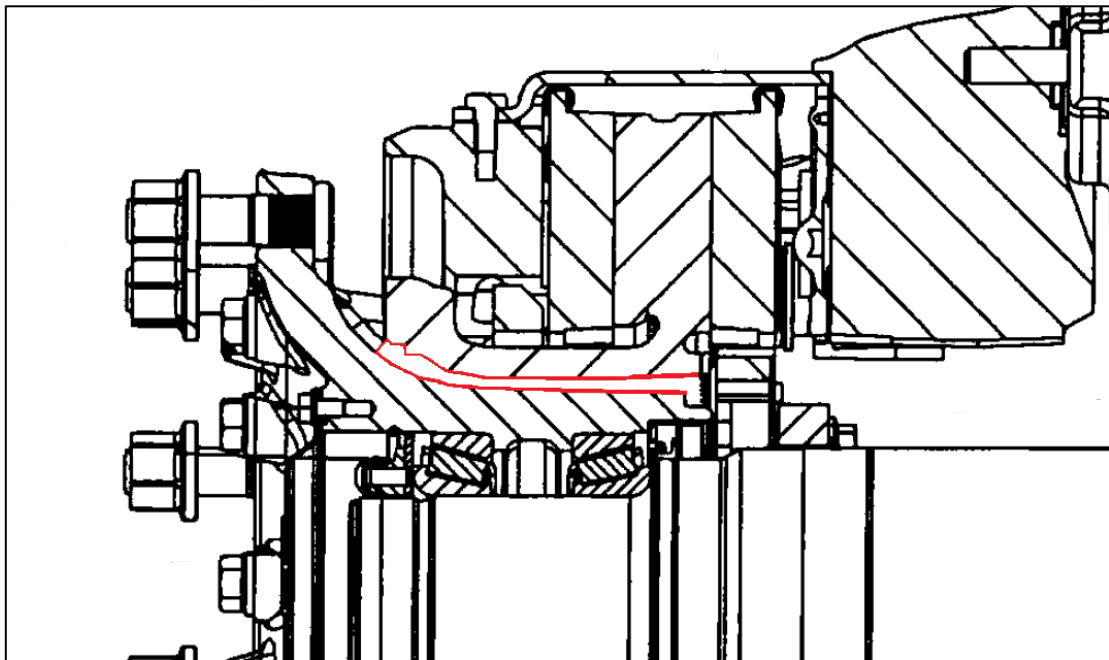


Figure 10.5: Surfaces selected for a radiation interaction between the disc brake and wheel carrier.

A mesh containing 111,516 elements was used for the disc brake, with only 0.48% of them generating skew warnings. Where possible, hexahedral elements were used to create a structured mesh. Contacting surfaces between the disc brake and wheel carrier (Figure 10.3) were forced to contain a structured mesh, with a small region on the flange region requiring tetrahedral elements to connect the two dissimilar meshes together. There was a slight increase in the proportion of skewed elements in the wheel carrier, with 1.83% of 405,508 predominately tetrahedral producing warnings. More complex geometry was the driver for the increased element count in the latter component, requiring a much finer mesh.

Starting from an ambient temperature of 20°C, the heating simulation was run for a two hour time period, making temperature calculations in increments of 10 seconds. In total, the simulation took 14 hours and 19 minutes, using 16 processors on a high power computing cluster, which is based on a dedicated Linux platform. For what is essentially a very simple model, as only the temperature degree of freedom is active on two components, this simulation is very computationally expensive. Developing the mesh to such a fine degree, particularly the wheel carrier, is the primary reason for the vast computation time.

Nevertheless, predicted results from FE modelling generated a temperature distribution, shown in the contour plot in Figure 10.6. The rotor section of the disc brake has a fairly evenly distributed surface temperature, as would be expected from the model setup. A small band depicted in grey surpasses the contour limit, set at 400°C to represent the target heating temperature, with the maximum temperature within the hot band reaching 401°C. Heat soaking through the hat and into the wheel carrier is also evident, with a predicted temperature gradient of 46°C between the thermocouples positions Hat 1 and Hat 3 (see Figure 9.2.b).

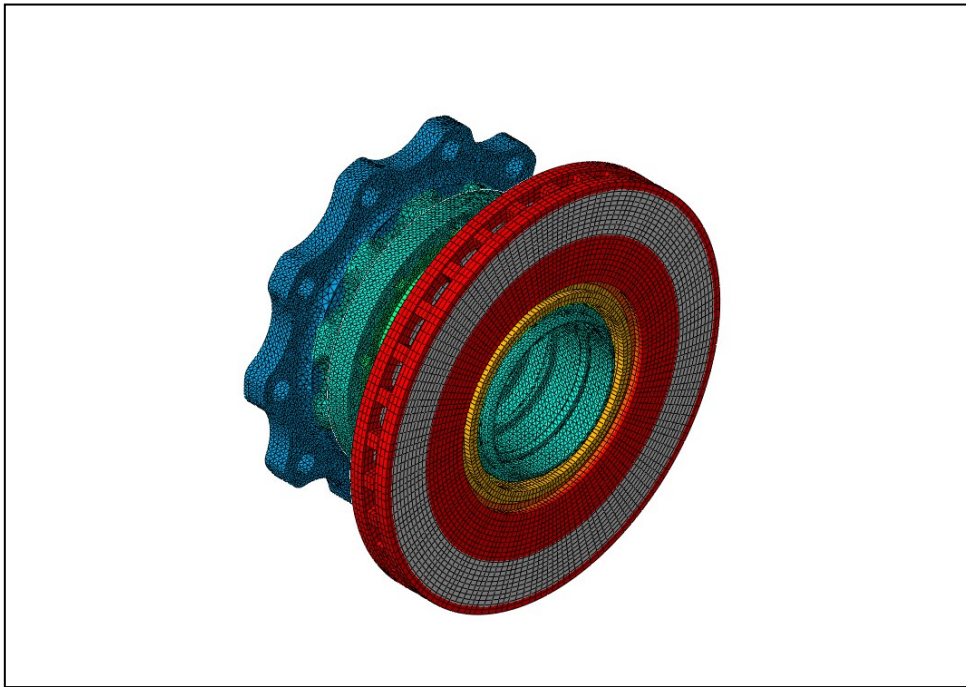


Figure 10.6: Predicted FE disc brake and wheel carrier temperature distribution at thermal equilibrium (initial cooling temperatures)

Accuracy of these temperature predictions can be compared to the experimental heating data taken during the disc brake only testing (experiment 1). Table 10.2 displays the experimental and the FE generated temperature predictions, along with the percentage difference between the two, for all 30 locations (these are the same temperatures as those displayed in Figure 10.1, Figure 10.2 and Figure 10.6). It was shown in Chapter 9 that three thermocouples have been deemed faulty, reducing the number of thermocouples available for FE validation down to 27. All thermocouples conformed to the desired $\pm 20\%$ accuracy limitation. Encouragingly, 23 predicted node temperatures matched the measured data to within $\pm 10\%$, in relative terms. Confidence is further gained with 22 of these thermocouples matched recorded data within only $\pm 5\%$.

Table 10.2: Final heating (initial parking) temperature comparisons – 01 Disc.

Component	Thermocouple Position	Measured Temperature (°C)	FE Prediction (°C)	Difference (%)
Disc	+000 DOO	403	405	0.5
	+000 DOM	400	409	2.3
	+000 DOI	379	404	6.5
	+045 DOO	396	405	2.2
	+045 DOM	405	409	1.1
	+045 DOI	355	404	13.6
	+090 DOO	413	404	-2.1
	+090 DOM	398	409	2.8
	+090 DOI	354	404	13.9
	+135 DOO	/	405	/
	+135 DOM	383	409	6.9
	+135 DOI	341	404	18.5
	+180 DOO	414	405	-2.3
	+180 DOM	395	409	3.6
	+180 DOI	382	404	5.8
	+000 DIO	408	395	-3.3
	+000 DIM	405	397	-2.0
	+000 DII	344	370	7.4
	+045 DIO	392	395	0.7
	+045 DIM	390	397	1.9
	+045 DII	365	370	1.3
	+090 DIO	405	395	-2.6
	+090 DIM	384	397	3.3
	+090 DII	334	370	10.8
	+135 DIO	414	395	-4.6
	+135 DIM	/	397	/
	+135 DII	/	370	/
	+180 DIO	414	395	-4.6
	+180 DIM	408	397	-2.8
	+180 DII	360	370	2.6

10.1.3 Effect of Additional Brake Components on the Disc Brake

Before moving onto the next experiment, where attention will be focused on the pad carrier temperatures, an examination of how the disc brake temperatures change as a result of adding caliper components to the assembly. Of the 30 rubbing thermocouples used in the initial experiment, only nine were used for more than just the disc only experiment. Placement of the pad carrier onto the Thermal Rig eliminated the possibility of mounting any thermocouples in

the 45° and 135° positions, as well as the 90° ID thermocouples; introduction of the bridge and housing also required further disassembly of the latter thermocouples.

A comparison of disc brake temperatures can be made between the experiment one (disc only) to experiment four (with the pad carrier). The first observation to point out with the caliper experiments is that to reach the thermal equilibrium position, the input power setting of the IHC had to be lowered to 6.4 kW, whilst the reference thermocouple remained at approximately 400°C.

When the disc brake was allowed to spin in free air, the flowfield generated around the disc brake were smooth and repeatable. Consequently, airflow into the will transpires uninterrupted, allowing for maximum cooling. Disruption of the flowfield must occur with the introduction of the pad carrier, causing a reduction in the convective cooling. This statement is reflected in the results as less power was required to heat the disc brake to the same temperature.

Introducing the pad carrier to the assembly interrupts the airflow around the disc brake. Angelinas *et al.* (2012) showed that the unified airflow stream exiting the channels, whilst in a dynamic scenario is hindered when the wheel is in close proximity to the disc brake OD creating secondary recirculation regions. With the design of the caliper being such that it must fit inside the wheel when assembled, the pad carrier is likely to have a greater local stifling effect than the wheel, preventing the air from exiting the channel. Consequently, the disc brake was unable to dissipate heat energy as effectively on the caliper side, causing the rise in temperature seen as the disc brake rotates through the caliper components. Adding more caliper components worsens the disc cooling as half of the outboard thermocouples demonstrate a significant rise, without any reductions for experiment five. Only three inboard thermocouples were used on the disc brake, two of which showed no significant change in temperature.

An area of further investigation has subsequently been developed here. Standard brake assembly development is usually focused on minimising component weight for an equal performance level. The challenge set out here is to develop caliper components that not only reduce weight but to also improve assembly cooling characteristics by minimising the impact on the flowfield, whilst maintaining the stiffness required to deliver the high clamp forces needed during a braking application.

10.2 Brake Pad Temperatures

Experiment two was for the FER 4567 pad friction material. A slight modification had to be made to the practical procedure, outlined earlier in the chapter, for the second experiment. As

the pad carrier was removed from the assembly, the pads were kept in contact with the disc brake with a G clamp, tighten by hand with just enough force to prevent the pads from falling (Figure 10.7). Clamp force has already been shown to impact the thermal properties of the brake pad (see section 5.7.3). However, considering the caliper provides a clamp force in the region of 150 kN, hand tightening the G clamp will put an insignificant amount of force through the pads, resulting in a negligible effect on the pad conduction properties during the cooling phase.

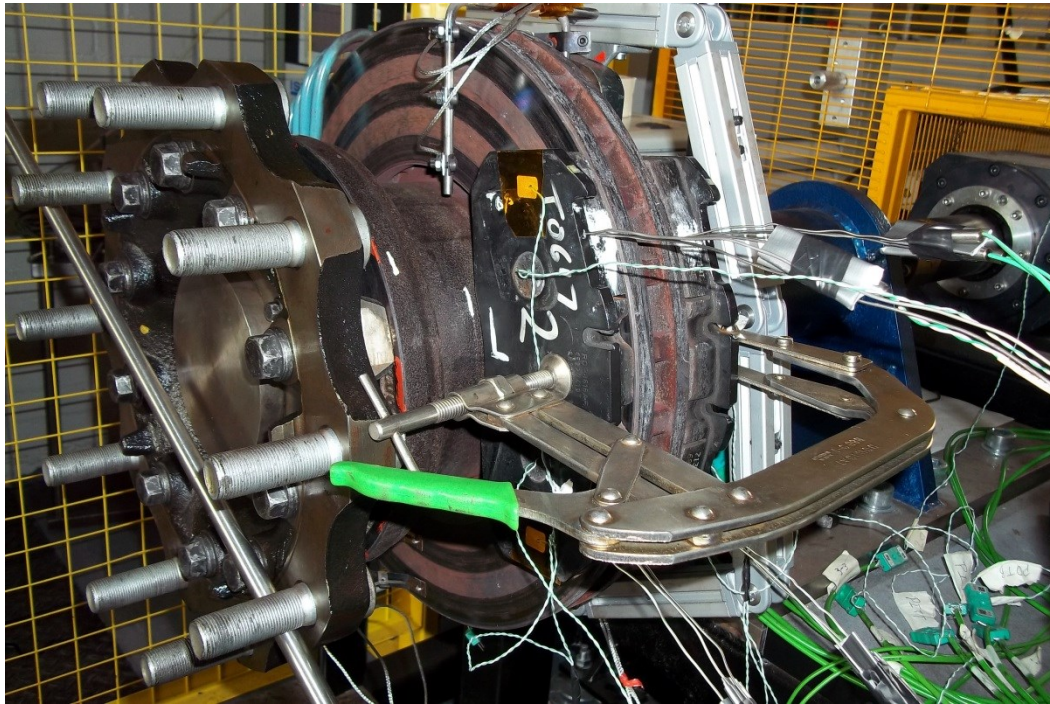


Figure 10.7: FER 4567 brake pads being held against the disc brake with a G clamp – experiment two

A change in procedure which did impact the experimental result is the fact that the pads could not be attached to the disc brake during the heating phase. On the Thermal Rig, heating of the pads can only be done via conduction from the disc brake. With the G clamp method of securing the pads, it became impossible to rotate the disc brake as the pads would come into contact with the IHC. Consequently, the pads were clamped against the disc brake immediately after the disc brake had reached the thermal equilibrium state and the motor and IHC had been switched off.

The pads were only at room temperature rather than a realistic operational temperature so no experimental heating results will be shown. However, the initial FE disc brake and wheel carrier temperatures could be taken from test one, with the pads set to the ambient 20°C. As with all boundary conditions, inputting accurate material properties is essential for accurate temperature predictions, demonstrated already in section 10.3. Material properties supplied by Meritor for the FER 4567 friction material (Table 5.4) were incomplete; most significantly, no value of

thermal conductivity was supplied. Without it, the FE coding would be unable to determine the internal heat flow through the material and therefore, it was necessary to use the method of iteration to find a suitable value. Considering peak surface temperature was not the focus of this model, the proposed actual contact ratio, proposed by Qi and Day (2007), was not used. Instead, the idealised smooth contact interaction was applied between the disc brake and friction material surfaces.

10.3 Pad Carrier Temperatures

Returning to the initial temperature analysis, section 10.3 will now focus on initial pad carrier temperatures. A similar layout will be used as before with the surface temperatures explored first, then the corresponding thermal interactions used in the FE modelling process and finishing with the effects of introducing additional brake assembly components.

Surface temperatures are presented in Figure 10.8 and Figure 10.9, for the outboard and inboard sides respectively. To reiterate, these surface temperatures are the average of five individual experiments. Upon inspection of the results, a temperature distribution indicates that the upper half of the pad carrier is warmer than the lower half by an approximate 20°C. The close proximity of the pad carrier's internal surfaces to the heat source (disc brake) enables a large proportion of the heat dissipated from the disc brake to be absorbed by the pad carrier. With the disc brake shown to be hottest on the upper section, more heat is transferred to the upper half of the pad carrier and hence, the thermal gradient recorded. To a lesser degree, as the pad carrier is stationary, internal buoyancy effects are able to materialise, increasing to the measured thermal gradient within the component.

Another noticeable pattern derived from the experimental results was that the outboard pad carrier side had consistently higher temperatures than the opposite, inboard side. For example, when only the pad carrier was introduced (experiment four) the maximum temperature on the upper outboard internal surface (PC O Int Top) was 240°C, compared to 220°C for its inboard counterpart (PC O Int Top). The former was actually the highest recorded on the pad carrier during that particular experiment, with the minimum recorded at 153°C on the lower inboard external surface, on the bottom of the pad carrier (PC I Ex Bottom). In general, the temperature difference between the two sides of the pad carrier is approximately 10°C.

Differences in the opposing sides arise because of the asymmetry in the component geometry. When fixed onto either a CV or the Thermal Rig, the caliper assembly is mounted onto the chassis via six bolts from pad carriers, which are broken into two sets of three. Each set of bolts

fasten on the inboard side of the pad carrier through two flanges. A conduction path is created, taking heat out of the inboard side. Additional mass is also added to the inboard side for these flange surfaces, providing additional thermal mass for the heat to be dissipated to, resulting in the temperature differences recorded.

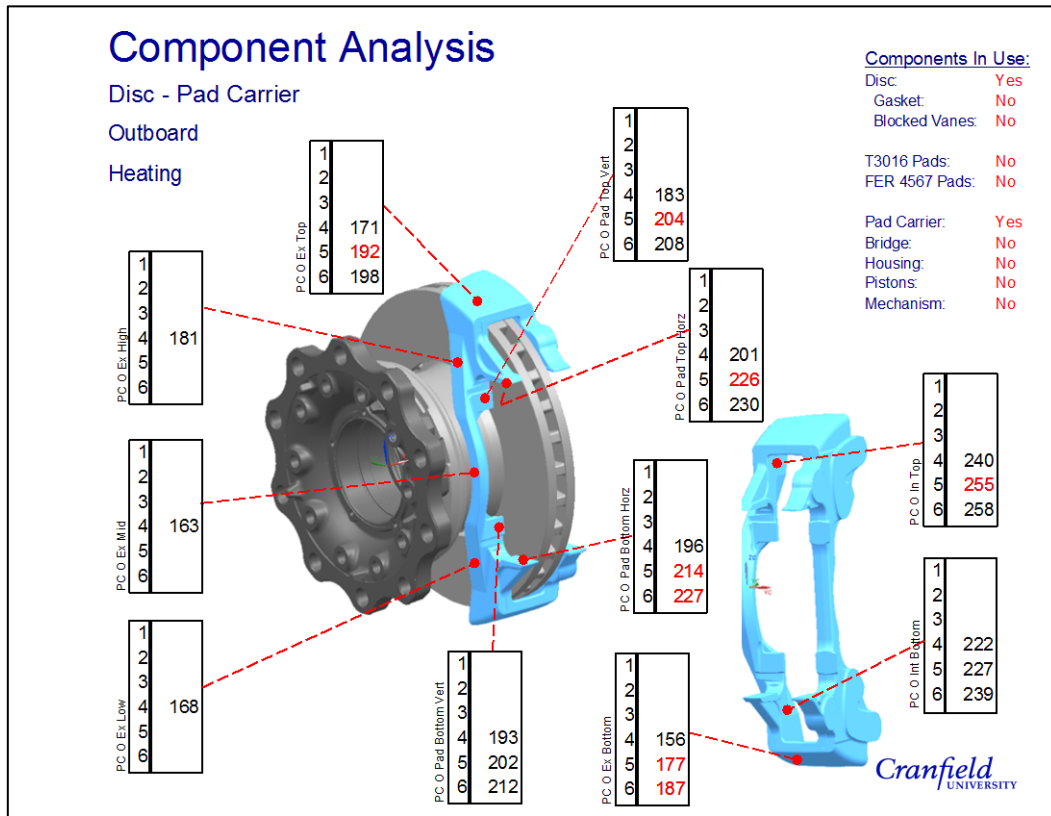


Figure 10.8: Average outboard pad carrier surface temperatures.

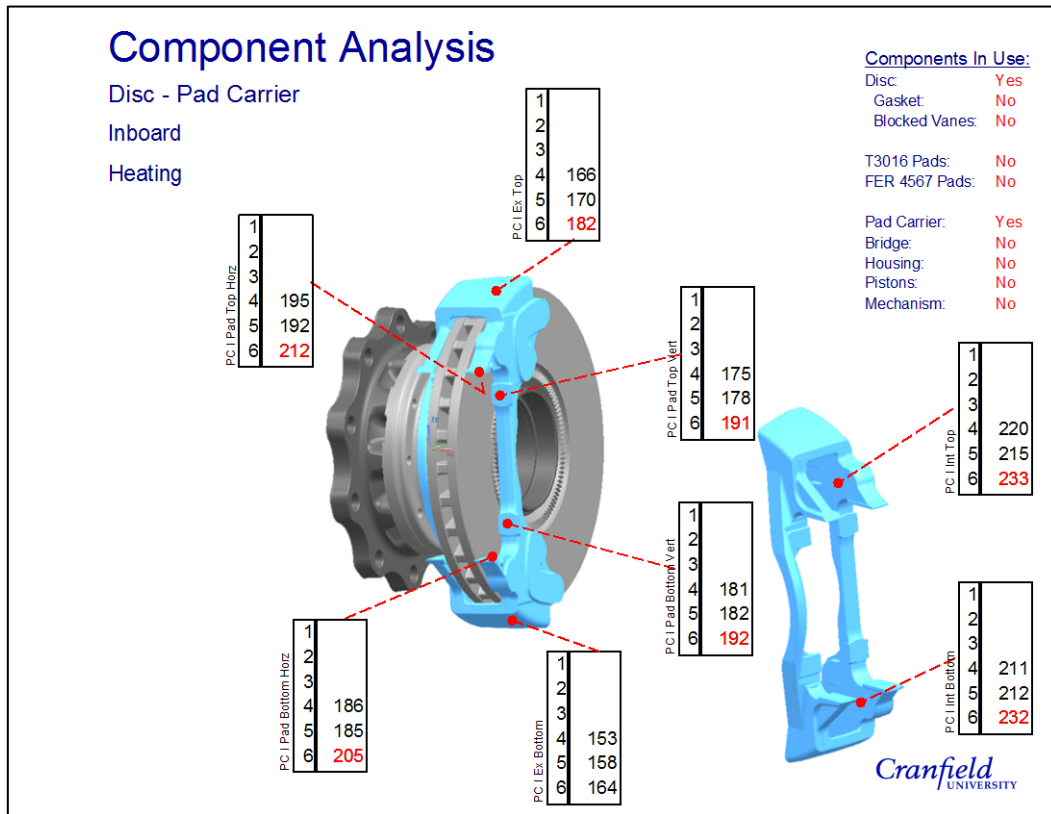


Figure 10.9: Average inboard pad carrier surface temperatures.

10.3.1 FE Model Alterations

With the pad carrier now in the brake assembly, the FE assembly model (presented in section 10.1.2) was developed further. Discussions shall start by describing the changes made before assessing the final heating (initial cooling) predicted temperatures. Starting with the fundamentals, during testing, thermal equilibrium was achieved from a reduced IHC power setting (and all subsequent experiments). The new value was set to 6.40 kW of heating power, with the disc ultimately receiving 5.76 kW. Using this value of input power, the new input flux was calculated at 27,447 W/m². An evenly distribution of the input energy was once again assumed.

Assuming an even distribution of radiation and convection coefficients across the disc brake friction surfaces is no longer a viable option. Results have shown the impact of the pad carrier on the disc brake's cooling characteristics, previously attributed to disturbing the airflow pattern, whilst the physical presence of the pad carrier blocks the radiation path to free air. Actions were taken to incorporate this into the FE model. Figure 10.10 shows the reduction in friction surface area devoted to dissipation via the radiation mode (highlighted in red). Where the pad carrier overlaid the friction surfaces, the radiation to air interaction was removed,

creating two separate areas on either side. The h_{conv} value used for both sections remained at $10 \text{ W/m}^2\text{K}$ (from Voller, 2003).

Figure 10.11 displays a new interaction added to capture the heat transfer between the disc brake friction surfaces and the pad carrier. An open type cavity radiation interaction was set for these surfaces, allowing the disc brake to radiate heat to the pad carrier. It was not just on the friction surfaces where the area of radiation had an alteration, due to the pad carrier introduction. In a similar fashion, an interaction was added for the outer disc brake circumferential surface. Again, an open type cavity radiation interaction was used for the surfaces depicted in Figure 10.12.

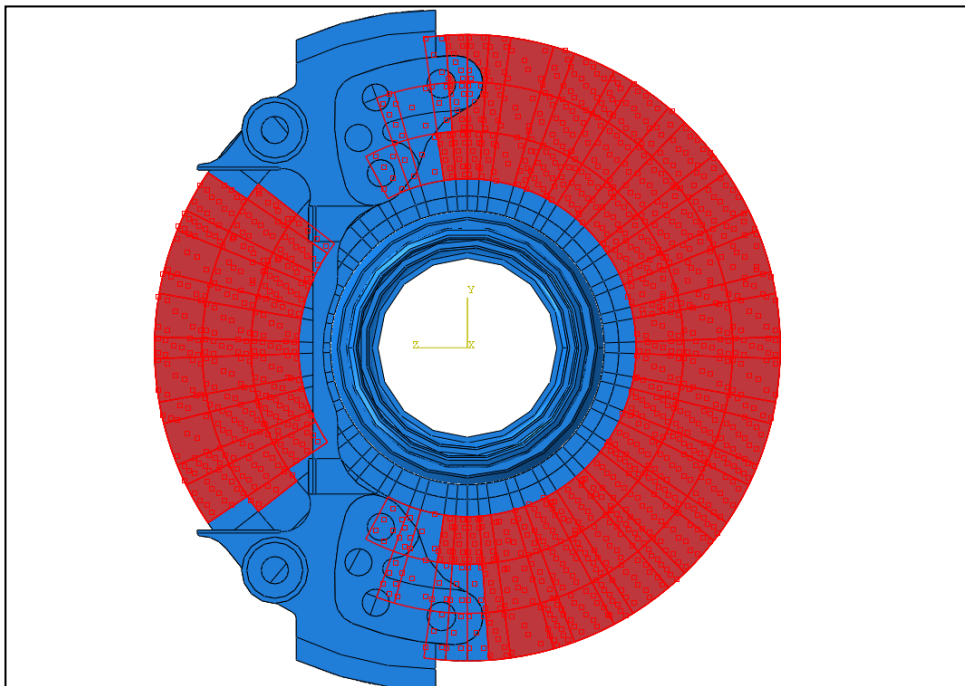


Figure 10.10: Reduction in disc surface area available for radiation with installation of the pad carrier

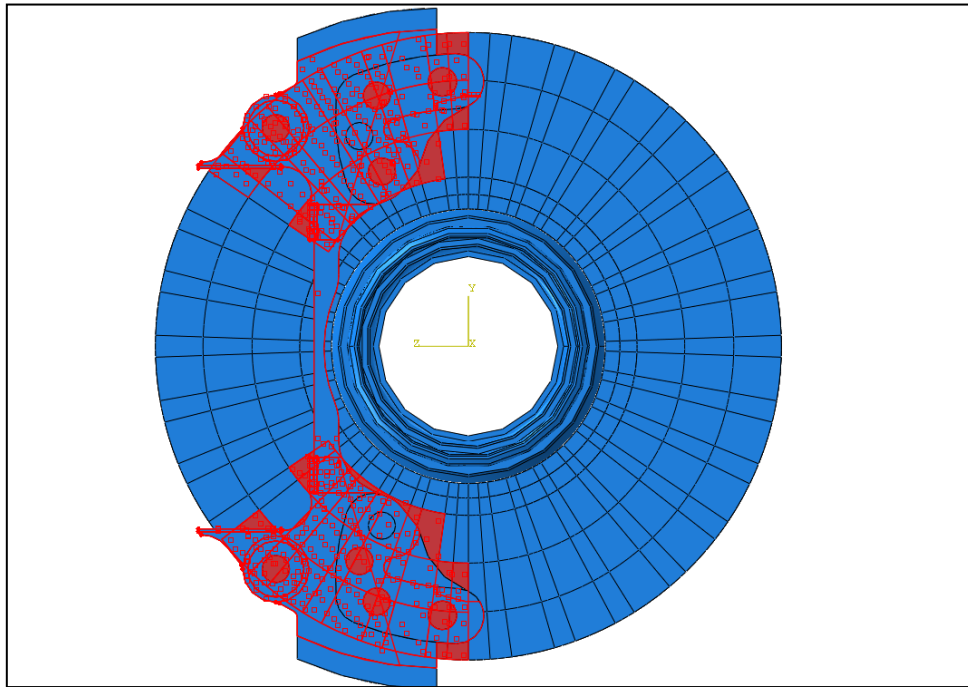


Figure 10.11: Radiation interaction between the disc and the pad carrier surfaces.

Convective heat transfer between the previous two sets of surfaces was much more complex to model. ABAQUS is an FE program, energy leaving a solid surface can be calculated. However, this type of heat transfer requires energy to be transferred through a fluid medium, a process outside the capability of FE analysis. During heating, warm air exiting the vane channels comes into contact with the pad carrier's internal surfaces. In an attempt to capture the convective heat flow within ABAQUS, gap conduction interactions were used on between the surfaces (Figure 10.11 and Figure 10.12). This approach was used simply to simulate the fluid heat transfer so was therefore adequate to use. A list of all the h_{cond} values used for the fourth experiment are shown in Table 10.3.

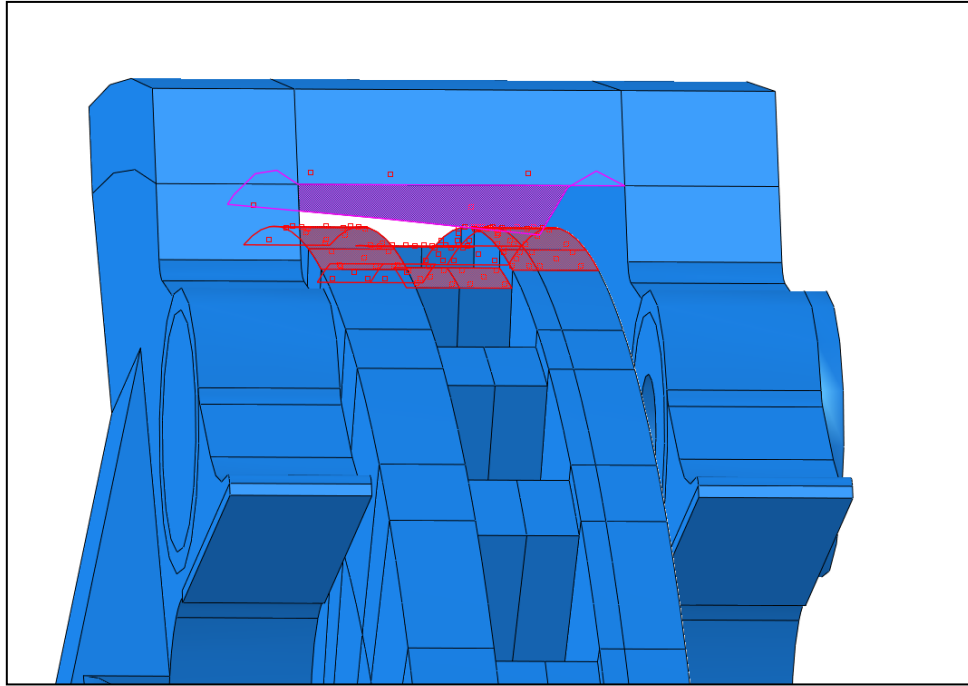


Figure 10.12: Surface area used for both the radiation and gap conduction interactions between the disc brake circumferential surface and the pad carrier

Table 10.3: Gap conductance values used – 04 Disc, Pad Carrier

Introduced	Gap Conductance Interaction	h_{cond} (W/m ² K)	Figure Reference
Experiment 4	Disc Circumferential Surface to Pad Carrier - Top	50	Figure 10.12
	Disc Circumferential Surface to Pad Carrier - Bottom	50	Figure 10.12
	Friction Surface To Internal Pad Carrier - Inboard - Top	50	Figure 10.11
	Friction Surface To Internal Pad Carrier - Inboard - Bottom	50	Figure 10.11
	Friction Surface To Internal Pad Carrier - Outboard - Top	50	Figure 10.11
	Friction Surface To Internal Pad Carrier - Outboard - Bottom	50	Figure 10.11
Experiment 5	Disc Circumferential Surface to Bridge Internal - Top	100	Figure 10.19
	Disc Circumferential Surface to Bridge Internal - Bottom	100	Figure 10.19
	Friction Surface To Internal Bridge	100	Figure 10.20a
	Friction Surface To Internal Housing	100	Figure 10.20b
	Pad Carrier To Housing – Top (Tappet)	100	/
	Pad Carrier To Housing – Bottom (Tappet)	100	/
Experiment 6	Friction Surface Inboard to Piston – Top	50	/
	Friction Surface Outboard to Piston - Bottom	50	Figure 10.23
	Friction Surface To Internal Mechanism	400	/

The final interaction between the disc brake and the pad carrier is shown in Figure 10.13, where another open type cavity radiation interaction was added between the surfaces. Unlike the

previous component interactions, no gap conductance was placed between the hat and the pad carrier. Although it was tested, FE results matched the experimental better when the gap conductance was removed. It was found in Chapter 8 that the airflow exiting the vanes in this region will have a degree of axial velocity, preventing fluid interaction here.

Heat transfer specifically from the pad carrier to the surrounding air was also included. A radiation to air interaction was given to all external surfaces without a cavity radiation interaction already attached to it. The emissivity value used once again matched the value found for the disc brake.

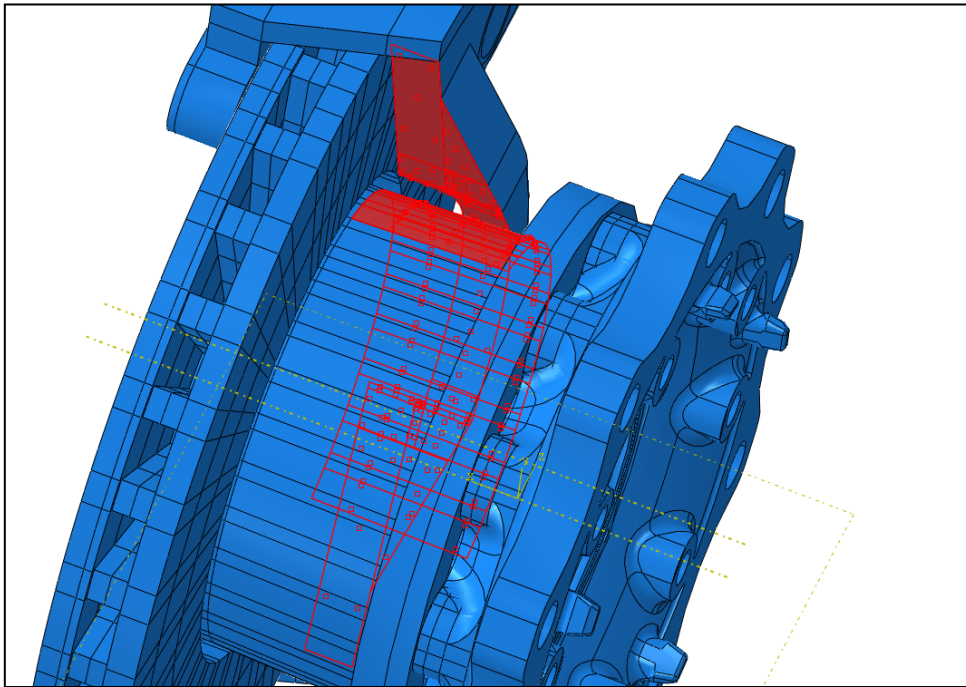


Figure 10.13: Radiation interaction between the hat and pad carrier

It was found experimentally that the pad carrier had an internal temperature gradient, making the top warmer than the bottom. Another superficial modelling technique was attempted to simulate this temperature distribution. Figure 10.14 has the bottom pad carrier surface, located in the $X - \theta$ plane, highlighted. All external pad carrier surfaces were initially given a h_{conv} value of $20 \text{ W/m}^2\text{K}$, except the highlighted bottom surface and the reciprocal top surface. To make the bottom cooler than the top, an increased value h_{conv} equalling $40 \text{ W/m}^2\text{K}$ was used on the bottom, whilst on the top the value remained at $20 \text{ W/m}^2\text{K}$.

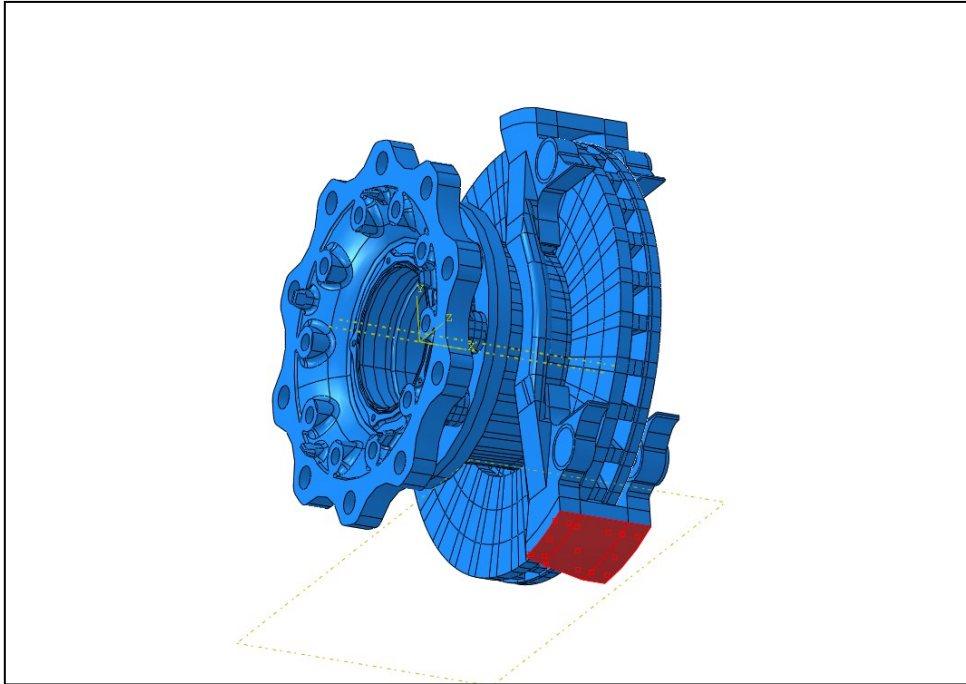


Figure 10.14: Surfaces used in attempt to artificially create a vertical thermal gradient

The final interaction added to the FE model was to simulate conduction from the two pad carrier flange surfaces to the axle. Importance of the additional mass in this area has already been shown to cause the inboard pad carrier side to be cooler than the outboard side. As the FE model does not include the axle attachment plates, a conduction interaction cannot be made. Instead, an artificial convection interaction was added to the model to capture the axial thermal gradient. Figure 10.15 displays the flange surfaces where this convection interaction was placed. Calculations were made initially to find the value of h_{conv} that would generate an equivalent amount of heat transfer as the actual conduction process did on the Thermal Rig. Fourier's law of cooling for convection and conduction were equated and rearranged to make h_{cond} the subject of equation (10.1), subsequently ensuring the convective and conduction dissipation are equal. As the same surface area is used in both they cancelled and were removed.

$$h_{conv} = \frac{h_{cond}\Delta T}{(T_{surf} - T_{\infty})} \quad (10.1)$$

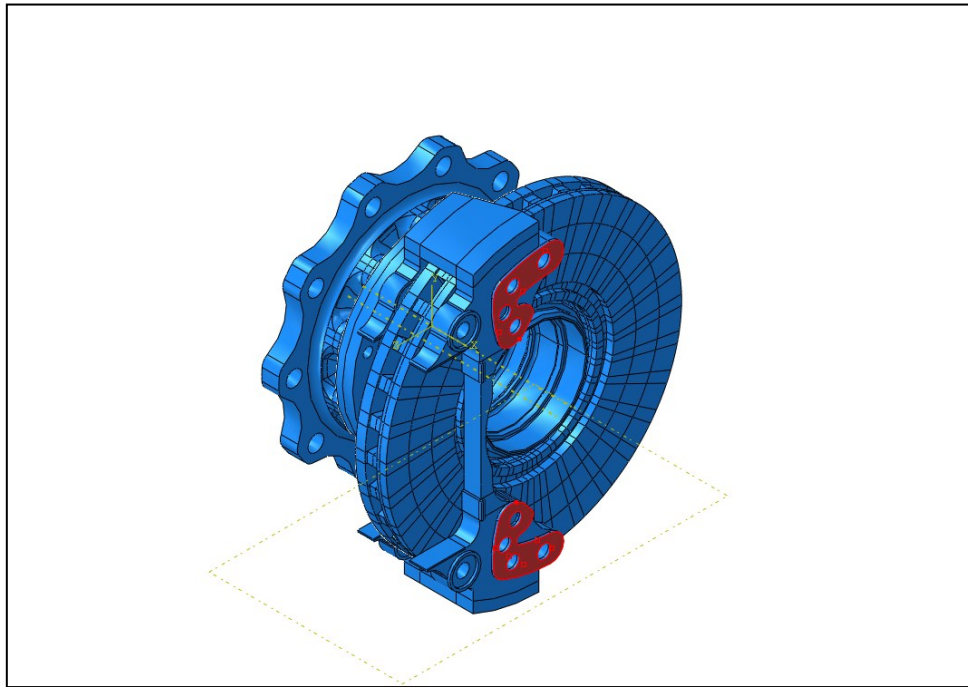


Figure 10.15: Pad carrier flange surface thermal boundary conditions

Evaluation of equation (10.1) requires the temperature difference between the mating surfaces to be known. As this was not recorded, it was assumed 1°C initially simulating a low thermal contact resistance. Using Tirović and Voller’s method, the h_{cond} value was calculated at 2,314 W/m²K. An estimation of 180°C could be made for the flange surface temperature, based on the results presented in Figure 10.9. Placing these values into equation (10.1) generated an initial h_{conv} value of 14.5 W/m²K. This value was rounded up to 15 W/m²K, which delivered well matched results.

10.3.2 Pad Carrier Final Heating FE Temperatures

Once again, predicted temperatures produced by the FE modelling are shown in Table 10.4, and match well with the experimental data. Of the nine rubbing thermocouples used on the disc brake, seven nodal positions predicted temperatures within $\pm 8\%$ of the measured data, with two predictions being slightly less accurate but still within $\pm 14\%$. Pad carrier temperature predictions also proved to have a close match. In total, of 11 thermocouples placed on the pad carrier surfaces, only one nodal temperature had a temperature difference larger than $\pm 20\%$ with the measured data, generally showing a good agreement.

Table 10.4: Final heating (initial parking) temperature comparisons – 04 Disc, Pad Carrier.

Component	Thermocouple Position	Measured Temperature (°C)	FE Prediction (°C)	Difference (%)
Disc	+000 DOO	403	390	-3.3
	+090 DOO	387	396	2.1
	+090 DOM	383	398	4.1
	+090 DIO	378	395	4.6
	+090 DIM	350	396	13.1
	+180 DOO	367	384	4.6
	+180 DOM	371	388	4.6
	+180 DOI	341	388	13.9
	+180 DIO	401	385	-4.0
	+180 DIM	358	385	7.6
	+180 DII	359	363	1.2
Pad Carrier	PC O Ex Top	171	205	19.7
	PC O Ex High	181	200	10.3
	PC O Int Top	240	209	-12.8
	PC O Pad Top Vert	183	190	3.9
	PC O Pad Top Horz	201	204	1.5
	PC O Ex Mid	163	156	-4.1
	PC O Pad Bottom Vert	193	181	-6.0
	PC O Pad Bottom Horz	196	192	-2.2
	PC O Ex Low	168	187	11.1
	PC O Int Bottom	222	197	-11.7
	PC O Ex Bottom	156	182	16.1
	PC I Ex Top	166	206	24.4
	PC I Int Top	220	219	-0.5
	PC I Pad Top Vert	175	199	13.8
	PC I Pad Top Horz	195	207	6.3
	PC I Pad Bottom Vert	181	192	6.5
	PC I Pad Bottom Horz	186	196	5.6
PC I Int Bottom	211	206	-2.3	
PC I Ex Bottom	153	183	19.7	

Making the pad carrier match was not straightforward. Paying close attention to the top and bottom surfaces in the $X - \theta$ plane (see Figure 10.14), nodal temperatures here were less accurate than the other locations. Early modelling trials utilised the SG Steel properties given in Table 5.1. Produced results had the $X - \theta$ surfaces overestimating by 100%, whilst the remaining nodal temperatures were significantly underestimating the temperature. The material properties were individually increased and decreased in 5% increments but ultimately,

modelling proved insensitive to individual property changes. These large differences were the main reasoning for implementing the bolt fastening flange surface gap conductances. By lowering the inboard temperature, axial heat flow took some of the excess heat away from the pad carrier top surface.

10.3.3 Influence of Other Caliper Components on Pad Carrier

Similarly with the disc brake, adding additional caliper components altered the average surface temperatures. Referring back to Figure 10.8 and Figure 10.9, the same colour coding scheme has been used to easily distinguish significant temperature changes. This section will briefly describe how adding the remaining caliper components influence pad carrier temperatures.

The outboard side of the pad carrier was most affected by the introduction of the bridge and housing (experiment 5). Six of the eight outboard thermocouples used in all the experiments showed significant increases. Conversely, there were no significant temperature changes on the inboard side of the pad carrier. By enclosing the pad carrier's outboard surface, the ability to convectively dissipate heat away is limited. The location of the bridge also restricts the radiation dissipation mode. Surfaces on the inboard side of the pad carrier, however, remain relatively open to passing airflow, keeping the convection rate relatively high.

A different pattern is seen when the pistons and mechanism component are placed inside the housing unit (experiment 6). Seven out of the eight inboard pad carrier thermocouples produced significant temperature changes compared to just three on the outboard pad carrier side. Introduction of the mechanism and pistons gives additional thermal mass to the housing unit, providing a greater sink for heat to be conducted away from the pad carrier. However, the opposite occurs, demonstrated by the pad carrier temperature rises.

A change to convection is attributed to this temperature increase. The bridge has been shown to act as an airflow barrier for the friction surfaces (see smoke machine testing, section 8.3.3.3), explaining the temperature rise. Further reduction of friction surface airflow once the mechanism has been installed can be explained by the schematic diagram shown in Figure 10.16. In the absence of the mechanism, air can funnel through the opening in the inboard housing side and over the friction surface as well as the internal bridge surfaces. Once installed, this airflow path is blocked, further reducing the convection potential. The situation is likely to be worsened by the presence of the pistons, as they will further impede the airflow within this channel.

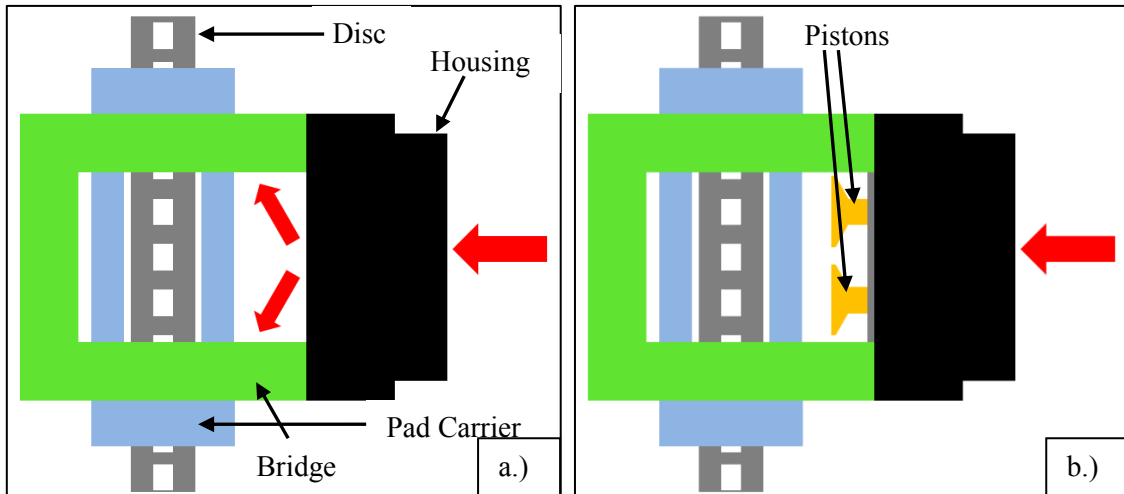


Figure 10.16: Schematic diagram of airflow a.) flowing through the housing or b.) being blocked by the mechanism.

10.4 Bridge and Housing Temperatures

In the fifth experiment, both the bridge and housing components were installed onto the Thermal Rig together. Discussion will continue on an individual basis, with attention focused on the bridge temperatures first.

10.4.1 Bridge Final Heating Temperatures

Recorded temperatures are presented in Figure 10.17. Like with the pad carrier, a temperature gradient is present between the upper and lower half of the component, albeit not a considerable one. For example, the external outboard temperatures only differ by 9°C , with the internal surfaces measuring a difference no greater than 5°C .

However, the difference between the internal surfaces, located directly over the vane channel exits (Br Mid Int Top/Bottom), and the immediate external surface only a few millimetres away (Br Mid Ex Top/Bottom) produces a far larger gradient, which were 34°C and 56°C on the upper and lower bridge parts respectively. Exiting air being pumped out the vane channels impact these internal surfaces, heating these regions up beyond any other point on the bridge. Conduction then disperses the heat around the remaining areas of the bridge.

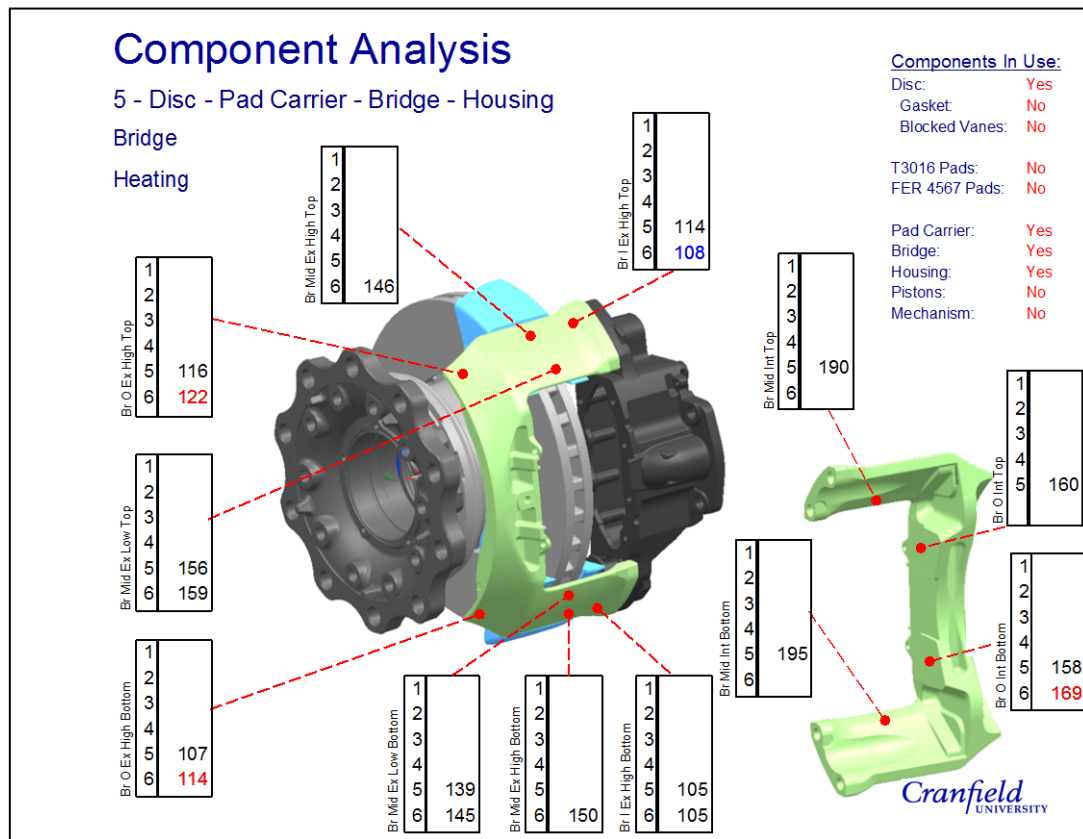


Figure 10.17: Average recorded bridge temperatures

It can also be seen in Figure 10.17 that installation of the mechanism and pistons does indeed impact on bridge temperatures. Of the four thermocouples located on the outboard side, three of them display a rise greater than 5°C. The remaining bridge temperatures remain approximately equal apart from a single thermocouple showing a decrease in temperature (Br I Ex High Top) by 6°C.

10.4.2 Housing Final Heating Temperatures

Next is the turn of the housing unit. Only six thermocouples were used on the housing, reducing to three when the mechanism was added. Figure 10.18 demonstrates that there is a temperature gradient on the flange (internal) surface, but it has a slightly different characteristic than what has been seen on previous components. Indeed, the top of the flange is warmer than the bottom by 8°C, yet the difference is much less than that from the central flange thermocouple to either of the top or bottom, 32°C and 24°C respectively. This result is a function of conduction from both the bridge and the pad carrier. Heat from the bridge predominately enters the housing through two individual contact regions, warming both the upper and lower sections of the component. Likewise, heat leaves the pad carrier through two tappets, which is then conducted

through to the housing. Thermal energy therefore enters at two extremities of the housing and hence, generating the displayed heating profile in Figure 10.18.

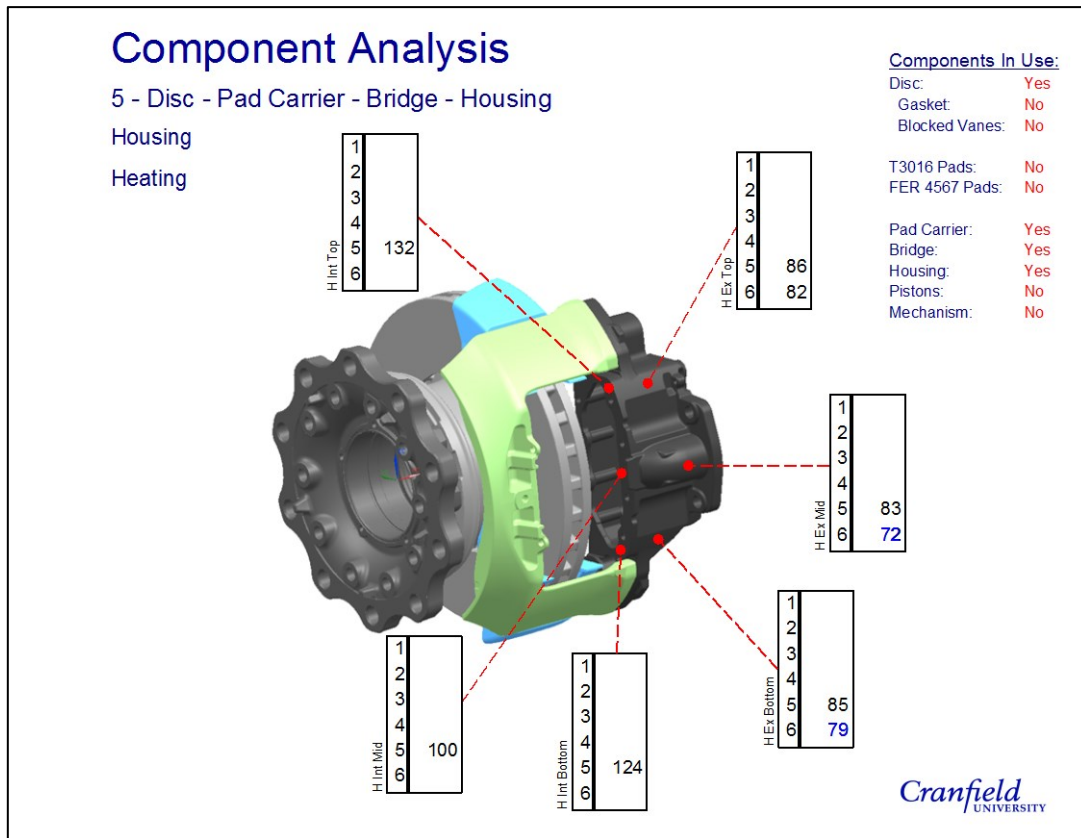


Figure 10.18: Housing final heating (initial cooling) temperatures

An obvious but important result is shown in Figure 10.18, with regards to the change in heating profile when the mechanism and pistons are installed on the assembly. Heat appears to be drawn from the housing's external surface and into the mechanical parts, due to the additional thermal capacity offered by their presence. With more heat going into the mechanism components rather than the housing unit, the chances of the secondary brake failure increase (a concept introduced in Chapter 8).

10.4.3 FE Model Development – Bridge and Housing

With the addition of the bridge and housing to the assembly, additional interactions and further changes were needed to the FE model. Interactions specific to the bridge will be discussed first before moving onto the housing unit. In a similar fashion to the pad carrier, placement of an open type cavity radiation interaction was placed between a section of the disc brake's outer circumferential surface and the internal top and bottom bridge surfaces (Figure 10.19). As before, the local ambient temperature used for this relationship remained at room temperature.

Both the bridge and housing unit had a rough, painted surface finish over the external surfaces. The emissivity would therefore be high, approaching unity and so the same emissivity value for the bridge and housing unit external surfaces were given the same emissivity value as the disc brake. Pumping of air through the channels also required a gap conductance interaction here to account for fluid interactions (see Table 10.3 for h_{cond} values).

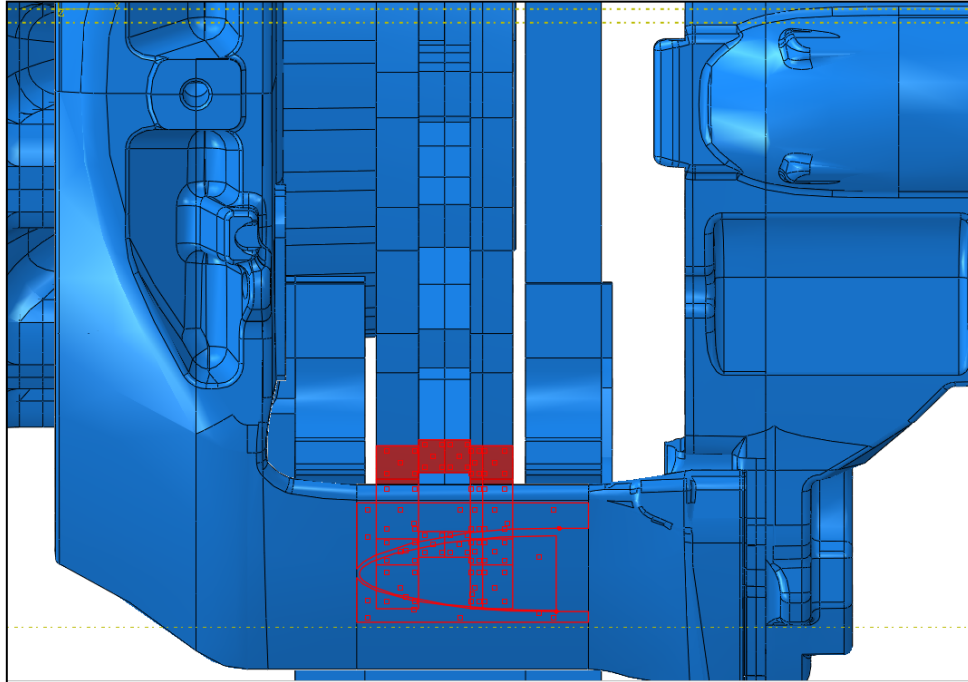


Figure 10.19: Radiation and gap conduction surfaces between bridge and disc brake outer surface

This was not the only place where radiation energy dissipated by the disc brake was captured by the bridge. Without a set of brake pads present in the assembly, there was a direct path between the disc brake outboard friction surface and the internal bridge surfaces (Figure 10.20.a). Again, a cavity type radiation interaction was placed on these surfaces with the same ambient temperature and emissivity values used as before. Interactions were set up the same for heat being passed from the disc brake inboard friction surface to the housing flange surface (Figure 10.20.b).

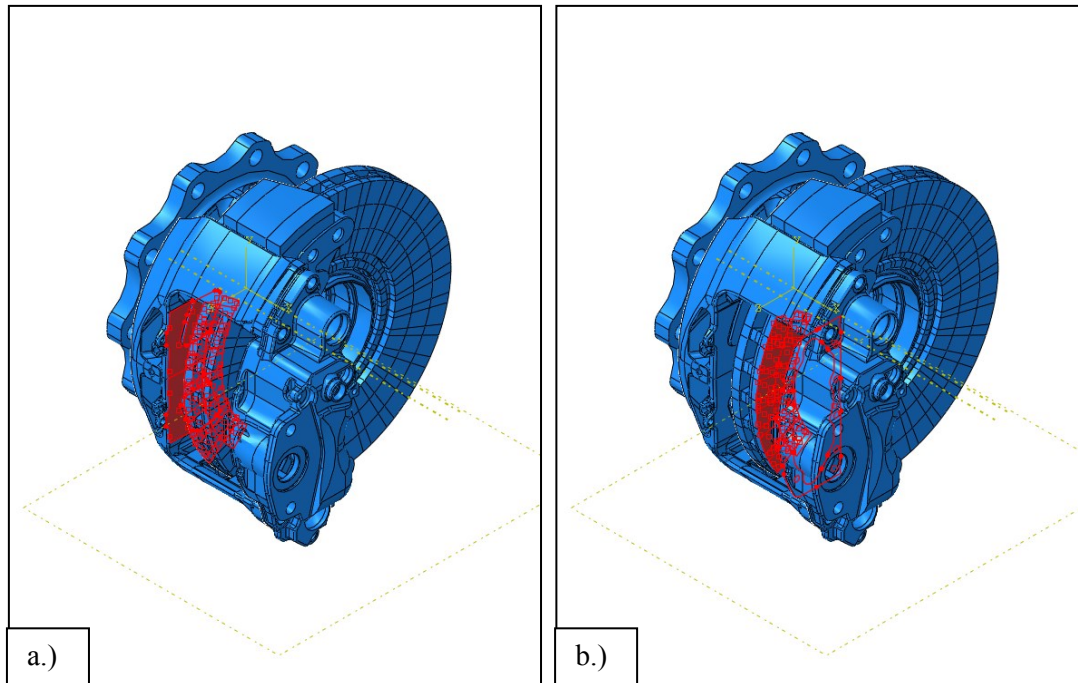


Figure 10.20: Radiation from disc brake friction surface a.) outboard to internal bridge surfaces, and b.) inboard to housing flange surface

The final alteration to the FE model was to add convection cooling to the inboard internal bridge surfaces, as described by the schematic diagram (Figure 10.16). Air being sucked through the housing meets the deflected exiting vane channel air and passes under the bridge. Therefore, it was necessary to add a high h_{conv} value to these surfaces. All other bridge and housing external surfaces were subject to both a radiation to air and standard convection interactions, for both the bridge and the housing. The same emissivity and convective coefficient values were used as with the pad carrier.

10.4.4 Bridge and Housing Heating FE Results

By this stage, the modelling procedure for the disc brake components had become relatively mature. It is therefore unsurprising that good agreement was generally found between the experimental data and FE predictions for the disc brake as only one of the seven nodal temperatures were misaligned to the thermocouple reading. The same can be stated for the pad carrier as all 16 predicted nodal temperatures match very well to with recorded data.

Unfortunately, even with all the global and localised thermal interactions placed on the bridge, it proved extremely difficult to achieve accurate bridge temperatures. This is reflected in Table 10.5 as only one of the eight nodal temperatures matched recorded data relatively well. It would appear that the global bridge temperature is too high as six nodal temperatures differences are in

excess of 20%, with only one below. Values presented in Table 10.5 were the best results after 32 attempted simulations.

Modelling of the housing was somewhat more successful. Three of the five node temperatures showed good agreement, with two having differences greater than 20%. It can be assumed therefore that the global heating profile is approximately correct for this component. It was decided that the investigation would continue without rectifying the bridge modelling at this stage, since additional components (mechanism, pistons, pads) may introduce difference thermal interaction mechanisms.

Table 10.5: Final heating (initial parking) temperature comparisons – 05 Disc, Pad Carrier, Bridge, Housing

Component	Thermocouple Position	Measured Temperature (°C)	FE Predicted Temperature (°C)	Difference (%)
Disc	+000 DOO	400	383	-4.2
	+180 DOO	378	378	0.2
	+180 DOM	386	383	-0.8
	+180 DOI	340	378	11.1
	+180 DIO	395	380	-3.9
	+180 DIM	301	381	26.9
	+180 DII	344	352	2.4
Pad Carrier	PC O Ex Top	195	190	-2.7
	PC O Int Top	254	215	-15.3
	PC O Pad Top Vert	210	196	-6.8
	PC O Pad Top Horz	230	214	-6.8
	PC O Pad Bottom Vert	206	173	-16.1
	PC O Pad Bottom Horz	215	180	-16.0
	PC O Int Bottom	232	187	-19.5
	PC O Ex Bottom	178	179	0.6
	PC I Ex Top	175	182	4.2
	PC I Int Top	218	186	-14.5
	PC I Pad Top Vert	179	171	-4.5
	PC I Pad Top Horz	191	180	-5.6
	PC I Pad Bottom Vert	181	163	-10.3
	PC I Pad Bottom Horz	188	166	-11.5
	PC I Int Bottom	214	174	-18.9
PC I Ex Bottom	159	177	11.1	
Bridge	Br O Ex High Top	119	147	23.7
	Br Mid Int Top	193	141	-26.5
	Br O Int Top	160	187	16.8
	Br O Int Bottom	159	199	25.4
	Br O Ex High Bottom	111	181	63.3
	Br I Ex High Bottom	105	146	39.0
	Br Mid Ex Low Bottom	141	230	63.1
	Br Mid Int Bottom	190	233	22.9
Housing	H Ex Top	87	89	1.5
	H Ex Bottom	85	103	21.0
	H Int Top	131	97	-25.8

H Int Mid	101	105	4.7
H Int Bottom	124	112	-9.5

10.5 Piston Temperatures

The brake assembly initial temperature analysis and FE model development work was completed by introducing the mechanism and the piston, which were the final components in the assembly. Figure 10.21 indicates that only pistons temperatures were recorded during the experimental process. It was hoped that surface temperatures on the mechanism would be investigated but unfortunately it proved physically impossible to secure any thermocouples to it. Consequently, it was only able to monitor piston surface temperatures.

Results show there is little temperature difference between the two pistons. The top piston is marginally warmer by only 7°C, at 162°C. Having previously noted that there is little airflow in the region between the inboard friction surface and the mechanism, which is also encased by the bridge, it is reasonable to assume that radiation is the dominant source of piston heat input.

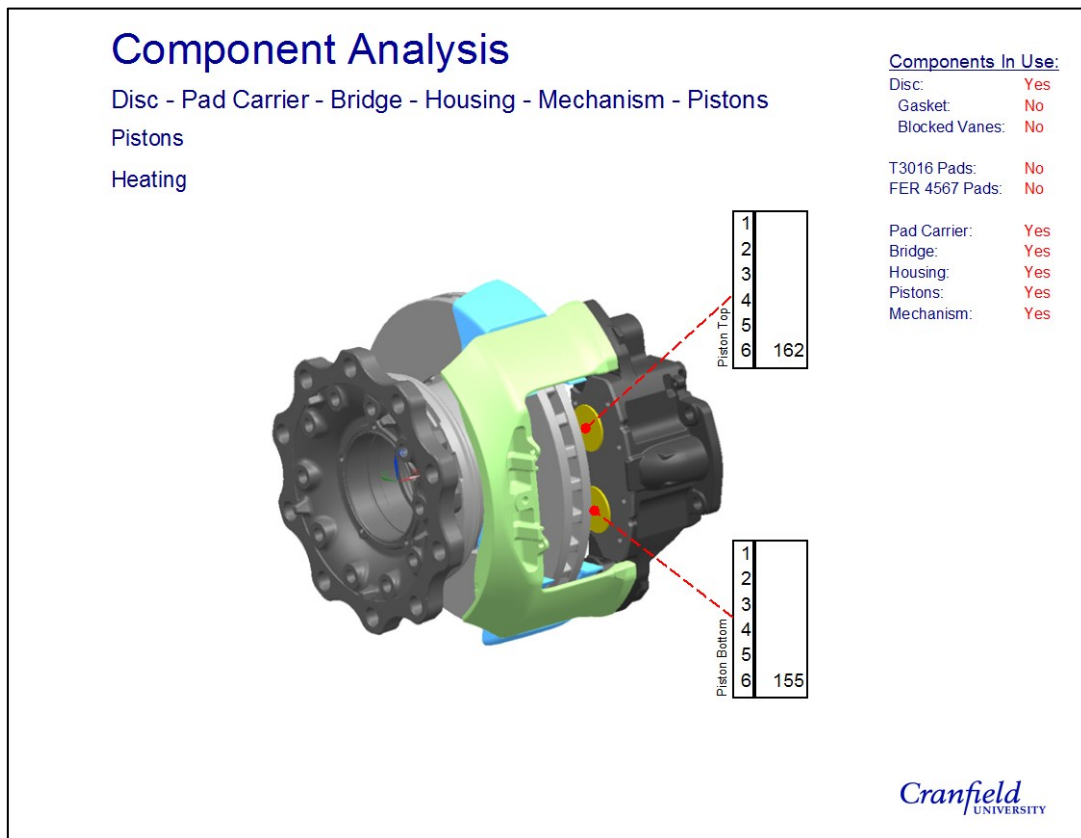


Figure 10.21: Piston temperatures from experiment 6

10.5.1 FE Development and Results

FE model development started with modelling the mechanism and piston components. No CAD model of these parts were supplied, consequently simplified geometry models for both parts were made. To ensure the simplified parts were representative, the mechanism and both pistons were weighed, giving a combined mass of 2.8 kg. Volume was added to the components such that when the material density was inputted into the NX modelling software, the correct combined mass was achieved. This was important to ensure the thermal heat sink added to the assembly was representative. With all components completed, the final FE model could be meshed, presented in Figure 10.22. In total, the mesh contained 1.15 million elements for the eight components it is assembled from, remembering there are two pistons. From Table 10.6 it can also be seen that the mesh quality is generally good, with only a low percentage of skewed elements in each of the components. The piston mesh does have a slightly higher proportion of skewed elements but being the smallest component in the assembly, it has minimal impact.

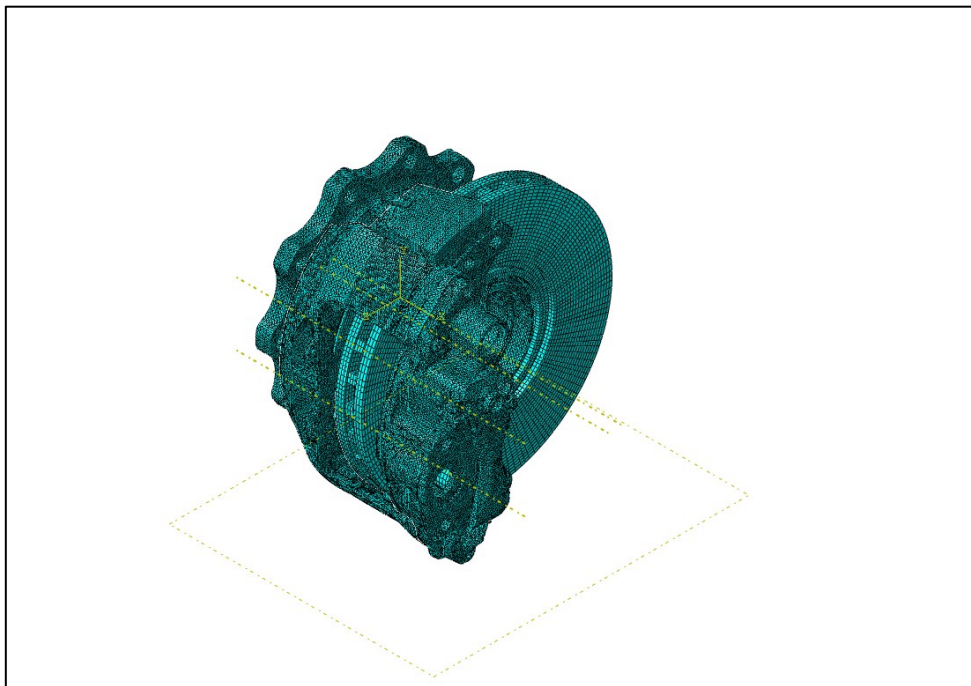


Figure 10.22: Full FE caliper assembly model – experiment 6

Table 10.6: Breakdown of the number of elements in the full FE model.

Component	Number of Elements	Skew Warnings
Disc	113,893	0.47%
Wheel Carrier	405,523	1.83%
Pad Carrier	166,916	0.15%
Bridge	217,450	1.20%
Housing	241,027	1.46%
Mechanism	8,442	0.17%
Piston	1,312	7.32%
Total	1,155,875	

Only two new radiation interactions were necessary to develop the FE model for this section. Both were from the disc brake's inboard friction surface, firstly to each of the pistons surfaces and also to the surface region of the mechanism, which is not being block by the pistons. This latter interaction is demonstrated in Figure 10.23. From the experimental results, it has been implied that there is little airflow within the space between the inboard friction surface and the mechanism, which is encased by the bridge. Consequently, there was no need to add a gap conduction interaction. Furthermore, despite the overheated bridge predictions in the previous section, a lack of airflow required removal of the high h_{conv} values placed on the inboard internal bridge surfaces. Brake assembly temperatures in the thermal equilibrium state are shown in Table 10.7.

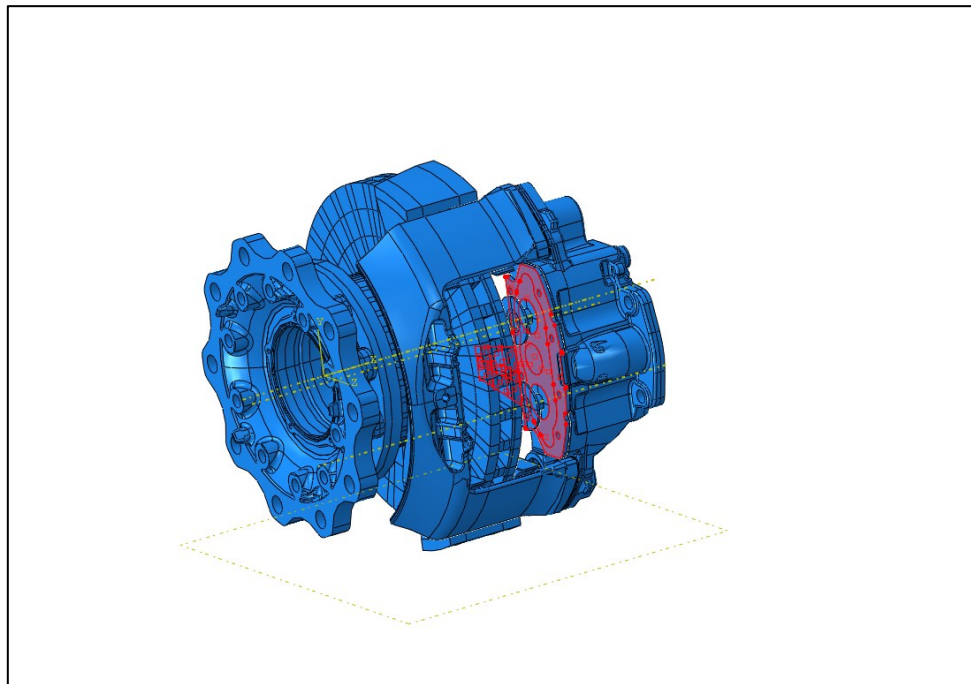


Figure 10.23: Radiation interaction between inboard friction surface and the mechanism

Table 10.7: Final heating (initial parking) temperature comparisons – 06 Disc, Pad Carrier, Bridge, Housing, Mechanism, Pistons

Component	Thermocouple Position	Measured Temperature (°C)	FE Predicted Temperature (°C)	Difference (%)
Disc	+000 DOO	399	377	-5.6
	+180 DOO	392	376	-4.1
	+180 DOM	399	380	-4.7
	+180 DOI	347	364	4.8
	+180 DIO	412	361	-12.4
	+180 DIM	292	378	29.7
	+180 DII	352	373	6.0
Pad Carrier	PC O Ex Top	198	289	46.4
	PC O Int Top	258	249	-3.8
	PC O Pad Top Vert	208	228	9.6
	PC O Pad Top Horz	230	241	4.8
	PC O Pad Bottom Vert	212	219	3.3
	PC O Pad Bottom Horz	227	229	1.3
	PC O Int Bottom	239	233	-2.4
	PC O Ex Bottom	187	273	45.8
	PC I Ex Top	182	287	58.1
	PC I Int Top	233	242	4.0
	PC I Pad Top Vert	191	227	18.8
	PC I Pad Top Horz	212	233	10.0
	PC I Pad Bottom Vert	192	216	12.9
	PC I Pad Bottom Horz	205	218	6.1
	PC I Int Bottom	232	232	0.1
Bridge	Br O Ex High Bottom	115	169	47.8
	Br Mid Ex High Top	146	135	-7.3
	Br Mid Ex High Bottom	151	136	-9.6
	Br O Int Top	178	217	21.3
	Br O Int Bottom	169	215	26.9
	Br I Ex High Bottom	105	111	5.4
	Br Mid Ex Low Bottom	145	137	-5.2
	Br O Ex High Top	122	169	38.2
	Br I Ex High Top	108	106	-1.2
	Br Mid Ex Low Top	159	136	-14.4
				0.0
Housing	H Ex Top	82	89	8.3
	H Ex Mid	72	86	18.4

	H Ex Bottom	79	94	19.6
				0.0
Piston	Piston Top	162	160	-1.3
	Piston Bottom	155	163	5.3

10.6 Full Assembly Cooling Temperatures and FE Predictions

In Chapter 6, the complexity associated with thermal modelling a stationary, parking brake application became apparent. The use of dynamically derived heat transfer coefficients for these long scenarios was identified as the greatest source of error. Subsequently, the following chapters were devoted to finding accurate convection data, which could be inputted in to the FE model as boundary conditions. Thus far in Chapter 10, values for h_{cond} and the emissivity were identified before generating representative initial values for the FE, validated against experimental results. This final section attempts to improve the stationary parking application modelling by pulling together all the technical research presented in this thesis, completing the research aims for the project.

Altering the previously made heating FE model into the cooling FE model was relatively easy. Removal of the thermal fluxes placed on the friction surfaces and changing the convective interaction properties was all that was required complete the modifications. The former was a trivial operation, however, the latter proved more problematic. CFD analysis work, presented in Chapter 8, generated variable values of h_{conv} over the four separate disc brake surface area regions. When these values were compared to the analytical values produced from in Chapter 7, it suggested they were too high with edge effects being attributed for high surface average h_{conv} values.

Regardless, the first attempts at modelling a stationary parking application used the CFD average surface h_{conv} values displayed in Figure 8.35. Indeed, it was proven that the cooling rate was too quick with these figures. In an attempt to reduce the disc brake's cooling rate, the CFD generated h_{conv} values were reduced in increments of 5% until experimental results match was achieved. Table 10.8 presents h_{conv} values that have been reduced by a factor of 15% from the original CFD estimates, which is close to the calculate 17.5% difference. Both CFD and the analytical modelling were completed for a free disc in open air, whereas the FE model impairs some of the surface cooling with the caliper, making neither set the true values to use for the full brake assembly.

Table 10.8: Final h_{conv} values used in the stationary parking simulations – reduced values by 15%.

Friction Surface Temperature (°C)	Inboard (W/m ² K)	Outboard (W/m ² K)	Hat (W/m ² K)	Vanes (W/m ² K)
20	0.0	0.0	0.0	0.0
49	8.9	7.3	3.4	5.3
112	9.5	8.7	3.9	5.7
213	10.2	10.0	5.2	5.6
350	10.1	10.4	5.3	6.1
500	10.2	10.9	5.4	6.0

Figure 10.24 displays the results from the FE modelling. As can be seen, the temperature prediction for the +000 DOO thermocouple now matches the experimentally found cooling profile, a common result for all rubbing thermocouple locations. A temperature difference of approximately 11% between the 0.5 and 1.0 hours is seen, which is considered within the allowable region. Although the h_{conv} values used were defined for a different scenario, it can be concluded that they are appropriate to use as the predictions match well.

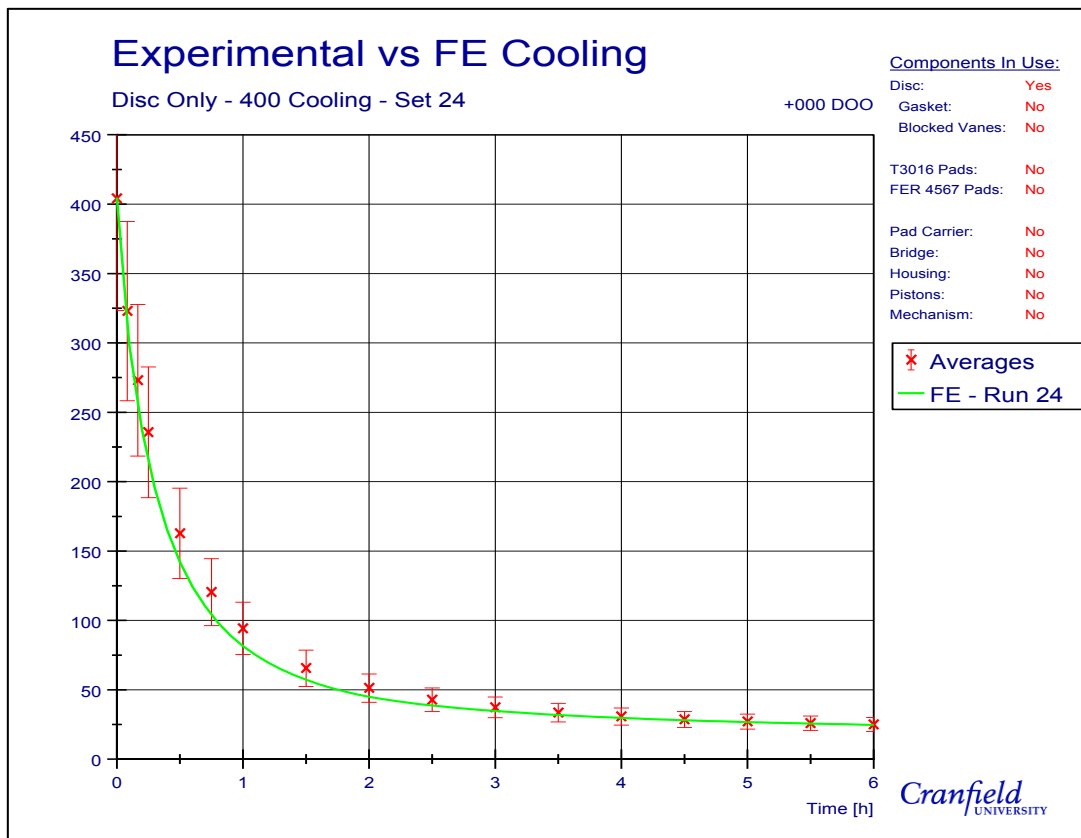


Figure 10.24: FE modelling of a stationary application – experiment 06

It should be noted that two separate step times were use in the modelling. Initially, temperatures were calculated at five second intervals at the beginning of the cooling phase, as the greatest

temperature changes are seen here. Using such a fine step time caused the computational time to be extremely large and it was therefore decided that after 30 minutes it would be reduced. Using equation (4.7) was used to determine an acceptable step time. With the target Fourier number set at unity, the step size was calculated to be 390 seconds. For post-processing convenience, it was reduced to 360 seconds. Being only a small change, the value remained in the identified acceptable range of values, ensure conduction was calculated adequately.

The next FE model saw the introduction of the brake pads against the held against the friction surfaces. As described previously, a slight change to the experimental process was necessary for experiment number two and therefore the modelling procedure had to reflect this. The same initial temperatures for the disc brake and wheel carrier were used, with the brake pads set to 20°C. Confidence will be gained in the modelling conditions if both the heating and then the subsequent cooling of the pads were aligned to experimental data.

Figure 10.25 was produced by applying the same variable h_{conv} value to all external brake pad surfaces as the inboard friction surface, a h_{cond} value at the friction interface in line with Table 9.3 and using a conductivity value of 6 W/m K for FER 4567 friction material. The predicted nodal temperature profile, for the back friction material thermocouple location (POBT), matches impeccably with experimental data throughout the simulation; this was common amongst all nodal predictions. Evidence is therefore presented to confirm that the method of finding h_{cond} values, derived by Tirović and Voller (2005), is accurate and it can be used for the longer parking application simulations.

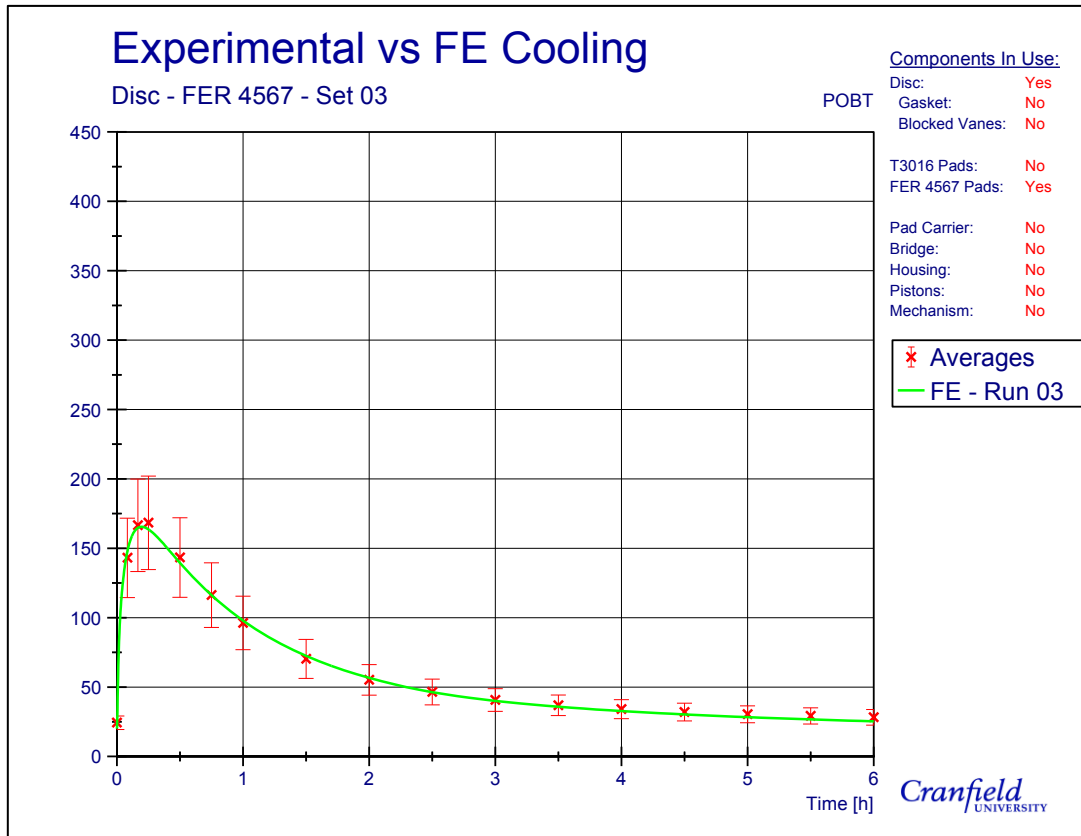


Figure 10.25: FE modelling of a parking– 02 Disc, FER 4567

A similar high degree of accuracy can be described when discussing the modelling results from experiment four. Again, very little work was involved in transforming the heating FE model into a cooling simulation. Once removal of the thermal flux had been completed, all that was required was to modify the h_{conv} values again. Like with the brake pads, external pad carrier surfaces used the same h_{conv} profile as the inboard friction surface, whilst the internal surfaces had no convection attributed to them as it is likely there would be a lack of airflow in this region.

Figure 10.26 validates the assumption made as the internal pad carrier surface temperature profile, for the PC I Int Top thermocouple, is aligned to the experimental data extremely well. Keeping the thermal fluid interaction (gap conduction) would have seen an increase in nodal temperatures towards the early part of the simulation, or at least maintaining its initial temperature for longer.

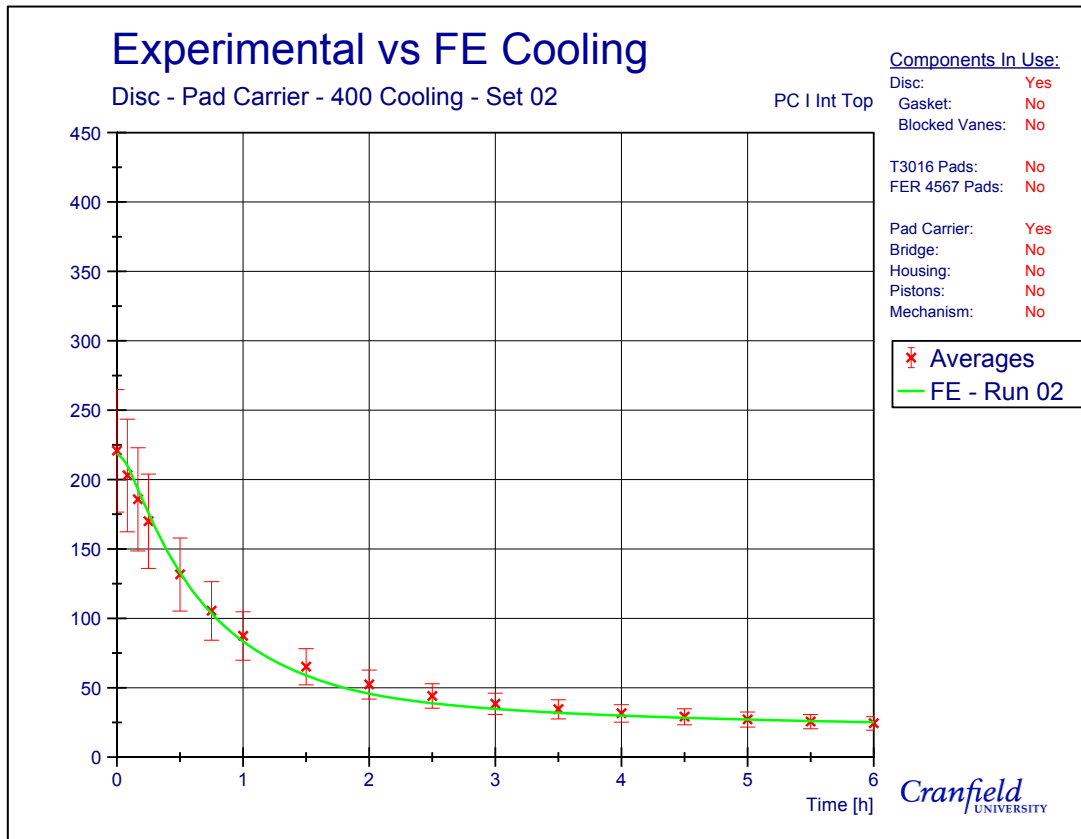


Figure 10.26: FE modelling of a stationary application – 04 Disc, Pad Carrier

In total, 15 of the 19 pad carrier nodal temperatures matched the thermocouple profile for the entire cooling phase. This result proves that the global temperature distribution can be accepted as accurate, due to the majority of nodal temperatures conforming to the prescribed standards. Four pad carrier predictions altered slightly from the pattern displayed in Figure 10.26 and they were the $X - \theta$ plane. Predicted node temperatures increased sharply for the first five minutes of the simulation before decreasing and realigning with the thermocouple within the first hour of cooling. Slight localised inaccuracies in the initial temperatures are shown here to have little impact on the global simulation accuracy. The amount of energy in the system was approximately correct at the start of the cooling phase. Equalisation of the thermal energy occurred after a period of time, bringing the predictions back in line with the measured cooling profile.

The penultimate FE simulation was for experiment five; inclusion of the bridge and housing components. Results from the initial temperature modelling procedure were less accurate than for other models, specifically the bridge temperatures. Similar model alterations were made as before, turning the previous heating FE model into the cooling model that will simulate the parking application.

Surprisingly, temperature predictions from the parking application FE model are shown in Figure 10.27 to match those of the middle internal bridge thermocouple (BR Mid Int Bottom) exceptionally accurately. Within the first five minutes the initial excess heat is dissipated and thereafter, the cooling profile remains within the modelling limitation. Having identified the thermal interactions between the components relatively well, component temperatures were able to stabilise once the heat flux was removed. During the early stage of the cooling application, having approximately the correct amount of heat in the system allows the model to self-compensate for the localised high/low regions of initial temperature.

Correspondingly, the housing unit surface temperature distribution also demonstrated conformity with the experimental data; one of the six thermocouple profile predictions is shown in Figure 10.28. Of those nodal positions that had poorly matched initial temperatures, like with the bridge component, all temperature prediction were accurate within an hour of the cooling application started.

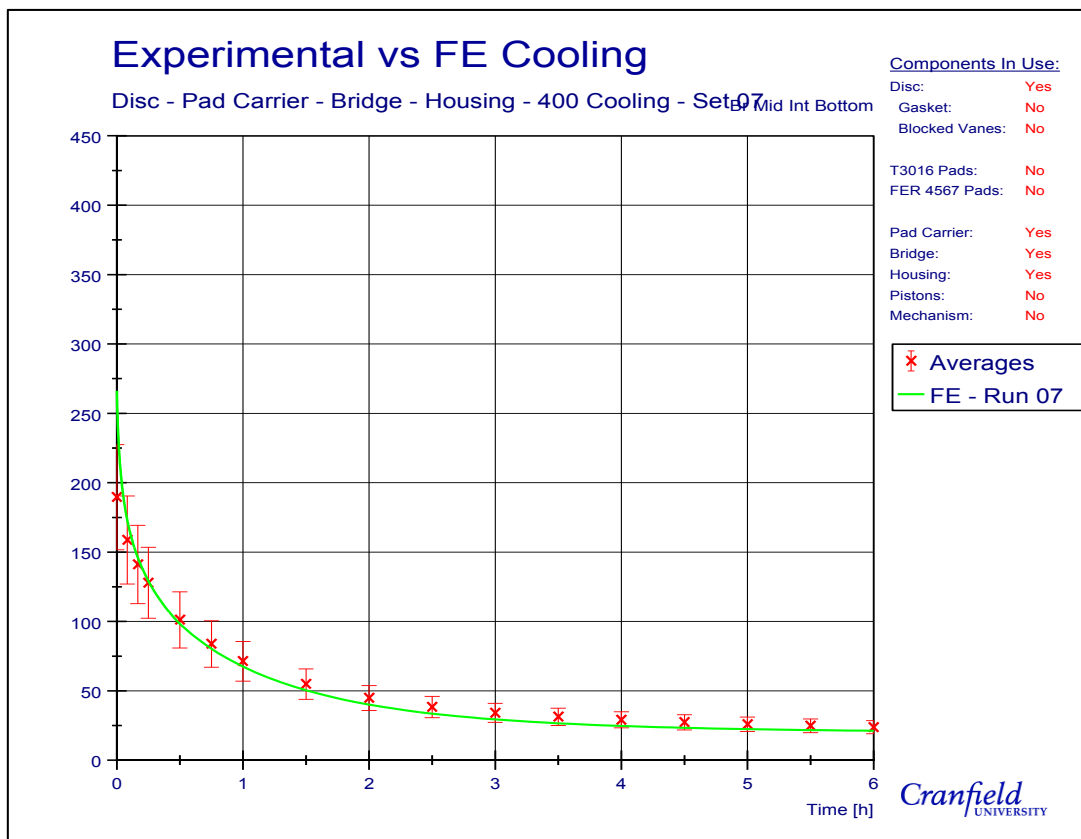


Figure 10.27: Predicted bridge temperatures compared to experimental data – experiment 5

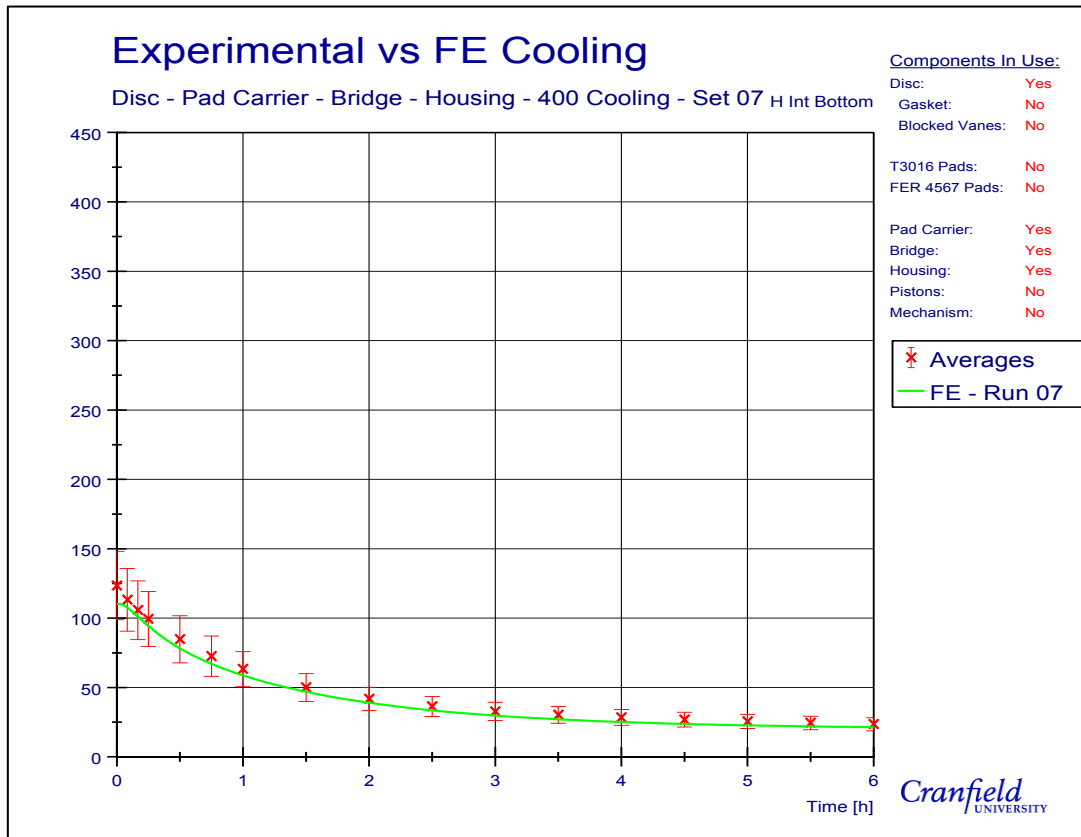


Figure 10.28: Predicted housing temperatures compared to experimental data – experiment 6

The final graph presented was created using FE predicted temperature results from the final full assembly model (experiment 6). Displayed results in Figure 10.29 are those for the lower piston surface. For completeness, results for the reference thermocouple (+000 DOO) have also been included. Evidence presented here therefore proves that the addition of caliper components and the reduction of surface cooling from the disc brake still enabled an accurate disc brake cooling profile prediction.

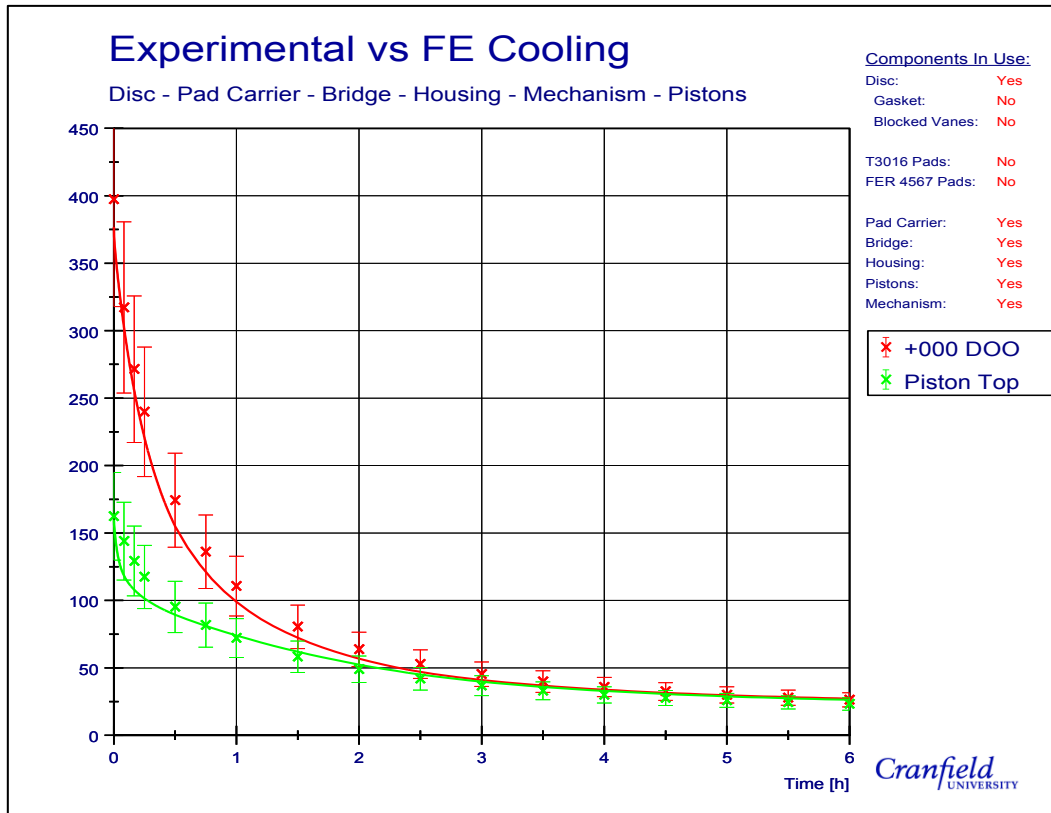


Figure 10.29: Piston and disc brake predicted temperatures from the final FE model – experiment 6.

10.7 Brake Assembly Showcase Model

To complete the research objectives in this investigation, one final FE model was run. A set of FER 4567 friction material brake pads was added to the last model presented in the previous section, making the simulation representative of a full stationary parking application. As stated previously, limitations of the Thermal Rig prevented model validation. However, confidence in the parking simulation is gained through the successful development of previous modelling that incorporated the specific heat transfer coefficients for this modelling scenario.

Figure 10.30 displays brake assembly temperature contour plots at various points throughout the cooling phase. The same preheating step was used to generate the initial model temperatures. Only a slight modification was necessary as the pads were not in contact with the disc, resulting in a gap conductance being used at the disc brake/friction material interface; the same value of 150 W/m²K, found in Chapter 6, was use. It is interested to see the temperature development in the pad carrier, becoming the hottest component in the assembly between 45 minutes and hour. It was shown experimentally in Chapter 9 that other brake components become hotter than the disc, matching the displayed prediction.

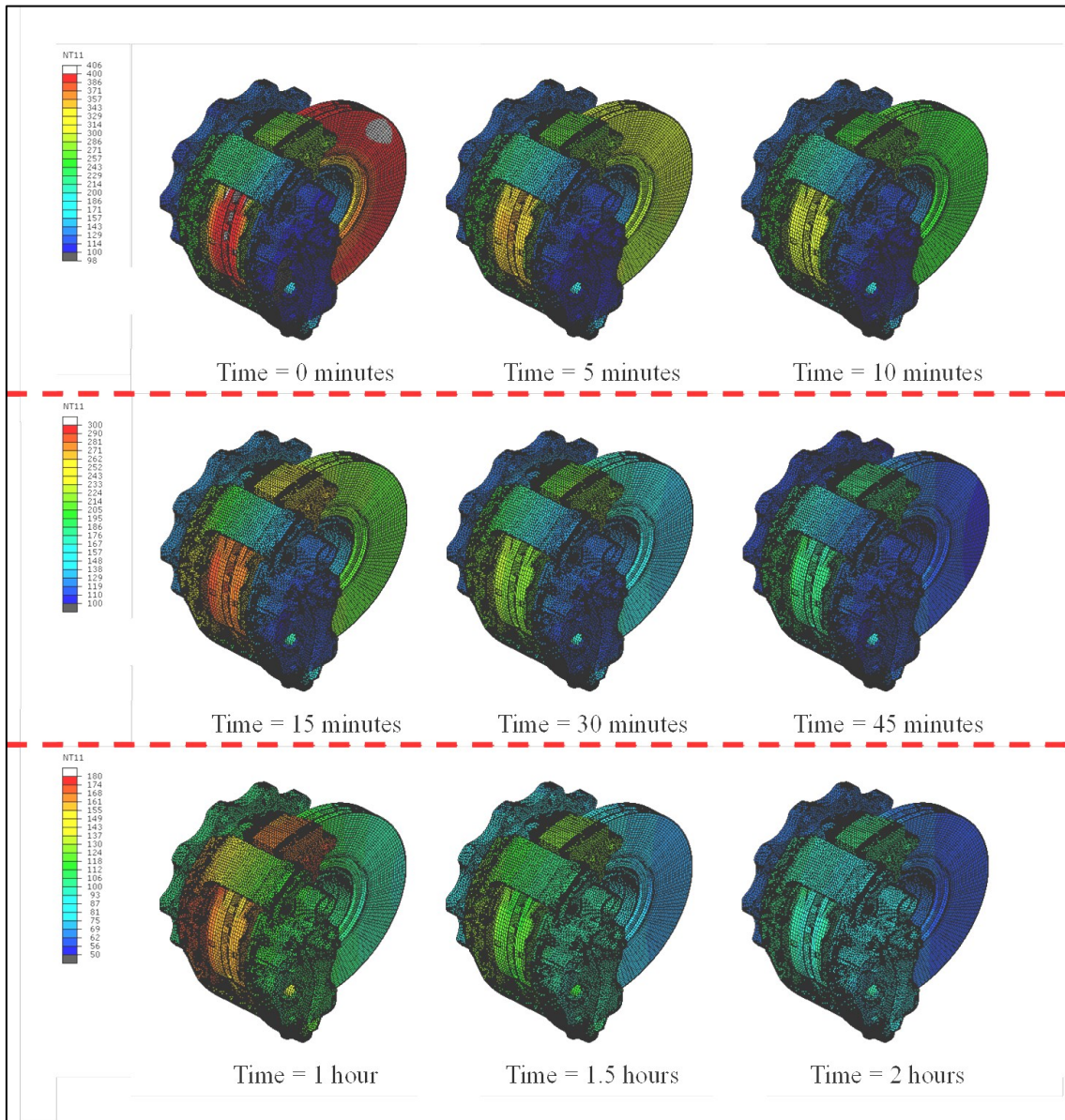


Figure 10.30: Temperature contour plots of brake assembly during the first 2 hours of the cooling phase

An observation from Figure 10.30 that could impede the EPB performance is the surface temperatures of the housing unit. The maximum housing temperature predicted was 178°C, with the internal surfaces that surround the mechanism approximately 150°C. The advanced heating is a result of the additional heat able to conduct into the component through the pads and pistons. Consideration of the thermal effects on the other components located inside the housing unit at these temperatures and how their failure would impact the EPB; as in the slack adjuster example presented in Chapter 8.

In conclusion, what has been demonstrated in this Thesis is a method of developing an engineering tool that will aid the design process. To enable this, a complete investigation into the heat dissipation from the disc brake was necessary, as well as the thermal interactions of the between the caliper components. Resultantly, a combination of practical experimentation and modelling, in the form of numerical and CFD, generated a complete set of boundary conditions for the CV parking brake application. These boundary condition values, and the method of obtaining them, are unique to this project.

10.8 Chapter Summary

In Chapter 10 a method was developed for generating reliable temperature predictions for the complete brake assembly, over the entire cooling phase of a parking braking application, using the ABAQUS FE program. Model complexity was increased slowly by adding caliper components separately. Thermal interactions between components could therefore be captured with this technique. At each stage temperature predictions were validation was conducted by comparing the surface heating temperatures of the assembly, which had the added advantage of generating an accurate initial cooling temperature distribution pattern. It was found by this process that slight inaccuracies in the initial temperature distribution are naturally overcome early in the cooling stage provided the total amount of energy in the assembly is approximate correct. Ultimately, the complete assembly model will aid Meritor in their development of the EPB and to identify and investigate possible situations where secondary brake failure may occur.

11 Summary and Conclusions

11.1 Summary

Introduction of the EPB into CV's necessitated the completion of the presented research. With a strong business case submitted internally, research commercial aspects focused on discovering the EPB advantages offered to the various benefit segments. A recommendation as to how to successfully market the EPB to the different segments was made based on the research results. The most valuable benefit of the EPB is that it partially separates the braking assembly from the common pneumatic airlines, which are susceptible to air leakage and ultimately causes brake failure.

Technical aspects were focused on heat flow through the brake assembly. Chapter 5 discusses the experimental apparatus used throughout this investigation for testing and validation. Using the developed Thermal Rig, it was discovered that the condition of the brake pads affect the total amount of brake assembly contraction during a parking application. A new set of pads having been through a complete thermal cycle delivers the most contraction.

Chapter 6 attempted to model a parking brake application with the FE technique. In the absence of superior information, the same modelling assumptions were used as dynamic brake modelling. Inaccurate results were the outcome as the heat transfer coefficients were not free to vary with temperature, over the full cooling range. Consequently, Chapter 7 developed a unique equation that predicts the average surface h_{conv} for a standard disc, positioned vertically in air and subjected to natural convection, by using a simplified geometry assumption. The derived equation is not limited to disc brakes, but to any generic disc under this condition.

Chapter 8 continued to examine the convective properties of the disc brake by utilising CFD capabilities, to analyse the airflow through and around it. A study into the effectiveness of a laminar and a number of turbulence models was undertaken. It was that the SST model is the most appropriate to use when modelling parking applications as it provides a good combination of accuracy and computation time. Airflow simulations required a new validation technique to be developed as the commonly used hot wire anemometry technique available was not sufficiently sensitive to detect the low flow velocities resulting from natural convection. Through the CFD modelling and then validated against the novel flow visualisation technique, it was shown that the straight vane, anti-coning disc brake does not cool optimally during a parking brake application as large recirculation regions form, preventing convective cooling. Further heat transfer properties were found in Chapter 9 with the emissivity of the fully oxidised

grey cast iron disc brake shown to remain approximately constant over the cooling temperature range, at a value 0.92. This finding simplifies modelling complexity, reducing computational time.

To complete the undertaken thermal interaction investigation, Chapter 10 outlines the production of a full CV brake assembly FE model. It was developed using an iteration technique and incorporated the newly discovered heat dissipation knowledge for boundary conditions. Temperature predictions obtained from the model were proved accurate to within $\pm 20\%$ against experimental validation. Ultimately, this investigation has demonstrated a complete process for developing a tool that accurately predicts the temperature of all the brake assembly components, over the entire cooling phase of a parking brake application.

11.2 Discussion

Work presented in this investigation was separated into two subdivisions, commercial aspects of the CV EPB and technical aspects based upon heat transfer. An individual research aim underpinned the direction of work conducted in each of the sections. It is discussed here how these aims were achieved.

11.2.1 Commercial Aspects

The research aim of for the commercial aspects was:

To understand the benefits of the EPB and how to successfully market them.

A benefit analysis was undertaken in Chapter 2 based on the author's knowledge of the product and the market where it would be sold. Eight end benefits were found, however, the total number of possible benefits was constrained as opinions from all segments were not considered. Resultantly, two questionnaires were conducted in Chapter 3 to examine whether any further benefits could be identified. Each questionnaire was sent to the three benefit segments downstream of Tier 1 suppliers for opinions which had thus far not been interrogated. It proved to be a successful approach as the benefit of pneumatic independence was found from the downstream beneficiaries. This ultimately proved to be the most important benefit to all beneficiaries and it was suggested any marketing campaign should be anchored against this.

The limitations of this procedure were also explained. Power analysis calculated the sample size used was too small for high statistical confidence to be generated in the results. Results obtained from the questionnaires may not have been representative of the total population. The only method of improving the statistical confidence in the results would have been to obtain results

from a larger sample. Getting responses to the questionnaires proved difficult, especially with the End Customer segment as a people in specific roles were requested to respond rather than asking a larger quantity.

The structure of the questionnaire can have a large impact on the results offered by an individual. A large amount of consideration was given to the structure of the questionnaires in an attempt to prevent bias from affecting the results given by a respondent and to retain their attention by including a mixture of open ended and closed questions. The chances of a respondent completing the questionnaires were therefore maximised.

Two approaches were adopted for administering the questionnaires; self-completion questionnaires and web-based self-completion questionnaires. Merits of other questionnaire types were discussed and dismissed in preference for these two because of the ease of distribution and cost advantages. A deeper understanding of respondents' opinions in the End Customer segment would have been achieved via face-to-face interviews and/or telephone, due to the personal interaction and further probing of questions these methods allow. Time and monetary constraints prevented these preferential methods. However, the results attained still proved successful in achieving the first commercial research objective and hence, the research aim, at the expense of gaining additional knowledge.

Additional conclusions could be made as a result of this finding. A lack of confidence in the current technology was one of the identified factors that have the potential to break technical lock-in. Numerous reports of failure of the braking system caused by a faulty pneumatics were reported in the questionnaire responses. The presented evidence suggests the market does indeed lack confidence in the current technology and it is therefore ready to adopt a new solution. Barriers to market can resultantly be removed and thus, the second research objective was achieved.

11.2.2 Technical Aspects

The research aim of for the technical aspects was:

To understand the heat flow around a stationary brake assembly.

To achieve the aim, a full FE model was created and validated against experimental results, which can predict the temperature of the entire brake assembly to within $\pm 20\%$. Although being able to predict these temperatures is useful, it does not constitute a full understanding of

the occurring heat flow. This aim was realised by developing the understanding of the variability in the heat transfer coefficients over the temperature range of a parking application.

Change in the convection heat transfer coefficient was the subject of Chapters 7 and 8. A numerical approach was taken in the former, using assumptions of simplified geometry to allow existing vertical wall equations for flat plate to be modified for a disc. From this, it was possible to demonstrate the non-linear nature of the average h_{conv} value for the disc surface, in the 20°C to 400°C temperature range, when subjected to natural convection. The accuracy of the derived equation was limited as all 3-dimensional effects were neglected, which ignores flow interactions between the individual sections of the simplified geometry.

By implementing a CFD study on a straight vane, ventilated anti-coning disc brake the 3-dimensional effects were found and compared to the analytical derived solution. It was found that the equation over-predicted the in-channel average h_{conv} value whilst under-predicting the friction surface values. However, good agreement was achieved in the general shape of the mean h_{conv} against temperature curve, demonstrating the nature of the cooling disc cooling was well understood.

Experimental validation of thermal modelling throughout this investigation used an acceptance criteria of $\pm 20\%$. The validation range was selected as heat transfer knowledge between brake assembly components prior to the presented work being conducted was scarce, giving the modelling processes no basis to start from. There is no standard within the literature that establishes what the acceptance criteria should be for a given situation. The selected range was therefore wide enough to allow modelling processes to develop maturity whilst maintaining a reasonable degree of accuracy to produce useful temperature predictions. CFD and FE modelling methods were improved such that they both realised the accuracy necessary for the early stage of product development, justifying the decision to use the $\pm 20\%$ range.

During the CFD method development process, three turbulence models were selected and tested for its ability to predict natural convection flow, along with a laminar model. The three turbulence models were selected because of their ease of use, as only limited data needed inputting into the model during the setup process, and for commonality with previous CFD models presented in the literature. Other turbulence models were available but are much more complex in their setup and calculations. As only a tool to aid the early design phase of product development was required, these alternative turbulence models were discarded as being unsuitable due to the setup and computational time they demand.

How the change in temperature affects the friction coefficient was not investigated here due to it being out of scope of the project. Friction properties are dependent on the individual constituents that make up the friction material. Heat into the friction material was shown to alter the brake pad mechanical properties as different amounts of thermal contraction was recorded, depending on how many heat cycles the pad has been exposed to. The ability to accurately analyse the friction materials was not readily available at Cranfield University. It was therefore correct not to include this package of work as results could not have been validated.

Four technical research objectives were identified and were subsequently completed in this project. A deeper understanding of the heat transfer coefficients allowed an FE model to be created to examine the heat paths in the brake assembly, which completed the second and third technical objectives. The experimental technique developed was used to validate all models created, as well as discovering the scenario where the most pad contraction occurs and therefore, the greatest amount of variability in clamp force the CV EPB has to overcome and thus, completed the first and fourth technical research objectives.

11.3 Conclusions and Research Contributions

This investigation has produced a number of conclusions relating to scientific contributions that have not previously been shown in the literature. These are:

1. It is now possible to predict the average h_{conv} value over the surface of a vertically suspended disc situated in air by using equation (4.12). Although found in a braking context, it is appropriate this equation in any scenario where an ordinary disc is subjected to natural convection. This equation holds true for cylindrical surfaces too, provided the correct coefficients are used.
2. When modelling cooling scenarios, where the body is subjected to natural convection, it has been shown that the heat transfer coefficients must vary over the specific temperature range to generate accurate results. This conclusion is relevant when the temperature range is large during the cooling period. Subsequently, the common assumptions used during dynamic brake modelling cannot be used for park braking applications.
3. The emissivity of a fully oxidised cast iron disc brake can be assumed approximately constant throughout a parking brake application.
4. When using generic CFD programmes for simulating natural convection applications, it was shown that the most appropriate turbulence model to use is the Shear Stress Transportation model. Of the ones tested, the combination of accuracy and computational time to convergence offers the best compromise to the user.

5. Initial temperature distribution on large FE models was proven relatively insensitive to the final accuracy of the predicted cooling profiles, provided the initial amount of energy in the assembly is approximately correct. Temperature equalisation occurs quickly, relative to the total time of a parking application.

In addition to these generic scientific conclusions, specific technical conclusions relating to CV EPB design and operation have also been made; which are:

1. The FER 4567 pad material gives the greatest amount of pad contraction during a parking application.
2. It takes four hours for contraction in the brake assembly to cease completely post application of the parking brake. It is the first hour after application that is most critical to the EPB design as 75% of the total contraction occurs during this period.
3. The amount of thermal contraction has been shown to be directly related to the thermal conditioning of the friction material. New pads having been exposed to a full thermal cycle produce the greatest amount of contraction. The total amount of contraction reduces and stabilises wears to an operational state.
4. It was identified that the CV EPB will reduce maintenance costs due to separation from the current problematic pneumatic system. This benefit should be exploited by making it the key selling point of the CV EPB.
5. Stationary cooling from anti-coning, straight vane disc brakes is hampered by the generation of large stagnation regions. Airflow is inhibited by the geometry of the disc brake, preventing convection and therefore optimal cooling from occurring. Presence of the caliper is likely to worsen stationary cooling performance further as large flow barriers are created.
6. An ε value of 0.92 was found for the fully oxidised grey cast iron disc brake.
7. Thermal conduction between the disc brake and wheel carrier proved to have a low influence on the disc brake cooling, with radiation and convection being the dominant sources of heat transfer to the wheel carrier.
8. The European braking market has been found accepting of electrical products in new CV's.

11.4 Recommendations for Future Work

By continuing the development of the FE model to incorporate mechanical effects will provide Meritor a tool capable of calculating the clamp force variability in all EPB operating conditions, as well as take into consideration the effects of modern technologies such as intelligent slack adjusters for low drag calipers. A continuation of the CFD investigation discussed in Chapter 8 is suggested as a disc brake in free air only was modelled, without any caliper components attached. It was found extremely difficult to mesh even this simplified case using the meshing

software Ansys Mesh 12.1, thwarting more complex modelling from being conducted. Since the completion of this study, conversations with an Ansys representative at the Euro Brake conference in Dresden, 2012, outlined the limitations with software. The author was assured that the new Ansys Mesh 14.0 software (due for release in quarter 3, 2012) would solve the issues, making full brake assembly modelling possible.

Performing buoyant CFD modelling of a full brake assembly would be advantageous to brake designers and researchers alike. Completion of this work would validate the assumptions made during the FE modelling procedure. Understanding the airflow around the full brake assembly would be the basis of an optimisation investigation for the caliper cooling performance. Traditional CFD modelling predicts the airflow around a body by numerically solving the Navier-Stokes equations. These equations are often unstable and computationally expensive. New software packages such as PowerFLOW, made by Exa, break from the norm by using the Lattice Boltzmann Method to analyse flow. Advantages arise with this method by not needing to full solve the equations for accurate flow analysis, reducing the computational time (<http://www.exa.com/technology-overview.html> 2013). No resource was available at the start or at any stage during this Thesis to use such a software package, restricting any assessment of generated surface h_{conv} values and airflow around a disc brake/assembly in stationary conditions, which remains an area of future work.

Properties of friction materials and how they changes with temperature is one of the key input data needed to convert the thermal FE model into a coupled thermomechanical model. Having such a predictive tool will enable Meritor to determine the EPB performance during development, making fine-tuning for best performance possible in early development stages. This will greatly assist in developing new design, its detailed features and allow objective comparison of different design concepts.

The μ level is directly proportional to the amount of disc brake torque delivered but different friction material constituents change the μ level variability with temperature. With this project investigating thermal aspects during the cooling phase, potential μ level drop with temperature was not investigated as it was a mechanical effect. Static μ level change can be pronounced and affected by atmosphere and other influences to the higher degree than dynamic μ levels. With a sufficient reduction in μ level, and subsequent braking torque, vehicle rollaway becomes a reality. Designed improvements to the Thermal Rig, shown in Figure 11.1, would allow the possibility to explore this phenomenon (further information on the proposed Thermal Rig modifications are given in Appendix F) and to find boundary conditions for a thermomechanical

FE model. Two pneumatic cylinders (Figure 11.1) apply a force to the bar attached to the wheel carrier. Initial designs utilise two cylinders with a diameter of 180 mm, capable of delivering a maximum of 16 kNm of torque, which simulates a brake force subjected by a fully laden CV parked on an 18% incline. Changes in clamp force, μ levels, initial torque slip and its further changes will be the information ultimately gained through this new testing procedure.

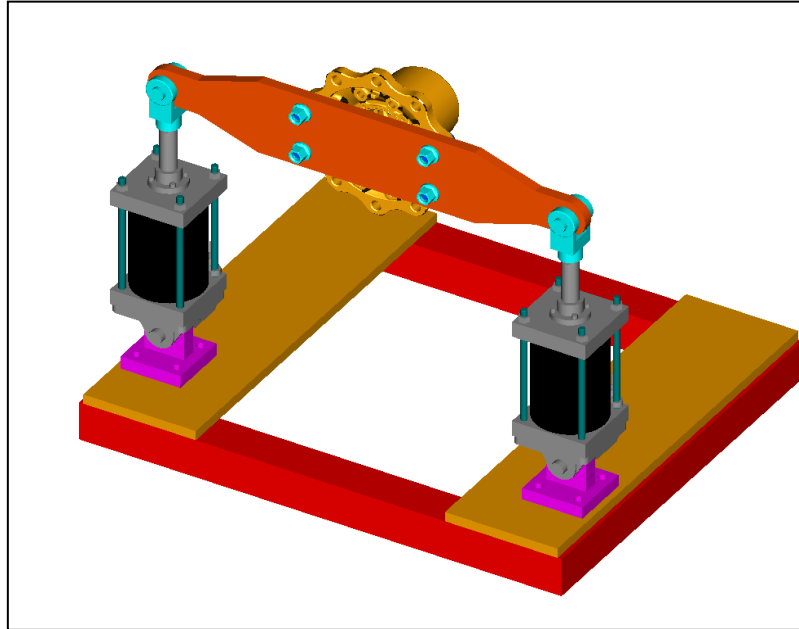


Figure 11.1: Designed pneumatic ram system for friction testing

Furthermore, these rig modifications will enable the Thermal Rig to test the parking performance on the Thermal Rig in a safe environment before being placed on a CV. Model validation will be achieved and initial EPB commissioning can be conducted with this setup. The FER 4567 friction material was identified as the most sensitive out of the two tested, in terms of thermal contraction. By using various pad configurations (friction material type and groove design) in combination with an EPB prototype, the full range of brake assembly combinations can be assessed. Information about the effect on EPB from different friction material compounds interacting with the disc brake and the amount of subsequent clamp force variation can also be realised through these tests.

The final extension to this research would be to incorporate software packages to simultaneously calculate the structural and thermal properties of the assemblies with the airflow around it. A growing trend over the past couple of years has seen the automotive industry increasingly utilise this type of prediction software packages. Because the airflow influences the surface temperatures, which in turn influences the airflow patterns, advantages are realised using an integrated approach. Modelling complexity vastly increases with such a technology as

structural and fluid calculations that impact each other are being calculated simultaneously. Furthermore, an adaptive meshing technique would also need to be incorporated in to the model at every iteration, as the changes in thermal loads will change the geometry due to thermal expansion. Basic computer systems will be unable to run such a model, requiring access to a “supercomputer” similar to the one used during this Thesis.

The latest version of ABAQUS has introduced CFD functionality, which potentially gives it the possibility of conducting an integrated calculation during parking. Exa’s PowerTHERM could be combined with PowerFLOW for the same purpose. Before such a technique can be used, the effectiveness and accuracy of temperature predictions during a stationary application needs assessing. Careful consideration to which software package needs purchasing, with the corresponding licences, as well as to what experimental procedures will be needed to validate predictions. Commercially available packages were extremely limited at the start of this Thesis. A decision to use such a technique must be made early in a project.

Appendix A - Minutes Of Meritor Survey Meeting With Thibaut Grosdemouge

Management meeting: Kevin Stevens, Thibaut Grosdemouge - 27/05/2010

Expectations from OEM - What they want you to do

- From the customer!

- In an industry that doesn't know what they want

- High level CEOs talking to one another making agreements that might not be possible

- Discussion - we want to save money

- weight etc.

- Added safety, cost + functionality from EPB

- No value, so no air to the cabin – Just a simple wire

- Try to be cost neutral

- Auto parking, bus parking etc. – functionality

- Safety linked to EPB

- “Customer perception is as important as legislation”

Costs

- 2 scenarios - System integrator

- Development of 5/6 new systems

- New values, integration of new ECB, etc.

- all at cost neutral

- Development costs ≈ \$450k

- Tooling \approx \$100k
- Develop actuators \approx \$900k
- Production Line \approx \$300k
- Testing \approx \$160k

Safety critical ECER13 regulation (Electronic Control for Brake System)

- ECU \approx \$900k
- Production Line \approx \$150k
- Software \approx \$3.5m
- “M.O.T” – regulator (TUV) company
- Working prototype
- Salaries

Total development cost \approx \$13.5m

- Design the product first before going to OEM
 - \approx \$2.5m of investment at this stage
- limits the risk by doing it this way. Maybe able to use competitor technology to drive EPB
- Original design, not fast enough hence needing to change design
 - Could use more powerful motor, but at a higher cost
 - Threat of new motors – Could produce a product that could rival the EPB design
- APQP - Advanced Planning Quality Planning
 - 6 phases

Development - Time – another year

- Only have 6 potential customers so has to be right when ArM go to them
- Concept Design
- Design for assemble -
- Design for manufacture - Best combination
- FECA - Failure Effect Compound Analysis
 - What is the effect of the failure
 - How often?
 - Must show to customer
 - they may find another mode
 - 0-10 scale - 10 = Safety critical
- DVP - Development Validation Process
 - Layout of initial test plan
 - Calcs, FE, Drawings
- ArV don't really have a supply chain for buying wires, gears etc.
- 252 days of development
- lesson learnt reports
 - What was good
 - What was bad
 - How can we improve - ½ page report if closed (internal) project
- May 2011 - start talking to customers
 - ≈\$200k investment at this point
- 85% of business comes from sales to Volvo
 - Not good customer portfolio

- want a small supplier portfolio as it is easier to manage

Forecasts

- 2020 - estimate 120k vehicles equipped with ArM EPB
- 2015-2025 - Sales to Volvo
 - 426k sales
 - \$226m turnover
 - \$63m gross profit (from 1 customer)
- EPB introduced to Medium sized CVs in 2018
- Competitor will have EPB implemented in 2016, resulting in them having 100% of the market, leaving ArM with 0% of the market share.
- Gross margin for 10 years \approx \$140m

Appendix B - Pilot Questionnaire

Intro

Thank you for opting to take this questionnaire. Completion of the questionnaire is self-explanatory and should take you approximately 10 minutes.

This questionnaire is being conducted as part my Doctorate research programme at Cranfield University. The sponsoring company for this research are currently developing a product that will be launched into specific market. It may become apparent (depending on your answers) what the product is during the questionnaire but as my aim is to investigate the current knowledge in the market, it is imperative from my results that I do not say what it is until the questionnaire has been completed!

Please be aware that throughout this questionnaire, the following acronyms are used:

- CV - Commercial Vehicles (all heavy goods vehicles, buses and coaches but not vans)
- OEM - Ordinary Equipment Manufacturer

Thank you again for taking the time to complete this questionnaire.

Regards

Kevin Stevens

Issues:

-

Q1 What is your current age?

- 25 or below (1)
- 26-35 (2)
- 36-45 (3)
- 46-55 (4)
- 56-65 (5)
- 66 or above (6)

Issues:

-

Q2 What is your gender?

- Male (1)
- Female (2)

Issues:

-

Q3 What industry do you work in?

- Logistics and Transportation (1)
- Retail (2)
- Engineering (3)
- Food (4)
- Agriculture (5)
- Other (6) _____
- Academia (7)

If Engineering Is Not Selected, Then Skip To In your opinion, which of the followi...

Issues:

-

Answer If What industry do you work in? Engineering Is Selected

Q4 Do you work in the automotive sector?

- Yes (1)
- No (2)

If No Is Selected, Then Skip To In your opinion, which of the followi...

Issues:

-

Answer If Do you work in the automotive sector? Yes Is Selected

Q5 Do you work for an OEM?

- Yes (1)
- No (2)

If Yes Is Selected, Then Skip To Which of the following qualification(...

Issues:

-

Answer If Do you work for an OEM? No Is Selected

Q6 Do you work for an OEM (a Tier 1, 2 or 3 supplier)?

- Yes (1)
- No (2)

If Yes Is Selected, Then Skip To End of Survey

Issues:

-

Q7 In your opinion, which of the following OEM's produces the best CV's?

- DAF (1)
- IVECO (2)
- MAN (3)
- Mercedes-Benz (4)
- Renault (5)
- Scania (6)
- Volvo (7)
- No opinion (8)
- Other (9) _____

Issues:

-

Answer If In your opinion, which of the following OEM's produces th... No opinion Is Not Selected

Q8 Please describe the vehicle features, from the selected OEM in the previous question, that you rate most highly when compared to the other manufacturers?

Issues:

-

Q9 How frequently does your company purchase/lease brand-new CV's?

- More frequently than every 2 years (1)
- Between every 2 and 4 years (2)
- Between every 4 and 6 years (3)
- Between every 6 and 8 years (4)
- Between every 8 and 10 years (5)
- Less frequently than every 10 years (6)
- Don't know (7)

Issues:

-

Q10 A 'new feature' adds functionality to a vehicle that was not present in previous models, delivering an enhancement in vehicle performance. From your experience, how frequently does your company receive CV's with 'new features'?

- More frequently than every 2 years (1)
- Between every 2 and 4 years (2)
- Between every 4 and 6 years (3)
- Between every 6 and 8 years (4)
- Between every 8 and 10 years (5)
- Less frequently than every 10 years (6)
- Don't know (7)

Issues:

-

Q11 Which of the following qualification(s) do you have? Mark as many as necessary.

- 5+ GCSE's (or equivalent) (1)
- A levels (or equivalent) (2)
- Driving licence: Category 'B' (standard passenger car) (3)
- Driving licence: Category 'C' or 'C1' (4)
- Driving licence: Category 'C + E' or 'C1 + E' (5)
- Driving licence: Category 'D' or 'D1' (6)
- Driving licence: Category 'D + E' or 'D1 + E' (7)
- Apprenticeship (8)
- BSc (or equivalent) (9)
- MSc (or equivalent) (10)
- MBA (11)
- Other (12) _____

Issues:

-

Answer If Which of the following qualification(s) do you have? Mark... Driving licence: Category 'C' or 'C1' Is Selected Or Which of the following qualification(s) do you have? Mark... Driving licence: Category 'C + E' or 'C1 + E' Is Selected Or Which of the following qualification(s) do you have? Mark... Driving licence: Category 'D' or 'D1' Is Selected Or Which of the following qualification(s) do you have? Mark... Driving licence: Category 'D + E' or 'D1 + E' Is Selected

Q12 How many years' experience do you have driving CV's?

- Less than 5 years (1)
- 5 years or more but less than 10 years (2)
- 5 years or more but less than 10 years (3)
- 5 years or more but less than 10 years (4)
- 20 years or more (5)

Issues:

-

Answer If Which of the following qualification(s) do you have? Mark... Driving licence: Category 'C' or 'C1' Is Selected Or Which of the following qualification(s) do you have? Mark... Driving licence: Category 'C + E' or 'C1 + E' Is Selected Or Which of the following qualification(s) do you have? Mark... Driving licence: Category 'C + E' or 'C1 + E' Is Selected Or Which of the following qualification(s) do you have? Mark... Driving licence: Category 'D + E' or 'D1 + E' Is Selected

Q13 Do you currently drive a CV on a day-to-day basis?

- Yes (1)
- No (2)

Issues:

-

Q14 Please read through the list of CV features below then rank their importance to you; where 1 is the most important and 9 is the least important.

_____ Cab ergonomics and comfort (1)

_____ Improved vehicle efficiency and fuel consumption (2)

_____ Reduced CO2 emissions (3)

_____ High payload capabilities (4)

_____ Vehicle cost (5)

_____ Ease, frequency and cost of maintenance (6)

_____ Manufacturers' reputation (7)

_____ Ability to customise the vehicle (8)

_____ Quality of driver aids (9)

Issues:

-

Q15 Over the past 5 years, what new CV feature(s) have you found to be the best or the most useful, and why? Please identify up to 3 new features.

Issues:

-

Q16 Over the past 5 years, what new CV feature(s) have you found to be the worst or the least useful, and why? Please identify up to 3 new features.

Issues:

-

Q17 Vehicle systems are increasingly becoming electronically controlled. Do you have any concerns over the electrification of any of the CV systems listed?

	Yes (1)	No (2)	Not sure (3)
Clutch (1)	<input type="radio"/>	<input type="radio"/>	<input type="radio"/>
Brakes (2)	<input type="radio"/>	<input type="radio"/>	<input type="radio"/>
Engine turbo's (3)	<input type="radio"/>	<input type="radio"/>	<input type="radio"/>
Steering (4)	<input type="radio"/>	<input type="radio"/>	<input type="radio"/>
Suspension (5)	<input type="radio"/>	<input type="radio"/>	<input type="radio"/>

Issues:

-

Answer If Vehicle systems are increasingly becoming electronically ... Clutch - Yes Is Selected

Q18 What are your concerns with the electrification of the CV clutch system?

Issues:

-

Answer If Vehicle systems are increasingly becoming electronically ... Brakes - Yes Is Selected

Q19 What are your concerns with the electrification of the CV brake system?

Issues:

-

Answer If Vehicle systems are increasingly becoming electronically ... Engine turbo's - Yes Is Selected

Q20 What are your concerns with the electrification of the engine turbo's in a CV?

Issues:

-

Answer If Vehicle systems are increasingly becoming electronically ... Steering - Yes Is Selected

Q21 What are your concerns with the electrification of the CV steering system?

Issues:

-

Answer If Vehicle systems are increasingly becoming electronically ... Suspension - Yes Is Selected

Q22 What are your concerns with the electrification of the CV suspension system?

Issues:

-

Q23 Are there any external issues that are currently having a positive effect on the efficiency of your CV operations? (e.g. government policy)

- Yes (1)
- No (2)

Issues:

-

Answer If Yes Is Selected

Q24 Please explain what these positive external issues are.

Issues:

-

Q25 Are there any external issues that are currently having a negative effect on the efficiency of your CV operations? (e.g. government policy)

- Yes (1)
- No (2)

Issues:

-

Answer If Are there any external issues currently negatively affect... Yes Is Selected

Q26 Please explain what these negative external issues are.

Issues:

-

Q27 What are the biggest problems with the CV's in your company? (You may identify up to 3 issues)

- High emissions (1)
- Poor driver comfort (2)
- High maintenance costs (3)
- Poor fuel economy (4)
- Insufficient payload capacity (5)
- Initial price (6)
- CV performance (7)
- Other (8) _____

Issues:

-

Q28 Vehicle weight reduction is becoming a key focus on many new CV designs. What do you believe is the minimum vehicle weight reduction would be before a useful benefit is gained?

- Up to 10 kg (1)
- 11-20 kg (2)
- 21-30 kg (3)
- 31-40 kg (4)
- 41-50 kg (5)
- 51-60 kg (6)
- 61-70 kg (7)
- 71-80 kg (8)
- 81-90 kg (9)
- 91-100 kg (10)
- More than 100 kg (11)

Issues:

-

Q29 How would you use this this weight saving?

Issues:

-

Q30 CV brake systems are pneumatically operated. Have you ever had a pneumatic brake failure?

- Yes (1)
- No (2)

Issues:

-

Answer If CV brake systems are pneumatically operated. Have you eve... Yes Is Selected

Q31 Please explain what the issues were with the pneumatic braking system.

Issues:

-

Q32 Have you ever experienced a problem with the parking brake on a CV?

- Yes (1)
- No (2)

Issues:

-

Answer If Have you ever experienced a problem with the parking brak... Yes Is Selected

Q33 Please explain what the issues were with the CV parking brake.

Issues:

-

Q34 Which of the following braking features are you aware of?

- ABS - Anti-Locking Brakes (1)
- ESP - Electronic Stability Control (2)
- TCS or ASR - Traction Control System, also known as Anti-Slip Regulation (3)
- EPB - Electronic Parking Brake (4)
- BBW - Brake-By-Wire (5)
- Other (6) _____

If EPB - Electronic Parking Brake Is Not Selected, Then Skip To End of Block

Issues:

-

Q35 Please describe how you became aware of the EPB.

Issues:

-

Q36 Based on your knowledge of EPB's, do you believe the EPB would be a beneficial product in CV's?

- Yes (1)
- No (2)
- Don't know (3)

Issues:

-

Q37 Do you foresee any benefits being received with the installation of an EPB in CV?

- Yes (1)
- No (2)

Issues:

-

Answer If Do you foresee any benefits being received with the insta... Yes Is Selected

Q38 What do you think these benefits will be?

Issues:

-

Q39 Do you think there will be any disadvantages of an EPB in a CV?

- Yes (1)
- No (2)

Issues:

-

Answer If Do you think there will be any disadvantages of an EPB in... Yes Is Selected

Q40 What do you think these disadvantages will be?

Issues:

-

Q41 Which of the following CV(s) do you have in your business?

- DAF (1)
- IVECO (2)
- MAN (3)
- Mercedes-Benz (4)
- Renault (5)
- Scania (6)
- Volvo (7)
- Other (8) _____

Issues:

-

Q42 Do you know which company manufactured the brakes on the CV's in your company?

- Yes (1)
- No (2)

Issues:

-

Q43 To each of these statements, please indicate whether you agree or disagree to each or them.

	Strongly Disagree (1)	Disagree (2)	Neither Agree nor Disagree (3)	Agree (4)	Strongly Agree (5)
The brake system is highly important to the overall CV performance. (1)	<input type="radio"/>	<input type="radio"/>	<input type="radio"/>	<input type="radio"/>	<input type="radio"/>
There is little difference in quality between brake systems from the various brake manufacturers. (2)	<input type="radio"/>	<input type="radio"/>	<input type="radio"/>	<input type="radio"/>	<input type="radio"/>

Issues:

•

Q44 Which of the following CV brake manufacturers are you aware of?

- Brembo (1)
- Haldex (2)
- Knorr-Bremse (3)
- Meritor (4)
- Wabco (5)
- Other (6) _____
- I'm not aware of any CV brake manufacturers (7)

Issues:

•

End

You have now completed the questionnaire. On behalf of the sponsoring company, Meritor Heavy Vehicle Braking Systems, and myself, I would like to thank you for your participation. Development of a CV electronic parking brake (EPB) will continue. A secondary, follow-up questionnaire will be sent out in early 2012 that will complete the data gathering process. This 2nd questionnaire should be shorter and more specific on the EPB. I would be grateful if you would be kind enough to complete this as well.

Thank you once again

Kevin Stevens

Issues:

-

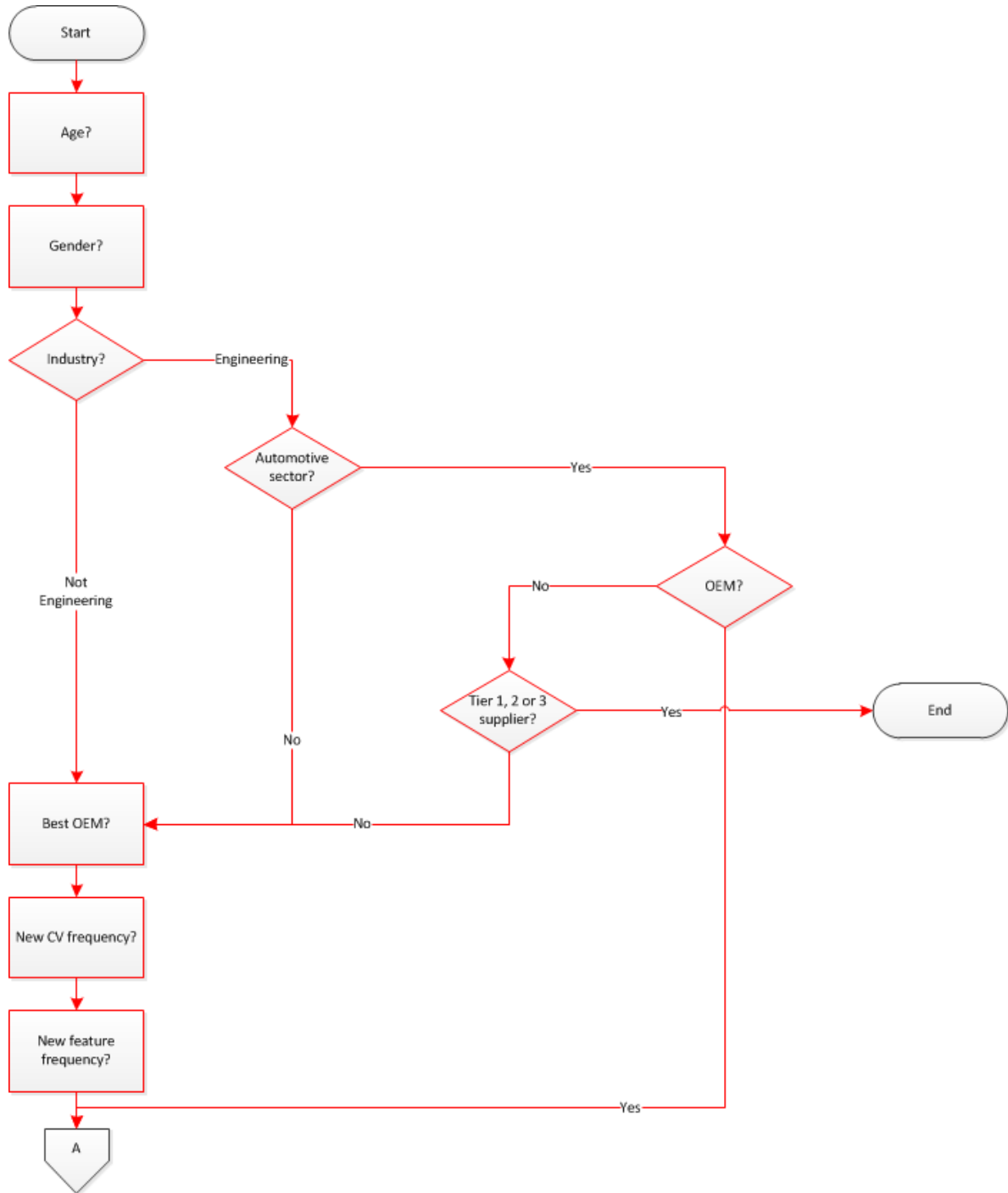
END

Any other Issues/comments?

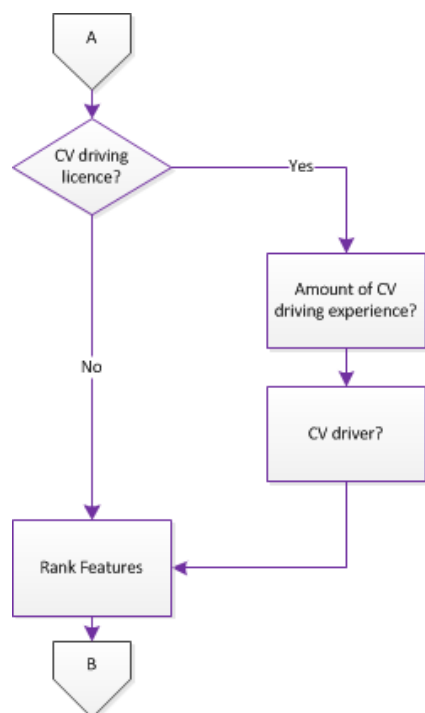
-

Appendix C – Pilot Questionnaire Flowchart

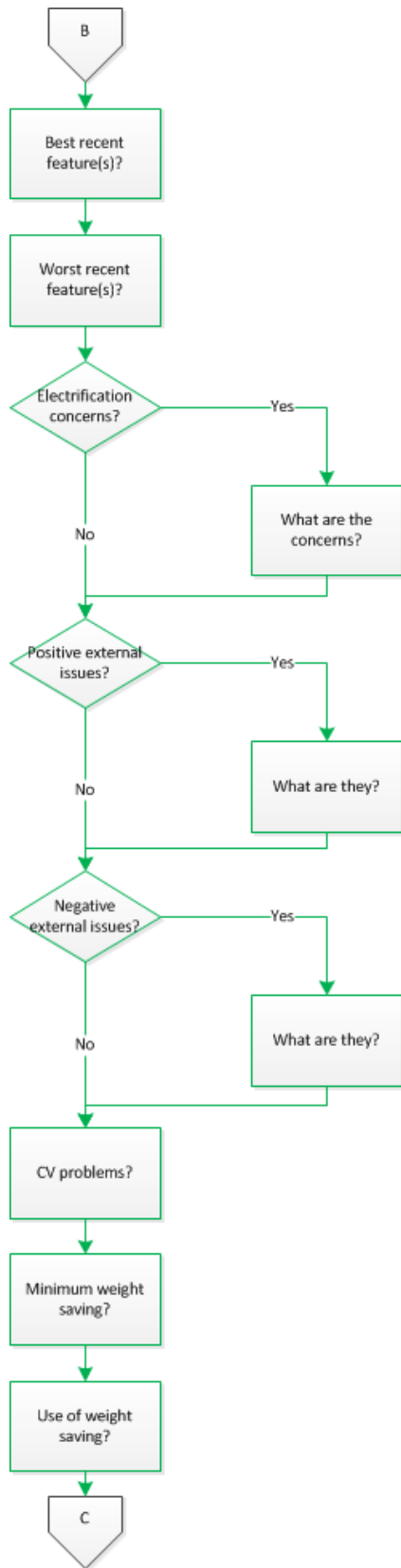
Appendix C.1 Personal Information



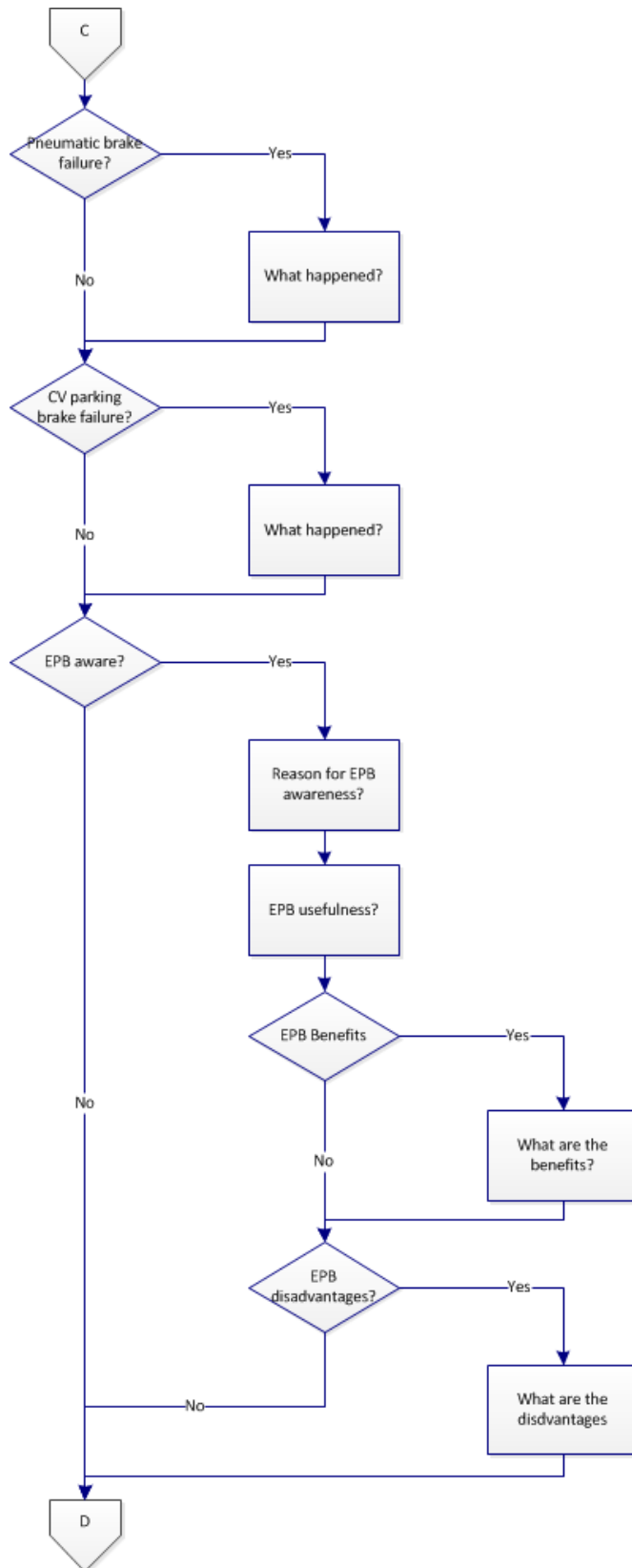
Appendix C.2 New Products



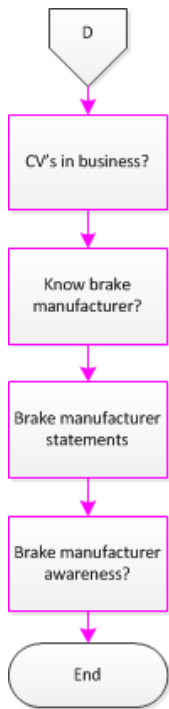
Appendix C.3 Customer Needs



Appendix C.4 Direct EPB



Appendix C.5 Brand Recognition



Appendix D - Explanatory Questionnaire



Market Research Questionnaire

Cranfield
UNIVERSITY
School of Management

An Investigation into Heat Dissipation from a Stationary Commercial Vehicle Disc Brake in Parked Conditions

Thank you for opting to complete this questionnaire – your participation is much appreciated and should only take you approximately 10 minutes.

This questionnaire is being conducted as part my Doctorate research at Cranfield University. The sponsoring company for this research is currently developing a product that will be launched into the commercial vehicle market. As this product is to be used in your sector, I would welcome you responses to this questionnaire.

Please be aware that throughout, the following acronyms are used:

- CV - Commercial Vehicles (buses, coaches and all heavy goods vehicles but not vans)
- OEM - Original Equipment Manufacturer

Instructions:

- There are two main types of questions being asked here; open questions and multiple choice questions.
 - A space has been left for each of the open questions for you to write your answer. If you need more space, a spare sheet at the back of the questionnaire is provided.
 - Multiple choice questions with circular tick boxes () require only one answer from the list of possible responses.
 - Multiple choice questions with rectangular tick boxes () means you can answer more than one of the options.
- Unless instructed to do so after each question, complete the questionnaire in a sequential order.

Thank you again for taking the time to complete this questionnaire.

Regards



Kevin Stevens

SECTION 1: Personal Information

Q1.1	What is your current age?		Instruction
	a.)	<input type="checkbox"/> 25 or below	
	b.)	<input type="checkbox"/> 26-35	
	c.)	<input type="checkbox"/> 36-45	
	d.)	<input type="checkbox"/> 46-55	
	e.)	<input type="checkbox"/> 56-65	
	f.)	<input type="checkbox"/> 66 or above	

Q1.2	What is your gender?		Instruction
	a.)	<input type="checkbox"/> Male	
	b.)	<input type="checkbox"/> Female	

Q1.3	What sector do you work in?		Instruction
	a.)	<input type="checkbox"/> Logistics and Transportation	If you did <u>not</u> select c.), go to Q1.7.
	b.)	<input type="checkbox"/> Retail	
	c.)	<input type="checkbox"/> Engineering	
	d.)	<input type="checkbox"/> Food	
	e.)	<input type="checkbox"/> Agriculture	
	f.)	<input type="checkbox"/> Academia	
	g.)	<input type="checkbox"/> Other	

If Other, please specify.

Q1.4	Do you work in the automotive sector?		Instruction
	a.)	<input type="checkbox"/> Yes	If b.), go to Q1.7.
	b.)	<input type="checkbox"/> No	

Q1.5	Do you work for an OEM?		Instruction
	a.)	<input type="checkbox"/> Yes	If a.), go to Q1.7.
	b.)	<input type="checkbox"/> No	

Q1.6	Do you work for a component or assembly supplier (a Tier 1, 2 or 3)?		Instruction
	a.)	<input type="checkbox"/> Yes	If a.), you have completed the questionnaire. Thank you for your participation.
	b.)	<input type="checkbox"/> No	

Q1.7	From the list below, which of the job titles is the closest to your own?		Instruction
	a.)	<input type="checkbox"/> Analyst	
	b.)	<input type="checkbox"/> Buyer	
	c.)	<input type="checkbox"/> Designer	
	d.)	<input type="checkbox"/> Driver	
	e.)	<input type="checkbox"/> Manager	
	f.)	<input type="checkbox"/> Mechanic	
	g.)	<input type="checkbox"/> Other	

If Other, please specify.

Q1.8	Which of the following qualification(s) do you have? Mark as many as necessary.		Instruction
	a.)	<input type="checkbox"/> 5+ GCSE's (or equivalent)	If you did <u>not</u> answer either d.), e.), f.) or g.), go to Q1.11.
	b.)	<input type="checkbox"/> A levels (or equivalent)	
	c.)	<input type="checkbox"/> Driving licence: Category 'B' (standard passenger car)	
	d.)	<input type="checkbox"/> Driving licence: Category 'C' or 'C1'	
	e.)	<input type="checkbox"/> Driving licence: Category 'C + E' or 'C1 + E'	
	f.)	<input type="checkbox"/> Driving licence: Category 'D' or 'D1'	
	g.)	<input type="checkbox"/> Driving licence: Category 'D + E' or 'D1 + E'	
	h.)	<input type="checkbox"/> Apprenticeship	
	i.)	<input type="checkbox"/> BSc (or equivalent)	
	j.)	<input type="checkbox"/> MSc (or equivalent)	
	k.)	<input type="checkbox"/> MBA	
	l.)	<input type="checkbox"/> PhD (or equivalent)	
	m.)	<input type="checkbox"/> Other	

If Other, please specify.

Q1.9	How many years' experience do you have driving CV's?		Instruction
	a.)	<input type="checkbox"/> Less than 5 years	If you work for an OEM (answered a.) to Q1.5), go to Q2.1.
	b.)	<input type="checkbox"/> 5 years or more but less than 10 years	
	c.)	<input type="checkbox"/> 10 years or more but less than 15 years	
	d.)	<input type="checkbox"/> 15 years or more but less than 20 years	
	e.)	<input type="checkbox"/> 20 years or more	
	f.)	<input type="checkbox"/> I have no CV driving experience	

Q1.10	Do you currently drive a CV on a day-to-day basis?		Instruction
	a.)	<input type="checkbox"/> Yes	
	b.)	<input type="checkbox"/> No	

Q1.11	From your experience, which of the following OEM's produce CV's that best satisfy your operating and/or performance requirements?	Instruction	
	a.) <input type="checkbox"/>	DAF	If you answered i.), go to Q2.1.
	b.) <input type="checkbox"/>	IVECO	
	c.) <input type="checkbox"/>	MAN	
	d.) <input type="checkbox"/>	Mercedes-Benz	
	e.) <input type="checkbox"/>	Renault	
	f.) <input type="checkbox"/>	Scania	
	g.) <input type="checkbox"/>	Volvo	
	h.) <input type="checkbox"/>	Other	
	i.) <input type="checkbox"/>	No opinion	

If Other, please specify.

Q1.12	Please describe what are the vehicle features, from the selected OEM in the previous question, which you rate most highly when compared to the other manufacturers?	

SECTION 2: New Products

Q2.1	How frequently does your company purchase/lease brand-new CV's?		Instruction
	a.)	<input type="checkbox"/> More frequently than every 2 years	
	b.)	<input type="checkbox"/> Between every 2 and 4 years	
	c.)	<input type="checkbox"/> Between every 4 and 6 years	
	d.)	<input type="checkbox"/> Between every 6 and 8 years	
	e.)	<input type="checkbox"/> Between every 8 and 10 years	
	f.)	<input type="checkbox"/> Less frequently than every 10 years	
	g.)	<input type="checkbox"/> Don't know	

Q2.2	An enhancement in vehicle performance is delivered when a 'new feature' is added to a vehicle that was not present in previous models. From your experience, how frequently does your company receive CV's with 'new features' that do deliver real enhancements in vehicle performance?		Instruction
	a.)	<input type="checkbox"/> More frequently than every 2 years	
	b.)	<input type="checkbox"/> Between every 2 and 4 years	
	c.)	<input type="checkbox"/> Between every 4 and 6 years	
	d.)	<input type="checkbox"/> Between every 6 and 8 years	
	e.)	<input type="checkbox"/> Between every 8 and 10 years	
	f.)	<input type="checkbox"/> Less frequently than every 10 years	
	g.)	<input type="checkbox"/> Don't know	

Q2.3	Please read through the list of CV features below then rank their importance to you; where 1 is the most important and 9 is the least important. (You should use each number between and including 1 to 9 once only)	Instruction	
	<input type="checkbox"/>	Cab ergonomics and comfort	
	<input type="checkbox"/>	Improved vehicle efficiency and fuel consumption	
	<input type="checkbox"/>	Reduced CO2 emissions	
	<input type="checkbox"/>	High payload capabilities	
	<input type="checkbox"/>	Vehicle cost	
	<input type="checkbox"/>	Ease, frequency and cost of maintenance	
	<input type="checkbox"/>	Manufacturers' reputation	
	<input type="checkbox"/>	Ability to customise the vehicle	
	<input type="checkbox"/>	Quality of driver aids	

Q2.4	Over the past 5 years, what new CV feature(s) have you found to be the best or the most useful, and why? Please identify up to 3 new features.	
------	--	--

Q2.5

Over the past 5 years, what new CV feature(s) have you found to be the worst or the least useful, and why? Please identify up to 3 new features.

Q2.6	Vehicle systems are increasingly becoming electronically controlled. Do you have any concerns over the electrification of any of the CV systems listed?			Instruction	
		Yes	No	Not sure	
	Clutch	<input type="checkbox"/>	<input type="checkbox"/>	<input type="checkbox"/>	If Yes, answer Q2.7, otherwise skip Q2.7.
	Brakes	<input type="checkbox"/>	<input type="checkbox"/>	<input type="checkbox"/>	If Yes, answer Q2.8, otherwise skip Q2.8.
	Engine turbos	<input type="checkbox"/>	<input type="checkbox"/>	<input type="checkbox"/>	If Yes, answer Q2.9, otherwise skip Q2.9.
	Steering	<input type="checkbox"/>	<input type="checkbox"/>	<input type="checkbox"/>	If Yes, answer Q2.10, otherwise skip Q2.10.
	Suspension	<input type="checkbox"/>	<input type="checkbox"/>	<input type="checkbox"/>	If Yes, answer Q2.11, otherwise skip Q2.11.

Q2.7

What are your concerns with the electrification of the CV clutch system?

Q2.8

What are your concerns with the electrification of the CV brake system?

Q2.9	What are your concerns with the electrification of the engine turbos in a CV?	
-------------	--	--

Q2.10	What are your concerns with the electrification of the CV steering system?	
--------------	---	--

Q2.11

What are your concerns with the electrification of the CV suspension system?

SECTION 3: Current Needs

Q3.1	Are there any factors, which are not under your company's control, that are having positive influences on your company's CV operations? (e.g. government policy)		Instruction
	a.)	<input type="checkbox"/> Yes	If you answered b.) or c.), go to Q3.3.
	b.)	<input type="checkbox"/> No	
	c.)	<input type="checkbox"/> Don't know	

Q3.2	Please explain what these positive influences are.	
-------------	---	--

Q3.3	Are there any pressures or issues, which are not under your company's control, that are negatively effecting your CV operations in any way?		Instruction
	a.)	<input type="checkbox"/> Yes	If you answered b.) or c.), go to Q3.5.
	b.)	<input type="checkbox"/> No	
	c.)	<input type="checkbox"/> Don't know	

Q3.4	Please explain what these negative pressures or issues are.	
-------------	--	--

Q3.5	What are the most important CV selection criteria within your company? You may identify up to 3 issues.		Instruction
	a.)	<input type="checkbox"/> High emissions	
	b.)	<input type="checkbox"/> Poor driver comfort	
	c.)	<input type="checkbox"/> High maintenance costs	
	d.)	<input type="checkbox"/> Poor fuel economy	
	e.)	<input type="checkbox"/> Insufficient payload capacity	
	f.)	<input type="checkbox"/> Initial price	
	g.)	<input type="checkbox"/> CV performance	
	h.)	<input type="checkbox"/> Other	
	i.)	<input type="checkbox"/> Don't know	

If Other, please specify.

Q3.6	Vehicle weight reduction is becoming a key focus on many new CV designs. How much weight has to be removed from a CV before you receive a useful benefit?		Instruction
	a.)	<input type="checkbox"/> Up to 20 kg	If you answered l.), go to Q4.1.
	b.)	<input type="checkbox"/> 21-40 kg	
	c.)	<input type="checkbox"/> 41-60 kg	
	d.)	<input type="checkbox"/> 61-80 kg	
	e.)	<input type="checkbox"/> 81-100 kg	
	f.)	<input type="checkbox"/> 101-120 kg	
	g.)	<input type="checkbox"/> 121-140 kg	
	h.)	<input type="checkbox"/> 141-160 kg	
	i.)	<input type="checkbox"/> 161-180 kg	
	j.)	<input type="checkbox"/> 181-200 kg	
	k.)	<input type="checkbox"/> More than 200 kg	
	l.)	<input type="checkbox"/> Don't know	

Q3.7	How would you use this this weight saving?		
------	--	--	--

SECTION 4: CV Braking Systems

Q4.1	CV brake systems are pneumatically operated. Have you ever had a pneumatic brake failure?		Instruction
	a.)	<input type="checkbox"/> Yes	If you answered b.), go to Q4.3.
	b.)	<input type="checkbox"/> No	

Q4.2	Please explain what the issues were with the pneumatic braking system.		
------	--	--	--

Q4.3	Have you ever experienced a problem with the parking brake on a CV?		Instruction
	a.)	<input type="checkbox"/> Yes	If you answered b.), go to Q4.5.
	b.)	<input type="checkbox"/> No	

Q4.4	Please explain what the issues were with the CV parking brake.
-------------	---

Q4.5	Which of the following braking features are you aware of? Mark as many as necessary.	Instruction
	a.) <input type="checkbox"/> ABS - Anti-Locking Brakes	If you did <u>not</u> answer d.), go to Q5.1.
	b.) <input type="checkbox"/> ESP - Electronic Stability Control	
	c.) <input type="checkbox"/> TCS or ASR - Traction Control System, also known as Anti-Slip Regulation	
	d.) <input type="checkbox"/> EPB - Electronic Parking Brake	
	e.) <input type="checkbox"/> BBW - Brake-By-Wire	
	f.) <input type="checkbox"/> Other	
	g.) <input type="checkbox"/> I'm not aware of any braking features	

If Other, please specify.

Q4.6	Please describe how you became aware of the EPB.	
-------------	---	--

Q4.7	Based on your current knowledge of EPB's, do you believe the EPB would be a beneficial product in CV's?	Instruction
	a.) <input type="checkbox"/> Yes	
	b.) <input type="checkbox"/> No	
	c.) <input type="checkbox"/> Don't know	

Q4.8	Do you expect any benefits to be received with the installation of an EPB in CV's?	Instruction
	a.) <input type="checkbox"/> Yes	If you answered b.) or c.), go to Q4.10.
	b.) <input type="checkbox"/> No	
	c.) <input type="checkbox"/> Don't know	

Q4.9	What do you think these benefits will be?	
-------------	--	--

Q4.10	Do you think there will be any disadvantages of an EPB in a CV's?	Instruction
	a.) <input type="checkbox"/> Yes	If you answered b.) or c.), go to Q5.1.
	b.) <input type="checkbox"/> No	
	c.) <input type="checkbox"/> Don't know	

Q4.11	What do you think these disadvantages will be?	
--------------	---	--

SECTION 5: Brand Awareness

Q5.1	Which of the following CV(s) do you operate in your business? Mark as many as necessary.	Instruction	
	a.) <input type="checkbox"/>	DAF	
	b.) <input type="checkbox"/>	IVECO	
	c.) <input type="checkbox"/>	MAN	
	d.) <input type="checkbox"/>	Mercedes-Benz	
	e.) <input type="checkbox"/>	Renault	
	f.) <input type="checkbox"/>	Scania	
	g.) <input type="checkbox"/>	Volvo	
	h.) <input type="checkbox"/>	Other	
	i.) <input type="checkbox"/>	Don't know	

If Other, please specify

Q5.2	To each of these statements, please indicate whether you agree or disagree					Instruction	
		Strongly Disagree	Disagree	Neither Agree or Disagree	Agree	Strongly Agree	
	The brake system is highly important to the overall CV performance.	<input type="checkbox"/>	<input type="checkbox"/>	<input type="checkbox"/>	<input type="checkbox"/>	<input type="checkbox"/>	
	There is little difference in quality between brake systems from the various brake manufacturers.	<input type="checkbox"/>	<input type="checkbox"/>	<input type="checkbox"/>	<input type="checkbox"/>	<input type="checkbox"/>	

Q5.3	Which of the following CV brake manufacturers are you aware of? Mark as many as necessary.		Instruction
	a.) <input type="checkbox"/>	Brembo	If g.), you have finished.
	b.) <input type="checkbox"/>	Haldex	
	c.) <input type="checkbox"/>	Knorr-Bremse	
	d.) <input type="checkbox"/>	Meritor	
	e.) <input type="checkbox"/>	Wabco	
	f.) <input type="checkbox"/>	Other	
	g.) <input type="checkbox"/>	I'm not aware of any CV brake manufacturers	

If Other, please specify

Q5.3	Do you know which company manufactured the brakes on the CV's in your company?		Instruction
	a.)	<input type="checkbox"/> Yes	
	b.)	<input type="checkbox"/> No	

Finish

You have now completed the questionnaire.

On behalf of the sponsoring company, Meritor Heavy Vehicle Braking Systems, and myself, I would like to thank you for your participation. Development of a CV electronic parking brake (EPB) is on-going. A secondary, follow-up questionnaire will be sent out in early 2012 that will complete the data gathering process. This second questionnaire should be shorter and more specific on the EPB. I would be grateful if you would be kind enough to complete this as well.

Thank you once again,

Kevin Stevens

Appendix E - Knowledge-Based Questionnaire



Market Research Questionnaire

A questionnaire to assess the advantages of the electric parking brake on commercial vehicles.



Thank you for opting to complete this questionnaire – your participation is much appreciated, this will take you no more than 10 minutes to complete.

This questionnaire is being conducted as part my Doctorate research at Cranfield University. The project sponsors, Meritor Heavy Vehicle Braking Systems, are currently developing an electric parking brake for commercial vehicles. As this product will be used in your sector, I would welcome your responses to this short questionnaire.

A brief introduction to the electric parking brake and how the current air parking system on commercial vehicles works is given first on the following pages before the questionnaire begins.

Please be aware that throughout, the following acronyms are used:

- CV - Commercial Vehicles (buses, coaches and all heavy goods vehicles but not vans)
- OEM - Original Equipment Manufacturer
- EPB - Electric Parking Brake

Thank you again for taking the time to complete this questionnaire.

Kind Regards



Kevin Stevens

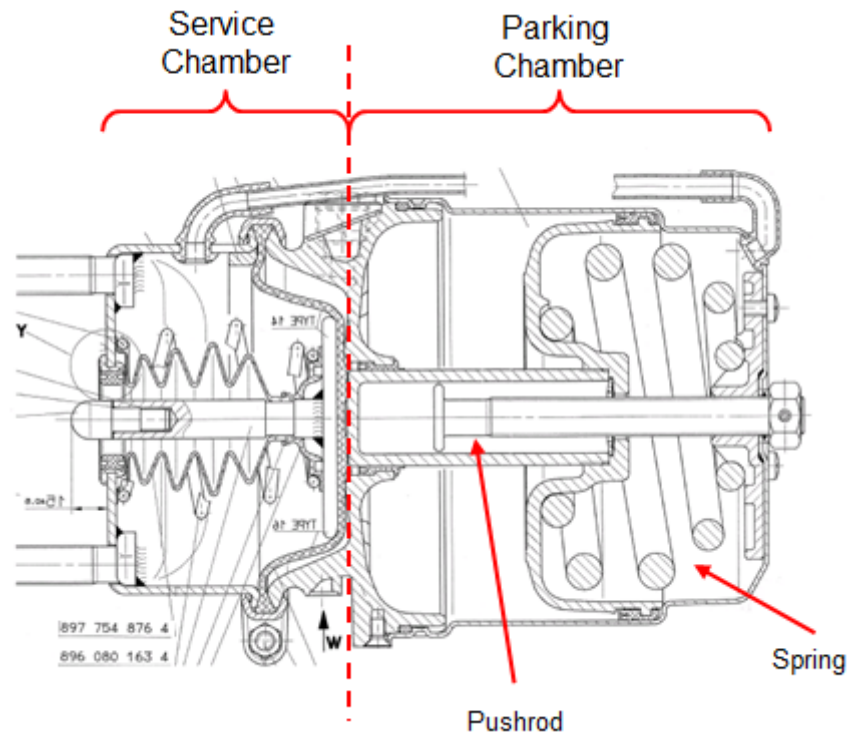
The EPB is a recent development in vehicle design. It was first introduced back in 2003, predominately on luxury cars, but recently they have become standard on some small to mid-range cars as well. They replace the existing handbrake lever with an electrical system, operated by a single on/off push button. Development of an EPB, to be placed on CV's, is currently being undertaken by brake manufacturers. The EPB unit attaches to the back of the brake caliper and uses a motor system to apply the brake.



(source: www.trw.com)

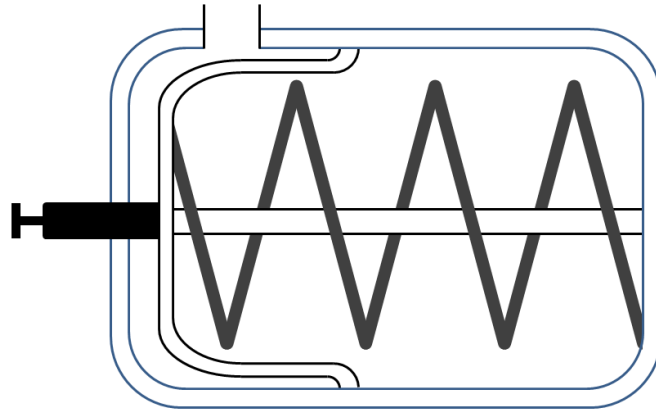
How Existing CV Parking Brakes Work

Existing CV parking brakes use a pneumatic (air) actuation system and is made up of two parts. The first is the service chamber, which is used to apply the brakes when the vehicle is in motion. Fixed to the back of the service chamber is the parking chamber, which holds a spring and a pushrod. As the name would suggest, the parking chamber is only applied when the vehicle is stationary.

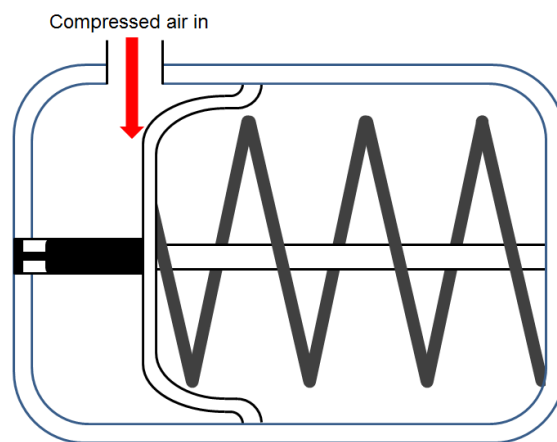


How Existing CV Parking Brakes Work

When the driver first enters the vehicle, the parking brake is in the *ON* position (see the simplified diagram below). No compressed air is in the parking chamber, allowing a large spring to fully extend. This pushes the pushrod out the parking chamber and into the service chamber to apply the brakes.



Once the level of compressed air has reached the required limit, the driver can release the brakes by moving the lever arm on the dashboard to the *OFF* position. When in this position, air is forced into the parking chamber, compressing the large spring and removes the pushrod from service chamber. The brakes are now released and the driver is free to drive away.



When a CV comes to rest, the driver returns the parking lever arm to the *ON* position. The air holding the large spring is "dumped" and the parking brakes are reapplied.

Electric brakes do exist in some CVs, but rather than fully embracing an electric braking system, they use a hybrid system where electronic signals control the air flow to/from the original spring parking chamber. Subsequently, many advantages proposed by the EPB system have been missed.

Q.2

Smaller brake component

The new EPB design for CV's would reduce both the size and the weight of the chamber parking unit.

Do you think this is a useful CV feature?

- Yes
- No
- Don't know

If yes, could you explain why this would be advantageous to you.

Q.3

Removal of Pneumatic Parts

Replacing the pneumatic parking component with an electrical system will mean airlines are removed and replaced with copper cables.

Do you think this is a useful CV feature?

- Yes
- No
- Don't know

If yes, could you explain why this would be advantageous to you.

Q.4

Smaller Air Reservoir

Reducing the compressed air capacity needed during CV operations will result in a smaller air reservoir being installed on CVs.

Do you think this is a useful CV feature?

- Yes
- No
- Don't know

If yes, could you explain why this would be advantageous to you.

Q.5

Aided Hill Starts

Being connected to the vehicles central electronic control unit (ECU), the EPB system has the ability to utilise other vehicle instrumentation. In this instance, when the vehicle sensors detect it is not moving whilst positioned on a hill, the parking brake will be applied automatically. Release of the parking brake will only happen when the accelerator pedal is being pressed by the driver, indicating they wish to continue driving.

Do you think this is a useful CV feature?

- Yes
- No
- Don't know

If yes, could you explain why this would be advantageous to you.

Q.6

Immobiliser

The brake system can be forced to remain on until the keys have been put in the ignition and a driver is requesting power. This function can be used either as a solitary immobiliser or as a secondary immobiliser, supplementing the original.

Do you think this is a useful CV feature?

- Yes
- No
- Don't know

If yes, could you explain why this would be advantageous to you.

Q.7

Single Button Operation

Being an electronic component, a single push on/off button can be used to operate the EPB, replacing the lever arm system.

Do you think this is a useful CV feature?

- Yes
- No
- Don't know

If yes, could you explain why this would be advantageous to you.

Q.8

Independence From Air Supply

The parking chamber will no longer need an air supply to operate.

Do you think this is a useful CV feature?

- Yes
- No
- Don't know

If yes, could you explain why this would be advantageous to you.

Q.9

Can you think of any further advantages the EPB could deliver, which have not yet been mentioned?

- Yes
- No
- Don't know

If Yes, please give details of the proposed advantages.

What end benefits would these functions give to you?

Q.10

Having read through the added features offered by the EPB, overall do you think it would be a beneficial product on CV's?

- Yes
- No
- Don't know

Finally, just to understand where your views are coming from, I would like a little information about yourself.

Q.11

What is your age?

- 25 or below
- 26-35
- 36-45
- 46-55
- 56-65
- 66 or above

Q.12

What is your gender?

- Male
- Female

Q.13

Do you have experience driving CVs?

- Yes
- No

Q.14

Would you consider yourself a CV driver?

- Yes
- No

If you answer “No” to question 14, please move to question 15. Otherwise, you have now completed the questionnaire, please go to the end.

Q.15

Do you work for an automotive OEM?

- Yes
- No

If you answer “No” to question 15, please move to question 16. Otherwise, you have now completed the questionnaire, please go to the end.

Q.16

Do you work for an automotive component supplier (Tier 1, 2 or 3 supplier)?

- Yes
- No

You have now completed the questionnaire.

On behalf of the sponsoring company, Meritor Heavy Vehicle Braking Systems, and myself, I would like to thank you for your participation. Development of a CV electronic parking brake is on-going and hoped to be available in the near future.

Thank you once again,

Kevin Stevens

Appendix F - Designed Pneumatic Ram Modification

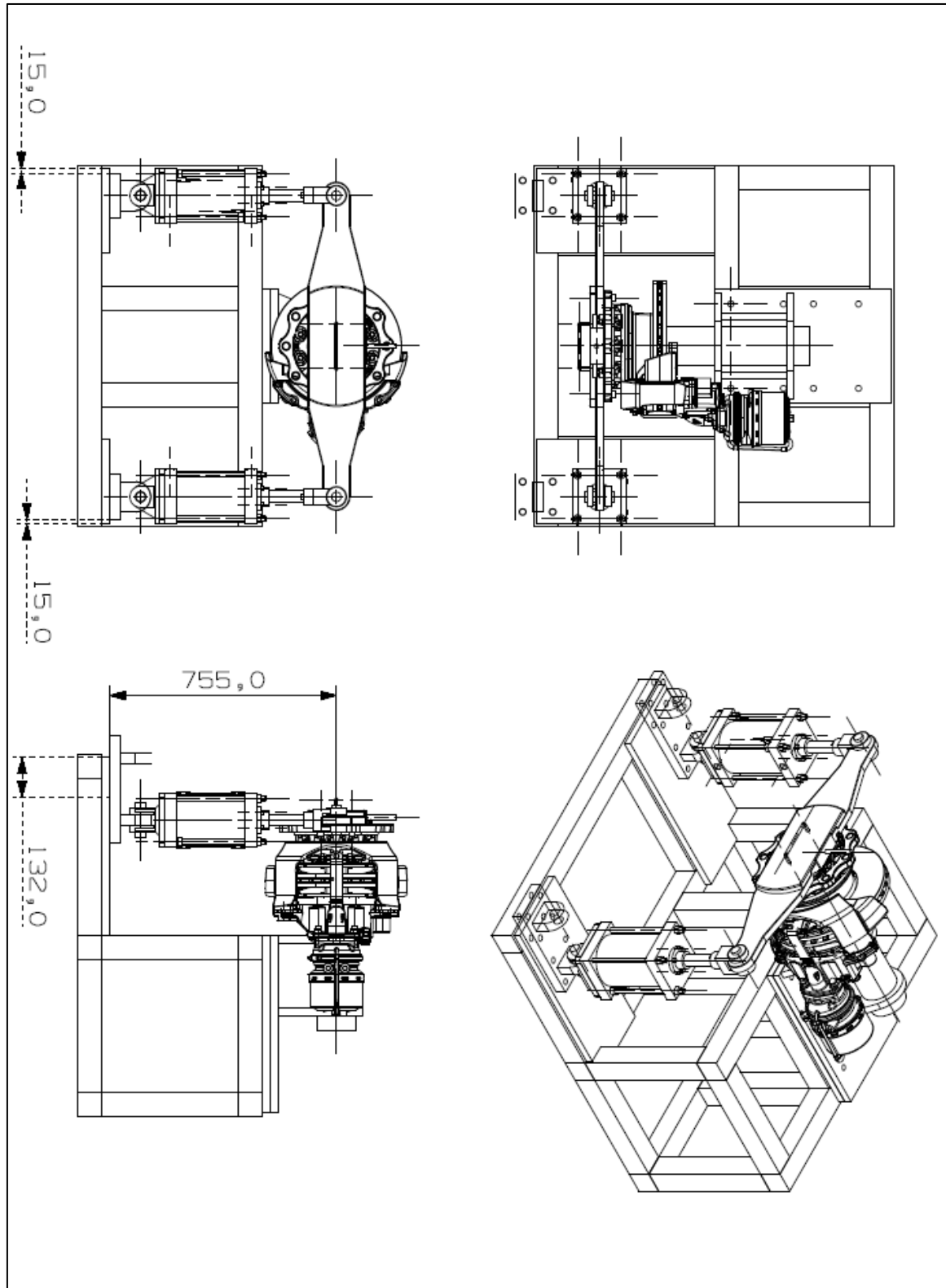


Figure F.1: Thermal Rig modification to drawing incorporating the pneumatic ram feature



Target delivery date:	Quantity: 1	SS5Y9-MCNI06
Ref:	Quotation Ref:	Special: <input type="checkbox"/>
		Issue date: 10/12/2009

Manifold Specification Sheet SERIES SY9000 / Type 43	Company: Cranfield University	
	Contact person: Dr Marko Tirovic	
	Address:	
	Town: Milton Keynes	Country Code:
	Phone: 01234758264	Fax:
	e-mail:	

0. Simple Special Details

Delivery time: 10 days	Selling Price: <input type="text"/>	Simple Special Ref: SS5Y9-MCNI06
-------------------------------	-------------------------------------	---

1. Manifold model



D side U side

2. Manifold specifications

Description	Model	Station nr.	Qty						
Type 43 Bar stock type, common external EXH, individual wiring	SS5Y9-43-03DR-C10F-D-Q		1						
Silencer for R ports (D side)	AN300-KM12		1						
EV - 3 position pressure center	SY9540R-5LOU-Q	<table border="1" style="display: inline-table;"> <tr><td>1</td><td>2</td><td>3</td></tr> <tr><td>X</td><td></td><td></td></tr> </table>	1	2	3	X			1
1	2	3							
X									
Plug connector with lead wire (3 m.)	SY100-30-4A-30	<table border="1" style="display: inline-table;"> <tr><td>X</td><td>X</td><td>X</td></tr> </table>	X	X	X	4			
X	X	X							
EV - 2 position single	SY9140R-5LOU-Q	<table border="1" style="display: inline-table;"> <tr><td></td><td>X</td><td>X</td></tr> </table>		X	X	2			
	X	X							
Individual SUP spacer	SY9000-38-2FA-Q	<table border="1" style="display: inline-table;"> <tr><td>X</td><td>X</td><td></td></tr> </table>	X	X		2			
X	X								
One touch fitting Ø10		<table border="1" style="display: inline-table;"> <tr><td>X</td><td>X</td><td>X</td></tr> </table>	X	X	X	6			
X	X	X							

Figure F.3: Air regulator components required for Thermal Rig ram modifications

Stock Number	Part Number	Description	Quantity	Price Per Unit (£)	Discount	Total
2000010000	ITV2050-31F2BL3-Q	Electro-pneumatic regulator	2	403.89	0.20	646.22
2000010000	AC40-MCMI07	Airline unit	1	242.80	0.20	194.24
2000010000	SS5YA-MCNI06	Manifold	1	393.23	0.20	314.58
2000010000	CDS1DN160-200	Standard Pneumatic cylinders	2	605.26	0.20	968.42
2000010000	CDS1DN160-201-XB6	Heat treated Pneumatic cylinders	2	811.37	0.20	1298.19
2000010000	CS1-C16	Single clevis base	2	76.99	0.20	123.18
2000010000	Y-16	Double knuckle clews	2	135.17	0.20	216.27
2000010000	TH1008B-20	Heat treated tubing	1	320.94	0.20	256.75
2000010000	TJ1065B-20	Standard tubing	1	42.12	0.20	33.70
2000010000	2530-3/4-1/2	Port reducers	4	2.57	0.20	8.22
2000010000	AS2201F-04-10S	Speed controllers for cylinders (estimated price)	4	10.00	0.20	32.00
2000010000	KQ2H10-02S	ITV fittings	2	3.08	0.20	4.93
		Total				4096.71
		V.A.T				716.92
		Total inc. V.A.T				4813.64

Table F.1: Quote received for Thermal Rig ram modifications

Appendix G - National Instruments Module Data Sheets



Technical Sales
United Kingdom
01635 523545
info.uk@ni.com

NI cRIO-9022

Real-Time Controller with 256 MB DRAM, 2 GB Storage

- Embedded controller runs LabVIEW Real-Time for deterministic control, data logging, and analysis
- 533 MHz processor, 2 GB nonvolatile storage, 256 MB DDR2 memory
- Dual Ethernet ports with embedded Web and file servers for remote user interfacing
- Hi-Speed USB host port for connection to USB flash and memory devices
- RS232 serial port for connection to peripherals; dual 9 to 35 VDC supply inputs
- -20 to 55 °C operating temperature range



Overview

The NI cRIO-9022 embedded real-time controller is part of the high-performance CompactRIO programmable automation controller (PAC) platform. It features an industrial 533 MHz Freescale MPC8347 real-time processor for deterministic, reliable real-time applications and contains 256 MB of DDR2 RAM and 2 GB of nonvolatile storage for holding programs and logging data.

This rugged, reliable controller is designed for low power consumption with dual 9 to 35 VDC supply inputs that deliver power to the CompactRIO chassis/modules and a -20 to 55 °C operating temperature range. The cRIO-9022 accepts 9 to 35 VDC power supply inputs on power-up and 6 to 35 VDC power supply inputs during operation, so it can function for long periods of time in remote applications using a battery or solar power.

The controller provides two Ethernet ports - 10/100 and 10/100/1000 - that you can use to conduct programmatic communication over the network and built-in Web (HTTP) and file (FTP) servers. The ports also are compatible with the NI 9144 C Series expansion chassis, so you can achieve more deterministic I/O for your application.

To create additional storage capability for your embedded logging applications, the cRIO-9022 has a Hi-Speed USB host port to which you can connect external USB-based storage media (flash drives and hard drives). In addition, the controller features a fault-tolerant file system that provides increased reliability for data-logging applications.

Specifications

Specifications Documents

- Specifications
- Data Sheet

Specifications Summary

General

Product Name	cRIO-9022
Product Type	Controller (Computing Device)

Form Factor	CompactRIO
Part Number	780718-01
Operating System/Target	Real-Time
LabVIEW RT Support	Yes
CE Compliance	Yes
Controller	
Controller Type	High Performance
Processor Core Type	533 MHz PowerPC
CPU Clock Frequency	533 MHz
System Memory	256 MB
Legacy Product	No
Ethernet (# of ports)	2
Serial Ports (RS232)	1
USB Ports	Yes
Chassis	
Number of Slots	0
Integrated Controller	No
Input Voltage Range	9 V , 35 V
Recommended Power Supply: Power	55
Recommended Power Supply: Voltage	24
Power Consumption	35
Physical Specifications	
Length	77.3 mm
Width	90.2 mm
Height	88.1 mm
Weight	609 gram
Minimum Operating Temperature	-20 °C
Maximum Operating Temperature	55 °C
Maximum Altitude	2000 m

Pricing



Technical Sales
United Kingdom
01635 523545
info.uk@ni.com

NI cRIO-9112

8-Slot, Virtex-5 LX30 CompactRIO Reconfigurable Chassis

- 8-slot reconfigurable embedded chassis that accepts any CompactRIO I/O module
- Xilinx Virtex-5 reconfigurable I/O (RIO) FPGA core for ultimate processing power
- Ability to automatically synthesize custom control and signal processing circuitry using LabVIEW
- DIN-rail mounting options
- -40 to 70 °C operating range



Overview

The NI cRIO-9112 eight-slot, reconfigurable embedded chassis is part of the CompactRIO high-performance programmable automation controller (PAC) platform. It features a user-programmable Xilinx Virtex-5 FPGA, giving you high processing power and the ability to design custom hardware using NI LabVIEW software. The cRIO-9112 provides low-level hardware access to any NI CompactRIO I/O module, so you can create unprecedented timing, triggering, control, and synchronization schemes for embedded and industrial applications.

Panel mounting holes are included in all CompactRIO chassis. For DIN-rail or panel mounting options, you can purchase a CompactRIO mounting kit separately.

Specifications

Specifications Documents

- Specifications
- Data Sheet


Specifications Summary

General	
Product Name	cRIO-9112
Form Factor	CompactRIO
Product Type	Chassis
Part Number	780916-01
Operating System/Target	FPGA
LabVIEW RT Support	Yes

An Investigation into Heat Dissipation from a Stationary Commercial Vehicle Disc Brake in Parked Conditions

CE Compliance	Yes
Reconfigurable FPGA	
FPGA	LX 30
Specific FPGA	Virtex-5 LX30
Chassis	
Number of Slots	8
Integrated Controller	No
Power Consumption	2.6 W
Physical Specifications	
Length	274 mm
Width	88.1 mm
Height	93.1 mm
Weight	880 gram
Minimum Operating Temperature	-40 °C
Maximum Operating Temperature	70 °C
Maximum Altitude	2000 m

Pricing

 Prices shown reflect Academic Discounts.
 Note: All academic discounts are subject to final verification and approval by National Instruments. Academic discounts are not applicable in the Middle East, North Africa, and GCC countries.

Part Number	Description	Est Ship	Pounds Sterling*	Qty
780916-01	cRIO-9112, 8-slot Virtex-5 LX 30 Reconfigurable Chassis for cRIO	1 - 2	£ 999.00 £ 899.10	0
198917-01	NI 9877 C Series Filler Module for Empty Slot	5 - 10	£ 29.00 £ 26.10	0
779473-01	NI 9901 Desktop Mounting Kit	5 - 10	£ 39.00 £ 35.10	0
779558-01	NI 9905 Horizontal Panel Mounting Kit for 8-slot Chassis	5 - 10	£ 29.00 £ 26.10	0
779018-01	NI 9915 DIN Rail Kit for 8-slot Chassis	5 - 10	£ 29.00 £ 26.10	0
779102-01	NI 9910 Industrial Sliding Rack Mounting Kit for cRIO/cDAQ	5 - 10	£ 119.00 £ 107.10	0



Technical Sales
 United Kingdom
 01635 523545
 info.uk@ni.com

NI 9211

4-Channel, 14 S/s, 24-Bit, ± 80 mV Thermocouple Input Module

- 4 thermocouple or ± 80 mV analog inputs
- -40 to 70 °C operating range
- 24-bit resolution; 50/60 Hz noise rejection
- Hot-swappable operation
- NIST-traceable calibration



Overview

The National Instruments NI 9211 thermocouple input module for use with NI CompactDAQ and CompactRIO chassis includes a 24-bit delta-sigma ADC, antialiasing filters, open-thermocouple detection, and cold-junction compensation for high-accuracy thermocouple measurements. The NI 9211 contains NIST-traceable calibration and channel-to-earth ground double isolation barrier for safety, noise immunity, and high common-mode voltage range.

Specifications

Specifications Documents

- Detailed Specifications
- Data Sheet

Specifications Summary

General	
Form Factor	CompactDAQ, CompactRIO
Operating System / Target	Windows, Real-Time
Measurement Type	Thermocouple, Voltage
Isolation Type	Ch-Earth Ground Isolation
Analog Input	
Number of Channels	4 DI
Sample Rate	14 S/s
Resolution	24 bits

Simultaneous Sampling	No
Maximum Voltage Range	-80..80 mV
Minimum Voltage Range	-80..80 mV
Signal Conditioning	Cold-junction compensation
Analog Output	
Number of Channels	0
Digital I/O	
Number of Channels	0
Counter/Timers	
Number of Counter/Timers	0
Timing/Triggering/Synchronization	
Triggers cDAQ Chassis	No

Pricing

Select one of the following options for product configuration and pricing:

Select Module and Accessories Below »
OR
Configure and Price a Complete CompactDAQ/CompactRIO System »



Module



Accessories



Chassis, Controllers, Modules



Software & Services

Step 1: Verify Device and Quantity Selection

Part Number	Description	Est Ship Days	Pounds Sterling*	Qty
779001-01	NI 9211	1 - 2	£ 239.00	1

Step 2: Select Optional Accessories

Part Number	Description	Est Ship Days	Pounds Sterling*	Qty
Screw Terminals				
779017-01	NI 9932 Backshell with 10-pos connector block (qty 1)	1 - 2	£ 29.00	0



Technical Sales
United Kingdom
01635 523545
info.uk@ni.com

NI 9213

16-Channel Thermocouple Input Module

- Built-in CJC (cold-junction compensation)
- High-speed mode for 75 S/s/ch (per channel rate after mux)
- 250 Vrms channel-to-earth ground safety isolation
- Autozero channel for offset error compensation
- 24-bit ADC for up to 0.02 °C measurement sensitivity
- J, K, T, E, N, B, R, and S types supported



Overview

The NI 9213 is a high-density thermocouple module for NI C Series carriers designed for higher-channel-count systems. With this module, you can add thermocouples to mixed-signal test systems without taking up too many slots.

The NI 9213 is similar to the NI 9211 four-channel thermocouple module except it features four times the channel count and almost 100 times the sample rate. In high-speed mode each channel can sample at 75 S/s. When 12 or fewer channels are used, the max sample rate per channel can increase to 100 S/s.

You can use up to eight NI 9213 modules in an NI CompactDAQ chassis or CompactRIO chassis for 128 thermocouple measurements in a single chassis, or deploy a single module in any of the USB, Ethernet, or Wi-Fi carriers for C Series modules.

Each shipping kit contains:

- NI 9213 module with spring-terminal connectivity
- NI 9940 backshell for cabling and strain relief
- Spring-terminal tool for signal wire insertion

Specifications

Specifications Documents

- Specifications
- Data Sheet

Specifications Summary

General

Product Name	NI 9213
--------------	---------

An Investigation into Heat Dissipation from a Stationary Commercial Vehicle Disc Brake in Parked Conditions

Product Family	Industrial I/O
Form Factor	CompactDAQ , CompactRIO
Part Number	780493-01 , 780493-02
Operating System/Target	Real-Time , Windows
LabVIEW RT Support	Yes
Measurement Type	Temperature , Thermocouple
RoHS Compliant	Yes
Signal Conditioning	Open thermocouple , Cold-junction compensation
Analog Input	
Channels	0 , 16
Single-Ended Channels	0
Differential Channels	16
Resolution	24 bits
Sample Rate	1200 S/s
Bandwidth	78 Hz
Max Voltage	78.125 mV
Maximum Voltage Range	-78.125 mV , 78.125 mV
Maximum Voltage Range Accuracy	38 μ V
Simultaneous Sampling	No
Analog Output	
Channels	0
Digital I/O	
Bidirectional Channels	0
Input-Only Channels	0
Output-Only Channels	0
Counter/Timers	
Counters	0
Physical Specifications	
Length	88.11 mm
Width	22.86 mm
I/O Connector	36-position spring terminal



Technical Sales
United Kingdom
01635 523545
info.uk@ni.com

NI 9214

16-Channel Isothermal Thermocouple Input Module

- Isothermal terminal block (included) for measurement accuracy up to 0.45 °C
- Several cold-junction compensation (CJC) sensors
- 250 Vrms channel-to-earth ground safety isolation
- Autozero channel for offset error compensation
- 24-bit ADC for up to 0.02 °C measurement sensitivity
- J, K, T, E, N, B, R, and S types supported



Overview

The NI 9214 is a high-density thermocouple module for NI C Series carriers designed for higher-channel-count systems that also need higher accuracy than the NI 9213 offers.

The NI 9214 has several features that increase overall accuracy including the following:

- Front-mounting metal terminal block (NI TB-9214)
- Several CJC sensors in the terminal block
- Component layout to minimize thermal gradients

You can use up to eight NI 9214 modules in an NI CompactDAQ chassis or CompactRIO chassis for 128 thermocouple measurements in a single chassis.

Each shipping kit contains the following:

- NI 9214 module with spring-terminal connectivity
- TB-9214 front-mounting terminal block
- Printed manual

Note that the NI 9214 isothermal thermocouple module does not work with the legacy NI cDAQ-9172 chassis or any of the legacy 1-slot C Series carriers (NI USB-9162, NI ENET-9163, and NI WLS-9163).

Specifications

Specifications Documents

- Specifications
- Data Sheet

Specifications Summary

General	
Product Name	NI 9214
Product Family	Industrial I/O
Form Factor	CompactDAQ , CompactRIO
Part Number	781510-01
Operating System/Target	Real-Time , Windows
LabVIEW RT Support	Yes
Measurement Type	Temperature , Thermocouple
Isolation Type	Ch-Earth Ground Isolation
RoHS Compliant	Yes
Signal Conditioning	Cold-junction compensation , Open thermocouple
Analog Input	
Channels	0 , 16
Single-Ended Channels	0
Differential Channels	16
Resolution	24 bits
Sample Rate	1088 S/s
Bandwidth	68 Hz
Max Voltage	78.125 mV
Maximum Voltage Range	-78.125 mV , 78.125 mV
Maximum Voltage Range Accuracy	25 μ V
Simultaneous Sampling	No
Analog Output	
Channels	0
Digital I/O	
Bidirectional Channels	0
Input-Only Channels	0
Output-Only Channels	0
Counter/Timers	
Counters	0



Technical Sales
United Kingdom
01635 523545
info.uk@ni.com

NI 9219

24-Bit Universal Analog Input

- 250 Vrms channel-to-channel isolation
- Built-in quarter, half, and full-bridge support
- Built-in voltage and current excitation
- Thermocouple, RTD, resistance, voltage, and current measurements
- CJC per channel for accurate thermocouple measurement
- 100 S/s/ch simultaneous inputs (50S/s/ch for Thermocouple)



Overview

The National Instruments 9219 is a 4-channel universal C Series module designed for multipurpose testing in any NI CompactDAQ or CompactRIO chassis. With the NI 9219, you can measure several signals from sensors such as strain gages, RTDs, thermocouples, load cells, and other powered sensors. The channels are individually selectable, so you can perform a different measurement type on each of the four channels. Measurement ranges differ for each type of measurement and include up to ± 60 V for voltage and ± 25 mA for current. Please see the manual for detailed specifications and ranges.

Because of the driver design, the NI 9219 does not limit the overall speed of an NI CompactDAQ system when used with faster sampling modules.

With 250 Vrms of channel-to-channel isolation, the NI 9219 protects not only the surrounding modules, chassis, and connected computer system but also the other channels within the same module. In addition to increased safety, channel-to-channel isolation eliminates problems associated with ground loops.

The NI 9219 uses 6-position spring terminal connectors in each channel for direct signal connectivity. You can purchase additional connectors to reduce signal connection time for multiple test units. In addition to extra connectors, a strain relief kit is available to secure the signal wires.

Strain relief backshells for signal wire security and high-voltage protection (qty 4): NI 9972

Extra connectors for 6-position connector modules (qty 10): NI 9973

Specifications

Specifications Documents

- Detailed Specifications
- Data Sheet

Specifications Summary

General

An Investigation into Heat Dissipation from a Stationary Commercial Vehicle Disc Brake in Parked Conditions

Form Factor	CompactDAQ, CompactRIO
Operating System / Target	Windows, Real-Time
Measurement Type	Bridge-based sensor, Current, Resistance, RTD, Thermistor, Thermocouple, Voltage
Isolation Type	Ch-Ch Isolation
Analog Input	
Number of Channels	4 DI
Sample Rate	100 S/s/ch
Resolution	24 bits
Simultaneous Sampling	Yes
Maximum Voltage Range	-80..80 V
Range Accuracy	243 mV
Minimum Voltage Range	-0.125..0.125 V
Range Accuracy	271 μ V
Maximum Current Range	-0.0025..0.0025 A
Range Accuracy	152 μ A
Minimum Current Range	-0.0025..0.0025 A
Range Accuracy	152 μ A
Signal Conditioning	0-20 mA current input, Bridge completion, Cold-junction compensation, Current excitation, Voltage excitation
Excitation Voltage	2.5 V
Bridge Configurations	Full Bridge, Half Bridge, Quarter Bridge
Analog Output	
Number of Channels	0
Digital I/O	
Number of Channels	0
Counter/Timers	
Number of Counter/Timers	0
Timing/Triggering/Synchronization	
Triggers cDAQ Chassis	No

Pricing



Technical Sales
 United Kingdom
 01635 523545
 info.uk@ni.com

NI 9263

4-Channel, 100 kS/s, 16-bit, ± 10 V, Analog Output Module

- 4 simultaneously updated analog outputs, 100 kS/s
- 16-bit resolution
- Hot-swappable operation
- NIST-traceable calibration
- -40 to 70 °C operating range



Overview

The National Instruments NI 9263 is a 4-channel, 100 kS/s simultaneously updating analog output module for any NI CompactDAQ or CompactRIO chassis. The NI 9263 also features ± 30 V overvoltage protection, short-circuit protection, low crosstalk, fast slew rate, high relative accuracy, and NIST-traceable calibration. The NI 9263 module includes a channel-to-earth ground double isolation barrier for safety and noise immunity.

Specifications

Specifications Documents

- Detailed Specifications
- Data Sheet

Specifications Summary

General	
Form Factor	CompactDAQ, CompactRIO
Operating System / Target	Windows, Real-Time
Measurement Type	Voltage
Isolation Type	Ch-Earth Ground Isolation
Analog Input	
Number of Channels	0
Analog Output	
Number of Channels	4

Update Rate	100 kS/s
Resolution	16 bits
Maximum Voltage Range	-10..10 V
Range Accuracy	0.11 V
Minimum Voltage Range	-10..10 V
Range Accuracy	0.11 V
Digital I/O	
Number of Channels	0
Counter/Timers	
Number of Counter/Timers	0
Timing/Triggering/Synchronization	
Triggers cDAQ Chassis	No

Pricing

Select one of the following options for product configuration and pricing:

Select Module and Accessories Below »
OR
Configure and Price a Complete CompactDAQ/CompactRIO System »



Module



Accessories



Chassis, Controllers, Modules



Software & Services

Step 1: Verify Device and Quantity Selection

Part Number	Description	Est Ship Days	Pounds Sterling*	Qty
779012-01	NI 9263	1 - 2	£ 289.00	1

Step 2: Select Optional Accessories

Part Number	Description	Est Ship Days	Pounds Sterling*	Qty
Screw Terminals				
779017-01	NI 9932 Backshell with 10-pos connector block (qty 1)	1 - 2	£ 29.00	0
779105-01	NI 9936 10-pos screw term connector block (qty 10)	1 - 2	£ 49.00	0



Technical Sales
United Kingdom
01635 523545
info.uk@ni.com

NI 9401

8 Ch, 5 V/TTL High-Speed Bidirectional Digital I/O Module

- 8-channel, 100 ns ultrahigh-speed digital I/O
- 5 V/TTL, sinking/sourcing digital I/O
- Bidirectional, configurable by nibble (4 bits)
- Industry-standard 25-pin D-SUB connector
- Hot-swappable operation
- -40 °C to 70 °C operating range



Overview

The NI 9401 is an 8-channel, 100 ns bidirectional digital input module for any NI CompactDAQ or CompactRIO chassis. You can configure the direction of the digital lines on the NI 9401 for input or output by nibble (4 bits). Thus, you can program the NI 9401 for three configurations - eight digital inputs, eight digital outputs, or four digital inputs and four digital outputs. With reconfigurable I/O (RIO) technology (CompactRIO only), you can use the NI LabVIEW FPGA Module to program the NI 9401 for implementing custom, high-speed counter/timers; digital communication protocols; pulse generation; and much more. Each channel is compatible with 5 V/TTL signals and features 1,000 Vrms transient isolation between the I/O channels and the backplane.

The NI 9934 (or other 25-pin D-SUB connector) is required for use with the NI 9401 module. The module includes a screw-terminal connector with strain relief as well as a D-SUB solder cup backshell for creating custom cable assemblies.

EMC Performance

To ensure EMC compliance, you must use a ferrite bead, such as NI part number 782803-01.

Specifications

Specifications Documents

- Specifications
- Data Sheet

Specifications Summary

General	
Product Name	NI 9401
Product Family	Industrial I/O
Form Factor	CompactDAQ , CompactRIO

An Investigation into Heat Dissipation from a Stationary Commercial Vehicle Disc Brake in Parked Conditions

Part Number	782401-01 , 779351-01
Operating System/Target	Real-Time , Windows
Measurement Type	Digital
Isolation Type	Ch-Earth Ground Isolation
RoHS Compliant	Yes
Analog Input	
Channels	0
Single-Ended Channels	0
Differential Channels	0
Analog Output	
Channels	0
Digital I/O	
Bidirectional Channels	8
Input-Only Channels	0
Output-Only Channels	0
Timing	Hardware
Maximum Clock Rate	10 MHz
Logic Levels	TTL
Input Current Flow	programmableCurrent
Output Current Flow	programmableCurrent
Supports Handshaking I/O?	Yes
Supports Pattern I/O?	Yes
Maximum Input Range	0 V , 5.25 V
Maximum Output Range	0 V , 5.25 V
Counter/Timers	
Counters	0
Physical Specifications	
Length	9 cm
Width	2.3 cm
I/O Connector	25-pin D-Sub
Minimum Operating Temperature	-40 °C

Appendix H - LM 120 Offset D-Elsa 225 Brake

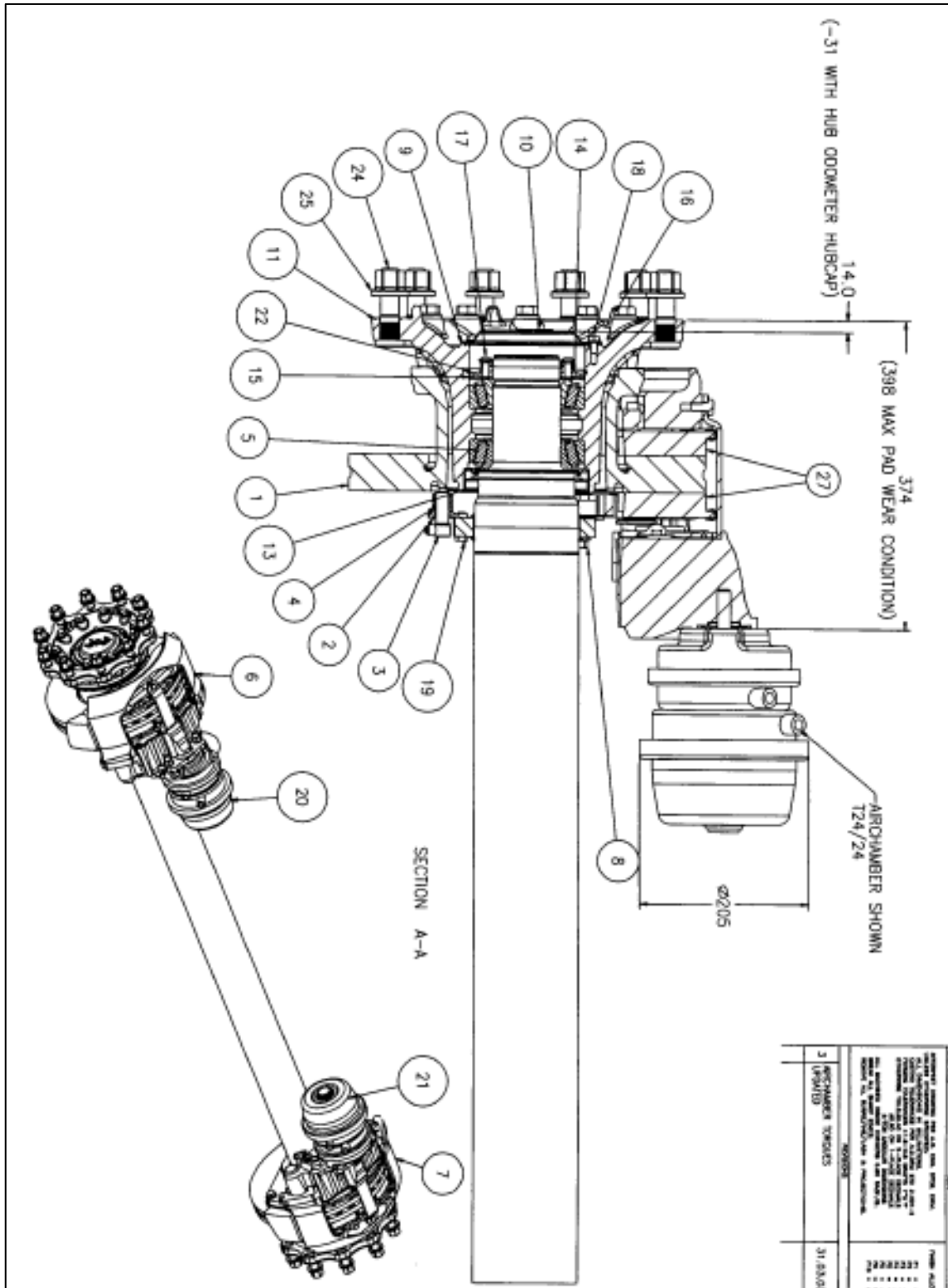
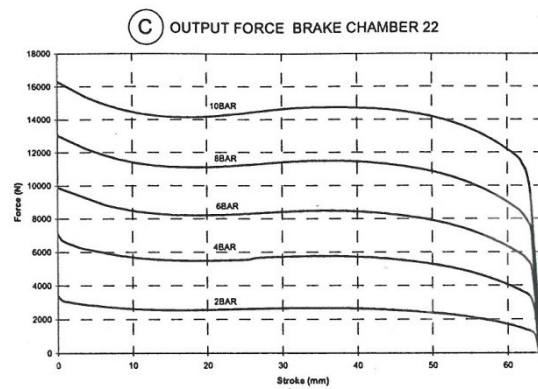
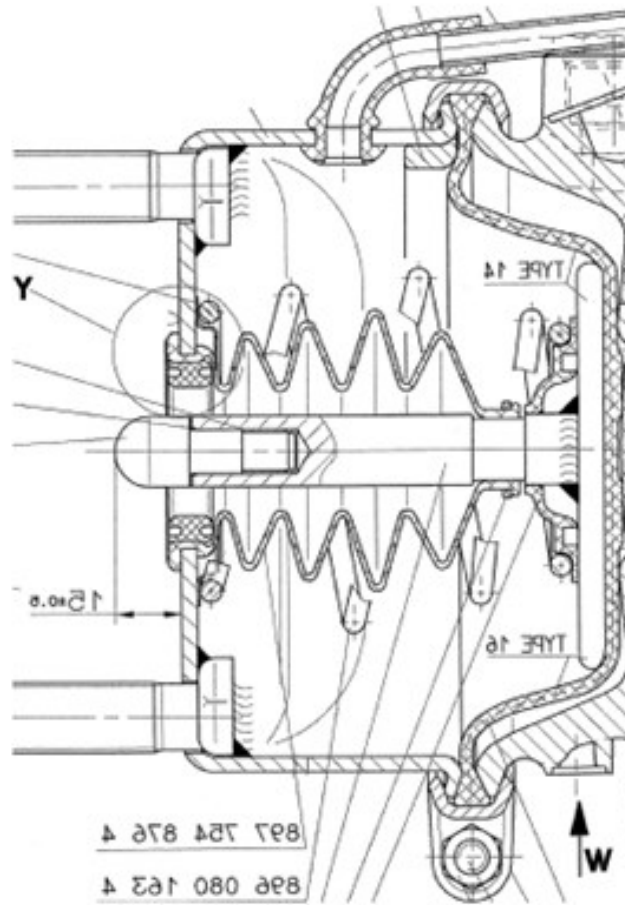


Figure H.1: Elsa 225 brake caliper assembly

Appendix J - Service Chamber



Appendix K - Analytical Disc Cooling Modelling, Cases 1 and 2

Appendix K.1 - Lumped HTC - Case 1

In this first section, the assumptions regularly used when dealing with dynamic braking applications will be used to demonstrate its inadequacy for parking applications. Both the radiation and convection dissipation modes will be held constant, corresponding to a lumped cooling model. First principles were used to generate the cooling equation. Recalling and differentiating the energy balance equation (equation (K.1)) where the rate of internal energy change is directly proportional to the energy entering the system (or work done on the system).

$$\Delta E = mC_p\Delta T \quad (\text{K.1})$$

Applying equation (K.1) to a parking application, as no energy is entering the disc during a parking application (due to the lack of frictional heating) the work done on the system is negative, hence a decrease in disc brake temperature.

$$\begin{aligned} Q_{in} - Q_{out} &= m_d C_{p,d} \frac{dT_d}{dt} \\ -Q_{out} &= m_d C_{p,d} \frac{dT_d}{dt} \end{aligned} \quad (\text{K.2})$$

With the presence of a gasket conduction can be neglected, allowing the heat dissipation term in equation (K.2) to be broken down into the two active modes. Consequently, the fundamental energy balance equation that needs to be solved is:

$$m_d C_{p,d} \frac{dT_d}{dt} = -(Q_{conv} + Q_{rad}) \quad (\text{K.3})$$

Fourier's law of cooling defines the nature of thermal dissipation. By applying Fourier's law to each of the dissipation terms in equation (K.3) a first order differential equation (ODE) was generated. Equation (K.4) is in the time domain with respect to temperature in the time domain. Because both radiation and convection is assumed constant in this particular case, it is possible to lump both the terms together into a total disc brake HTC, h_{total} .

$$\begin{aligned} m_d C_{p,d} \frac{dT_d}{dt} &= -[h_{conv} A_{surf} (T_d - T_\infty) + h_{rad} A_{surf} (T_d - T_\infty)] \\ m_d C_{p,d} \frac{dT_d}{dt} &= -(h_{conv} + h_{rad}) A_{surf} (T_d - T_\infty) \end{aligned} \quad (\text{K.4})$$

$$m_d C_{p,d} \frac{dT_d}{dt} = -h_{total} A_{surf} (T_d - T_\infty)$$
$$\frac{dT_d}{dt} = -\frac{h_{total} A_{surf} (T_d - T_\infty)}{m_d C_{p,d}}$$

Appendix K.1.1 - Numerical Solution

By integrating equation (K.4), an exact solution of the first order differential equation that predicts bulk disc brake temperature drop over time will be achieved. However, before this process is conducted, a numerical solution to the problem will be presented. When calculating radiation, by definition the energy change is proportional to the fourth power of disc temperature, which is highly nonlinear. Subsequently, in anticipation of a more complex equation than that shown in equation (K.4) when varying HTCs are used, a numerical analysis for each of the three disc only cases shall be conducted. By completing the numerical study, comparisons of the equations with varying complexities can be made.

Appendix K.1.1.1 - Solver

To solve equation (K.4) numerically, one of MatLab's inbuilt differential solvers was used. The decision to use the generic standard differential solver built into MatLab, rather than writing a specific numerical code, was made to allow greater effort to be directed towards achieving the aims of the overall project. MatLab has six inbuilt differential solvers to offer ode23, ode45, ode113, ode15s, ode23ts and ode23tb. The first three are explicit solvers whereas the later three are implicit. As implicit methods use both the current time-step result plus the future time-step to produce the result, they have a higher order of accuracy but inherently require greater computational resources. With all the assumptions made in the derivation of equation (K.4), provided that the function is not stiff an explicit method would suffice, rejecting the three implicit solvers. A function is stiff if a solver is unable to solve the ODE unless the time-step is sufficiently small, drastically increasing the computational time.

The ode113 solver could also be rejected as it was designed to solve ODEs of multiple orders, leaving either the ode23 or ode45 1st ODE solver. Both remaining solvers are capable of estimating the error in the time-step during all iterations, making the solver as efficient as possible without losing accuracy in the results. This also means that the built-in solver used is likely to be more accurate than any programmed solver specifically made. Comparing the remaining two options, the ode45 solver is the more accurate solver as it has 4th or 5th order accuracy whilst the ode23 solver is only 2nd or 3rd order accuracy (depending on the problem).

For this reason, the ode45 solver was chosen to run the numerical problems presented in equation (K.4), as well as all future numerical analysis.

Appendix K.1.1.2 - Results

Table 11.1 shows the average rotor, hat and subsequent disc bulk temperatures measured in section 9.2.1. The bulk disc temperature started at 257.8°C and fell to 29.5°C over the six hour cooling period; it should be noted that the average ambient temperature during these experiments was 24.1°C. An error of ±20% from the numerical results when compared to these experimental results would be deemed sufficiently close to the actual for acceptance but a desired level of precision was ±10% to generate a more accurate outcome.

Table 11.1: Average disc brake temperature taken from averaged experimental data – blocked vanes, gasket installed. Ambient temperature = 24.1°C

Time (h)	Rotor Temperature (°C)	Hat Temperature (°C)	Bulk Disc Temperature (°C)
0	335.3	180.3	257.8
0.08	290.8	176.5	233.7
0.17	255.6	169.8	212.7
0.25	227.3	161.5	194.4
0.5	167.7	136.5	152.1
0.75	130.8	116.6	123.7
1.0	106.3	101.1	103.7
1.5	77.0	79.2	78.1
2.0	60.9	65.0	62.9
2.5	51.0	55.1	53.0
3.0	44.3	47.9	46.1
3.5	39.5	42.6	41.1
4.0	36.1	38.7	37.4
4.5	33.5	35.7	34.6
5.0	31.5	33.4	32.5
5.5	29.9	31.6	30.8
6.0	28.8	30.2	29.5

In the absence of better information, the disc brake specific heat was kept at a constant value of 48 W/m.K instead of varying it with temperature, which would happen in reality. The variation in specific heat of grey cast iron is likely to be small though, so this assumption is legitimate. All but one variable in equation (K.4) was known at this point, leaving just the value of h_{total} outstanding. By supplying various h_{total} values to the 1st ODE, multiple cooling curves were generated and displayed in Figure K.1. Although there are a number of different cooling curves

presented, it would appear the actual cooling characteristics of the disc brake is not captured by any of the values used for the total HTC. Early on in the cooling phase, the magnitude of h_{total} is high, approximately 30 W/m²K but falls below 15 W/m²K towards the end.

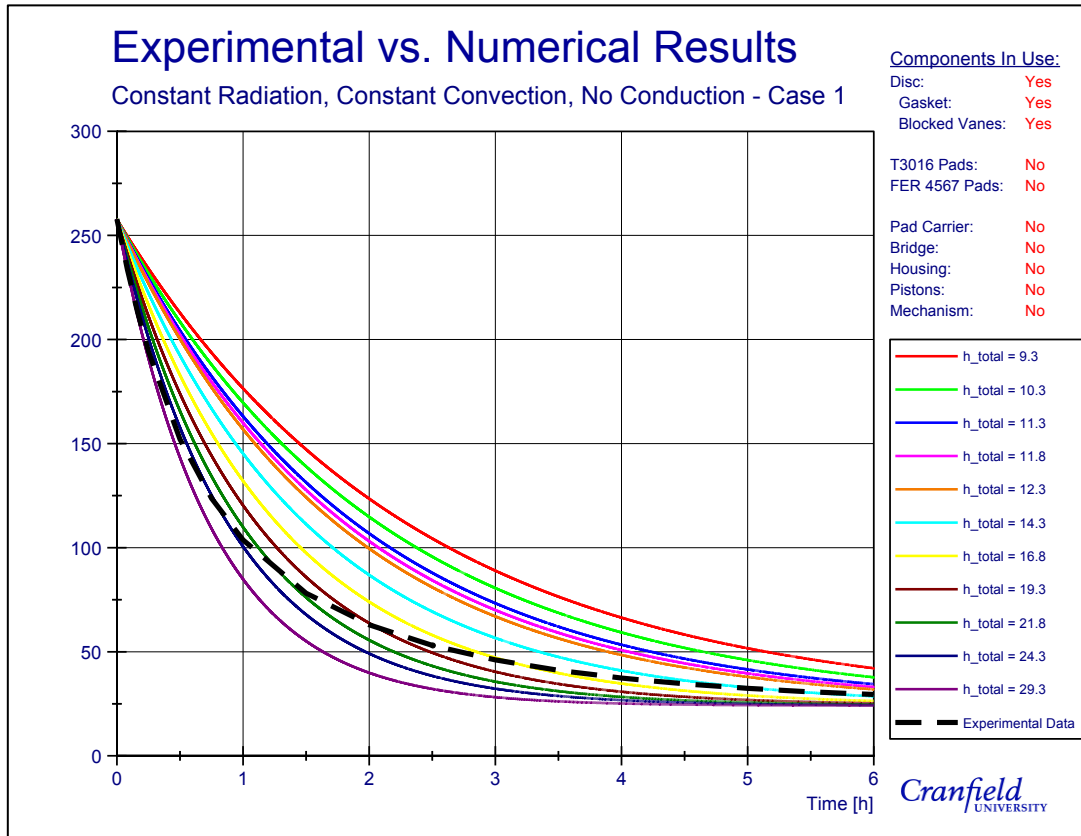


Figure K.1: 1st ODE results for case 1, bulk temperature drop

Separation of the radiation HTC from the total HTC was required to find the values of h_{conv} . Remembering h_{total} is the sum of the convection and radiation coefficients, it was possible to calculate h_{conv} by subtracting a value of h_{rad} from the total HTC value. Of course, this relies on knowing the value of h_{rad} . Having completed emissivity work previously, it is known that a fully oxidised grey cast iron disc brake has an emissivity value of 0.92, which can be assumed constant throughout the duration of the cooling phase. By using equation (K.5) a value of h_{rad} can be calculated for a single temperature only. Simple inspection of equation (K.5) leads to the conclusion that as the temperature falls, h_{rad} will fall nonlinearly with the temperature. Nonetheless, the procedure in motion for constant HTC's will commence to find the lumped case 1 estimation for a value of h_{conv} using the derived 1st ODE.

$$h_{rad} = \varepsilon\sigma(T_d^3 + T_\infty^3 + T_d^2T_\infty + T_dT_\infty^2) \quad (K.5)$$

When calculating the value of h_{rad} , if the initial disc brake bulk temperature value is used then an accurate value of h_{rad} value will be achieved for the initial instance only, continually becoming an overestimate of the real value as temperature drops. Overestimating the cooling values will lead to rapid cooling rate. Conversely, if a value recorded towards the end is used then an underestimation of h_{rad} is made for the majority of the cooling phase, generating an elongated cooling phase. Consequently, an average of the initial and final temperature was taken for the calculation in an attempt to counterbalance the changeable radiation effect. The average temperature 143.7°C (416.7 K) produces a h_{rad} value of 9.8 W/m²K when emissivity is taken to be 0.92.

In Figure K.1, the first line corresponds to a h_{total} value of 9.8 W/m²K, which can be considered as pure radiation cooling as the convection HTC equalled to zero. With the radiation being assumed constant, further incrimination of h_{total} will effectively only increase the h_{conv} value. Figure K.2 shows essentially the same data as Figure K.1 but now with different h_{conv} values as the subject of each line. Again, the predicted value h_{conv} value is elevated at the beginning of the cooling phase with a magnitude approximately 15 W/m²K then reduces close to 5 W/m²K.

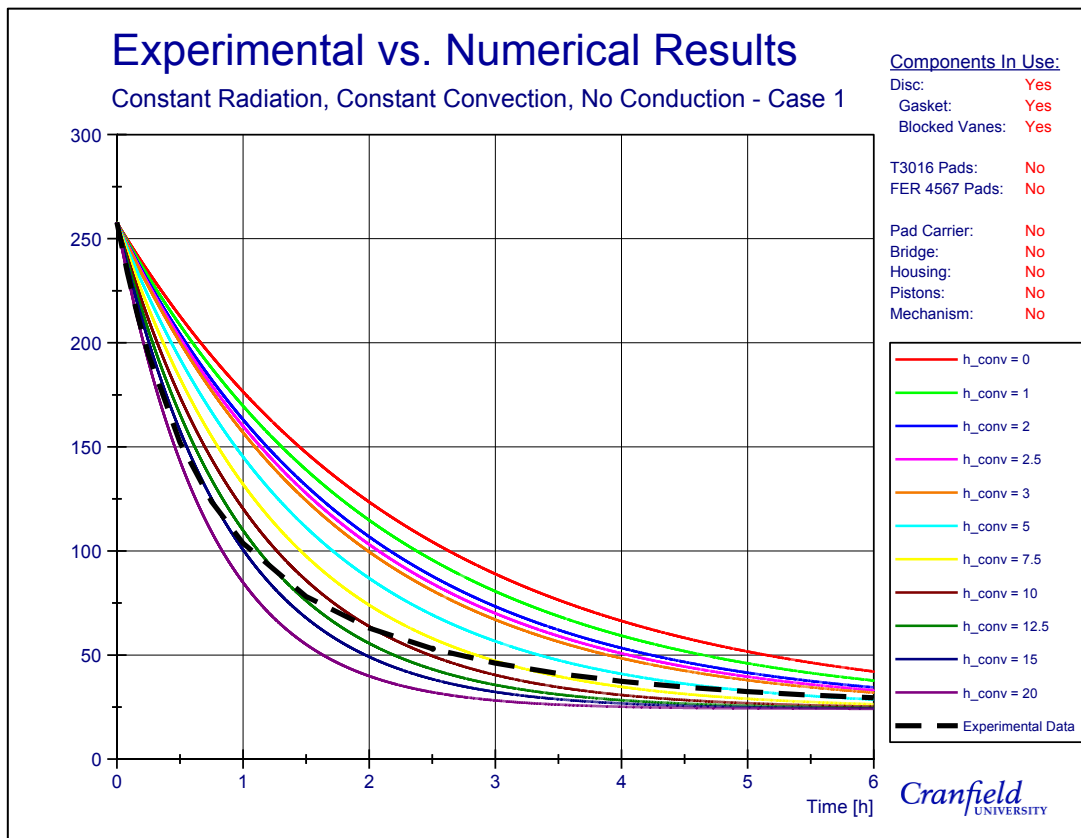


Figure K.2: Effect of increasing the convective HTC on disc brake cooling – Case 1

When extrapolating the experimental values of h_{conv} produced by Voller (2003), it was expected that a value in the region of $2.5 \text{ w/m}^2\text{K}$ would be found for stationary cooling application. At the end of the cooling phase the initial estimate was half that of the lumped numerical value and six times smaller than at the beginning of the cooling phase. Several reasons for the discrepancy between the expected and computed values of h_{conv} are offered. Firstly, Voller conducted dynamic cooling tests at various rotational velocities where forced convection flow eradicates any buoyant airflow through and around the disc. As the rotational velocity approaches zero, forced convection becomes less dominant with buoyancy driven flow becoming more pronounced. Unfortunately, Voller did not collect data at sufficiently low rotational speeds to test the buoyant flow. As a consequence, the conducted extrapolation of Voller's results was unreasonable; the airflow in this case relates to unrealistic static air.

Alternatively, a second offered reasoning for the misalignment could be that the buoyancy effect, ignored by Voller, had a varying magnitude during the experiment. At a high temperature, the buoyant force driving the airflow could be sufficiently large to deliver much greater h_{conv} value than previously expected, whilst decreasing with temperature with the reduction in the buoyant force.

Then again, the buoyant force could performance only a minor role in disc brake dissipation, with radiation being the principal mode. It was previously assumed radiation remained constant throughout the cooling phase but it is easy to see that in fact, the relationship is highly nonlinear. By applying a varying radiation with temperature, the cooling characteristics which the 1st ODE produces may align the numerical data to the experimental data. A final possibility could be that the physics governing disc brake cooling during the cooling phase is so complex that a combination of varying radiation and convection may be required to achieve an accurate temperature profile estimate. Investigations will continue after finding the exact solution to equation (K.4) into improving the predicted temperature profiles predicted by the numerical equation, but there is little merit in testing all the above possibilities. It has already been stated that radiation is highly nonlinear, thus any further numerical analysis holding radiation constant would be irrelevant, resulting in two potential further experiment; constant convection with a variable radiation coefficient and if necessary, both variable convection and radiation coefficients.

Appendix K.1.1.3 - Cooling Equation

Having the ability to produce numerical solutions to differential equations is a powerful tool to an Engineer as they can find approximations to time dependent problems quickly. The

disadvantage with ODE solvers in computer packages, such as MatLab, is the Engineer must have a computer present and sufficient skill to program it. During the initial design stage, an Engineer may wish to know the cooling properties without having to go through the process of programming a computer; it would be more convenient to place values into an equation and get an indication of how the design will perform. It is easy to integrate equation (K.4) as the only variable changing with the independent variable (time) is a single first order term for the bulk disc temperature (the dependent variable). Therefore, the solution will be an exact solution to the 1st ODE. Standard integration of equation (K.4) gives:

$$\int_a^b \frac{dT_d}{(T_d - T_\infty)} = \int_{t_1}^{t_2} -\frac{h_{total}A_{surf}}{m_d C_{p,d}} dt$$

$$\int_a^b \frac{dT_d}{(T_d - T_\infty)} = -\frac{h_{total}A_{surf}}{m_d C_{p,d}} \int_{t_1}^{t_2} dt$$

$$\ln \frac{(T_{d,b} - T_\infty)}{(T_{d,a} - T_\infty)} = -\frac{h_{total}A_{surf}}{m_d C_{p,d}} (t_2 - t_1) + K \quad (K.6)$$

where K is the constant of integration and can only be determined by substituting known values into equation (K.6). There was only a single unknown in this equation (K) so only a solitary set of boundary conditions were needed to complete the cooling equation. By using the initial temperature in Table 11.1 (257.8°C) for both the start and finish point for the integration, a 0°C temperature gradient will be present. Consequently, the constant of integration must also be zero for this to hold true; reducing the Case 1 cooling equation to:

$$\ln \frac{(T_{d,b} - T_\infty)}{(T_{d,a} - T_\infty)} = -\frac{h_{total}A_{surf}}{m_d C_{p,d}} (t_2 - t_1) \quad (K.7)$$

Limitations of the cooling equation derived in equation (5.1) are that both temperatures $T_{d,a}$ and $T_{d,b}$ must be greater than T_∞ , and $T_{d,a}$ must be larger than $T_{d,b}$ to ensure the solution is cooling.

Equation (5.1) was originally developed by Galindo-Lopez (2008) as part of an investigation into convective cooling optimisation of a disc brake. Galindo-Lopez used the equation in conjunction with experimental data to determine h_{conv} values for rotating disc brakes. By using the results presented in Table 11.1, the same method can be used to find the exact value of h_{conv} . For the entire six hour period, equation (5.1) generates a h_{total} value of 13.7 W/m²K, which corresponds to a h_{conv} value of 3.9 W/m²K. Compared to the expected value, the Galindo-Lopez cooling equation produces a h_{conv} value 54% larger. Yet, from the numerical results, a h_{conv} value of 5 W/m²K was shown to be reasonable at the end of the cooling but too

low for the majority of the cooling time. Considering the Galindo-Lopez equation calculates an even lower h_{conv} value than this, it can be rejected as an accurate method of predicting h_{conv} values over long time periods.

Appendix K.2 Case 2 - Variable Radiation

Having proven that assuming static values for both convection and radiation HTC is an insufficient technique for estimating accurate disc brake cooling, this section incrementally increases the cooling equation complexity by allowing radiation to vary with temperature whilst continuing to hold convection constant. This action will test one of the misalignment possibilities discussed in section Appendix K.1.1.2. Radiation is highly nonlinear with temperature. It is hoped that by allowing the radiation HTC to alter with the temperature drop the cooling estimation will be more representative of actual disc brake cooling.

Appendix K.2.1 - Numerical Solution

To begin, let the energy balance shown in equation (K.3) be recalled. With conduction continuing to be neglected, the energy balance remains unchanged. However, lumping of the HTCs will not occur, with the thermal work terms replaced by their respective Fourier cooling equation alternatives. A new energy balance that allows for a varying radiation was created and shown in equation (K.8).

$$m_d C_{p,d} \frac{dT_d}{dt} = -(Q_{conv} + Q_{rad})$$

$$m_d C_{p,d} \frac{dT_d}{dt} = -[h_{conv} A_{surf} (T_d - T_\infty) + \sigma \varepsilon A_{surf} (T_d^4 - T_\infty^4)] \quad (K.8)$$

Multiplying out of the brackets and then separating of the variables signifies two separate dependent variable terms in equation (K.9); a linear term (from convection) and a nonlinear, fourth order term (from radiation).

$$m_d C_{p,d} \frac{dT_d}{dt} = -[h_{conv} A_{surf} T_d - h_{conv} A_{surf} T_\infty + \sigma \varepsilon A_{surf} T_d^4 - \sigma \varepsilon A_{surf} T_\infty^4]$$

$$m_d C_{p,d} \frac{dT_d}{dt} = A_{surf} (h_{conv} T_\infty + \sigma \varepsilon T_\infty^4) - A_{surf} (h_{conv} T_d + \sigma \varepsilon T_d^4) \quad (K.9)$$

To generate the differential equation for case 2, dividing equation (K.9) through by both the disc brake mass and its specific heat capacity is required. The resultant 1st ODE is presented in equation (K.10).

$$\frac{dT_d}{dt} = \frac{A_{surf}}{m_d C_{p,d}} (h_{conv} T_\infty + \sigma \varepsilon T_\infty^4) - \frac{A_{surf}}{m_d C_{p,d}} (h_{conv} T_d + \sigma \varepsilon T_d^4) \quad (K.10)$$

However, this above equation can be simplified into a more convenient form by introducing a couple of factors. With specific heat capacity, mass and surface area remaining constant throughout, the term before each bracket can be lumped together as a single constant, γ , which is a function of the disc brakes physical attributes. Additionally, the product of the Stefan-Boltzmann constant and the emissivity equate to make the relative constant of proportionality⁶, β .

let $\beta = \sigma \varepsilon$ (K.11a)

$$\gamma = \frac{A_{surf}}{m_d C_{p,d}} \quad (K.11b)$$

By placing the two constants from equation (K.11) into equation (K.10), the final 1st ODE is derived for second cooling case.

$$\frac{dT_d}{dt} = \gamma (h_{conv} T_\infty + \beta T_\infty^4) - \gamma (h_{conv} T_d + \beta T_d^4) \quad (K.12)$$

Substituting equation (K.12) into the same MatLab ode45 solver generates the results shown in Figure K.3. The effect of variable radiation has improved the results somewhat as the nonlinearity of the experimental data is followed better than those in Figure K.2. Initially, heat dissipates at a rate corresponding to a h_{conv} value of 15 W/m²K and reduces to 7.5 W/m²K at the conclusion of the cooling phase. The increase in h_{conv} at the low temperature end can be attributed to the variability in the radiation as little energy can be radiated as the temperatures approach the ambient. Keeping radiation constant in the previous lumped case gave an overestimation of emitted radiation energy, consequently producing an undervaluation of the convection. The relative change in h_{conv} is less than for case 1. It can therefore be concluded that the variation in radiation must be considered highly significant as its presence in the cooling ODE improved the quality of the numerically generated results.

⁶ σ is known as the constant of proportionality whilst ε is the relative ability of a surface to emit energy. Combining these two definitions give the name relative constant of proportionality.

Although an improvement is evident, it cannot be said that the numerically generated cooling profiles match the experimental profile well. Combining the fact that the numerical data is still misaligned to that of the experimental data and that the h_{conv} value is falling with temperature, a final case was necessary where both radiation and convection varied with temperature.

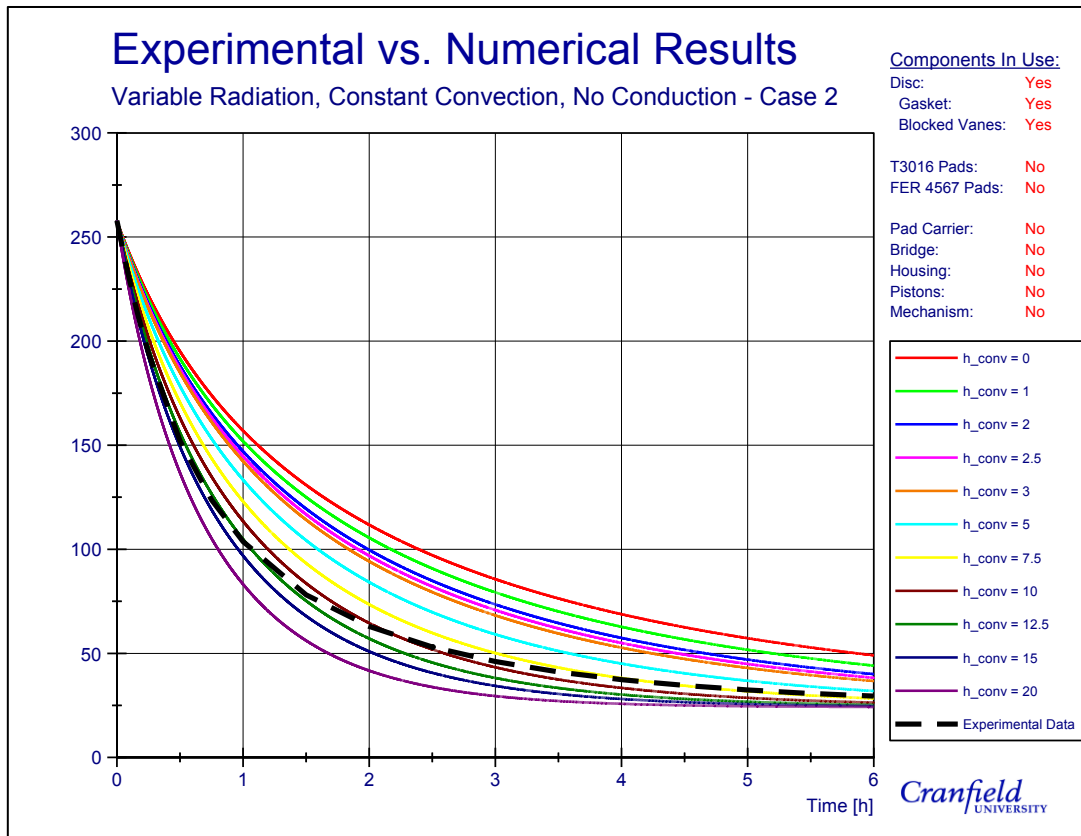


Figure K.3: 1st ODE results for case 2 with variable radiation, bulk temperature drop

Appendix K.2.2 - Improved Cooling Equation

Before pursuing further an ODE with a higher precision output, by allowing more variables to change with temperature, an attempt to derive a cooling equation that would have higher accuracy than the Galindo-Lopez cooling equation was made. The integral form of equation (K.12) would appear at first glance to be solvable via the method of integration factors (Stroud 2001). However, because this method is only applicable for linear, first order equations this cannot be used. Unfortunately, there is no alternative for exactly solving equation (K.12), therefore an attempt to find an approximated solution was conducted instead.

Appendix K.2.2.1 - Asymptotic Assumption

A common technique for determining approximations to ODEs, when it is not possible to achieve an exact analytical solution, is to deploy an asymptotic expansion. Asymptotic expansions are functions that describe the nature of an existing function with increasing accuracy with every term that is added to the expansion. An infinite number of terms are possible in any expansion, increasing the precision of the function. A disadvantage of increasing accuracy though is additional time needed to calculate the function. For this reason, the function is truncated after a desired number of terms, giving the desired level of accuracy whilst remaining solvable within a respectable time period.

The nature of asymptotic expansions are that the first term is close to the actual result, with every higher order term acting as correction functions to the initial prediction. Each correction term has a coefficient, known as a gauge factor, that either tends the coefficient to zero or infinity depending on what type of function is present. In real thermal problems the correction terms adjust the initial temperature towards a real temperature, therefore the coefficients should reduce in size in every term. Equation (K.13) shows a power asymptotic expansion used to estimate the bulk disc temperature with the β function used as the gauge factor. Raising the exponential β value does indeed tend the gauge factor towards zero or is an acceptable expansion to make.

$$T_d = T_{d_0} + \beta T_{d_1} + O(\beta^2) \tag{K.13}$$

Convergence of asymptotic functions is only guaranteed if the power being raised is multiplied by a sufficiently small parameter, such that their product is less than unity. The relative constant of proportionality was the gauge factor in the expansion and has an order of magnitude equal to 10^{-8} . The bulk disc temperature term multiplying the gauge factor from convection (linear) will have an order of magnitude of 10^2 , making the product in the region of 10^{-6} , clearly much smaller than one. However, when considering the nonlinear radiation term, which has an order of magnitude equal to 10^{11} , making the order of the product larger than unity. A working solution is therefore not guaranteed to be achieved. The investigation continued however, as there was still a chance the approximate solution would return reasonable results and because no other known approximation would work for the function derived in equation (K.12).

Considering the expansion in powers of β was used to approximate disc temperature, the expansion was truncated after two terms, making the bulk temperature error proportionate to square of β . Multiplying β^2 by a third temperature, as shown in the error term (equation (K.14)), with a magnitude of 10^{11} will result in a correction term in the order of 10^{-5} . With a

value so small, the β^2 term would alter the predicted temperature by a magnitude of 10 μK , so will have an insignificant impact on the bulk disc temperature. Consequently, truncating the expansion after only two terms is adequate to achieve a high level of accuracy.

$$O(\beta^2) = \beta^2 T_{d_2} \quad (\text{K.14})$$

Using the same logic, the correction term in the order of β will modify the original temperature by a magnitude of 1000 K, when the bulk disc temperature is at 400°C. As a consequence, the resultant approximation equation can only be used when initial temperatures satisfy the inequality shown in equation (K.15).

$$\beta > T_d^4 \quad (\text{K.15})$$

Substituting the asymptotic expansion in equation (K.13) into the 1st ODE yields:

$$\frac{dT_d}{dt} + \gamma \left[h_{conv}(T_{d_0} + \beta T_{d_1}) + \beta(T_{d_0} + \beta T_{d_1})^4 \right] = \gamma(h_{conv}T_\infty + \beta T_\infty^4) \quad (\text{K.16})$$

Expanding the left-hand bracket creates an equation with multiple terms, most of which combine T_{d_0} and T_{d_1} . Unfortunately, it is still impossible to integrate equation (K.17) in its current form as both T_{d_0} and T_{d_1} are functions of dependent variable T_d ; without separation, integration is impossible.

$$\begin{aligned} \frac{dT_d}{dt} + \gamma \left[h_{conv}T_{d_0} + h_{conv}\beta T_{d_1} + \beta T_{d_0}^4 + 4T_{d_0}^3\beta^2 T_{d_1} + 6T_{d_0}^2\beta^3 T_{d_1}^2 \right. \\ \left. + 4T_{d_0}\beta^4 T_{d_1}^3 + \beta^5 T_{d_1}^4 \right] = \gamma(h_{conv}T_\infty + \beta T_\infty^4) \end{aligned} \quad (\text{K.17})$$

Appendix K.2.2.2 - Comparing β Coefficients

It has already been shown that the order of any term including a squared β term would produce a value of little significance to the overall bulk disc temperature. For this reason, equation (K.17) can be reduced to equation (K.18) by removing all terms that include a β^n term, where n is equal to or greater than two.

$$\frac{dT_d}{dt} + \gamma \left[h_{conv}T_{d_0} + h_{conv}\beta T_{d_1} + \beta T_{d_0}^4 \right] = \gamma(h_{conv}T_\infty + \beta T_\infty^4) \quad (\text{K.18})$$

All the mixed terms containing T_{d_0} and T_{d_1} have been removed, making it possible to integrate the function. However, the integration is not straightforward due to the dependencies on T_d . By equating powers of β coefficients, it is possible to remove the issues of dependencies and solve

equation (K.18) (Shivamoggi 2003). Two separate equations will be generated, the first for T_{d_0} and the other for T_{d_1} .

Appendix K.2.2.2.1 - Order 1

Firstly, let all terms multiplying a β coefficient of order one be compared. As only T_{d_0} variables are present, it can replace T_d as the dependent variable. The resultant is equation (K.19):

$$O(1) \quad \frac{dT_{d_0}}{dt} + \gamma h_{conv} T_{d_0} = \gamma h_{conv} T_{\infty} \quad (K.19)$$

The above equation is a linear equation that can be integrated using the method of integrating factors (Stroud 2001). This method can be used when a linear equation taking the form shown in (K.20a), where both G and H are constants. Its solution is achieved by completing the integral in (K.20b).

$$\frac{dT_d}{dt} + GT_d = H \quad (K.20a)$$

$$T_d IF = \int H \cdot IF dt \quad (K.20b)$$

The integrating factor, IF , is found by integrating the exponent (the G constant) of the exponential function with respect to the independent variable;.

$$IF = e^{\int G dt} = e^{\int \gamma h_{conv} dt} = e^{\gamma h_{conv} t} \quad (K.21)$$

Having determined the IF , it is possible to solve equation (K.20a) by substituting equation (K.21) into it.

$$\begin{aligned} T_{d_0} e^{\gamma h_{conv} t} &= \int \gamma h_{conv} T_{\infty} e^{\gamma h_{conv} t} dt \\ T_{d_0} e^{\gamma h_{conv} t} &= T_{\infty} e^{\gamma h_{conv} t} + K_1 \\ T_{d_0} &= T_{\infty} + K_1 e^{-\gamma h_{conv} t} \end{aligned} \quad (K.22)$$

K_1 is the constant of integration that requires determining from boundary conditions. By using the experimental data for a bulk disc temperature at a time equal to zero for the initial boundary condition, it can be found that K_1 has the value of 233.7. Making the final equation for T_{d_0} :

$$T_{d_0} = T_{\infty} + 233.7e^{-\gamma h_{conv}t} \quad (K.23)$$

To confirm equation (K.23) produces results of the correct format, a few simple checks were completed. Firstly, the equation should describe disc brake cooling over time. Inspection confirms that as time increases, the negative power of e will ensure the disc brake temperature will always decay. Secondly, the presence of the constant ambient temperature term guarantees that for any time value put into the equation (K.23), the disc brake temperature can never fall below the ambient temperature. Resultantly, the equation conforms to the first law of thermodynamics.

With a reliable first approximation term equation completed, temperatures recorded at the end of the cooling phase were used to calculate an initial estimate of 13,67 W/m²K value for h_{conv} over the entire cooling phase. Based on work previously completed, a value of 13.67 W/m²K appears much more realistic than previous estimates as the this values falls in the region of 7.5 to 15 W/m²K suggested by the numerical analysis. Evidence supports a conclusion that the improved cooling equation generates better estimates of convective HTC's than the original Galindo-Lopez equation does.

Appendix K.2.2.2.2 - Order β

By repeating the previous method but for β coefficients of order β , a correction factor to the initial estimation could be made. On this occasion, the dependent variable is now replaced with T_{d_1} . The comparison leaves:

$$O(\beta) \quad \frac{dT_{d_1}}{dt} + \gamma h_{conv}T_{d_1} + \gamma T_{d_0}^4 = \gamma T_{\infty}^4 \quad (K.24)$$

Having already derived an equation for T_{d_0} , the fact that there are two separate dependent temperature variables in equation (K.24) does not cause concern. Substitution of equation (K.22) into it, formed an equation with only a single temperature dependent variable. Subsequently, the correction term equation was also linear in T_{d_1} , meaning the integration factors method could once again be used. Equation (K.25) shows linear equation with initial predictor equation substituted in and the right-hand bracket expanded.

$$\begin{aligned}
 \frac{dT_{d_1}}{dt} + \gamma h_{conv} T_{d_1} + \gamma \beta (T_{\infty} + K_1 e^{-\gamma h_{conv} t})^4 &= \gamma \beta T_{\infty}^4 \\
 \frac{dT_{d_1}}{dt} + \gamma h_{conv} \beta T_{d_1} &= \gamma \beta T_{\infty}^4 - \gamma \beta (T_{\infty} + K_1 e^{-\gamma h_{conv} t})^4 \\
 \frac{dT_{d_1}}{dt} + \gamma h_{conv} T_{d_1} &= \gamma T_{\infty}^4 - \gamma T_{\infty}^4 - 4\gamma T_{\infty}^3 K_1 e^{-\gamma h_{conv} t} \\
 &\quad - 6\gamma T_{\infty}^2 K_1^2 e^{-2\gamma h_{conv} t} - 4\gamma T_{\infty} K_1^3 e^{-3\gamma h_{conv} t} \\
 &\quad - \gamma K_1^4 e^{-4\gamma h_{conv} t}
 \end{aligned} \tag{K.25}$$

Inspection of equation (K.25) will reveal that the G coefficient is identical to that found in the equation for the order of β equal to 1. The solvable integral was therefore:

$$\begin{aligned}
 T_{d_1} e^{\gamma h_{conv} t} &= \int (-4\gamma T_{\infty}^3 K_1 e^{-\gamma h_{conv} t} - 6\gamma T_{\infty}^2 K_1^2 e^{-2\gamma h_{conv} t} \\
 &\quad - 4\gamma T_{\infty} K_1^3 e^{-3\gamma h_{conv} t} - \gamma K_1^4 e^{-4\gamma h_{conv} t}) e^{\gamma h_{conv} t} dt
 \end{aligned} \tag{K.26}$$

To integrate the above equation separation of the variables was required. Multiplying out the bracket provided four separate terms which could be integrated simply.

$$\begin{aligned}
 T_{d_1} e^{\gamma h_{conv} t} &= - \int 4\gamma T_{\infty}^3 K_1 dt - \int 6\gamma T_{\infty}^2 K_1^2 e^{-\gamma h_{conv} t} dt \\
 &\quad - \int 4\gamma T_{\infty} K_1^3 e^{-2\gamma h_{conv} t} dt - \int \gamma K_1^4 e^{-3\gamma h_{conv} t} dt
 \end{aligned} \tag{K.27}$$

Conducting the integration gives:

$$\begin{aligned}
 T_{d_1} e^{\gamma h_{conv} t} &= -4\gamma T_{\infty}^3 K_1 t + \frac{6T_{\infty}^2 K_1^2}{h_{conv}} e^{-\gamma h_{conv} t} + \frac{2T_{\infty} K_1^3}{h_{conv}} e^{-2\gamma h_{conv} t} \\
 &\quad + \frac{K_1^4}{3h_{conv}} e^{-3\gamma h_{conv} t} + K_2
 \end{aligned} \tag{K.28}$$

Finally, dividing all terms by the IF left equation (K.29), an expression for the T_{d_1} .

$$\begin{aligned}
 T_{d_1} &= -4\gamma T_{\infty}^3 K_1 t e^{-\gamma h_{conv} t} + \frac{6T_{\infty}^2 K_1^2}{h_{conv}} e^{-2\gamma h_{conv} t} + \frac{2T_{\infty} K_1^3}{h_{conv}} e^{-3\gamma h_{conv} t} \\
 &\quad - \frac{K_1^4}{3h_{conv}} e^{-4\gamma h_{conv} t} + K_2 e^{-\gamma h_{conv} t}
 \end{aligned} \tag{K.29}$$

As described in equation (K.13), the bulk temperature approximation can be calculated by a simple summation. An improved cooling equation that now includes the effects of varying radiation, was found by substituting both equations (K.22) and (K.29) into equation (K.13). The final cooling equation derived for the second case is:

$$\begin{aligned}
 T_d = T_\infty + K_1 e^{-\gamma h_{conv} t} - 4\beta\gamma T_\infty^3 K_1 t e^{-\gamma h_{conv} t} + \frac{6\beta T_\infty^2 K_1^2}{h_{conv}} e^{-2\gamma h_{conv} t} \\
 + \frac{2\beta T_\infty K_1^3}{h_{conv}} e^{-3\gamma h_{conv} t} - \frac{\beta K_1^4}{3h_{conv}} e^{-4\gamma h_{conv} t} + \beta K_2 e^{-\gamma h_{conv} t}
 \end{aligned} \tag{K.30}$$

Appendix L - Temperature Dependent Air Properties

Air properties values were taken from Necati Özisik (1985). Characteristic property changes with temperatures were generated from these graphs and used in the MatLab formulae during the analytical dimensionless number investigations.

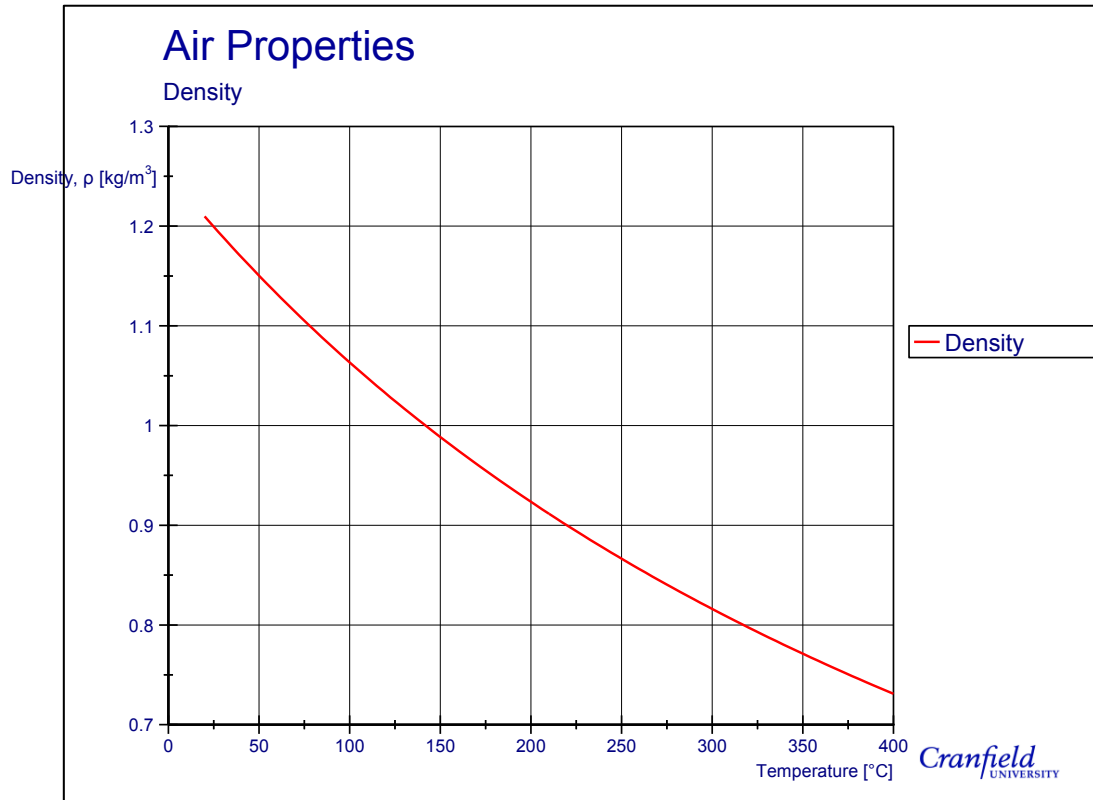


Figure L.1: Change in density with temperature change

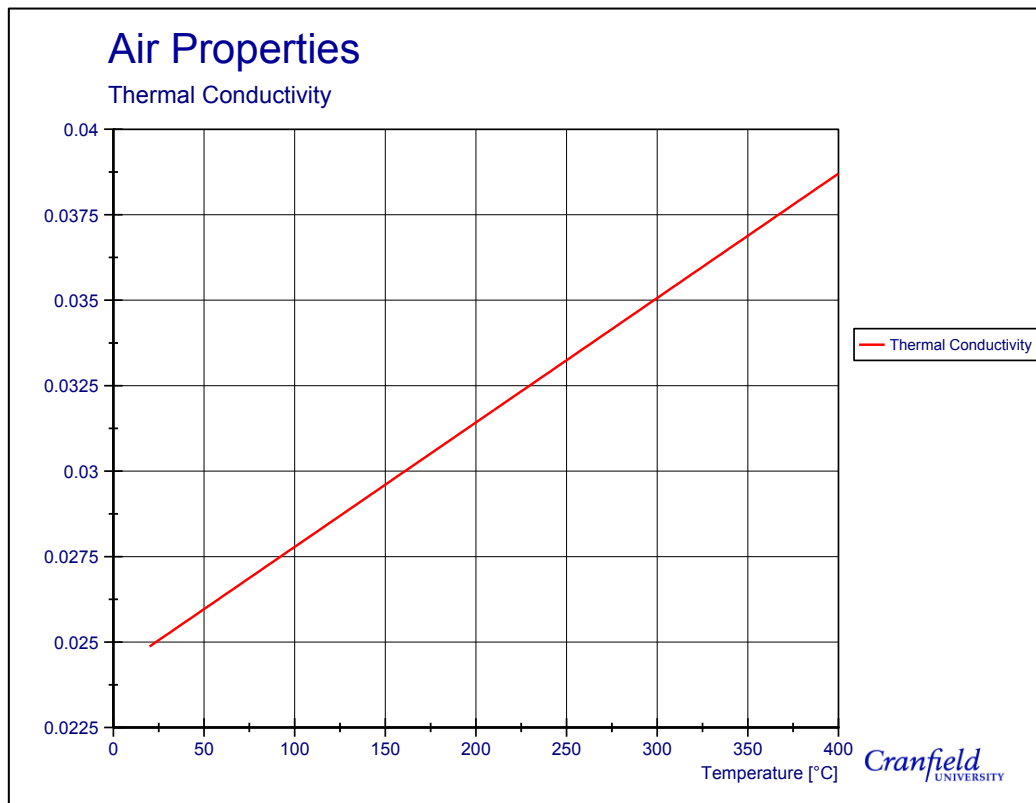


Figure L.2: Change in thermal conductivity with temperature change

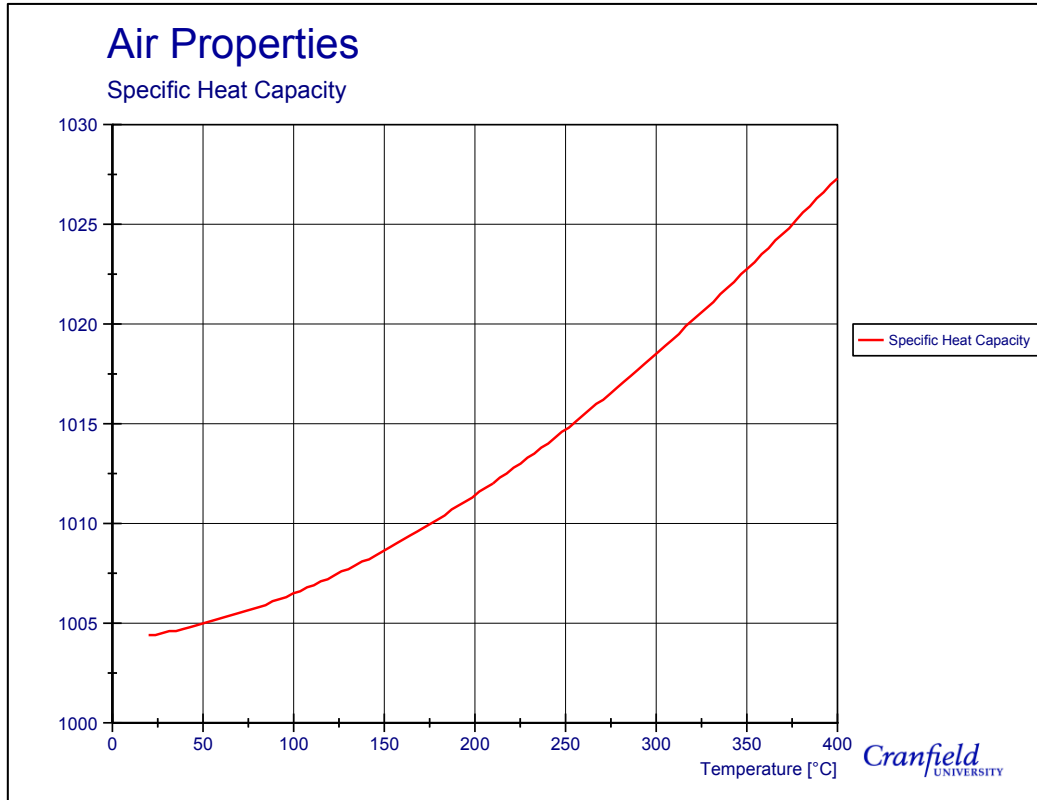


Figure L.3: Change in specific heat capacity with temperature change

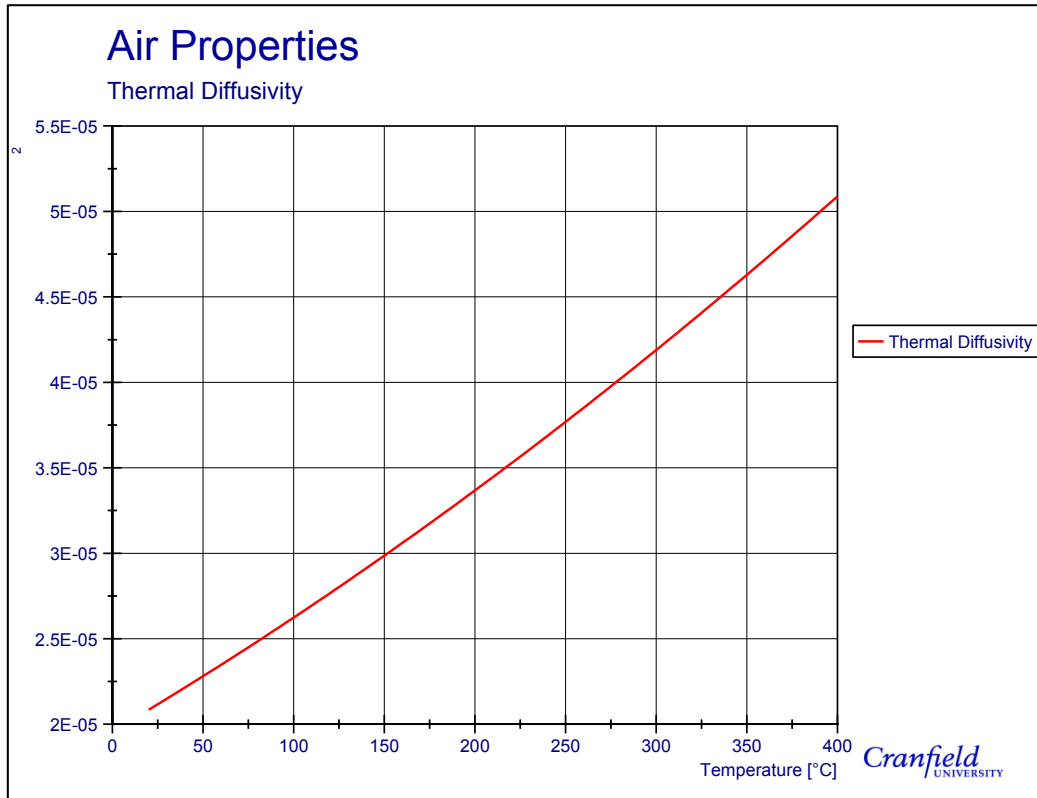


Figure L.4: Change in thermal diffusivity with temperature change

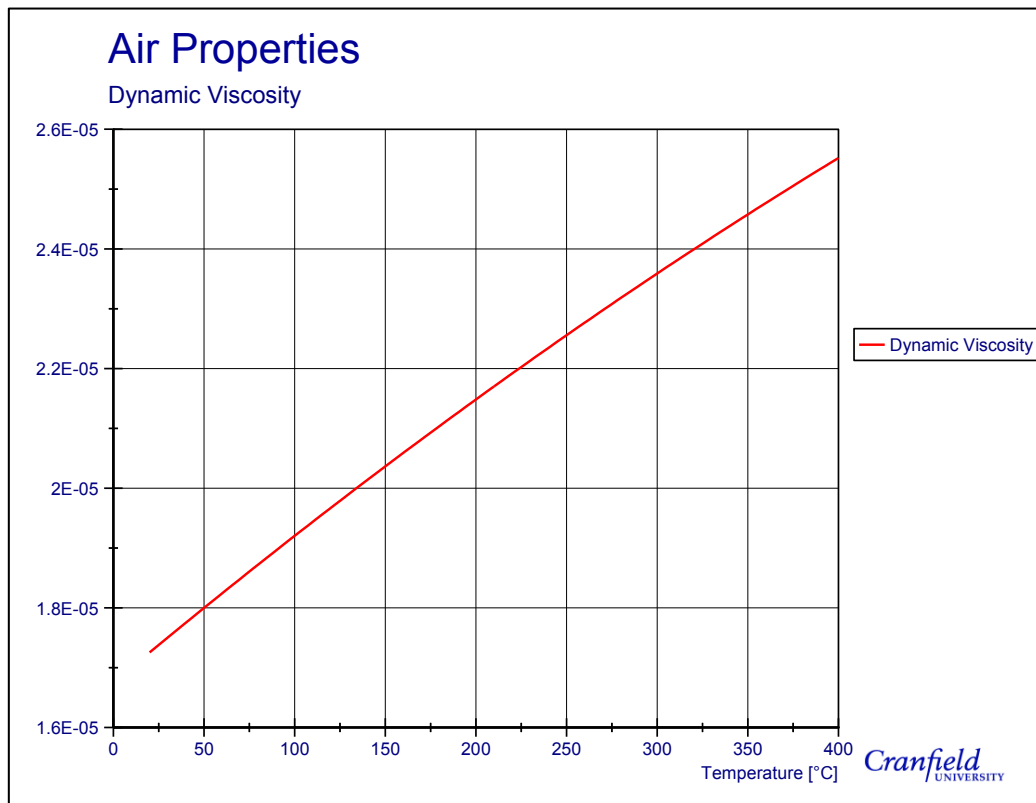


Figure L.5: Change in dynamic viscosity with temperature change

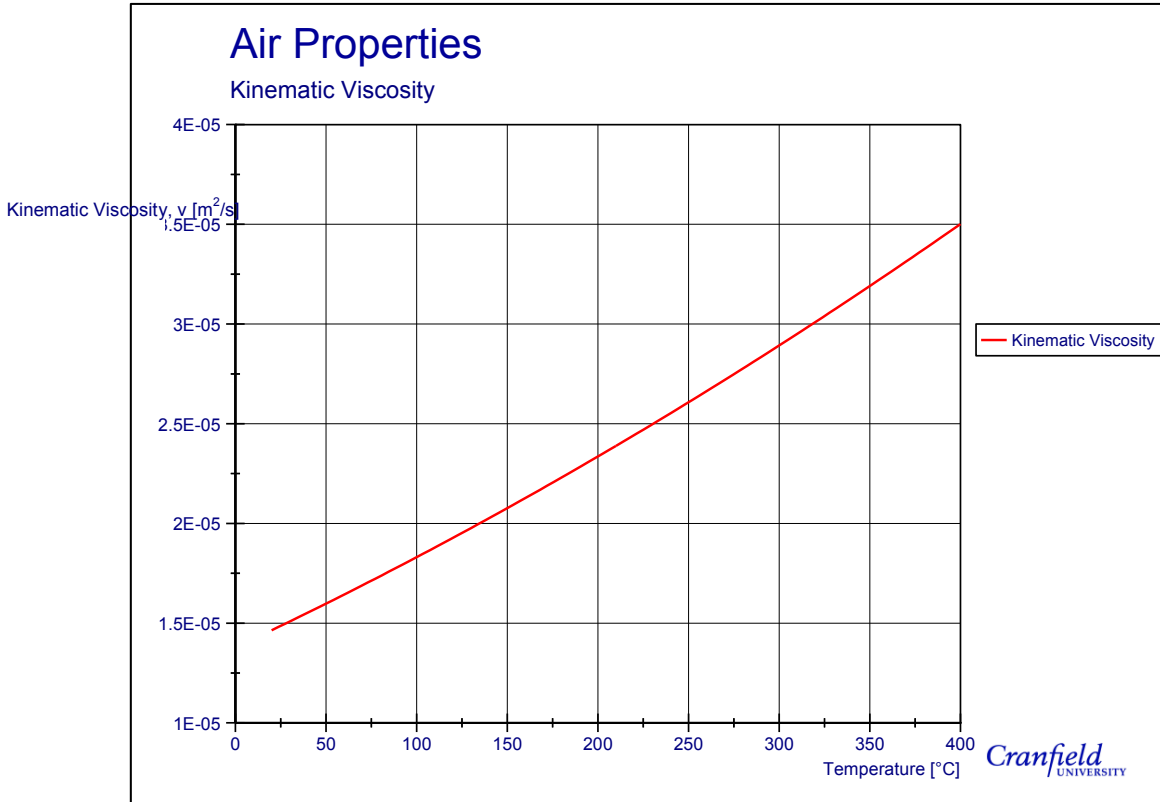


Figure L.6: Change in kinematic viscosity with temperature change

Appendix M - Contact Pressure

With an accurate thermal FE model, understanding some fundamental mechanical properties will enable a sequentially coupled thermomechanical model to be fabricated. The most important mechanical interaction for any braking scenario is the interaction between the disc brake and pads. A retarding friction force is generated here, generating heat energy into the system. Real contact area, as defined by Qi and Day (2007), is the ratio actual contact between the disc brake and pad, to the brake pad surface area. The lower the real contact area, the more heat is pushed into the brake pad locally (total energy remains constant) causing extremely high surface temperatures. Reduced contact also causes the area of friction generation to decrease, which ultimately increases the local torque applied.

Pressure distribution between the brake pads and the disc brake has been studied numerous times, for example Vianello (2011). Physical measurements are usually taken by pressure sensitive paper, which is then converted to a digital image. Once in digital form, the image can have calculations made on it to produce numerical estimations for the pressure and localised force magnitudes. This process was used to find the pressure distribution between the disc brake and both the FER 4567 and T3016 brake pads when a 6 bar pneumatic pressure is applied to the service chamber.

Figure M.1 shows a scanned copy of the raw image created from the pressure paper when the FER 4567 friction material was pressed against the disc brake. Many imperfections are present on paper, for example all the edging has a deeper red from where it was cut to size. To turn the scanned picture into calculated pressure distributions, a MatLab program was written (see Appendix N). The basis of how the program works is that the scanned colour image was converted into a black and white image using the inbuilt `rgb2gray` MatLab functions. Calculations are based on the intensity of the black levels of the image. By having the imperfections still in the picture during calculations, areas of black will be picked up, showing contact where there is none. Each image was therefore prepared before being put into the MatLab program to remove darkened areas. Figure M.2 shows the prepared image of raw pressure paper scan in Figure M.1.

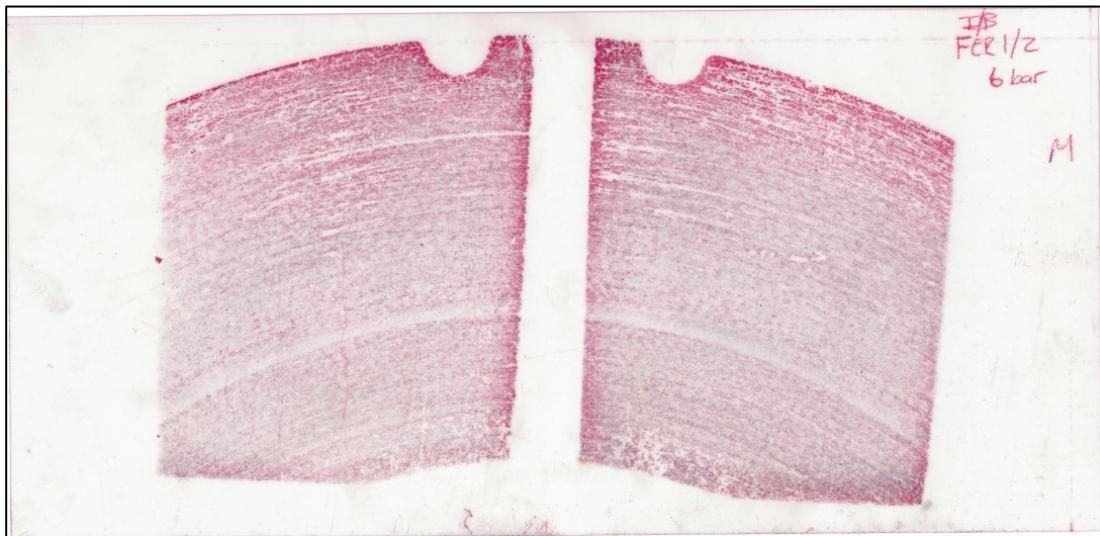


Figure M.1: Pressure distribution paper before editing

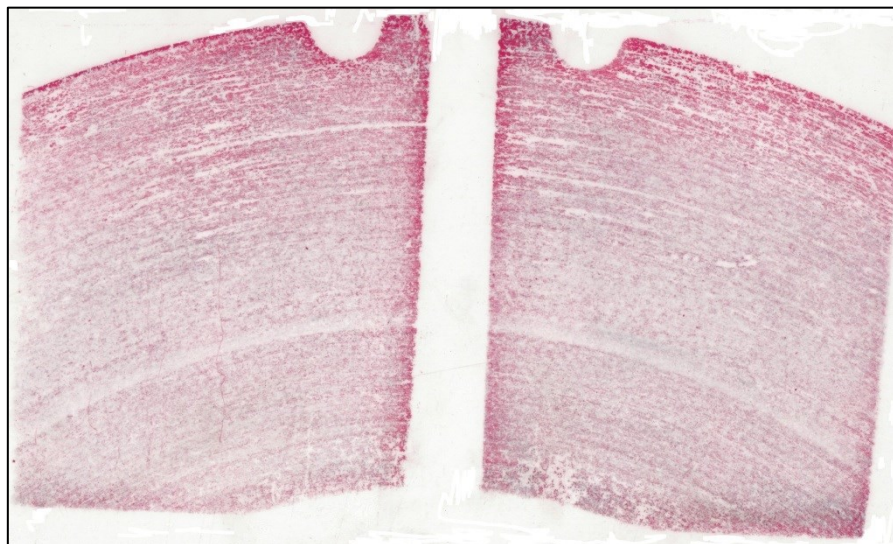


Figure M.2: Pressure distribution paper edited and ready for analysis

Pressure paper comes in a variety of predefined pressure ranges. The Medium paper was used for the 6 bar pneumatic pressure tests, which has a range of 350 to 1400 bar. For each range of pressure paper, the intensity of the red colouring had a slightly different scale. This was important when setting up the MatLab program as the intensity level seen on the paper was required for calculation purposes. Likewise was the humidity of the room when the test was carried out. Different humidity levels will impact on the light intensity generated on the pressure paper. A value of 70% humidity was taken for all tests due to having no instrumentation available at the time of testing to take the reading.

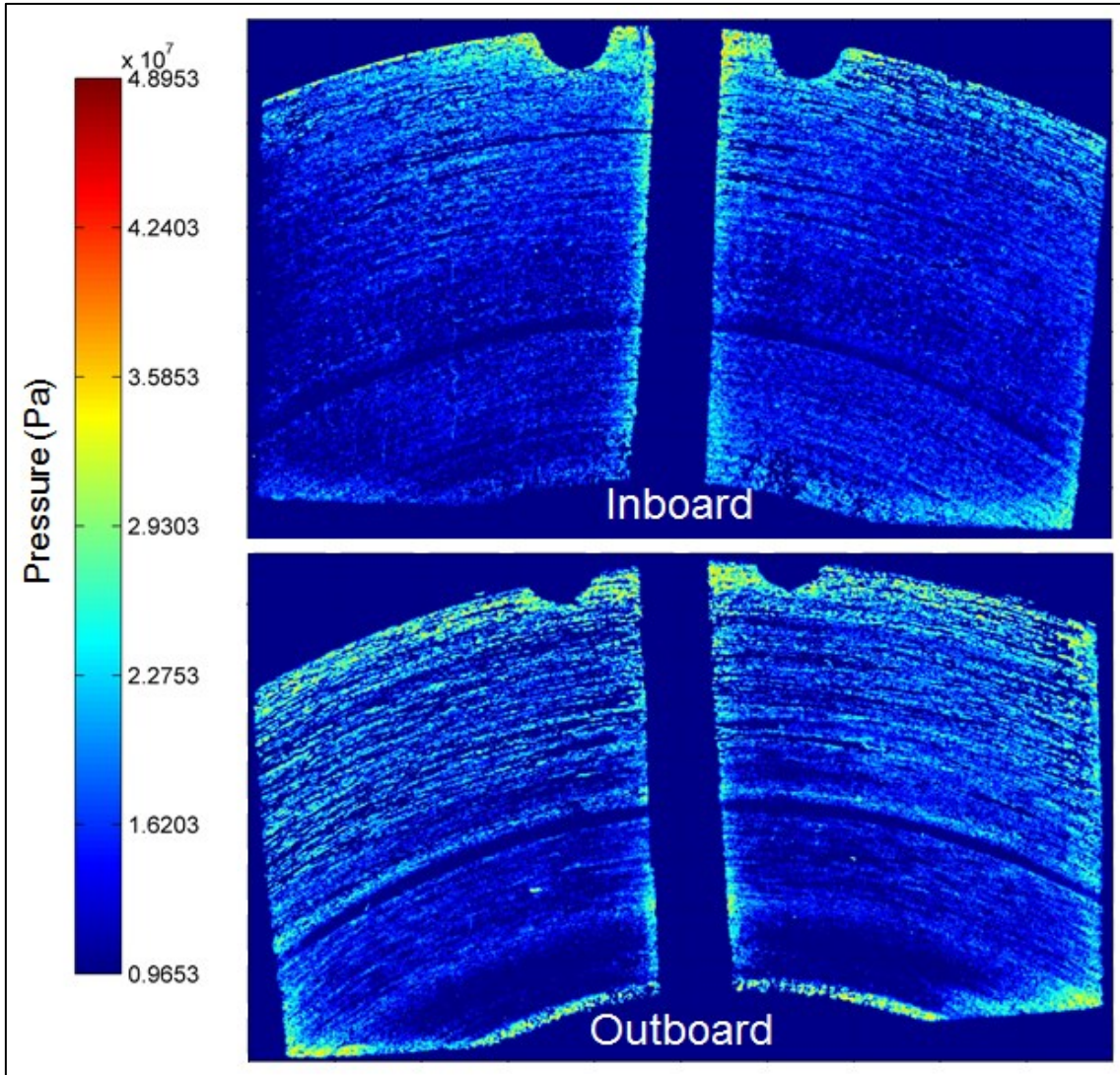


Figure M.3: Pressure distribution pattern between the FER 4567 friction material brake pads and the disc brake, subjected to 6 bar pneumatic actuating pressure

The output from the derived MatLab program can be seen in Figure M.3 for the FER 4567 friction material, whilst subjected 6 bar pneumatic actuating pressure.

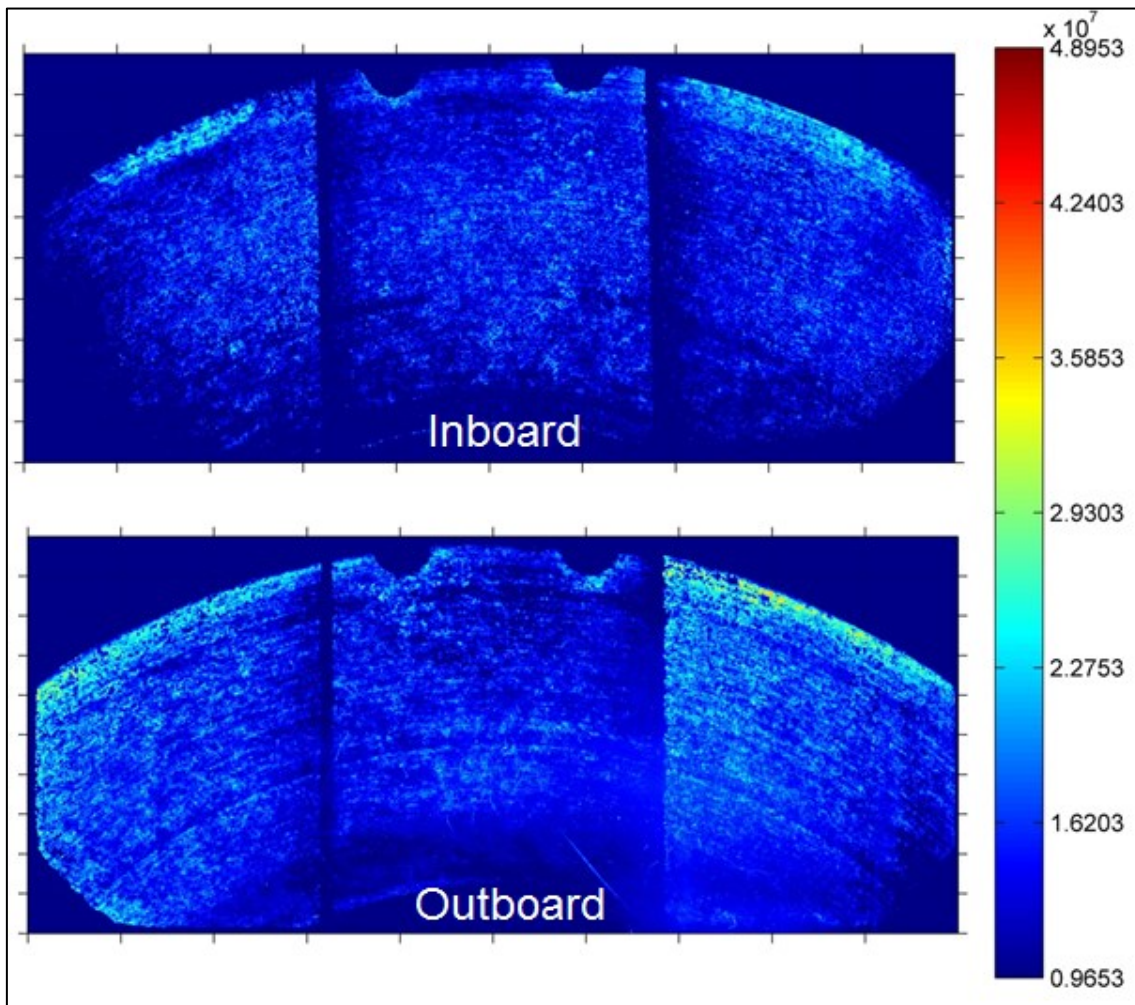


Figure M.4: Pressure distribution pattern between the T3016 friction material brake pads and the disc brake, subjected to 6 bar pneumatic actuating pressure

Appendix N - MatLab Program

```

clear all
format long
format loose

%%%%% Select Variables
Pad_Type=0; %FER4567 = 0, T3016 = 1

%%%%% Controlable variables
White_Set = 220; % make is 255,
Max_Density = double(1.4); % Max density of the PressureX paper - judgement call.
m=10;
n=10;
Conv = 6894.75728; %Conversion rate from 1 PSI to Pa
Pmin_PSI = 1400; %Minimum pressure paper rating
Pmax_PSI_set = 7100;
P_Range_PSI=Pmax_PSI_set-Pmin_PSI;
Pmin_Pa = Pmin_PSI*Conv;
Pmax_Pa_set = Pmax_PSI_set*Conv;
Pixel_Area = (0.210/2481)*(0.296/3481); % Area of 1 pixel ---- Did a simple test to see how many pixels
were scanned in from a piece of A4 paper
P_Range_Pa=Pmax_Pa_set-Pmin_Pa;

% if Pad_Type==0
% Pad='FER 4567';
% else
% Pad='T3016';
% end

Pad_Area_FER4567=14764*0.000001; %Actual pad area in square meters
Pad_Area_T3016=20989*0.000001; %Actual pad area in square meters

if Pad_Type==0
    Pad_Area_Ideal=Pad_Area_FER4567;
else
    Pad_Area_Ideal=Pad_Area_T3016;
end

% Read Image
I1 = imread('Image001 - Cropped and edited.jpg');
figure(1)
imshow(I1); % Display Image

% Convert colour image to grayscale
I2 = rgb2gray(I1);

% Make light whites actually white
a=size(I2);
for j=1:a(1,1)
    for i=1:a(1,2)
        if I2(j,i)>=White_Set
            I2(j,i)=255;
        else

```

```

    I2(j,i)=I2(j,i);
end
end
end
figure(2)
imshow(I2); % Display Image
set(gca, 'visible', 'on', 'XGrid', 'on', 'YGrid', 'on');
set(gca, 'XTick', 0:(a(1,2)/m):a(1,2), 'XTickLabel', []) % etc.
set(gca, 'YTick', 0:(a(1,1)/n):a(1,1), 'YTickLabel', []) % etc.

% Invert Image
I3 = 255-I2;

% Increase picture matrix size
XY = size(I3);
X = XY(1,2);
Y = XY(1,1);

Xx=X/10;
xx=ceil(Xx); % rounds up to the next integer
Yy=Y/10;
yy=ceil(Yy);
I3((yy*n),(xx*n))=0;

Max_Black = double(max(max(I3))); %Finds the maximum black value for percentage

for j=1:yy*n
    for i=1:xx*m
        r=double(I3(j,i));
        R=double(r*Max_Density/Max_Black); %Puts black into a percentage of paper density
        I3a(j,i)=R; %Matrix of colour densities

        B=double(I3a(j,i)); %Extracts density figure
        S=(2901.5*B*B*B)-(5608.6*B*B)+(8274.2*B); %from excel y = 2901.5x3 - 5608.6x2 + 8274.2x ----
        - R2 = 0.9982
        I3_PSI(j,i)=S; % Matrix of pressures in PSI
        T=S*Conv; % Convert Pressure to Pa from PSI
        I3_Pa(j,i)=T; % Matrix of pressures in Pa
    end
end

% Apply two-dimensional Gaussian filter
x = 2;
y = 2;
h = fspecial('gaussian',x,y); I4_PSI=imfilter(I3_PSI,h); % Increase x, y values for reducing detail
Pmax_PSI=max(max(I4_PSI));
h = fspecial('gaussian',x,y); I4_Pa=imfilter(I3_Pa,h); % Increase x, y values for reducing detail
Pmax_Pa=max(max(I4_Pa));

% %Calculate maximum pressure
% max_pressure_PSI = double(max(max(I4_PSI)));
% max_pressure_Pa = double(max(max(I4_Pa)));

for j=1:yy*n
    for i=1:xx*m

```

```

if I4_PSI(j,i)<=Pmin_PSI
    I5_PSI(j,i)=0;
else
    I5_PSI(j,i)=I4_PSI(j,i);
end
if I4_Pa(j,i)<=Pmin_Pa
    I5_Pa(j,i)=0;
else
    I5_Pa(j,i)=I4_Pa(j,i);
end

end
end

% Create Quadrants
for j=1:n
    for i=1:m
        x=xx*i;
        y=x-xx+1;
        z=x-y+1;

        XX = I5_PSI((((j-1)*yy)+1):(j*yy),(((i-1)*xx)+1):(i*xx));
        C = find(XX); %Returns the number of 0 values in matrix
        A = sum(sum(XX));
        D = size(C);
        Pixel_Count = D(1,1);
        if Pixel_Count==0
            Pixel_Count_plus_one=1;
            Value_PSI = A/Pixel_Count_plus_one;
        else
            Pixel_Count_plus_none = Pixel_Count;
            Value_PSI = A/Pixel_Count_plus_none;
        end
        Matrix_PSI(j,i)= Value_PSI;
        Pixel_Matrix(j,i)=Pixel_Count;

        XX = I5_Pa((((j-1)*yy)+1):(j*yy),(((i-1)*xx)+1):(i*xx));
        C = find(XX);
        A = sum(sum(XX));
        D = size(C);
        Pixel_Count = D(1,1);
        if Pixel_Count==0
            Pixel_Count_plus_one=1;
            Value_Pa = A/Pixel_Count_plus_one;
        else
            Pixel_Count_plus_none = Pixel_Count;
            Value_Pa = A/Pixel_Count_plus_none;
        end
        Matrix_Pa(j,i)= Value_Pa;
        ForceMatrix_N(j,i)=Value_Pa*Pixel_Count*Pixel_Area;
        Surface_Area_Actual(j,i) = Pixel_Area*Pixel_Matrix(j,i);

    end
end
end

```

```
Matrix_PSI; % m x n matrix of average pressure distribution
Pixel_Matrix; % No of pixels which have a value directly relating to the amount of surface contact
Surface_Area_Actual;
%% Calculate Mean %%%
Mean_PSI=sum(sum(I5_PSI))/sum(sum(Pixel_Matrix))
Mean_Pa=sum(sum(I5_Pa))/sum(sum(Pixel_Matrix))

%% Calculate Standard Deviation %%%
for j=1:(yy*n)
    for i=1:(xx*m)
        X=double(I5_PSI(j,i));
        Y=double(Mean_PSI);
        if I5_PSI(j,i)==0
            I6_PSI(j,i)=0;
        else
            I6_PSI(j,i)=double((X-Y)^2);
        end
        X=double(I5_Pa(j,i));
        Y=double(Mean_Pa);
        if I5_Pa(j,i)==0
            I6_Pa(j,i)=0;
        else
            I6_Pa(j,i)=double((X-Y)^2);
        end
    end
end
Q=sum(sum(I6_PSI));
W=find(I6_PSI);
Z=size(W);
Standard_Dev_PSI=sqrt(Q/Z(1,1));

Q=sum(sum(I6_Pa));
W=find(I6_Pa);
Z=size(W);
Standard_Dev_Pa=sqrt(Q/Z(1,1));

%Calculate Force - Full Matrix
A=find(I6_Pa);
B=size(A);
C=max(B);
D=double(Pixel_Area);
Contact_Area_Actual=C*D; %square meters
for j=1:(yy*n)
    for i=1:(xx*m)
        E=double(I5_Pa(j,i));
        Force_N_Actual(j,i)=E*Contact_Area_Actual;
        Force_N_Ideal(j,i)=E*Pad_Area_Ideal;
    end
end
Force_N_Actual;
Force_N_Ideal;
Fmax=max(max(Force_N_Actual));
Fmin=min(min(Force_N_Actual));

%% Export to excel
```



```

xlswrite('Pressure Distribution.xlsx', I5_PSI, 'PSI Full', 'B2');
xlswrite('Pressure Distribution.xlsx', I5_Pa, 'Pa Full', 'B2');
xlswrite('Pressure Distribution.xlsx', Matrix_PSI, 'PSI 10x10', 'B2');
xlswrite('Pressure Distribution.xlsx', Matrix_Pa, 'Pa 10x10', 'B2');
xlswrite('Pressure Distribution.xlsx', Force_N_Actual, 'N Act Force Full', 'B2');
xlswrite('Pressure Distribution.xlsx', Force_N_Ideal, 'N Ide Force Full', 'B2');
xlswrite('Pressure Distribution.xlsx', ForceMatrix_N, 'N Act Force 10x10', 'B2');

```

```

xlswrite('Pressure Distribution.xlsx', Mean_PSI, 'Stats', 'B2');
xlswrite('Pressure Distribution.xlsx', Mean_Pa, 'Stats', 'C2');
xlswrite('Pressure Distribution.xlsx', Mean_Pa, 'Stats', 'B3');
xlswrite('Pressure Distribution.xlsx', Mean_Pa, 'Stats', 'C3');
xlswrite('Pressure Distribution.xlsx', StDev_PSI, 'Stats', 'B4');
xlswrite('Pressure Distribution.xlsx', Standard_Dev_PSI, 'Stats', 'C4');
xlswrite('Pressure Distribution.xlsx', StDev_Pa, 'Stats', 'B5');
xlswrite('Pressure Distribution.xlsx', Standard_Dev_Pa, 'Stats', 'C5');
xlswrite('Pressure Distribution.xlsx', Actual_Contact_Area, 'Stats', 'B6');
xlswrite('Pressure Distribution.xlsx', Contact_Area_Actual, 'Stats', 'C6');
xlswrite('Pressure Distribution.xlsx', Ideal_Contact_Area, 'Stats', 'B7');
xlswrite('Pressure Distribution.xlsx', Pad_Area_Ideal, 'Stats', 'C7');

```

```

%%%%%%%%%%%%%%%%%% Just for pictures %%%%%%%%%%%%%

```

```

for j=1:yy*n
    for i=1:xx*m
        if I5_PSI(j,i)==0
            I9_PSI(j,i)=Pmin_PSI;
        else
            I9_PSI(j,i)=I4_PSI(j,i);
        end
        if I5_Pa(j,i)==0
            I9_Pa(j,i)=Pmin_Pa;
        else
            I9_Pa(j,i)=I5_Pa(j,i);
        end
    end
end
end

```

```

figure(3), imshow((abs(I9_PSI)),[]), colormap(jet(128)), colorbar % Apply 128-level colormap
title('Pressure Distribution - PSI', 'FontWeight','bold')
set(gca, 'visible', 'on', 'XGrid', 'on', 'YGrid', 'on');
set(gca, 'XTick', 0:xx:(xx*m), 'XTickLabel', []) % etc.
set(gca, 'YTick', 0:yy:(yy*n), 'YTickLabel', []) % etc.
colorbar('Ylim', [Pmin_PSI Pmax_PSI], 'YTick', Pmin_PSI:(Pmax_PSI-Pmin_PSI)/6):Pmax_PSI)
p = figure(3);
print(p, '-r600', '-djpeg', 'Pressure Distribution - PSI.jpeg')

```

```

figure(4), imshow((abs(I9_Pa)),[]), colormap(jet(128)), colorbar % Apply 128-level colormap
title('Pressure Distribution - Pa', 'FontWeight','bold')
set(gca, 'visible', 'on', 'XGrid', 'on', 'YGrid', 'on');
set(gca, 'XTick', 0:xx:(xx*m), 'XTickLabel', []) % etc.
set(gca, 'YTick', 0:yy:(yy*n), 'YTickLabel', []) % etc.
colorbar('Ylim', [Pmin_Pa Pmax_Pa], 'YTick', Pmin_Pa:(Pmax_Pa-Pmin_Pa)/6):Pmax_Pa)
p = figure(4);

```

```

print(p, '-r600', '-djpeg', 'Pressure Distribution - Pa.jpeg')

figure(5), imshow((abs(Force_N_Actual)),[]), colormap(jet(128)), colorbar % Apply 128-level colormap
title('Force Distribution - Actual (N)', 'FontWeight','bold')
set(gca, 'visible', 'on', 'XGrid', 'on', 'YGrid', 'on');
set(gca, 'XTick', 0:xx:(xx*m), 'XTickLabel', []) % etc.
set(gca, 'YTick', 0:yy:(yy*n), 'YTickLabel', []) % etc.
colorbar('Ylim', [Fmin Fmax], 'YTick', Fmin:((Fmax-Fmin)/6):Fmax)
p = figure(5);
print(p, '-r600', '-djpeg', 'Force Distribution - N.jpeg')

figure(6), imshow((abs(Force_N_Ideal)),[]), colormap(jet(128)), colorbar % Apply 128-level colormap
title('Force Distribution - Ideal (N)', 'FontWeight','bold')
set(gca, 'visible', 'on', 'XGrid', 'on', 'YGrid', 'on');
set(gca, 'XTick', 0:xx:(xx*m), 'XTickLabel', []) % etc.
set(gca, 'YTick', 0:yy:(yy*n), 'YTickLabel', []) % etc.
colorbar('Ylim', [Fmin Fmax], 'YTick', Fmin:((Fmax-Fmin)/6):Fmax)
p = figure(6);
print(p, '-r600', '-djpeg', 'Force Distribution - N.jpeg')

%%%%%%%%%%%%%%%%%%%%%%%%%%%%%%%%%%%%%%%%%%%%%%%%%%%%%%%%%%%%%%%%%%%%%%%%
%%%%%%%%%%%%%%%%%%%%%%%%%%%%%%%%%%%%%%%%%%%%%%%%%%%%%%%%%%%%%%%%%%%%%%%%
I9_PSI(1,1)=Pmax_PSI_set;
I9_Pa(1,1)=Pmax_PSI_set*Conv;

for j=1:yy*n
    for i=1:xx*n
        if I9_PSI(j,i)>=Pmax_PSI_set
            I9_PSI(j,i)=Pmax_PSI_set;
        else
            I9_PSI(j,i)=I9_PSI(j,i);
        end

        if I9_Pa(j,i)>=Pmax_Pa_set
            I9_Pa(j,i)=Pmax_Pa_set;
        else
            I9_Pa(j,i)=I9_Pa(j,i);
        end
    end
end

figure(7), imshow((abs(I9_PSI)),[]), colormap(jet(128)), colorbar % Apply 128-level colormap
title('Pressure Distribution - PSI', 'FontWeight','bold')
set(gca, 'visible', 'on', 'XGrid', 'on', 'YGrid', 'on');
set(gca, 'XTick', 0:xx:(xx*m), 'XTickLabel', []) % etc.
set(gca, 'YTick', 0:yy:(yy*n), 'YTickLabel', []) % etc.
colorbar('Ylim', [Pmin_PSI Pmax_PSI_set], 'YTick', Pmin_PSI:(P_Range_PSI/6):Pmax_PSI_set)
p = figure(7);
print(p, '-r600', '-djpeg', 'Pressure Distribution - PSI - Scaled.jpeg')

figure(8), imshow((abs(I9_Pa)),[]), colormap(jet(128)), colorbar % Apply 128-level colormap
title('Pressure Distribution - Pa', 'FontWeight','bold')
set(gca, 'visible', 'on', 'XGrid', 'on', 'YGrid', 'on');
set(gca, 'XTick', 0:xx:(xx*m), 'XTickLabel', []) % etc.

```

```
set(gca, 'YTick', 0:yy:(yy*n), 'YTickLabel', []) % etc.  
colorbar('Ylim', [Pmin_Pa Pmax_Pa_set], 'YTick', Pmin_Pa:(P_Range_Pa/6):Pmax_Pa_set)  
p = figure(8);  
print(p, '-r600', '-djpeg', 'Pressure Distribution - Pa - Scaled.jpeg')
```

References

- ABAQUS User's Manual (2004) 'ABAQUS User's Manual, Version 6.5.
- Abbas, S. A., Cubitt, N. J. and Hooke, C. J. (1969) 'Temperature Distributions in Disc Brakes', *Proceedings of the Institution of Mechanical Engineers*, 184, 185-194.
- Abdul, R. 'AMD vs Intel - Market Share and Revenue Comparative Study', [online], Available: www.robabdul.com/amd-vs-intel-market-share-revenue.asp [Accessed 07/12/2011].
- Abu Bakar, A. R., Ouyang, H. and Siegel, J. E. (2005) 'Brake Pad Surface Topography Part I: Contact Pressure Distribution', *SAE Technical Paper 2005-01-3941*.
- Adloff, L. (2007) *Experimental and Theoretical Investigation on Heating and Cooling Properties of a Pillared Brake Disc*, Thesis, Cranfield University.
- Albaum, G. (1997) 'The Likert scale revisited', *Journal of the Market Research Society*, 39(2), 331-348.
- Allen, J. E. (1982) *Aerodynamics The Science of air in motion*, Second Edition, McGraw-Hill.
- Amin, A. M., Seri, S. M. and Raghavan, V. R. (2007) 'Study of the Temperature Distribution in Disc Brakes by the Method of Order of Magnitude Analysis', in *al., A. Z. e., Edition Regional Conference on Engineering Mathematics, Mechanics, Manufacturing & Architecture*, 202-211.
- Anderson, J. D. (2007) *Fundamentals of Aerodynamics*, Fourth Edition, McGraw-Hill.
- Angelinas, S. (2009) *Analysis and Improvement of Brake Disc Cooling using Computational and Experimental Methods*, Thesis, Cranfield University.
- Angelinas, S., Tirović, M., Gibbens, P., Roberts, P., Taylor, M. and Stevens, K. (2012) 'Improvement of Convective Heat Dissipation from Commercial Vehicle Disc Brakes by Implementing Geometric Design Alternative', in *EuroBrake 2012*, Dresden, Germany.

Apte, A. A. and Ravi, H. (2006) 'FE Prediction of Thermal Performance and Stresses in a Disc Brake System', *SAE Technical Paper 2006-01-3558*.

Arthur, W. B. (1989) 'Competing Technologies, Increasing Returns, and Lock-In by Historical Events', *The Economic Journal*, 99(394), 116-131.

ArvinMeritor (2009) '2009 Annual Report', [online], *Available:*

<http://phx.corporate-ir.net/phoenix.zhtml?c=122961&p=irol-reportsannual> [Accessed 15/12/2010].

ArvinMeritor (2010) '2010 Annual Report', [online], *Available:*

<http://phx.corporate-ir.net/phoenix.zhtml?c=122961&p=irol-reportsannual> [Accessed 25/01/2011].

Azwadi, C. S. N., Fairus, M. Y. M. and Syahrullail, S. (2010) 'Virtual study of natural convection heat transfer in an inclined square cavity', *Journal of Applied Sciences*, 331-6.

Bagnoli, F., Dolce, F. and Bernabei, M. (2009) 'Thermal fatigue cracks of fire fighting vehicles gray iron brake discs', *Engineering Failure Analysis*, 16(1), 152-163.

Barigozzi, A. and Perdichizzi, A. (2008) 'Combined Experimental and CFD Investigation of Brake Discs Aero-thermal Performances', *SAE Technical Paper 2008-01-2550*.

Barrow, G. (2010) 'Hannover 2010: MAN Concept S claims 25% CO2 reduction', [Online], www.roadtransport.com, [online], *Available:*

<http://www.roadtransport.com/Articles/2010/09/13/136874/Hannover-2010-MAN-Concept-S-claims-25-CO2-reduction.htm>, [Accessed 07 September 2011].

Basi, R. K. (1999) 'WWW response rates to social-demographic items', *Journal of the Market Research Society*, 41(4), 397-402.

Bernon, M. (2008) 'Defining Sustainable Supply Chain Management', in *Supply-Chain World Europe*, Budapest.

-
- Boone, K. *How to conduct a survey*, [online], Available: <http://www.migindia.biz/How-to-conduct-a-survey.pdf> [Accessed 22/12/2011].
- Brace, I. (2004) *Questionnaire Design: How to Plan, Structure and Write Survey Material for Effective Market Research*, First Edition, Kogan Page.
- Bradley, N. (1999) 'Sampling for Internet surveys. An examination of respondent selection for Internet research', *Journal of the Market Research Society*, 41(4), 387-395.
- Carrillo-Hermosilla, J. (2006) 'A policy approach to the environmental impacts of technological lock-in', *Ecological Economics*, 58(4), 717-742.
- Carver, P. R. (1978) 'The Case Against Statistical Significance Testing', *Harvard Educational Review*, 48(3), 378-399.
- Çengel, Y. A. and Boles, M. A. (2007) *Thermodynamics An Engineering Approach*, Sixth Edition, McGraw-Hill.
- Çengel, Y. A. and Cimbala, J. (2004) *Fluid Mechanics: Fundamentals and Applications*, International, Sixth Edition, McGraw-Hill.
- Churchill, S. W. and Chu, H. H. S. (1975) 'Correlating Equations for Laminar and Turbulent Free Convection from a Horizontal Cylinder', *International Journal of Heat Mass Transfer*, 18(9), 1049-1053.
- Corcione, M., Habib, E. and Campo, A. (2011) 'Natural convection from inclined plates to gases and liquids when both sides are uniformly heated at the same temperature', *International Journal of Thermal Sciences*, 50, 1405-1416.
- Cowan, R. and Gunby, P. (1996) 'Sprayed to death: Path dependence, lock-in and pest control strategies', *Economic Journal*, 106(436), 521-542.
- Cowan, R. and Hulten, S. (1996) 'Escaping lock-in: The case of the electric vehicle', *Technological Forecasting and Social Change*, 53(1), 61-79.

- Culierat, J. (2008) *Experimental Investigation of Commercial Vehicle Disc Brake in Respect to Parking Braking*, Thesis, Cranfield University.
- D'Souza, S. (2010) 'Intel's Advertisements: A Critical Analysis of 5 ads', [online], Available: <http://www.scribd.com/doc/36951757/Intel-Advertisements-Critical-Analysis> [Accessed 22/11/2011].
- Damodaran, V., Cherukuru, R. and Jayasundera, A. (2003) 'CFD Based Lumped Parameter Method to Predict the Thermal Performance of Brake Rotors in Vehicle', *SAE Technical Paper 2003-01-0601*.
- Daniel, L. G. (1998) 'Statistical Significance Testing: A Historical Overview of Misuse and Misinterpretation with Implications for the Editorial Policies of Educational Journals', *Research In The Schools*, 5(2), 23-35.
- Das, M. K. and Reddy, K. S. K. (2006) 'Conjugate natural convection heat transfer in an inclined square cavity containing a conducting block', *International Journal of Heat and Mass Transfer*, 49(25-26), 4987-5000.
- Datamonitor (2010a) 'Knorr-Bremse AG, Company Profile', [online], Available: <http://360.datamonitor.com/> [Accessed 06/11/2010].
- Datamonitor (2010b) 'WABCO Holding Inc, Company Profile', [online], Available: <http://360.datamonitor.com/> [Accessed 28/01/2010].
- David, P. A. (1985) 'Clio and the Economics of QWERTY', *American Economic Review*, 75(2), 332-337.
- Department for Transport (2010) *Transport Statistics Bulletin: Vehicle Licensing Statistics 2009*, Department for Transport.
- Desai, C. and Vafai, K. (1992) '3-DIMENSIONAL BUOYANCY-INDUCED FLOW AND HEAT-TRANSFER AROUND THE WHEEL OUTBOARD OF AN AIRCRAFT', *International Journal of Heat and Fluid Flow*, 13(1), 50-64.

-
- Di Pasquale, D., Rona, A. and Garrett, S. J. (2009) 'A selective review of CFD transition models', in *39th AIAA Fluid Dynamics Conference*, San Antonio, Texas, American Institute of Aeronautics and Astronautics.
- Dijk, M. and Yarime, M. (2010) 'The emergence of hybrid-electric cars: Innovation path creation through co-evolution of supply and demand', *Technological Forecasting and Social Change*, 77(8), 1371-1390.
- Dufrénoy, P. (2004) 'Two-/three-dimensional hybrid model of the thermomechanical behaviour of disc brakes', *Proceedings of the Institution of Mechanical Engineers Part F-Journal of Rail and Rapid Transit*, 218(1), 17-30.
- Dufrénoy, P. and Weichert, D. (1995) 'Prediction of railway disc brake temperatures taking the bearing surface variations into account', *Proceedings of the Institution of Mechanical Engineers Part F-Journal of Rail and Rapid Transit*, 209(2), 67-76.
- ECE Regulation No. 13 (2008) 'Concerning the adoption of uniform technical prescriptions for wheeled vehicles, equipment and parts which can be fitted and/or be used on wheeled vehicles and the conditions for reciprocal recognition of approvals granted on the basis of these prescriptions*', *Addendum 12*,
- Emery, A. F. (2003) 'Measured and Predicted Temperatures of Automotive Brakes under Heavy or Continuous Braking', *SAE Technical Paper 2003-01-2712*.
- ENDS (1999) *Ministers agree control on heavy vehicles, ozone depleters*, [online], Available: www.endsreport.com [Accessed 02/10/2010].
- Eppler, S. and Klenk, T. (2002) 'Thermal Simulation within the Brake System Design Process', *SAE Technical Paper 2002-01-2587*.
- Erlston, L. J. and Miles, M. D. (2005) 'A practical solution to full circle brake pad actuation', *SAE Technical Paper 2005-01-3932*.
- European Social Survey (2012) *Exploring public attitudes, informing public policy*.

Faul, F., Erdfelder, E., Lang, A. and Buchner, A. (2007) 'G*Power 3: A flexible statistical power analysis program for the social, behavioral, and biomedical sciences', *Behavior Research Methods*, 39(2), 175-191.

Fluent Inc. (2006) *Release Notes for FLUENT 6.3*, Fluent Inc.

Fox, R. W., McDonald, A. T. and Pritchard, P. J. (2004) *Introduction to Fluid Mechanics*, John Wiley & Sons.

Foxon, T. J. (2002) 'Technological and Institutional 'Lock-In' as a Barrier to Sustainable Innovation', in *International Summer School on Innovations for Sustainable Development: Institutions, Incentives and Economic Policy*, Seeon, Germany, 7-11 September.

Freudenberger, B. (1999) 'Brake Hydraulic System Principles & Service Tips', [online], Available: <http://e-searcher.com/literature-research-papers/breaks/> [Accessed 21/09/2010]

Galindo-Lopez, C. H. (2008) *Optimisation of Convective Heat Dissipation from Ventilated Brake Discs*, Thesis, Cranfield University.

Gao, C. and Kuhlmann-Wilsdorf, D. (1990) 'On stick-slip and the velocity dependence of friction at low speeds', *Transactions of the ASME. Journal of Tribology*|*Transactions of the ASME. Journal of Tribology*, 112(2), 354-60.

Griebel, H. J., Treyde, T. and Kaster, T. (2004) *NVH optimization of an electrical parking brake*, translated by Barton, D. and Blackwood, A., Leeds, England: Professional Engineering Publishing Ltd, 199-207.

Haley, R. I. (1968) 'Marketing Segmentation: A Decision-Oriented Research Tool', *The Journal of Marketing*, 32, 30-35.

Hartsock, D. L., Dinwiddie, R. B., Fash, J. W., Dalka, T., Smith, G. H., Yi, Y. B. and Hecht, R. (2000) 'Development of a high speed system for temperature mapping of a rotating target', *Thermosense Xxii*, 4020, 2-9.

Hassan, M. Z., Brooks, P. C. and Barton, D. C. (2008) 'Thermo-Mechanical Contact Analysis of Car Disc Brake Squeal', *SAE Technical Paper 2008-01-2566*.

-
- Haugen, F. (2010) 'Ziegler–Nichols' Closed-Loop Method', [online], Available: http://teach.no/publications/articles/zn_closed_loop_method/zn_closed_loop_method.pdf [Accessed 21/05/2010]
- Hecht, R. L., Dinwiddie, R. B. and Wang, H. (1999) 'The effect of graphite flake morphology on the thermal diffusivity of gray cast irons used for automotive brake discs', *Journal of Materials Science*, 34(19), 4775-4781.
- Heffernan, M. E. (2006) 'Analyzing and Simulation Brake Rotor Temperatures: A technique Applied to a Formula SAE Vehicle', *SAE Technical Paper 2006-01-1974*.
- Hirose, T., Tanaka, N., Kojima, T., Hatano, T. and Taniguchi, T. (2010) *Study of Activation Timing of Automatic Braking for Vehicle-Infrastructure Cooperative Driving Support System*, translated by Budapest, Hungary.
- Hoem, J. M. (2008) 'The reporting of statistical significance in scientific journals', *Demographic Research*, 18(15), 437-442.
- Hooley, G., Piercy, N. F. and Nicoulaud, B. (2008) *Marketing Strategy and Competitive Positioning*, Fourth Edition, FT Prentice Hall.
- <http://www.exa.com/technology-overview.html> (2013) 'Technology Overview', [online], Available: <http://www.exa.com/technology-overview.html> [Accessed 12/01/2012].
- Incropera, F. P., DeWitt, D. P., Bergman, T. L. and Lavine, A. S. (2006) *Fundamentals of Heat and Mass Transfer*, 6th Edition, John Wiley & Sons.
- International Energy Agency (2008) *Energy technology perspectives 2008: scenarios & strategies to 2050*, International Energy Agency.
- Jang, H., Ko, K., Kim, S. J., Basch, R. H. and Fash, J. W. (2004) 'The effect of metal fibers on the friction performance of automotive brake friction materials', *Wear*, 256(3-4), 406-414.

Jean Callebaut, L. (2007) 'Induction Heating', *Power Quality and Utilization Guide*, Section 7: Energy, Efficiency, pp2-9.

Jerhamre, A. and Bergstrom, C. (2001) 'Numerical Study of Brake Disc Cooling Accounting for Both Aerodynamic Drag Force and Cooling Efficiency', *SAE Technical Paper 2001-01-0948*, 1156-1163.

Jha, A. (2009) 'Labour's £5,000 sweetener to launch electric car revolution', *The Guardian*,

Kalton, G. and Schumen, H. (1982) 'The effect of the question on the survey responses: a review', *Journal of the Royal Statistical Society*, 145(1), 42-73.

Kellner, P. (2004) 'Can online polls produce accurate findings?', *International Journal of Market Research*, 46(1), 3-21.

Kim, S. J. and Jang, H. (2000a) 'Friction and wear of friction materials containing two different phenolic resins reinforced with aramid pulp', *Tribology International*, 33(7), 477-484.

Kim, S. J. and Jang, H. (2000b) 'Friction Characteristics of Non-Asbestos Organic (NAO) and Low-Steel Friction Materials: The Comparative Study', *KSTLE International Journal*, 1(1), 1-7.

Kim, S. W. (2006) 'Thermophysical properties of automotive brake disk materials', *IHOST 2006: 1st International Forum on Strategic Technology, Proceedings*, 163-166.

Kim, S. W., Park, K., Lee, S. H., Kang, K. H. and Lim, K. T. (2008) 'Thermophysical Properties of Automotive Metallic Brake Disk Materials', *International Journal of Thermophysics*, 29(6), 2179-2188.

Lang, P. M. (1962) 'Calculating Heat Transfer Across Small Gas-Filled Gaps', 20(1), 62-63.

Lee, C. W., Chung, H. B., Lee, Y. O., Chung, C. C., Son, Y. S. and Yoon, P. (2010) 'Fault detection method for electric parking brake (EPB) systems with sensorless estimation using current ripples', *International Journal of Automotive Technology*, 11(3), 387-394.

-
- Lee, K. and Barber, J. R. (1993) 'Frictionally Excited Thermoelastic Instability in Automotive Disk Brakes', *Journal of Tribology-Transactions of the Asme*, 115(4), 607-614.
- Lee, K. and Dinwiddie, R. B. (1998) 'Conditions of Frictional Contact in Disc Brakes and Their Effects on Brake Judder', *SAE Technical Paper 980598*, 1077-1086.
- Liang, L., Jian, S. and Xuele, Q. (2005) 'Study on Vehicle Braking Transient Thermal Field Based on Fast Finite Method Simulation', *SAE Technical Paper 2005-01-3945*.
- Limpert, R. (1975) 'The Thermal Performance of Automotive Disc Brakes', *SAE Technical Paper 750873*.
- Limpert, R. (1999) *Brake Design and Safety*, Second Edition, Society of Automotive Engineers.
- Lu, Y. F., Tang, C. F. and Wright, M. A. (2002) 'Optimization of a commercial brake pad formulation', *Journal of Applied Polymer Science*, 84(13), 2498-2504.
- Mackin, T. J., Noe, S. C., Ball, K. J., Bedell, B. C., Bim-Merle, D. P., Bingaman, M. C., Bomleny, D. M., Chemlir, G. J., Clayton, D. B., Evans, H. A., Gau, R., Hart, J. L., Karney, J. S., Kiple, B. P., Kaluga, R. C., Kung, P., Law, A. K., Lim, D., Merema, R. C., Miller, B. M., Miller, T. R., Nielson, T. J., O'Shea, T. M., Olson, M. T., Padilla, H. A., Penner, B. W., Penny, C., Peterson, R. P., Polidoro, V. C., Raghu, A., Resor, B. R., Robinson, B. J., Schambach, D., Snyder, B. D., Tom, E., Tschantz, R. R., Walker, B. M., Wasielewski, K. E., Webb, T. R., Wise, S. A., Yang, R. S. and Zimmerman, R. S. (2002) 'Thermal cracking in disc brakes', *Engineering Failure Analysis*, 9(1), 63-76.
- Majcherczak, D., Dufrenoy, P. and Berthier, Y. (2007) 'Tribological, thermal and mechanical coupling aspects of the dry sliding contact', *Tribology International*, 40(5), 834-843.
- Majcherczak, D. and Dufrénoy, P. (2006) 'Dynamic analysis of a disc brake under frictional and thermomechanical internal loading', *Archive of Applied Mechanics*, 75, 497-512.
- Majcherczak, D., Dufrénoy, P. and Naït-Abdelaziz, M. (2005) 'Third Body Influence on Thermal Friction Contact Problems: Application to Braking', *Journal of Tribology*, 127, 89-95.
- McAdams, W. H. (1954) *Heat Transfer*, Third Edition, McGraw-Hill.

- McDonald, M. and Christopher, M. (2003) *Marketing A Complete Guide*, Palgrave Macmillan.
- McPhee, A. D. and Johnson, D. A. (2008) 'Experimental heat transfer and flow analysis of a vented brake rotor', *International Journal of Thermal Sciences*, 47(4), 458-467.
- Mendenhall, W. and Sincich, T. (2007) *Statistics For Engineering And The Sciences*, Fifth Edition, Pearson Prentice Hall.
- Menter, F. R. (1994) 'Two-equation eddy-viscosity turbulence models for engineering applications', *AIAA Journal*, 32(8), 1598-1605.
- Menter, F. R., Langtry, R. and Volker, S. (2006) 'Transition Modelling for General Purpose CFD Codes', in *6th International Symposium on Engineering Turbulence Modelling and Measurements*, Dordrecht, Netherlands, 277-303.
- Meritor (2010) 'ArvinMeritor Plans to Invest \$42 Million to Aggressively Enhance Its Foundation Brake Position in Europe', [Press Release], 07 September 2011, [online], Available: <http://investors.meritor.com/phoenix.zhtml?c=122961&p=irol-newsArticle&ID=1473155&highlight=> [Accessed 15/01/2012].
- Minseok Jang, authorLink("Lee, Y. O., Lee, Y. O., Lee"), a. W., Lee, W., authorLink("Lee, C. W., Lee, C. W., authorLink("Chung, C. C., Chung, C. C., Son"), a. Y. and Son, Y. (2009) 'Novel clamping force control for electric parking brake systems', in *Asian Control Conference, 2009. ASCC 2009. 7th*, Hong Kong, China, 1588-1593.
- Moffat, R. J. (1985) 'Using Uncertainty Analysis in the Planning of an Experiment', *Journal of Fluids Engineering-Transactions of the Asme*, 107(2), 173-178.
- Moffat, R. J. (1988) 'Describing the Uncertainties in Experimental Results', *Experimental Thermal and Fluid Science*, 1(1), 3-17.
- Morgan, V. T. (1975) 'The Overall Convective Heat Transfer from Smooth Circular Cylinders' in *Advances In Heat Transfer*, New York, 199-264.

-
- Naji, M. and Al-Nimr, M. (2001) 'Dynamic thermal behavior of a brake system', *International Communications in Heat and Mass Transfer*, 28(6), 835-845.
- Nakos, J. T. (2004) *Uncertainty Analysis of Thermocouple Measurements Used in Normal and Abnormal Thermal Environment Experiments at Sandia's Radiant Heat Facility and Lurance Canyon Burn Site*, SAND2004-1023.
- National Instruments (NI 9211 Datasheet) www.ni.com.
- National Instruments (NI 9213 Datasheet) www.ni.com.
- National Instruments (NI 9214 Datasheet) www.ni.com.
- Necati Özisik, M. (1985) *Heat Transfer A Basic Approach*, First Edition, McGraw-Hill.
- Newcomb, T. P. (1969) *Automobile Brakes and Braking Systems*, Bentley Pub.
- NIST ITS Thermocouple Database (1999), [online], Available:
http://srdata.nist.gov/its90/main/its90_main_page.html, [Accessed 10/08/2011].
- Norris, D. G. (1993) "'Intel Inside" Branding A Component In A Business Market', *Journal of Business & Industrial Marketing*, 8(1), 14-24.
- Office of National Statistics (2011) *Performance and Quality Monitoring Report: April to June 2011*.
- Okamura, T. and Yumoto, H. (2006) 'Fundamental Study on thermal Behavior of Brake Discs', *SAE Technical Paper 2006-01-3203*.
- Olphe-Galliard, M. (2011) *Study of the Thermodynamics and Fluid Mechanics Involved in the Cooling of Brake Discs*, Thesis, Cranfield University.

- Orendacova, A., Tibenska, K., Cizmar, E., Orendac, M. and Feher, A. (2007) 'A method for accurate thermal conductivity measurements of small samples at ultra-low temperatures', *Cryogenics*, 47(1), 61-63.
- Ouyang, H., Abu-Bakar, A. R. and Lijie, L. (2009) 'A combined analysis of heat conduction, contact pressure and transient vibration of a disk brake', *International Journal of Vehicle Design*, 190-206.
- Palmer, E., Mishra, R. and Fieldhouse, J. D. (2006) *Analysis of air flow and heat dissipation from high performance passenger car front brake rotor*, translated by University of Huddersfield, Huddersfield: 1-6.
- Panier, S., Dufrénoy, P. and Weichert, D. (2004) 'An experimental investigation of hot spots in railway disc brakes', *Wear*, 256(7-8), 764-773.
- Parker, W. J., Jenkins, R. J., Butler, C. P. and Abbott, G. L. (1961) 'Flash Method of Determining Thermal Diffusivity, Heat Capacity, and Thermal Conductivity', *Journal of Applied Physics*, 32(9), 1679-1684.
- Parry-Husbands, H., Cucka, J. and Smith, S. (2010) "'It's Not Me, It's You: People-centric Media Planning": Leveraging involvement, mind & mood to improve media effectiveness', *ARF Re:think*.
- Pavlidis, V. and Siskos, D. (2010) 'Current Trends in Post-Processing of FEA Results in the Automotive Industry', in *FISITA*, Budapest, Hungary,
- Peng, Y. Q., Li, W. and Ieee (2009) *Research on Fuzzy Control Strategies for Automotive EPB System with AMESim/Simulink Co-simulation, Ccdc 2009: 21st Chinese Control and Decision Conference, Vols 1-6, Proceedings*, New York: IEEE.
- Peter, A. (2012) 'Electric park brake for commercial vehicles', in *ATZlive, Edition Chassis.TechPlus 3rd International Munich Chassis Symposium*, Munich, Germany, 191-201.
- Qi, H. S. and Day, A. J. (2007) 'Investigation of disc/pad interface temperatures in friction braking', *Wear*, 262(5-6), 505-513.

-
- Richardson, P. D. (1963) 'Studies of Flow and Heat Transfer Associated With a Rotating Disc', *Mechanical Engineering Science*, 5(4), 336-342.
- Rickard, S. (2008) *Introduction to Probability*, Cranfield University School of Management, Cranfield University.
- Robinet, B. (2008) *Thermo-mechanical modelling of commercial vehicle disc brake in respect to parking braking*, Thesis, Cranfield University.
- Sakamoto, H. (2004) 'Heat convection and design of brake discs', *Proceedings of the Institution of Mechanical Engineers Part F-Journal of Rail and Rapid Transit*, 218(3), 203-212.
- Savvides, N. and Goldsmid, H. J. (1972) 'MEASUREMENT OF THERMAL-CONDUCTIVITY BY A PARALLEL FLOW SANDWICH TECHNIQUE USING PELTIER EFFECT', *Journal of Physics E-Scientific Instruments*, 5(6), 553-&.
- Schuette, H. and Waeltermann, P. (2005) 'Hardware-in-the-Loop Testing of Vehicle Dynamics Controllers – A Technical Survey', *SAE Technical Paper 2005-01-1660*, 1-19.
- Seglő, F. and Svendenius, J. (2010) 'Electro Mechanical Brake System on Heavy Vehicles', in *FISITA 2010*, Budapest, Hungary,
- Sheridan, D. C., Kutchev, J. A. and Samie, F. (1988) 'Approaches to the Thermal Modeling of Disc Brakes', *SAE Technical Paper 880256*.
- Shivamoggi, B. K. (2003) *Perturbation methods for differential equations*, Birkhauser.
- Sisson, A. E. (1978) 'Thermal Analysis of Vented Brake Rotors', *SAE Technical Paper 780352*.
- Slosarczyk, K., Linden, J. G., Burnham, K. J., Cockings, K. and Capolongo, R. (2008) *Implementation of an electronic park brake feature with limited data availability, Icseng 2008: International Conference on Systems Engineering*, Los Alamitos: IEEE Computer Soc.
- Stevens, K. (2009) *Investigation of Thermal Characteristics for Commercial Vehicle Braking Systems*, Report, Cranfield University.

- Stevens, K., Leiter, R., Taylor, M., Gibbens, P., Roberts, P., Jackson, J., Thomas, P. and Tirović, M. (2010) 'Thermal Aspects in Electronic Parking Braking of Commercial Vehicles', in GRRT, Edition *6th European Conference on Braking*, Lille, France, 327-334.
- Stevens, K., Tirović, M., Roberts, P., Taylor, M. and Gibbens, P. (2012) 'Heat Transfer from Commercial Vehicle Brake Disc Assemblies in Parked Conditions', in ATZlive, Edition *chassus.tech plus*, Munich, Germany, Springer, 721-739.
- Stroud, K. A. (2001) *Engineering Mathematics*, Fifth Edition, Palgrave MacMillan.
- Sun, H. (2006) 'Sensitivity Study on Brake Cooling Performance', *SAE Technical Paper 2006-01-0694*.
- Svrcek, W. Y., Mahoney, D. P. and Young, B. R. (2007) *A Real Time Approach to Process Control*, Second Edition, John Wiley & Sons, Ltd.
- Talati, F. and Jalalifar, S. (2008) 'Investigation of heat transfer phenomena in a ventilated disk brake rotor with straight radial rounded vanes', *Journal of Applied Sciences*, 3583-92.
- Talati, F. and Jalalifar, S. (2009) *Analysis of heat conduction in a disk brake system*, 45, Heat Mass Transfer.
- Taylor, J. R. (1982) *An Introduction to Error Analysis The Study of Uncertainties in Physical Measurements*, University Science Books.
- Thomas, P. and Jackson, J. (2007) *Modular approach to disc brake adjusters and disc brake design*, translated by Frankfurt, Germany.
- Tirović, M. and Galindo-Lopez, C. H. (2008) 'Understanding and improving the convective cooling of brake discs with radial vanes', *Proceedings of the Institution of Mechanical Engineers Part D-Journal of Automobile Engineering*, 222(D7), 1211-1229.
- Tirović, M. and Sergent, N. (2010) 'Lightweight, High Performance Disc Brake Calipers', in *FISITA*, Budapest, Hungary, F2010-B-115.

-
- Tirović, M., Sergent, N., Campbell, J., Roberts, P. and Vignjevic, R. (2012) 'Structural Analysis of Commercial Vehicle Disc Brake Caliper', *Proceedings of the Institution of Mechanical Engineers, Part D: Journal of Automobile* 226, 613-622.
- Tirović, M. and Voller, G. P. (2005) 'Interface pressure distributions and thermal contact resistance of a bolted joint', *Proceedings of the Royal Society a-Mathematical Physical and Engineering Sciences*, 461(2060), 2339-2354.
- Tretsiak, D. and Kliuzovich, S. (2006) 'Research in Self-Boosting Disc Brakes for Commercial Vehicles', in *FISITA 2006*, Yokohama, Japan,
- Tritt, T. M. (2005) *Thermal Conductivity Theory, Properties and Applications*, New York: Springer.
- Valvano, T. and Lee, K. (2000) 'An Analytical Methods to Predict Thermal Distortion of a Brake Rotor', *SAE Technical Paper 2000-01-0445*.
- Vianello, M. (2011) *Analisi termo-meccanica di un freno a disco automobilistico con funzione integrata di freno elettrico di parcheggio*, Thesis, Universita' di Pisa.
- Vishay Micro-Measurements (2007) 'Strain Gage Thermal Output and Gage Factor Variation with Temperature', www.vishaymg.com, Tech Note TN-504-1.
- Voller, G. P. (2003) *Analysis of Heat Dissipation From Railway and Automotive Friction Brakes*, Thesis, Brunel University.
- Voller, G. P., Tirović, M., Morris, R. and Gibbens, P. (2003) 'Analysis of automotive disc brake cooling characteristics', *Proceedings of the Institution of Mechanical Engineers Part D-Journal of Automobile Engineering*, 217(D8), 657-666.
- Wang, Z. L., Tang, D. W. and Zhang, W. G. (2007) 'Simultaneous measurements of the thermal conductivity, thermal capacity and thermal diffusivity of an individual carbon fibre', *Journal of Physics D-Applied Physics*, 40(15), 4686-4690.
- Wawrzonek, L. and Bialecki, R. A. (2008) 'Temperature in a disk brake, simulation and experimental verification', *International Journal of Numerical Methods for Heat & Fluid Flow*, 18(3-4), 387-400.

Wilde, B. and Leiter, R. (2007) *EPB for CV case study*, ArvinMeritor Internal Report, Cwmbran.

Woisard, E. L. (1961) 'Pulse Method for the Measurement of Thermal Diffusivity of Metals', *Journal of Applied Physics*, 32(1), 40-45.

Wu, J. (2010) *An Investigation of Asset Management in Supply Chains*, Thesis, Cranfield University.

Yevtushenko, A. and Kuciej, M. (2010) 'Temperature and thermal stresses in a pad/disc during braking', *Applied Thermal Engineering*, 30(4), 354-359.

Zawilski, B., Littleton, R. T. I., Pope, A. and Tritt, T. M. (1999) 'Parallel thermal conductance technique for measuring thermal conductivity of smaller thermoelectric materials', *Eighteenth International Conference on Thermoelectrics. Proceedings, ICT'99 (Cat. No.99TH8407)*|*Eighteenth International Conference on Thermoelectrics. Proceedings, ICT'99 (Cat. No.99TH8407)*, 10.1109/ICT.1999.843420.